

Conceptual Design and Experimental Investigation of Polymer Matrix Composite Infill Panels for Seismic Retrofitting

by
Wooyoung Jung, Methee Chiewanichakorn
and Amjad J. Aref

Technical Report MCEER-06-0010

September 21, 2006

NOTICE

This report was prepared by University at Buffalo, State University of New York as a result of research sponsored by MCEER through a grant from the Earthquake Engineering Research Centers Program of the National Science Foundation under NSF award number EEC-9701471 and other sponsors. Neither MCEER, associates of MCEER, its sponsors, University at Buffalo, State University of New York, nor any person acting on their behalf:

- a. makes any warranty, express or implied, with respect to the use of any information, apparatus, method, or process disclosed in this report or that such use may not infringe upon privately owned rights; or
- b. assumes any liabilities of whatsoever kind with respect to the use of, or the damage resulting from the use of, any information, apparatus, method, or process disclosed in this report.

Any opinions, findings, and conclusions or recommendations expressed in this publication are those of the author(s) and do not necessarily reflect the views of MCEER, the National Science Foundation, or other sponsors.

Conceptual Design and Experimental Investigation of Polymer Matrix Composite Infill Panels for Seismic Retrofitting

by

Wooyoung Jung¹, Methee Chiewanichakorn¹ and Amjad J. Aref²

Publication Date: September 21, 2006

Submittal Date: September 14, 2005

Technical Report MCEER-06-0010

Task Number 04-2002

NSF Master Contract Number EEC 9701471

- 1 Post Doctoral Research Associate, Department of Civil, Structural and Environmental Engineering, University at Buffalo, The State University of New York
- 2 Associate Professor, Department of Civil, Structural and Environmental Engineering, University at Buffalo, The State University of New York

MULTIDISCIPLINARY CENTER FOR EARTHQUAKE ENGINEERING RESEARCH
University at Buffalo, State University of New York
Red Jacket Quadrangle, Buffalo, NY 14261

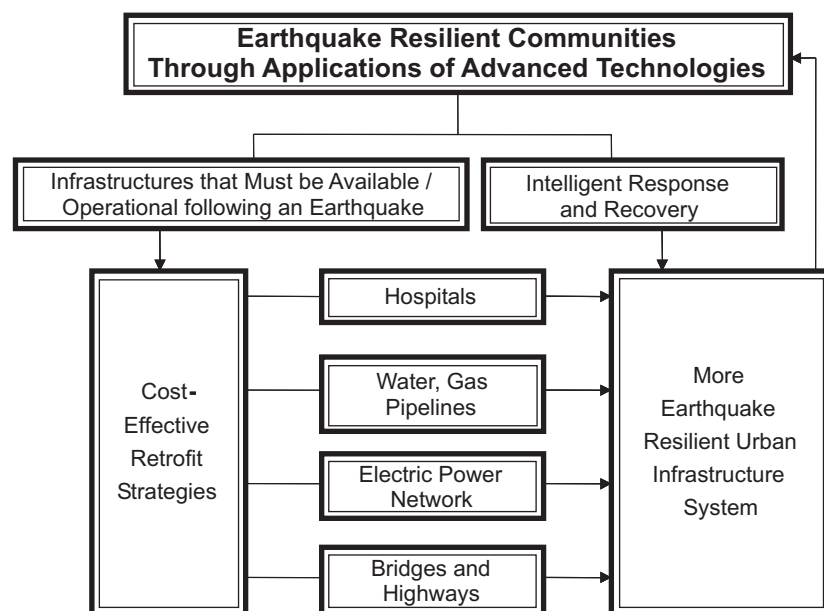
Preface

The Multidisciplinary Center for Earthquake Engineering Research (MCEER) is a national center of excellence in advanced technology applications that is dedicated to the reduction of earthquake losses nationwide. Headquartered at the University at Buffalo, State University of New York, the Center was originally established by the National Science Foundation in 1986, as the National Center for Earthquake Engineering Research (NCEER).

Comprising a consortium of researchers from numerous disciplines and institutions throughout the United States, the Center's mission is to reduce earthquake losses through research and the application of advanced technologies that improve engineering, pre-earthquake planning and post-earthquake recovery strategies. Toward this end, the Center coordinates a nationwide program of multidisciplinary team research, education and outreach activities.

MCEER's research is conducted under the sponsorship of two major federal agencies: the National Science Foundation (NSF) and the Federal Highway Administration (FHWA), and the State of New York. Significant support is derived from the Federal Emergency Management Agency (FEMA), other state governments, academic institutions, foreign governments and private industry.

MCEER's NSF-sponsored research objectives are twofold: to increase resilience by developing seismic evaluation and rehabilitation strategies for the post-disaster facilities and systems (hospitals, electrical and water lifelines, and bridges and highways) that society expects to be operational following an earthquake; and to further enhance resilience by developing improved emergency management capabilities to ensure an effective response and recovery following the earthquake (see the figure below).



A cross-program activity focuses on the establishment of an effective experimental and analytical network to facilitate the exchange of information between researchers located in various institutions across the country. These are complemented by, and integrated with, other MCEER activities in education, outreach, technology transfer, and industry partnerships.

In this research, three prefabricated PMC infill panel systems for seismic retrofitting were studied using experimental and analytical methods to assess their effectiveness and response under simulated earthquake loading. The concept of combined interface damping layers, which include honeycomb and solid viscoelastic materials, was applied to these panel systems and was found to be highly feasible for use in seismic applications. Design and fabrication procedures for each PMC infill panel are presented, as well as the results from a conceptual trial design using finite element (FE) analysis. Both monotonic and cyclic loading tests were performed on full-scale models to validate these systems in real situations. The results show that PMC infill panel systems offer the potential to increase the damping as well as the lateral resistance of steel frames, with a relatively low cost of retrofitting.

ABSTRACT

By using polymer matrix composite (PMC) material, new conceptual designs for seismic retrofitting were developed for application in existing buildings. Similar to partial rehabilitation techniques using composite material such as column wrapping, the use of prefabricated PMC infill panel systems is a very efficient way to achieve seismic retrofitting of existing facilities because of the efficiency of the material and its ease of use in construction. PMC material has high stiffness-to-weight and strength-to-weight ratios. Thus, the addition of PMC infill panels into existing structures will not significantly alter the weight of the structure while providing substantial structural enhancement.

In this research, three prefabricated PMC infill panel systems for seismic retrofitting were proposed. The PMC infill panels were studied using experimental methods to assess their effectiveness and response under simulated earthquake loading. Applying the concept of combined interface damping layers to the proposed panel systems was found to be highly feasible in the seismic applications. Design and fabrication procedures for each PMC infill panel were presented, and a conceptual trial design was performed using finite element (FE) analysis. To validate the proposed systems in real situations, both monotonic- and cyclic-loading tests were performed on full-scale models. The results obtained from this research showed that the systems offer the potential to increase the damping as well as the lateral resistance of steel frames, with a relatively low cost of retrofitting.

ACKNOWLEDGEMENTS

This research was funded by the Earthquake Engineering Research Centers Program of the National Science Foundation under Award Number EEC-970147 to the Multidisciplinary Center for Earthquake Engineering Research (MCEER). The financial support in the form of a research assistantship is greatly appreciated. Special thanks go to An-Cor Industrial Plastics, Inc. and 3M Corp., Japan for their support and valuable advice on the fabrication of the test specimen.

Furthermore, considerable thanks are due to the supporting staff in the laboratory in Ketter Hall at University at Buffalo, including Mr. Mark Pitman, Late, Mr. Richard Cizdziel, Mr. Scott Weinreber, Mr. Duane Kozlowski. Without their help and advice, the experimental studies would not have successfully completed.

TABLE OF CONTENTS

SECTION	TITLE	PAGE
1	INTRODUCTION	1
1.1	Motivation for This Study	1
1.2	Literature Review of Infilled Frame Structures	3
1.3	Structural Applications of Polymer Matrix Composite Materials	6
1.4	Rehabilitation Strategies and Objectives	7
1.5	Research Background and Objectives	11
1.6	Organization of The Report	15
2	MATERIAL CHARACTERISTICS	17
2.1	Polymer Matrix Composite Material	17
2.1.1	Fiber, Matrices, and Fabrication of Composites	17
2.1.2	Test Description of FRP Composite Material	21
2.1.3	Selection of FRP Composite Laminate	24
2.1.4	Volume and Weight Fractions	25
2.1.5	Results of FRP Material Tests	26
2.2	Steel Members	36
2.2.1	Material Description and Test Results	36
2.3	Polymer Honeycomb Material	40
2.3.1	Description of the Material	40
2.3.2	Results of the Polymer Honeycomb Material Tests	41
3	TESTING OF SEMI-RIGIDLY CONNECTED STEEL FRAME	49
3.1	Introduction	49
3.2	The Configuration of Semi-rigid Steel Frame	50
3.3	Testing of Semi-rigidly Connected Steel Frame	53
3.3.1	Test Specimen Setup	53

TABLE OF CONTENTS (cont'd)

SECTION	TITLE	PAGE
3.3.2	Supplementary Test Setup	54
3.3.3	Discussion of Test Results	57
4	MULTI-LAYER PMC INFILL PANEL SYSTEM	67
4.1	Introduction	67
4.1.1	Typical Structural System of Composite Panel	67
4.1.2	Selecting Proper Construction Materials	68
4.1.3	Simplified Design Cases of FRP Laminates	69
4.2	Design of a Multi-layer PMC Infill System	72
4.2.1	Design Concept and Configuration	72
4.2.2	Construction	87
4.3	Test Specimens and Experimental Setup	91
4.4	Experimental Description and Procedure	96
4.5	Discussion of Test Results	97
4.6	Summary	114
5	ENERGY DISSIPATING INTERFACE DAMPING LAYERS	115
5.1	Introduction	115
5.2	Basic Material Description	116
5.3	Description of Test Setup	123
5.4	Experimental Results	125
5.4.1	Polymer Honeycomb Material Testing	125
5.4.2	Testing of Combined Honeycomb and Viscoelastic Material	135
5.4.3	A Study of Combining Ratio Between Materials	148
5.5	Summary	158
6	ENHANCED PMC DAMPING INFILL PANEL SYSTEMS	163
6.1	Introduction	163

TABLE OF CONTENTS (cont'd)

SECTION	TITLE	PAGE
6.2	Design of a Multi-panel PMC Infill System	164
6.2.1	Design Concept and Structural Configuration	164
6.2.2	Construction	180
6.3	Design of FRP Box Infill Systems	186
6.3.1	Design Concept and Structural Configuration	186
6.3.2	Construction	193
6.4	Test Cases and Specimen Setup	197
6.5	Experimental Description	202
6.5.1	Instrumentations	202
6.5.2	Loading System and History Protocol	207
6.6	Results and Discussions	210
6.6.1	Results of Multi-panel PMC Infilled Frame Test	210
6.6.2	Result of FRP Box Infill Panel Testing	241
6.6.3	Honeycomb Effect of the Interface Damping Layers	258
6.7	Summary	260
7	CONCLUSIONS AND RECOMMENDATIONS	265
7.1	Conclusions	265
7.1.1	General Advantages of Proposed PMC Infill Panel Systems	265
7.1.2	Multi-layer PMC Infilled Frame	266
7.1.3	Combining Interface Constrained Damping Layer	268
7.1.4	PMC Infill Panel Systems with Passive Energy Dissipation Mechanisms	270
7.2	Recommendation for Future Works	275
	REFERENCES	279
	APPENDICES	287
	Appendix A: Classical Lamination Theory	288

LIST OF ILLUSTRATIONS

FIGURE	TITLE	PAGE
1-1	Types of Renewal Strategies	7
1-2	Design Approach of Rehabilitation Techniques (Moehle, 2000)	8
1-3	Geometric Configuration of the Damping Panel	14
2-1	Longitudinal Stress–Strain Diagram for Hypothetical Composite	21
2-2	Coupon Dimensions of Each Test (unit = inch)	22
2-3	The Shear Test Fixtures	24
2-4	Test Results of Two FRP Material Systems	25
2-5	The First & Second Test of Tensile Coupon (0°)	28
2-6	The Third & Fourth Test of Tensile Coupon (0°)	28
2-7	The First & Second Test of Tensile Coupon (90°)	29
2-8	The Third & Fourth Test of Tensile Coupon (90°)	29
2-9	The First Test of Compression Coupon (0°)	30
2-10	The Second Test of Compression Coupon (0°)	30
2-11	The First Test of Compression Coupon (90°)	31
2-12	The Ultimate Stress of Compression Test	31
2-13	The First Test of Shear Coupon (0°)	33
2-14	The Second Test of Shear Coupon (0°)	33
2-15	The Third Test of Shear Coupon (0°)	33
2-16	The First Test of Shear Coupon (90°)	34
2-17	The Second Test of Shear Coupon (90°)	34
2-18	The Third Test of Shear Coupon (90°)	34
2-19	Steel Coupon Test for Unused Joint Angle Connections	37
2-20	Steel Coupon Test for Existing Steel Frame Members	37
2-21	Stress–strain Results of Previous test (Mander et al., 1993)	39
2-22	Honeycomb Carrying Load on the Surface Normal to Z Axis	41
2-23	The Dimension of Polymer Honeycomb Test Coupon (unit = inch)	42

LIST OF ILLUSTRATIONS (cont'd)

FIGURE	TITLE	PAGE
2-24	Polymer Honeycomb Test Coupon (Side View)	42
2-25	Loading and Unloading Test of the Polymer Honeycomb Material	43
2-26	Shear Modulus of the Polymer Honeycomb Material	44
2-27	Full Stress-strain Behavior of the Polymer Honeycomb Material	44
2-28	Setup of Polymer Honeycomb Test Coupon	45
2-29	The Small Deform Shape of Polymer Honeycomb Material ($\epsilon = 0.28$ in/in)	46
2-30	The Large Deform Shape of Polymer Honeycomb Material ($\epsilon = 0.79$ in/in)	46
2-31	The Failure of Polymer Honeycomb Material ($\epsilon = 1.60$ in/in)	47
2-32	The Bonding Scrim Failure of Polymer Honeycomb Material Coupon	47
3-1	Detailed Configuration of Top and Seat Angle Connections (unit = inch)	51
3-2	The Configuration of Hinge Support (unit = inch)	51
3-3	The Configuration of Steel Frame (unit=inch)	52
3-4	Steel Frame Setup	53
3-5	Configuration of Stabilizing Frames	55
3-6	Setup of Steel Frame Structure (unit = inch)	56
3-7	Configuration of Out-of-plane Supporting Steel Plate (unit=inch)	57
3-8	Result of Push-over Loading Test for Steel Frame (Case 1, 1.0%)	59
3-9	Result of Cyclic Loading Test for Steel Frame Tests (Case 1, 1.0 & 1.5% drift)	59
3-10	Result of Push-over Loading Test for Steel Frame (Case 2)	62
3-11	Comparison of Stiffness of Semi-rigid Steel Frame (1.0% drift)	63

LIST OF ILLUSTRATIONS (cont'd)

FIGURE	TITLE	PAGE
3-12	Stiffness Degradation of Test Frame under Progressive Test Cases	63
3-13	Comparison of In-plane Behavior for Semi-rigid Steel Frame before and after Joint Angle Connection Damage under Push-over Loading	64
3-14	Moment-Rotation Relation of Steel Frame Tests at Left Top Joint Connection	64
3-15	Result of Cyclic Loading Test for Steel Frame Tests (Case 2, 1.0 & 1.5% drift)	65
3-16	Comparison of Hysteretic Behavior for Semi-rigid Steel Frame Before and After Joint Angle Connection Damage Under Cyclic Loading	65
4-1	Simplified Stacking Sequence Cases of Typical Composite Laminate	71
4-2	The Mechanical Concept of Composite Infilled Frame	73
4-3	The Schematic Representation of the Energy Mechanism for the Composite Infilled Frame	74
4-4	Overall Configuration of the Multi-layer PMC Infill Panel	75
4-5	The Shape of Each Components of Composite Panel	75
4-6	Geometric Configuration of an Inner PMC Sandwich Panel	77
4-7	Geometric Configuration of the Polymer Honeycomb Layer	78
4-8	Geometric Configuration of Outershell Layers	78
4-9	Detailed Cross Section of the Multi-layer PMC Infill Panel	79
4-10	Detailed Rounded Edge of a Multi-layer PMC Infill Panel (unit = inch)	80
4-11	The Results of Combined Simplified Stacking Sequences for Composite Wall Laminate Design	82
4-12	Orientation Codes of Coreshell	84
4-13	Orientation Codes of Outershell	85
4-14	The Axis of Each lamina Orientation (unit=inch)	86

LIST OF ILLUSTRATIONS (cont'd)

FIGURE	TITLE	PAGE
4-15	Fabricating Procedure of a Multi-layer PMC Infill Panel	87
4-16	Inner PMC Sandwich Composite Panel	88
4-17	Completed Fabrication of the Multi-layer PMC Infill Panel	89
4-18	Specific Cross Section of the Multi-layer PMC Infill Panel	90
4-19	FRP Anchor Tab for Experimental Setup	90
4-20	Multi-layer Infill Panel Setup	91
4-21	Strain Gages on an Inner PMC Sandwich Panel	92
4-22	Location of Linear Potentiometers	93
4-23	Typical Instruments for Experiments	93
4-24	Epoxy Grouting in the Initial Gap	94
4-25	The Column to Infill Connection	95
4-26	Force-Displacement Relationship of the Multi-layer PMC Infilled Frame under Push-over Loading (1.0% drift)	97
4-27	Comparison of Force-displacement Response for the Steel Frame and the Multi-layer PMC Infilled Frame under Push-over Test (1% drift)	98
4-28	Estimation for Net Response of the Multi-layer PMC Infill within Elastic Range of the Structure	99
4-29	Hysteretic Response of the Multi-layer PMC Infilled Frame under Successively Cyclic Loading Drift	100
4-30	Comparison of Hysteretic Response for Steel and Multi-layer PMC Infill Frames (different scales) : (a) 0.5%; (b) 1.0%; (c) 1.5% drift	101
4-31	Test Result of Initial Gap Effect	102
4-32	The Result of Hysteretic Loops for Steel Frame Test for Each Cycle under Cyclic Load	104
4-33	The Result of Hysteretic Loops for Multi-layer PMC Infilled Frame Test for Each Cycle under Cyclic Load	104
4-34	Energy Dissipation Capacity for the Multi-layer PMC Infilled Frame (different scales) (unit = kips-in)	105

LIST OF ILLUSTRATIONS (cont'd)

FIGURE	TITLE	PAGE
4-35	Behavior of the Multi-layer PMC infill Wall with Top and Side Gaps	106
4-36	The Schematic of Possible Force Path and Detail of Localized Damage (C: Comp; T: Tension)	106
4-37	Out-of-plane Buckling Displacement of the PMC Sandwich Infill	106
4-38	Test Observation for Out-of-plane Buckling Displacement of the PMC Sandwich Infill	107
4-39	The Comparison of the Shear Deformation of polymer Honeycomb Layer under Applied Loading	110
4-40	The Comparison of Test Results for the PMC Infilled Frame with and without Connection under Monotonic Loading (1.0 %)	111
4-41	The Comparison of Test Results for the PMC Infilled Frame with and without Connection under Cyclic Loading (1.0 %)	111
4-42	The Damage of the Multi-layer PMC Infilled Frame with the Column-to-Infill Connection (1)	112
4-43	The Damage of the Multi-layer PMC Infilled Frame with the Column-to-Infill Connection (2)	113
5-1	The Structure of the Honeycomb Material	117
5-2	Material Monotonic Test Results for Honeycomb	118
5-3	Creep Test Results for 3M Viscoelastic Material (3M Corp., Japan)	119
5-4	Schematic Presentation of the Idealized Force–Displacement Relation	122
5-5	Test Coupon (a) Design; (b) Configuration (unit = inch)	123
5-6	Longitudinal Force on Each Surface (Direct Shear) : (a) polymer Honeycomb; (b) 3M Viscoelastic Solid	124
5-7	The Comparison of the Stiffness for Different Thicknesses	127
5-8	The Comparison of the Shear Modulus for Each Thickness	127
5-9	The Variation of Stiffness for Different Frequencies (5% Strain)	128

LIST OF ILLUSTRATIONS (cont'd)

FIGURE	TITLE	PAGE
5-10	The Variation of Strength for Different Frequencies (5% Strain)	128
5-11	Deformed Shape of Polymer Honeycomb Material Tests at Different Frequencies (10% strain)	129
5-12	Hysteresis Loops of Sinusoidal Test for Different Frequencies (10% strain, 0.394 in. thickness)	130
5-13	Hysteresis Loops of Sinusoidal Test for Different Frequencies (10% strain, 0.512 in. thickness)	130
5-14	The Result of Honeycomb Material with Different Area (Case 1, 10% strain)	131
5-15	The Result of Honeycomb Material with Different Area (Case 1, 30% strain)	131
5-16	The Result of Honeycomb Material with Different area (Case 2, 10% strain)	132
5-17	The Result of Honeycomb Material with Different Area (Case 2, 30% strain)	132
5-18	The Result of Honeycomb Material with Different area (Case 3, 10% strain)	133
5-19	The Result of Honeycomb Material with Different Area (Case 3, 30% strain)	133
5-20	The Variation of Effective Stiffness for the Area Ratio	134
5-21	Test Samples (H = Polymer Honeycomb, V = Solid Viscoelastic, unit=inch)	137
5-22	Results of the Initial and Post Stiffness for Combining Composite Materials with Different Thickness (Viscoelastic/Honeycomb/Viscoelastic): (a) 0.197 in (b) 0.394 in (c) 0.512 in	138
5-23	Results of the Hysteresis Loops for Combining Composite Materials with Different Thickness (10% Strain, 1.0 Hz)	139
5-24	Results of the Hysteresis Loops for Combining Composite Materials with Different Thickness (10% Strain, 3.0 Hz)	139

LIST OF ILLUSTRATIONS (cont'd)

FIGURE	TITLE	PAGE
5-25	Comparison of the Stiffness of Each Combination: Initial Stiffness	140
5-26	Comparison of the Stiffness of Each Combination: Post Failure Stiffness	140
5-27	Test Results for Stiffness Degradation	141
5-28	Test Results for each case ($f = 1.0$ Hz)	142
5-29	The Combined Honeycomb/Viscoelastic (H-V) Specimen Test	143
5-30	The Combined Honeycomb/Viscoelastic/Honeycomb (H-V-H) Specimen Test	144
5-31	The Combined Viscoelastic/Honeycomb/Viscoelastic (V-H-V) Specimen Test	145
5-32	The Effect of the 3M Viscoelastic Materials for Different Frequencies: (a) 0.1 Hz (b) 1.0 Hz (c) 3.0 Hz	146
5-33	Comparison of the Behavior for the Honeycomb Damper and the Combined Composite Damper: (a) 0.1 Hz (b) 1.0 Hz (c) 3.0 Hz	147
5-34	Configuration of Test Specimen (unit = inch)	148
5-35	Idealized Stress versus Strain Relation	150
5-36	Shear Stress-Strain Relation of 3M Viscoelastic Solid Material	151
5-37	Hysteretic Energy of 3M Viscoelastic Solid Material for Different Frequencies (30% strain rate)	151
5-38	Comparison of Analytical and Experimental Results for the 3M Viscoelastic Material	152
5-39	Variation of the Stiffness for Different Applied Strain Rates	154
5-40	Variation of the Stiffness for Different Applied Frequencies	154
5-41	Energy Dissipation Capacity for Several Combined Cases: (a) 10% strain (b) 30% Strain (c) 50% Strain	155
5-42	Variation of Energy Dissipation for Various Viscoelastic Mixing Ratio: (a) 10% strain (b) 30% Strain (c) 50% Strain	156
5-43	Test Specimen Setup	157

LIST OF ILLUSTRATIONS (cont'd)

FIGURE	TITLE	PAGE
5-44	Deformation of the Combining Interface Layers	157
5-45	Honeycomb Failure of the Combined Interface Layers	157
5-46	Hysteretic Energy of Different Damper Cases (10% strain, 1.0 Hz)	159
5-47	Comparison of Energy Dissipation for Different Cases	160
6-1	The Geometric Configuration of the Multi-panel PMC Infill Panel	165
6-2	Numerical Design Examples for Maximum Buckling Force of Several Stacking Sequence Arrangements	168
6-3	Simplified Numerical Analysis for the PMC Sandwich Infill Design	169
6-4	The Detailed Dimension of PMC Sandwich Panel (unit=inch)	171
6-5	The Orientation of Stacking Sequence of Inner Panel (unit=inch)	172
6-6	Force-displacement Relation of the PMC Infilled Frame for Different Contact Distance	173
6-7	Numerical Results for the Initial Gap Distance and Contact Lateral Displacement Relationship	173
6-8	Geometric Configuration of the Damping Panel	174
6-9	Deformed Geometry of the Damping Panel during Inter-story Drift	175
6-10	The Detail Dimension of a Damping Panel (unit=inch): (a) Interface Damping Layer (b) FRP Laminated Plate	177
6-11	The Detail Configuration of Each Cross Section	178
6-12	The Detail Dimension of Outer Panel (unit = inch)	179
6-13	Fabrication of the PMC Sandwich Infill Panel	180
6-14	Detailed Fabrication of the Interface Damping Layer	181
6-15	Typical Failure Mechanisms for the Pinned-joint Configuration	182
6-16	Top Connection of the Outer Damping Panel (Slot)	184
6-17	Bottom Connection of Outer Damping Panel (Pin)	184

LIST OF ILLUSTRATIONS (cont'd)

FIGURE	TITLE	PAGE
6-18	Sandwiched Steel Plate in the Outer Damping Panel Laminate	185
6-19	View of the Outer Damping Panel	185
6-20	The Configuration of FRP Box Infill System (unit=inch)	186
6-21	The Detail Dimension of Interface Layer (unit=inch)	187
6-22	The Configuration of Two Types of FRP Box Infill Systems	188
6-23	The Detailed Description of the FRP Box Infill System (unit=inch)	190
6-24	The Basic Orientation of FRP Box Infill (Each ply layer = 0.03 inch)	191
6-25	The Configuration of the FRP Box Infill (Each layer = 0.03 inch)	192
6-26	Fabricated FRP Box Infill Panel	194
6-27	Cross Section of FRP Box Infill	194
6-28	Top Connection of the FRP Box Infill (Slot)	195
6-29	Bottom Connection of the FRP Box Infill (Pin)	195
6-30	Sandwiched Steel Plate in the FRP Box Panel	196
6-31	Configuration of the Proposed Stiff Layer of the Interface	196
6-32	PMC Sandwich Infill Setup	198
6-33	Wood and Rubber Spacers	198
6-34	Design of Outer Damping Panel Connectors (unit=inch)	199
6-35	Fabrication Process of Beam-to-Panel Connector	200
6-36	Multi-panel PMC Infill Panel Setup	201
6-37	FRP Box Infill System Setup	202
6-38	Strain Gage Location at the Inner Panel and the Steel Members (Cp: Composite strain pairs, ST: Steel strain pairs, unit=inch)	203
6-39	Calculation of the Steel Straining Actions	204
6-40	Strain Gage Setup of the Test Specimen	205
6-41	Joint Angle Connection Instrumentation	205

LIST OF ILLUSTRATIONS (cont'd)

FIGURE	TITLE	PAGE
6-42	Linear Potentiometers for Special Measurements	206
6-43	Linear Potentiometer Setup at the Interface Layers	206
6-44	Design of Diagonal and Out-of-plane LVDTs	207
6-45	Displacement Pattern Applied Cyclic Loading	208
6-46	Force-displacement Relationship of the PMC Sandwich Infill Panel under Push-over load	211
6-47	Loading and Unloading Relation of the PMC Sandwich Infill	211
6-48	Comparison of Inter-story Drift - Rotation Relation of Each Joint Angle Connection	212
6-49	Moment-Rotation Relation of Top Joint Connection (PMC Sandwich Infilled Frame Test, Push-over Load)	212
6-50	Maximum Moment Distribution of Steel Column under Push-over Test (2.0%)	214
6-51	Maximum Moment Distribution of Steel Beam under Push-over Test (2.0%)	214
6-52	Reduction of Bending Moment at the Column after the Contact Point	215
6-53	Reduction of Bending Moment at the Beam after the Contact Point	215
6-54	Strain Variation of the PMC Infill Panel	216
6-55	Strut Angle Distribution of the PMC Infill Panel along Principal Material Coordinate Direction	216
6-56	Strut Angle Distribution of the PMC Infill Panel along Global Coordinate Direction	217
6-57	Initial Stiffness of the Multi-panel Infilled Frame Test (1% Drift, Push-over Test)	221
6-58	Enhanced Stiffness Effect of the Interface Damping Layers	221
6-59	Shear Deformation of the Interface Damping Layer under Push-over Load (1.0%)	222

LIST OF ILLUSTRATIONS (cont'd)

FIGURE	TITLE	PAGE
6-60	Comparison of Moment-Rotation Behavior of the Bare Frame before and after the the Multi-panel Infilled Frame Tests (1.0%, Push-over)	222
6-61	Moment-Rotation Relation of the Top and Seat Angle Connection in the Multi-panel Infill System (1.0%, Push-over)	223
6-62	Top Joint Rotation Response of the Multi-panel PMC Infilled Frame under Cyclic Loading	223
6-63	Bottom Joint Rotation Response of the Multi-panel PMC Infilled Frame under Cyclic Loading	224
6-64	Comparison of Top Joint Rotation Response before and after the Infill contact in the Multi-panel PMC Infilled Frame	224
6-65	Comparison of Moment Distribution of the Left Steel Column (1.0%, Push-over)	225
6-66	Comparison of Moment Distribution of the Right Steel Column (1.0%, Push-over)	225
6-67	Comparison of Moment Distribution of the Top Steel Beam (1.0%, Push-over)	226
6-68	Hysteretic Response of the Multi-panel PMC Infilled Frame Before Making Contact with the PMC Sandwich Infill Panel	230
6-69	Hysteretic Response of the Multi-panel PMC Infilled Frame in Contact with the PMC Sandwich Infill Panel	230
6-70	Comparison of Damping Performance between the Steel Frame and the Multi-panel Infill System (0.16%, $f = 0.5$ Hz)	231
6-71	Comparison of Damping Performance between the Steel Frame and the Multi-panel Infill System (0.16%, $f = 0.25$ Hz)	231
6-72	Comparison of Damping Performance between the Steel Frame and the Multi-panel Infill System (1.0%, $f = 0.08$ Hz)	232
6-73	Comparison of Damping Performance between the Steel Frame and the Multi-panel Infill System (1.0%, $f = 0.04$ Hz)	232
6-74	Comparison of Damping Performance between the Steel Frame and the Multi-panel Infill System (1.5%, $f = 0.054$ Hz)	233

LIST OF ILLUSTRATIONS (cont'd)

FIGURE	TITLE	PAGE
6-75	Comparison of Damping Performance between the Steel Frame and the Multi-panel Infill System (1.5%, $f = 0.027$ Hz)	233
6-76	Comparison of Hysteretic Energy Dissipation Under Various Frequencies (1.0% drift)	234
6-77	High Frequency Effect of the Outer FRP Damping Panel Systems (1.0% drift, $f = 3.0$ Hz)	234
6-78	Variation of Shear Deformation of the Left Interface Damping Layer under Increasing Cyclic Loading Drift	235
6-79	Variation of Shear Deformation of the Right Interface Damping Layer under Increasing Cyclic Loading Drift	235
6-80	The Rate Effect of the Interface Damping Layer of the Multi-panel Infilled Frame: (a) 0.16%; (b) 0.5%; (c) 1.0% drift	236
6-81	Frequency Effect of the Multi-panel Infill System under Cyclic Loading (1.0% drift)	237
6-82	Comparison of Energy Dissipation Capacity for the Multi-panel Infill System and the Steel Frame (1.0% drift)	237
6-83	Stiffness Degradation of the Multi-panel Infill System under Successively Applied Cycles	238
6-84	Destructive Test of the Multi-panel PMC Infilled Frame under Push-over Loading (Up to 3.0% drift)	238
6-85	Schematic Representation of the Failure Caused by Impact Pressure Between the Bolted Angle Connection and the Infill	239
6-86	The Failure of the Multi-panel PMC Infilled Frame Structure	240
6-87	Force-Displacement Response of the FRP Box Infill Systems under Push-over Loading (1% drift)	243
6-88	Variation of Shear Deformation of the Interface Layer in the FRP Box Infill Systems under Push-over Loading (1% drift)	243
6-89	Hysteretic Response of the FRP Box Infill System (Case 1, High Frequency (3.0 Hz))	244
6-90	Hysteretic Response of the FRP Box Infill System (Case 2, High Frequency (3.0 Hz))	244

LIST OF ILLUSTRATIONS (cont'd)

FIGURE	TITLE	PAGE
6-91	Shear Deformation of the Interface Layers of the Test Structure Case 1 (1.5% Drift)	245
6-92	Shear Deformation of the Interface Layers of the Test Structure Case 2 (1.5% Drift)	245
6-93	Variation of the Shear Deformation on the Combining Interface Layer under Cyclic Loading Tests (Case 1)	246
6-94	Variation of the Shear Deformation of the Interface Damping Layer under Cyclic Loading Tests (Case 2)	246
6-95	Frequency Effect of the Combining Interface Layer in the FRP Box Infill (Case 1, 1.5%)	248
6-96	Frequency Effect of the Combining Interface Layer in the FRP Box Infill (Case 2, 2.0%)	248
6-97	Comparison of the Hysteretic Energy for the FRP Box Infill (Case 1) and the Steel Frame (1.0% drift, $f = 0.08$ Hz)	249
6-98	Comparison of the Hysteretic Energy for the FRP Box Infill (Case 2) and the Steel Frame (1.0% drift, $f = 0.08$ Hz)	249
6-99	Comparison of the Hysteretic Energy for the FRP Box Infill (Case 1) and the Steel Frame (1.5% drift, $f = 0.054$ Hz)	250
6-100	Comparison of the Hysteretic Energy for the FRP Box Infill (Case 2) and the Steel Frame (1.5% drift, $f = 0.054$ Hz)	250
6-101	Comparison of Energy Dissipation Capacity for the FRP Box Panel Cases and the Steel Frame (1.0% drift, $f = 0.08$ Hz)	251
6-102	Failure of the FRP Box Infill having a Stiff and a Flexible Interface Layers under Cyclic Load (2.0% drift, $f = 0.04$ Hz)	251
6-103	Schematic Representation of the FRP Box Infill Geometry	254
6-104	Shear Deformation of the Interface Layer at B Location (1.0% drift)	255
6-105	Comparison of Shear Deformation for the Interface Layers at B Location in Both Cases (1.0% drift)	255
6-106	Comparison of Hysteretic Response for Both Cases of the FRP Box Infill Systems (0.16% drift)	256

LIST OF ILLUSTRATIONS (cont'd)

FIGURE	TITLE	PAGE
6-107	Comparison of Hysteretic Response for Both Cases of the FRP Box Infill System (1.0% drift)	256
6-108	Comparison of Hysteretic Response for Both Cases of the FRP Box Infill System (1.5% drift)	257
6-109	Failure of Joint Angle Connection by Preventing Shear Deformation of the FRP Box Infill System (Case 1, 1.5% Drift)	257
6-110	Stiffness Variation through the Honeycomb Effect of the Interface Layer (Case 1, 1.5% drift)	259
7-1	Plastic Hinge Mechanism: (a) Single-story Steel Frame; (b) Multi-story Steel Frame	276
A.1	Bending of Line Element in x-z Plane	291
A.2	Geometry and Resultant Forces of a Laminate	295

LIST OF TABLES

TABLE	TITLE	PAGE
2-1	Typical Laminate Comparison Data. (Fiber Glast Corp., 1999)	18
2-2	The Properties of Boat and Tooling Glass Fabric (Style 7781)	18
2-3	Typical Properties of DERA KANE 411 (Dow Chemical Comp., 1999)	20
2-4	The Results of Each Test for FRP Materials	25
2-5	The Other Properties of Used FRP laminate	26
2-6	The Dimension of Each Test Coupon for Composite Panel	27
2-7	The Result of Tensile Coupon (0°)	27
2-8	The Result of Tensile Coupon (90°)	27
2-9	The Result of Compression Coupon (0°)	30
2-10	The Result of Compression Coupon (90°)	30
2-11	The Result of Shear Coupon (0°)	32
2-12	The Result of Shear Coupon (90°)	32
2-13	The Summary of Material Test Results	35
2-14	Properties of Polymer Honeycomb Material (Nida-Core Corp.)	40
2-15	Tested Properties of Polymer Honeycomb Material	45
2-16	Real Properties of Polymer Honeycomb Material (Nida-Core Corp., FL)	45
4-1	The Properties of Vinyl Foam (An-Cor plastic Inc.)	69
4-2	The Properties of Divinycell H100 (Divinycell Corp.)	69
4-3	The Results of Various Laminate Layups of the Composite Infill	83
4-4	The Designing Stacking Sequence for Coreshell	84
4-5	The Designing Stacking Sequence for Outershell	85
4-6	The Modified Stacking Sequence of Composite Laminates (Unit = inch)	88
4-7	Comparison of Test Results for the Column-to-Infill Connections	109

LIST OF TABLES (cont'd)

TABLE	TITLE	PAGE
5-1	The Properties of 3M Viscoelastic Material (3M, Japan)	120
5-2	The Dimensions of Test Specimens	124
5-3	The Loading Patterns Based on the Displacement Control	124
5-4	The Results of Monotonic Loading Tests	127
5-5	The Summary of the Effective Stiffness for Area & Combination (kips/in)	134
5-6	The Dimension of Test Samples (Total Length = 2.0 inch)	149
5-7	Constant Value for the Honeycomb Stiffness Relation (0.39 in thickness)	158
6-1	The Summary of FRP Material Test Results Used in the Multi-panel Infill Panel System (Kitane, 2003)	167
6-2	The Orientation Code of the Skin Laminate (Total thickness = 0.21 inch)	171
6-3	The Applied Displacements of the Tests	208
6-4	Possible Frequency for Assigned Displacements	209
6-5	The Comparison of the Initial Stiffness for the Steel Frame and Two Cases of the FRP Box Damping Panel Systems under Push-over Load	242

SECTION 1

INTRODUCTION

1.1 Motivation for This Study

Worldwide, civil infrastructure related to bridges and buildings represents an investment of trillions of dollars, and increasingly the security of this investment is being questioned going into the 21st century. The infrastructure of constructed facilities is now reaching a critical age with widespread signs of deterioration and inadequate functionality. Some disadvantages associated with many of the traditional strengthening techniques have led researchers to develop innovative methods utilizing advanced composite materials.

Many existing structures located in seismic zones lack strength and damping. One approach for correcting these deficiencies is the construction of infilled walls to strengthen and stiffen the structure. As such, large number of buildings throughout the United States are structural frames infilled with unreinforced clay brick, concrete masonry, or structural clay tile. This infill construction has been prevalent since the late 1800s and still quite popular in moderate seismic regions of the central and eastern United States. However, there are conditions in cast-in-place construction where cost, time constraints, or limiting disruptions to building operations may dictate other solutions. A new rehabilitation scheme is needed that will simplify the construction process, reduce time, cost and inconvenience of construction, and reduce the obstruction to the functional use of structure both during and after construction.

In recent years, polymer matrix composite (PMC) materials have received considerable attention for use in civil infrastructure applications ranging from the retrofit and rehabilitation of buildings and bridges to the construction of new structural systems. Due to their light weight, high stiffness-to-weight and strength-to-weight ratios and potentially high resistance to environmental degradation that leads to lower life-cycle costs, civil engineers are recognizing the potential of advanced polymer composites as an alternative construction material, and fiber reinforced polymer (FRP) composites are playing an increasingly important role in civil engineering applications. Even greater promise

exists for the advanced concept of joining composites with traditional materials to form hybrid structures. The reason for the increasing prominence of these materials relates to the ability of these materials to be tailored to suit particular environments in different conditions compared with conventional materials.

As an example of practical application, PMC materials are being used to retrofit structural elements such as columns, beams, and bridges to enhance strength and ductility. The most popular application of FRP composites for seismic retrofitting is FRP composite jacketing of concrete columns. Recent earthquakes have shown the vulnerability of existing old concrete columns in bridges and buildings. The 1971 San Fernando earthquake led to a growing concern for seismic rehabilitation of existing structures, and the development of steel jacket systems for retrofitting the RC columns with substantial details had emerged in many applications. The seismic retrofitting of concrete columns requires that the shell/casting provide additional hoop reinforcement in order to develop sufficient confinement. The use of steel results in additional strength and stiffness both in the hoop and axial directions, with the additional axial stiffness often causing further distress due to the attraction of forces during a seismic event to the stiffened axial member. In contrast with composites, it is possible to tailor properties to comply only in the directions required, thereby improving efficiency and economy. The structural effectiveness had been established by the excellent performance during the 1994 Northridge earthquake. It was evident that the FRP composites were very suitable for retrofit purposes. Various column-jacketing techniques using advanced composites have been studied since then.

There are still challenges with new FRP composite material technology. Those challenges should be viewed as opportunities to study and improve the materials to ensure that the products will be durable and reliable. Especially, the term “advanced composite structures” still carries a sense of mystique and an association with high costs and high performance application. It must be mentioned that the applications of composites do suffer from some disadvantages, primary among them being; (1) higher initial materials cost, (2) lack of existing comprehensive standards and design guidelines, and (3) the need for an integrated materials-process-design structure in product development, which

entails a critical change in paradigm. Recently, in a marketplace where demands for product performance are ever increasing, composite materials have potentials in reducing costs and improving performance. The resulting need for new markets has spurred renewed efforts in manufacturing processes and making it highly feasible to use composites in civil infrastructure on a competitive basis.

1.2 Literature Review of Infilled Frame Structures

Typically, some low- and mid-rise building frames have infill wall systems that are built and installed as partitions after the frame of a structure is constructed, and in some cases infill walls are part of the structural system. There is no resemblance between the structural response of the infilled frame and the empty frame, as the former is substantially stronger and stiffer than the latter. In the 1950s, the behavior of infilled frames with monotonically increasing lateral force had been investigated by Benjamin and Williams (1957).

Since that time, many researchers (Mainstone, 1971; Barua and Mallick, 1977; Dawe and Seah, 1989; Mehrabi, et al., 1994) studied the behavior and associated analytical models of the infilled frames with different materials under monotonic loading. The role of infill walls in strengthening and stiffening the structure as a whole under cyclic and earthquake loading was also investigated by a number of researchers (Klingner and Bertero, 1976; Kahn and Hanson, 1979; Liauw and Kwan, 1985; Valiasis and Stylianidis, 1989; Manos, et al., 1993; Mosalam, et al., 1997a, Mosalam, et al., 1997b, Berman and Bruneau, 2003, Kesner and Billington, 2005, Vian and Bruneau, 2005). The effects of neglecting the infill walls are highlighted in high-seismicity regions where the frame-and-wall interaction may cause a substantial increase of stiffness, resulting in possible changes in the seismic demand, and the infilled frame structure exhibits changes in the magnitude and distribution of stresses in the frame members.

To control structural frame vibration, Gasparini, et al. (1981) explored the damping of frames with visco-elastic infill panels as a means of increasing damping and minimizing vibration. The concept of constrained viscoelastic layers was employed and the feasibility of adding a viscoelastic layer to a braced frame to enhance its damping, and thus passively control wind induced vibrations was ex-

amined. It was found by analytical studies that significant increases in the damping of a steel frame may be realized by incorporating viscoelastically damped infill panels.

Mander, et al. (1993), and Harris, et al. (1993) addressed the effects of retrofitting infilled frames by studying retrofitting techniques and infilled frames repaired by ferrocement or lightly reinforced concrete. Under seismic excitations, stiffness affects the natural period of vibration and attracts additional loads, while the strength capacity affects the ductility demand on the elements.

Recently, numerous research activities have been devoted towards the use of FRPs in structural applications. Although composites may offer unique properties ideal for seismic retrofitting, the research dealing with fully prefabricated PMC infill wall systems is very scarce. Most of the research for rehabilitative strategies using FRP materials have been focused on the enhancement of the performance (strengthening) for existing masonry or reinforced concrete infill walls. Structural weakness or overloading, dynamic vibrations, settlement, and in-plane and out-of-plane deformations can cause failure of masonry structure. Available literature on masonry infill shows that each of these causes can be prevented and/or reduced by using FRP composites. A number of previous research investigations for strengthening have been conducted and they are briefly stated here.

Laursen et al. (1995) performed shear and flexural tests on masonry walls strengthened with carbon overlays. In the case of the shear tests the primary objective was to change the mode of failure from a brittle failure to a ductile failure. For the shear test specimens, it was observed that the presence of carbon overlays improved the wall performance by changing the failure from a shear failure mode to a flexural failure mode. This change in the mode of failure caused an increment in ductility of approximately 100%, and prevented a brittle failure mode.

Schwegler (1995) investigated strengthening methods for masonry shear walls corresponding to the lowest building story. The goal of this research was to increase the system ductility, generate uniform crack distribution, and increase the load carrying capacity of the system. In the walls strengthened with Carbon Fiber Reinforced Polymer (CFRP) sheets, the deformation was increased; however, due to delamination of the CFRP sheets from the masonry, significant increases in the load carrying

capacity compared to walls strengthened with conventional woven was not observed. It was observed that if only one side of the masonry wall is strengthened, the capacity could be halved.

Hartley et al. (1996) reported the feasibility of using CFRP sheets for repairing block walls used in residential construction due to settlement. Test specimens were subjected to a simulated foundation settlement. The settlement loads were similar to the cantilevered weight of the walls. By comparing the control wall and the retrofitted wall, an increase in capacity of 80% was observed.

Haroun et al. (1997), studied the effects of strengthening and repairing masonry-infilled reinforced concrete frames using fiberglass composites. As-built frames as well as those strengthened and repaired by external layers of FRP composite were examined to assess their relative seismic resistance attributable to the strengthening and repair techniques. The results indicated that the strengthening and repair techniques that employed composite materials prevented diagonal tension and shear failure of the infill wall.

Ehasni et al. (1996) investigated the behavior of unreinforced masonry (URM) walls with glass fiber reinforced polymer (GFRP) sheets. The test results indicated that retrofitting of unreinforced masonry structures with composite fabrics is a very effective technique for increasing the flexural and shear strength as well as ductility of these elements. The retrofitted beams could resist loads as high as twenty four times their weight and exhibited deflections of up to 1/48 times the span. The shear specimens also carried significantly high loads and failed in a ductile manner. Similar to reinforced concrete structures where the mode of failure is governed by the amount of the reinforcement provided, in these applications the strength of the fabric controlled the mode of failure.

A strengthening method for existing buildings and particularly for infill masonry walls with bending loading induced by earthquakes was studied by Kolsch (1998). An experimental program with strengthened concrete beams and masonry walls with bending loading was carried out. The experimental studies showed that a significant enhancement of the load-bearing capacity of the tested members was achieved.

Hamilton, III et al. (2001) studied flexural capacity of glass FRP strengthened concrete masonry walls. Six unreinforced concrete masonry walls were tested in out-of-plane flexure up to capacity. The walls were strengthened with glass FRP composite composed of unidirectional E-glass fabric with an epoxy matrix. It was concluded that FRP can provide a strengthening alternative for unreinforced masonry.

1.3 Structural Applications of Polymer Matrix Composite Materials

Manufacturers, designers, and engineers recognize the ability of PMC composite materials to produce high-quality, durable products. Composite materials are found in many of the products used in our day-to-day lives. In the United States, composites manufacturing is a 25 billion dollar a year industry, and it is one of the few industries in which the U.S. is more advanced than most competitors abroad. There are five to seven thousand composites related manufacturing plants and materials distributors across the U.S.

The composite industry can be generally characterized by the market that uses composite products. Industry has identified three major new application areas for composite materials — namely, infrastructure, industrial facilities, and offshore exploration and production.

Within the scope of composites civil applications, the structural applications can be classified as shown in Fig. 1-1. These new materials are applicable to both construction of new structures, and maintenance and rehabilitation of existing structures. In particular, the structural rehabilitation can be divided into three categories in terms of objective; repair, strengthening and retrofit. In '*repairing*' a structure, the FRP composite material is used to fix a structural or functional deficiency so that the structure can regain its originally expecting performance level. In contrast, the '*strengthening*' of structures is specific to those cases in which the addition of the FRP composite would enhance the existing designed performance level. The term '*retrofit*' is specifically used as related to upgrading the seismic capacity of facilities by the use of FRP composites, such as in the case of the use of FRP composite jackets for the confinement of columns. The differentiation is important not only on the basis of structural functionality, but also because the specifics related to the use of the material in

conjunction with existing conventional materials, and its expected life have a significant effect on the selection of fiber-resin combinations from a variety of alternatives.

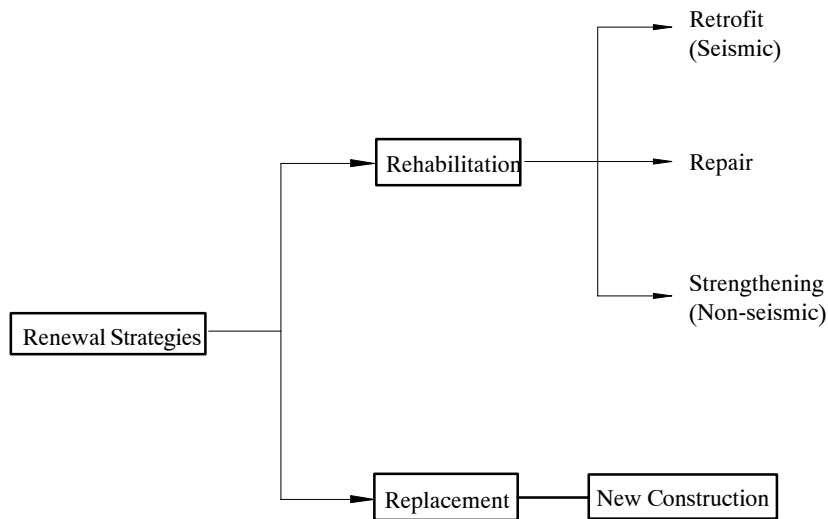


Figure 1-1 Types of Renewal Strategies

As such, the primary objective of using composites for the rehabilitation of civil structures is to restore or enhance the functionality and/or safety of existing structural components or systems. Hence, rehabilitation measures must be designed such that within the intended period of operation and cost, (1) the structures remain functional with an accepted probability of functionality, and (2) they are capable of sustaining all actions and influences likely to occur and have adequate durability with an appropriate degree of reliability.

Although a significant number of research, related to the use of composites for rehabilitation of civil structures, has been performed, there is still a lack of uniformly accepted philosophy for using a new technology. Especially, additional studies on the effective applications of composites for retrofit of building structures and on the feasibility of these concepts are still remain to be seen.

1.4 Rehabilitation Strategies and Objectives

Concerns for seismic rehabilitation of existing structures grew considerably following the 1971 San Fernando earthquake and resulted in several programs to identify and mitigate seismic risks. The 1989 Loma Prieta and 1994 Northridge earthquakes provided significant new impetus for seismic

rehabilitation of building and bridge structures in the U.S. Earthquakes in other parts of the world provide a continual reminder of the need for seismic mitigation programs underpinned by research to demonstrate their effectiveness and improve the efficiency. In the 1990s the Federal Emergency Management Agency (FEMA) and the State of California separately began to develop seismic rehabilitation guidelines. These efforts were guided by research reported to date or under way at the time. The guidelines of rehabilitation strategies (FEMA 356) are briefly demonstrated in the following section.

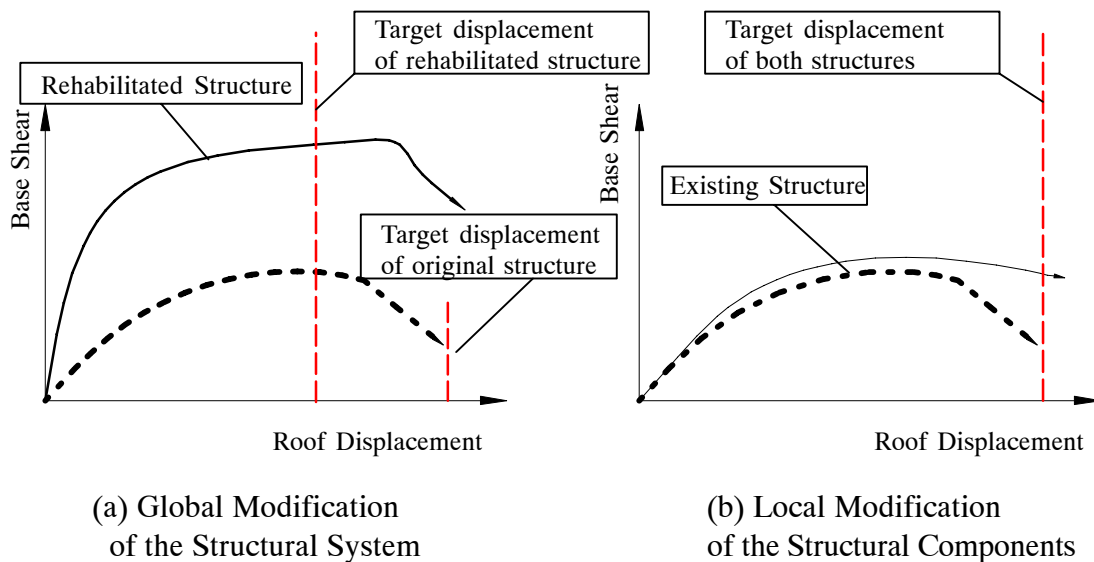


Figure 1-2 Design Approach of Rehabilitation Techniques (Moehle, 2000)

Global and Local Modification of Components

Two general approaches are usually considered for a seismic rehabilitation project in the U.S. The first involves global modification of the structural system, and the other is related to local modification of isolated components of the structural and nonstructural system. In the first approach, the modifications to the structural system are designed so that the design demands, often denoted by target displacement, on the existing structural and nonstructural components are less than their capacities. Common approaches include addition of structural walls, steel braces, or base isolators. Passive energy dissipation schemes are not common for reinforced concrete frames because the dis-

placements required for them to be effective often are beyond the displacement capacities of the existing components.

In the second approach, the objective is to increase the deformation capacity of deficient components so that they will reach their specified limit state as the building responds at the design level. Common approaches include addition of concrete, steel, or fiber reinforced polymer composite jackets. Fig. 1-2 illustrates two approaches of proposed rehabilitation techniques.

Removal or Lessening of Existing Irregularities

Removal or lessening of existing irregularities may be an effective rehabilitation strategy if a seismic evaluation shows that the irregularities result in the inability of the building to meet the selected structural performance level, described in FEMA. Such irregularities are often, but not always, caused by the presence of a discontinuity in the structure, for example – termination of a perimeter shear wall above the first story. Simple removal of the irregularity may be sufficient to reduce demands predicted by the analysis to acceptable levels. However, removal of discontinuities may be inappropriate in the case of historic buildings, and the effect of such alteration on important historic features should be considered carefully.

Mass Reduction

Mass reduction may be an effective rehabilitation strategy if the results of a seismic evaluation show deficiencies attributed to excessive building mass, global structural flexibility, or global structural weakness. Mass and stiffness control the amount of force and deformation induced in a structure by ground motion. Reductions in mass can result in direct reductions in both the amount of force and deformation demand produced by earthquakes and, therefore, can be used in lieu of structural strengthening and stiffening. Mass can be reduced through demolition of upper stories, replacement of heavy cladding and interior partitions, or removal of heavy storage and equipment loads.

Seismic Isolation

Seismic isolation may be an effective rehabilitation strategy when the results of a seismic evaluation show deficiencies pertaining to excessive seismic force or deformation demands, or if it is desired to protect important contents and nonstructural components from damage. When a structure is seismically isolated, compliant bearings are inserted between the superstructure and its foundations. This produces a system with a nearly rigid body translation of the structure above the bearings. Most of deformation induced in the isolated system by ground motion occurs within the compliant bearings, which are specifically designed to resist these concentrated displacements. Most bearings also have excellent energy dissipation characteristics. Together, this results in greatly reduced demands on the existing elements of the structure, including contents and nonstructural components. For this reason, seismic isolation is often an appropriate strategy to achieve enhanced rehabilitation objectives that include the protection of historic structures, valuable contents, and equipment, or for buildings that contain important operations and functions. This technique is most effective for relatively stiff buildings with low profiles and large mass. It is less effective for light, flexible structure.

Supplemental Energy Dissipation

Installation of supplemental energy dissipation devices may be an effective rehabilitation strategy if the results of a seismic evaluation show deficiencies attributable to excessive deformations due to global structural flexibility in a building. Many available technologies allow the energy imparted upon a structure by ground motion to be dissipated in a controlled manner through the action of special devices — fluid viscous dampers, yielding plates, or friction pads — resulting in an overall reduction in the displacements of the structure. The most commonly used devices dissipate energy through frictional, hysteretic, or viscoelastic processes. In order to dissipate substantial energy, dissipation devices must typically undergo significant deformation, which requires that the structure undergoes substantial lateral displacements. Therefore, these systems are most effective in structures that are relatively flexible and have some inelastic deformation capacity. Energy dissipators are most commonly installed in structures as components of braced frames. Depending on the char-

acteristics of the device, either static or dynamic stiffness is added to the structure as well as energy dissipation capacity.

For each structure, a decision for rehabilitation must be made as to the acceptable behavior for different levels of seismic hazard, balanced with the cost of rehabilitating the structure to obtain that behavior. For many buildings, multiple rehabilitation objectives are often adopted – ranging from negligible damage and occupancy interruption for earthquake events with a high probability of occurrence, to substantial damage but protection of life safety for events with a low probability of occurrence. In general, rehabilitation objectives that expect relatively low levels of damage for relatively infrequent earthquake events will result in more extensive rehabilitation work and greater expense than the objectives with more modest goals of controlling damage.

A rehabilitation objective shall be achieved by implementing rehabilitation measures based on a strategy of addressing deficiencies identified by a prior seismic evaluation. Each rehabilitation measure shall be evaluated in conjunction with other rehabilitation measures, and the existing structure as a whole, to assure that the complete rehabilitation scheme achieves the target building performance level for the selected earthquake hazard level. The effects of rehabilitation on stiffness, strength, and deformability shall be taken into account in an analytical model of the rehabilitated structure.

1.5 Research Background and Objectives

In conventional seismic design of existing structures, energy dissipation occurs in specially detailed ductile plastic hinge regions of beams and column bases, which also form part of the gravity load carrying systems. Plastic hinges are regions of concentrated damage to the gravity frame, which are often irreparable. Situations exist in which the conventional design approach is not applicable. When a structure must remain functional after an earthquake, as is the case of important structures such as hospitals and their critical facilities, the conventional design approach is inappropriate. For such cases, the structure may be designed with sufficient strength so that inelastic action is either prevented or is minimal; an approach that is very costly. Moreover, in such structures, special precau-

tions need to be taken in safeguarding against damage or failure of important secondary systems, which are needed for continuing serviceability. Conventional upgrading techniques usually include the addition of walls and strengthening of existing frames.

From the 1980s, the U.S. National Science Foundation (NSF) began to fund research on seismic rehabilitation. The objectives of the program were to provide information for evaluation of the vulnerability of existing structures for various levels of seismicity, and to develop advanced strategies for repair and retrofitting. Nonstructural rehabilitation was accomplished through replacement, strengthening, repair, bracing, or other attachments. The NSF research efforts had been supplemented by many research activities carried out at the National Center for Earthquake Engineering Research (NCEER). Recently, due to additional research needs, new rehabilitation approaches for critical facilities have been identified. Hospitals are classified as one element of the most important public facilities and important part in the hazard emergency management. Hospitals are expected to provide uninterrupted and efficient medical services during and after an earthquake or any natural hazard.

As part of Multidisciplinary Center for Earthquake Engineering Research (MCEER) research initiatives in the area of advanced analyses and protective technologies for seismic retrofit of critical facilities, FRP composite materials have been investigated as a new seismic strategy. The proposed methods may provide the solution in dealing with life cost-effective and stake holder – acceptable retrofitting strategies for maintaining functionality of critical facilities and their contents during earthquakes. As an innovative alternative, the light-weight FRP composite components has the potential to emerge as an alternative material for non-structural elements such as infill walls that can be used as seismic retrofitting strategy in regions of moderate to high seismicity.

The basic design philosophy and structural technique considered herein focus on increasing the efficiency for retrofitting a structure before and after earthquake damages. The prefabricated PMC infill systems are proposed and their properties can be easily modified to suit any particular functional purpose. Fiber orientations and stacking sequence in the PMC infill system can be adjusted to en-

hance structural behavior without any limitations given by existing configurations. Also, ductile behavior of PMC infill systems can prevent the catastrophic failure of the overall structure. From a construction point of view, PMC infill systems can be easily installed during the strengthening and retrofitting process of the existing structures.

The research applications of full-scale PMC infill systems have been scarce so far due to economical factors, and the lack of guidelines available for designing these systems. However, recent efforts for developing composite fabrication skills and related issues to dramatically increase investment in maintenance and upgrade facilities could make the research of full-size movable PMC infill application more attractive in the retrofit or replacement projects. The research described here represents one of the early and pioneering work that considers the novel applications of PMC infill panels for seismic retrofitting. This research primarily focuses on studying the effectiveness and feasibility of various PMC infill panel systems. Conceptual designs for three types of PMC infill systems are presented and the feasibility of the proposed PMC infill systems has been verified by both experimental and analytical studies. Figure 1-3 illustrates one of the PMC infill systems that has been investigated in this study. The following is the scope of the research.

1. Characterization of properties of composite materials used in the design and fabrication: (1) FRP composite, (2) new and existing steel frame members, and (3) polymer honeycomb materials.
2. The proposal of conceptual design criteria and manufacturing techniques for the structural PMC panel systems.
3. The introduction of energy dissipation effects produced by novel combined interface damping layers along with the investigation of several design parameters.
4. Full-scale testing of the proposed three types of PMC infill wall systems when incorporated in a steel frame having semi-rigid bolted connections. Several test specimens were considered: (1) steel frame, (2) multi-layer PMC infill, (3) multi-panel PMC infill, and (4) FRP box infill panels were carried out under both push-over and a multi-step quasi-static loading tests.

In the cases of (3) and (4), frequency effect of the interface layers material was investigated under various loading rates.

Through these investigations, final conclusions are given for the effectiveness and behavior of the proposed PMC infill panel systems in terms of the stiffness, strength, energy dissipation, and the possible failure modes. In addition, the results provide information on areas where more research efforts would be needed.

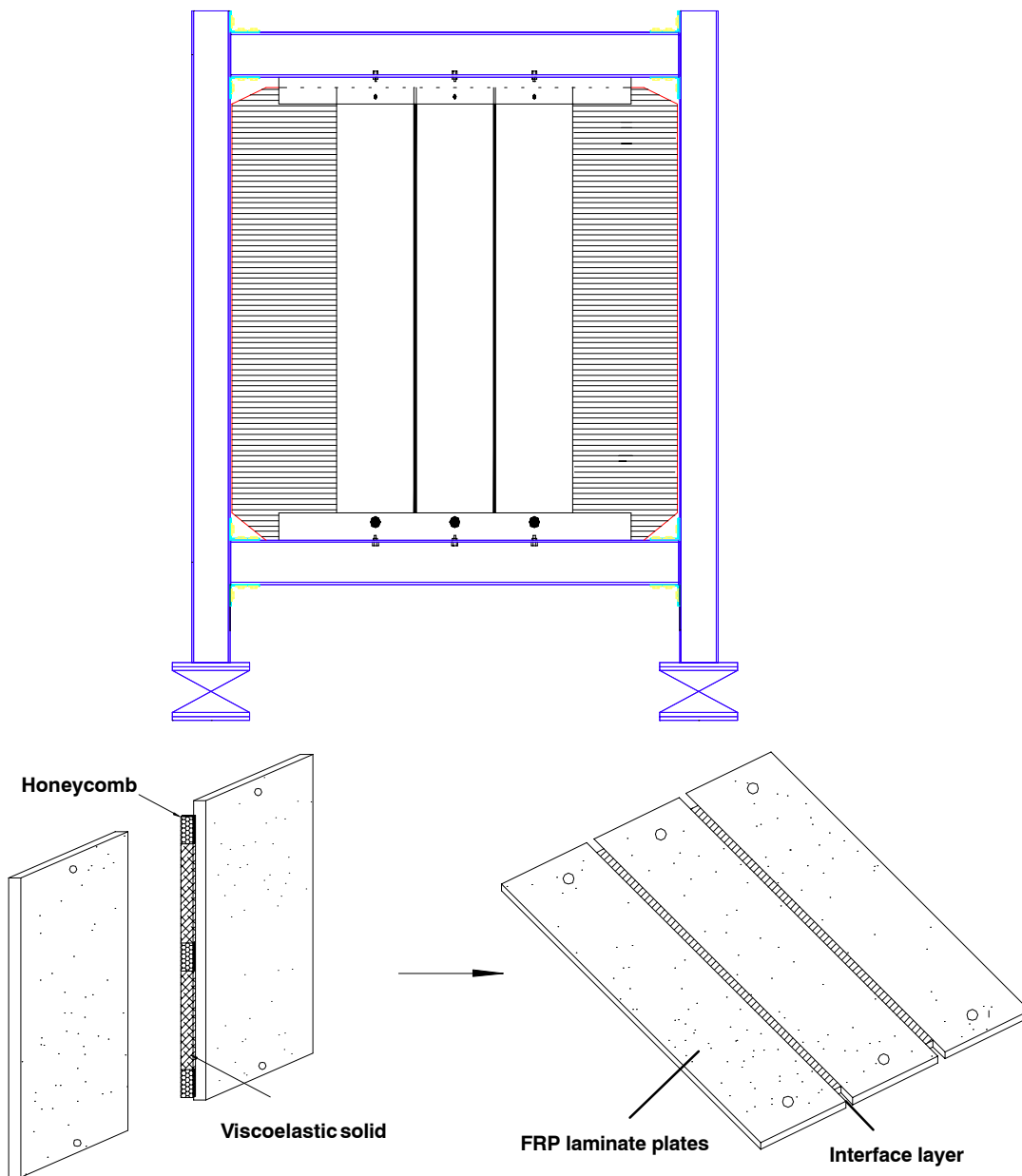


Figure 1-3 Geometric Configuration of the Damping Panel

1.6 Organization of The Report

This report comprises of seven sections and an appendix. In the following section, material properties of both FRP composites, and new and existing steel frame members are investigated. Based on the ASTM testing specifications, the results of each experimental coupon test are presented and brief description of the tests with comments is given. The results obtained by the material tests are summarized as follow; (1) the orthotropic properties of FRP composite materials, (2) basic mechanical properties of the polymer honeycomb, and (3) elastic, plastic properties of steel members. Section 3 presents an overview of steel frame used in the experiments that has semi-rigid top and seat angle connections. Geometric configuration of steel frame and fundamental experimental setup are introduced. As the first study among three PMC seismic infill panels, a multi-layer PMC infill panel, is investigated in section 4. This section discusses the effectiveness of the multi-layer PMC infill panel under monotonic and cyclic loading conditions and presents the specific needs for structural applications. The observed behaviors of a multi-layer PMC-infill panel system are assessed on the bases of stiffness, strength, modes of failure, and energy dissipation output. The results obtained in this section provides important information for studying further research related to the seismic PMC infill panels. In section 5, based on the results obtained by section 4, a passive energy dissipation mechanism designed by the combination of interface damping layers between fabricated solid FRP panels is introduced and investigated. The effectiveness and design parameters of combining composite materials are proposed by experimental studies. In section 6, we present conceptual design and tests of the enhanced PMC infill panels considering passive energy dissipation mechanism. Two types of PMC infill panel systems – namely, multi-panel PMC infill and FRP box infill systems, are investigated by experimental studies. In the last section, the conclusions of this study and recommendations for future work are summarized.

SECTION 2

MATERIAL CHARACTERISTICS

2.1 Polymer Matrix Composite Material

This section mainly presents the composite material testing to evaluate the mechanical properties that are needed for analysis and design. The evaluation of the mechanical properties of composites includes their strength and stiffness characteristics.

The word “composite” signifies that two or more materials are combined together on a macroscopic scale to form a useful third material. The field of composite materials is fairly new. Only since the early 1960s, engineers and scientists exploited seriously the vast potential of fabricated fibrous composite materials. The evolution of composite materials is basically an extension of man’s continuing curiosity of searching for new materials with better properties.

2.1.1 Fiber, Matrices, and Fabrication of Composites

2.1.1.1 Fiber

A great majority of materials are stronger and stiffer in the fibrous form than bulk materials. A high fiber aspect ratio permits very effective transfer of load via matrix materials to the fibers, thus taking advantage of their excellent properties. The physical properties of FRP composites are fiber dominant. When the resin and fiber are combined, their performance remains mostly like the individual fiber properties. Fiber selection is critical when designing composite structures. Practically, the average fabricator has a choice of several types of materials. These are fiberglass, carbon fiber, and Kevlar among others. Fiberglass tends to be the all-purpose choice, while carbon/graphite offers high stiffness and Kevlar has high abrasion resistance. Table 2-1 shows laminate comparison data for three types of materials.

In this study, two types of fiber glass were used. First, E-glass in the form of a fiberglass fabric (plain weave pattern – fibers are arranged in bi-directional pattern) was chosen as reinforcement of FRP of the multi-layer infilled panel application. The multi-layer infilled panel is a sandwich-type panel

that can be illustrated Section 4.2.1. The principal advantages of glass fibers are the low cost and high strength even if there are many other high strength fibers. The selected fiberglass fabric is frequently used in mold-building, sandwich core panels, and high strength lay-up like boat floors and roofs. The glass fabric physical properties that we adopted in this research are listed in Table 2-2.

Table 2-1 Typical Laminate Comparison Data. (Fiber Glast Corp., 1999)

Specification	Fiberglass Fabric	Graphite Fabric	Kevlar Fabric
Laminate Construction	10 Plies Glass	10 Plies Carbon	10 Plies Kevlar
Laminate/Resin Content	50% / 50%	56% / 44%	51% / 49%
Elongation @ Break, %	1.98	0.91	1.31
Tensile Strength (psi)	45,870	75,640	45,400
Tensile modulus (psi)	2,520,000	8,170,000	3,770,000
Flexural Strength (psi)	66,667	96,541	34,524
Flexural Modulus (psi)	3,050,000	6,480,000	2,500,000

Table 2-2 The Properties of Boat and Tooling Glass Fabric (Style 7781)

Width	Thread Count (Warp x Fill)	Weight (oz / sq. yard)	Thickness Inches	Weave
38" – 72"	16 x 14	9.70	0.014	plain

After completing the multi-layer infilled frame test, it was found that the number of yarns in each direction is very important for the construction of full-scale products. As such, E-glass in the form of a woven fabric was chosen considering the variability in the number of yarns. The selected woven roving is composed of direct roving woven into a fabric. The input rovings are designed to give a rapid wet-out and excellent laminate properties. It is commonly denoted as “Style 7781” in the industry and has similar number of yarns, approximately 65 and 68 yarns per foot in the fill and wrap directions. The style 7781 is frequently used in aerospace and military application due to its excellent strength and formability. In this study, it was applied for fabricating the multi-panel sandwich infill and FRP box infill sections. The multi-panel infilled panel system dissipates energy by shearing of interface layer between panels, can be illustrated in Section 6.2.1. The fabric weight and thickness

is 8.69 oz. per square yard and 0.009 inch, respectively. Material tests for the woven roving (style 7781) were not performed here. Previous test results for this material (Kitane, 2003) were used, and they are presented in section 6.

2.1.1.2 Matrix (Resin)

Since fibers can not transmit loads from one to the other, they are limited in the use for engineering applications. When they are embedded in a matrix material, the matrix serves to bind the fibers together, transfer loads to the fibers, and protect them against environmental factors and damage due to handling. The matrix has a strong influence on several mechanical properties of the composite such as transverse modulus and strength, shear properties, and properties in compression.

One of the obstacles hindering the acceptance of polymer composites in civil engineering applications is the susceptibility of the polymer matrix to degradation initiated by moisture, temperature, and ultraviolet light. From a discussion with the composite fabricator (An-Cor Industrial plastics), a matrix of vinyl ester resin (DERAKANE 411) produced by the Dow plastic company, was chosen in the fabrication of PMC wall systems. The DERAKANE vinyl ester resin is a premium-quality thermosetting product that can be used to fabricate a wide range of corrosion-resistant FRP applications. FRP structures made of polyester resin (DERAKANE) are easily fabricated by all conventional fabricating techniques and requires little maintenance over a long service life. In addition, they offer significant cost advantages during construction, installation, and continuing use.

Structures made of vinylester resin (DERAKANE) provide a number of advantages over those made of conventional metal, and they are:

- Outstanding resistance to corrosion from several chemicals and excellent temperature stability.
- High impact and fatigue resistance.
- High strength to low weight ratio.
- Excellent electrical and thermal insulation properties.

Table 2-3 presents properties of 1/8" clear casting at room temperature.

Table 2-3: Typical Properties of DERA KANE 411 (Dow Chemical Comp., 1999)

<i>Properties</i>	<i>At Room Temperature</i>
Tensile strength (psi)	11 – 12,000
Tensile modulus (psi, x 10 ⁵)	4.9
Elongation %	5.0 – 8.0
Flexural Strength (psi)	16 – 18,000
Flexural modulus (psi, x 10 ⁵)	4.5
Heat Distortion Temp (°F)	210 – 220
Specific gravity of Liquid	1.040
Specific gravity of Solid	1.126
Cure shrinkage (%)	8.3
Poisson's ratio	0.35 – 0.38

2.1.1.3 Fabrication of Composites

The fabrication or shaping of composites into finished products often combines the formation of the material itself during the fabrication process. The formation of the composite involves the combination of the matrix and fiber such that the matrix impregnates, surrounds, and wets the fibers. The relative properties of the matrix and fiber are one of the most important factors determining the properties of a composite structure. Theoretically, the composite stress–strain curves would lie somewhat between the stress–strain curve of both constituent materials as shown in Fig. 2-1.

If the fiber volume fraction is high, the composite stress–strain curve will be closer to the fiber stress–strain curves. The actual location of the composite stress–strain curve will depend on the relative volume fractions of the constituents. On the other hand, the composite stress–strain curve may be closer to the matrix stress–strain curve for a higher matrix volume fraction. The void content of a composite may significantly affect some of its mechanical properties. Higher void content usually means lower fatigue resistance, greater susceptibility to water penetration and weathering, and increased variation or scatter in strength properties. The knowledge of void content is desirable for the estimation of the quality of composites. A good composite should have less than 1 % voids.

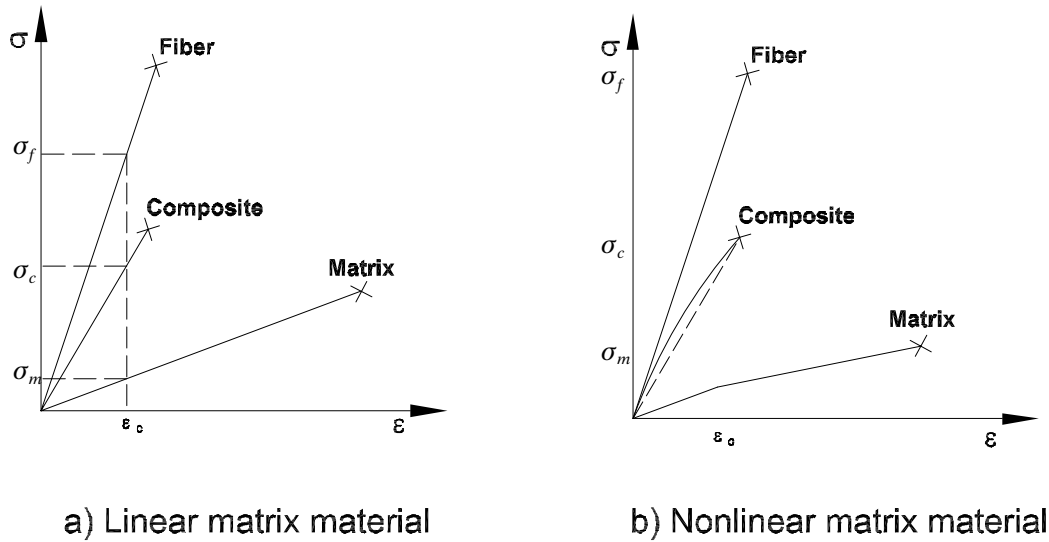


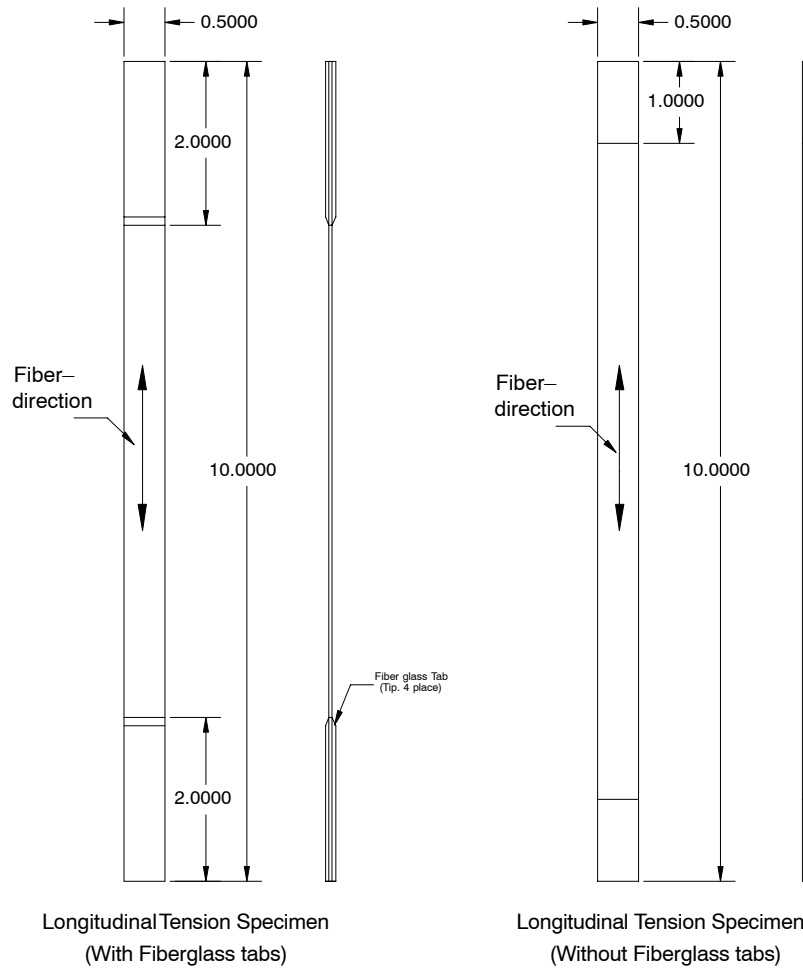
Figure 2-1 Longitudinal Stress–Strain Diagram for Hypothetical Composite

2.1.2 Test Description of FRP Composite Material

This section is concerned with test methods to measure basic composite mechanical properties that are needed in the analysis and design. Based on displacement control test procedures, all coupon tests were performed using an MTS universal testing machine. Load is applied to the specimen at the specified rate of 1.0 Hz until failure. According to the specification of the ASTM, dimensions of each test coupon are shown in Fig. 2-2.

Tensile Test

Ultimate tensile strengths (σ_L , σ_T), Young's moduli (E_1 , E_2) and Poisson's ratios (ν_{12} , ν_{21}) may be measured by testing longitudinal (0°) and transverse (90°) directional specimens according to the ASTM D3039 standard test method. The D3039 test method works well for orthotropic specimens because a uniform state of stress would produce across the specimens as they are loaded in tension. The D3039 specimen geometry is shown in Fig. 2-2. Laminated load transfer tabs are adhesively bonded to the ends of the specimen in order to have the load transferred from the grips of the tensile testing machine to the specimen without damaging the specimen.



Tension Test Specimen

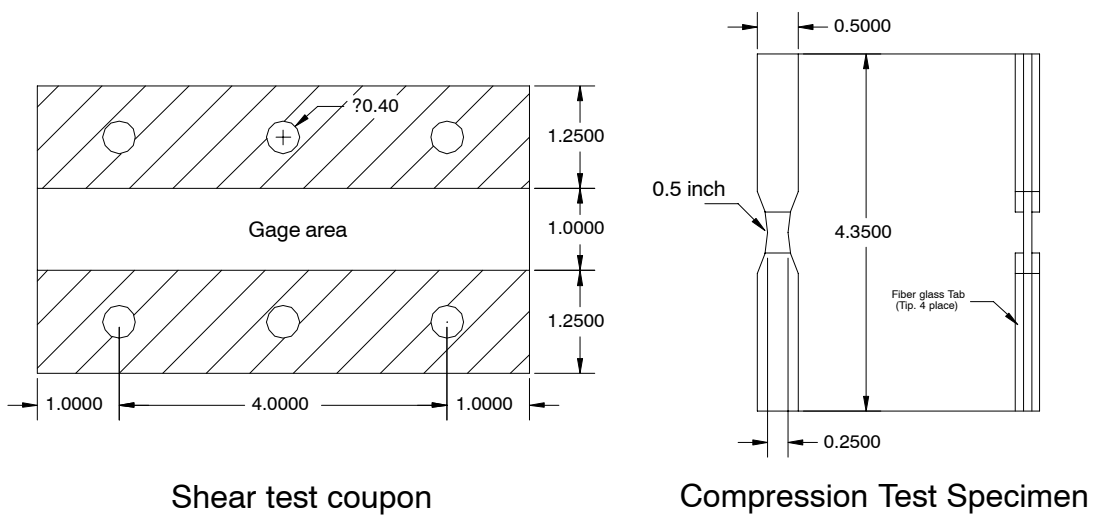


Figure 2-2 Coupon Dimensions of Each Test (unit = inch)

Compression Test

Compression testing has proved to be one of the most interesting and difficult challenges. In this study, an ASTM standard D3410 has been applied to evaluate ultimate compression strengths (σ_L' , σ_T'), compression Young's moduli (E_1' , E_2'), and Poisson's ratios (ν_{12} , ν_{21}) and the fixture, which was originally known as the Illinois Institute of Technology Research Institute (IITRI) fixture, was used to produce compression in the specimen through side-loading. The side-loading of the specimen was accomplished by pyramidal wedges inside a heavy-housing. In order to avoid local buckling and the reduction of in-plane compressive strength after delamination due to transverse impact, the compression test coupon was redesigned to be a little thicker.

In-Plane Shear Test

For evaluating in-plane shear properties, a test method which generates pure shear loading is needed. There are four widely used test methods for measuring in-plane shear properties of a unidirectional composite lamina and they are (1) [± 45]_s laminate tensile test method, (2) the off-axis tensile test method, (3) the 2-rail shear test method, and (4) the torsion test method (Whitney et al., 1982). In this research, we used the 2-rail shear test method, as described in ASTM D4255. Fig. 2-3(a) and Fig. 2-3(b) show the two-rail fixture and the three-rail fixture, respectively.

In both methods, a flat rectangular plate specimen is clamped in between the rail fixtures and the fixture is subjected to uniaxial load from the testing machine. The uniaxial loading on the fixture generates in-plane shear loading on the specimen, and the resulting strains are monitored by the strain gages shown in Fig. 2-3. Simple equilibrium requires that the average shear stress along the specimen loading axes (x , y) for the 2-rail shear test method to be

$$\tau_{xy} = \frac{P}{Lt} \quad (2-1)$$

where L = specimen length along x direction

P = applied load along the x direction

t = specimen thickness

The shear strain along the x, y directions can be determined from the measured normal strain, $\epsilon_{x'}$, along the x' axis, which is oriented at 45° from the x axis. From the strain transformation relationship for a state of pure shear along the x, y axes, we have

$$\gamma_{xy} = 2\epsilon_{x'} \quad (2-2)$$

Finally, the data can be generated from the above equations, and the corresponding modulus and strength can be found from the resulting stress–strain curve.

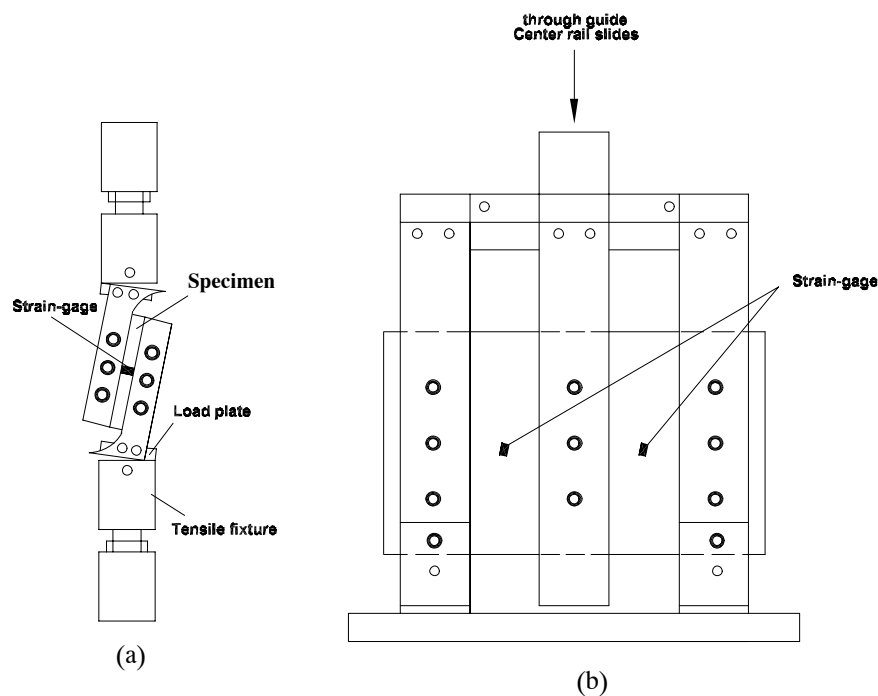


Figure 2-3 The Shear Test Fixtures

2.1.3 Selection of FRP Composite Laminate

In the tests, two systems of fiber glass–reinforced polyester were investigated for possible use in the composite panels. One system incorporated a multi–layer glass fabrics (plain weave) in a matrix of vinylester resin (DERAKANE 411). The second system incorporated a multi–layer woven roving glass fabric (CertainTeed, 302-2B) in a similar matrix. Sheets approximately 1 ft^2 were fabricated using hand layup techniques. The thickness of each sheet was 0.24 in. Its thickness varied slightly along longitudinal direction. To evaluate the stiffness property between both systems, two tension

coupons, according to the specification of the ASTM shown in Fig. 2-2, were cut from each sheet of FRP laminates. Test results of tension specimens are compared in Fig. 2-4. Based on the results, we evaluated that the material system containing a multi-layer glass fabric (plain weave) had higher stiffness than material system containing a multi-layer CertainTeed woven roving glass fabric as shown in Table 2-4.

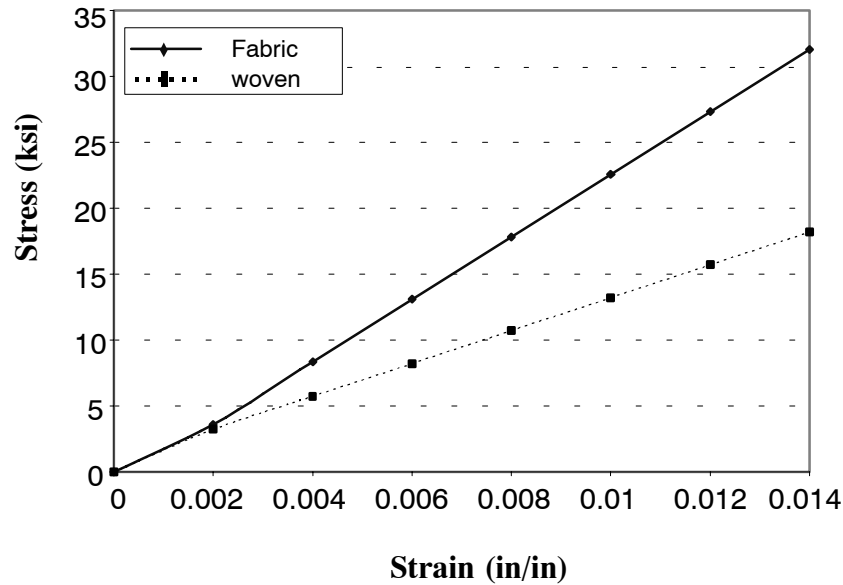


Figure 2-4 Test Results of Two FRP Material Systems

Table 2-4 The Results of Each Test for FRP Materials

<i>Material Type</i>	<i>Stiffness (Elastic modulus)</i>	<i>poisson's ratio</i>
Plain Weave Fabric FRP	2370.6 ksi	0.15
Woven Roving Fabric FRP	1246.7 ksi	0.28 – 0.3

2.1.4 Volume and Weight Fractions

As mentioned before, one of the most important factors determining the properties of composites is the relative proportions of the matrix and reinforcing materials. The relative proportions can be given in terms of the weight fractions or the volume fractions. The weight fractions can be easily obtained during fabrication process or by one of the experimental methods after fabrication. The

fiber volume fraction of a laminate can be obtained by a burn test. In the burn test, a piece of a FRP laminate is burned in an oven. After the burning, fiber weight fraction, w_f , can be obtained by comparing total weight of FRP laminate and the fibers left in the oven. Finally, the volume fractions, v_f , are obtained by the expressions for conversion between the weight fractions and volume fractions. These expressions are derived for a two-phase material and then generalized to a multiphase material.

To measure the density of the laminate, several pieces of laminate samples were cut from the tested laminate sheets. The density of E-glass fiber was 0.102 lb/in³ for the multi-layer infill model and 0.092 lb/in³ for the multi-panel infill model, respectively. The density of the matrix was 0.041 lb/in³. Table 2-5 shows a summary of these properties.

Table 2-5 The Other Properties of Used FRP laminate

	W_f / W_c	V_f / V_c	<i>Density (lb/in³)</i>
Material Test Coupon	0.65	0.425	0.067
Multi-layer Model (2000)	0.55	0.327	0.061
Multi-panel Model (2002)	0.41	0.236	0.053

2.1.5 Results of FRP Material Tests

Experimental techniques for each test to obtain the mechanical properties of laminate made of plain weave style were conducted. The stress–strain curves (see Figs. 2-5 to 2-8, 2-9 to 2-12, 2-13 to 2-18) of laminates reveal the modulus, poisson’s ratio and the ultimate stress. The tested material coupon dimensions are shown in Table 2-6, and the results for each test are presented in Table 2-7 to 2-12.

Table 2-6 The Dimension of Each Test Coupon for Composite Panel

<i>Method</i>	<i>Thickness (in)</i>	<i>Dimension (in x in)</i>
Tension(0)	0.0545	0.498 x 10
Tension(90)	0.053	0.4945 x 10
Compression(0)	0.0575	0.497 x 5.5
Compression(90)	0.0535	0.497 x 5.5
Shear(0)	0.064	1.0 x 6.0
Shear(90)	0.0615	1.0915 x 6.0

Tension Test (0° tensile coupon)**Table 2-7 The Result of Tensile Coupon (0°)**

	Elastic Modulus		Poisson's ratio
Test 1	3239.5 ksi	22.32 GPa	0.199
Test 2	2667.5 ksi	18.4 GPa	0.21
Test 3	2372.5 ksi	16.3 GPa	0.203
Test 4	2426.6 ksi	16.72 GPa	2.76
Average value	2676.52 ksi	18.4 GPa	0.204
Ultimate Stress	34.89 ksi	240.4 MPa	

Tension Test (90° tensile coupon)**Table 2-8 The Result of Tensile Coupon (90°)**

	Elastic Modulus		Poisson's ratio
Test 1	1861.1 ksi	12.82 GPa	0.18
Test 2	1745.3 ksi	12.03 GPa	0.12
Test 3	1703.6 ksi	11.74 GPa	0.16
Test 4	1578.3 ksi	10.87 GPa	0.13
Average value	1722.1 ksi	11.87 GPa	0.14
Ultimate Stress	28.6 ksi	197 MPa	

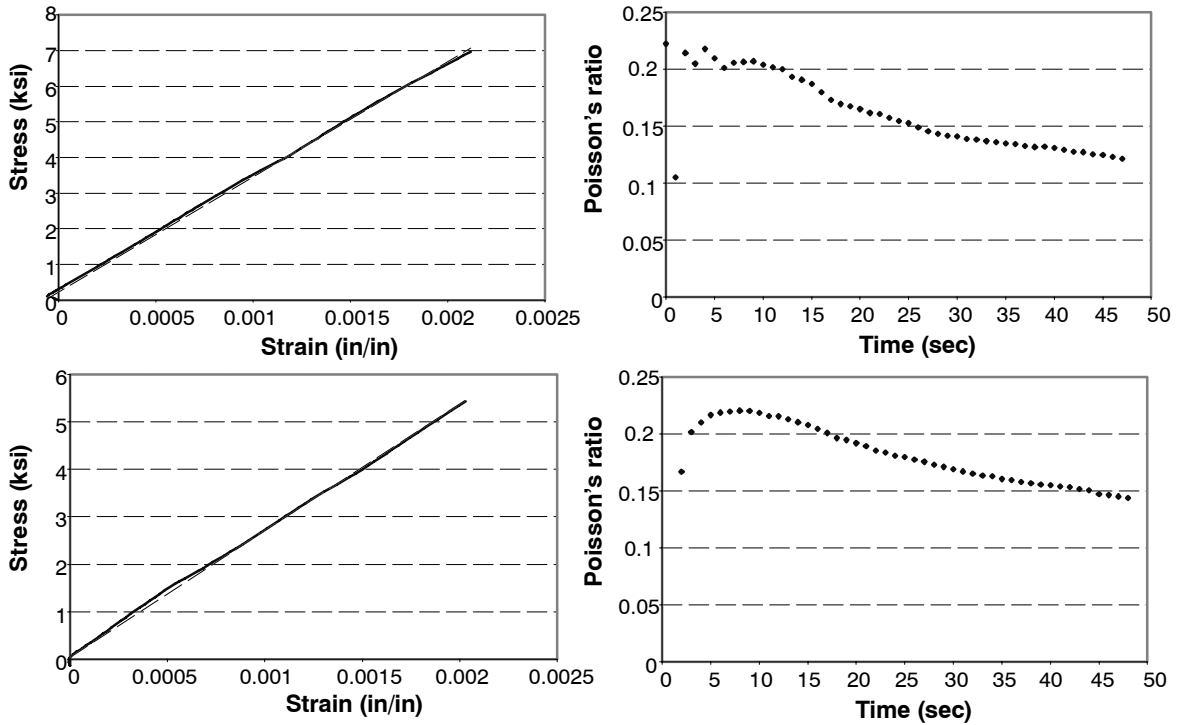


Figure 2-5 The First & Second Test of Tensile Coupon (0°)

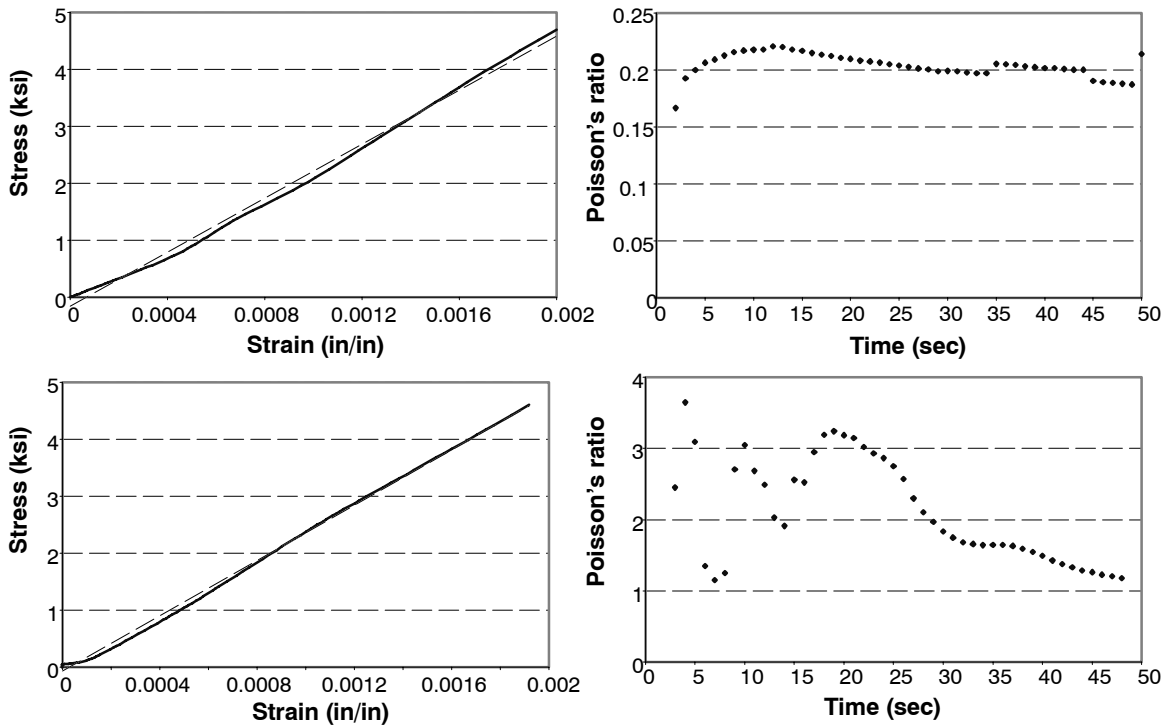


Figure 2-6 The Third & Fourth Test of Tensile Coupon (0°)

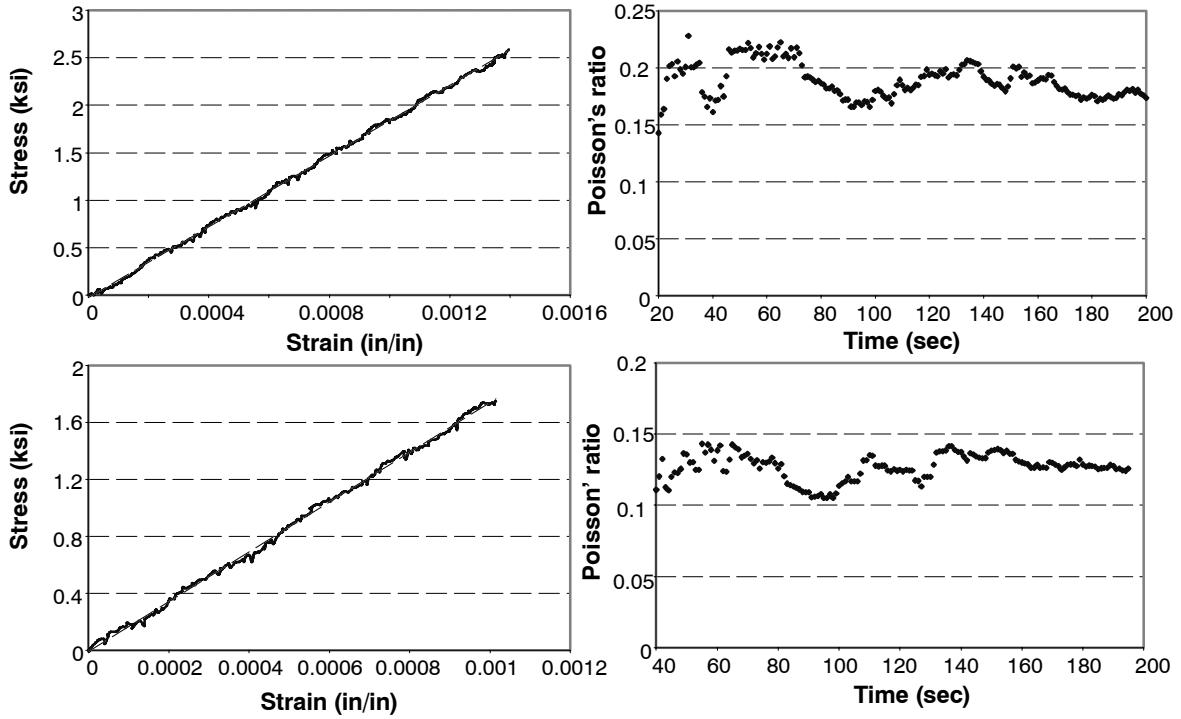


Figure 2-7 The First & Second Test of Tensile Coupon (90°)

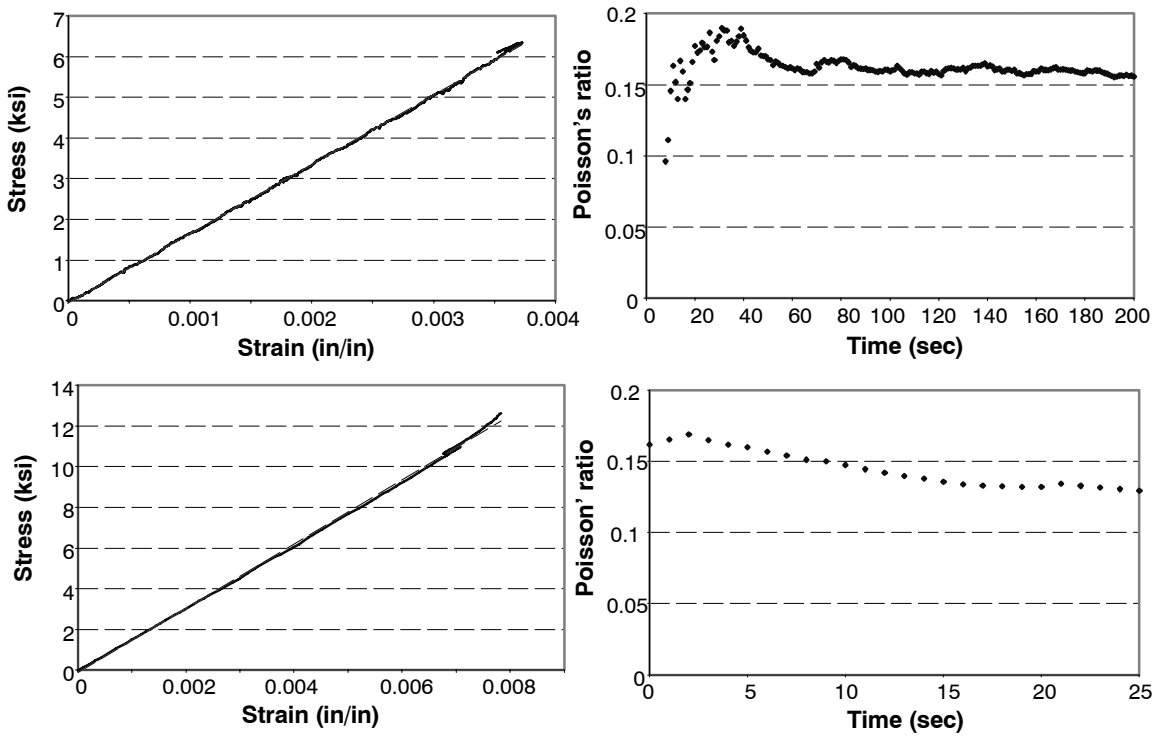


Figure 2-8 The Third & Fourth Test of Tensile Coupon (90°)

Compression Test (0° compression coupon)

Table 2-9 The Result of Compression Coupon (0°)

	Elastic Modulus		poisson's ratio
Test 1	2423.2 ksi	16.7 GPa	0.15
Test 2	1922.6 ksi	13.2 GPa	0.1 – 0.2
Average value	2172.9 ksi	15.0 GPa	0.15
Ultimate Stress	37.0 ksi	254.9 GPa	

Compression Test (90° compression coupon)

Table 2-10 The Result of Compression Coupon (90°)

	Elastic Modulus		poisson's ratio
Test 1	1091.8 ksi	7.52 GPa	0.12
Ultimate Stress	18.1 ksi	124.71 MPa	

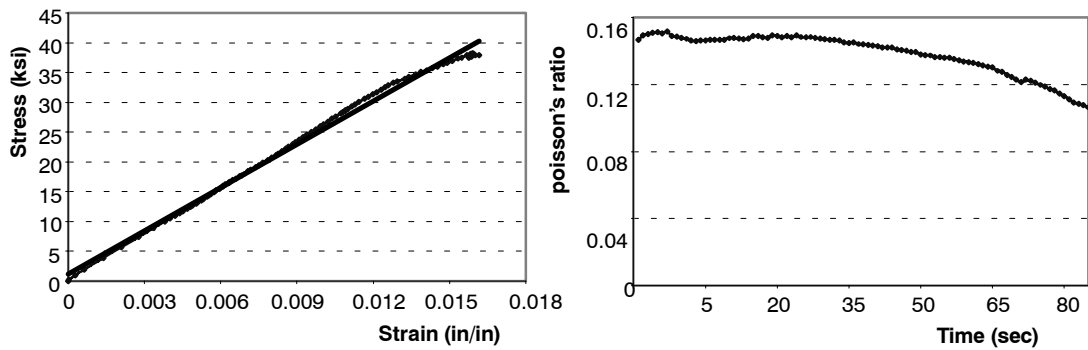


Figure 2-9 The First Test of Compression Coupon (0°)

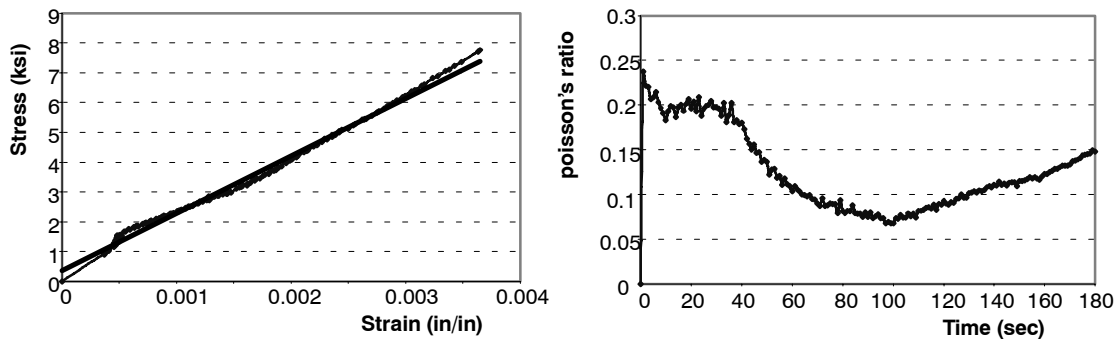


Figure 2-10 The Second Test of Compression Coupon (0°)

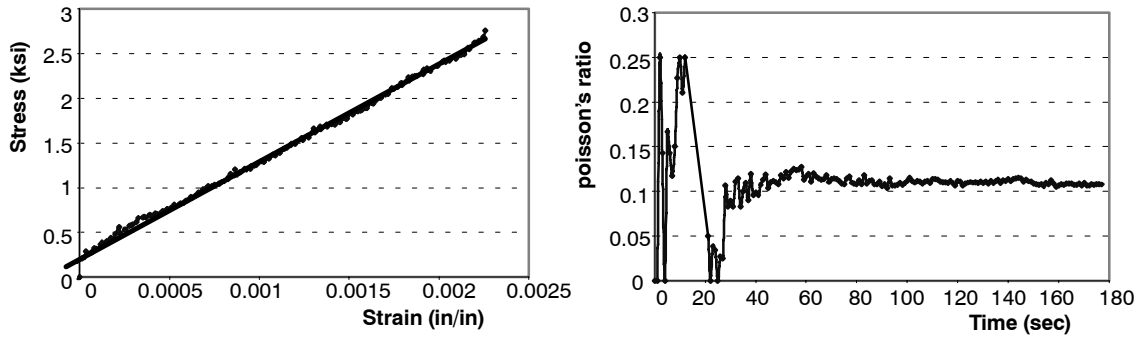


Figure 2-11 The First Test of Compression Coupon (90°)

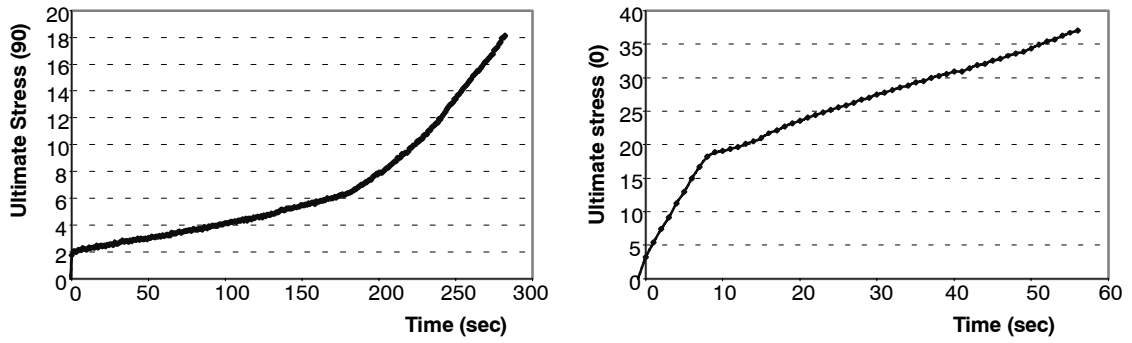


Figure 2-12 The Ultimate Stress of Compression Test

Shear Test (0° Shear coupon)

Table 2-11 The Result of Shear Coupon (0°)

	Shear Modulus	
Test 1	646.42 ksi	4.453 GPa
Test 2	540.44 ksi	3.72 GPa
Test 3	582.14 ksi	4.01 GPa
Average value	589.67 ksi	4.062 GPa
Ultimate Stress	9.09 ksi	62.63 MPa

Shear Test (90° Shear coupon)

Table 2-12 The Result of Shear Coupon (90°)

	Shear Modulus	
Test 1	756.98 ksi	5.215 GPa
Test 2	759.83 ksi	5.235 GPa
Test 3	756.58 ksi	5.212 GPa
Average value	757.8 ksi	5.22 GPa
Ultimate Stress	8.65 ksi	59.6 MPa

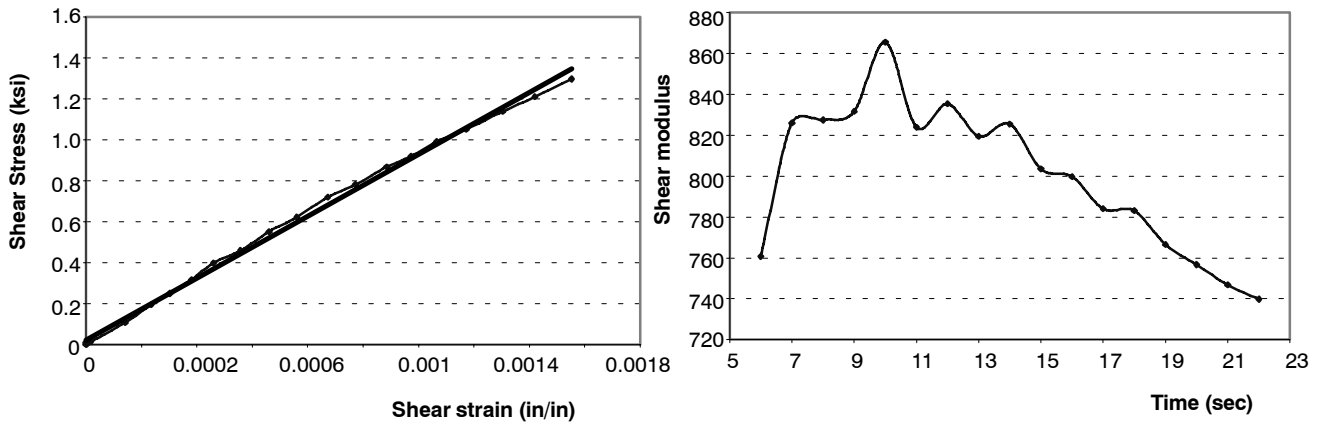


Figure 2-13 The First Test of Shear Coupon (0°)

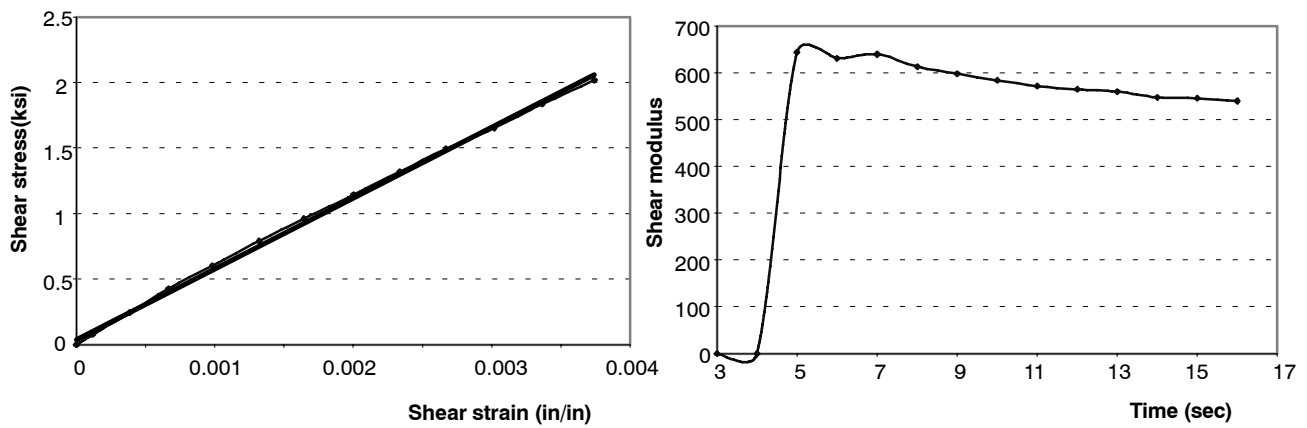


Figure 2-14 The Second Test of Shear Coupon (0°)

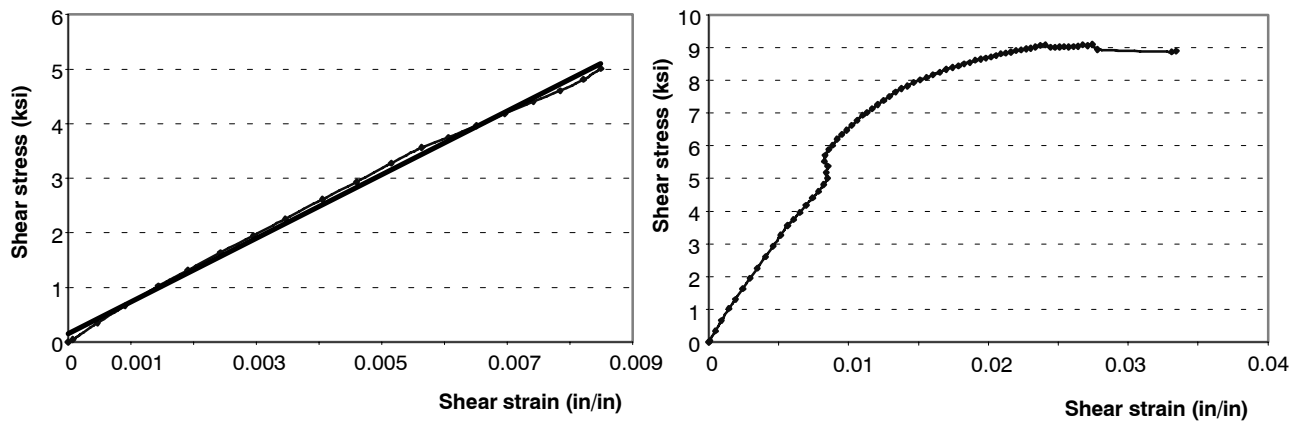


Figure 2-15 The Third Test of Shear Coupon (0°)

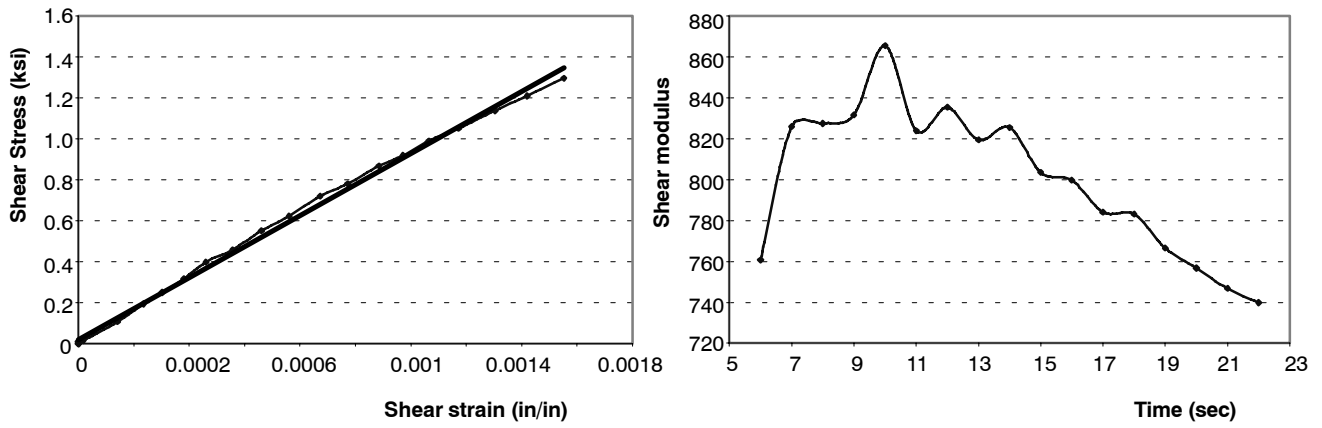


Figure 2-16 The First Test of Shear Coupon (90°)

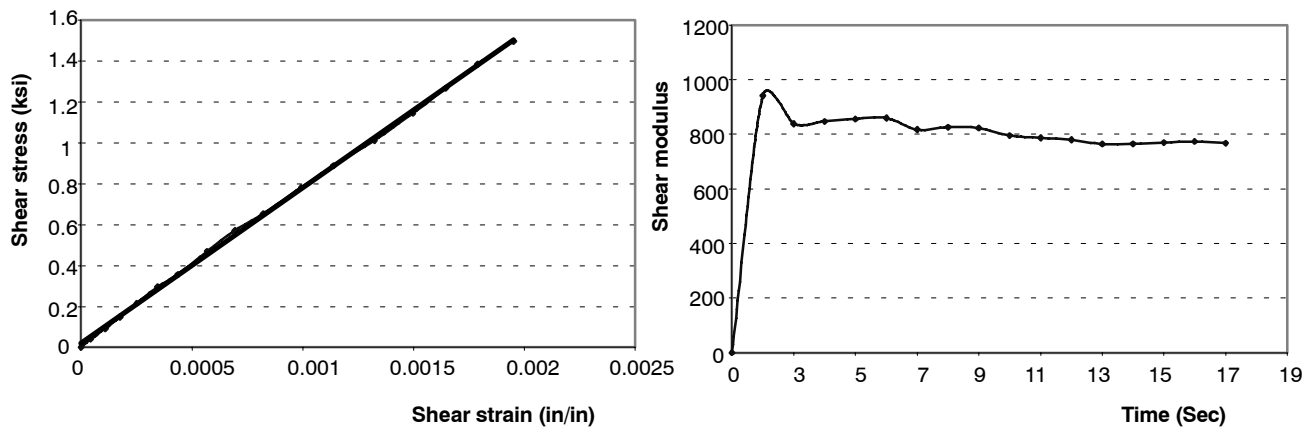


Figure 2-17 The Second Test of Shear Coupon (90°)

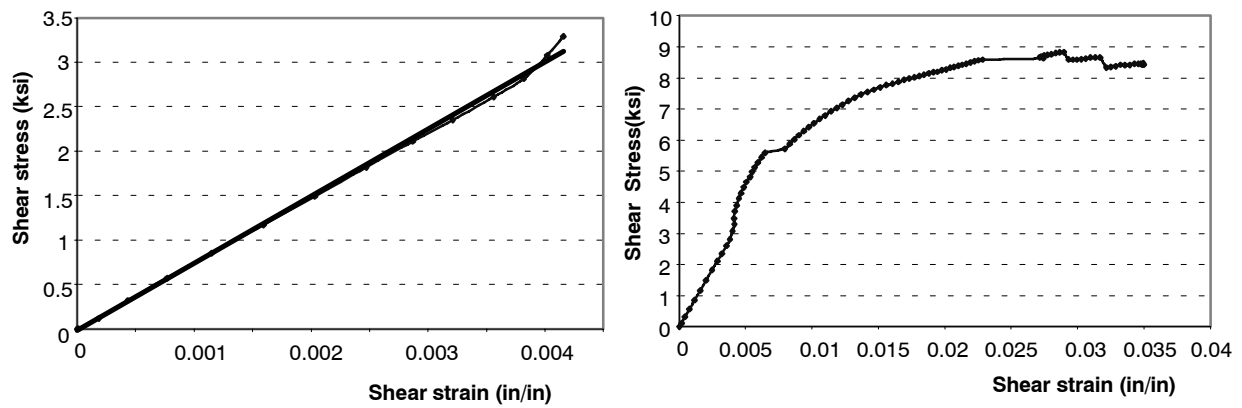


Figure 2-18 The Third Test of Shear Coupon (90°)

Finally, Table 2-13 summarizes the results experimentally obtained for a multi-layer plain-weave glass fabric in a matrix of vinylester resin, Derakane 411®. In the tests, the linear stress-strain curve was used for measuring mechanical properties. In fact, FRP composite material that was tested exhibited nonlinearity, especially for shear test data. However, it was assumed to be linear in this study. Data within linear range were utilized for the purpose of simplified design. Material nonlinearity has to be considered in order to accurately predict the failure mode and inelastic behavior of a structure.

Table 2-13 The Summary of Material Test Results

	Longitudinal direction (L)			Transverse direction (T)		
	Tension (E_{tL}, σ_{tL})	Compression (E_{cL}, σ_{cL})	Shear (G_{sL}, τ_{sL})	Tension (E_{tT}, σ_{tT})	Compression (E_{cT}, σ_{cT})	Shear (G_{sT}, τ_{sT})
Width (in)	0.498	0.256	1.0	0.4945	0.25	1.09
Thickness (in)	0.0545	0.197	0.064	0.053	0.2	0.0615
Elastic modulus (ksi)	2676.5	2172.9		1722.1	1091.8	
Shear modulus (ksi)			757.8			589.6
poisson's ratio	0.204	0.15		0.14	0.12	
Ultimate stress (ksi)	34.89	37	8.65	28.6	18.1	9.09

2.2 Steel Members

2.2.1 Material Description and Test Results

Two types of steel members, A36 for steel frame members and A50 for the top and seat angle plates, were chosen in the tests. Several samples were tested to evaluate the stress-strain behavior and a total of five coupons were tested to establish the material properties of the steel members. Three of which were cut from the existing steel frame members after finishing all experimental works and the others were taken from an unused portion of the same piece of steel from the top and seat angle specimens. Due to possible anisotropy of the rolled steel in the longitudinal and transverse directions, two of five specimens were taken perpendicular to the rolling direction. All coupon tests were conducted in accordance with American Society of Testing and Material (ASTM)–E8, “Standard Methods of Tension Testing of Metallic Materials”.

The coupons were machined into standard test specimen shapes and tested using a 60–kip capacity MTS universal testing machine. Both load and displacement readings were automatically recorded during testing and an axial force vs. axial deformation curve for each of the several coupons were measured using linear extensometer. The results of the coupon tests is also given in Fig. 2-19 and 2-20.

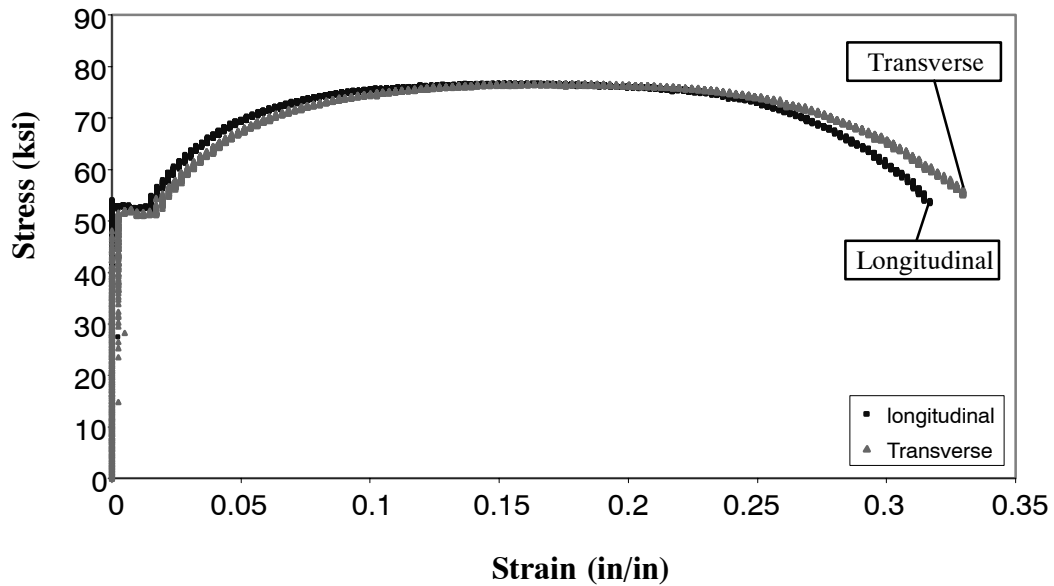


Figure 2-19 Steel Coupon Test for Unused Joint Angle Connections

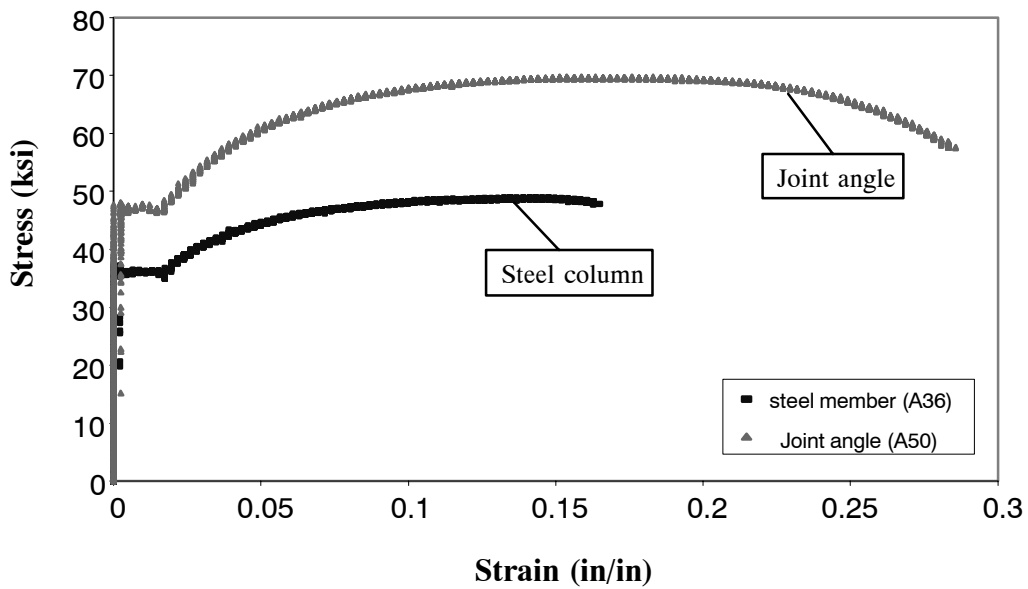
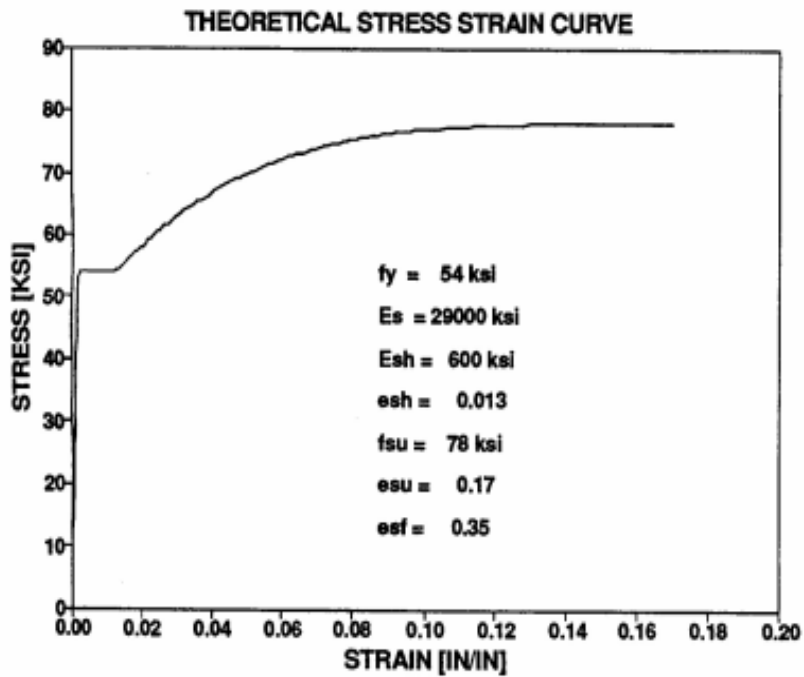
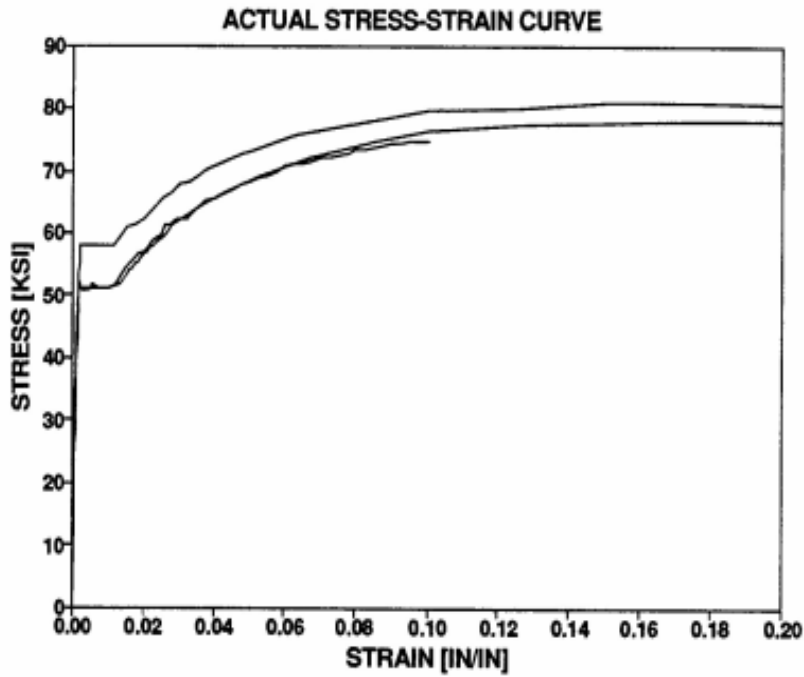


Figure 2-20 Steel Coupon Test for Existing Steel Frame Members

According to these coupon tests, the yield stress for existing steel frame members was approximately 36 ksi and ultimate stress was between 48 ksi and 50 ksi. In this case, the ultimate stress was not accurately measured because the test was not completed due to the premature failure at the instru-

mented area. For new bolted top and seat angle connections, the yield stress varied between 48 ksi and 55 ksi, while the ultimate strength varied between 68 ksi and 78 ksi. It was observed that the ultimate strain at the bolted angle connections taken from the existing steel frame was less than the new ones because the used ones may have been subjected to a large number of previous loading cycles. For the older steel frame used in the multi-layer PMC infilled frame test, a stress-strain relation (depicted in Fig. 2-21 and previously tested by Mander et al. (1993)) was used in the design and analysis.

In the cyclic loading test, the effect of cyclic loading resulted in a difference in the stress–strain response compared to monotonic loading. The reason being that the cyclic load may have caused the material to harden in the compression and to soften in tension especially at high temperature. Furthermore, cyclic loading caused fracture at lower strain at the same temperature. The inelastic behavior of metal model under cyclic conditions can be represented by two kinematic hardening models that are available in the commercial numerical analysis ABAQUS.



**Figure 2-21 Stress-strain Results of Previous test
(Mander et al., 1993)**

2.3 Polymer Honeycomb Material

2.3.1 Description of the Material

Damping materials used in structural applications are typically co-polymers or glass substances which dissipate energy when subjected to shear deformation. A variety of materials are now available as honeycomb structures. Aluminum, paper and “Nomex” honeycombs are made of expanding bonded sheet material. More recently polypropylene has been extruded with a honeycomb section. This material has different stress-strain response from aluminum alloys, and higher elastic strains.

The selected polymer material is composed of H8-PP Polypropylene Honeycomb which was produced by Nida-Core Corp., FL, combined with a resin-rich layer on each surface of the honeycomb. This is a true hexagonal cell honeycomb extruded from polypropylene and the color is clear translucent. To facilitate this honeycomb with adhesive and laminating resins, a non-woven polyester scrim has been thermo-fused to both sides of the core. To prevent filling the cells with resin during construction, a polypropylene barrier film is bonded under the scrim. The properties of H8-PP polypropylene honeycomb are presented in Table 2-14. The honeycomb material used in this research offers the following characteristics:

- The walls of the cells are solid along their whole length, affording the unit excellent compressive strength and good shear strength
- The thicknesses of cell walls vary from 0.2” (5 mm) to 20” (500 mm)
- Ideal for a very wide variety of facings, whether conventional like wood, laminates, metals or more innovative like fiber glass reinforced thermoplastics.
- Possible to construct either non-woven polyester scrims thermofused on both sides of honeycomb to facilitate conventional wet lamination, or open cells for use with thermoplastic skins.

Table 2-14 Properties of Polymer Honeycomb Material (Nida-Core Corp.)

Mechanical properties	SI unit	English
Cell size	8 mm	5/16 inch
Density	80kg/m ³	4.8 lb/ft ³
Compressive strength	1.3 MPa	188 psi
Modulus of Elasticity	15 MPa	2175 psi
Tensile Strength	0.5 MPa	72.5 psi
Shear Strength	0.5 MPa	72.5 psi
Shear modulus	8 MPa	1160 psi
Effective temperature range	-40 to +110 C °	-40 to +230 F
Standard dimensions (1)	2134 mm x 1219 mm	84 “ x 48 “

2.3.2 Results of the Polymer Honeycomb Material Tests

Commercial polymer honeycomb was tested to evaluate various material properties. The application of the polymer honeycomb material is to dissipate the energy through in-plane shear deformation. For design purposes, when this material is used at the interface between skin laminate plates. It would undergo shear deformation and dissipate energy when the structure vibration induces relative motion between the honeycomb and adjacent layers. To investigate the mechanical properties of polymer honeycomb materials, pure shear test was conducted along the cell axis (normal to Z-direction) in Fig. 2-22. Test coupon and adaptor are depicted in Figs. 2-23 and 2-24, respectively. The tests were performed using displacement control MTS universal machines.

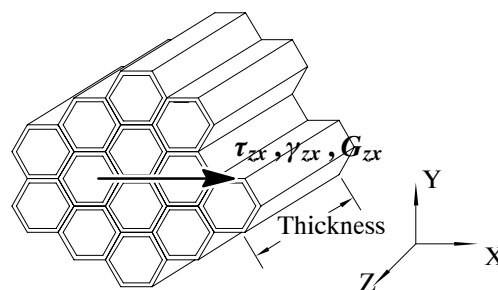


Figure 2-22 Honeycomb Carrying Load on the Surface Normal to Z Axis

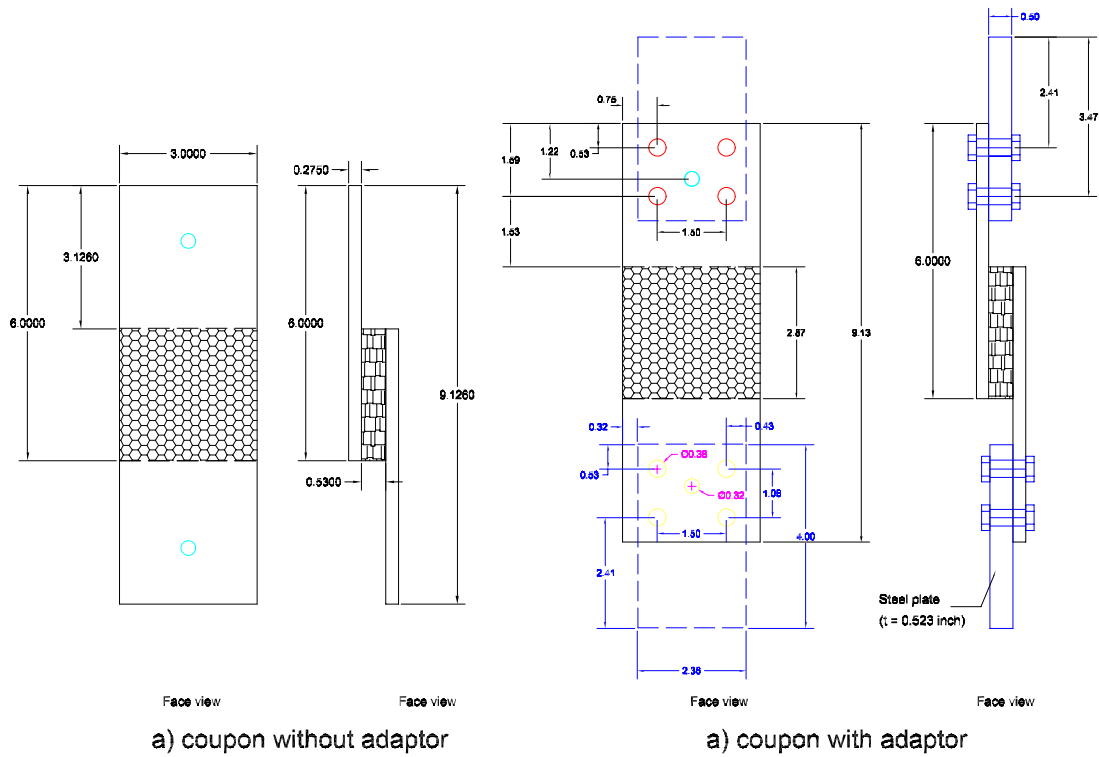


Figure 2-23 The Dimension of Polymer Honeycomb Test Coupon (unit = inch)

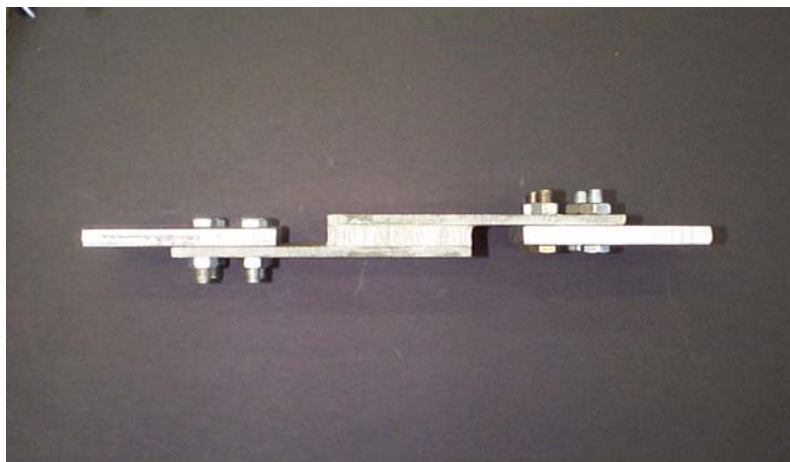


Figure 2-24 Polymer Honeycomb Test Coupon (Side View)

Test results for pure shear stress–strain curves are shown in Fig. 2-25 to 2-27. As shown in Fig. 2-25, energy absorption was found from the loading and unloading test for the polymer honeycomb. According to previous research (Zhu et al., 2000), similar shape of the loading and unloading curves was also observed in the tensile and compressive tests and the behaviors were also similar to those of polyurethane which was found to have viscosity. It was proved that hysteresis occurs when high-

strain deformation bands propagated or unfolded in the honeycomb when average strain exceeded 30%, due to interface friction. From Fig. 2-26, shear modulus was measured, and Fig. 2-27 shows full stress-strain relation of the honeycomb. Tested honeycomb deformation was visible in the cells when the strain reached 15% or 20%. Beyond approximately 30% strain, large shear deformation occurs through the honeycomb with the scrim failure between the skin plates and the honeycomb. It was observed that there was no regularity in cell shape between 50% and 60% strains. The previous research (Zhu et al., 2000) indicated that there is inhomogeneity in the recovery process, as a result of interface friction after the honeycomb structure collapses.

Table 2-15 and 2-16 present the 2-layer material test results in this study and the material properties of the honeycomb provided by the Nida-core Corp., FL, respectively. In the 2-layer shear test, the pure shear strength sometimes introduces eccentricity into the bonding material as well as the polymer materials, in spite of the attempt aimed at minimizing eccentricity in the specimen design. Accordingly, by comparing with the manufacturing values, the results obtained from the 2-layer shear test were verified. Both results showed good agreement. Finally, Fig. 2-29 to 2-32 show the deformation level at various stages of loading.

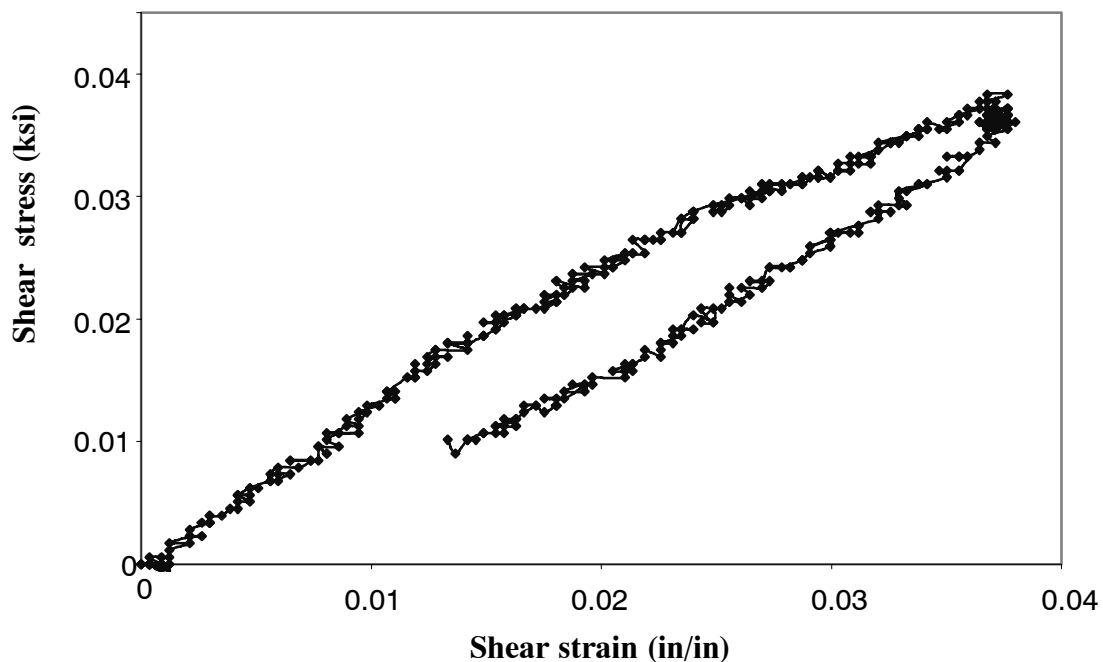


Figure 2-25 Loading and Unloading Test of the Polymer Honeycomb Material

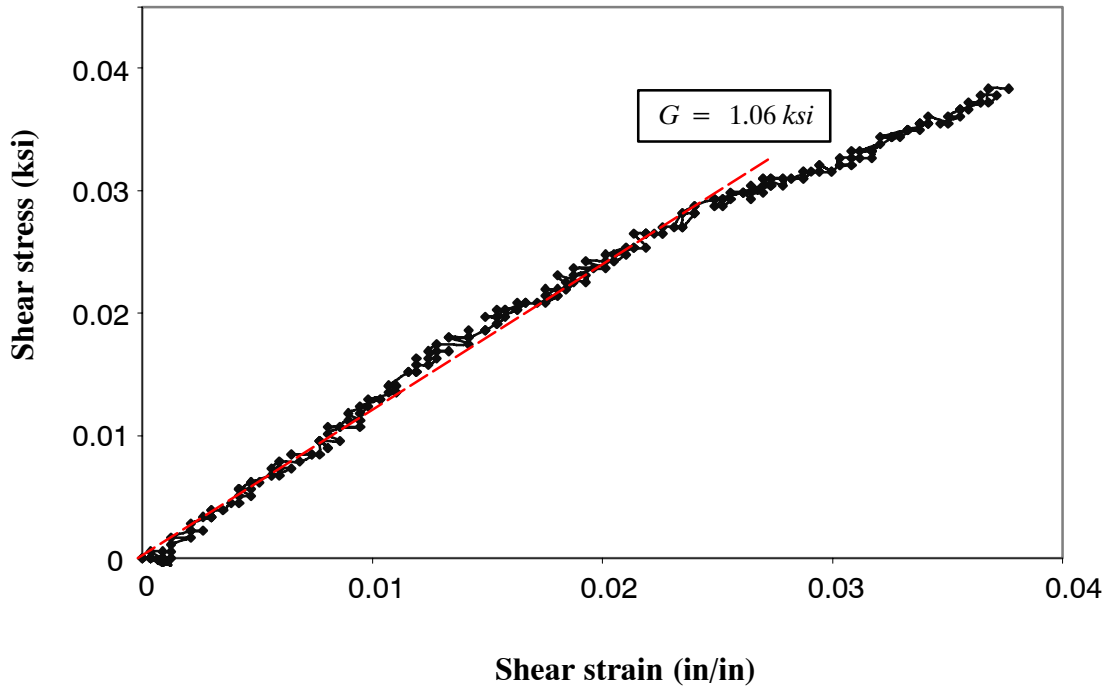


Figure 2-26 Shear Modulus of the Polymer Honeycomb Material

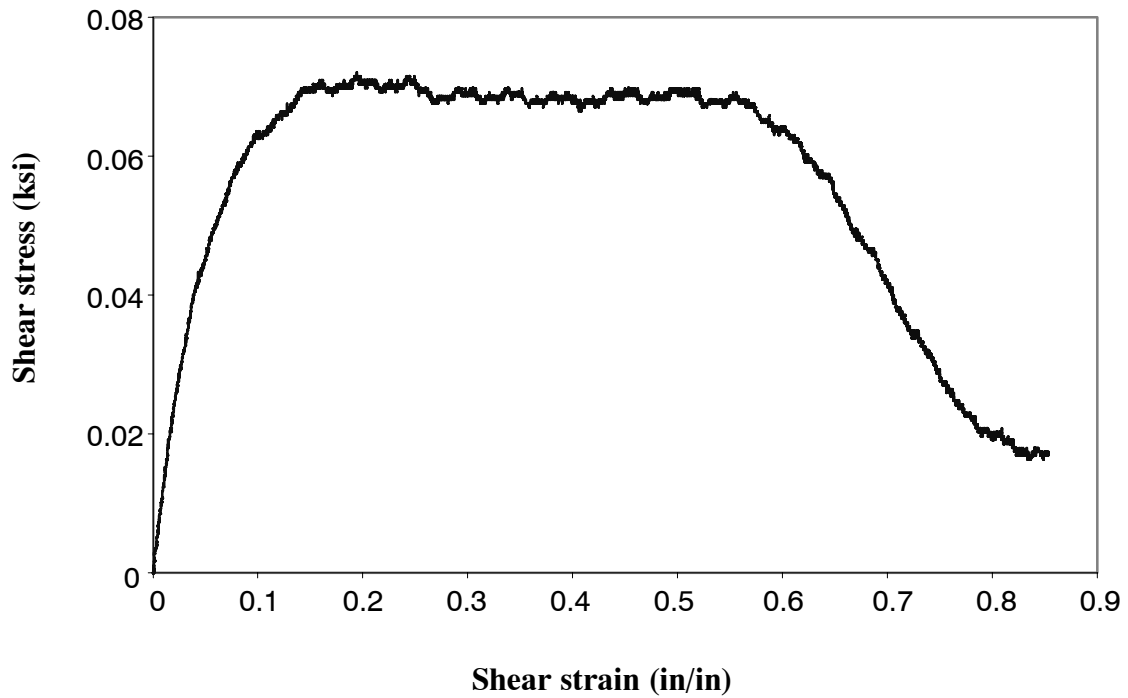


Figure 2-27 Full Stress-strain Behavior of the Polymer Honeycomb Material

Table 2-15 Tested Properties of Polymer Honeycomb Material

Property	Value
Shear modulus (G)	1.0608 ksi
Ultimate shear stress	0.07154 ksi
Ultimate shear strain	0.55 in/in

Table 2-16 Real Properties of Polymer Honeycomb Material (Nida-Core Corp., FL)

Mechanical Property	Value
Density	4.8 lb/ft ³
Shear Modulus (G)	1160 psi
Ultimate shear stress	72.5 psi
Ultimate shear strain	0.625
Modulus of Elasticity	2175 psi
Tensile Strength	72.5 psi
Compressive Strength	188 psi



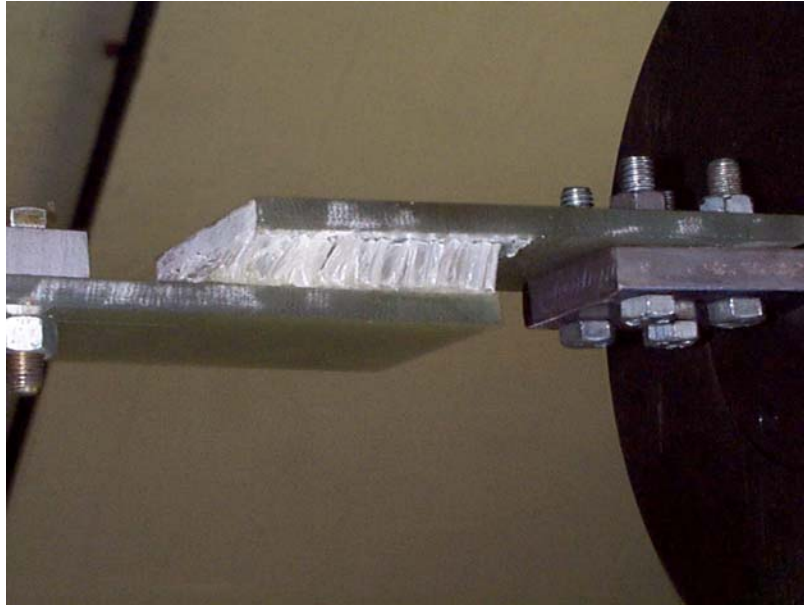
Figure 2-28 Setup of Polymer Honeycomb Test Coupon



Figure 2-29 The Small Deform Shape of Polymer Honeycomb Material
($\epsilon = 0.28$ in/in)



Figure 2-30 The Large Deform Shape of Polymer Honeycomb Material
($\epsilon = 0.79$ in/in)



**Figure 2-31 The Failure of Polymer Honeycomb Material
($\epsilon = 1.60$ in/in)**

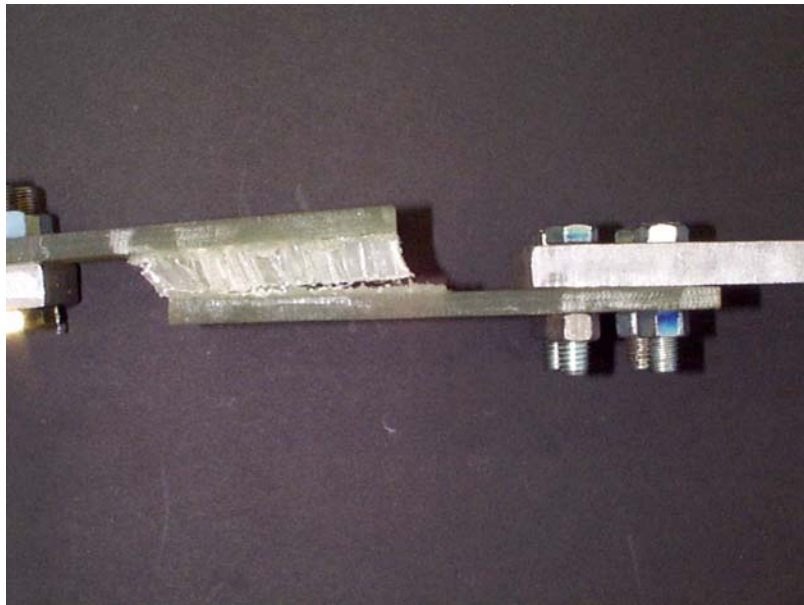


Figure 2-32 The Bonding Scrim Failure of Polymer Honeycomb Material Coupon

SECTION 3

TESTING OF SEMI-RIGIDLY CONNECTED STEEL FRAME

3.1 Introduction

For design purposes, beam-to-column connections of steel frames are usually considered to be either fully restrained (FR) or perfectly pinned. However, the connections in a typical steel frame are essentially partially restrained (PR) with different rigidities. The most recent trend is to make connections in a steel frame flexible to reduce the risk of damage during seismic loading (Salazar et al., 2001). This requires that the connection behavior has to be considered as realistically as possible in the evaluation of the nonlinear seismic response of steel frames. Thus, the presence of PR connections reduces the lateral stiffness, but increases the energy dissipation capacity of the frames. However, there are evidences that frames with PR connections would undergo larger lateral displacement compared to frames with FR connections. Consequently, the $P - \Delta$ phenomenon may produce detrimental effects on the performance of the frames.

Critical facilities such as most hospitals in the eastern U.S. generally have steel frame system, the older ones (designed prior to seismic code provisions) having frames assembled using flexible semi-rigid connections, the newer ones (designed after seismic code provisions) having more conventional steel frame with rigid connections. For the purpose of effective retrofit, a semi-rigid steel frame was employed as a primary structure in this study. Tests of semi-rigidly connected steel frame can provide significant information for understanding the beneficial effects provided by the proposed retrofit strategy. Two types of existing semi-rigid steel frames were considered here – (1) investigation of the progressive angle connection behavior under stiffened PMC infill structure, and (2) occurrence of the existing original joint angle connection failure during the tests. Both types of frames are identical in general except that the steel frame that was assembled by past researcher (Mander et al., 1993) used bolted angle connections in the first specimen (case 1) and the same steel frame with new bolted angle connections in the other specimen (case 2). In the experimental, multi-layer infilled frame was employed for case 1. During the tests, new bolted top and seat angle connections

were replaced after completing the multi-layer PMC infilled frame tests (case 1) for the subsequent tests. The sizes of steel frame members for all test cases are the same. Accordingly, tests of two types of semi-rigid steel frames are presented in this section.

3.2 The Configuration of Semi-rigid Steel Frame

The components of steel frame were columns, beams, braces, and connections. The columns, beams, and braces were built up with angles and/or plates connected together with rivets, bolts or welds. Because the focus here is to provide infill retrofit strategies for old construction that often made of steel with a yield stress of 30 - 36 ksi.

The members of the frame that were used in the experiments were designed using A36 steel for gravity load and constructed according to the specifications of the American Institute of Steel Construction (AISC) which represented common design and construction practices of old building structures. The cross-sectional dimensions (U.S.) of beam and column members were W8x21 and W8x24, respectively.

Both beam and column members were assembled by bolted semi-rigid (top and bottom angle seat) connections. Two bolt rows were used in the angle-leg connected to the beam flange, and one bolt row was used for the outstanding angle-leg connected to the column flange. The semi-rigid top and seat angle plates were designed to have the capacity of approximately 50% of the connecting member. Thus, yielding in the frame would be concentrated in the angle connections to prevent main members from damages. According to AISC specification, the seat angle is intended to transfer only vertical reaction and should not provide significant restraining moment at the end of the beam. Top angle only provided lateral stability and was designed not to carry any gravity load. Details of the top and seat angle connections are illustrated in Fig. 3-1. The columns were also connected to the two pin connectors of steel plates which were strongly connected to the concrete reaction beam using anchor rods and all bolts were torqued. Fig. 3-2 shows a hinge support of the steel frame.

Finally, Fig. 3-3 presents a sketch of the steel frame used in this study and a picture of the completely fabricated structure. All fabrications of steel members were carried out at the Structural Engineering Earthquake Simulation Laboratory at the University at Buffalo.

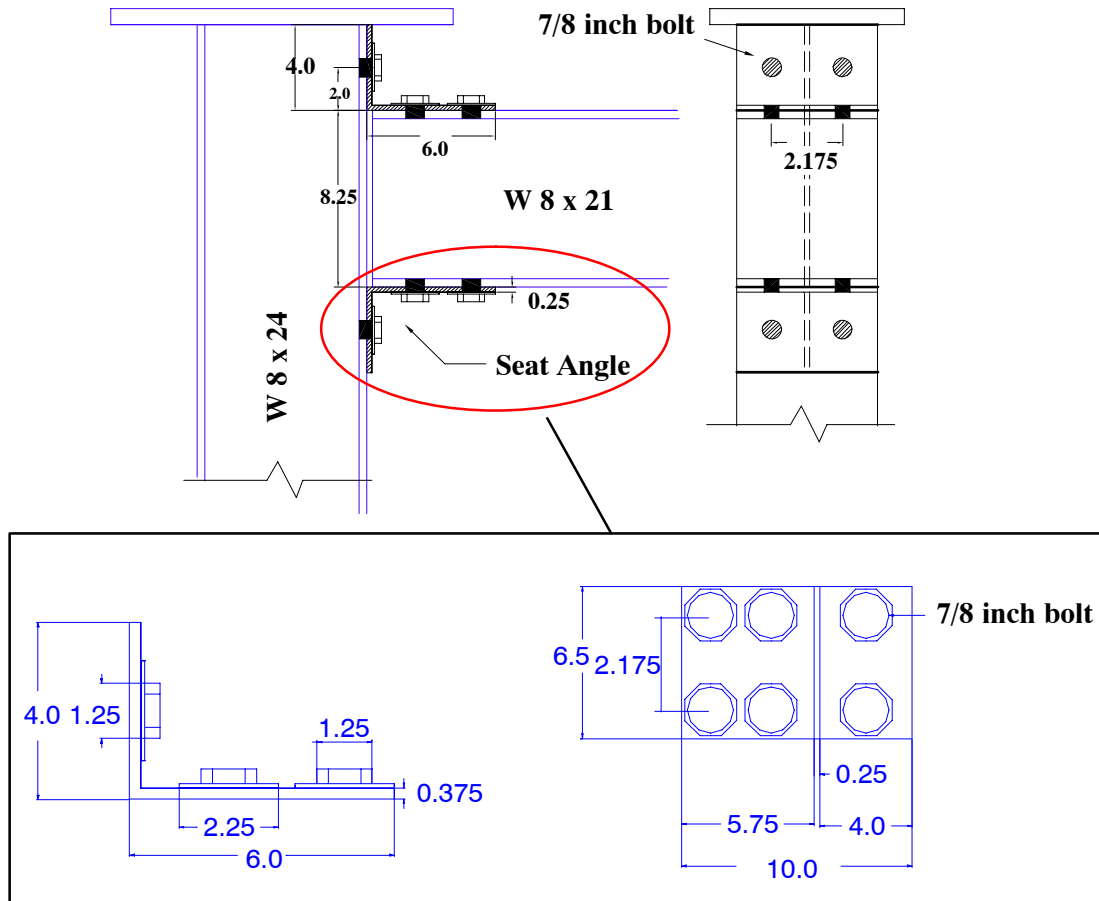


Figure 3-1 Detailed Configuration of Top and Seat Angle Connections (unit = inch)

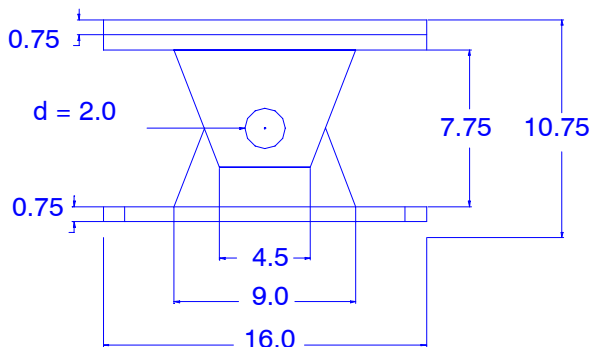
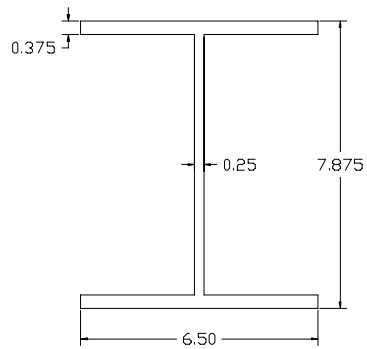
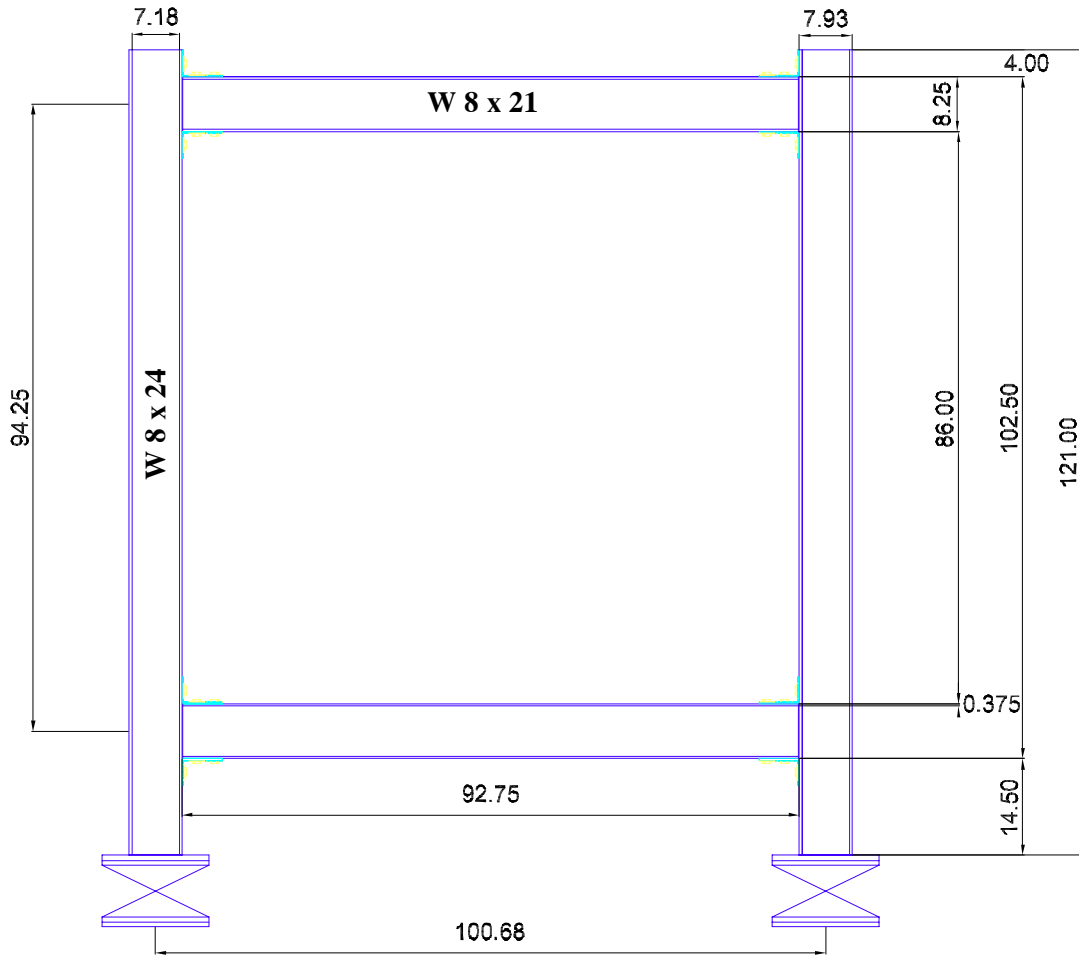
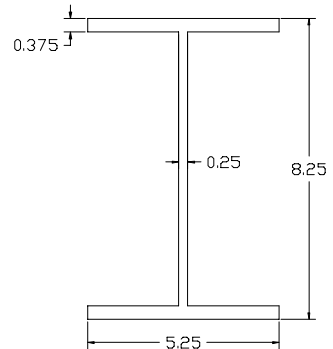


Figure 3-2 The Configuration of Hinge Support (unit = inch)



Cross Section (W 8 x 24)



Cross Section (W 8 x 21)

Figure 3-3 The Configuration of Steel Frame (unit=inch)

3.3 Testing of Semi-rigidly Connected Steel Frame

3.3.1 Test Specimen Setup

In the experimental stage, an existing steel frame was employed to save construction time and material costs. The old top and seat angle connections in the frame underwent beyond the yield point when they were tested before. As such, a steel frame without the PMC infill panel was tested to obtain the response of the steel frame and evaluate the potential enhancements after the infill wall was installed. As mentioned before, a stress-strain relationship, tested by Mander et al. (1993), was adopted for mechanical properties of existing joint angle connections. Fig. 3-4 illustrates the tested steel frame setup.



Figure 3-4 Steel Frame Setup

To investigate the strength and stiffness of steel frame under monotonic and cyclic loading, push-over and fully reversed cyclic loading were applied to the upper W8x21 beams at 0.0167 Hz (2 cycles per 120 second). The displacement amplitudes of cycles for each drift level were 0.56, 1.13 and 2.26 inch. In the steel frame tests, a non-destructive test program was carried out to avoid damaging the steel frame. The linear variable differential transformers (LVDTs) were used to measure the absolute lateral displacements of the test specimen. More detailed experimental instrumentations will be discussed later.

3.3.2 *Supplementary Test Setup*

A full-scale test specimen without an infill panel was placed on the concrete foundation beam after finishing parts of supplementary experimental setup. Fig. 3-5 shows the configuration of the stabilizing frame that was designed and constructed to resist any accidental out of plane forces, transverse to the plane of the test specimens, of less than $\pm 10\%$ of the in-plane test load applied to the test specimen.

Figure 3-6 shows a sketch of the test specimen setup. The test specimen was anchored to a foundation beam, which was designed to resist the maximum expected load during the test. Each hinge joint of the test specimen was connected to the foundation beam by four 22 mm (0.875-inch) high-strength A325 bolts. After an installation of composite infill panel, the out-of-plane instability of the infill panel was prevented by supports perpendicular to the plane of loading using six steel plates. These steel supports enclosed composite panel at the interface of both columns and beams to reduce any in-plane friction and allow free lateral displacements of the specimen. Steel plates used in the experimental setup were PL 6.0 x 5.25 x 0.625 inch and they are shown in Fig. 3-7.



(a) 4 - Guide Wheels

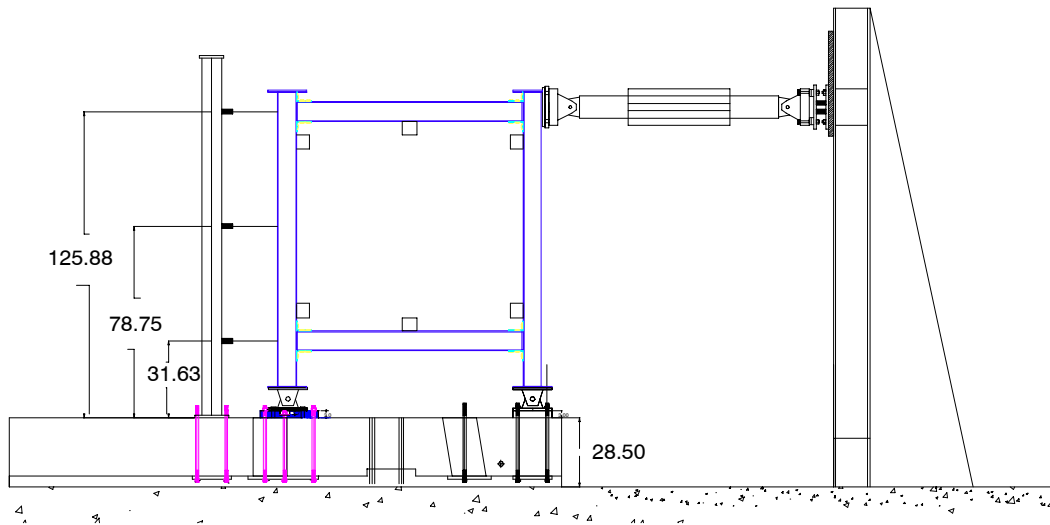


(b) Steel Rod

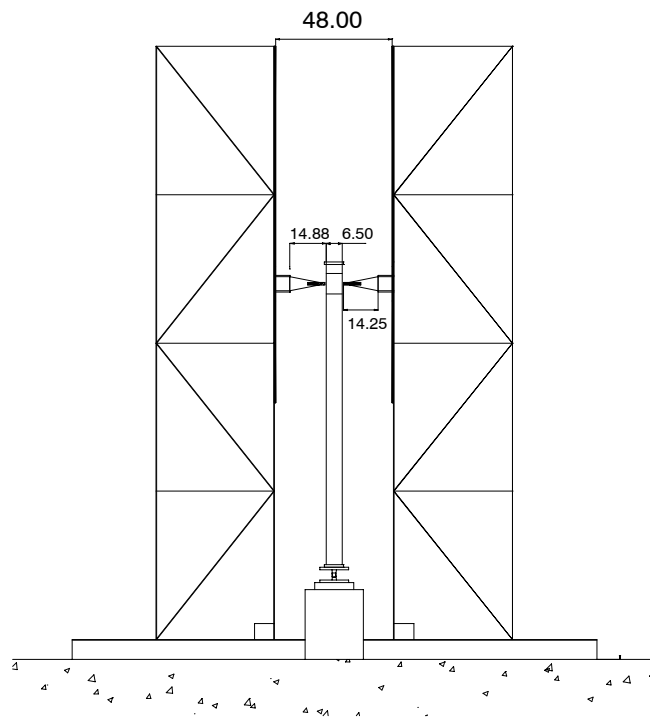


(c) Stabilizing Frame Setup

Figure 3-5 Configuration of Stabilizing Frames



Front view



Side view

Figure 3-6 Setup of Steel Frame Structure (unit = inch)

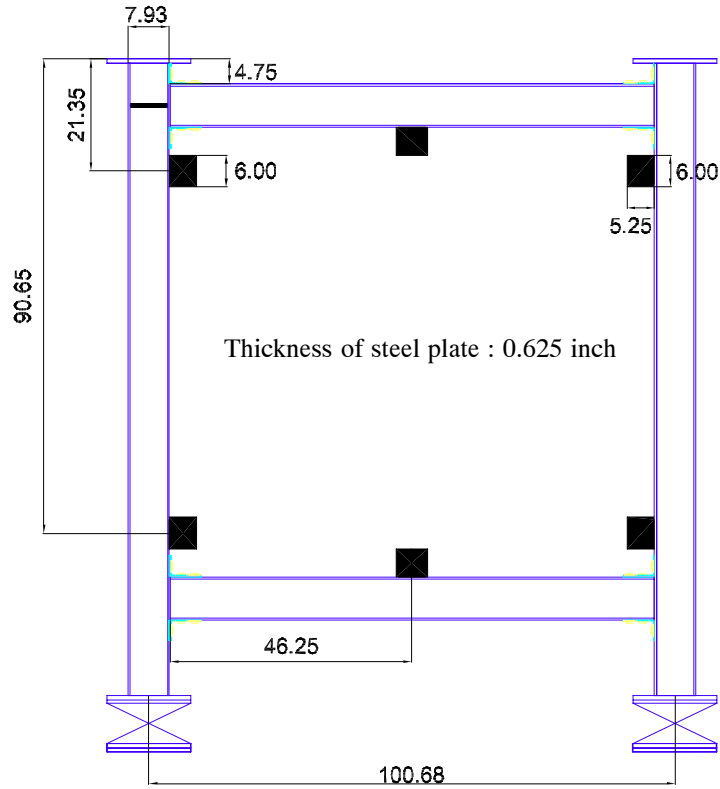


Figure 3-7 Configuration of Out-of-plane Supporting Steel Plate (unit=inch)

3.3.3 Discussion of Test Results

This section presents test results for the bare steel frame. Earlier studies (Elnashai et al, 1994; Salazar et al, 2001) indicated that frame with semi-rigid connections exhibits energy absorption capacity, and may be used effectively for earthquake resistant design. It indicates that semi-rigid connections in the frame is a dominant factor for determining its behaviors. As such, the behavior of bolted angle connections in the frame must be investigated under monotonic and cyclic loads.

As mentioned before, two testing cases of steel frame were considered in this study. One is a steel frame that possessed old semi-rigid angle connection (Type 1) and the other is a steel frame with newly replaced top and seat angle connections (Type 2). In the steel frame tests, the hydraulic actuator was driven to a displacement less than the expected elastic limit (up to 1.5%) to avoid damaging the bolted semi-rigid angle connections and to ensure that this frame can be reused in the multi-layer

PMC infilled frame tests. Therefore, the quasi-static cyclic experiment of the steel frame was conducted in displacement control for lateral drifts of 0.5%, 1.0%, and 1.5%.

Steel frame with old semi-rigid angle connections (Type 1)

The force-displacement response under monotonically increasing lateral load for Type 1 frame is shown in Fig. 3-8. It must be noted that a Type 1 steel frame has been used by previous research program and being re-used again in this study. It can be observed that the stiffness of the specimen is slowly decreased after the displacement of 0.3 inch. It is due to the fact that the strain hardening of the old connection and/or existing bolt and angle connection slip may have occurred during the test. From this test, the initial stiffness was computed to be 6.27 kips/in.

In cyclic loading tests, it can be seen that the stiffness degradation started to be evident as the slope of the curve decreased. Significant hysteresis within the cycles is apparent indicating that the angle connections had yielded, thus dissipated energy. Fig. 3-9 shows the results of cyclic loading tests.

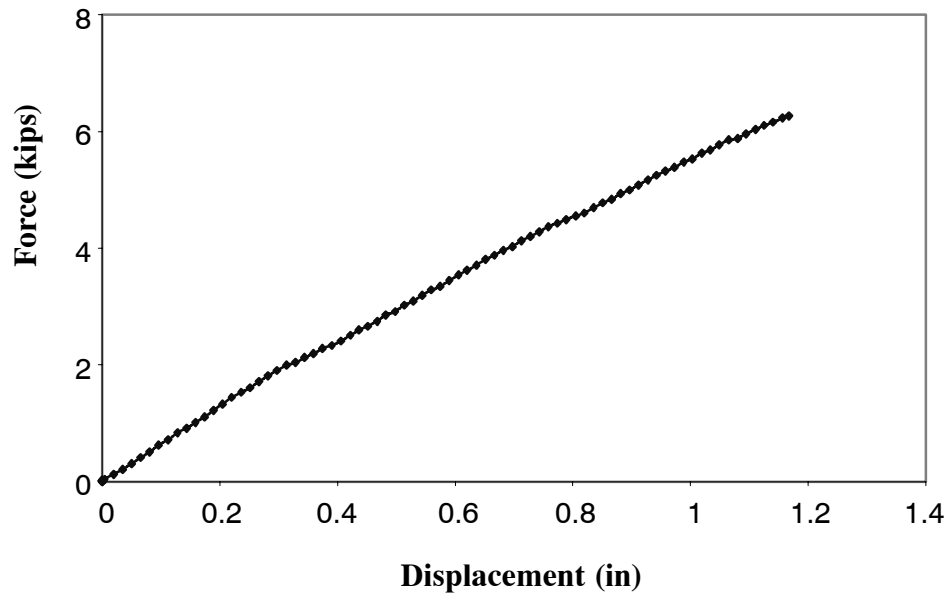


Figure 3-8 Result of Push-over Loading Test for Steel Frame (Case 1, 1.0%)

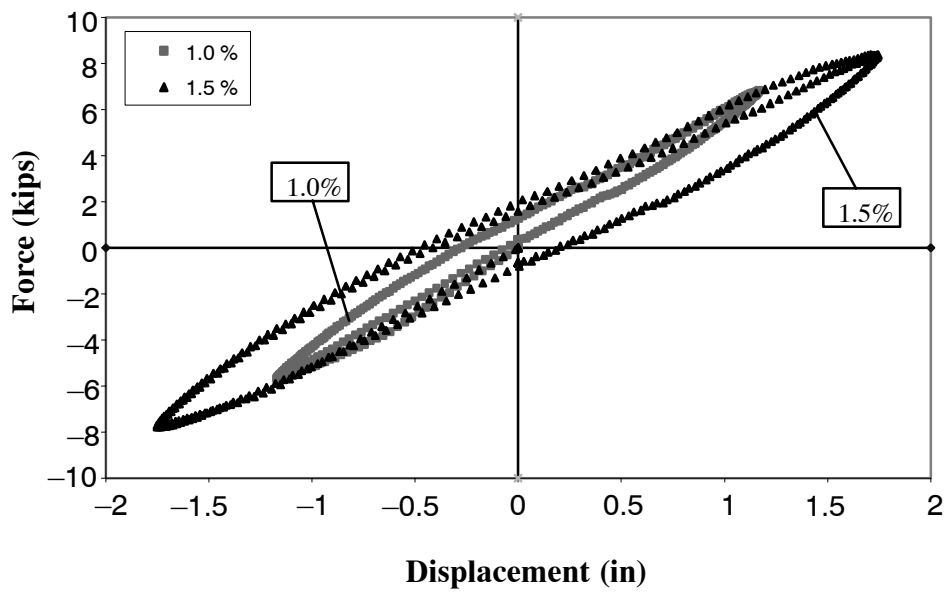


Figure 3-9 Result of Cyclic Loading Test for Steel Frame Tests (Case 1, 1.0 & 1.5% drift)

Steel frame with new semi-rigid angle connections (Type 2)

For Type 2 frame, new bolted top and seat angle connections were installed. The behavior of new bolted angle connections in the frame was studied briefly before and after testing of the PMC infill systems. After completing all experimental tests including seismic PMC infill tests, bare steel frame was tested again to investigate the post-testing behaviors of the bare frame. It must be noted that a Type 2 steel frame was a Type 1 steel frame with newly replaced semi-rigid angle connections.

The force-displacement response for the test specimen (Type 2) subjected to push-over loading is shown in Fig. 3-10 and 3-11. In these figures, the values of elastic stiffness from the initial and stabilized envelope curves obtained from cyclic loading test are presented. As shown in Fig. 3-10, there is minor difference between successive test results. In the initial stage (Test 1), it was assumed that there is no slip and the leg of angle adjacent to the column behaves as linear-elastic, while the leg of angle adjacent to the beam behaves as a rigid body. Also, initial higher restraint between the angle and the column face may arise from the perfect clamping action of bolts which prevents any slip between the components. Because of an insignificant difference among three test cases in Fig. 3-10, the overall stiffness was determined by the average value. As the lateral drift increases, stiffness degradation may also arise in the structure as the result of material yielding and/or slipping in the connections.

The force-displacement response of the bare steel frame after the PMC infill system tested and removed is presented and compared with bare steel frames before the PMC infill system tested in Fig. 3-11. It is clearly shown that there is a significant difference between their behaviors. The reason being that the existing joint angle connections were subjected to an successively increasing number of cyclic bending moments. Differences in stiffness of semi-rigid steel frame for a given displacement level appear to be due to several reasons: (1) elastic deformation of the frame after the infill yields, (2) cyclic slips in the bolted-angles and between loading actuator and long steel adaptors adjacent to the loading reaction frame, and (3) cumulative damage of the connections at variable amplitude tests. Especially, cyclic bolt slip is one of the major characteristics at the large deformation lev-

els. The slip load of the bolted members depends on the distribution of the clamping forces, which in turn relies on bolt tensions and friction condition of contact surfaces. Variation of the stiffness for the test frame was summarized in Fig. 3-12.

Fig. 3-13 shows the comparison of in-plane behaviors of the steel frame with or without the damage in the bolted top and seat angle connections. Semi-rigid steel frame with the infill induced larger lateral force due to the infill's contribution which resulted in an increase in frame stiffness. However, larger induced lateral forces are also attracted to the frame, which could result in failure of the infill wall and more importantly failure of the frame itself. In many cases, the bolted angle connections sustain damage due to induced larger vertical reaction forces. With damages in the bolted top and seat angle connections, the stiffness of overall structure was significantly reduced as shown in Fig. 3-13. For the bolted angle connections, the moment-rotation behavior obtained by monotonic loading tests is presented in Fig. 3-14. This result provides information for the initial stiffness of newly replaced top and seat angle connections (Type 2).

The force-displacement responses for the structure of type 2 were also studied under applied cyclic loads. Test results at different lateral drifts are compared in Fig. 3-15. In the cyclic loading tests, there is no significant stiffness degradation. This is due to new angle connection setup without slip and material yield. Fig. 3-16 shows comparison of hysteretic behavior for semi-rigid steel frame before and after joint angle connection damage under cyclic loading. Generally, the dissipation of energy at partially restrained (PR) connections is estimated by considering the hysteretic behavior of bending moment, shear, and axial forces. It has been shown that the energy dissipation due to shear and axial forces is negligible compared to that due to bending moment (Salazar et al., 2001). This is because the shear and axial force deformation behaviors are virtually linear, and the corresponding energy dissipation due to hysteretic behavior can be neglected.

As shown in Fig. 3-16, similar hysteresis within the cycles is apparent and it indicates that all or part of angle connections in the structure had yielded by the bending moment at the connections and the corresponding relative rotation. After damage at the joint angle connections, it would be predicted

that the presence of plastic hinges, if developed, will produce additional axial deformation and relative rotation in a particular element.

The semi-rigidly connected steel frame was tested whenever new seismic retrofitting strategy was applied, with particular attention directed towards understanding the comparative in-plane behavior of semi-rigid frame at each stage. It is because the behavior of the semi-rigid connection varied following the effects of slippage and applied loading cycles. Steel frame tests were very important for this study in order to understand and quantify the contribution of the PMC infill panel systems to energy dissipation and stiffness enhancements.

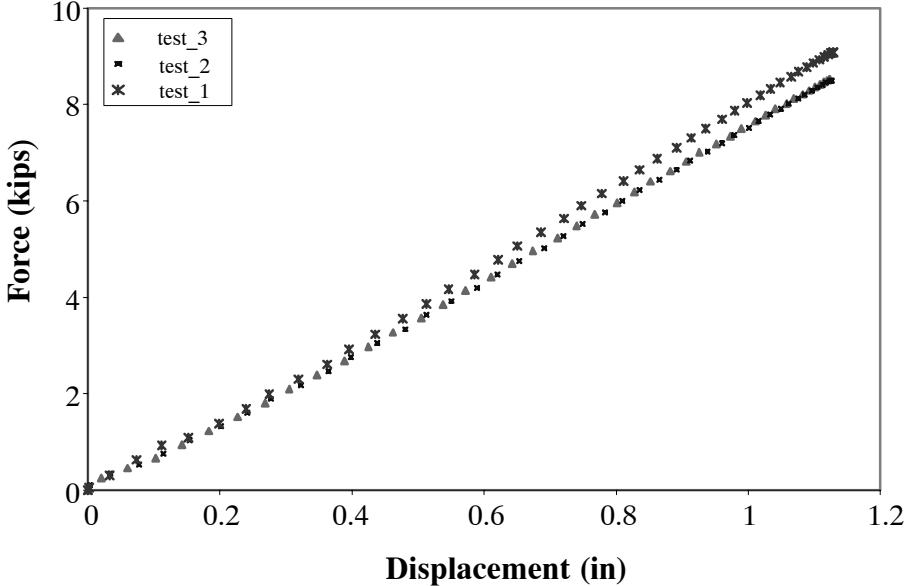


Figure 3-10 Result of Push-over Loading Test for Steel Frame (Case 2)

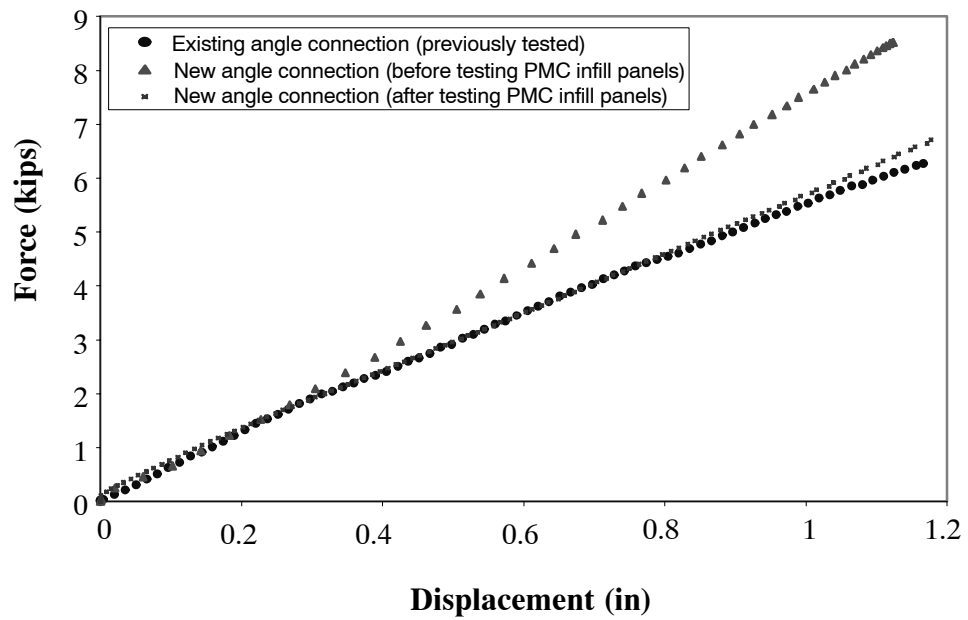


Figure 3-11 Comparison of Stiffness of Semi-rigid Steel Frame (1.0% drift)

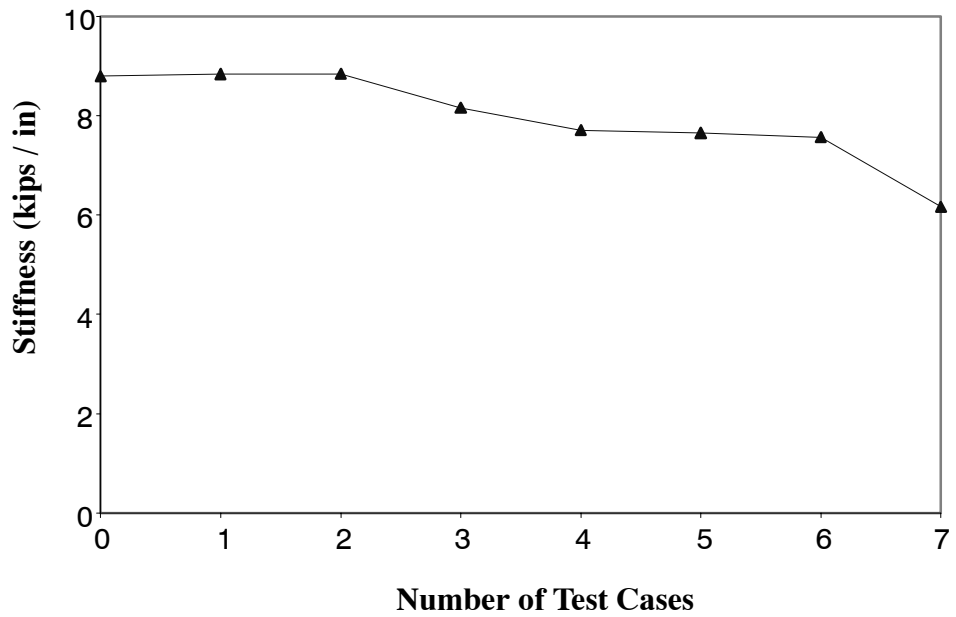


Figure 3-12 Stiffness Degradation of Test Frame under Progressive Test Cases

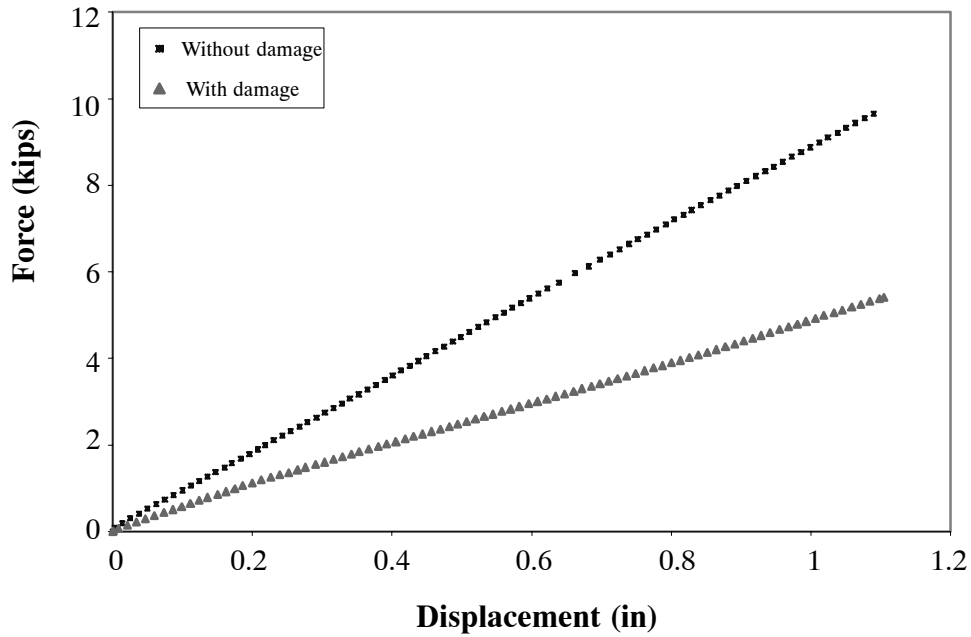


Figure 3-13 Comparison of In-plane Behavior for Semi-rigid Steel Frame before and after Joint Angle Connection Damage under Push-over Loading

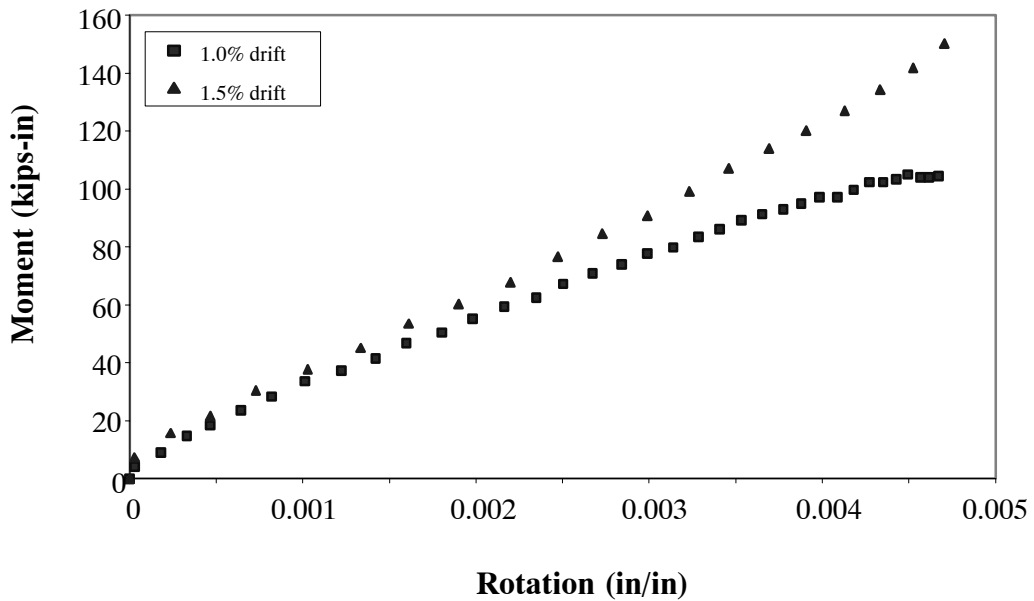


Figure 3-14 Moment-Rotation Relation of Steel Frame Tests at Left Top Joint Connection

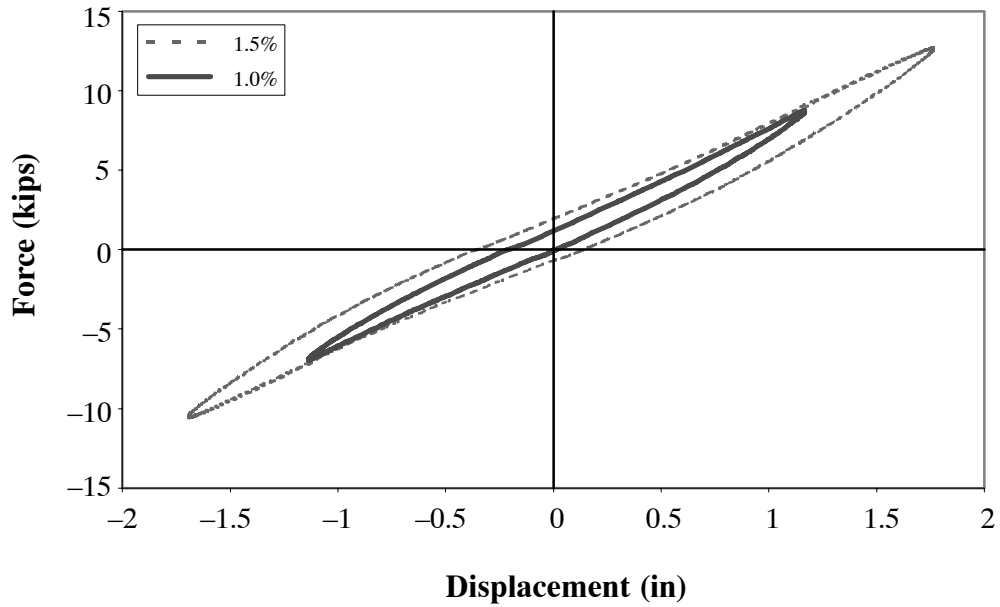


Figure 3-15 Result of Cyclic Loading Test for Steel Frame Tests (Case 2, 1.0 & 1.5% drift)

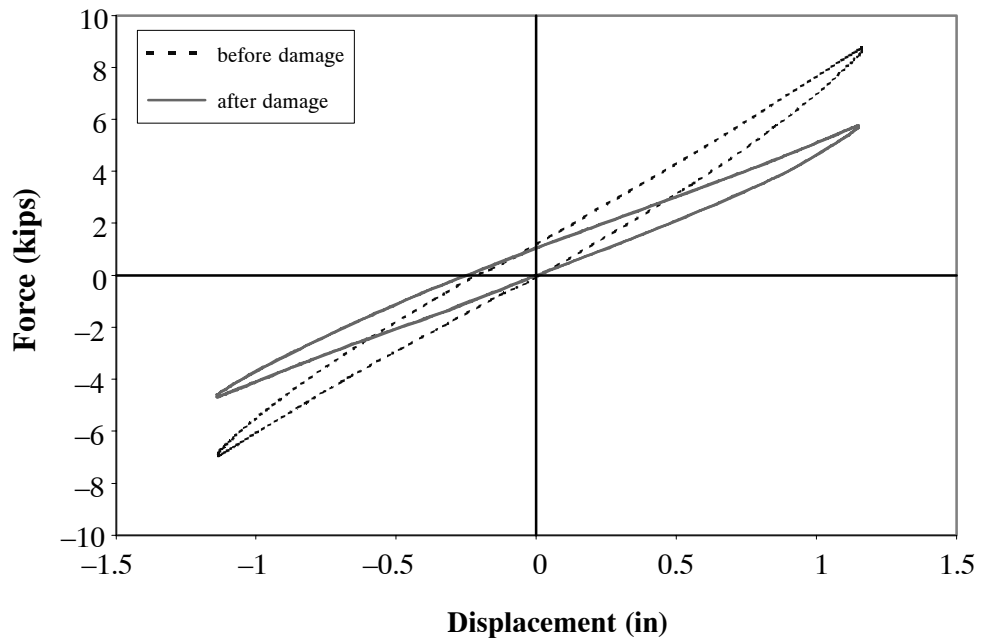


Figure 3-16 Comparison of Hysteretic Behavior for Semi-rigid Steel Frame Before and After Joint Angle Connection Damage Under Cyclic Loading

SECTION 4

MULTI-LAYER PMC INFILL PANEL SYSTEM

4.1 Introduction

This section describes the concept of a multi-layer PMC infill panel system which is introduced as a seismic retrofitting strategy. An experimental study was performed to explore the effectiveness of this seismic retrofitting strategy, and to examine the behavior of this PMC infill wall system when subjected to monotonic and cyclic loading. A steel frame retrofitted with a multi-layer PMC infill wall was monitored to assess the resultant enhancements to its seismic-energy dissipation. In testing the multi-layer PMC infill wall system, a large-scale steel frame was used to avoid the typical uncertainties associated with scaling effects. Details of the steel frame were described in the previous section. The optimal design for the stacking sequence of a multi-layer PMC infill wall panel was determined based on performance and material cost using finite element analysis. Finally, the observed behavior of the PMC-infilled frame was assessed on the bases of stiffness, strength, modes of failure, and energy dissipation.

4.1.1 Typical Structural System of Composite Panel

A typical laminated structure that is widely used in aeronautical/aerospace, marine, and civil engineering constructions is the sandwich-type construction. The sandwich-type structures are constructed of three layers. Two of them, called face sheets, constitute the external layers treated as thin shells, which are separated by a thick mid-layer playing the role of the core. The new and exotic high modulus, high strength, low weight fiber-reinforced composite materials are likely to be widely employed in these structures, especially when the condition of least weight is of vital concern, as is the case with the aeronautical/aerospace flight vehicle structures. In the sandwich construction, the faces are generally made up of high strength materials (steel, aluminum, or glass-reinforced plastic), the core layer is made of a low specific weight material (balsa, porous rubber, corrugated metal sheet, metallic honeycomb) which may be much more flexible and stronger than the face sheets. In addition to the possibility of achieving high flexural-stiffness characteristics with little resultant

weight penalty, sandwich-type construction also exhibits many properties of exceptional importance for aerospace and civil engineering constructions. They provide: (a) excellent thermal and sound insulation; (b) a longer service life as compared to stiffened-reinforced structures which are weakened by the appearance of stress-concentrations; (c) possibility of being designed to meet very close thermal distortion tolerances.

Although standard sandwich panel construction consists of two strong outer faces and a weaker inner core, in a continuing effort to achieve higher stiffness-to-weight and strength-to-weight ratios, traditional materials have evolved from metallic face sheets and aluminum honeycomb core to composite materials. For the face sheets, composite materials offer high stiffness and low specific weight. For the core, non-metallic honeycomb and plastic foam materials are now available and widely used.

4.1.2 Selecting Proper Construction Materials

All the FRP composites (glass, graphite, Kevlar) can be used for energy absorbing applications and all are usually weight effective, when compared with mild steel, under stable collapse conditions. Of particular importance for large-scale commercial applications, the skin sheet materials using glass fibers for reinforcement offer significant energy absorption capability, as good as that demonstrated by conventional fabric or type lay-ups. The energy absorbing characteristics of a structure made from FRP composites were thoroughly presented by Thornton et al.(1985). It is clear that the type and nature of the fiber and resin, the geometry of the structure, and the fiber arrangement affect significantly the energy absorbing capability. However, currently available data are not sufficient to give a clear and unambiguous answer for energy estimation. The difficulty arises simply because energy absorption in composite material is largely by fracture, buckling, fiber debonding and breaking, or matrix damage rather than by plastic deformation as in metals.

The main purpose of combining strong thin facings with a thick core is to produce a highly stressed-skin construction, which leads to great bending stiffness and strength for the structure's weight. For the sandwich construction to be lightweight for infill wall applications, the core must be a lightweight material of a low density cellular construction. In this study, the vinyl sheet foam and Diviny-

cell H materials were chosen as the core in all PMC infill panel construction. Closed cell vinyl foam provided by An-Cor Plastic Corp. is an excellent core material with proper mechanical properties. When vinyl foam was used as a structural sandwich core, it provides low weight, excellent stiffness as well as high insulation.

For the Divinycell H material, it is a semi-rigid PVC foam used as a core material in conjunction with high-strength skins, to produce strong, stiff, lightweight composite structures. This construction has a high strength-to-weight ratio, exceptional dynamic strength, excellent insulating properties, and a closed-cell structure that makes it impervious to water. A grade H among several types of Divinycell grades produced by DIAB international company was chosen and it has all the properties expected for a high-performance, lightweight construction material. The properties of a vinyl sheet foam and a Divinycell H are shown in Table 4-1 and 4-2.

Table 4-1 The Properties of Vinyl Foam (An-Cor plastic Inc.)

Density (lb/ft ³)	Modulus			Strength		
	Compression (psi)	Flexure (psi)	Shear (psi)	Compression (psi)	Flexure (psi)	Shear (psi)
2	730	630	360	36	50	31

Table 4-2 The Properties of Divinycell H100 (Divinycell Corp.)

Density (lb/ft ³)	Modulus			Strength		
	Compression (psi)	Tension (psi)	Shear (psi)	Compression (psi)	Tension (psi)	Shear (psi)
6.2	18125	15225	5800	245	450	200

4.1.3 Simplified Design Cases of FRP Laminates

The material architecture of each laminate offers unique properties and characteristics and, hence, must be distinctly identified whenever it is associated with specific quantitative or numerical analyses. Positive and concise identification of a laminate can be achieved through the use of a laminate orientation code. An adequate code must be able to specify as concisely as possible – (1) the orienta-

tion of each lamina relative to a reference axis, (2) the number of laminae at each orientation, and (3) the exact geometric sequence of laminae. In this research, the stacking sequence of a laminate was combined based on the simplified design cases (shown in Fig. 4-1) and evaluated their structural performance. The results for each combination of stacking sequence are shown in Table 4-3 and the simplified design cases are shown in Fig. 4-1.

Symmetrical Laminates

A laminate is called symmetric if the material, angle, and thickness of plies are the same above and below the midplane. An example of symmetric laminates is $[0/30/\overline{60}]_s$.

Cross-ply Laminates

A laminate is called a cross-ply laminate (also called laminates with specially orthotropic layers) if only 0° and 90° plies were used to make a laminate. An example of a cross-ply laminate is $[0/90/90/0/90]$.

Angle-ply Laminates

A laminate is called an angle ply laminate if it has plies of same material and thickness, and only oriented at $+\theta$ and $-\theta$ directions. An example of an angle ply laminate is $[-40/40/-40/40]$.

Antisymmetric Laminates

A laminate is called antisymmetric if the material and thickness of the plies are the same above and below the midplane, but the ply orientations at the same distance above and below of the midplane are negative of each other. An example of an antisymmetric laminate is $[45/60/-60/-45]$.

Balanced Laminates

A laminate is balanced when it consists of pairs of layers of the same thickness and material where the angles of plies are $+\theta$ and $-\theta$. If the number of plies in a balanced laminate is odd, it can be made symmetric. An example of a balanced laminate is $[30/40/-30/30/-30/-40]$.

Quasi-Isotropic Laminates

A laminate is called quasi-isotropic if its extensional stiffness matrix $[A]$ behaves like that of an isotropic material. An example of quasi-isotropic laminates is $[0/\pm 45/90]_s$.

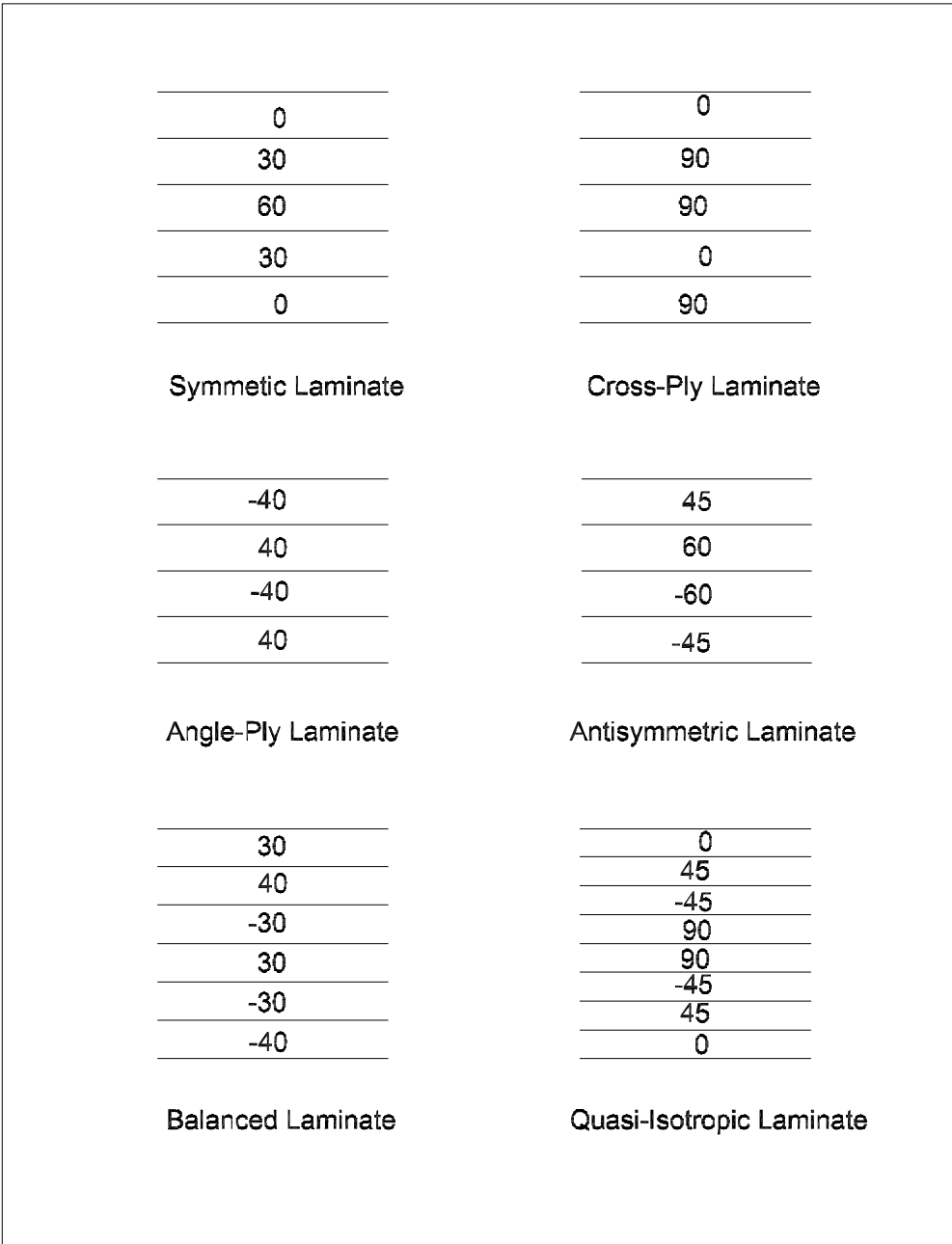


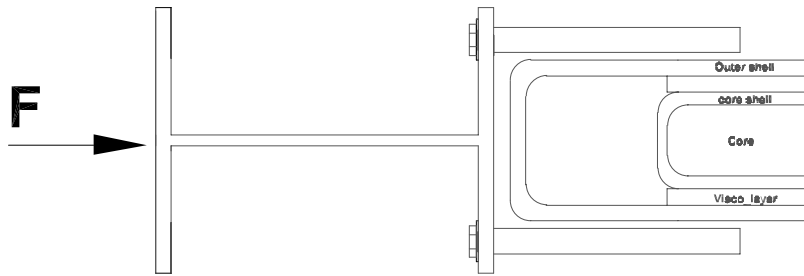
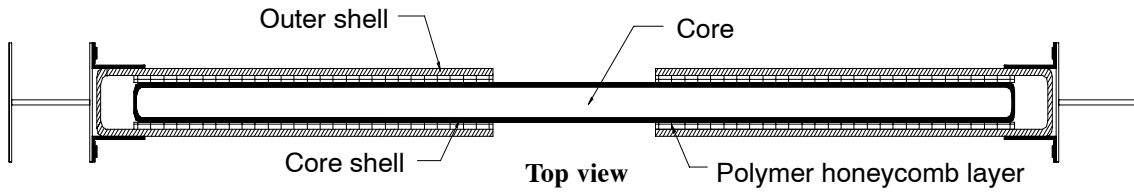
Figure 4-1 Simplified Stacking Sequence Cases of Typical Composite Laminate

4.2 Design of a Multi-layer PMC Infill System

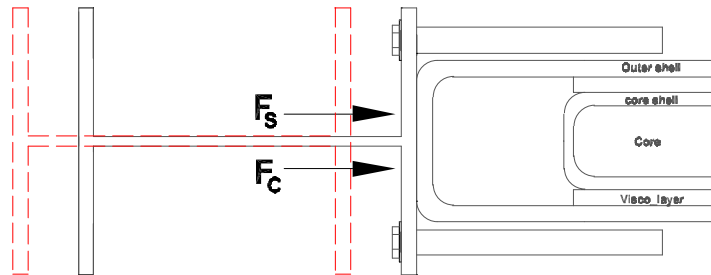
4.2.1 Design Concept and Configuration

Several technical and cost-saving challenges are associated with the design of PMC infill walls in structural applications such as buildings. Some of the most serious questions surrounding the viability of PMC structures relate to four major considerations: first, the availability of PMC structural systems that have been tested to resist seismic loads; second, the cost of the construction; third, the availability of standards for their design; and fourth, the feasibility of their construction. In considering the design procedure of a PMC infill wall, many design variables must be specified. Such design variables include the thickness, fiber orientation, and stacking sequence of FRP plies and, above all, the determination of a number of geometrical parameters defining the damping interface layer configuration.

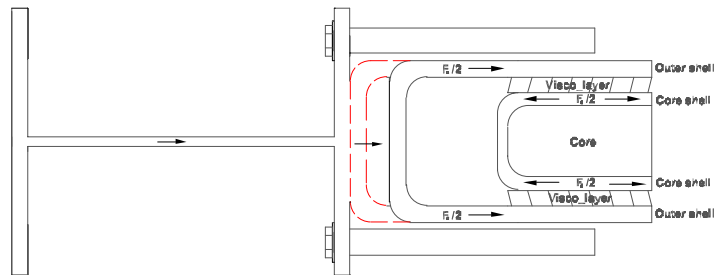
First, a conceptual multi-layer system is introduced to increase energy dissipation performance associated with the perfect bonding assumption. This multi-layer system will allow in-plane shear deformation and, therefore, sliding along specific layers to take place upon loading the frame. Fig. 4-2 shows the mechanical concept of the multi-layer panel system. The damage of the composite panel is expected to be concentrated in specific layers and, hence, energy dissipation will be produced within the multi-layer PMC infill wall panel. Fig. 4-3 presents the schematic representation of the energy mechanism for the multi-layer infilled frame. Fig. 4-4 illustrates an overall configuration of multi-layer PMC infilled panel. As shown in Figure 4-5, the conceptual design of the multi-layer PMC infill wall system consists of three panels forming the entire wall thickness: first, an inner panel composed of a core material and core shell; second, outer panels that consist of outer shells at both sides of the inner panel; and third, polymer honeycomb layers at the interface between the the core and outer shells. The role of the inner panel is to increase structural rigidity. In turn, the outer panels are designed to transfer applied lateral force to the polymer honeycomb layers as well as to resist large contact forces at the interface with the steel columns.



(a) Applied lateral force for infilled frame



(b) Transmit lateral force to composite panel



(c) Energy dissipation by polymer honeycomb layers

Figure 4-2 The Mechanical Concept of Composite Infilled Frame

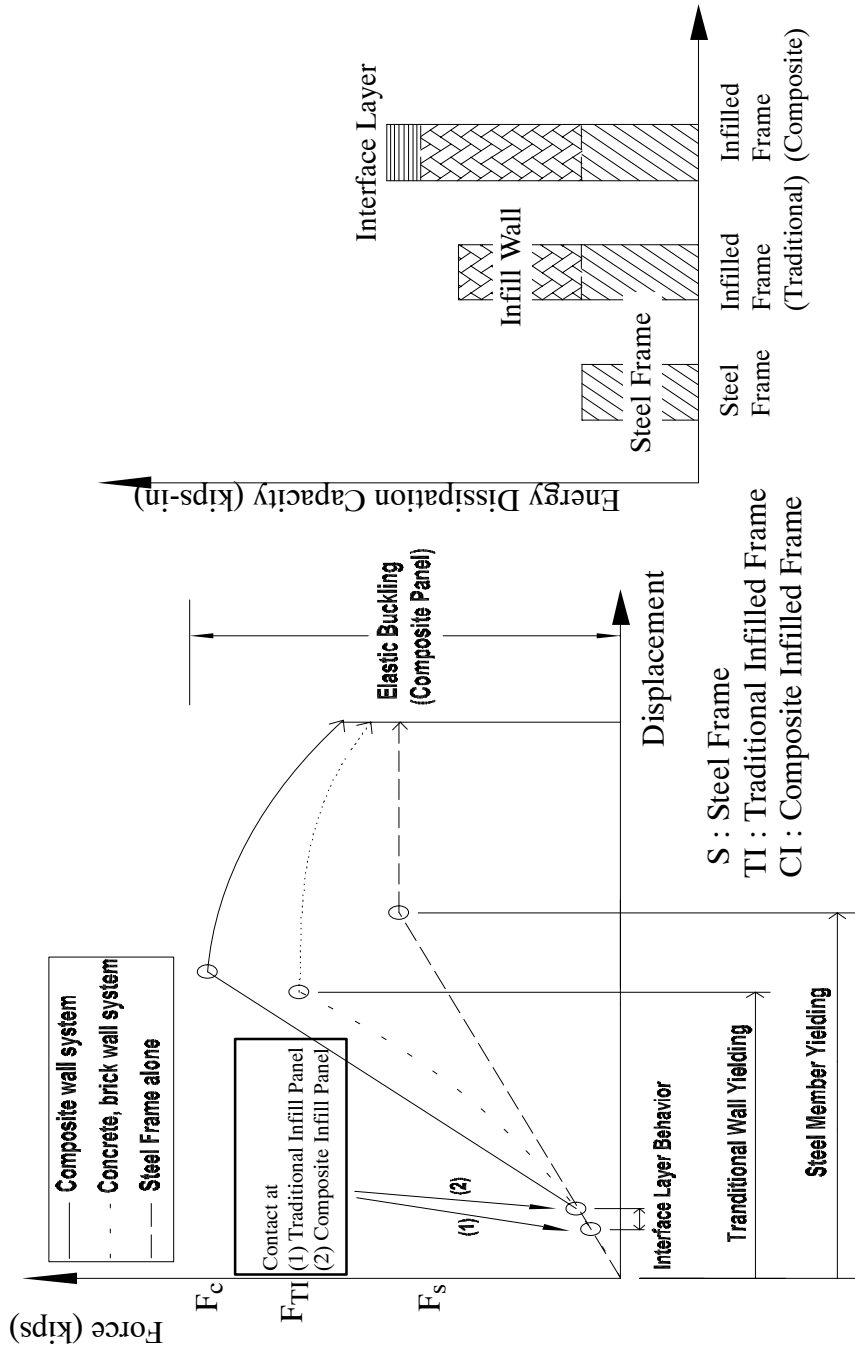


Figure 4-3 The Schematic Representation of the Energy Mechanism for the Composite Infilled Frame

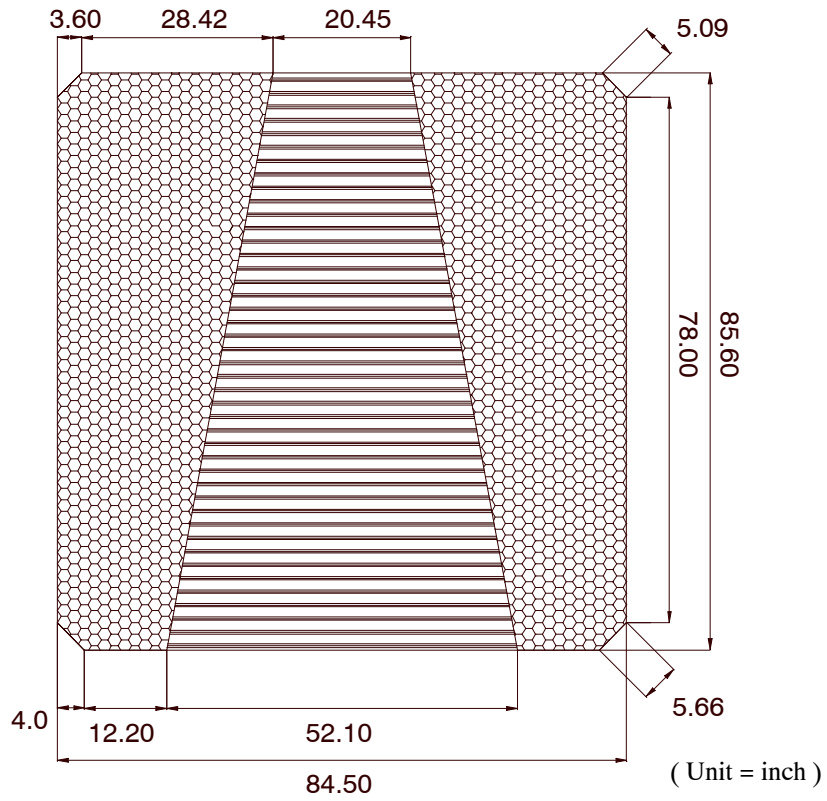


Figure 4-4 Overall Configuration of the Multi-layer PMC Infill Panel

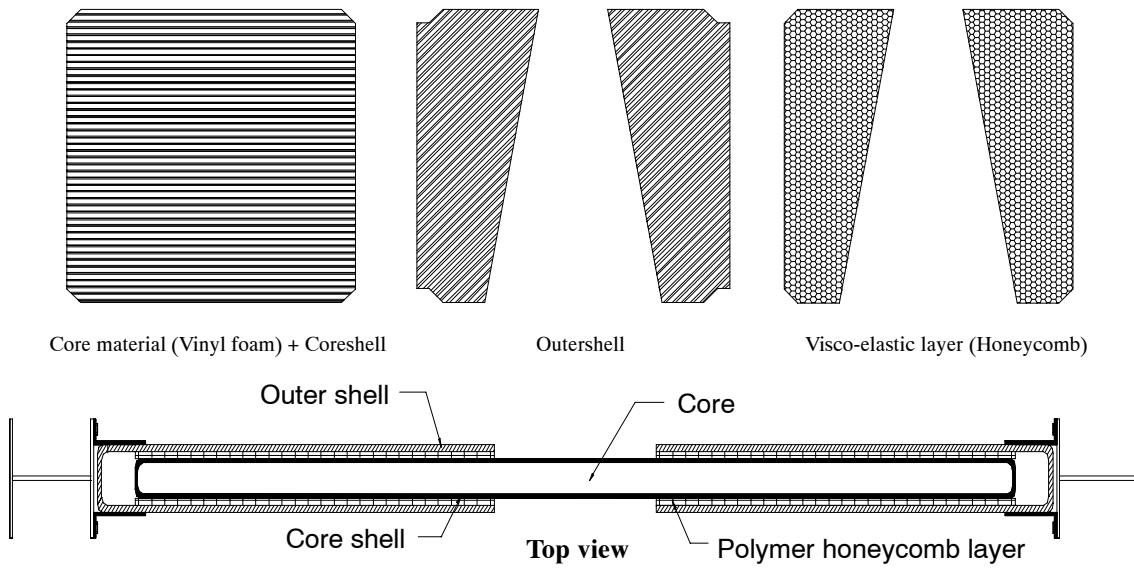


Figure 4-5 The Shape of Each Components of Composite Panel

This design concept of an inner PMC sandwich panel design is considered to reduce the weight, sound, and vibration as well as to improve the structural rigidity of the entire composite panel. To obtain high performance at low cost, the thinly spaced core-shell laminates were designed to provide bending rigidity, and the space between the laminates was filled with vinyl sheet foam. The vinyl foam core material provides most of the shear rigidity of this sandwich construction. In the design of sandwich element, it would be convenient to have simplified design procedures which could provide a starting point for the design process, i.e. initial thickness and material selection. In this study, the core to face thickness ratio was arbitrarily chosen to be 5.0. Fig. 4-6 presents the geometric configuration of the inner PMC sandwich infill of the multi-layer PMC infill system.

For the outer panel design, consideration was given to the deformed shape of the PMC infill wall from push-over analysis. As such, the geometry of the outer panels was designed to have a trapezoidal shape. The area of a trapezoidal shape was considered to provide enough stiffness of the interface layers in order to transfer applied force to inner PMC sandwich panel. Even if a trapezoidal shape of the outer panel is not appropriate under cyclic loading conditions, with adequate thickness this shape should provide sufficient capacity to transfer applied forces to cause symmetric shear deformation on both sides, which can be helpful in studying the interface layers' behavior at the interface surfaces. Moreover, rounded edges of the outer panels were designed to avoid any stress concentration, and to achieve the desired behavior.

Geometrical configurations of the multi-layer components and the overall structure are presented in Fig. 4-4 to Fig. 4-7. The interface thickness used in this study was determined by the availability of commercial product size of polymer honeycomb material. Fig. 4-9 and 4-10 illustrate a cross section and rounded edge of the multi-layer PMC infilled frame, respectively. Gap between the inner panel and rounded edge of the outer laminate was designed to allow maximum displacement of the polymer honeycomb material and to provide enough space for installing column-to-infill connections.

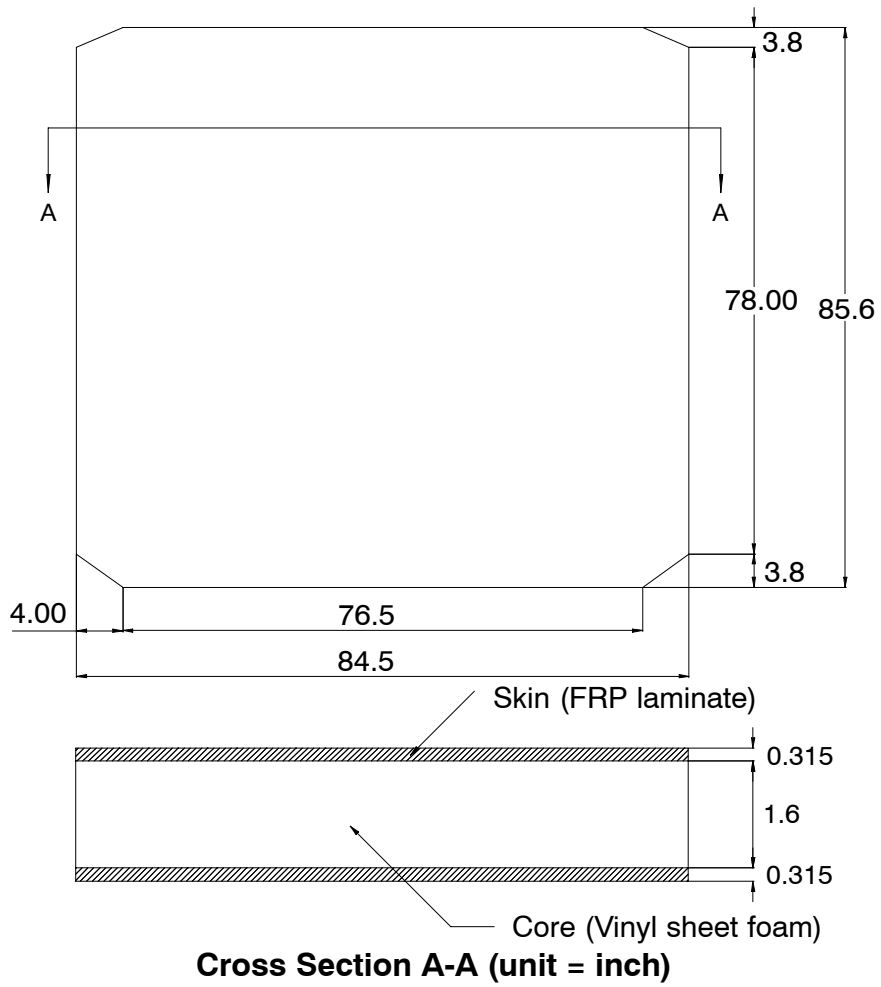


Figure 4-6 Geometric Configuration of an Inner PMC Sandwich Panel

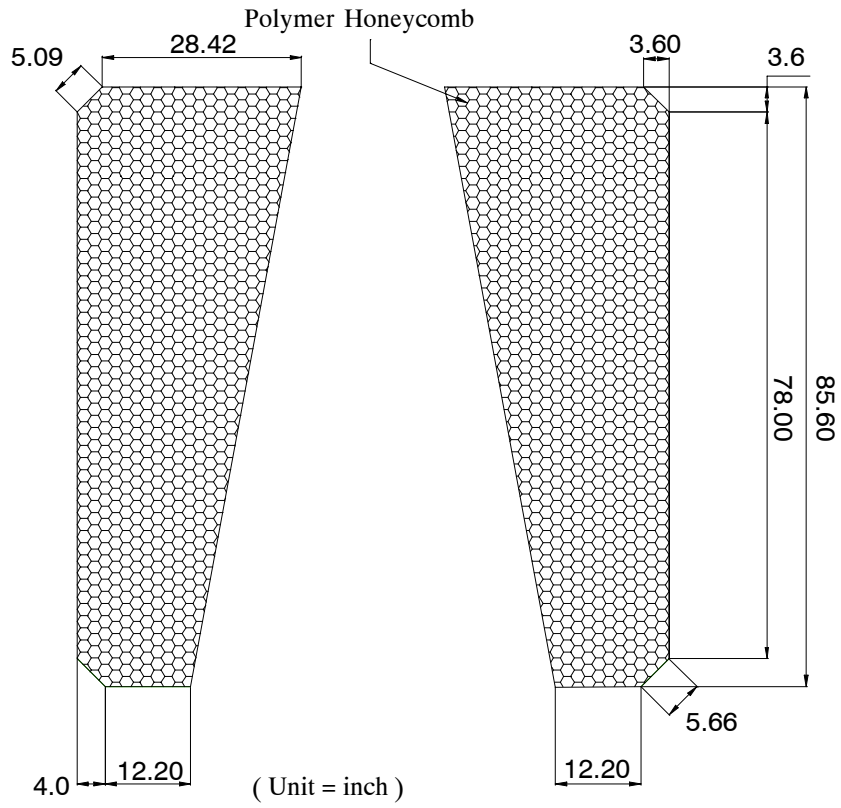


Figure 4-7 Geometric Configuration of the Polymer Honeycomb Layer

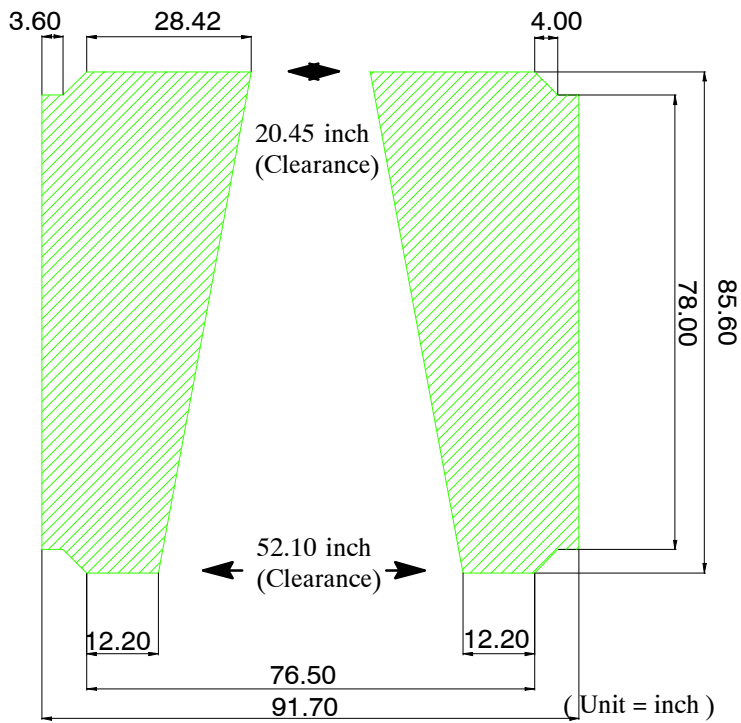


Figure 4-8 Geometric Configuration of Outershell Layers

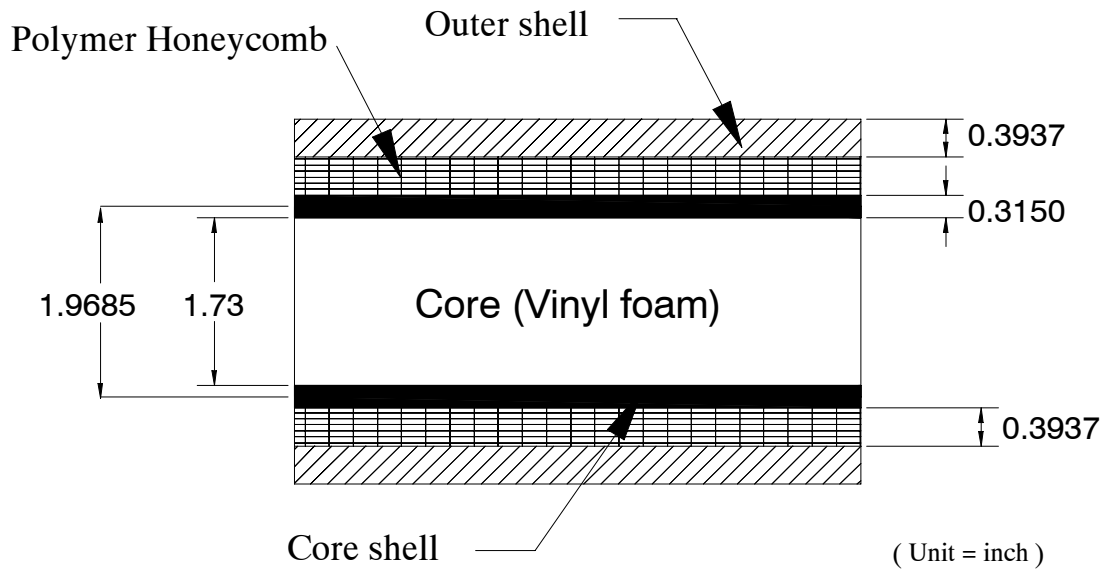


Figure 4-9 Detailed Cross Section of the Multi-layer PMC Infill Panel

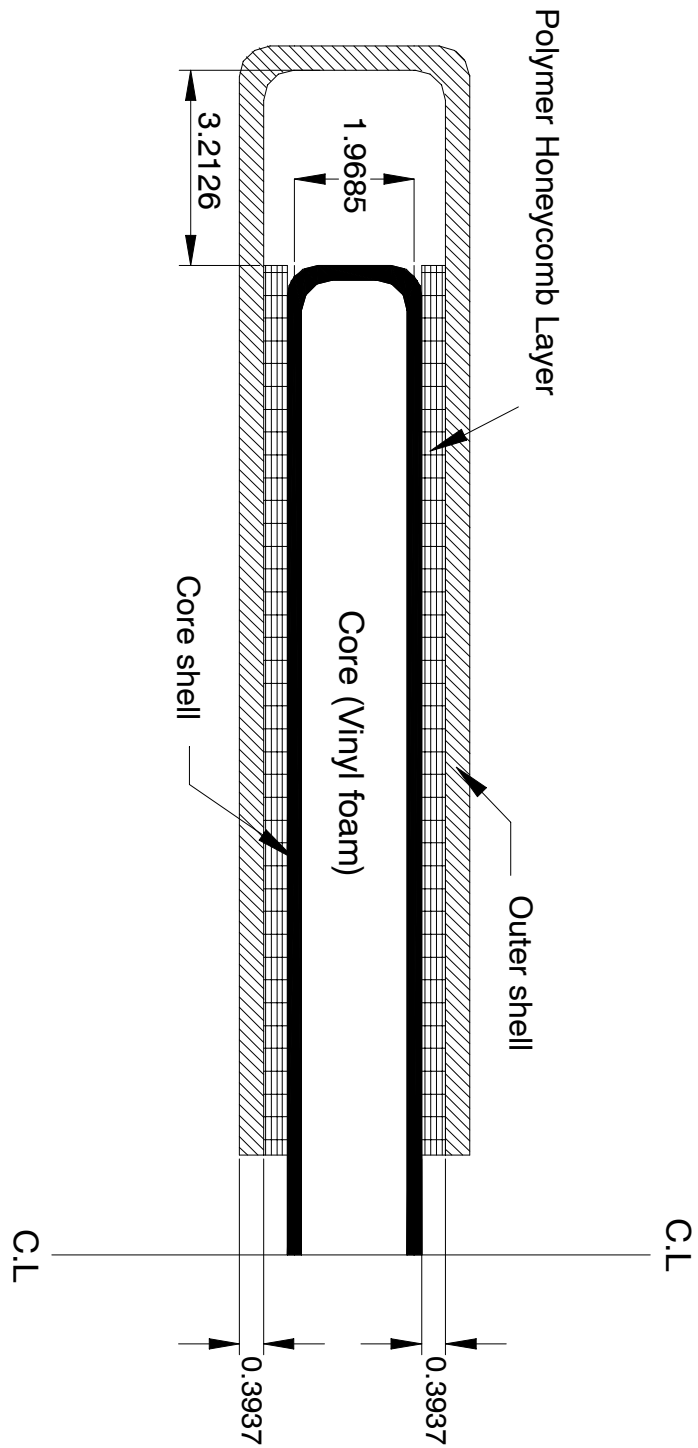


Figure 4-10 Detailed Rounded Edge of a Multi-layer PMC Infill Panel (unit = inch)

The optimal design of inner and outer panels composed of FRP laminates was governed by structural performance and cost. The most common and essential constraint of this structure is stiffness. The design considerations addressed three factors; first, selecting a material system or a group of material systems; second, optimizing the stacking sequence for the laminates based on applied loads; and third, constraints such as cost and stiffness. Actually, the stiffness and strength of a single lamina were determined by practical factors such as the choice of the fiber and matrix, processing technique, and the fiber volume fraction. In the design process, E-glass fiber was chosen as a proper reinforcement because of practical suitability and cost.

After selecting the reinforcement, the optimal design of stacking sequence for core-shell of the inner PMC sandwich panel and outer-shell laminates was obtained by finite element analysis. In this case, the total inner panel thickness was controlled by the buckling of the inner panel at high lateral drift (2.5%). The laminate for each component (outer shell or core shell) was then designed by considering several possible stacking sequences (i.e., orientation and thickness of each lamina). Generally, when laminated composite plates are symmetric and orthotropic, their in-plane and flexural stiffnesses become a function of the lamination parameters, which are functions of the stacking sequences. By using numerous finite element simulations representing the lay-up and geometric combinations of various materials, force-displacement relationship of the infill panel and steel frame was evaluated, leading to the final choice of laminate architecture. As shown in Fig. 4-11, commonly used stacking cases of FRP laminates were considered as a starting point. Various combinations of stacking sequences were applied in the design process and the results are summarized in Table 4-3.

The selected optimal wall design parameters with respect to the fiber orientation are $[0_3/30_4/45_6/60_2/90_2/-60_2/-45_4/-30_6/0_2]_s$ for coreshell, and $[0_5/30_8/45_4/90_5/-45_4/-30_8/0_5]_s$ for outer-shell laminate, and thickness of each ply is 0.005 in. The detailed optimum stacking sequences are shown in Tables 4-4 and 4-5. And, geometric configuration of each laminate and orientation axis along applied loading direction are presented in Fig. 4-12, 4-13, and 4-14, respectively.

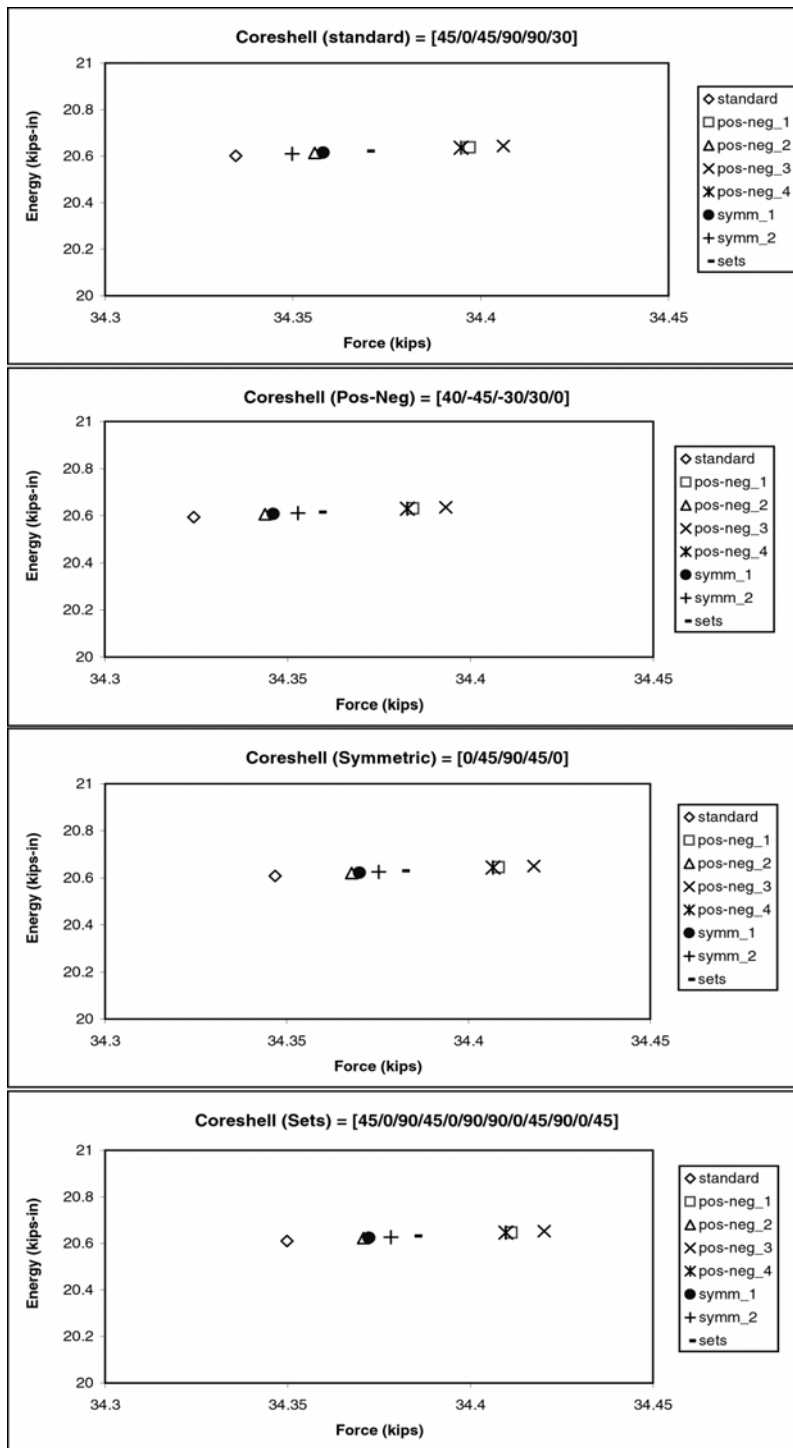


Figure 4-11 The Results of Combined Simplified Stacking Sequences for Composite Wall Laminate Design

Table 4-3 The Results of Various Laminate Layups of the Composite Infill

1) General cases

	Core shell	Outer shell	Force(kips)
Standard	[45/0/45/90/90/30]	[45/45/-45/-45/0]	46.07
Pos_neg	[45/45/-45/-45/0]	[45/45/-45/-45/0]	46.92
Symmetric	[0/45/90/45/0]	[45/45/-45/-45/0]	46.04
Symmetric_1	[90/0/0/45]s	[45/45/-45/-45/0]	45.80
Set	[45/0/90/45/0/90]s	[45/45/-45/-45/0]	45.93
Case1	[0/45/90/-45/0]s	[0/45/90/-45/0]s	46.65
Case2	[0/30/90/-30/0]s	[0/30/90/-30/0]s	46.22
Case3	[0/30/45/90/-45/-30/0]s	[0/30/45/90/-45/-30/0]s	47.03
Case4	[0/-30/90/30/0]s	[0/-30/90/30/0]s	46.22
Case5	[0/30/90/30/0]s	[0/-30/-90/-30/0]s	45.61
Case6	[0/30/45/-45/-30/0]s	[0/30/45/-45/-30/0]s	47.17

2) Detailed cases

	Core shell	Outer shell	Force(kips)
ex1	[0/30/45/90/-45/-30/0]s	[0/30/45/90/-45/-30/0]s	47.03
ex2	[0/30/45/90/-45/-30/0]s	[0/-30/90/-30/0]s	46.24
ex3	[0/30/45/90/-45/-30/0]s	[0/30/90/-30/0]s	46.69
ex4	[0/30/45/90/-45/-30/0]s	[0/45/90/-45/0]s	46.88
ex5	[0/30/45/90/-45/-30/0]s	[0/30/45/-45/-30/0]s	47.03

3) choose best cases

	Core shell	Outer shell	Force(kips)
ex_1	[0/30/45/-45/-30/0]s	[0/30/90/-30/0]s	46.86
ex_2	[0/30/45/-45/-30/0]s	[0/60/90/-60/0]s	46.68
ex_3	[0/30/45/-45/-30/0]s	[0/45/90/-45/0]	47.05
ex_4	[0/30/45/-45/-30/0]s	[0/30/60/90/-60/-30/0]s	47.04
ex_5	[0/30/45/-45/-30/0]s	[0/30/45/90/-45/-30/0]s	47.19
ex_6	[0/30/45/-45/-30/0]s	[0/30/45/90/0/-45/-30/0]s	47.03
ex_7	[0/30/45/-45/-30/0]s	[0/30/45/90/0/90/-45/-30/0]s	46.96
ex_8	[0/30/45/-45/-30/0]s	[0/30/45/60/90/-60/-45/-30/0]s	47.11
ex_9	[0/30/45/0/-45/-30/0]s	[0/30/45/90/-45/-30/0]s	47.02
ex_10	[0/30/45/45/0/-45/-45/-30/0]s	[0/30/45/90/-45/-30/0]s	47.24
ex_11	[0/30/30/45/0/-45/-30/0]s	[0/30/45/90/-45/-30/0]s	47.13
ex_12	[0/30/30/45/45/0/-45/-45/-30/0]s	[0/30/45/90/-45/-30/0]s	47.29
ex_13	[0/30/45/45/0/-45/-45/-30/0]s	[0/30/45/45/90/-45/-45/-30/0]s	47.26
ex_14	[0/30/45/45/0/-45/-45/-30/0]s	[0/30/45/45/60/90/-60/-45/-45/-30/0]s	47.15
ex_15	[0/30/30/45/45/0/-45/-45/-30/0]s	[0/30/45/90/0/-90/-45/-30/0]s	47.06
ex_16	[0/30/30/45/45/90/-45/-45/-30/0]s	[0/30/45/90/0/-90/-45/-30/0]s	47.05
ex_17	[0/45/45/60/60/0/-60/-60/-45/-45/0]s	[0/30/45/90/0/-90/-45/-30/0]s	47.03
ex_18	[0/45/45/60/60/90/-60/-60/-45/-45/0]s	[0/30/45/90/0/-90/-45/-30/0]s	47.00
ex_19	[0/30/30/45/45/60/0/-60/-45/-45/-30/0]s	[0/30/45/90/-45/-30/0]s	47.30
ex_20	[0/30/30/45/45/60/90/-60/-45/-45/-30/0]s	[0/30/45/90/-45/-30/0]s	47.29
ex_21	[0/30/30/45/45/60/0/-60/-45/-45/-30/0]s	[0/45/60/90/-60/-45/0]s	47.04
ex_22	[0/30/30/45/45/60/0/-60/-45/-45/-30/0]s	[0/30/45/90/0/-90/-45/-30/0]s	47.07
ex_23	[0/30/30/45/45/60/0/-60/-45/-45/-30/0]s	[0/45/45/60/60/90/-60/-60/-45/-45/0]s	46.84
ex_24	[0/30/30/45/45/60/0/-60/-45/-45/-30/0]s	[0/45/60/60/90/0/-90/-60/-60/-45/0]s	46.70
ex_25	[0/30/30/45/45/60/0/-60/-45/-45/-30/0]s	[0/60/90/-60/0]s	46.78
ex_26	[0/30/45/45/60/60/0/-60/-60/-45/-45/-30/0]s	[0/45/45/60/60/90/-60/-60/-45/-45/0]s	46.79
ex_27	[0/30/45/45/60/60/90/-60/-60/-45/-45/-30/0]s	[0/30/30/45/90/0/-90/-45/-30/0]s	46.98
ex_28	[0/30/30/45/45/60/90/0/-90/-60/-45/-45/-30/0]s	[0/30/45/45/60/60/90/0/-90/-60/-60/-45/-45/-30/0]s	46.81
ex_29	[0/30/45/45/60/60/90/0/-90/-60/-60/-45/-45/-30/0]s	[0/30/30/45/45/60/90/0/-90/-60/-45/-45/-30/0]s	46.67
ex_30	[0/30/30/45/45/60/90/-60/-45/-45/-30/0]s	[0/30/30/45/90/-45/-30/0]s	47.33
ex_31	[0/30/45/45/60/60/90/-60/-60/-45/-45/-30/0]s	[0/45/60/60/90/-60/-60/-45/0]s	46.61
ex_32	[0/30/30/45/45/60/90/-60/-45/-45/-30/0]s	[0/30/45/45/60/90/-60/-45/-45/-30/0]s	47.19
ex_33	[0/30/30/45/45/60/90/-60/-45/-45/-30/0]s	[0/45/-45/60/60/90/-60/60/-45/45/0]s	46.85
ex_34	[0/30/30/45/45/60/90/-60/-45/-45/-30/0]s	[0/30/30/45/60/90/-60/-45/30/0]s	47.28

4) Best cases

	Core shell	Outer shell	Force(kips)
ex_10	[0/30/45/45/0/-45/-45/-30/0]s	[0/30/45/90/-45/-30/0]s	47.24
ex_12	[0/30/30/45/45/0/-45/-45/-30/0]s	[0/30/45/90/-45/-30/0]s	47.29
ex_13	[0/30/45/45/0/-45/-45/-30/0]s	[0/30/45/45/90/-45/-45/-30/0]s	47.26
ex_19	[0/30/30/45/45/60/0/-60/-45/-45/-30/0]s	[0/30/45/90/-45/-30/0]s	47.30
ex_20	[0/30/30/45/45/60/90/-60/-45/-45/-30/0]s	[0/30/45/90/-45/-30/0]s	47.29
ex_30	[0/30/30/45/45/60/90/-60/-45/-45/-30/0]s	[0/30/30/45/90/-45/-30/0]s	47.33
ex_32	[0/30/30/45/45/60/90/-60/-45/-45/-30/0]s	[0/30/45/45/60/90/-60/-45/-45/-30/0]s	47.19

Table 4-4 The Designing Stacking Sequence for Coreshell

No.	Orientation angle	The number of layers	Total thickness (inch)
1	0	3	0.015 (0.381mm)
2	30	4	0.02 (0.508mm)
3	45	6	0.03 (0.762mm)
4	60	2	0.01 (0.254mm)
5	90	2	0.01 (0.254mm)
6	-60	2	0.01 (0.254mm)
7	-45	4	0.02 (0.508mm)
8	-30	6	0.03 (0.762mm)
9	0	5	0.025 (0.635mm)
10	-30	6	0.03 (0.762mm)
11	-45	4	0.02 (0.508mm)
12	-60	2	0.01 (0.254mm)
13	90	2	0.01 (0.254mm)
14	60	2	0.01 (0.254mm)
15	45	6	0.03 (0.762mm)
16	30	4	0.02 (0.508mm)
17	0	3	0.015 (0.381mm)

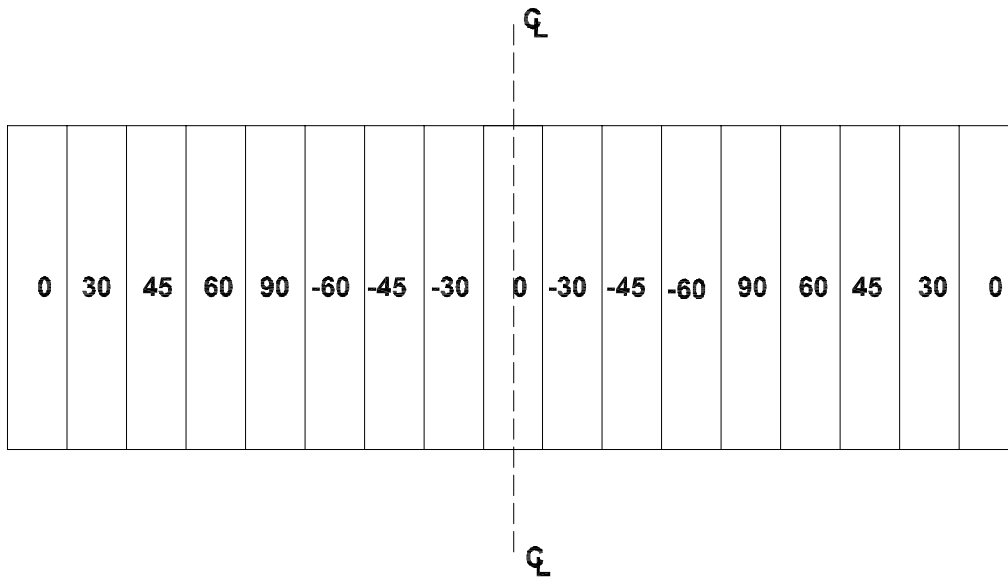


Figure 4-12 Orientation Codes of Coreshell

Table 4-5 The Designing Stacking Sequence for Outershell

No.	Orientation angle	The Number of layers	Total thickness
1	0	5	0.025 (0.635mm)
2	30	8	0.04 (1.016mm)
3	45	4	0.02 (0.508mm)
4	90	5	0.025 (0.635mm)
5	-45	4	0.02 (0.508mm)
6	-30	8	0.04 (1.016mm)
7	0	10	0.05 (1.27mm)
8	-30	8	0.04 (1.016mm)
9	-45	4	0.02 (0.508mm)
10	90	5	0.025 (0.635mm)
11	45	4	0.02 (0.508mm)
12	30	8	0.04 (1.016mm)
13	0	5	0.025 (0.635mm)

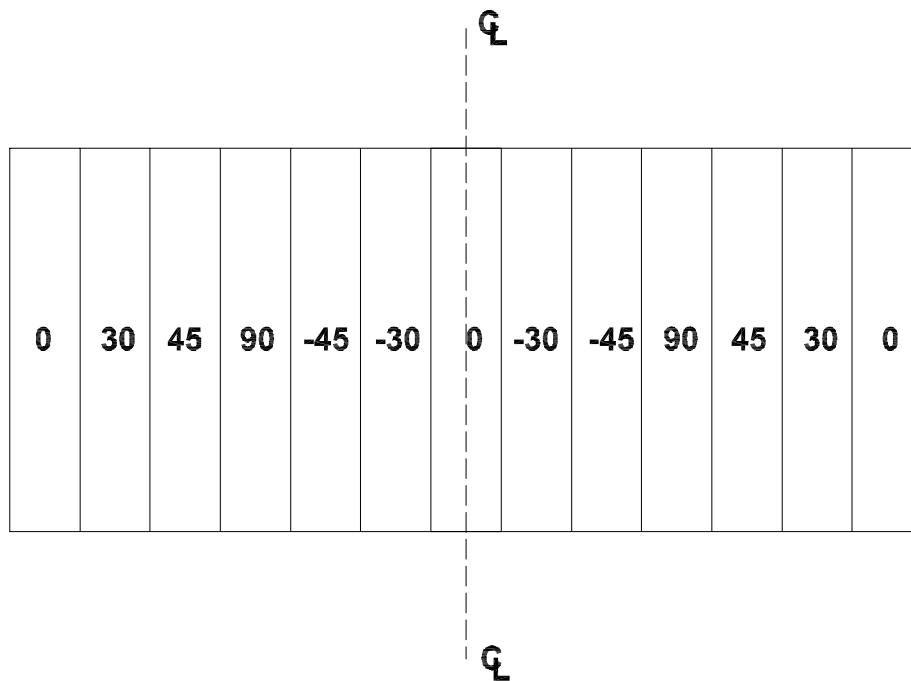
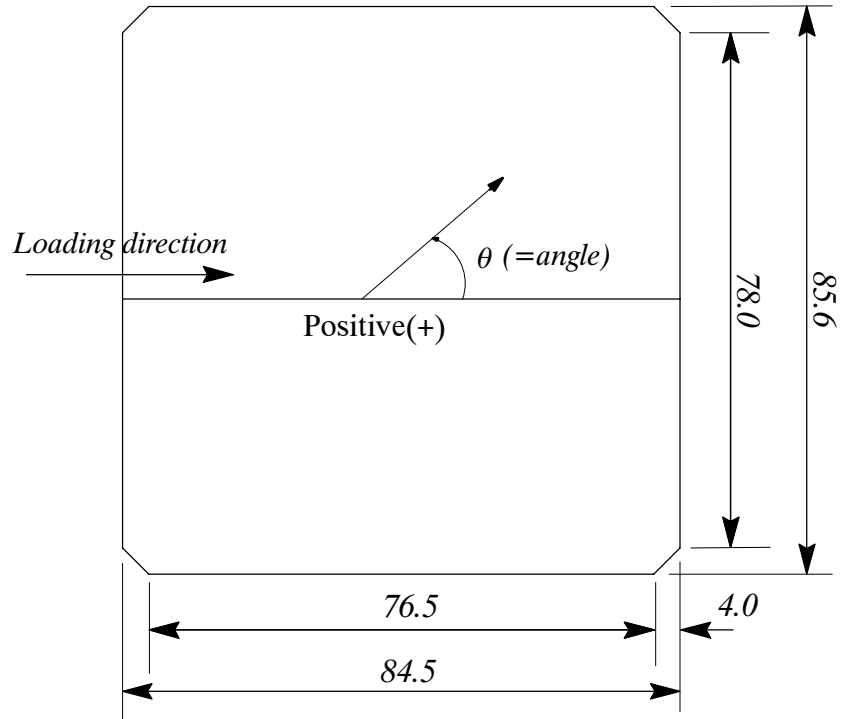
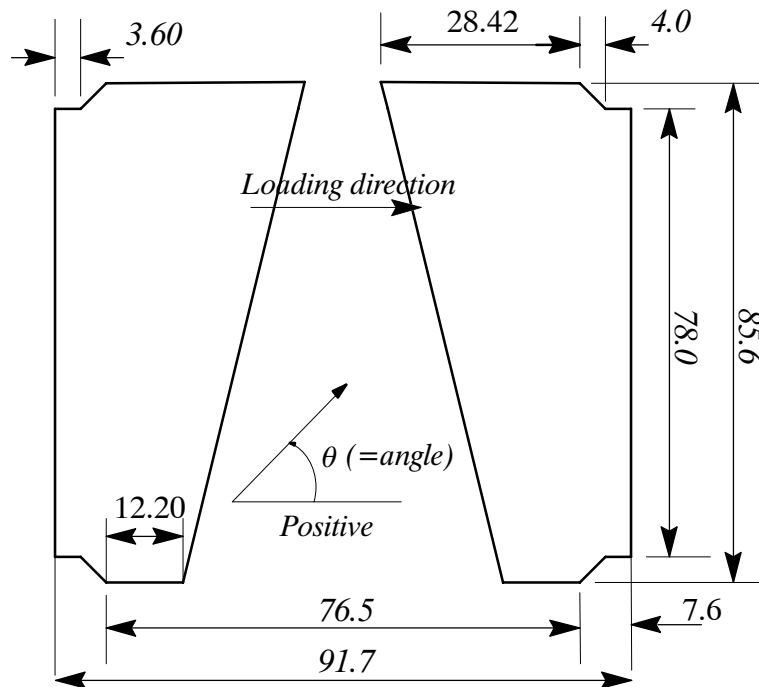


Figure 4-13 Orientation Codes of Outershell



(a) Standard Orientation of the Coreshell Element



(b) Standard Orientation of the Outershell Element

Figure 4-14 The Axis of Each lamina Orientation (unit=inch)

4.2.2 Construction

The PMC composite panel was constructed in collaboration with a local company (An-Cor Industrial Plastics, Inc., of Tonawanda, New York) to assess the most practical manufacturing solution. In the first phase, PMC sandwich panel which was composed of core and laminate facing was fabricated by hand lay-up process. After that, damping material (Honeycomb, Nida-Core Corp., FL) was delivered and attached to both side of PMC sandwich panel. Finally, outer FRP laminates were lay-up and installed on the surface of the polymer honeycomb layers. The flowchart of construction is shown in Fig. 4-15.

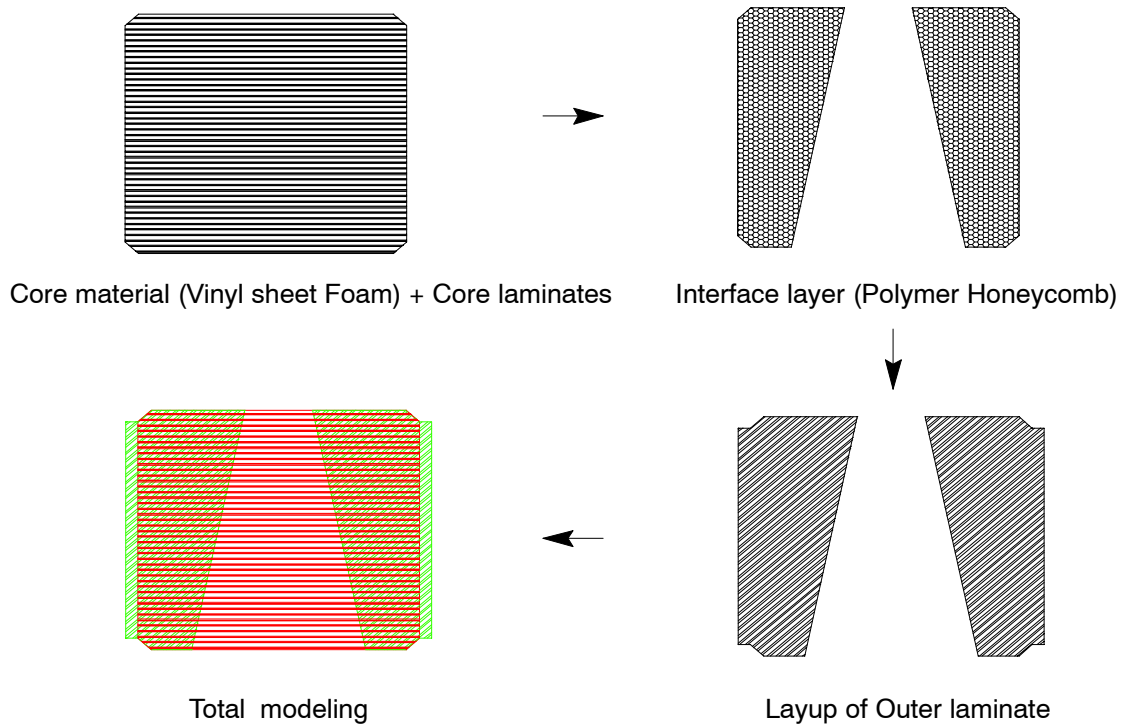


Figure 4-15 Fabricating Procedure of a Multi-layer PMC Infill Panel

In the construction process, some design parameters were modified based on commercially feasible techniques. A ply thickness was changed due to different fiber-resin volume fraction when compared to design data and additional adhesive fraction was inserted between skin and core materials. As such, the stacking sequence design was modified in the lay-up process. Modified ply stacking sequences are shown in Table 4-6 based on as built condition. Fig. 4-16 shows the completed fabrication of the PMC sandwich panel.

Table 4-6 The Modified Stacking Sequence of Composite Laminates (Unit = inch)

No.	Inner Laminate			Outer laminate		
	Orientation (degree)	No. of layers	Thickness (inch)	Orientation (degree)	No. of layers	Thickness (inch)
1	0	2	0.03	0	2	0.03
2	30	2	0.03	30	3	0.045
3	45	3	0.045	45	1	0.015
4	60	1	0.015	90	1	0.015
5	90	1	0.015	-45	1	0.015
6	-60	1	0.015	-30	3	0.045
7	-45	2	0.03	0	3	0.045
8	-30	3	0.045	-30	3	0.045
9	0	1	0.015	-45	1	0.015
10	-45	1	0.015	90	1	0.015
11	90	2	0.03	45	1	0.015
12				30	3	0.03
13				0	3	0.03
Total			0.285			0.36



Figure 4-16 Inner PMC Sandwich Composite Panel

Finally, the multi-layer PMC infill wall depicted in Figure 4-17 was completely fabricated. Fig. 4-18 (a) and (b) show the cross section of the PMC sandwich panel and the rounded edges of the outer panels intended to avoid any stress concentrations. For experimental setup, FRP anchor tab was installed at the top position on the surface of the inner PMC sandwich panel. Fig. 4-19 presents the FRP moving anchor tab for the experimental setup of the multi-panel PMC infilled frame test.

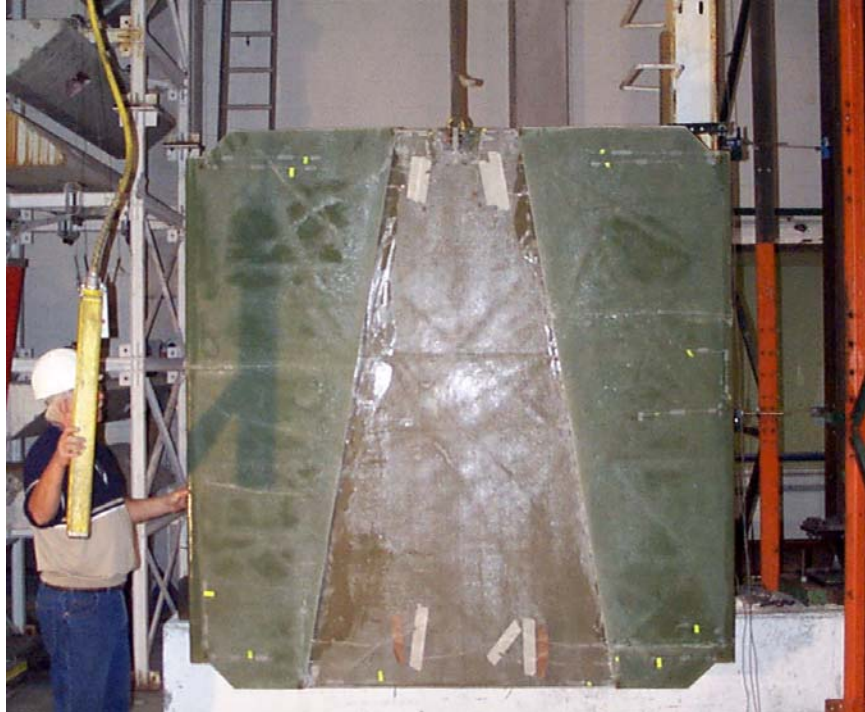


Figure 4-17 Completed Fabrication of the Multi-layer PMC Infill Panel



(a) Cross Section of the PMC Sandwich Panel



(b) Rounded Edge of the Multi-layer PMC Infill panel

Figure 4-18 Specific Cross Section of the Multi-layer PMC Infill Panel

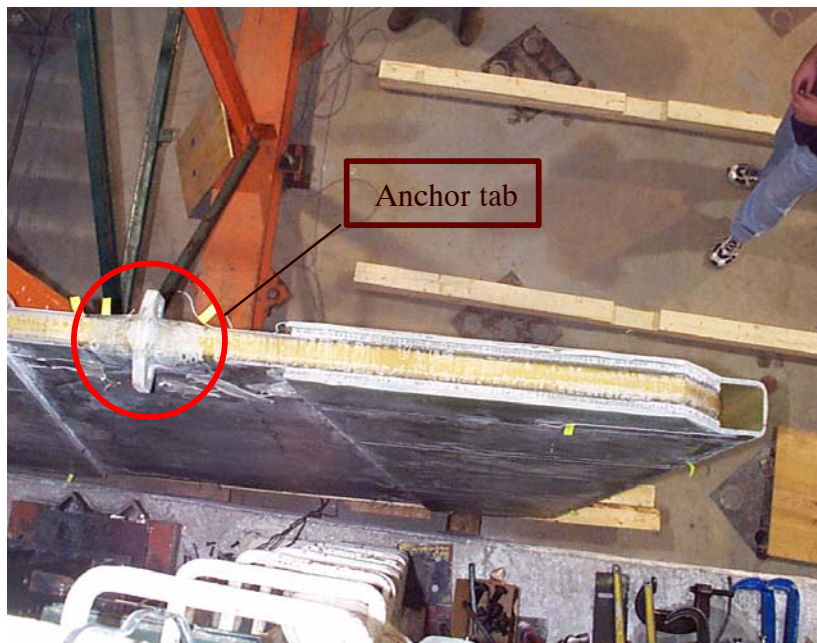


Figure 4-19 FRP Anchor Tab for Experimental Setup

4.3 TEST SPECIMENS AND EXPERIMENTAL SETUP

Figure 4-20 shows the test specimen setup. This test specimen consisted of a steel frame with the multi-layer PMC infill wall. Semi-rigidly connected steel frame members (A36 steel), which were designed for gravity loads and constructed according to the specifications of the American Institute of Steel Construction (AISC), were used to represent common design and construction practices of old building structures. The cross-sectional dimensions (U.S.) of beam and column members were W8x21 and W8x24, respectively. Gravity loading, which would be applied through the top beam, was not applied here. After manufacturing, the multi-layer PMC infill wall (85.6 by 92.0 inch) was placed within the steel frame opening (86.0 by 92.5 inch) to be tested.



Figure 4-20 Multi-layer Infill Panel Setup

Different instrumentations were attached on the specimen to capture key data and to characterize the structural response of the multi-layer PMC infill wall. These key data included four major measurements: first, longitudinal and transverse strain measurements obtained from gauges placed at critical points on the PMC infill wall panel (see Fig. 4-21); second, the shear deformation of the polymer honeycomb material obtained through linear potentiometers; third, the hysteresis behavior and the corresponding strength and stiffness degradation measured using displacement transducers; and

fourth, buckling of the PMC inner panel. Fig. 4-22 illustrates LVDTs' locations. Four sets of gauges were attached to the edge of each component in the PMC infill wall panel, and three linear variable differential transformers (LVDTs) were also placed on the column next to the test specimen using magnetic bases so that the LVDT tips touched the left column flange of the test specimen. Out-of-plane LVDT measurement was inconsistent and depended on the exact location of the buckling mode, and the data obtained from pairs of strain gauges located on the surface of the laminates were only marginally useful in tracing the stress contour because of the impact and vibration during testing. Fig. 4-23 illustrates various measuring instruments attached to the multi-layer PMC infill frame test.

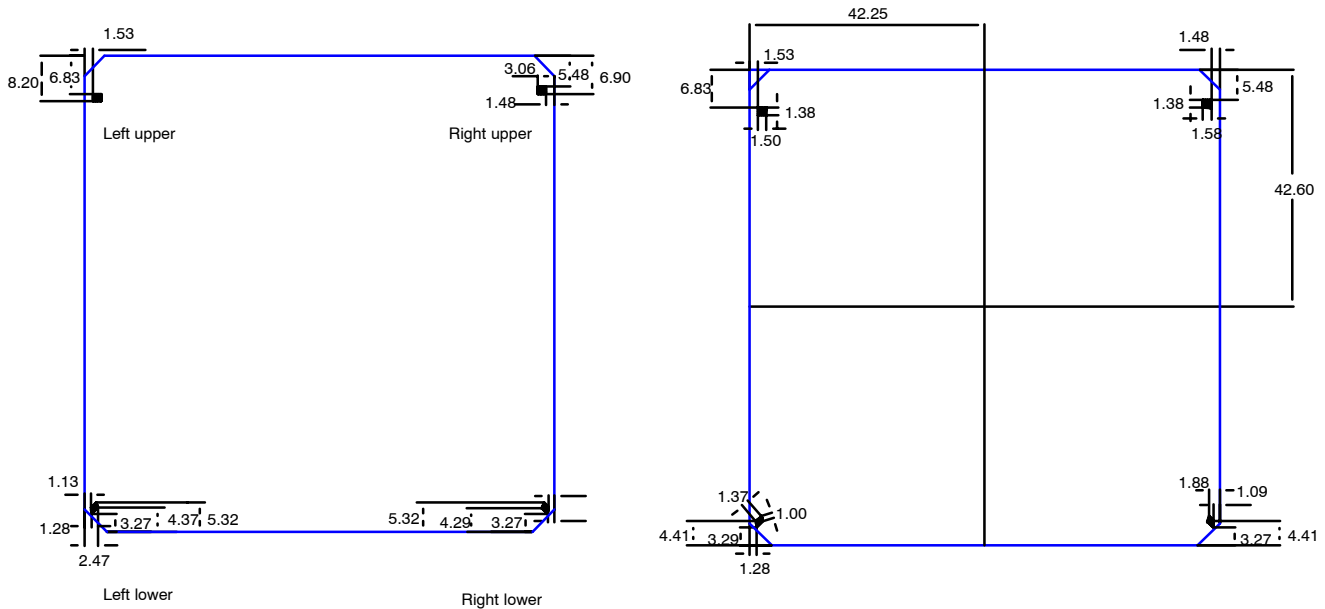


Figure 4-21 Strain Gages on an Inner PMC Sandwich Panel

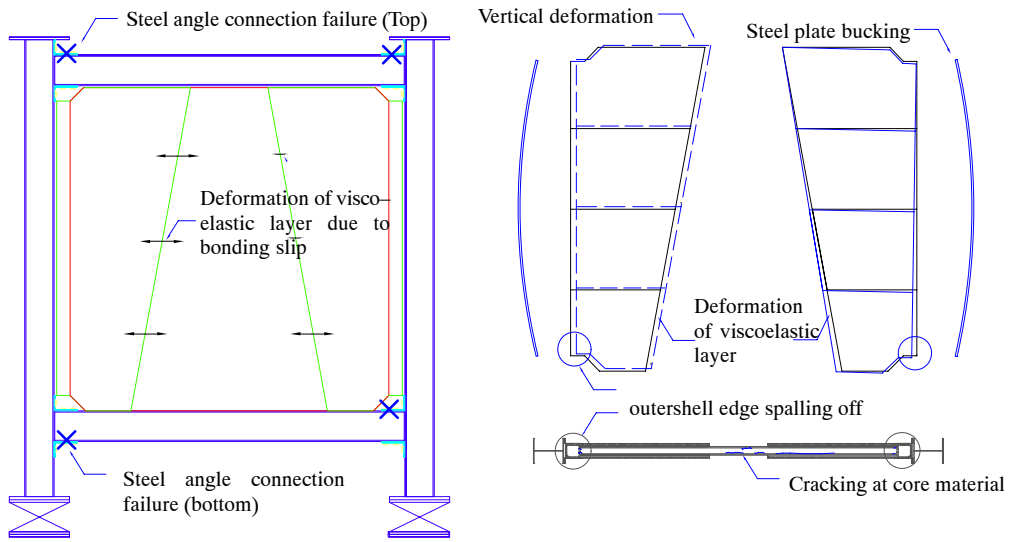


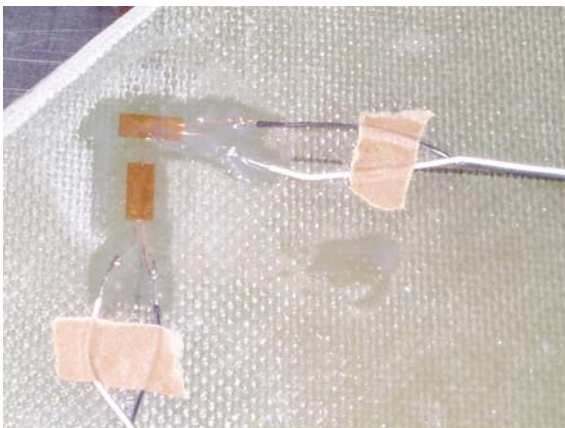
Figure 4-22 Location of Linear Potentiometers



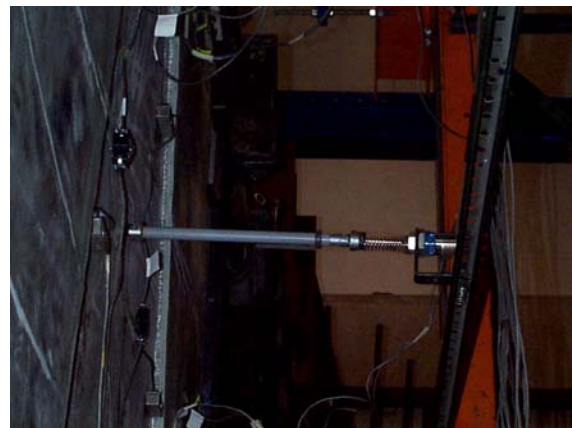
(a) Linear potentiometer



(b) Displacement transducer



(c) Strain gages (Long & Trans)



(d) Out-of-plane LVDT

Figure 4-23 Typical Instruments for Experiments

After erection of the steel frame, the multi-layer PMC infill wall was constructed and installed within the steel frame. In the case of the steel frame with infills, gaps of incomplete contact between the steel frame and the infill may negatively influence the stiffness. These gaps may be between the wall and columns of the frame or between the wall and the top beam enclosing the frame. Different strength and stiffness conditions must be expected with different discontinuity types and locations. Therefore, the presence of any gaps or discontinuities between the infills and the frame must be investigated for the design and rehabilitation process. The resistance provided by infill walls was also studied when the proper connection and interaction between the wall and the frame were made.

For the investigation of the effect of the initial gap at the initial stage of loading, the opening between the PMC infill wall panel and columns was grouted with epoxy resin (tensile modulus: $E = 4.9 \times 10^5$ psi; Poisson's ratio: $\nu = 0.2 - 0.4$). Fig. 4-24 shows epoxy grouting of the initial gap between the column and the infill.

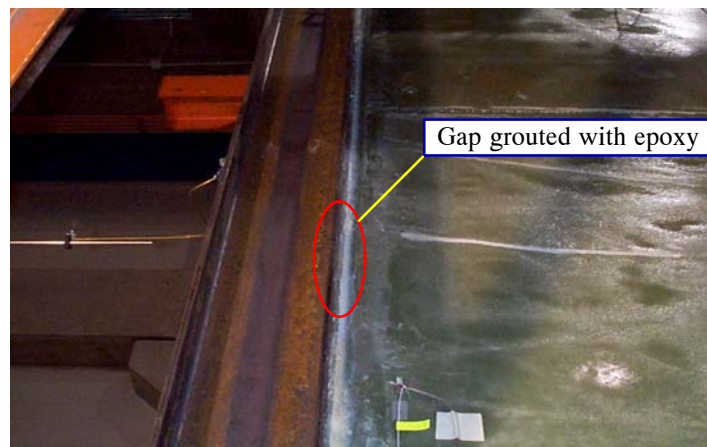


Figure 4-24 Epoxy Grouting in the Initial Gap

For the column-to-infill connections used in one of the multi-layer PMC infill wall frame tests, six 0.5-inch (12.7-mm) high-strength A325 bolts and a steel plate (3.0 x 78.0 x 0.5 inch) were used to connect the column to the PMC infill wall panel. Figure 4-25 shows a detailed illustration of the column-to-infill connection.

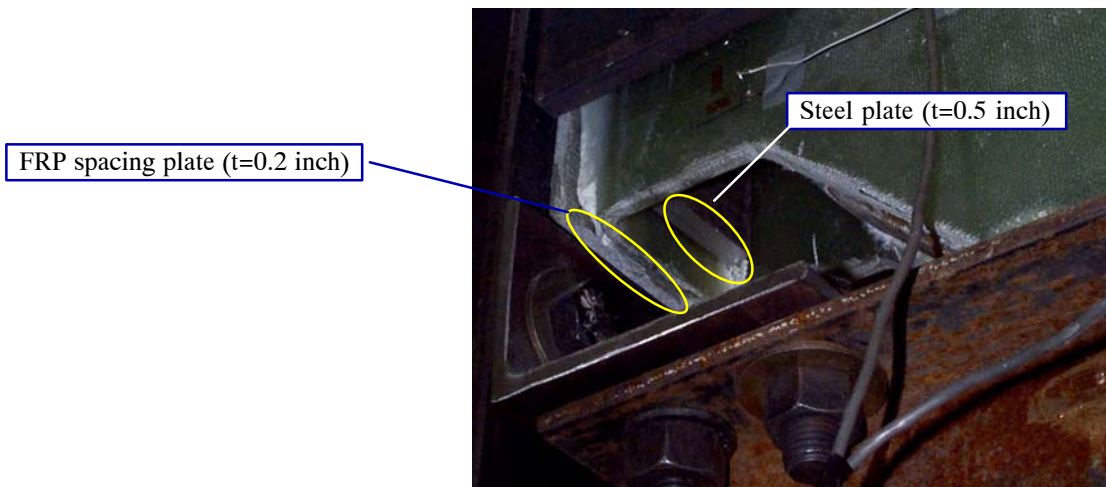
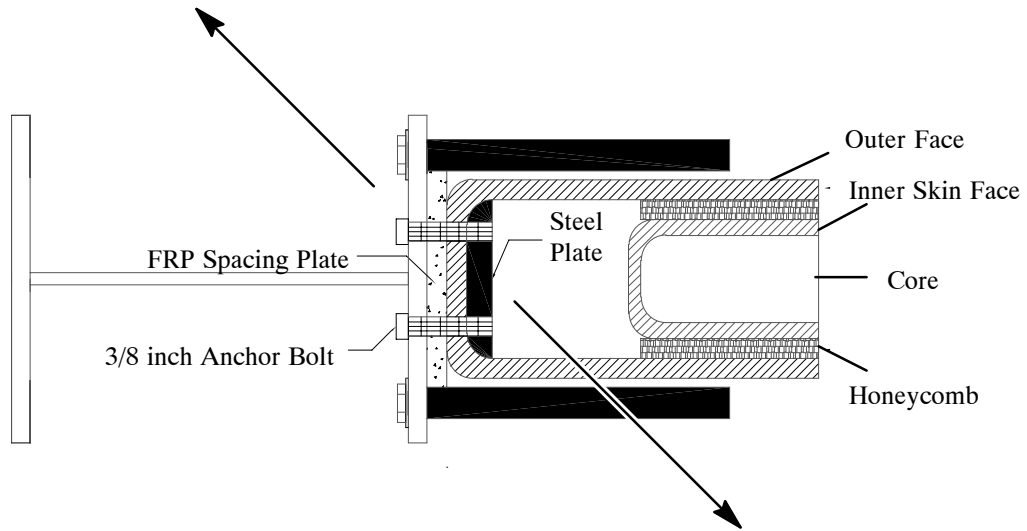
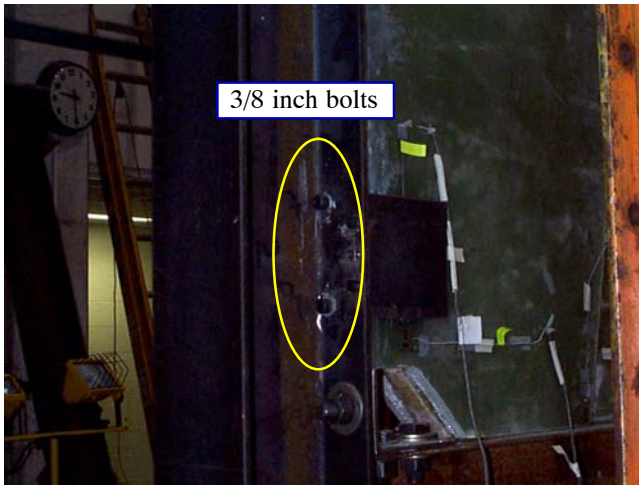


Figure 4-25 The Column to Infill Connection

4.4 EXPERIMENTAL DESCRIPTION AND PROCEDURE

This section presents testing procedures and loading histories that were employed in this study. Full-scale specimens were tested with both monotonic and cyclic loading. The multi-layer PMC infill wall system experiments described in this study were performed using two test specimens. The two test frames were identical in all respects except that the PMC infill wall was installed *without* connectors in one specimen test and *with* connectors to the frame in the other. The purpose of the first specimen test was to obtain the properties of the PMC infill wall system, and the second specimen was only tested to investigate the effect of the infill-to-column connections on the behavior. Accordingly, the selected test cases herein consisted of two test specimens: (1) the PMC-infilled frame without column-to-infill connections and (2) the PMC-infilled frame with the column-to-infill connections. Lateral force was applied to the top beam by a 250-kips MTS hydraulic actuator with a stroke of ± 4 inches. The displacement at the loading point of the structure and the corresponding load were monitored and displayed. Loading history was considered based on the previous infill wall test by Mander, *et al.* (1993), at the Structural Engineering and Earthquake Simulation Laboratory at the University at Buffalo. All cyclic tests for the multi-layer PMC-infilled frame were performed under displacement control, and the response were almost identical. The suggested loading history in this study consists of a series of stepwise incremental deformation cycles (multiple step). For each step, the test specimens were cycled two times at assigned lateral displacement, and the displacement level was increased gradually depending on the observed behavior. A sinusoidal wave form was then used to control the input displacement histories. The test was paused after every two cycles at the assigned displacement so that the PMC infill wall and frame could be visually inspected to examine the onset or progress of failure. Finally, the test was stopped when buckling occurred at the inner panel. Using 0.5% drift increments, the maximum lateral drift applied in the tests was 3.0%. These test procedures produced data to compare with steel frame tests performed at the lateral drifts of 0.5%, 1%, and 1.5%.

4.5 DISCUSSION OF TEST RESULTS

Based on the experimental results, the structural behavior of the PMC infill wall system when subjected to static and quasi-static tests without the column-to-infill connection is presented and compared with the results obtained for the same test conducted on the bare steel frame. For the PMC-infilled frame with the column-to-infill connection, the results are compared, but they are discussed separately because of the progressive angle connection damage during the test.

Force-displacement Relationship

The force-displacement behavior of both the bare frame and the PMC-infilled frame is presented here. Fig. 4-26 illustrates the push-over test results of the PMC-infilled frame. Several kinks show in Fig. 4-26 are attributable to the fact that the grouting epoxy, which was installed at the interface between the PMC infill wall and the column members at the beginning of the test, produced different boundary conditions while epoxy started to break at the interface during the test. Epoxy grouting at the previous test leads to an increase in initial stiffness of the overall structure by enhancing infill action and/or friction at the interface.

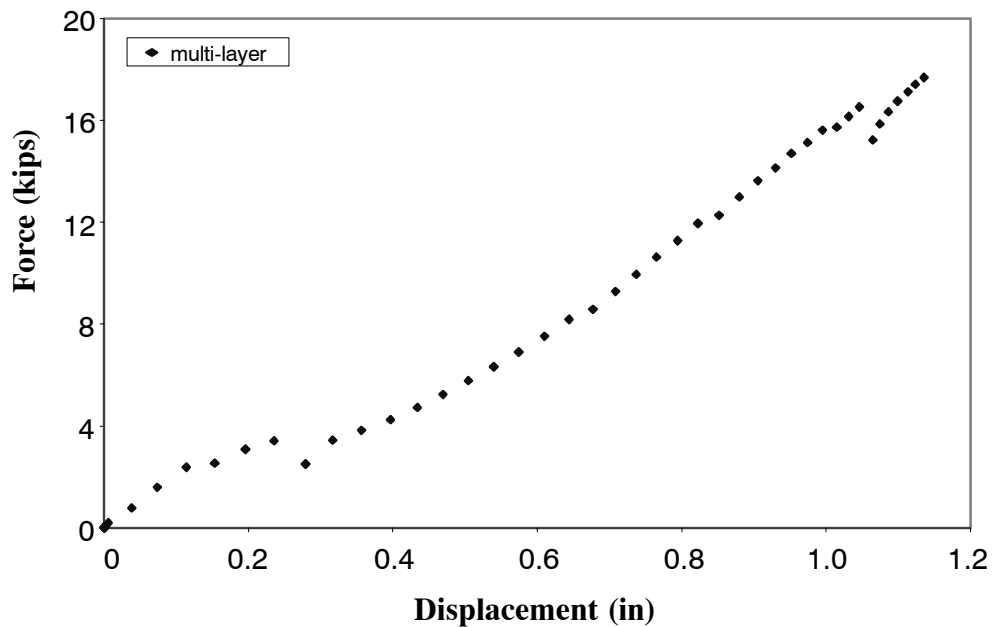


Figure 4-26 Force-Displacement Relationship of the Multi-layer PMC Infilled Frame under Push-over Loading (1.0% drift)

Due to the effect of the epoxy grout at the interface between the PMC infill wall panel and the steel column, stiffness can be defined from this experiment as the force per unit displacement in the range between 0.25 and 1.0% drifts. This drift range is considered primarily because, the initial stiffness attributable to epoxy grout at the wall-frame interface is higher than that obtained in the higher drift range (0.25-1.0%). Higher stiffnesses of the bare frame and the PMC-infilled frame were computed to be 5.54 kips/in and 18.15 kips/in, respectively. Fig. 4-27 illustrates force-displacement responses of the bare frame and the PMC-infilled frame.

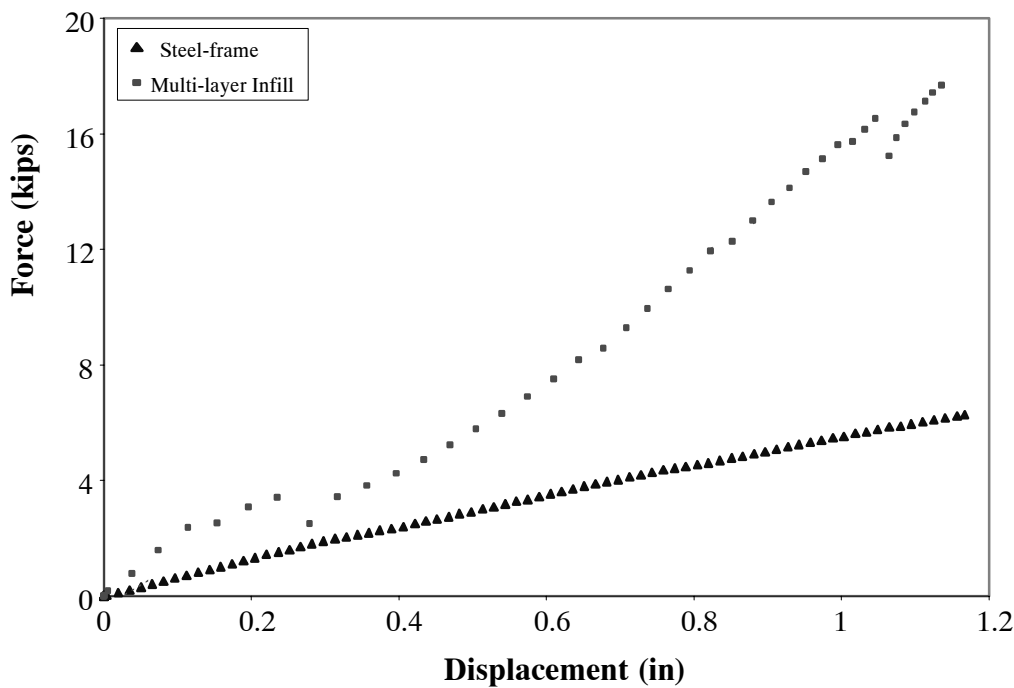


Figure 4-27 Comparison of Force-displacement Response for the Steel Frame and the Multi-layer PMC Infilled Frame under Push-over Test (1% drift)

The PMC-infilled frame specimens are approximately three times stiffer than the bare frame. The net response of the PMC infill wall is obtained by subtracting the bare-frame response at the given drift from the gross infill-frame response, because force-displacement relationships subjected to monotonic loading are derived for the net infill performance due to the diagonal strut and truss actions of the system. From Fig. 4-28, the relationship for net infill response is described as follow;

For strength of the net infill,

$$F_{\text{infill wall}} = F_{\text{infilled frame}} - F_{\text{steel frame}} \quad (4-1)$$

For stiffness of the net infill,

$$K_{\text{infill wall}} = K_{\text{infilled frame}} - K_{\text{steel frame}} \quad (4-2)$$

For energy capacity of the net infill,

$$E_{\text{Infill}} = E_{\text{Total}} - E_{\text{Steel frame}} \quad (4-3)$$

where, E_{total} is the energy capacity of the multi-layer PMC infilled frame.

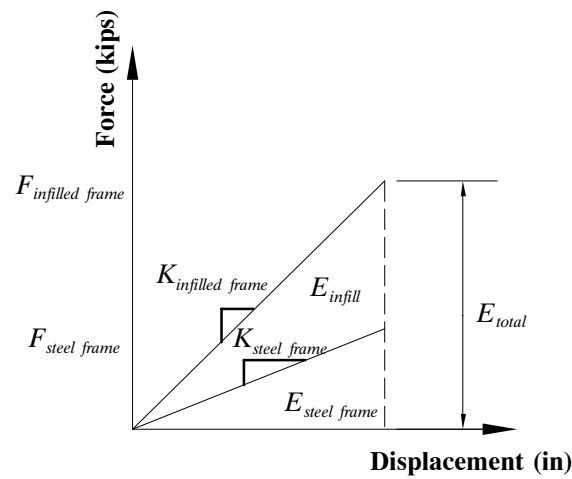


Figure 4-28 Estimation for Net Response of the Multi-layer PMC Infill within Elastic Range of the Structure

By using (4-1) and (4-2) in Fig. 4-27, it is evident that the PMC infill wall contributes two thirds of total stiffness, so the stiffness properties of the PMC infill wall can therefore be used to enhance the stiffness of the structure.

Figure 4-29 shows the hysteretic response of the PMC-infilled frame under successive loading drifts. Clearly, the behavior of the PMC infill wall was ductile, and the frame withstood large deformation without any significant strength or stiffness degradation before the buckling of the inner panel took place at 2.5% lateral drift. The pinching action appeared due to a loss in stiffness of the angle connection and damages imposed on the PMC infill wall during previous loading cycles. As the lateral drift level increased, pinching became more exacerbated because of excessive separation of the top and seat angle from the column flange and the consequently additional sliding took place.

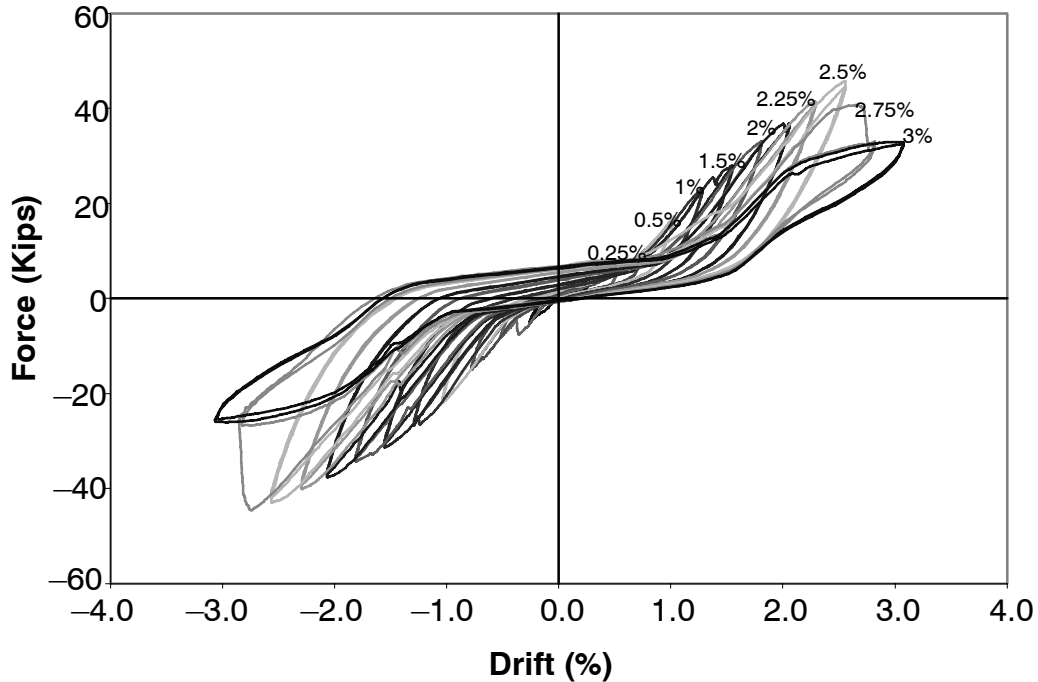


Figure 4-29 Hysteretic Response of the Multi-layer PMC Infilled Frame under Successively Cyclic Loading Drift

Fig. 4-30 shows the comparison of hysteretic response for steel and the multi-layer PMC infilled frame under different loadings. As shown in Fig. 4-30(a), significant pinching action appeared due to epoxy grouting during monotonic loading test. The force history for the multi-layer PMC infill frame during various cycles is also shown in this figure. The multi-layer PMC infilled frame was capable of withstanding larger force compared to the steel frame, which clearly indicated by higher capacity of the multi-layer PMC infilled frame. These results can be used to evaluate the contribution of the PMC infill wall in terms of the lateral stiffness as well as energy dissipation.

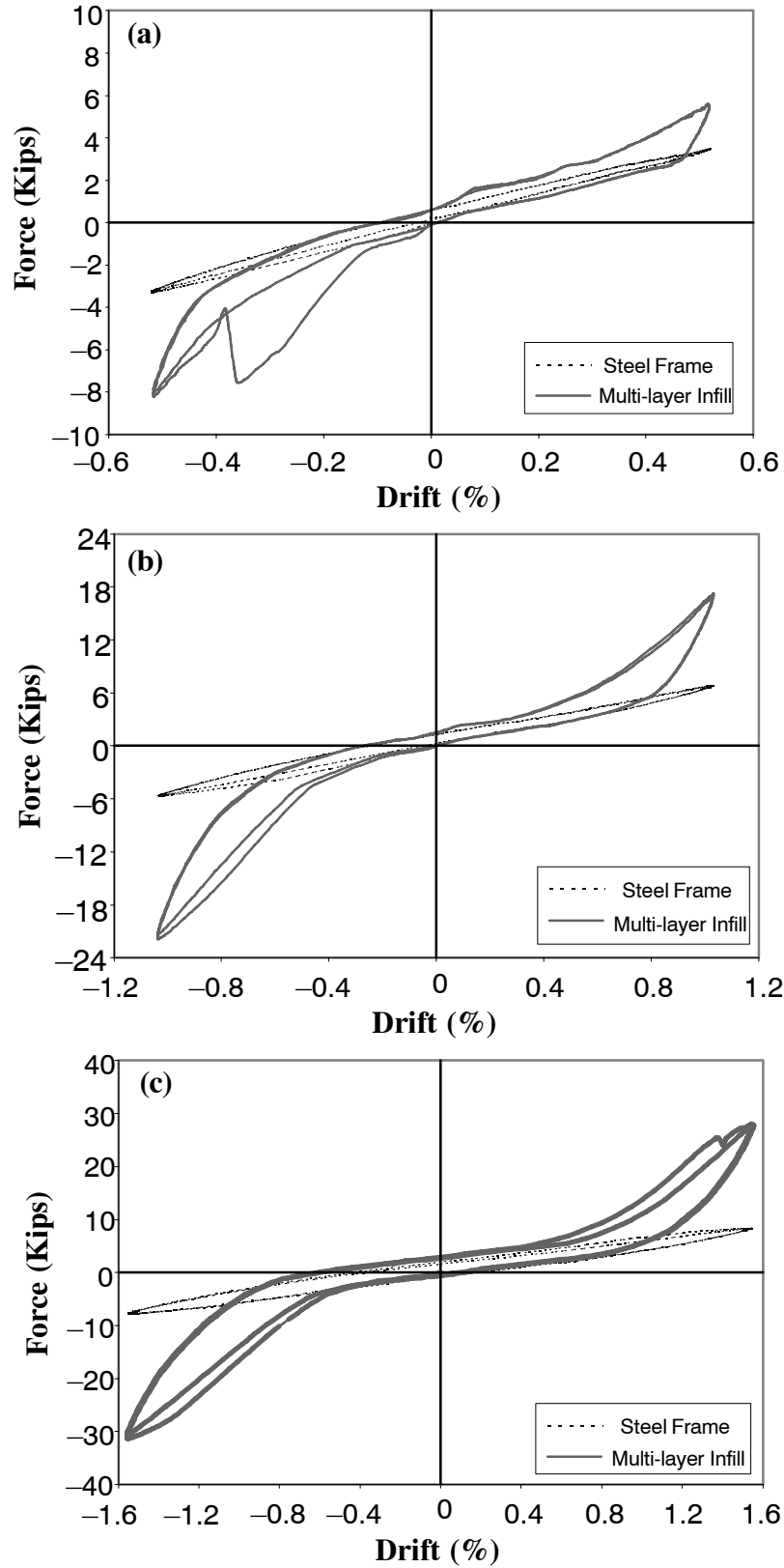


Figure 4-30 Comparison of Hysteretic Response for Steel and Multi-layer PMC Infill Frames (different scales) : (a) 0.5% ; (b) 1.0% ; (c) 1.5% drift

Initial Gap Effects

The behavior of the PMC infill wall system as the load was increased can be divided into two parts associated with initial gaps. According to Riddington (1984), the relatively smaller gaps used in the concrete-infilled frame test significantly affect the structural behavior of the infilled frame, and these effects are largely undesirable. The effects of the initial gap for the structural behavior of the PMC infill wall were investigated. Up to the breaking of epoxy grout at the initial gap, the PMC-infilled frame with and without any initial side gap was tested. After epoxy grout breaks, the PMC-infilled frame behaved like a test specimen with a 1.5-mm gap at the top and both sides. These results clearly indicate that the stiffness of the structure varied through the introduction of the initial gaps.

It was observed in Fig. 4-31 that the initial stiffness of the structure without and with an initial gap was 20.96 kips/in and 17.64 kips/in, respectively. The measured stiffness after breaking the epoxy grout was approximately 18.15 kips/in. The initial stiffness of the structure without an initial gap is 1.18 times greater than that of the structure with an initial gap. Therefore, similar to the traditional infilled frame structures, the effect of an initial gap on the structural performance of the PMC-infilled frame plays an important role and should be taken into design consideration.

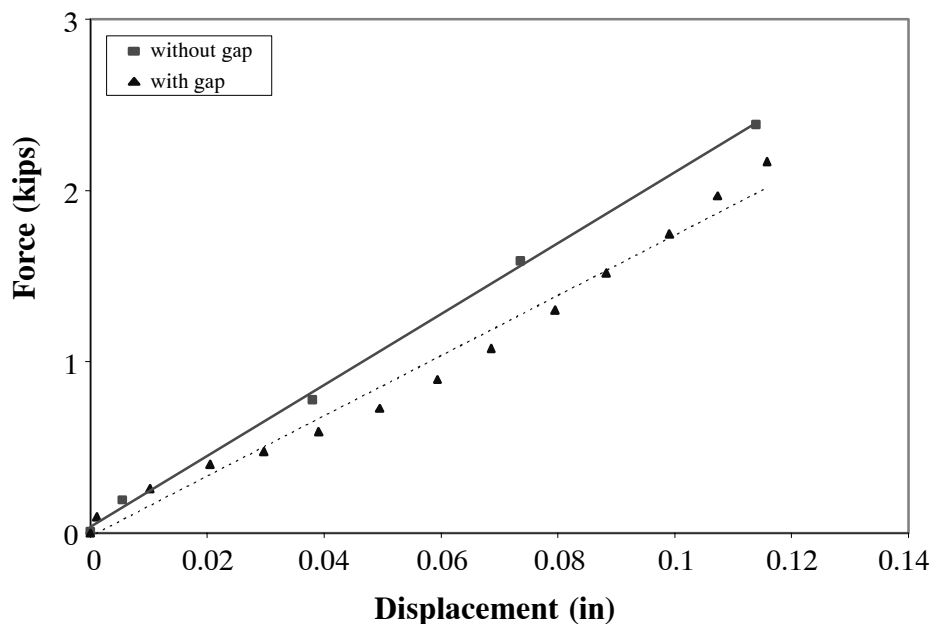


Figure 4-31 Test Result of Initial Gap Effect

Energy Dissipation Capacity and Mode of Failure

The energy dissipation during two load cycles was calculated based on the area within the hysteresis loops from the lateral load-versus-displacement diagram. Figure 4-32 and 4-33 present the hysteresis loops of each cycle for the steel and PMC-infilled frame at 0.5%, 1.0%, and 1.5%, respectively. Large amount of energy dissipation was contributed from the bolted top and seat angle connection, the polymer interface layers, and sliding shear of the multi-layer PMC infill wall. Finally, the energy dissipation of the PMC infill wall at the corresponding inter-story drift levels is evaluated and presented in Figure 4-34. It was evident that for the first cycle of loading, a considerable amount of energy was dissipated. Subsequently, the second cycle shows mechanism reduction in energy dissipation capacity due to a changed sliding shear response. The results of the experiments revealed that contact strength of the PMC infill wall at the interface with the steel frame in the compressive corners is important for the evaluation of the failure mode and the behavior of the polymer honeycomb layers.

The behavior of the structures as the load was increased can be divided into several stages. After loading, slippage occurred between the PMC infill wall panel and the left column, and the PMC infill wall panel lifted and wedged into the upper corner. Next, slippage successively occurred between the PMC panel and the bottom beam, causing the PMC wall to slide across and wedge into the lower corner. Different stages developed in the PMC infill panel system can be illustrated in Fig. 4-35. At higher drifts, contact forces gave rise to two failure modes—namely, localized crushing damage and buckling due to the diagonal compression strut. From these failure modes, it is evident that polymer honeycomb layers allowed contact force to be transmitted through the top and bottom beam. Figure 4-36 shows the localized damage and possible loading path of the PMC panel. This test was stopped because of buckling of the inner panel induced by the compressive contact force at the top and bottom beams. Fig. 4-37 and 4-38 present the measured data of out-of-plane displacement transducer and the buckling shape of the infill during the tests.

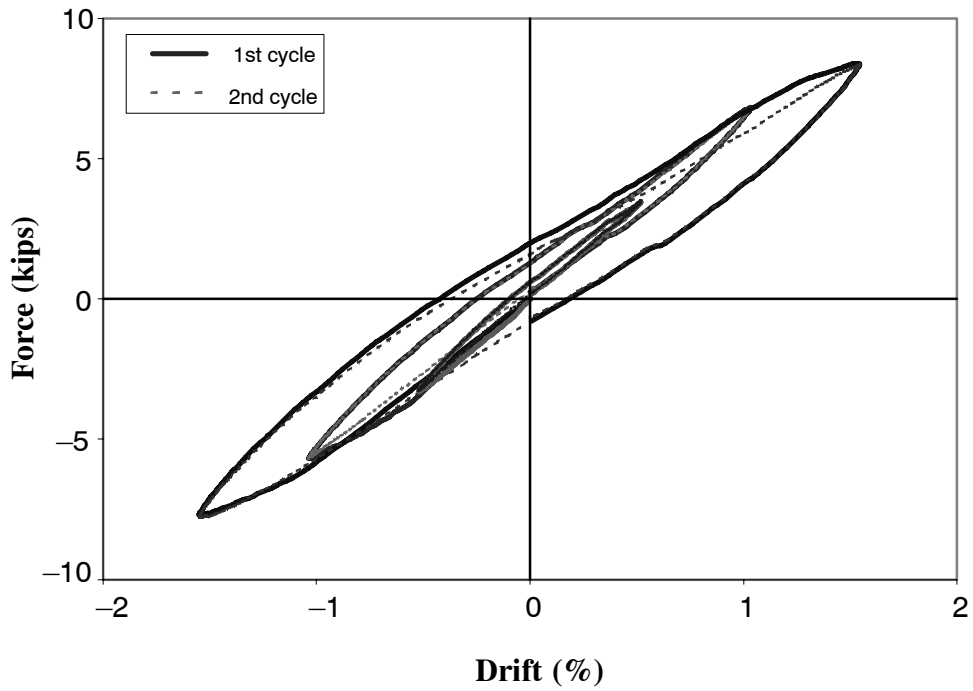


Figure 4-32 The Result of Hysteretic Loops for Steel Frame Test for Each Cycle under Cyclic Load

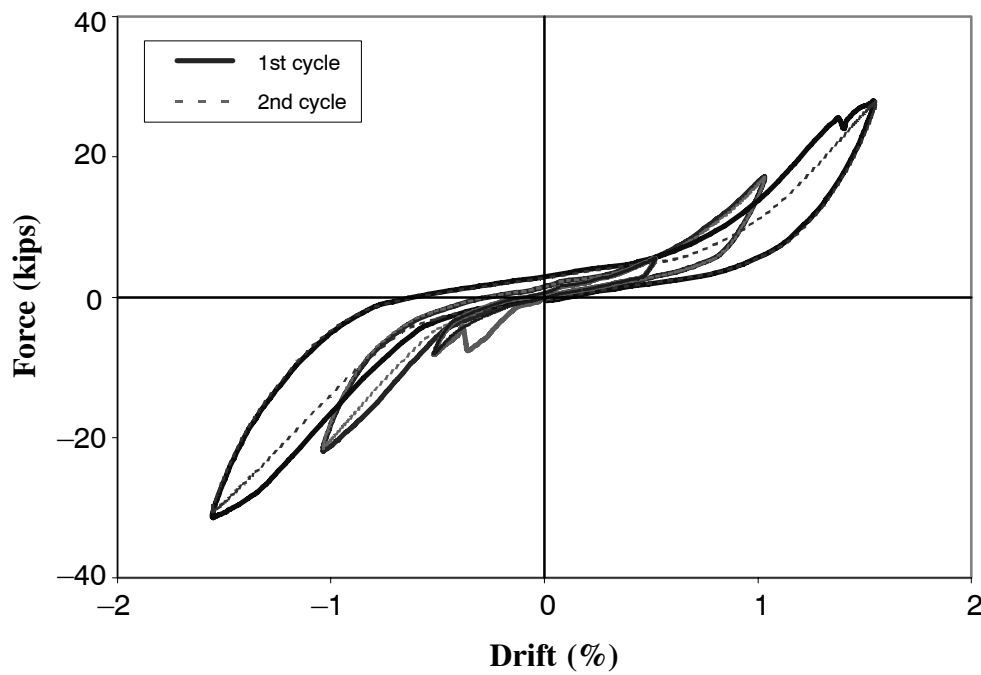
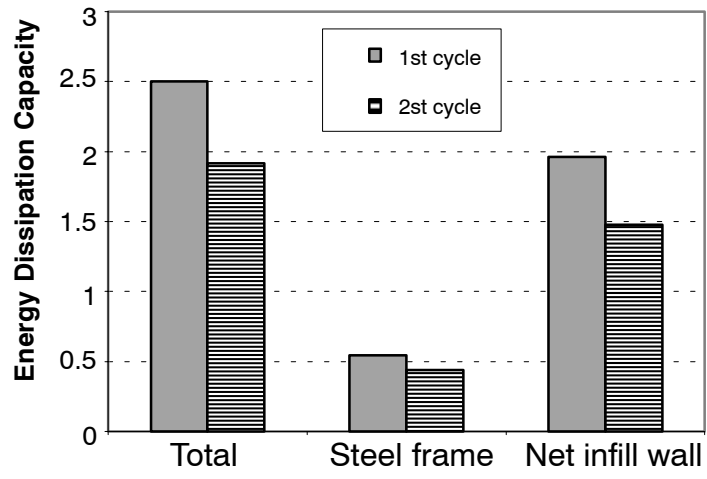
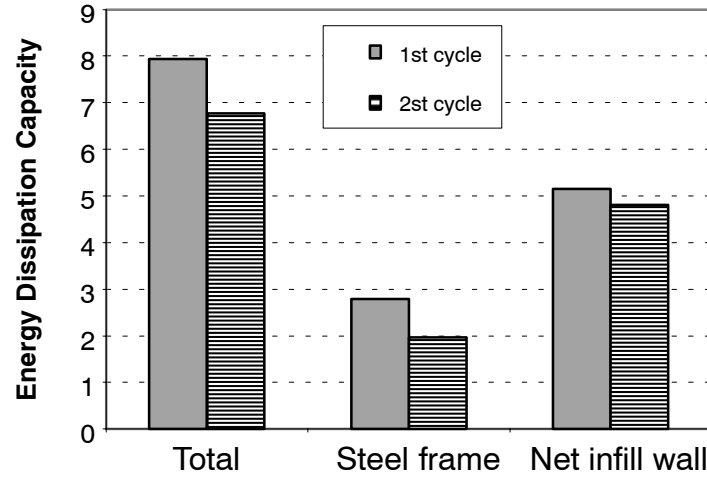


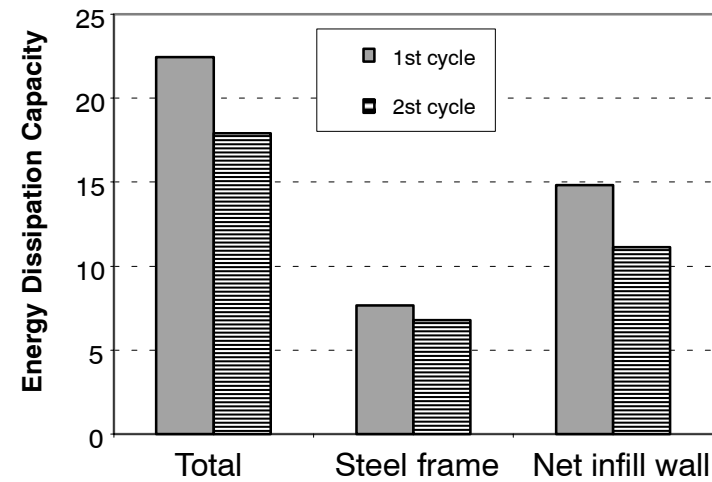
Figure 4-33 The Result of Hysteretic Loops for Multi-layer PMC Infilled Frame Test for Each Cycle under Cyclic Load



(a) Cycle Number at 0.5% Drift



(b) Cycle Number at 1.0% Drift



(c) Cycle Number at 1.5% Drift

Figure 4-34 Energy Dissipation Capacity for the Multi-layer PMC Infilled Frame (different scales) (unit = kips-in)

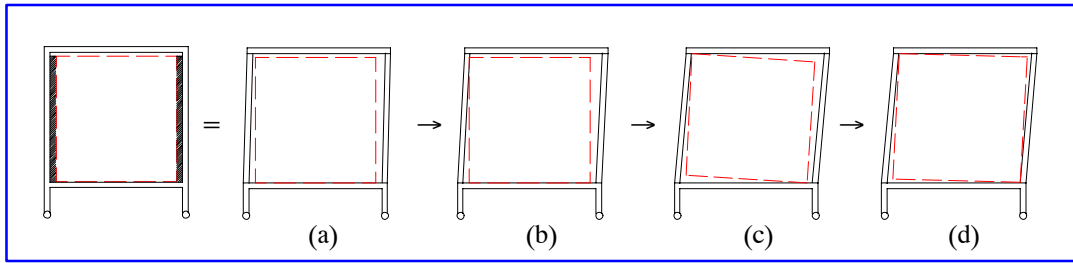


Figure 4-35 Behavior of the Multi-layer PMC infill Wall with Top and Side Gaps

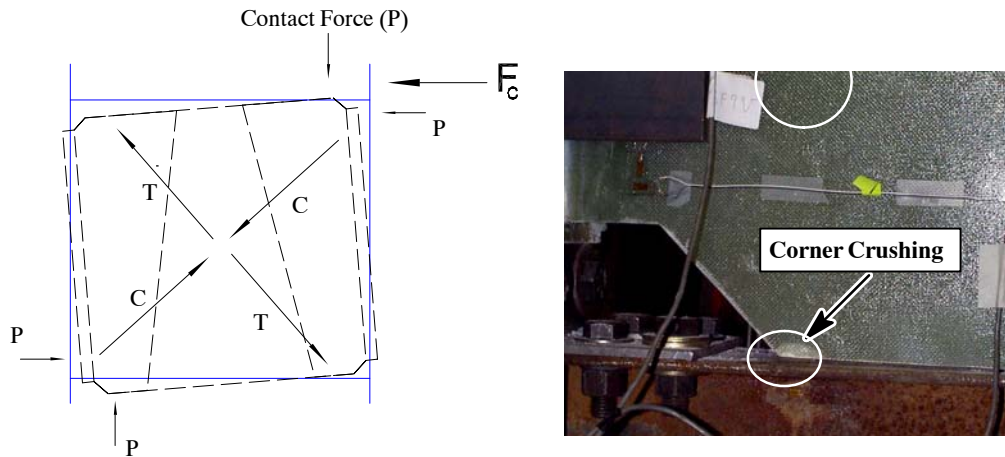


Figure 4-36 The Schematic of Possible Force Path and Detail of Localized Damage (C: Comp; T: Tension)

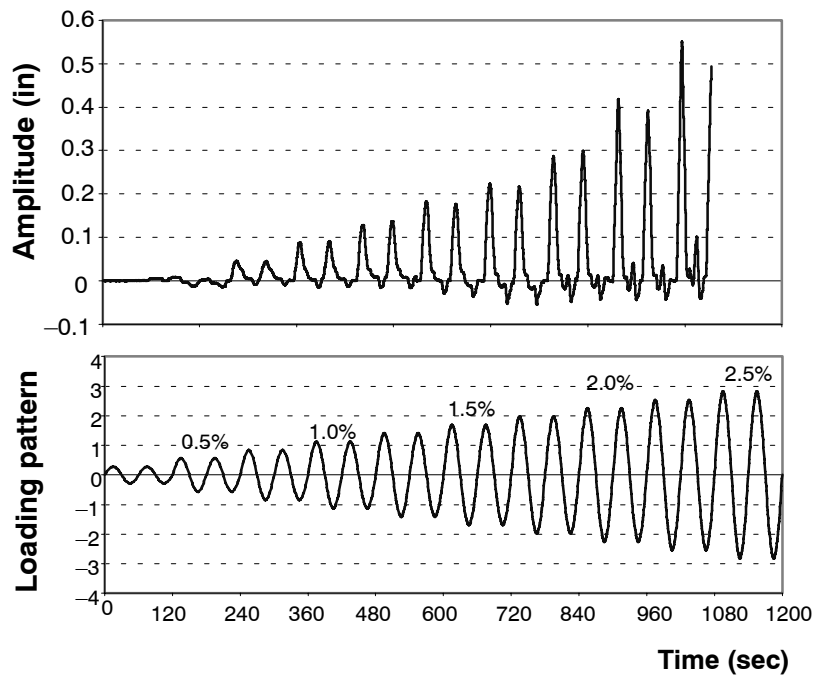


Figure 4-37 Out-of-plane Buckling Displacement of the PMC Sandwich Infill



(a) Before Buckling of the Inner PMC Sandwich Panel



(b) After Buckling of the Inner PMC Sandwich Panel

Figure 4-38 Test Observation for Out-of-plane Buckling Displacement of the PMC Sandwich Infill

Stress Distribution

The laminate strains and stresses were examined by considering the Tsai-Hill failure criterion, which takes into consideration the interaction between strengths along with longitudinal and transverse direction (Jones 1999). For the Tsai-Hill criterion, when failure index calculated from the laminate stress and strain at any position is greater than unity, failure at that location has occurred. The contours of the laminate stress and strain can be obtained from the strain gauges mounted on the PMC infill wall. In this case, the failure index evaluation of the multi-layer PMC infill panel was carried out by using the finite element analysis.

In the experiments, strain gages at the inner panel malfunctioned because strain-gages were damaged during outer laminate construction. For the outer laminates, the data obtained from strain gages located on the surface of the laminates were only marginally useful in tracing the stress contour because of the impact and vibration during testing. The maximum Tsai-Hill failure index of outer laminate at each drift occurred near contact corners between the beams and the PMC infill wall and less than unity, even at high drift levels.

Testing of the PMC Infilled Frame with Column-to-infill Wall Connection

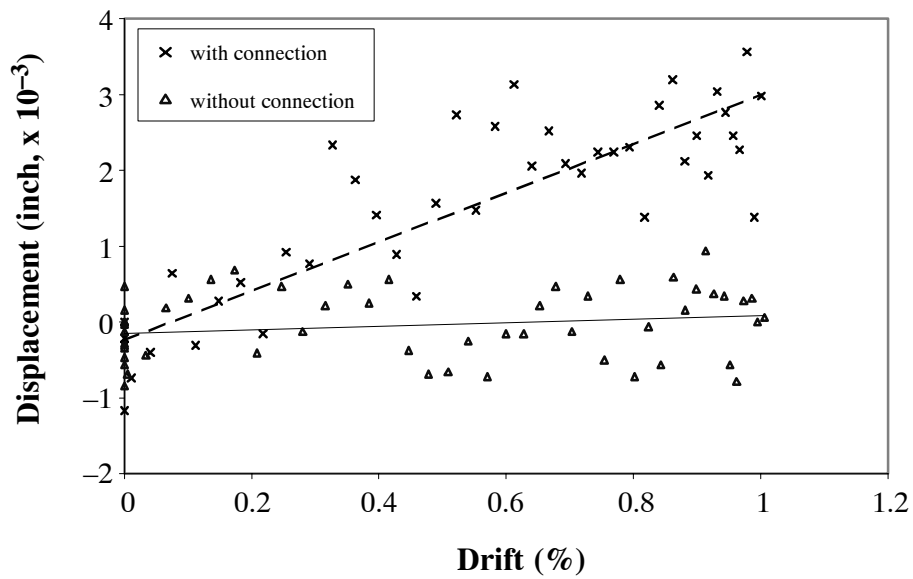
This test was intended to explore possible enhancements to the system when the PMC infill panel was connected to the columns. The results may provide an important basis for designing the new PMC infill panel. The test was stopped when the frame exhibited progressive angle-connection failure. Figure 4-39 shows the horizontal shear deformation at the polymer honeycomb layers for the PMC infill wall with or without the infill-to-column connections. Preventing sliding at the column face generated more horizontal shear deformation in the polymer honeycomb layers compared to the first test (without column-to-infill wall connection). As a result, the introduction of infill-to-column connection produced greater stiffness as well as larger hysteretic loops, which translates into larger energy-dissipation capacity. It also indicates that the contribution of the visco-elastic honeycomb layers to energy dissipation is further enhanced. This enhanced behavior is illustrated in Fig. 4-40 and 4-41. The measured stiffnesses are compared in Table. 4-7.

Table 4-7 Comparison of Test Results for the Column-to-Infill Connections

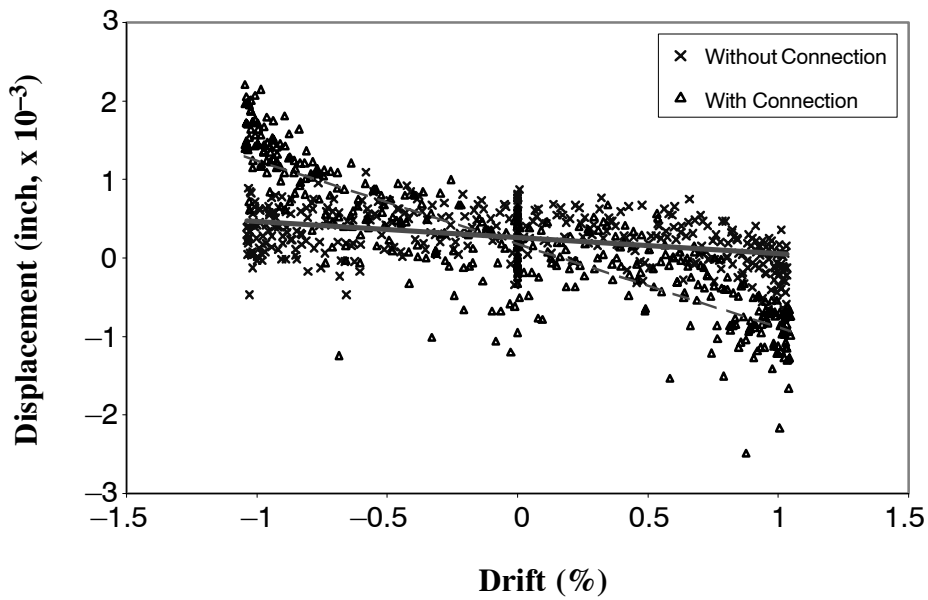
Test Types	Stiffness (kips/in)
Steel Frame Test	5.54
Multi-layer PMC Infilled Frame (Test Case 1) <i>without column-to-infill connection</i>	18.56
Multi-layer PMC Infilled Frame (Test Case 2) <i>with Column-to-Infill connection</i>	22.4

However, angle connections became critical components because, by preventing sliding shear, they attracted more forces. It was observed that the vertical deformation of the honeycomb layer was too small because the inner PMC sandwich and outer FRP laminate panels deform simultaneously due to contact with the steel frame at the same time. As a result, the high contact force caused by both panels produced a large rotational deformation on the angle connection.

Similarly, if the area of polymer honeycomb layers is increased (i.e., stiffness of the interface increases), additional demand will be imposed on the angle connections. If an increase in angle connection demands are neglected, it would lead to premature damage in the semi-rigid seat-angle connections. It is clear that careful consideration of the size and shape of the inner PMC sandwich, and outer laminate panel would help in reducing the damage to the overall structure. From the experiment, several damages caused by the column-to-infill connections of the multi-layer PMC infilled frame occurred. Fig. 4-42 to 4-43 show the failures during the second multi-layer PMC infilled frame tests.



(a) Monotonic Loading Test



(b) Cyclic Loading Test

Figure 4-39 The Comparison of the Shear Deformation of polymer Honeycomb Layer under Applied Loading

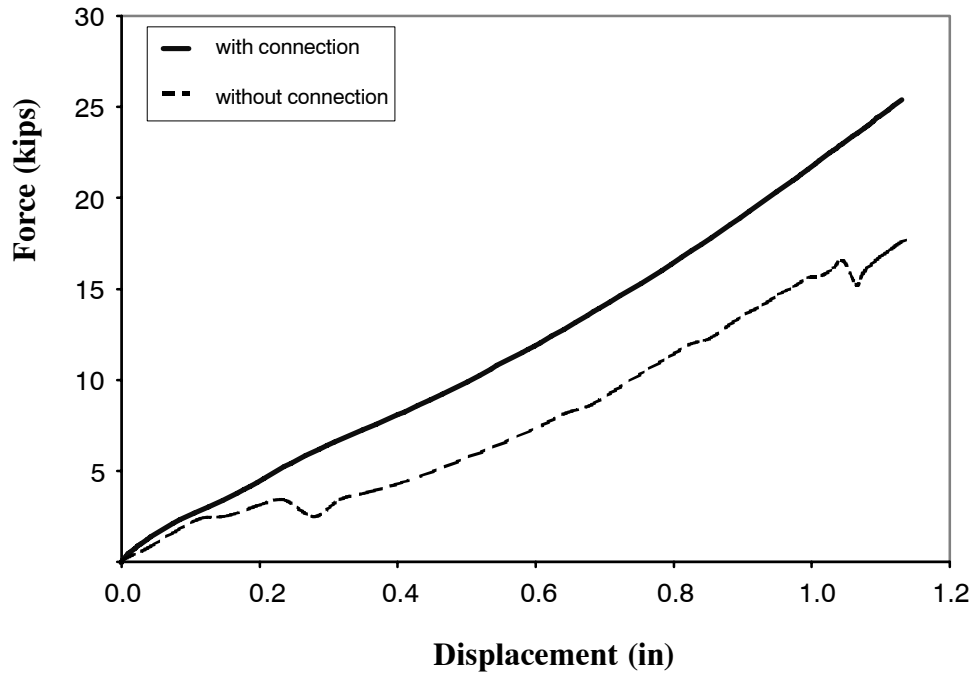


Figure 4-40 The Comparison of Test Results for the PMC Infilled Frame with and without Connection under Monotonic Loading (1.0 %)

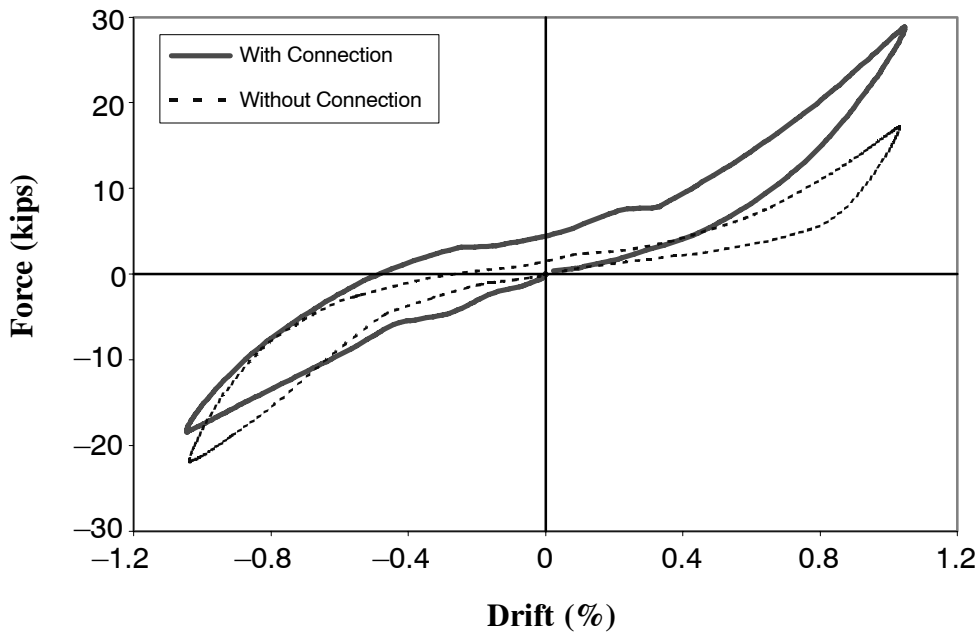
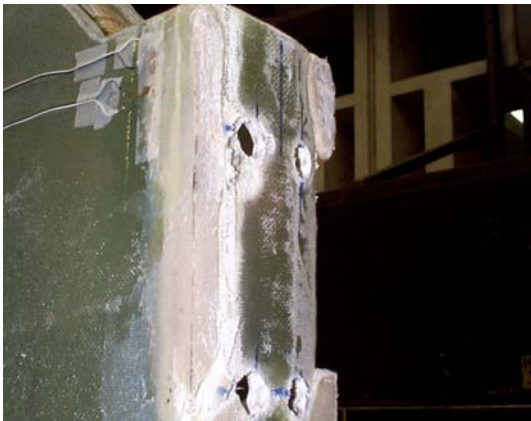


Figure 4-41 The Comparison of Test Results for the PMC Infilled Frame with and without Connection under Cyclic Loading (1.0 %)



(a) Angle connection failure at top and bottom joints



(b) bolting joint sliding of outershell



(c) outershell spalling off - bolting release

Figure 4-42 The Damage of the Multi-layer PMC Infilled Frame with the Column-to-Infill Connection (1)



(a) Elastic Buckling of Inner Panel



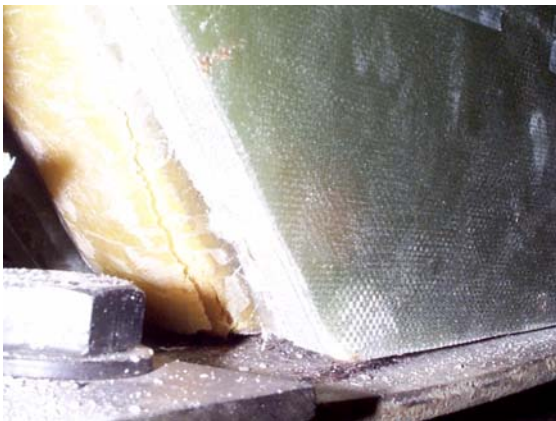
(b) Buckling of Steel Plate in the Edge of Outershell



(c) Deformation of Viscoelastic Layers



(d) Failure of Shear Connectors



(e) Cracking of Inner Core



(f) Breaking of Outershell

Figure 4-43 The Damage of the Multi-layer PMC Infilled Frame with the Column-to-Infill Connection (2)

4.6 Summary

Traditionally, infill wall systems have been used in seismic areas to resist lateral loads. The use of infill panels may be particularly suitable in regions where an implementation of advanced devices is less probable due to the lack of earthquake awareness. In recent year, light-weight materials have potentials to emerge as favorable solution for infill and partition walls in seismic retrofitting because reduced the overall mass of the structure, as well as simple and faster to construct.

In this section, the prefabricated multi-layer infill panels made of FRP composites were studied. The primary objectives of this study were to develop a conceptual design of the multi-layer infill system and investigate the effectiveness of such system under various loading conditions. A conceptual design for the multi-layer infill panel was presented and optimum design for the FRP composite material was performed based on finite element simulations. In the design process, sandwich construction was chosen as an inner component because the concept is very suitable for lightweight structure with high in-plane stiffness. To increase energy dissipation capability, the polymer honeycomb material was used at the interface between the inner and outer components. The geometric configuration of outer components was determined by push-over analysis and positioned at the both sides of the inner sandwich component.

An experimental study was also conducted on two types of multi-layer infilled frames, i.e., with and without the column-to-infill connections, under in-plane monotonic and cyclic loads. The experimental results were compared with the bare frame test results. It was shown that the contribution to total stiffness and strength by the infill was very large and the energy dissipation of the PMC infill was almost two-third of total capacity. Also, the influence of initial gap between the infill and the frame has been proved to significantly affect the behavior of the structures. Finally, the multi-layer PMC infill panel exhibited failure by elastic buckling. The experimental studies demonstrate that the introduction of a PMC infill wall panel in a semi-rigidly connected steel frame produces significant enhancements to stiffness, strength, and energy dissipation.

SECTION 5

ENERGY DISSIPATING INTERFACE DAMPING LAYERS

5.1 Introduction

To control excessive noise and vibration, the application of damping devices to structures is becoming a standard practice in many industries. There have been various methods developed to design structures with maximum possible damping capacity. In recent years, earthquake-resistant design and retrofitting of structures using various energy dissipation devices such as viscoelastic dampers (VEDs), viscous fluid dampers, friction dampers, and added damping and stiffness devices have received considerable attention. Based on the mechanical dissipation of energy, viscoelastic damping schemes offer many desirable characteristics. For instance, VEDs have shown to be capable of providing structures with considerable added damping to reduce the story shear, inter-story drift, and floor accelerations of structures produced by wind and seismic excitations.

Numerous useful design techniques and successful applications have been reported since the early 1950's. Oberst (1952) proposed to apply a thin layer of viscoelastic material to the surface of flexible structures for passive vibration control. Kerwin (1959) introduced the constrained viscoelastic damping, in which the viscoelastic layer is covered in turn by a high tensile stiffness constraining layer. The constraining layer induces shear strain in the viscoelastic layer, and thus greater damping is produced. Since the introduction of this basic concept, many modifications have been proposed to improve the damping performance. Ungar and Ross (1959) suggested a multiple constrained layer treatment, and Nelson (1977) proposed a useful design technique for highly damped structures. For the enhanced damping material, Alberts and Xia (1995) studied design and analysis of fiber enhanced viscoelastic damping polymers. The fiber enhanced viscoelastic damping treatment represents both substantial increase in damping and decrease in weight added when compared with conventionally constrained viscoelastic layered damping concept. Although several damping technologies may offer advanced properties ideal for the mechanical dissipation of energy, the research dealing with combining composite damping materials is very scarce.

The previously tested multi-layer composite panels in section 4 were characterized by having shear interface layers, composed of polymer honeycomb material, in between composite laminates consisting of a number of plies. A characteristic feature of this composite panel system was that significant damping can be obtained from interface slip at contact surfaces. However, on the basis of the results obtained from section 4, the design of composite infill panels as a seismic damping component faces two challenges: (1) the interface materials may be sufficiently stiff that will not allow deformation at the interface, thus, small sliding leads to relatively small energy dissipation. (2) whereas a solid viscoelastic material, which contribute significantly to energy dissipation, will make the structure very flexible. Therefore, we are considering a new interface damping system by combining both a honeycomb and solid viscoelastic material. The enhanced passive damping of this new interface system will involve the modification of key structural design parameters which affect the structural mass, stiffness, and damping characteristics.

In this section, the combined composite damping material system is explored. The effectiveness of this system to increase energy dissipation between FRP skin plates is our primary interest. In this configuration, two different styles of composite materials are considered for comparison; one is a polymer honeycomb material and the other is a solid viscoelastic material. Practically, the honeycomb material will be helpful to enhance the initial stiffness of the entire structure, and the solid viscoelastic material will provide more energy dissipation properties in the multi-layer panel systems when subjected to in-plane shear loading. In the design process, several cases were considered to find the best material combination, and practical factors such as cost and fabrication. Thus, numerous experimental studies were performed. Finally, based on these results, simplified design procedures are introduced for predicting the stiffness and the damping characteristics of the energy dissipating material.

5.2 Basic Material Description

There are several theoretical and practical challenges associated with the development of the new composite damping material. In this research, new applications for two composite energy absorbing

materials, such as the 3M solid viscoelastic and the honeycomb were studied to evaluate their stiffness as well as damping effects. Energy dissipation mainly arises from the relaxation and recovery of the polymer network after it has been deformed (Zhu et al., 2000). The following is the mechanical characterization of each material.

5.2.1 Polymer Honeycomb Material

Man-made polymer, metal and ceramic honeycomb are now available as standard products that can be used in a variety of applications. The polymer honeycomb material used in this study is composed of H8-PP Polypropylene Honeycomb produced by Nida-Core Corporation., FL, combined with a resin-rich scrim layer on each surface of the honeycomb as shown in Fig. 5-1. The properties of this material were presented in section 2 and it is the same material used in the multi-layer PMC infill system.



Figure 5-1 The Structure of the Honeycomb Material

The cells are true hexagonal cell honeycomb extruded from polypropylene and 0.315 in (8mm) across the cell, wall to wall. Wall thickness is nominally in the order of 0.005 in (0.127mm) range. One variance from typical hexagonal cell honeycomb is that there is no double wall effect in one axis. Based on the deformation mechanisms in honeycomb, their deformations can be analyzed more or less exactly to give equations which describe their properties because honeycombs have a regular geometry.

The properties of the solid cell wall material based on this approach can produce reliable data for both the Young's modulus and yield strength of the cell wall of common metal or aluminum honeycombs. However, ceramic and polymer honeycombs are more difficult to define their properties be-

cause the polymer cell walls no longer behave like linear elastic beams loaded in bending. Therefore, the behavior of the polymer honeycomb material was primarily defined by experimental results. A test specimen that consisted of constrained layers of honeycomb material with FRP plates was used in the study. Fig. 5-2 described the shear stress-strain relation of honeycomb material. From this figure, two observations can be made. First, at the beginning of loading, the energy dissipation is introduced through the inelastic deformation of the honeycomb material. Second, under extreme loading, when the layer reaches the bonding scrim slip, more energy is dissipated by the larger inelastic deformation of the honeycomb material but the stiffness at this stage is significantly reduced.

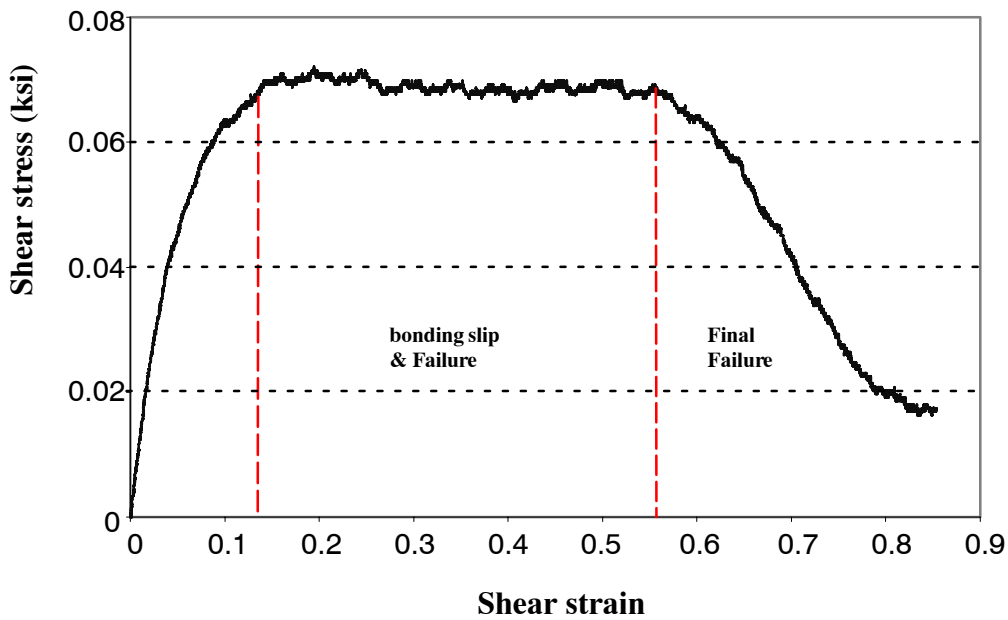


Figure 5-2 Material Monotonic Test Results for Honeycomb

5.2.2 Polymer Dissipative Solid (PDS) Material

Viscoelastic materials provide high energy dissipation and their application in the form of constrained layers is very effective in suppressing resonant vibration. Recently, they have been investigated for earthquake-resistant design applications. Pong and Tsai (1995) showed that several design parameters such as ambient temperature, thickness, and total area of viscoelastic material affect the seismic mitigation capacity. The thickness cannot be too small, which is not effective in vibration reduction, nor can it be too large, which not only increases the cost, but also reduces the seismic resistance. The total area of viscoelastic dampers should be determined properly for optimum damper performance to obtain the most economical design. The dissipative polymer solid material used in this study is 3M ISD 111 solid viscoelastic material which was fabricated by 3M corporation, Japan. Two different thicknesses were provided to match the thickness of honeycomb material and two different sample sizes (1.0 x 1.5 x 0.2 inch and 1.0 x 1.5 x 0.4 inch pads) were used. Table 5-1 and Fig. 5-3 show the 3M viscoelastic material data (obtained from the 3M company) for shear and the results for creep tests. In Table 5-1, the presented properties are the shear storage (G') and loss moduli (G''), and loss factor (η), which is defined as $\eta = \frac{G''}{G'}$.

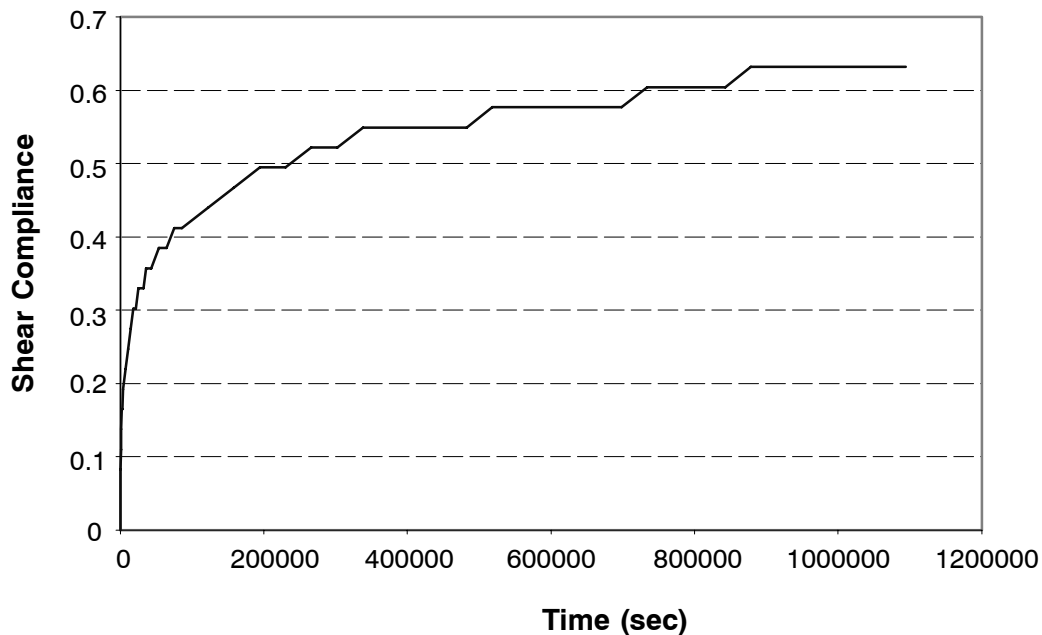


Figure 5-3 Creep Test Results for 3M Viscoelastic Material (3M Corp., Japan)

Table 5-1 The Properties of 3M Viscoelastic Material (3M, Japan)

		10% strain			50% strain			100% strain		
Temp.	Freq	G'(w)	G''(w)	η	G'(w)	G''(w)	η	G'(w)	G''(w)	η
°C	Hz	psi	psi		psi	psi		psi	psi	
0	0.1	50.84	56.86	1.12	48.5	54.47	1.12	45.0	49.53	1.1
	0.3	88.1	110.1	1.25	81.0	100.9	1.25	72.43	88.35	1.22
	1.0	170.3	222.9	1.31	143.8	195.2	1.36	117.2	157.5	1.34
	3.0	324.6	404.2	1.25	232.7	331.9	1.43	149.2	238.6	1.6
10	0.1	22.99	18.5	0.8	21.29	18.07	0.85	20.49	17.66	0.86
	0.3	34.09	33.78	0.99	33.03	32.84	0.99	31.96	32.1	1.0
	1.0	60.04	67.83	1.13	57.16	66.0	1.15	56.29	64.4	1.14
	3.0	104.3	130.3	1.25	98.55	125.1	1.27	91.86	116.6	1.27
20	0.1	12.34	7.23	0.59	12.0	7.16	0.6	11.4	6.95	0.61
	0.3	17.21	12.62	0.73	16.96	13.07	0.77	16.35	12.76	0.78
	1.0	26.76	24.42	0.91	26.91	25.4	0.94	26.25	24.83	0.95
	3.0	42.65	45.36	1.06	44.02	47.95	1.09	42.0	45.71	1.09
30	0.1	8.77	3.68	0.42	8.36	3.52	0.42	7.88	3.44	0.44
	0.3	11.22	6.11	0.54	10.8	6.07	0.56	10.26	5.93	0.58
	1.0	15.92	11.39	0.72	15.47	11.33	0.73	14.84	11.07	0.75
	3.0	23.49	20.63	0.88	23.17	20.7	0.89	22.36	20.31	0.91
40	0.1	7.43	2.43	0.33	6.76	2.33	0.35	6.31	2.23	0.35
	0.3	8.83	3.57	0.4	8.2	3.47	0.42	7.69	3.31	0.43
	1.0	11.44	6.09	0.53	10.74	5.99	0.56	10.2	5.68	0.56
	3.0	15.57	10.57	0.68	14.81	10.5	0.71	14.21	10.18	0.72

5.2.3 The Damping Material Configurations

The most serious questions surrounding the viability of combining composite materials with dissipative polymer solid material pertain to their fabrication and the availability of standards for their design. In the design process, damping materials are combined in series to deform together. As such, and the thickness has to be determined following the stiffness and damping relationship between the polymeric honeycomb and 3M solid viscoelastic material. Actually, the thickness of the damper will be carefully considered so that it will not be too small that will lead to large strains. Thus, the combining methods dealing with arrangement and mixing ratio between the two materials tend to be critical for the performance of the damper. The following assumptions are made in studying the combinations of both materials.

1. There is only in-plane shear deformation in the combined damping materials. Therefore, passive damping is only generated by the shear deformation.
2. Bonding is perfect; both honeycomb and solid viscoelastic materials should deform together.
3. There is no relative transverse motion between different layers.
4. FRP skin plates are elastic and dissipate insignificant amount of energy relative to the damping materials.

Based on these assumptions, simplified relationships for combining damping materials are established. Fig. 5-4 presents a schematic representation of idealized force-displacement relationship. For stiffness (K) and energy dissipation capacity (E),

$$\sum K_{\text{combine}} = K_{\text{honeycomb}} + K_{\text{viscoelastic}} \quad (5-1)$$

$$\sum E = E_{\text{honeycomb}} + E_{\text{viscoelastic}} \quad (5-2)$$

However, because $K_{\text{viscoelastic}}$ is too small relative to the stiffness of polymer honeycomb, it is assumed that K_{total} is equal to the honeycomb stiffness before the bonding scrim failure.

When combining viscoelastic composite materials, it is clear that one has to take into account the effect of ambient temperature and excitation frequency for an effective application of the material

in structural damping applications. The damper properties to a certain degree are dependent on the number of loading cycles and the range of deformation, especially under large strain due to temperature increases within the damper material. These are critical parameters that need careful consideration before applying the combined damper in a multi-layer panel system as well as other PMC infill systems having passive energy constrained damping layers.

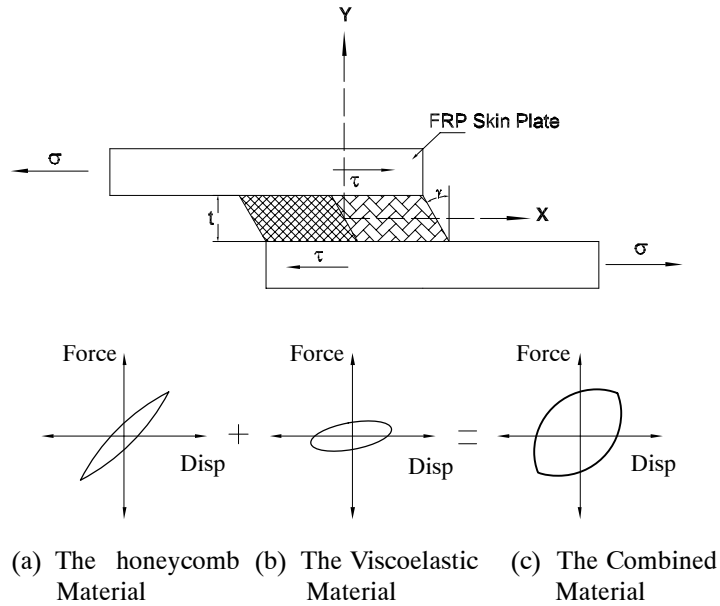
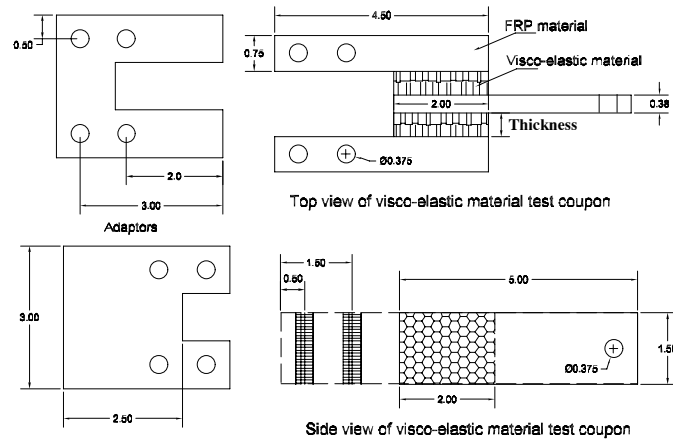


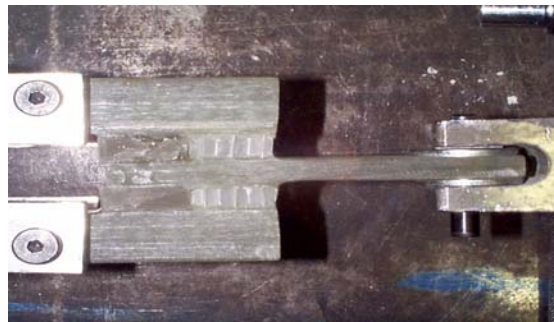
Figure 5-4 Schematic Presentation of the Idealized Force–Displacement Relation

5.3 Description of Test Setup

As mentioned earlier, the materials chosen for the combination were polymer honeycomb and 3M solid viscoelastic material. A typical test specimen consists of layers of such materials bonded with FRP skin plates as shown in Fig. 5-5.



(a)



(b)

Figure 5-5 Test Coupon (a) Design; (b) Configuration (unit = inch)

A test specimen subjected to longitudinal force dissipates energy through direct shearing of the combined composite materials as shown in Fig. 5-6. All tests were conducted in frequency domain on an MTS hydraulic actuator using a sinusoidal strain as input and measuring the stress output. The experiments described in this study consist of two cases ; (1) polymer honeycomb only, and (2) the combination of the polymer honeycomb and 3M viscoelastic solid. For the solid viscoelastic material, the test data were provided by 3M Japan Corp. The purpose of the first testing case was to assess the properties of the polymer honeycomb material, and to evaluate the potential enhancements when

combined with 3M viscoelastic material. These results should provide clear evidence for the effectiveness of combining polymeric materials, and serve as a means for validating the computational modeling of the polymer honeycomb. All tests were performed under both monotonic and cyclic loading condition with different strain and frequency ranges. Tables 5-2 and 5-3 present test specimen dimensions. The results show the first 20 cycles of the target displacement specified in Table 5-3 at the frequencies of 0.1, 1.0, and 3.0 Hz. For instance, Test 1 (5%) of Sample 1 means the specimen was subjected to 20 cycles of the maximum displacement amplitude of 0.01 in at the frequencies 0.1, 1.0, and 3.0 Hz, respectively.

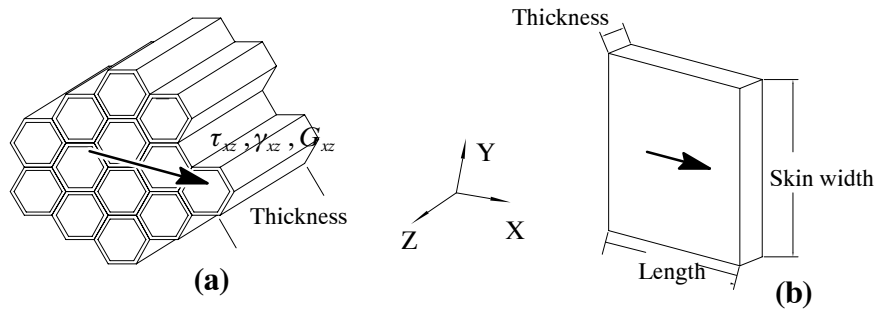


Figure 5-6 Longitudinal Force on Each Surface (Direct Shear) :
(a) polymer Honeycomb; (b) 3M Viscoelastic Solid

Table 5-2 The Dimensions of Test Specimens

	Dimension (Unit = inch)			
	Length	Width	Thickness	Skin plate's thickness
Sample 1	2.0	1.5	0.197	1.02
Sample 2	2.0	1.5	0.394	0.87
Sample 3	2.0	1.5	0.512	0.75

Table 5-3 The Loading Patterns Based on the Displacement Control

	Sample 1	Sample 2	Sample 3
Thickness Type	0.197 in (5 mm)	0.394 in (10 mm)	0.512 in (13 mm)
Test 1 (5%)	0.01 in	0.02 in	0.026 in
Test 2 (10%)	0.02 in	0.04 in	0.051 in
Test 3 (30%)	0.06 in	0.12 in	0.15 in
Test 4 (50%)	0.098 in	0.2 in	0.256 in

5.4 Experimental Results

Several parameters were studied in the experimental phase to evaluate the effective stiffness, ultimate strength, and the area of hysteretic loops, whereby the area enclosed in each loop represents the energy dissipated by the damper per cycle.

5.4.1 *Polymer Honeycomb Material Testing*

Several polymer honeycomb specimens with thickness of 0.197 inch, 0.394 inch, and 0.512 inch were tested under monotonic loading condition to evaluate the stiffness relative to thickness. Each selected thickness was determined by the commercial product dimensions. Fig. 5-7 and 5-8 present the test results of polymer honeycomb material for different thicknesses. Table 5-4 shows a summary of the results evaluated by the experimental force–displacement relationship.

Stiffness is defined here as the shear force required to cause a displacement that corresponds to 5% strain. From this table, one can observe that the stiffness is inversely proportional to the thickness. However, it is clearly shown that the thickness of the honeycomb has little effect on stiffness over 0.394 in thickness. Shear stress-strain relationships, for different thicknesses, are obtained to measure basic mechanical properties that are needed for analysis. At different frequencies of loading, the variations of stiffness and strength for each thickness are shown in Fig. 5-9 and 5-10. In addition, Fig. 5-11 shows the deformed shape of each test coupon during the tests.

From cyclic loading tests, the hysteretic behavior for various geometric conditions was studied, and basic relationships for the effective stiffness and damping were obtained. In the experimental phase, force-displacement relationship was monitored and evaluated under different frequencies. Fig. 5-12 and 5-13 show the hysteretic behavior of polymer honeycomb for different thicknesses at different frequencies. It is evident that the polymer honeycomb material is not dependent on the frequency even though it is made of a visco-elastic polymer. This is a significant difference between the polymer honeycomb and a solid polymeric material.

Fig. 5-14 to 5-19 present the behavior of the honeycomb for different honeycomb area. To investigate these effects, three specimens were tested to assess the contribution of various geometrical con-

figurations. These test results were divided into two strain ranges; before and after bonding scrim failure. Before bonding scrim failure, the effective stiffness of the honeycomb is proportional to the area. That is, the work put into material is proportional to the area under the stress-strain curve. Accordingly, the effective stiffness relationship will be drawn to correspond with honeycomb area ratio. Alternatively, after bonding scrim failure, the effective stiffness will be sustained by slight bonding and friction capacity.

Table 5-5 shows the summary of the test results for different geometrical honeycomb configurations. These results clearly show that the effective stiffness is proportional to the area regardless of arrangements. Based on the test results, Fig. 5-20 shows the relationship between the area ratio and effective stiffness.

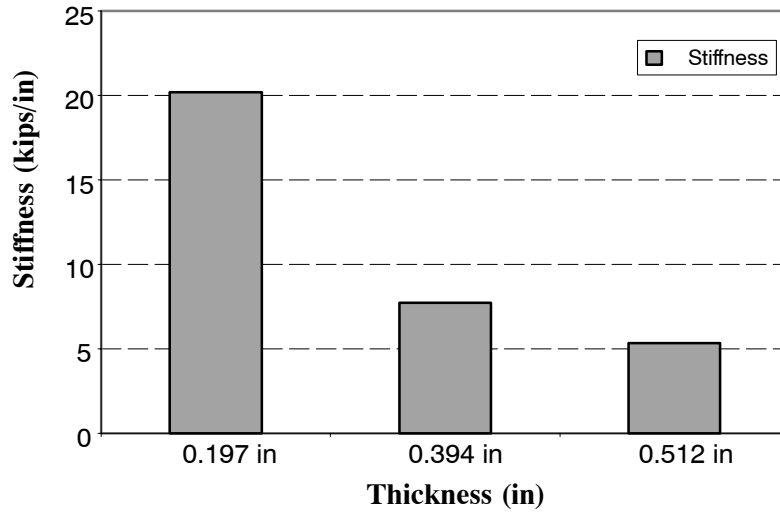


Figure 5-7 The Comparison of the Stiffness for Different Thicknesses

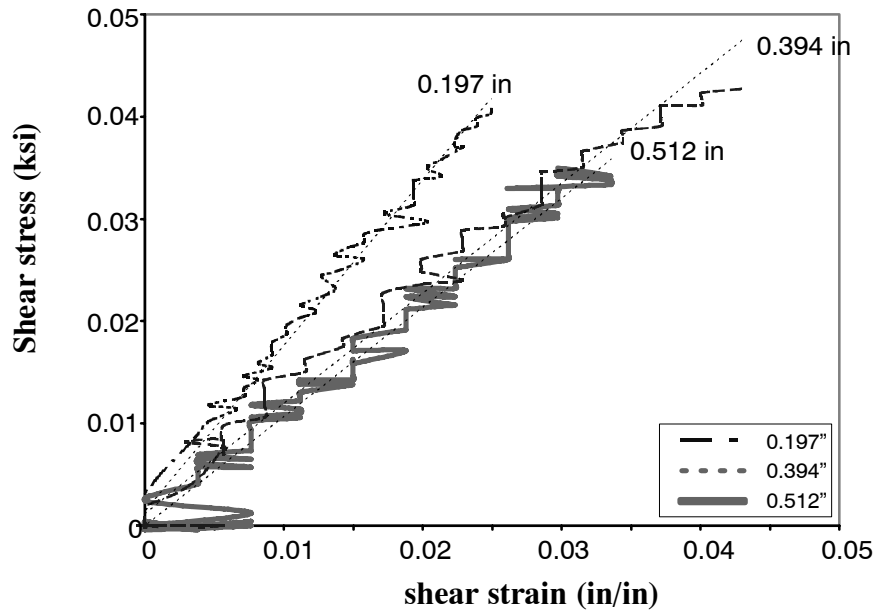


Figure 5-8 The Comparison of the Shear Modulus for Each Thickness

Table 5-4 The Results of Monotonic Loading Tests

Thickness	0.197 in	0.394 in	0.512 in
Initial Stiffness (kips/in)	20.17	7.71	5.32
Shear Modulus (ksi)	1.6	1.16	1.078

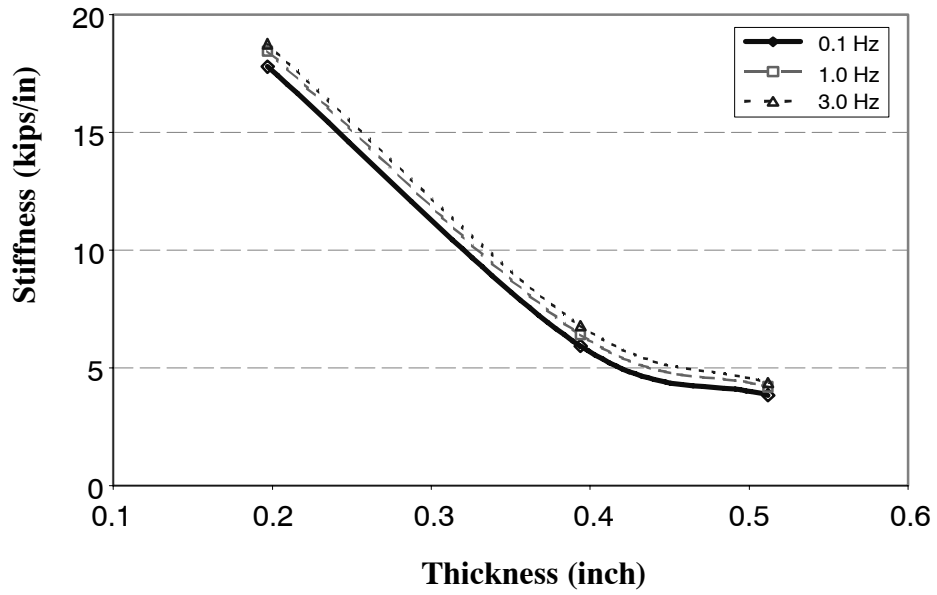


Figure 5-9 The Variation of Stiffness for Different Frequencies (5% Strain)

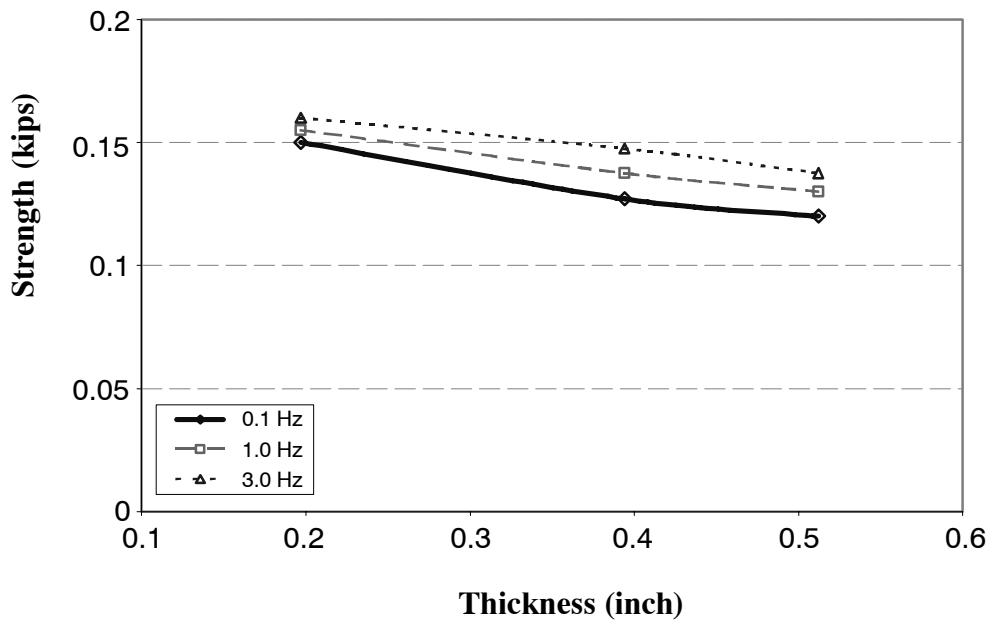
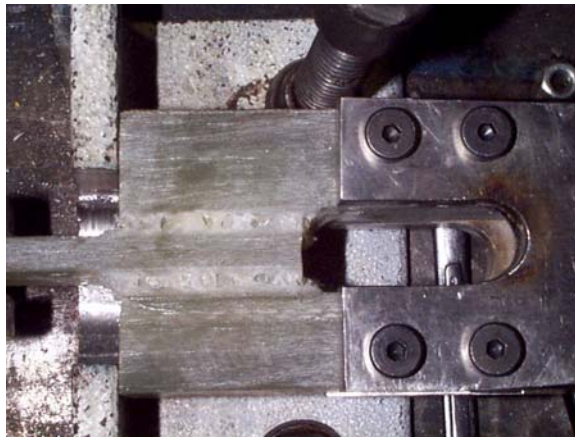
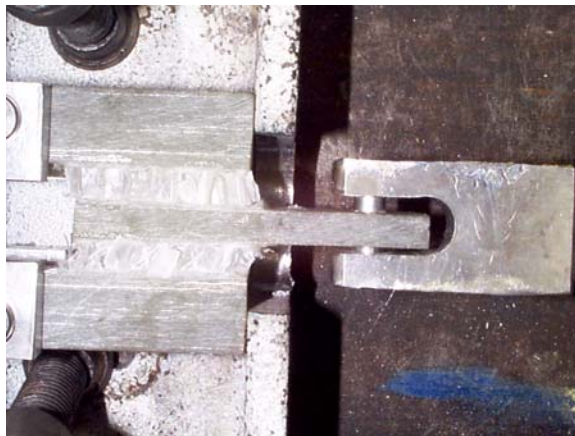


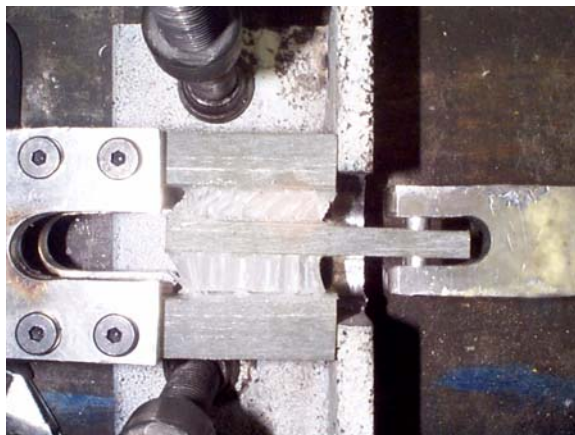
Figure 5-10 The Variation of Strength for Different Frequencies (5% Strain)



(a) 0.197 in Honeycomb Sample



(b) 0.394 in Honeycomb Sample



(c) 0.512 in Honeycomb Sample

Fig. 5-11. Deformed Shape of Polymer Honeycomb Material Tests at Different Frequencies (10% strain)

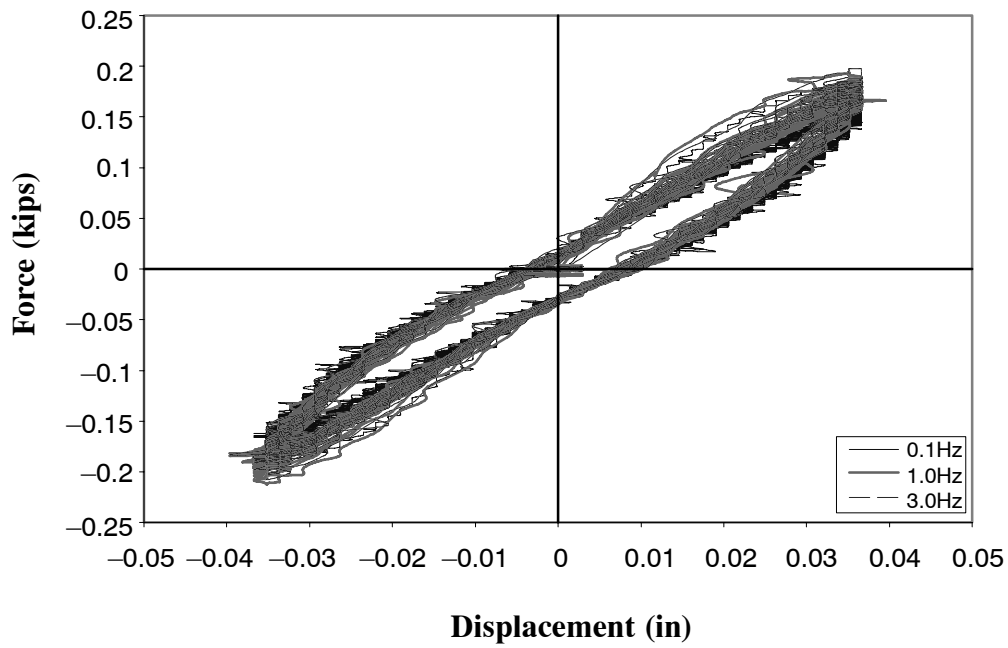


Fig. 5-12. Hysteresis Loops of Sinusoidal Test for Different Frequencies (10% strain, 0.394 in. thickness)

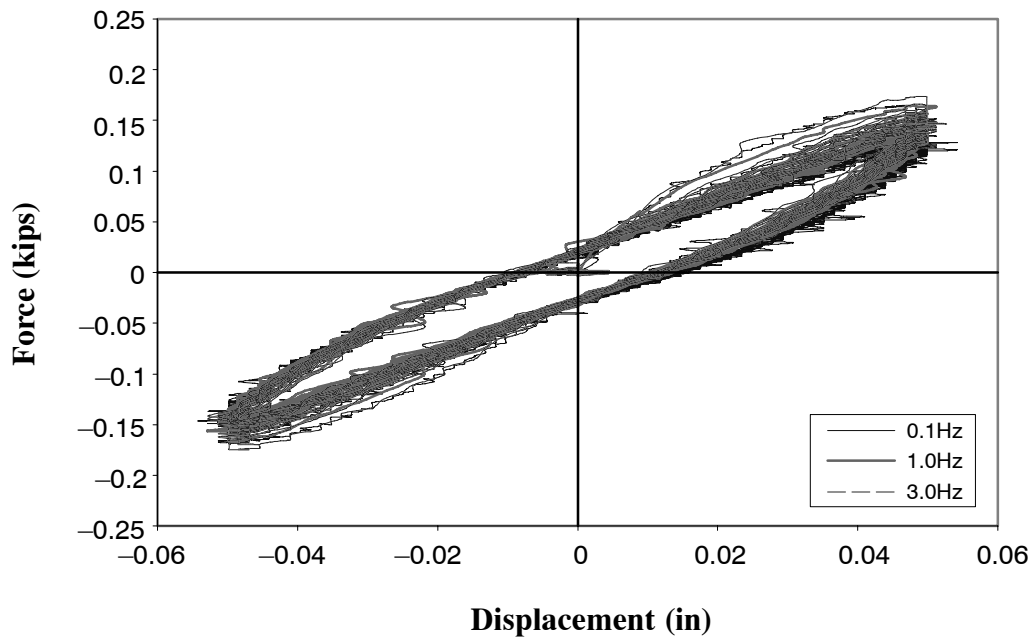


Fig. 5-13. Hysteresis Loops of Sinusoidal Test for Different Frequencies (10% strain, 0.512 in. thickness)

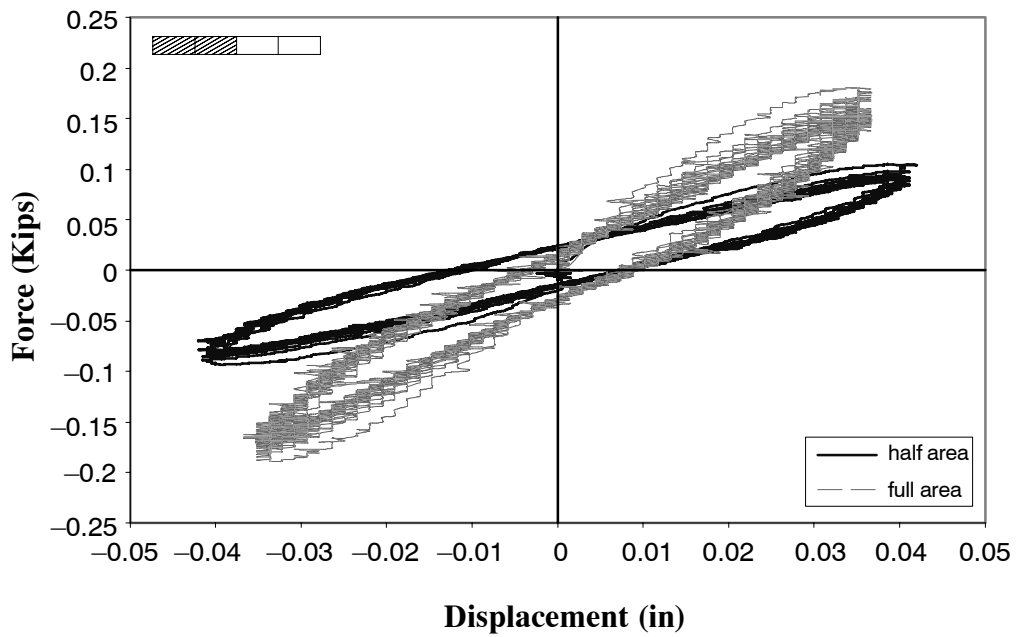


Fig. 5-14. The Result of Honeycomb Material with Different Area (Case 1, 10% strain)

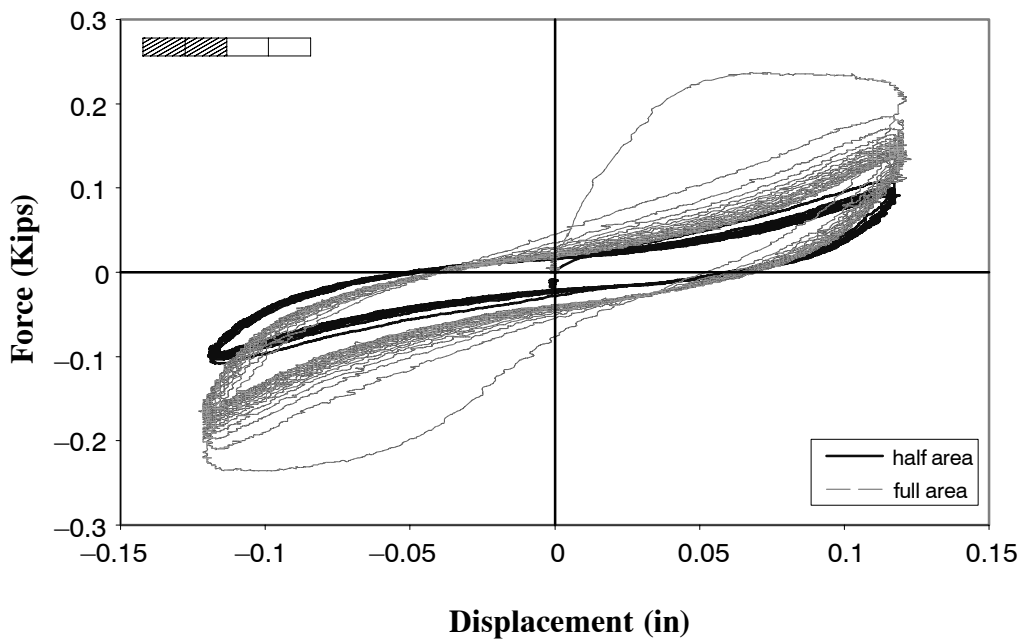


Fig. 5-15. The Result of Honeycomb Material with Different Area (Case 1, 30% strain)

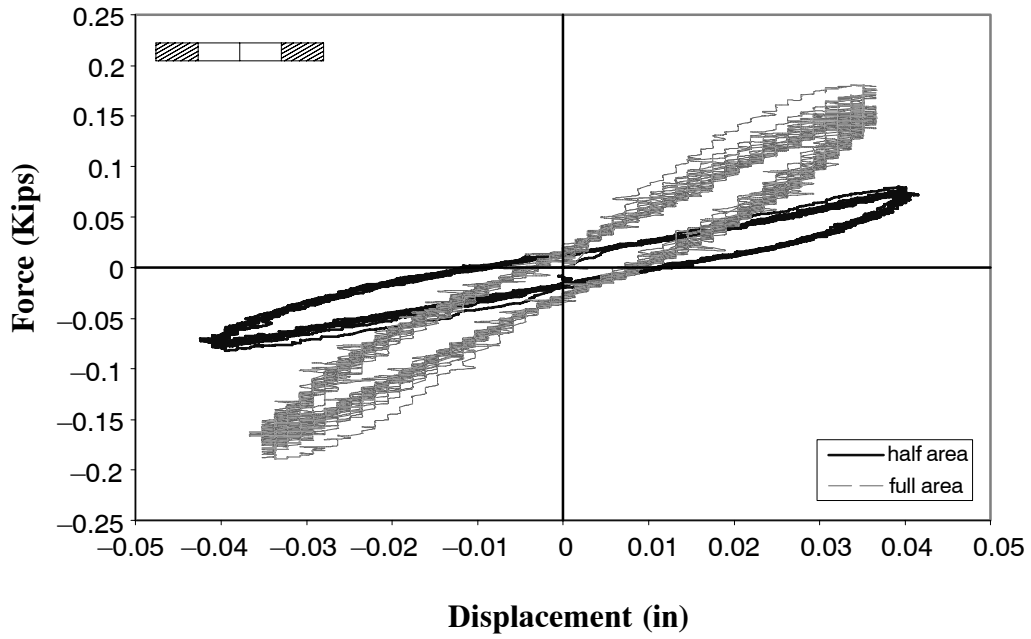


Figure 5-16 The Result of Honeycomb Material with Different area (Case 2, 10% strain)

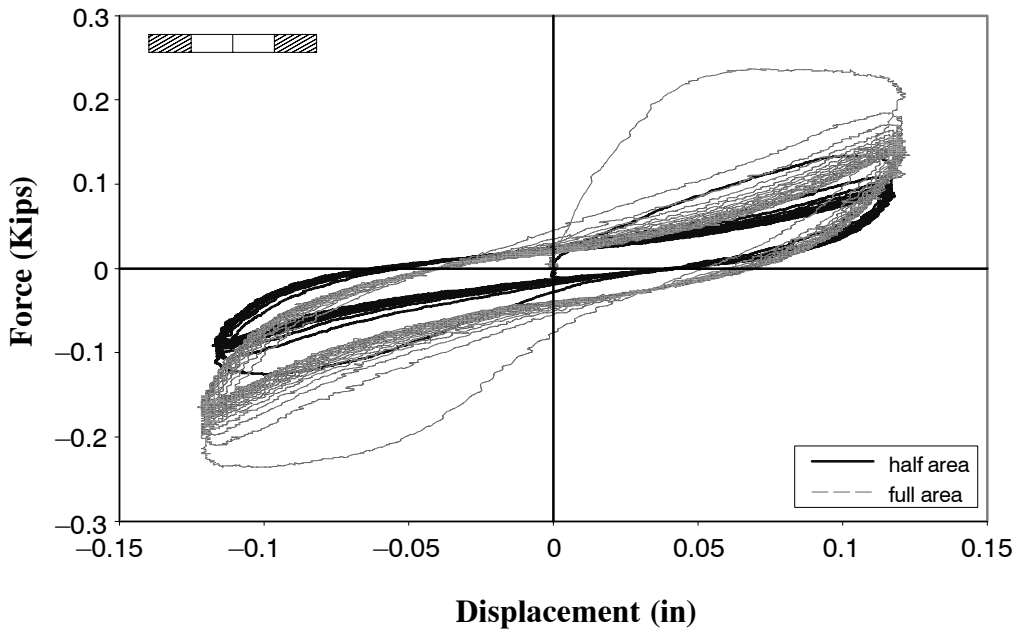


Figure 5-17 The Result of Honeycomb Material with Different Area (Case 2, 30% strain)

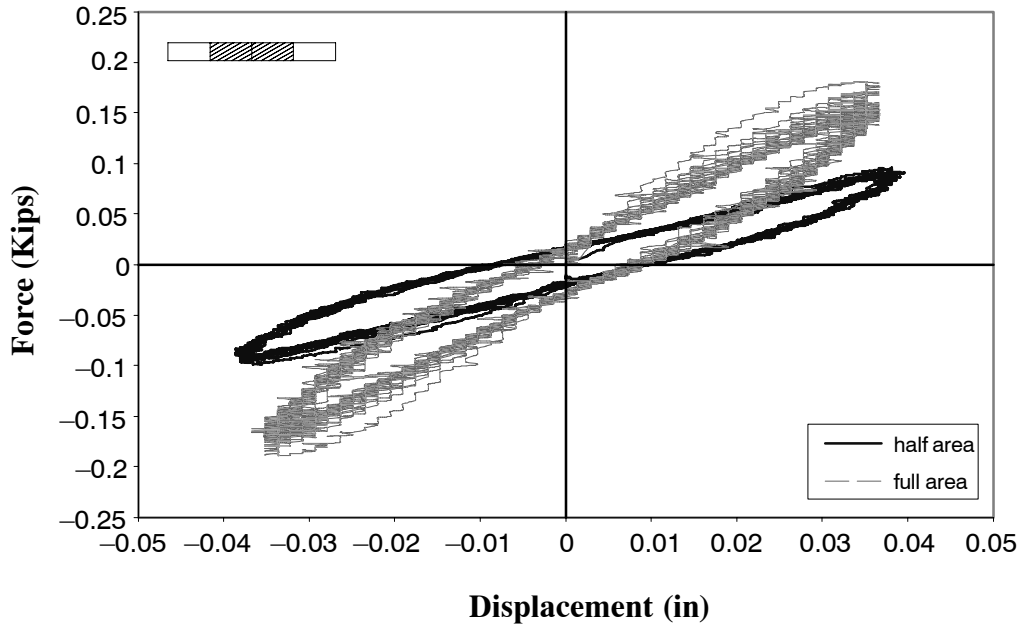


Figure 5-18 The Result of Honeycomb Material with Different area (Case 3, 10% strain)

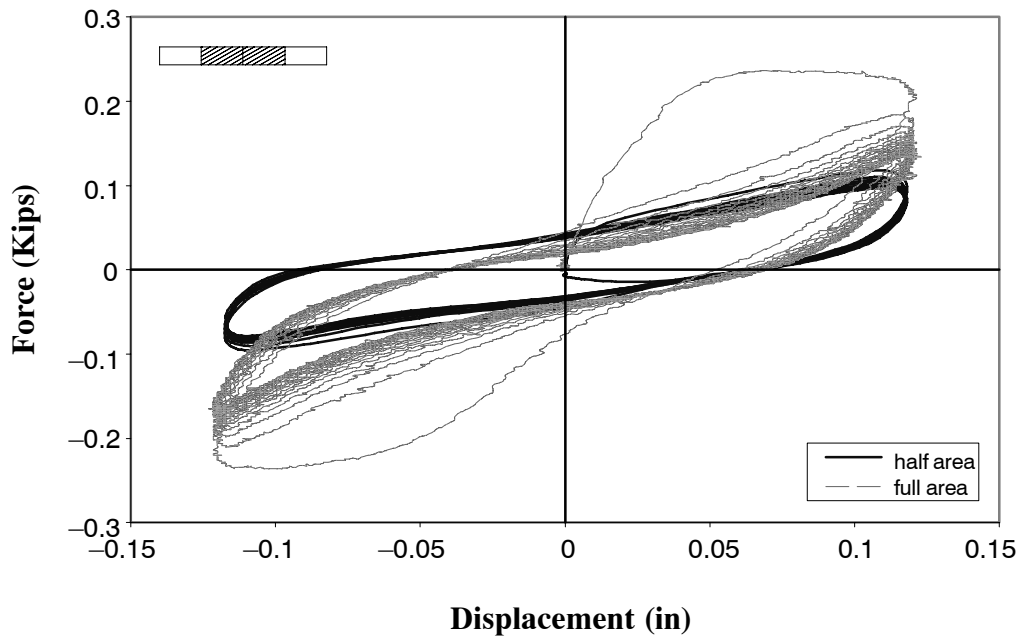

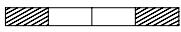



Figure 5-19 The Result of Honeycomb Material with Different Area (Case 3, 30% strain)

Table 5-5 The Summary of the Effective Stiffness for Area & Combination (kips/in)

Area Types	Magnitude	Half Area	Full Area
 (1)	Small Strain (10% Strain rate)	2.06	4.45
	Large Strain (30% Strain rate)	0.66	1.12
 (2)	Small Strain (10% Strain rate)	1.7	4.45
	Large Strain (30% Strain rate)	0.67	1.12
 (3)	Small Strain (10% Strain rate)	2.23	4.45
	Large Strain (30% Strain rate)	0.58	1.12

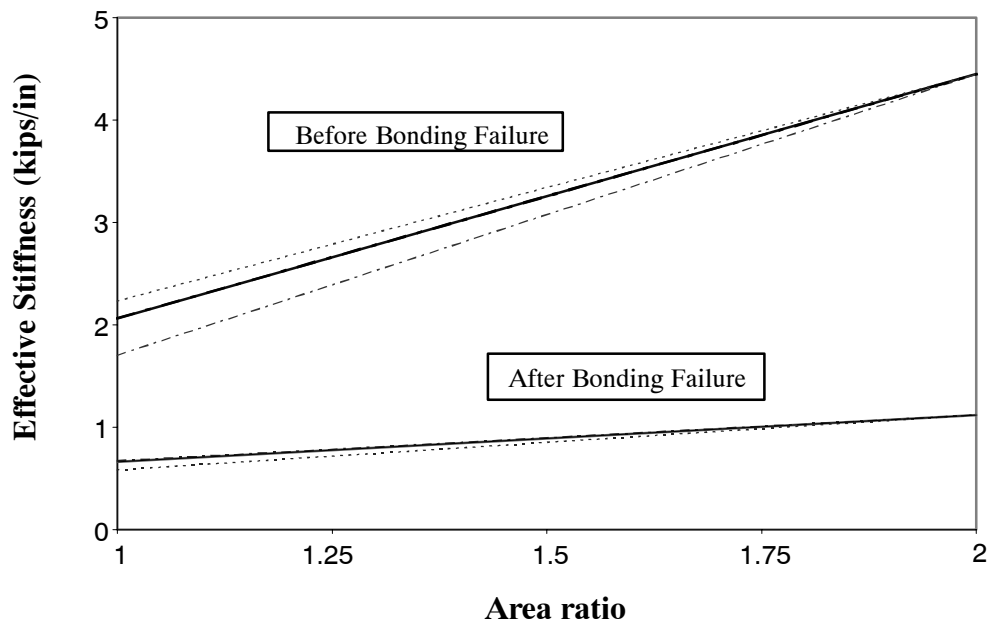


Fig. 5-20. The Variation of Effective Stiffness for the Area Ratio

5.4.2 Testing of Combined Honeycomb and Viscoelastic Material

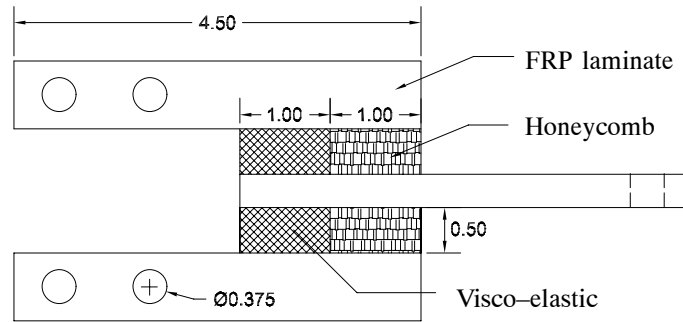
The testings used a sinusoidal loading protocol for the combined composite materials were performed on an MTS hydraulic loading actuator. The same procedures, similar to those employed in the testing of polymer honeycomb, were imposed on these tests in order to investigate the effects of combining honeycomb and viscoelastic material. Based on various fabrication considerations, three test coupons were chosen. Fig. 5-21 shows the configuration of each test coupon each of which is having a 0.394 inch thickness. For the investigation of the different thickness effect, an additional test coupon (V-H-V type) with 0.197 inch thickness was also fabricated, where V stands for viscoelastic material and H stands for polymer honeycomb material.

Fig. 5-22, 5-23, and 5-24 present the relationship between the stiffness and the energy dissipation for different thicknesses. As mentioned before, depending on the thickness, the stiffness of polymer honeycomb varies from very stiff to very flexible before its failure. To study the behavior of the multi-layered PMC infill panel proposed in section 4, a thickness of 0.394 inch sample was chosen in this study.

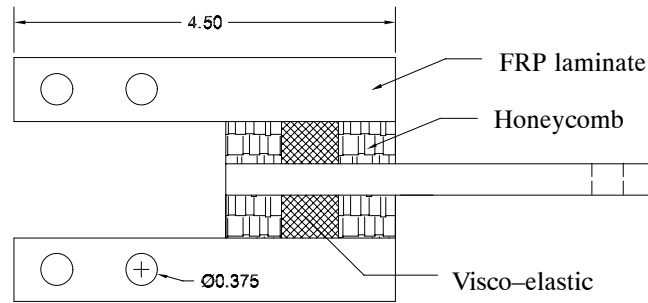
The initial and after scrim-breaking stiffness for different combination cases were evaluated under monotonic loading condition. Fig. 5-25 and 5-26 show the stiffness at the initial stage and post-breaking stages. The variation of the stiffness mainly resulted from the progressive loss of the honeycomb resistance. For an increased strain rate, the degradation of the stiffness for each system is also shown in Fig. 5-27. Similar to the behavior of the honeycomb, it was observed that the combined material system start to loose its stiffness at 15 to 20% strain. Beyond that point, the overall stiffness is reduced significantly. Based on the polymer honeycomb and the combined composite material tests, the results agree well and the overall stiffness will be primarily governed by honeycomb behavior. For the investigation of the behavior with respect to the different combining configurations, the specimens with different arrangements were tested using sinusoidal loading. By examining their hysteretic behavior, one can observe that there is no significant difference among the three cases. It is noted that energy absorbing capacity in the combined composite material system is not depen-

dent on their arrangement as evident in Fig. 5-27 and 5-28. Conclusively, two parameters such as bonding scrim capacity of the polymer honeycomb material and area are the primary factors affecting the behavior of the combined composite material system. Various test specimens having different arrangements and their shear deformations are shown in Fig. 5-29, 5-30, and 5-31.

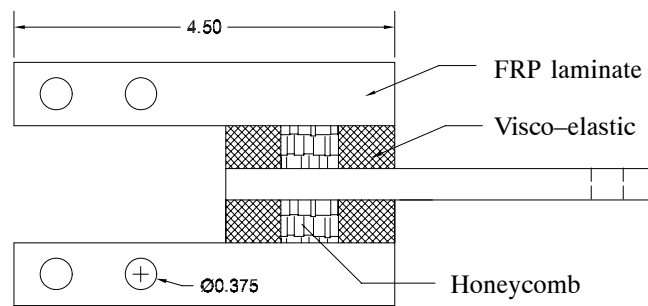
Furthermore, it is shown in Fig. 5-32 that by comparing the two test systems, combined with solid viscoelastic material, it is evident that energy dissipation of the combined solid viscoelastic damping system is significantly enhanced. Fig. 5-33 presents two different pure damping systems which were composed of (1) the original honeycomb, and (2) combined composite materials. The difference between both cases is the portion of honeycomb area. The frequency response of the systems was measured, and the area of each hysteretic loop was used to evaluate the damping characteristics.



(a) [V-H] layer



(b) [H-V-H] layers



(c) [V-H-V] layers

Fig. 5-21. Test Samples (H = Polymer Honeycomb, V = Solid Viscoelastic, unit=inch)

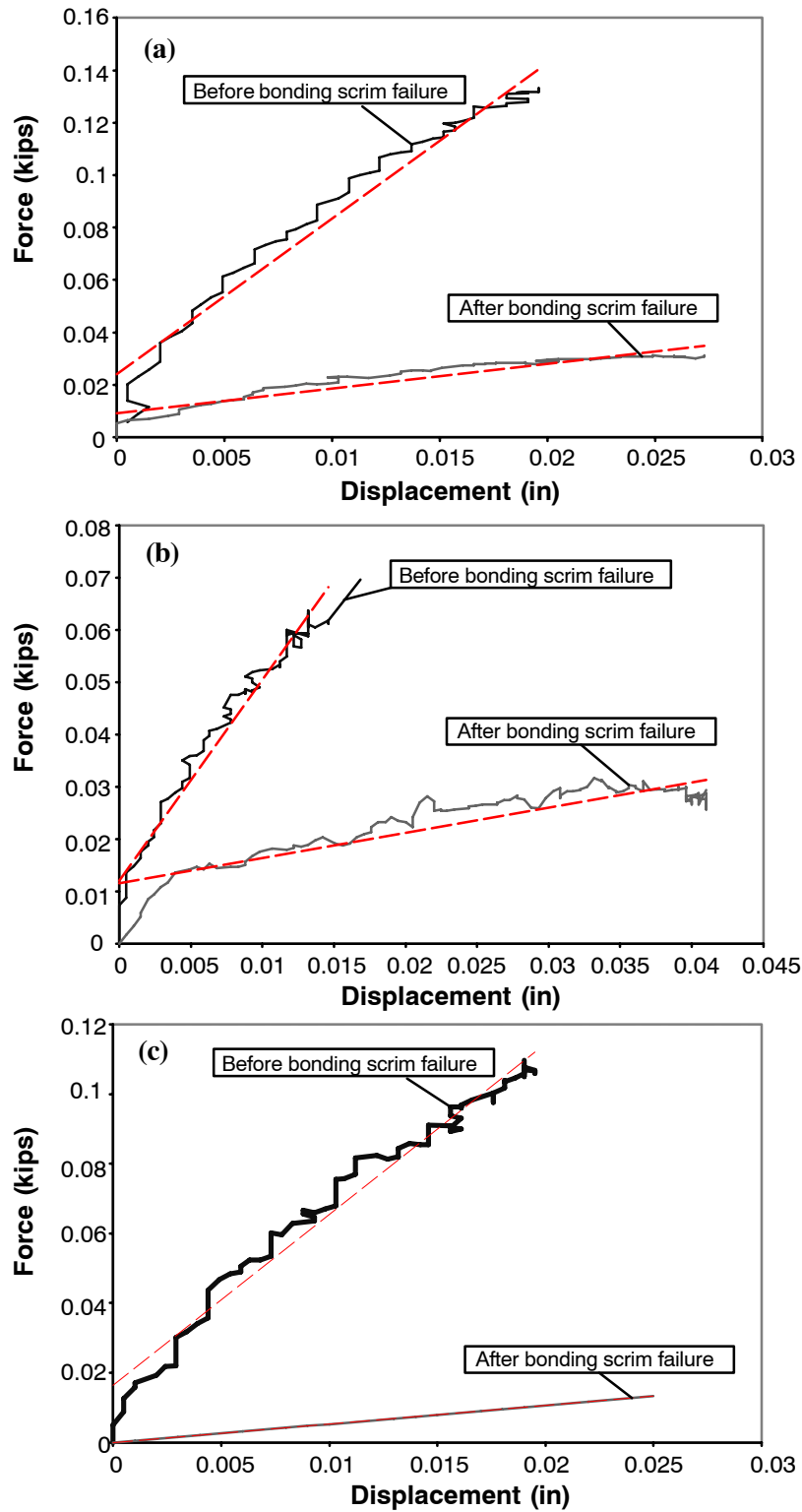


Fig. 5-22 Results of the Initial and Post Stiffness for Combining Composite Materials with Different Thickness (Viscoelastic/Honeycomb/Viscoelastic): (a) 0.197 in (b) 0.394 in (c) 0.512 in

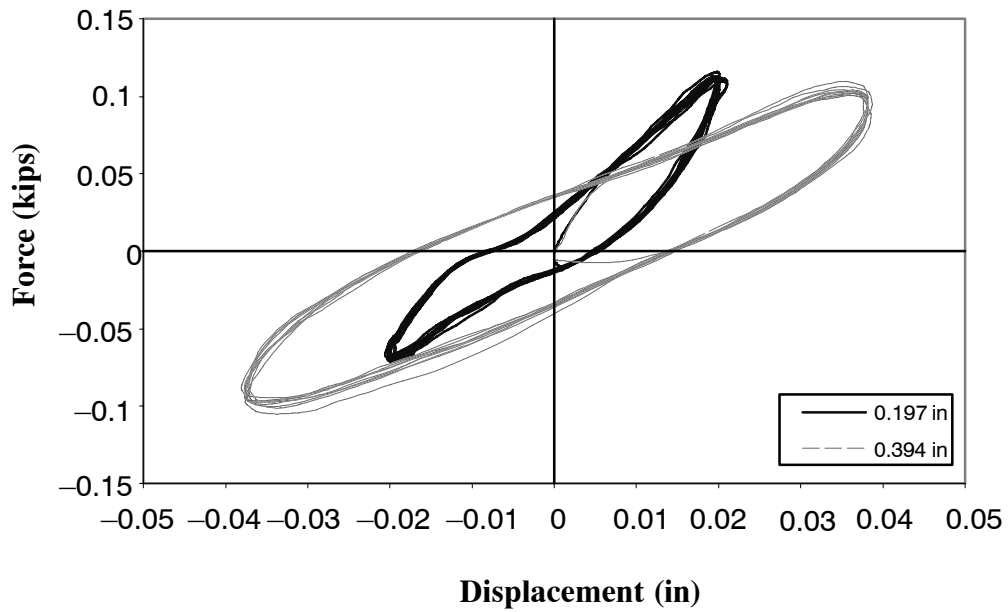


Fig. 5-23. Results of the Hysteresis Loops for Combining Composite Materials with Different Thickness (10% Strain, 1.0 Hz)

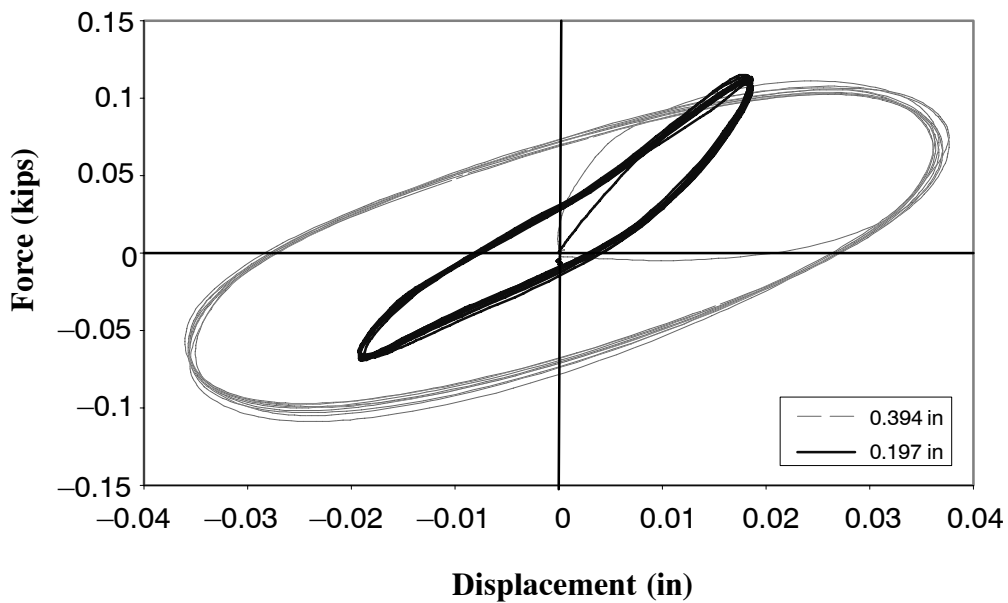


Fig. 5-24. Results of the Hysteresis Loops for Combining Composite Materials with Different Thickness (10% Strain, 3.0 Hz)

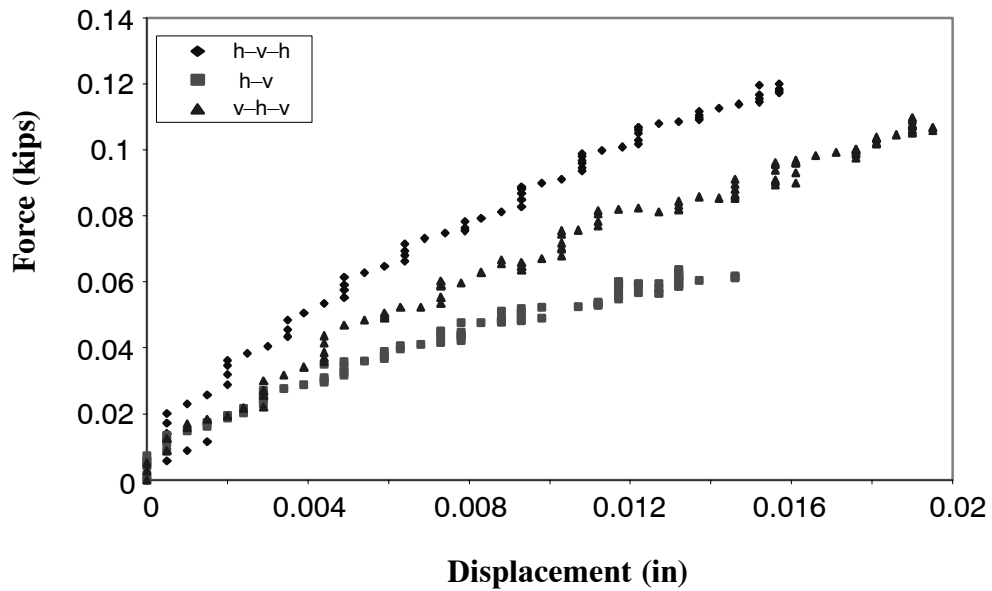


Fig. 5-25 Comparison of the Stiffness of Each Combination: Initial Stiffness

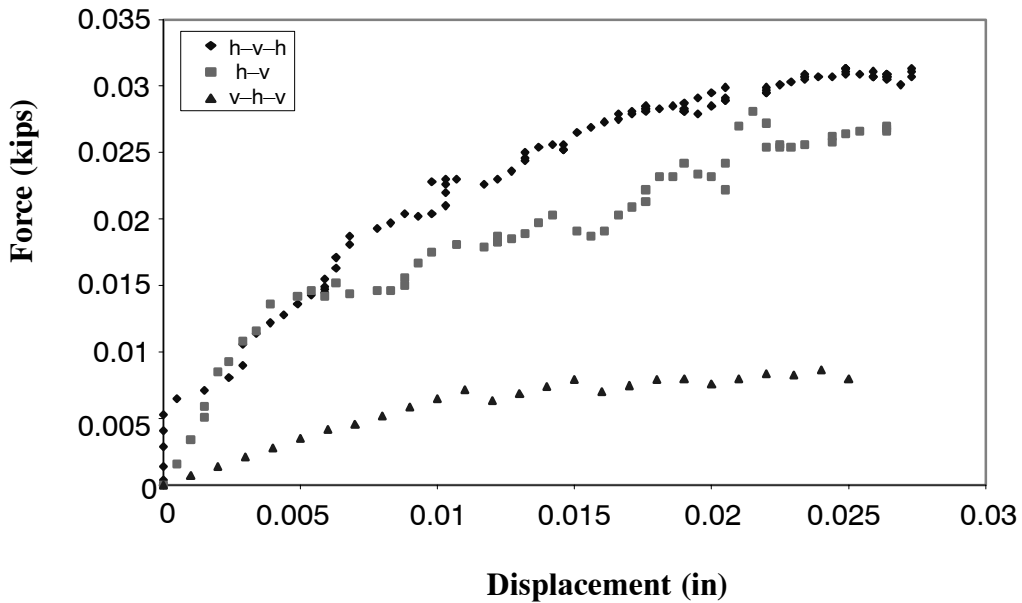


Fig. 5-26 Comparison of the Stiffness of Each Combination: Post Failure Stiffness

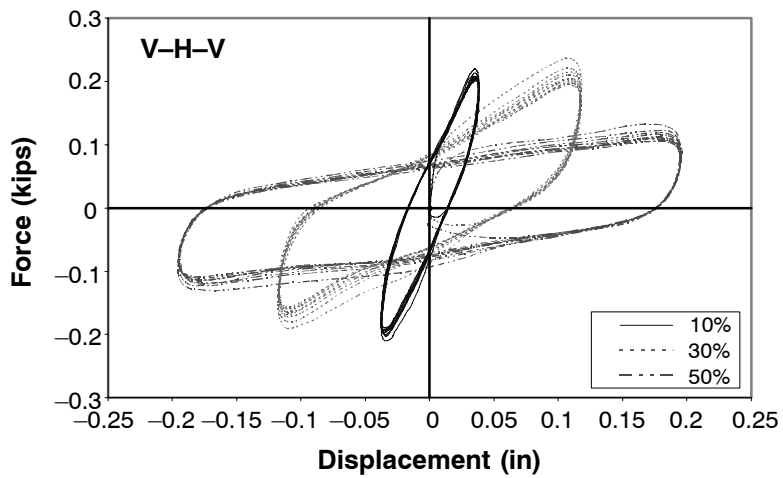
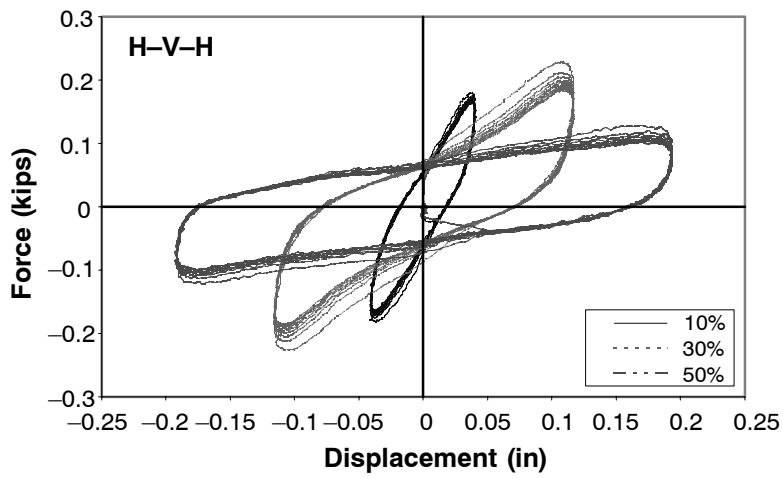
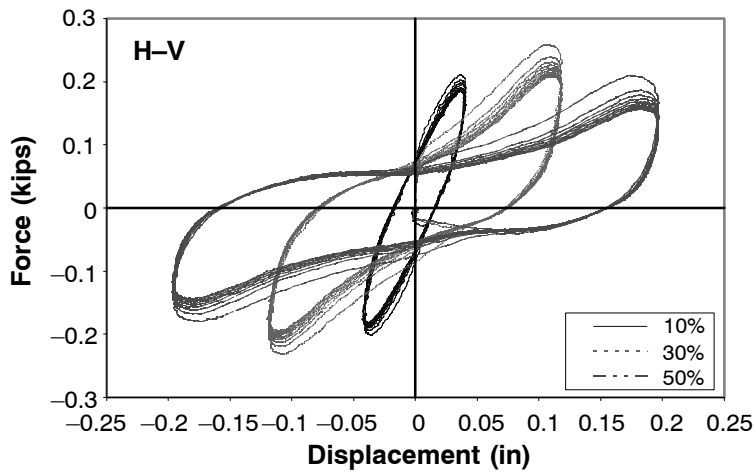


Figure 5-27 Test Results for Stiffness Degradation

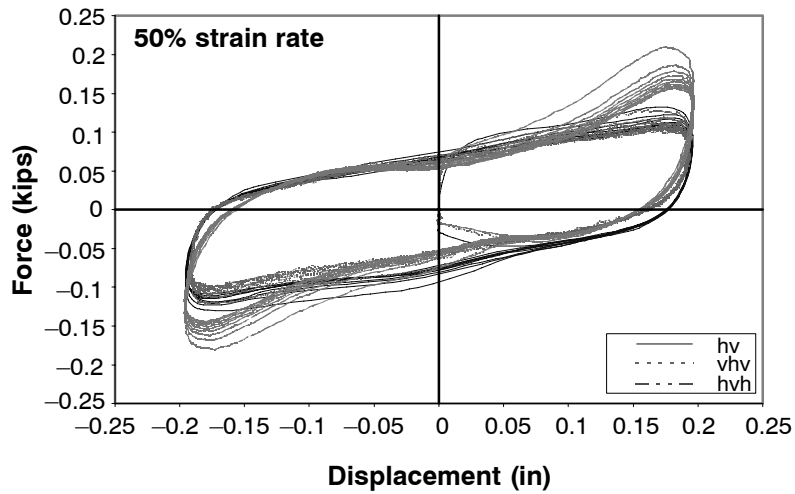
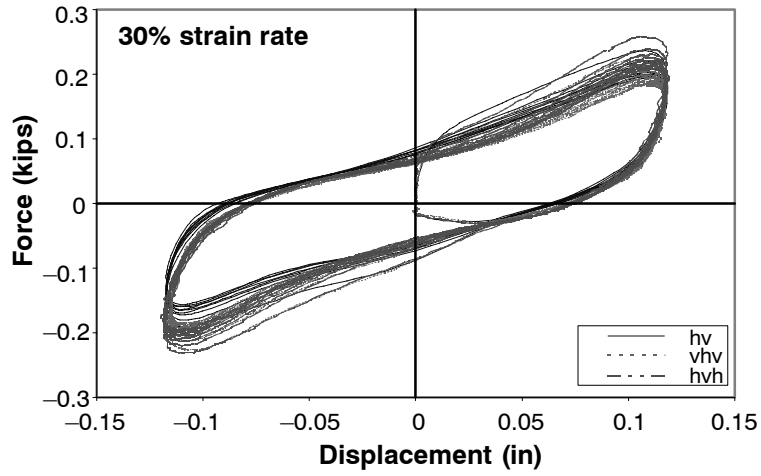
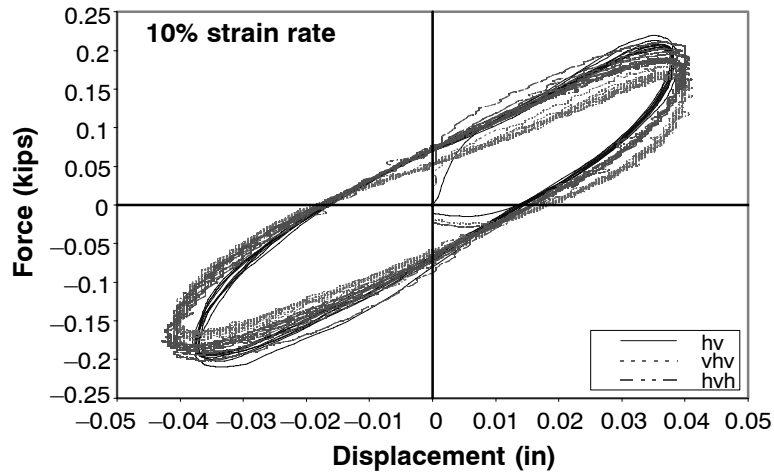
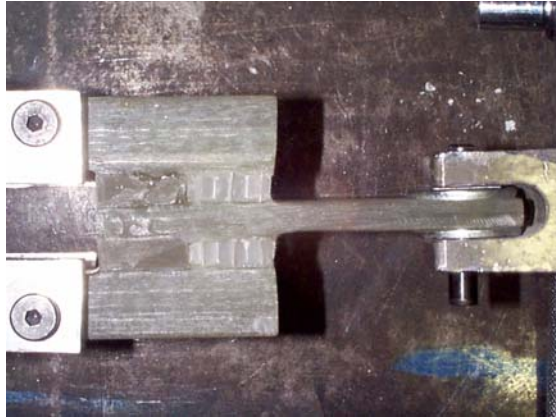
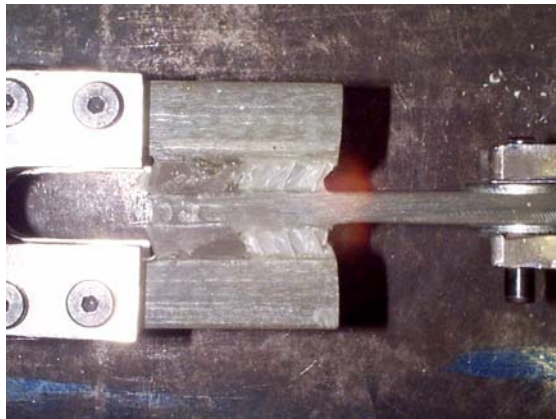


Figure 5-28 Test Results for each case ($f = 1.0$ Hz)



(a) Test Specimen Setup

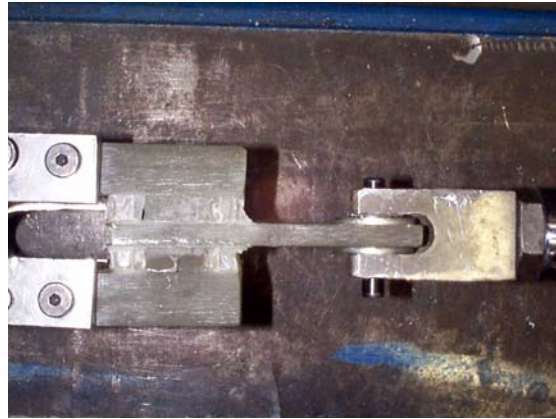


(b) Deformation of Test Sample

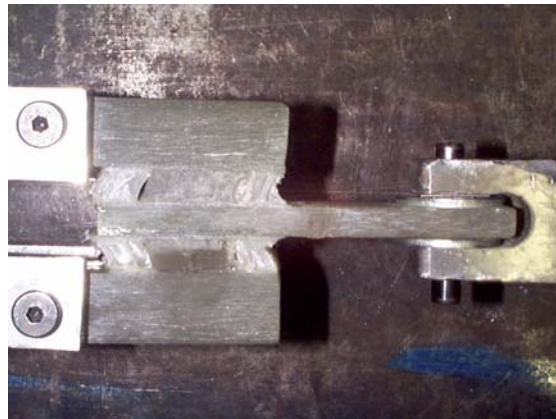


(c) Bonding Failure of Honeycomb

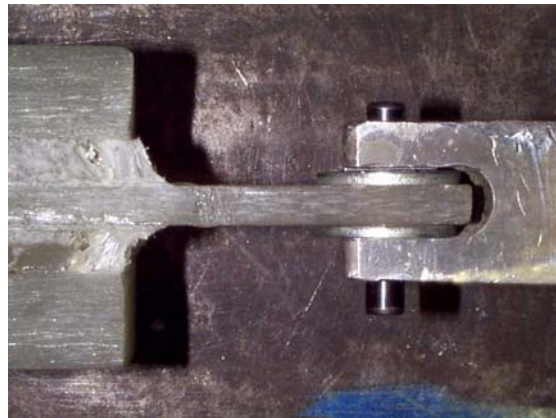
Figure 5-29 The Combined Honeycomb/Viscoelastic (H-V) Specimen Test



(a) Test Specimen Setup

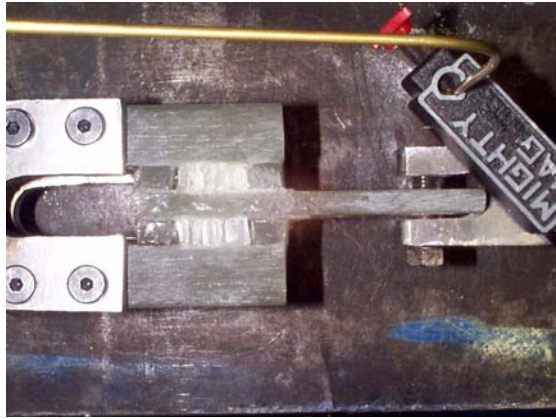


(b) Deformation of Test Sample

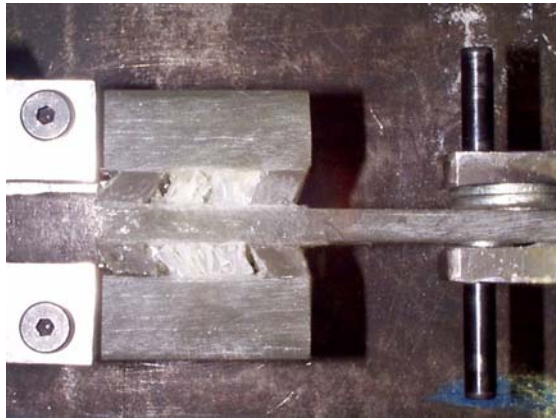


(c) Bonding Failure of the Honeycomb

Figure 5-30 The Combined Honeycomb/Viscoelastic/Honeycomb (H-V-H) Specimen Test



(a) Test Specimen Setup

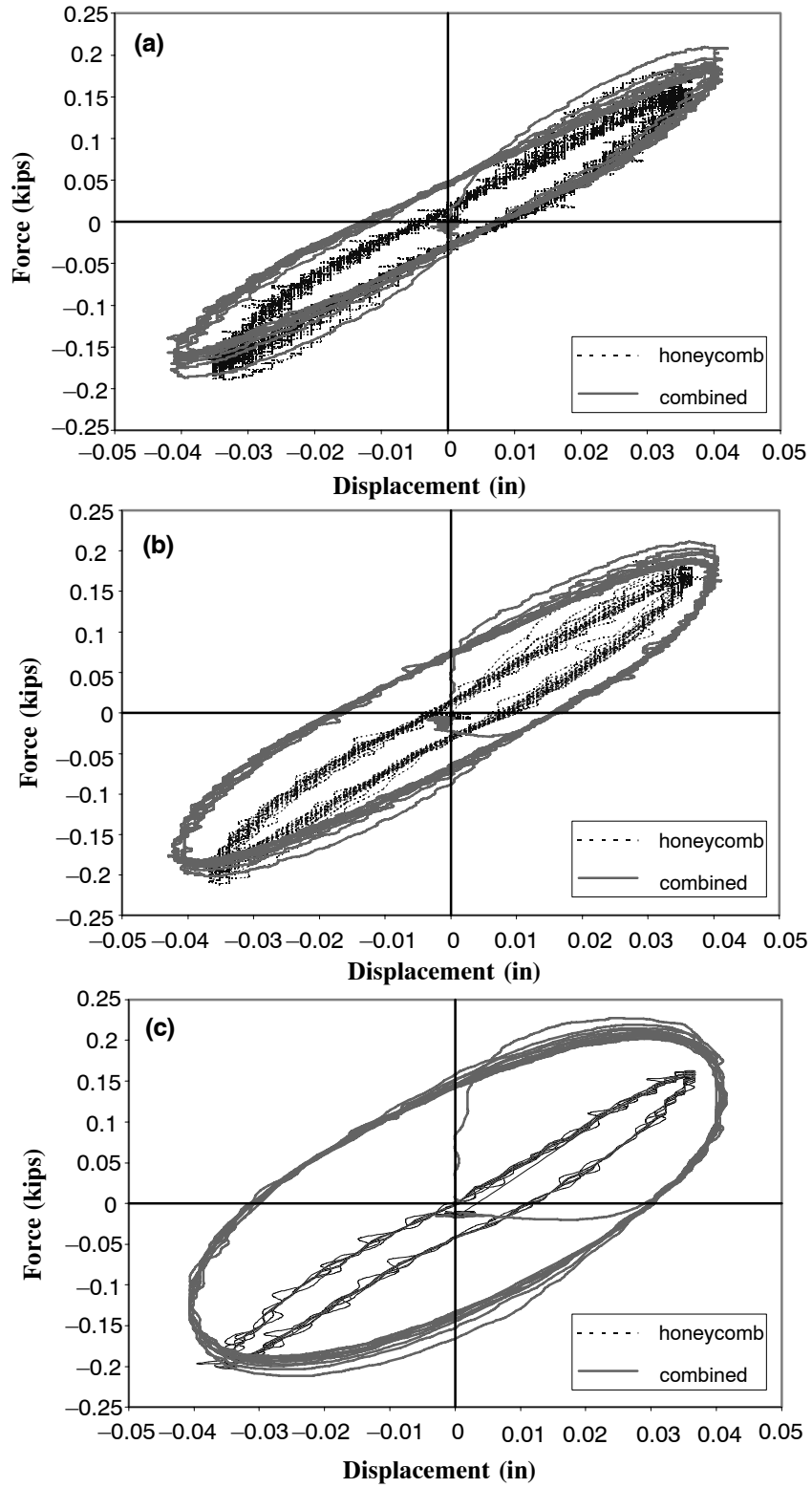


(b) Deformation of Test Sample



(c) Bonding Failure of the Honeycomb

Figure 5-31 The Combined Viscoelastic/Honeycomb/Viscoelastic (V-H-V) Specimen Test



**Figure 5-32 The Effect of the 3M Viscoelastic Materials for Different Frequencies:
 (a) 0.1 Hz (b) 1.0 Hz (c) 3.0 Hz**

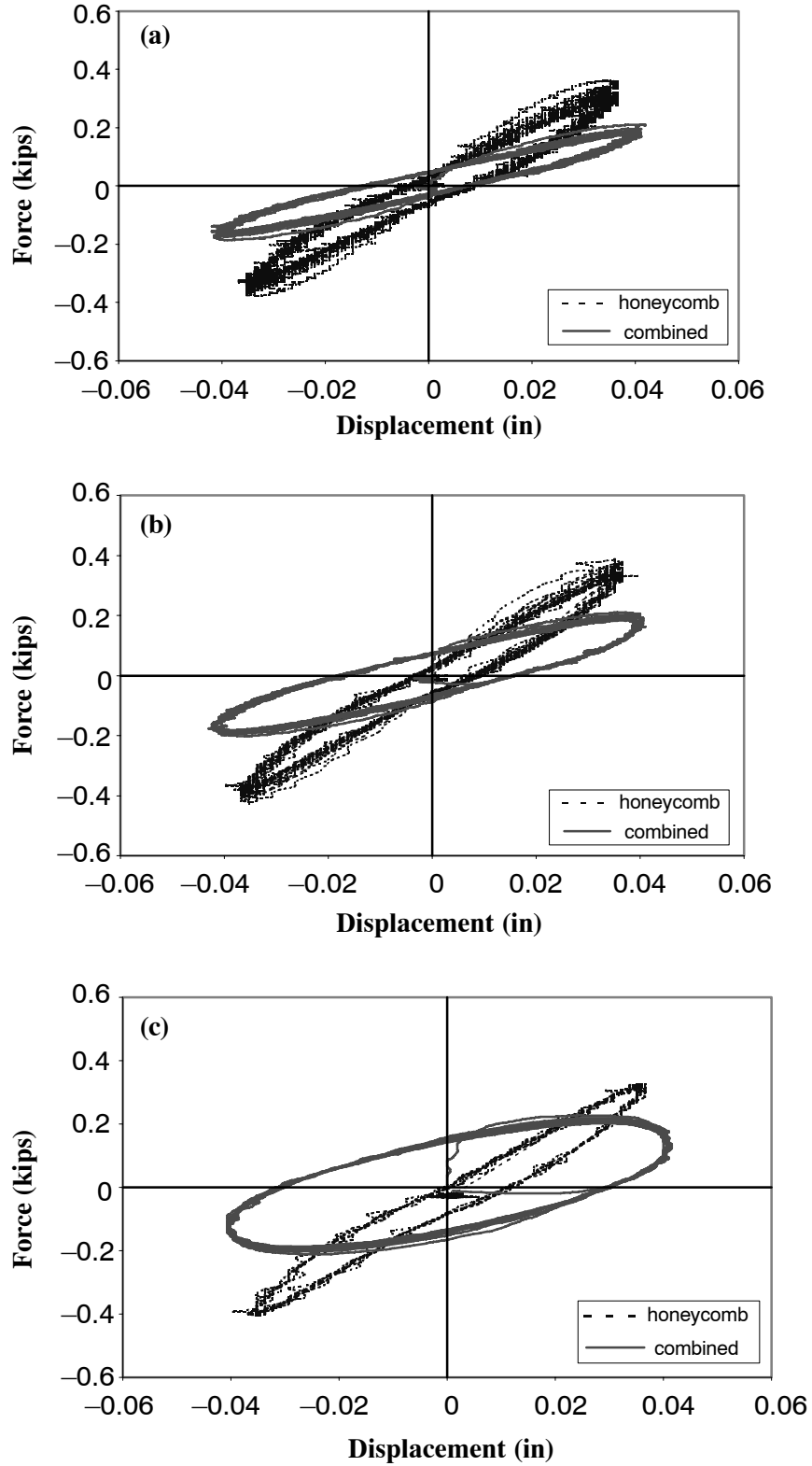
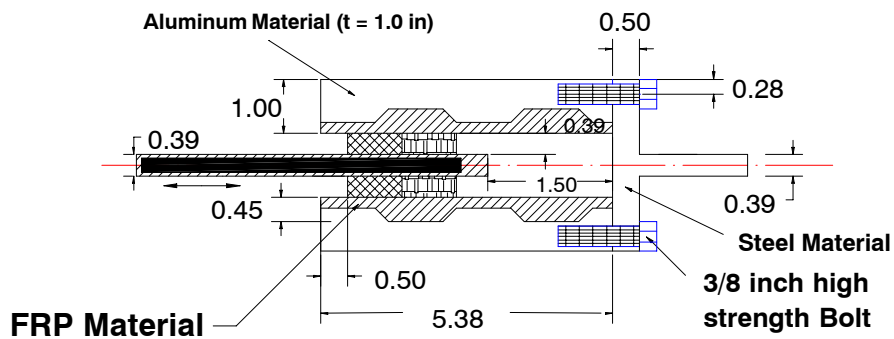


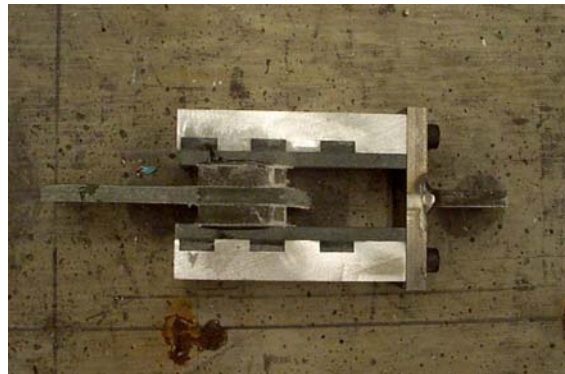
Figure 5-33 Comparison of the Behavior for the Honeycomb Damper and the Combined Composite Damper: (a) 0.1 Hz (b) 1.0 Hz (c) 3.0 Hz

5.4.3 A Study of Combining Ratio Between Materials

A new approach for increasing energy dissipation capacity was described in earlier studies by combining composite materials. The constituent materials chosen for the combination were polymer honeycomb and 3M Viscoelastic solid material. To investigate the combining ratio between these materials, different test specimens that consisted of layers of such materials bonded with Fiber Reinforced Polymer (FRP) skin plates (Fig. 5-34) were used.



(a) Design of the specimen (Top View)



(b) Fabrication of the specimen

Figure 5-34 Configuration of Test Specimen (unit = inch)

This test specimen subjected to longitudinal force dissipates energy through direct shearing of the combined composite materials as well as is able to prevent peeling action. All tests were conducted with different frequency rates on an MTS hydraulic actuator using a sinusoidal strain as input and measuring stress output. The results show the first 20 cycles of the hysteresis loops for the damping

material tested at the frequencies of 0.1, 1.0, and 3.0 Hz. The results in this section provide clear evidence for the effect of different combining ratios of the combined damping materials.

Several critical parameters from the different combining configurations were studied in the experimental phase and behavior in terms of the effective stiffness and the area of hysteretic loops were evaluated. All tests were performed under both monotonic and cyclic loading condition with different strain and frequency ranges. Table 5-6 presents the different combining patterns, and the combining ratio is simply described by the ratio of viscoelastic to the total area.

Table 5-6 The Dimension of Test Samples (Total Length = 2.0 inch)

	Dimension (Unit = inch)			
	Length	Width	Thickness	Combining Ratio
Sample 1	2.0	1.5	0.3937	1.0
Sample 2	1.61	1.5	0.3937	0.8
Sample 3	1.5	1.5	0.3937	0.75
Sample 4	1.22	1.5	0.3937	0.6
Sample 5	0.98	1.5	0.3937	0.5
Sample 6	0.79	1.5	0.3937	0.4
Sample 7	0.6	1.5	0.3937	0.3
Sample 8	0.51	1.5	0.3937	0.25

The purpose of the first sample test was to evaluate the properties of the viscoelastic solid material, and to compare with the data obtained by 3M, Japan. Viscoelastic material has properties of both viscous liquids and elastic solids when they undergo shear deformations. The measured shear modulus and hysteretic energy relation are shown in Fig. 5-36 and 5-37, respectively. Under a sinusoidal load with frequency ω , the shear strain $\gamma(t)$ and the shear stress $\tau(t)$ of a linear viscoelastic material oscillate at the same frequency ω but in general out-of-phase. A viscoelastic material that is placed in a sinusoidal shear loading exhibits hysteretic behavior. Zhang et al. (1989) presents the governing relationship as,

$$\gamma(t) = \gamma_0 \sin \omega t, \tau(t) = \tau_0 \sin(\omega t + \delta) \quad (5-3)$$

where, γ_0, τ_0 are the peak shear strain and peak shear stress, respectively. And, δ is the lag angle. The shear stress can be written as

$$\tau(t) = \gamma_0 [G'(\omega) \sin \omega t + G''(\omega) \cos \omega t] \quad (5-4)$$

where,

$$G'(\omega) = \frac{\tau_0}{\gamma_0} \cos \delta, \quad G''(\omega) = \frac{\tau_0}{\gamma_0} \sin \delta \quad (5-5)$$

Table 5-1 shows the test results of viscoelastic material (ISD 111 polymer material) subjected to sinusoidal shear loading. With $\sin \omega t$ given by (5-4) and using the identity $\sin^2 \omega t + \cos^2 \omega t = 1$, the stress-strain relationship can be rewritten

$$\tau(t) = G'(\omega)\gamma(t) \pm G''(\omega) [\gamma_0^2 - \gamma^2(t)]^{1/2} \quad (5-6)$$

which defines an ellipse as shown in Fig. 5-35, whose area gives the energy dissipated by the viscoelastic material per unit volume and per cycle of oscillation. As such, energy dissipation is given by

$$E_H = \int_0^{2\pi/\omega} \tau(t) \dot{\gamma}(t) dt = \pi \gamma_0^2 G''(\omega) \quad (5-7)$$

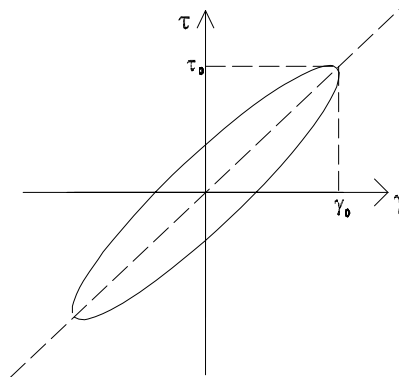


Figure 5-35 Idealized Stress versus Strain Relation

Based on Table 5-1 and (5-7), analytical prediction for energy dissipation capacity of ISD 111 polymer material was established. The comparison between the analytical and experimental results at different applied frequencies is shown in Fig. 5-38. It is shown that the analytical prediction has a

good agreement with experimental results at most strain rates and the data obtained from 3M Corp., Japan, is reliable.

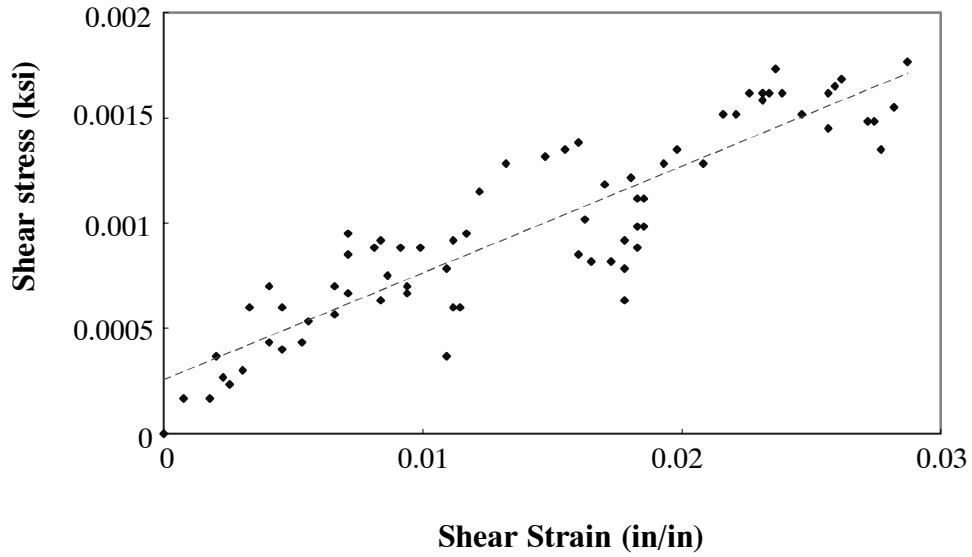


Figure 5-36 Shear Stress-Strain Relation of 3M Viscoelastic Solid Material

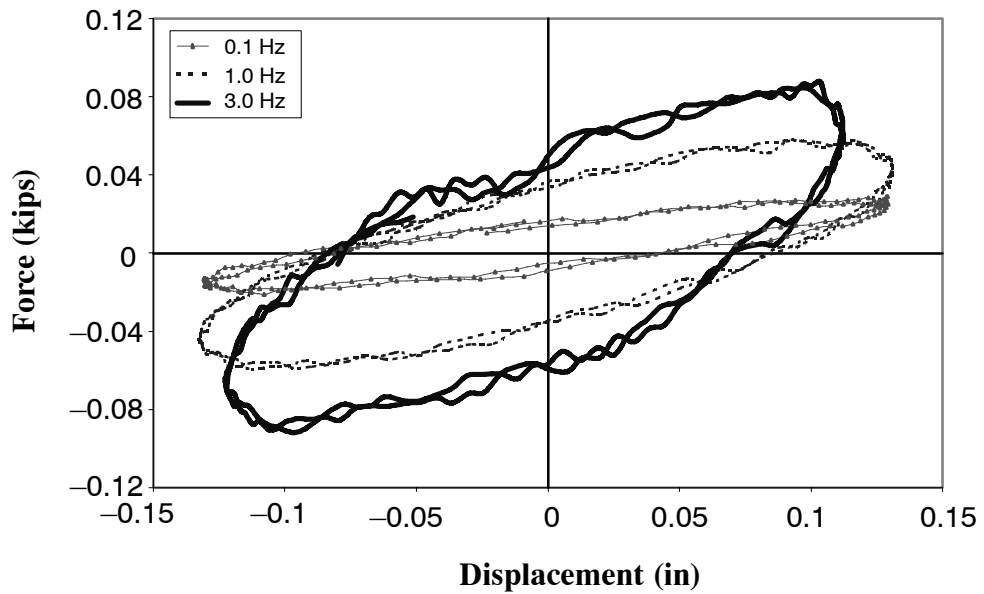


Figure 5-37 Hysteretic Energy of 3M Viscoelastic Solid Material for Different Frequencies (30% strain rate)

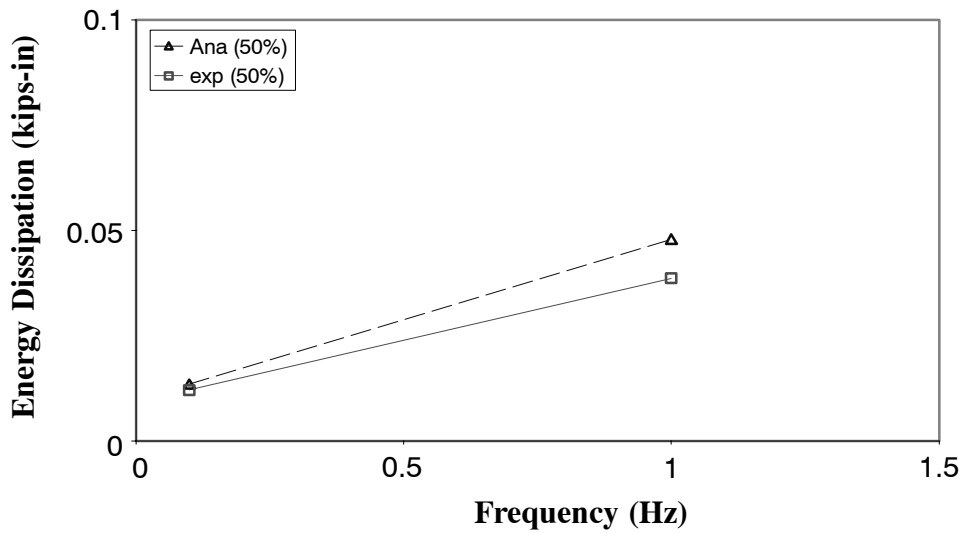
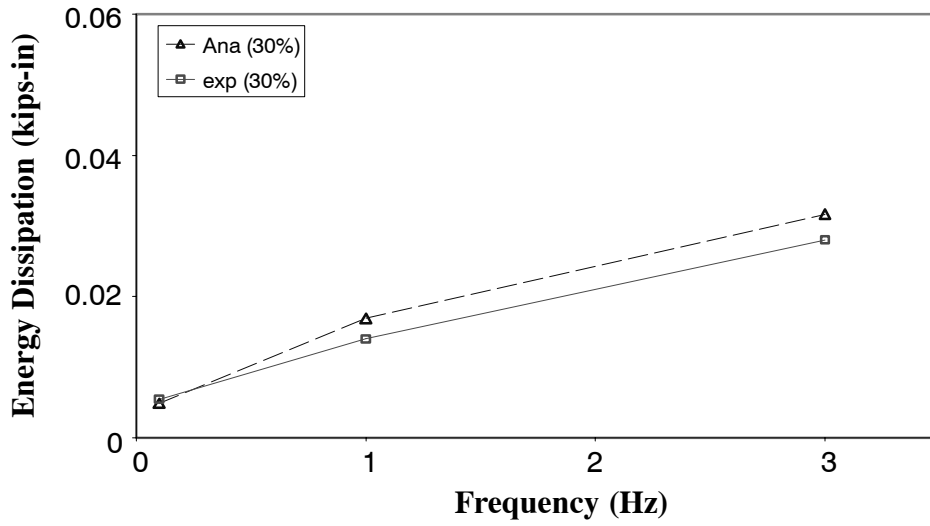
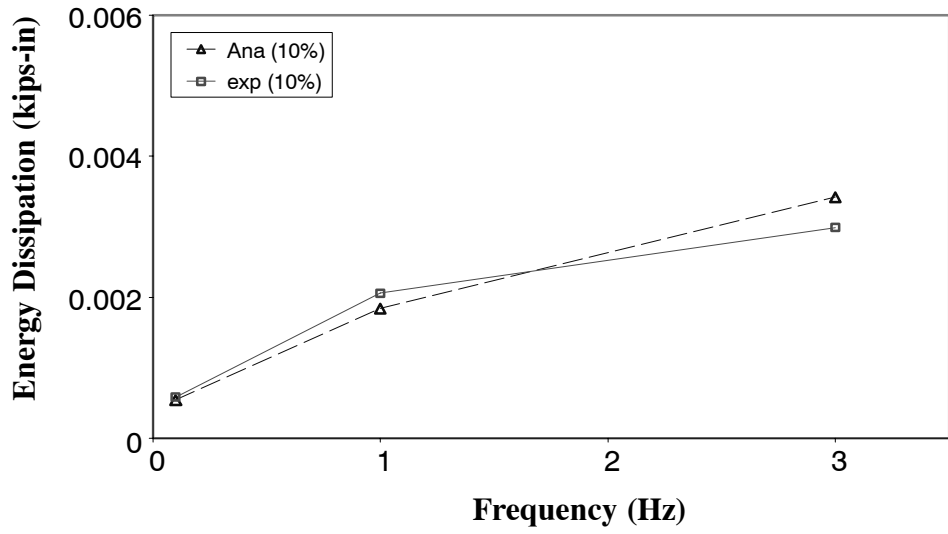


Figure 5-38 Comparison of Analytical and Experimental Results for the 3M Viscoelastic Material

From the monotonic and cyclic loading tests, the initial stiffness and energy dissipation capacity were investigated for different combination of the materials. For the initial stiffness, it is shown by Figure 5-39 that the stiffness is proportional to the percentage of honeycomb area. Particularly, case 4 has a relatively large value even though the honeycomb portion is smaller than the ones in cases 5, 6, 7 and 8. This derivation is due to the fabricating error, and it was observed that the test coupon in case 4 was coated slightly by epoxy bonding in the fabrication process. Fig. 5-40 illustrates the variation of the stiffness under different applied frequencies. It is shown that as the applied frequency was increased, the stiffness of the combined materials was enhanced by the contribution of the viscoelastic material around the mixing ratio 0.6, where the mixing ratio is defined as viscoelastic area-to-total area.

From the test results conducted at 10% strain, it is evident that up to case 4, i.e. mixing ratio = 0.61, energy dissipation increases as frequency increases. But, for cases 5 to 8, there was not significant effect from the change in frequencies on energy dissipation. This indicates that energy dissipation in these cases (case 5 to 8) is governed by honeycomb behavior. A small effect on the energy dissipation from added viscoelastic solid is apparent in this small strain range. At 30% strain rate, the observed behaviors are similar to those at 10% strain rate. However, the effect of enhanced energy dissipation capacity by the viscoelastic material becomes significant at high frequency as the honeycomb start to loose its capacity. For cases 5 to 8, the total energy dissipation has still increased because the damage in the polymer honeycomb still contributes some rate independent damping through the interface friction of the honeycomb cells. These results are presented in Fig. 5-41. At 50% strain rate, energy dissipation for cases 6 to 8 tends to be reduced because honeycomb failed completely so that it can not provide any damping through friction. After the honeycomb collapse, only viscoelastic material provides the stiffness as well as the damping properties in the structure. Finally, design guideline for different mixing ratios is suggested in Fig. 5-42 based on the test results. By considering the stiffness and energy dissipating performance, it is recommended for the purpose of design that the mixing ratio of viscoelastic solid is effective as long as at least 60% of total damper area. However, when the ratio is less than 60%, the stiff honeycomb material will prohibit the shear

deformation of the viscoelastic material from the applied loading and become a dominant factor for the overall behavior. Fig. 5-43 to 5-45 show test specimen setup and the progressive failure of the combined interface layers during tests for various mixing ratios.

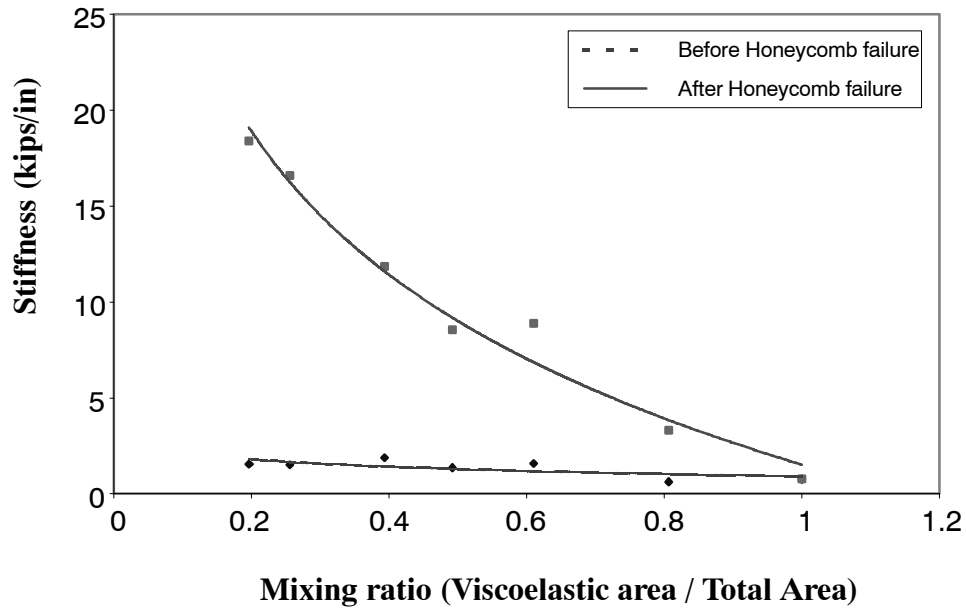


Figure 5-39 Variation of the Stiffness for Different Applied Strain Rates

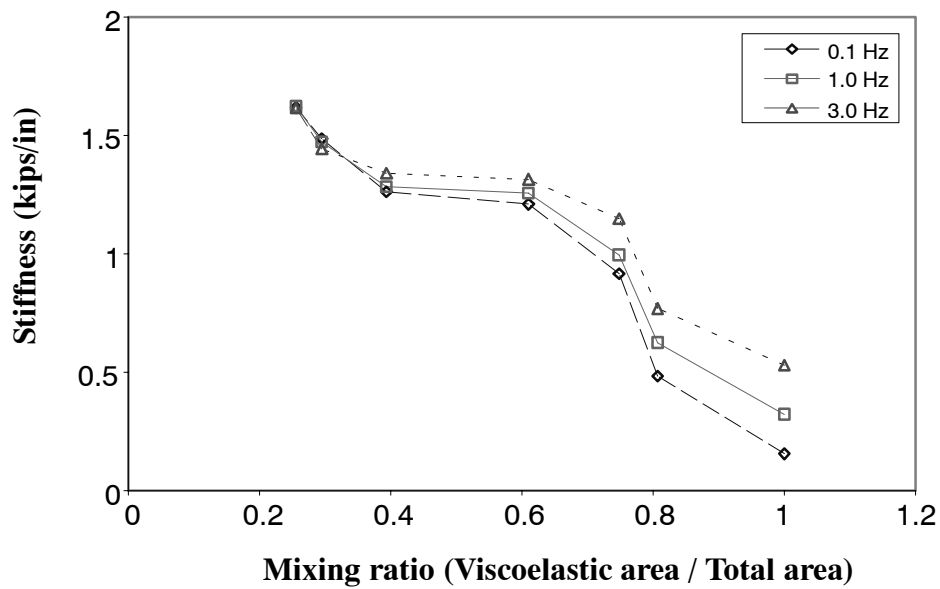


Figure 5-40 Variation of the Stiffness for Different Applied Frequencies

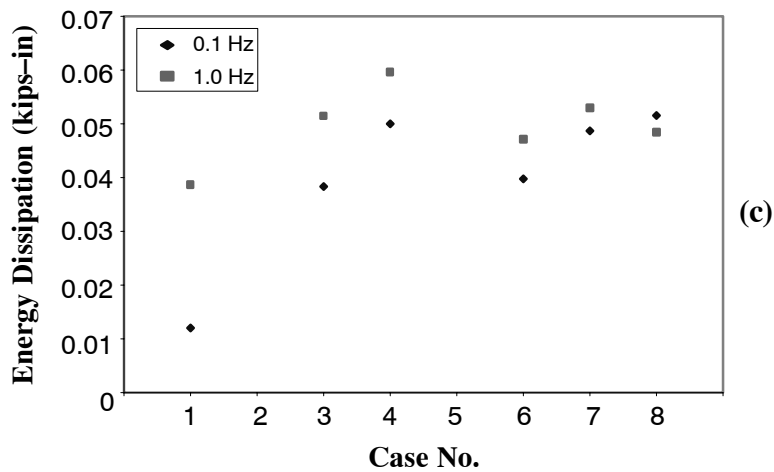
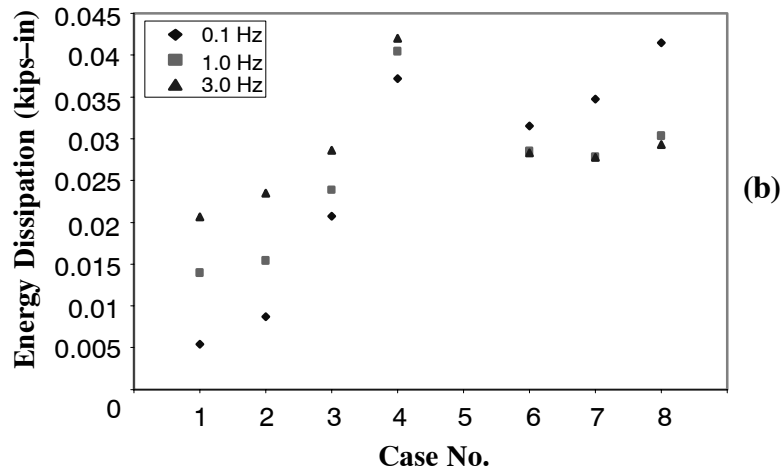
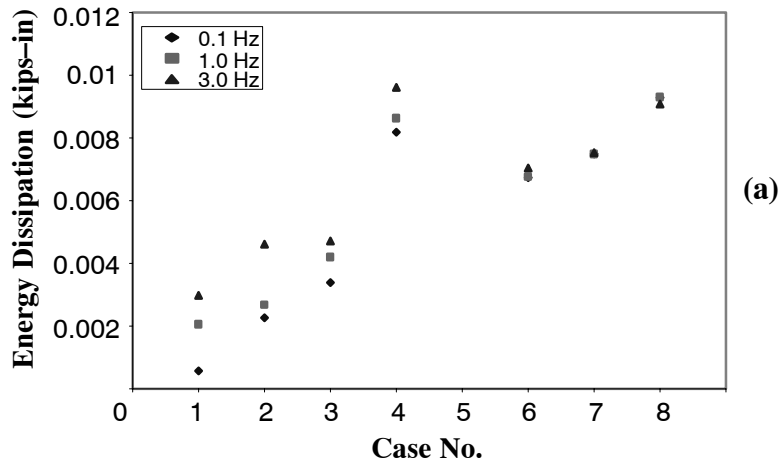


Figure 5-41 Energy Dissipation Capacity for Several Combined Cases:

(a) 10% strain (b) 30% Strain (c) 50% Strain

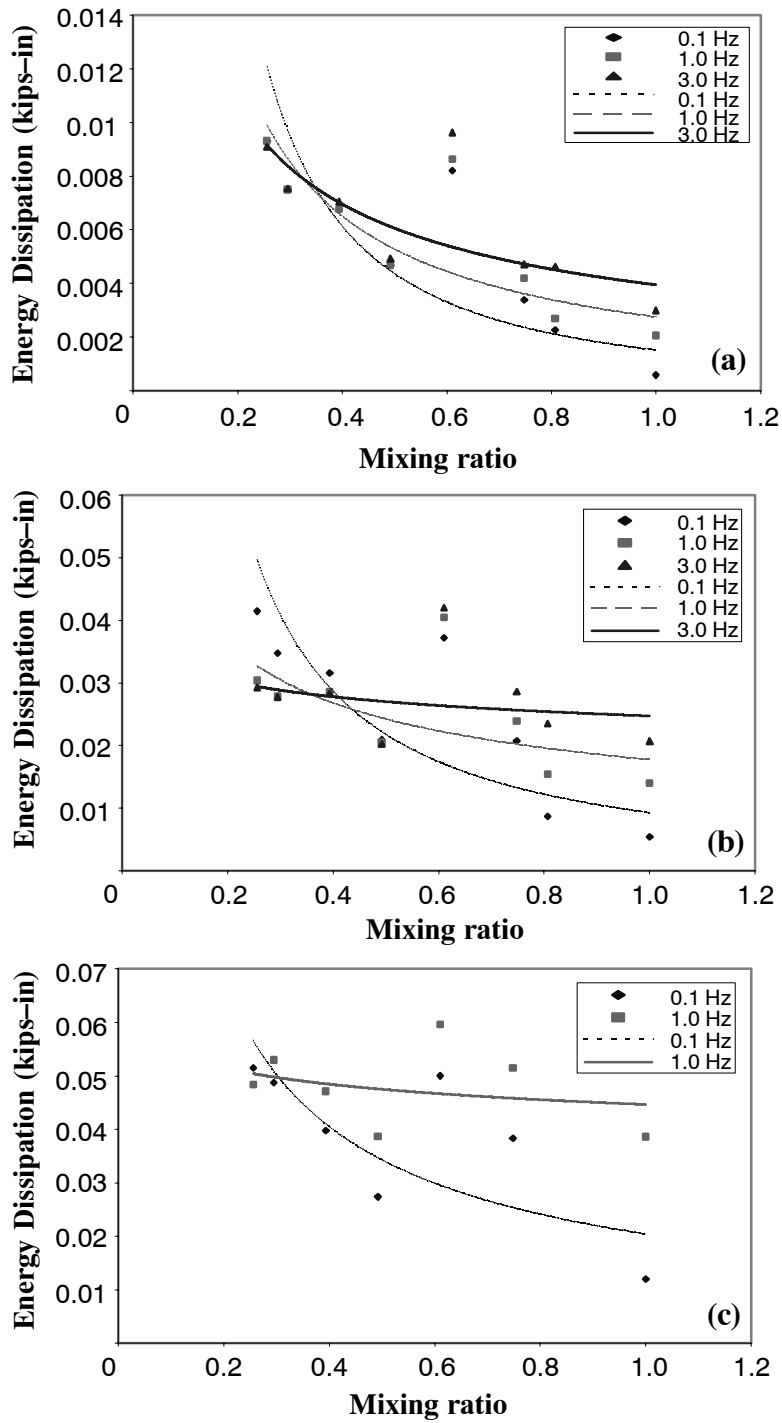


Figure 5-42 Variation of Energy Dissipation for Various Viscoelastic Mixing Ratio:

(a) 10% strain (b) 30% Strain (c) 50% Strain



Figure 5-43 Test Specimen Setup



Figure 5-44 Deformation of the Combining Interface Layers



Figure 5-45 Honeycomb Failure of the Combined Interface Layers

5.5 Summary

The stiffness and damping properties of the combined energy dissipating material system have been investigated, and the relationship between the geometric parameters (such as area and thickness) and frequency have been established based on the experimental and numerical results. For the overall stiffness, the combined system is governed by the polymer honeycomb. The parametric relation is applied using the assumption of a constant stress distribution in the honeycomb. Therefore, the proposed relationship is,

$$K_{\text{eff}} = C_0 * \left(\frac{A}{A_0} \right) \quad (5-8)$$

Where, C_0 = Constant value from experimental results (see Table 5-7), $\frac{A}{A_0}$ = Area ratio, A = Area of honeycomb material, and A_0 = total area.

Table 5-7 Constant Value for the Honeycomb Stiffness Relation (0.39 in thickness)

	C_0 (kips/in)	A_0 (in ²)
Before Bonding Scrim Failure	0.045	3.0
After Bonding Scrim Failure	0.011	3.0

Damping in actual structures is usually represented by equivalent viscous damping. The viscous damping is the simplest form of damping to use since the governing differential equation of motion is linear and, hence, amenable to analytical solution. The most common method for defining equivalent viscous damping is to equate the energy dissipated in a vibration cycle of the actual structure. The energy dissipated in the actual structure is given by the area (E_D) enclosed by the hysteresis loop. With the application of the combined damping layers, the equivalent damping in an actual structure is expressed by the force-displacement relation obtained from an experiment under cyclic loading with displacement amplitude u_o (Chopra, 2001)

$$\xi_{Eq} = \frac{1}{4\pi} \frac{1}{\omega/\omega_n} \frac{E_D}{E_{so}} \quad (5-9)$$

where ω = applied frequency, ω_n = natural frequency of the system, and the strain energy, $E_{s_o} = \frac{k u_o^2}{2}$, is calculated from the stiffness k determined by experiment.

For the polymer honeycomb material tests, the energy dissipation of a cycle of vibration is independent of frequency (ω). In contrast, the energy dissipated in the viscoelastic material increases linearly with the forcing frequency. Accordingly, the equivalent viscous damping ratio of the polymer honeycomb will be roughly the same for all frequencies, namely, rate-independent linear damping. This is associated with static hysteresis due to plastic strain and localized plastic deformation in a range of stresses within the apparent elastic limit. In this section, the energy dissipation capacity of each pure damping system is tested and presented in Fig. 5-46. The results indicate that the combined damping system has more energy dissipation capacity than other damping cases. Moreover, a new configuration of interface damping layers is proposed and analyzed in this section.

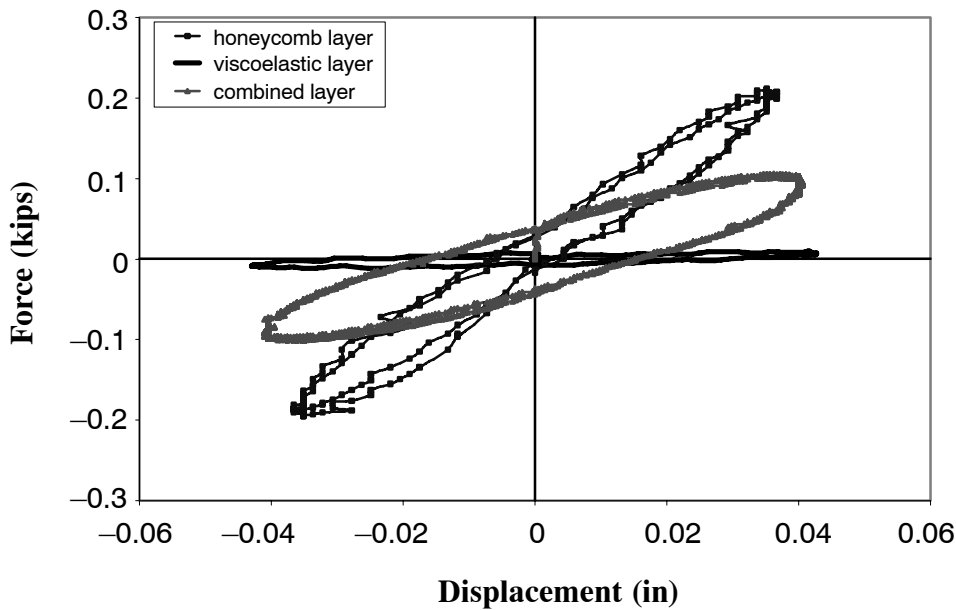


Fig. 5-46. Hysteretic Energy of Different Damper Cases (10% strain, 1.0 Hz)

The damping properties of the proposed combined damping layers and effective stiffness were investigated. In particular, it was clearly shown in Fig. 5-47 that the combined interface system provides significant energy dissipation when compared with the individual system of honeycomb or solid viscoelastic material. More importantly, this system is adjustable to design properties such

stiffness and energy dissipation. These advantages of combining such materials will be useful for increasing both the shear resistance and the energy dissipation at contact surfaces. And, it is shown that by combining both materials, i.e., honeycomb and solid viscoelastic, this new configuration could achieve more economical design for energy dissipating devices. However, it was found that there is little discrepancy between the energy dissipation capacities of viscoelastic layer under different frequencies. It is due to the fact that the viscoelastic damper properties remain somewhat constant and independent of strain (below 20%) for each temperature and frequency (Chang et al., 1993).

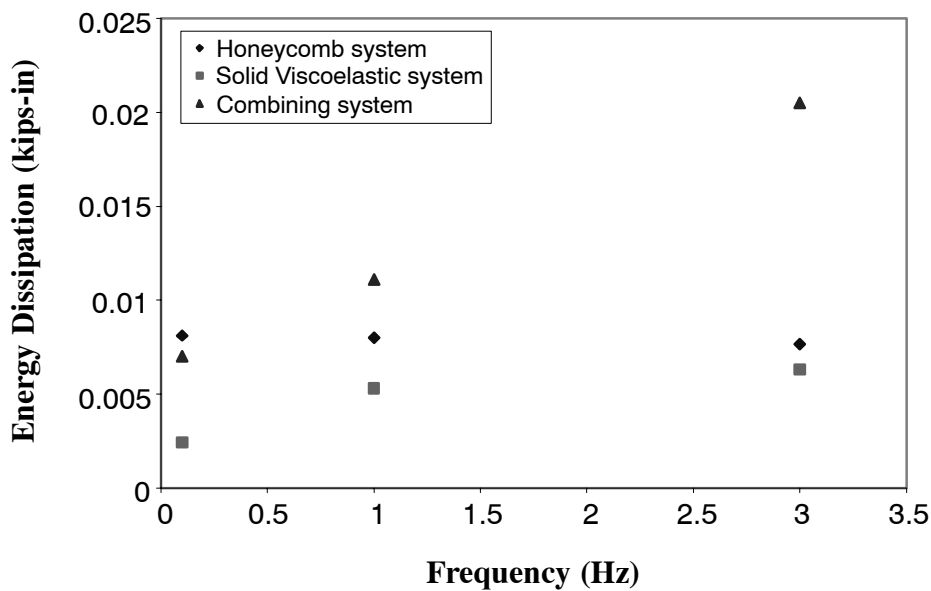


Fig. 5-47. Comparison of Energy Dissipation for Different Cases

For the proposed combined interface damping layers, numerous experimental studies were performed in this section. Nevertheless, more experimental tests are still needed to account for the variation in temperature in order to develop a more general equation. Also, it was observed that possible maximum resistant strain is about 10-20% for the honeycomb, while solid viscoelastic can undergo up to 100-200%.

In an earthquake, it has been shown (Gasparini et al., 1980) that constrained damping layers must have sufficient strength to preclude its failure during an extreme condition. For the application of the honeycomb material proposed herein, this material should have adequate fatigue strength for long term durability and sufficient deformation for extreme loading. Accordingly, it is expected that

the application of the honeycomb will be useful for increasing initial stiffness as well as damping of the structure subjected to wind loading.

SECTION 6

ENHANCED PMC DAMPING INFILL PANEL SYSTEMS

6.1 Introduction

Supplemental damping is often used effectively for seismic retrofitting of existing structures and/or structures damaged in past earthquakes. Many devices have been developed that can be used as part of a primary or secondary system of lateral resistance. Traditional seismic resistant design relies on energy dissipation by the inelastic action in various parts of the structure, which are suitably designed to provide significant energy dissipation potential. However, this energy dissipation, which is due primarily to material hysteresis, requires large plastic deformations in the primary structural members which causes substantial damage to non-structural components as well. Supplemental damping devices intended to dissipate the earthquake-induced energy by acting either parallel or in series with the primary structural system. As a result, the energy dissipation demand on primary structural members is minimized, thus reducing permanent deformations and damage to structural and non-structural components.

To make the effective use of supplemental damping devices, passive energy dissipation concept is an emerging technology that may be used to enhance the seismic performance of buildings by adding extra damping to the structure. As part of this research, two different PMC infill specimens with supplemental damping layers were studied to investigate their effectiveness for seismic retrofitting. The experimental phase performed was concerned with the response of a steel frame retrofitted by two infill panels — namely, (1) the multi-panel PMC infill panel, and (2) FRP box panel systems. Two systems were subjected to monotonic and cyclic loading.

A steel frame with new bolted top and seat angle connections was employed here to avoid uncertain failures due to prior damage in connections. The bare frame was tested before testing the PMC seismic panel in order to assess the resultant enhancements to the seismic-energy capacity. The observed behavior of the PMC-infill panel systems was assessed on the bases of stiffness, modes of failure, and energy dissipation output. This section describes the conceptual design, fabrication, and testing

of two infill systems; a multi-panel PMC infill wall panel, and FRP Box panel with different interface layers.

6.2 Design of a Multi-panel PMC Infill System

6.2.1 Design Concept and Structural Configuration

The horizontal components of earthquake ground motions are usually the most damaging to a structure (Yang et al., 1991). With respect to non-structural elements, there are two primary mechanisms that cause damage. The first is related to inter-story drifts, and the second is related to floor accelerations. Inter-story drift is defined as the relative displacement that occurs between two adjacent floors. Second, floor accelerations are the absolute accelerations that occur as a result of an earthquake. Clearly, a design concept that reduces both the inter-story drifts and floor accelerations combines the best aspects of these two design philosophies. Seismic isolation is such a concept, but it also can be costly and may not be appropriate for the retrofit of tall slender building structures.

Conventional upgrading techniques usually include the addition walls and foundations, and strengthening of frames. Most of these techniques often lead to costly consequences such as heavy demolition, lengthy construction time, reconstruction, and occupant relocation. Advanced composite materials and new technologies have been extensively researched and applied in seismic retrofitting projects. Considering both innovative structural design and construction philosophies, prefabricated light-weight nonstructural elements were proposed here as a new technology for seismic retrofitting.

The basic design philosophy and structural technique considered herein focus on increasing the efficiency for retrofitting a structure before and after earthquake damages. The properties of the prefabricated PMC infill systems can be easily modified to suit their functional purposes. Fiber orientations and stacking sequence of the PMC materials can be adjusted to enhance structural behavior without any limitations given by existing configurations. Also, ductile behavior of PMC infill systems can prevent the catastrophic failure of the overall structure. From the construction point of view, PMC

infill systems can be easily installed during the strengthening and retrofitting process of the existing structures. To perform these purposes, a full-scale multi-panel PMC infill system was examined.

The proposed multi-panel PMC infill panel system is composed of two separate basic structural components, and they are: inner PMC sandwich infill and outer FRP damping panels. Figure 6-1 shows the geometric configuration of these basic structural components.

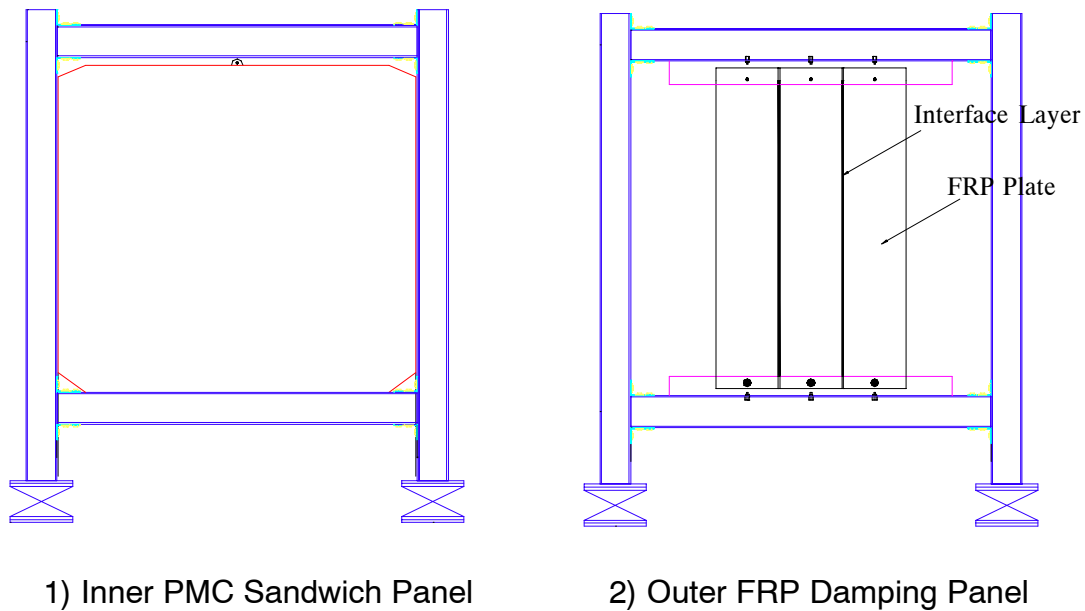


Figure 6-1 The Geometric Configuration of the Multi-panel PMC Infill Panel

This multi-panel PMC infill panel was designed to have constrained passive energy damping interface layers, which were made of both 3M viscoelastic solid and polymer honeycomb materials. The primary function of the constrained damping layers between the FRP panels is to provide the necessary energy dissipation. However, the inner PMC infill wall was considered to provide lateral resistance of the structure.

The primary design concept of the proposed multi-panel PMC infill system was focused on two aspects; (1) enhancement of damping properties from the passive interface damping layers, and (2) providing considerable lateral stiffness by the inner PMC sandwich infill at high drift level to resist severe earthquake excitation and avoid excessive relative floor displacements that cause both struc-

tural and non-structural damage. These two separate components along with the steel frame are intended to provide the desired stiffness or/and damping following different drift values.

For the inner component, a PMC sandwich infill was designed to reduce the weight, sound, and vibration as well as to improve the structural rigidity of the composite wall. The inner PMC sandwich infill consisted of two fiber-reinforced polymer (FRP) laminates with an infill of Divinycell H-100 sheet foam in between. For the selection of the FRP skin laminate materials, E-glass in the form of woven fabric was chosen as reinforcement of the FRP because of its cost performance, and vinyl ester resins were employed as the matrix (DERAKANE 411). The selected vinyl ester resins are typically used when high durability, thermal stability, and extremely high corrosion resistance are required. The Divinycell foam is a semi-rigid PVC used as a core material in conjunction with high-strength skins to produce strong, stiff, lightweight composite structures. Thus, Divinycell foam has a high strength-to-weight ratio, exceptional dynamic strength, and excellent insulating properties.

Finally, the FRP skin laminates were designed to have the same number of fibers along wrap and fill directions for easy construction. In this study, FRP laminates were used for both fabricating the skin layer of the PMC infill and the outer panels. For these FRP laminates, material properties were obtained from a previous research by Kitane (2003) because same FRP laminates were employed for the design and fabrication process. Accordingly, material properties are modeled as a homogeneous, linear elastic, and orthotropic material. Table 6-1 presents the obtained FRP laminate material properties.

Similar to the behavior of traditional infilled frame structures, when a PMC infilled frame is subjected to a racking load, the frame tends to separate from the infill over part of the length of each side. The remaining regions of contact between the frame and the infill occur in the corners at the end of the compression diagonal. Also, if the racking load is increased until the structure collapses, several modes of failure of the infill and of the frame are possible. In the traditional infilled frame

structures composed of concrete, masonry, or brick, these behaviors have led to the concept that the infill may be considered roughly as equivalent to a diagonal bracing strut.

**Table 6-1 The Summary of FRP Material Test Results
Used in the Multi-panel Infill Panel System (Kitane, 2003)**

Method	Fill direction			Wrap direction		
	Tension	Compression	Shear	Tension	Compression	Shear
Width (in)	0.498	0.256	1.0	0.4945	0.25	1.09
Thickness (in)	0.0545	0.197	0.064	0.053	0.2	0.0615
Elastic modulus (ksi)	2415	2303.3		2600	3264	
Shear modulus (ksi)			394.5			355.7
Poisson's ratio	0.129	0.1		0.13	0.25	
Ultimate stress (ksi)	41.3	35	8.13	48.7	38	9.26

Numerous analytical and experimental investigations of the behavior of diagonally-loaded traditional infilled frames have been performed by several researchers (Staford, 1966; Carter and Staford, 1967; Saneinejad et al., 1995). On the basis of the infill's failure mode, possible design methods were established for the infilled frame structures. However, in the case of the inner PMC sandwich infill panel, the empirical design formulae for the traditional infilled frame cannot be employed due to: (1) out of range in the proposed functions because of a thin panel thickness, (2) the effect of allowing initial gaps, and (3) anisotropic properties of the PMC infill. Therefore, a new approach for designing the PMC sandwich infill is derived in this section.

As observed in section 4, the dominant failure of the PMC sandwich infill panel was elastic buckling under racking load. By considering the observed failure mode, an iterative process by numerous finite element simulations was carried out. The maximization of buckling loads with respect to laminate configuration was the objective function of the inner PMC sandwich panel design. Since the structural behavior of sandwich constructions is strongly affected not only by the types of fiber reinforced composite materials, but also by fiber orientations and stacking sequences of individual plies constituting the sandwich faces, the determination of optimum stacking sequence is a significant key

parameter in the design process. By considering several stacking sequences, Fig. 6-2 shows the maximum buckling force that was obtained from finite element analysis.

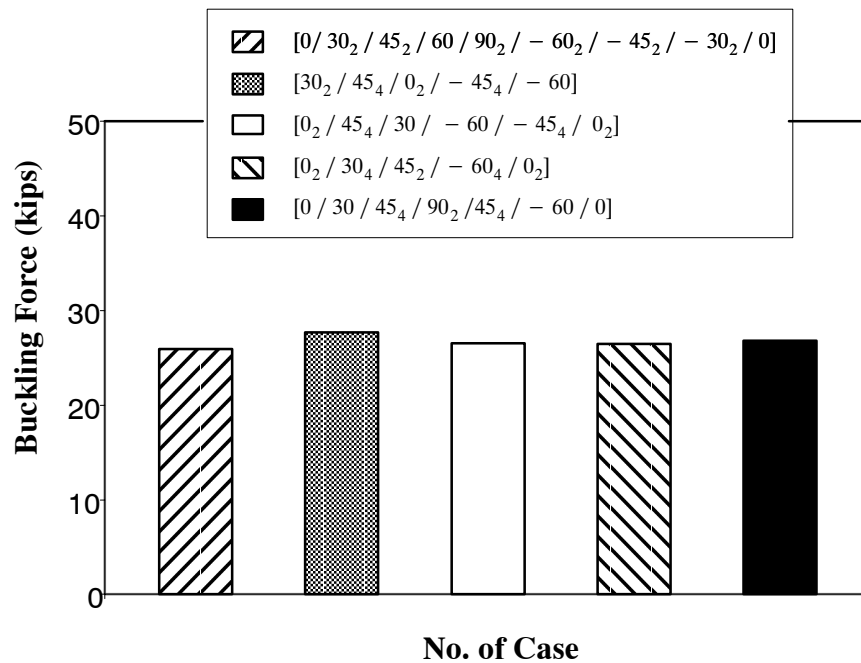


Figure 6-2 Numerical Design Examples for Maximum Buckling Force of Several Stacking Sequence Arrangements

The corresponding features involved in the buckling response of the PMC infill panel were obtained numerically by using linear buckling and geometrical non-linear analyses.

To simplify the analysis, the inner PMC sandwich infill was only modelled and analyzed under diagonally compressive forces as shown in Fig. 6-3(a). The interaction between the infill and frame members was represented by applying constraint conditions as depicted in Fig. 6-3(b). The applied stacking sequences were designed by iterative procedures while ply layer thicknesses are kept constant. Total thickness of the PMC sandwich was controlled by space on the steel beam, and the thickness ratio of the FRP skin and the core was designed to prevent local buckling failures.

Finally, the results obtained by numerous finite element simulations including different geometric combinations were evaluated for the static critical buckling load. Table 6-2 presents the designed stacking sequence of the inner PMC sandwich infill panel. Also, detailed dimensions of the PMC sandwich infill panel are shown in Fig. 6-4 and Fig. 6-5. These figures show the geometric configu-

ration of the PMC sandwich infill and fiber orientation along the loading direction. In this design, the core to skin thickness ratio was assumed to be 7.6.

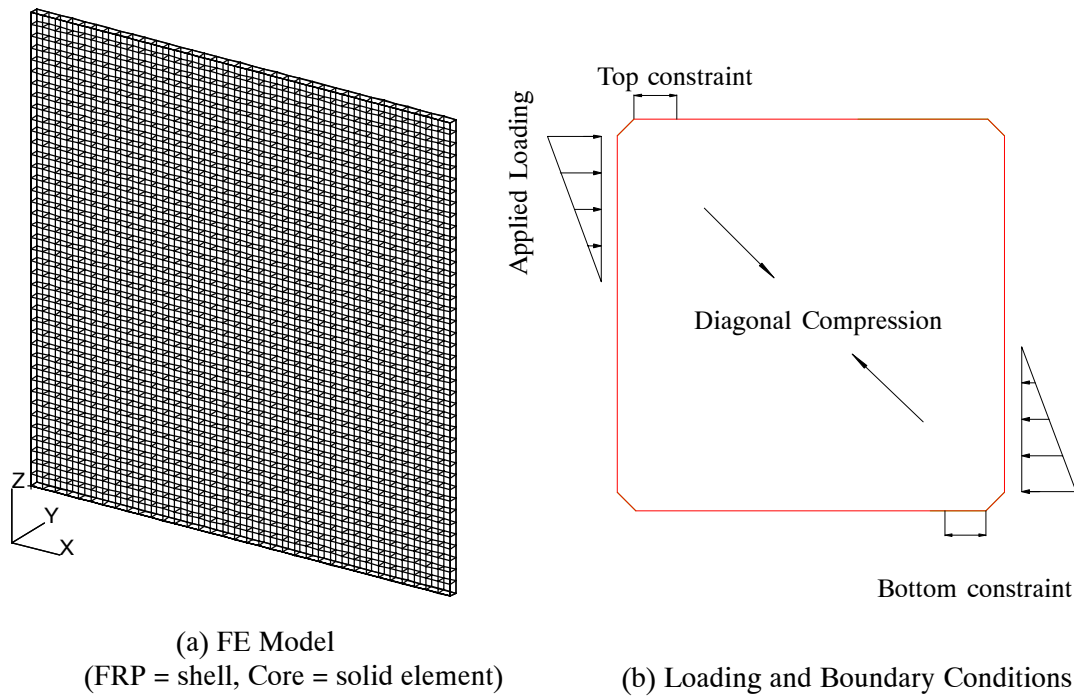


Figure 6-3 Simplified Numerical Analysis for the PMC Sandwich Infill Design

For the steel frame with infills, the presence of any gaps between the columns and the infill wall and/or between the top beam and the infill wall may be unavoidable. These gaps may negate some or all of the stiffness provided by the infill. In particular, large gaps are not practically tolerable for pure infilled frame structure, because they are normally subjected to alternating loads. As such, different strength and stiffness conditions must be expected with different gap types. Therefore, attention has to be given to the initial gaps between the infill and the opening of steel frame.

In designing the PMC sandwich infill, these unavoidable gaps between the infill and the opening of steel frame can be used as a key design parameter to achieve the considerable lateral resistance at specific drift. In practice, it would be expected that the post-action of the infill panel after closing the initial gaps may prevent excessive relative floor displacements, and the shear deformation of the combined interface damping layers in the outer FRP damping panels will be occurred until the initial gap closes.

For the gap effects on concrete or masonry infilled frames, Riddington (1984) concluded that a lack of fit equivalent to 0.1% of the infill dimensions did not appreciably change the collapse load, but significantly increased the horizontal deflection due to the infill sliding and jamming into the top loaded corner of the frame. However, Dawe and Seah (1989) found that a gap of 0.7% of the infill height dramatically decreased the collapse load up to 50% for a masonry infilled steel frame, due to significant decrease in the lengths of the contact. Generally, large gaps are not practically tolerable for infilled frame structure, because they are normally subjected to alternating loads.

In this study, although there should be little decrease in the stiffness and/or strength of the infill, it is assumed arbitrarily that the maximum side gap was allowed to have less than 0.4% of the infill dimensions. By using finite element simulations representing the PMC infilled frame with different side and top gap distances at the interface, the force-displacement relationship was evaluated. In the numerical analysis, it was found that there is a relation between different gap distances and the corresponding infill action by designed contact point of lateral displacement. Fig. 6-6 and 6-7 present the relation between the contact lateral displacement and initial side gap distance. It is evident that the gap distance may become a design parameter for initiating considerable stiffness in a structure.

In this study, the design target was chosen in the range between 2% and 2.5% drifts in order to allow maximum shear strain in the interface layers; thus, 0.37 inch of side gap and 0.6 inch as a top gap were chosen based on numerous finite element simulations. When the frame exhibits a lateral drift larger than 2.0% - 2.5%, the inner PMC sandwich infill panel will start to come in contact with the steel frame components. This onset of contact, however, produces additional lateral stiffness and the steel frame is prevented from undergoing a lateral drift larger than what it was designed for. Because now the inner PMC sandwich infill is providing significant stiffness, it will be eventually failed by buckling. The geometric configuration and laminate architecture of the PMC sandwich infill, depicted in Fig. 6-4 and 6-5 were determined based on the prescribed initial gap distance.

Table 6-2 The Orientation Code of the Skin Laminate (Total thickness = 0.21 inch)

No.	Orientation angle	The number of layers	Total thickness (inch)
1	30	1	0.015 (0.381mm)
2	45	2	0.03 (0.762mm)
3	0	1	0.015 (0.381mm)
4	-45	2	0.03 (0.762mm)
5	-60	1	0.015 (0.381mm)
6	-60	1	0.015 (0.381mm)
7	-45	2	0.03 (0.762mm)
8	0	1	0.015 (0.381mm)
9	45	2	0.03 (0.762mm)
10	30	1	0.015 (0.381mm)

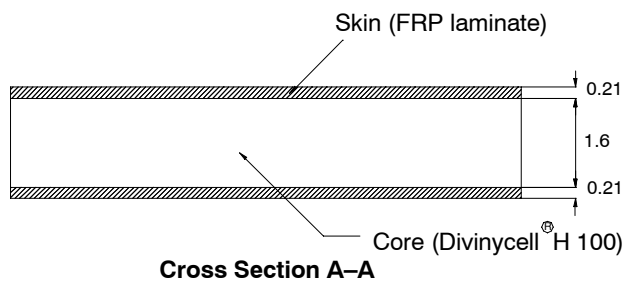
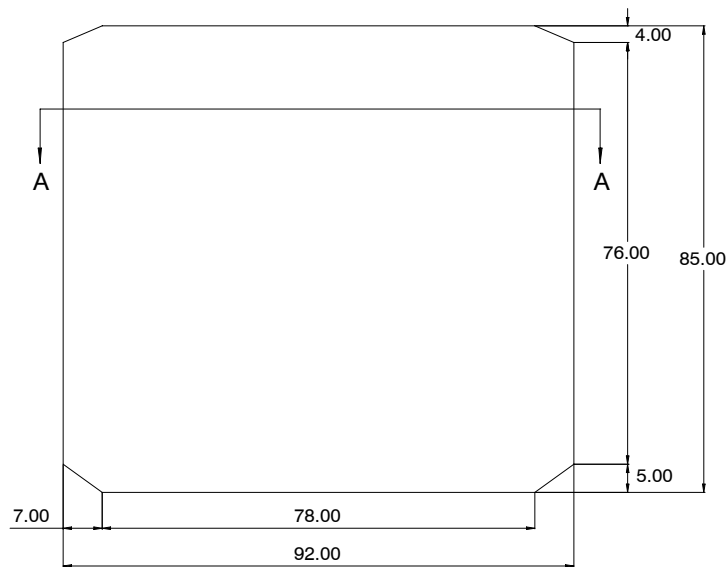


Figure 6-4 The Detailed Dimension of PMC Sandwich Panel (unit=inch)

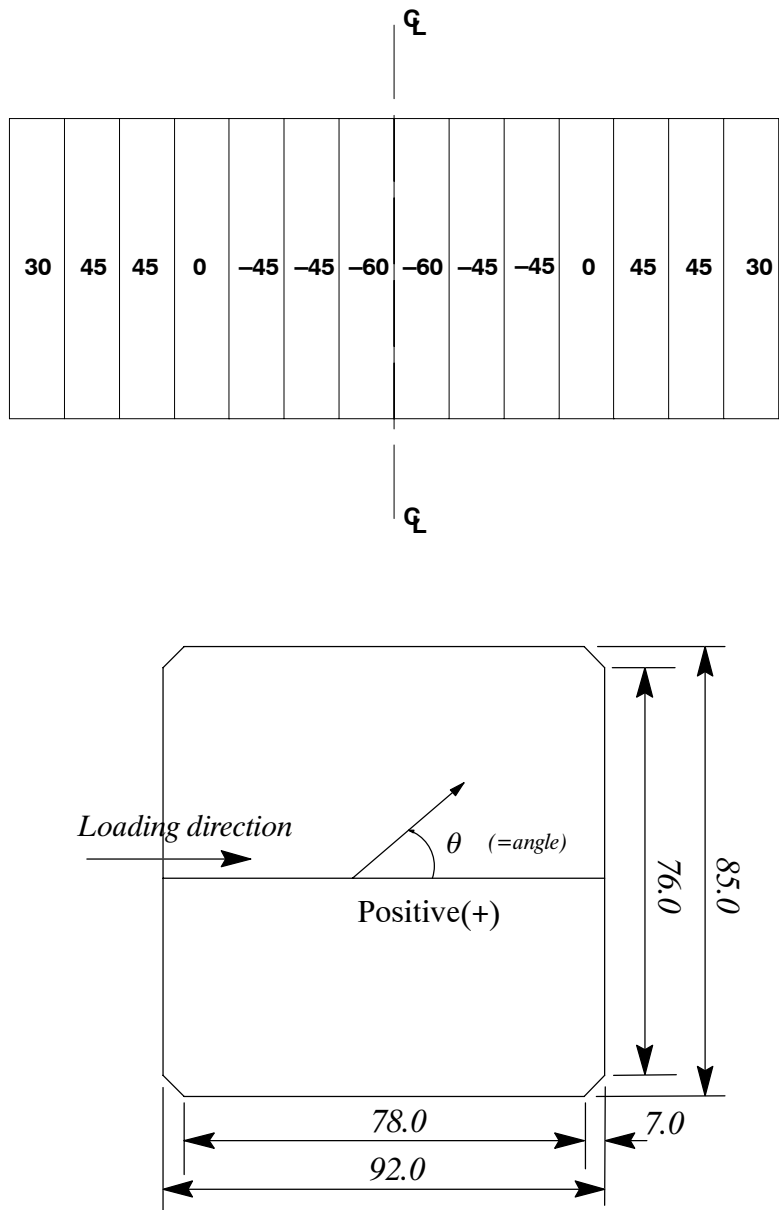


Figure 6-5 The Orientation of Stacking Sequence of Inner Panel (unit=inch)

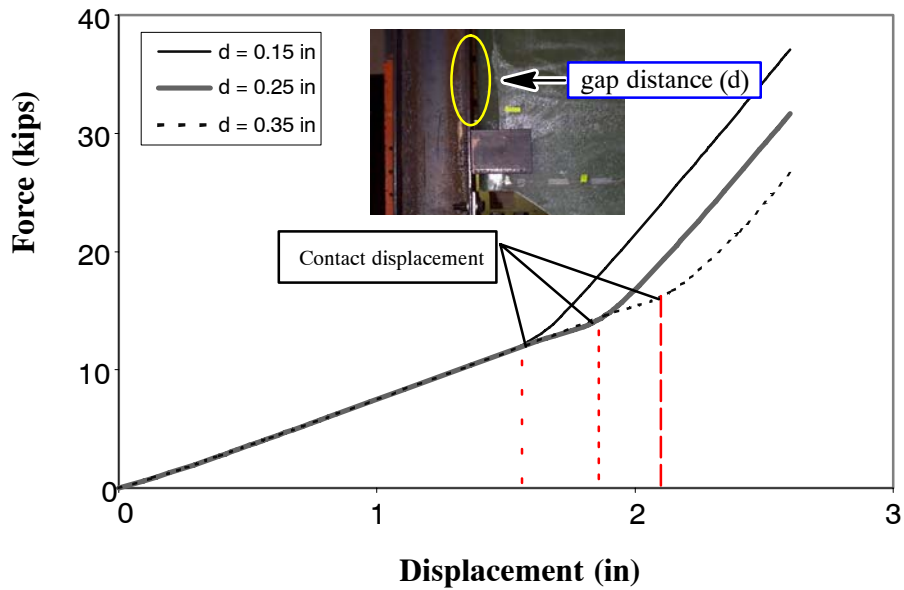


Figure 6-6 Force-displacement Relation of the PMC Infilled Frame for Different Contact Distance

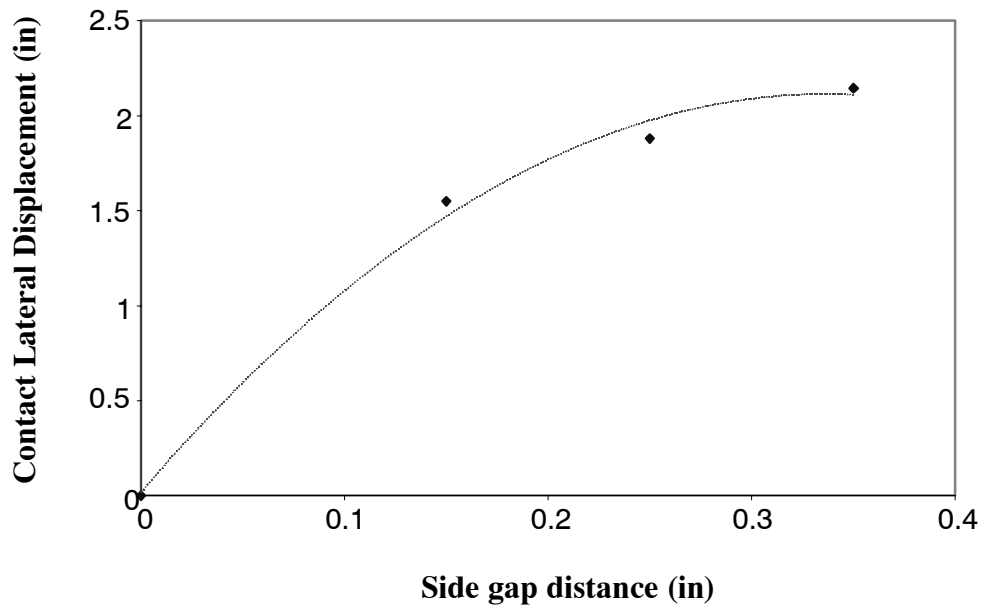


Figure 6-7 Numerical Results for the Initial Gap Distance and Contact Lateral Displacement Relationship

For the outer damping panel design, the damping concept of the previous research (Gasparini et al, 1981) was adopted and basic consideration was given to have shear deformation of the interface layers between FRP plates along the relative motion of the top and bottom beams. This passive energy

damping panels should be designed so as to achieve initial static stiffness and an acceptable maximum strain at the interface layers. Practically, the proposed damping system could be utilized in as many panels as necessary to achieve different levels of damping and stiffness. As shown in Fig. 6-8, the geometric configuration of the outer panels with constrained energy dissipating layers was designed in this study to have three FRP laminate plates and constrained passive damping materials at the interface between them.

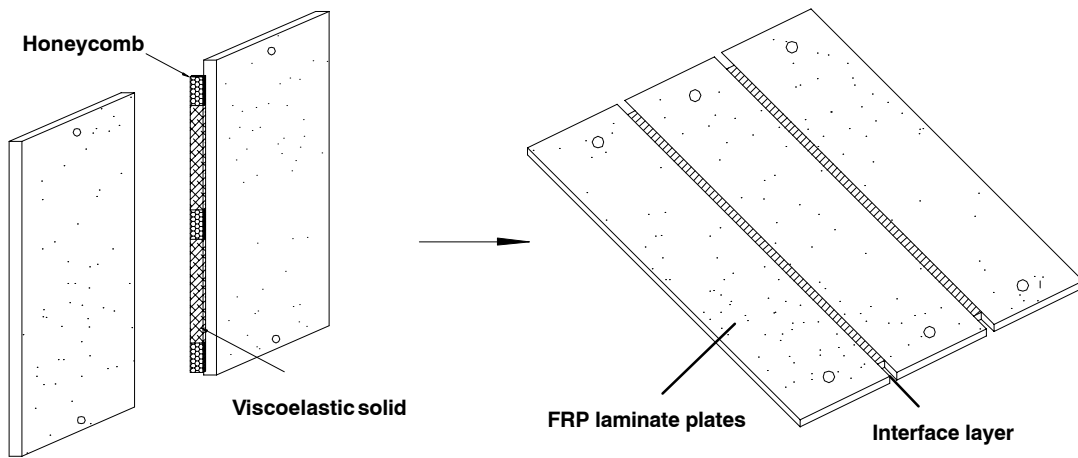


Figure 6-8 Geometric Configuration of the Damping Panel

In the design process of the FRP laminates, the vertical releases at the top panel to beam connections were considered to eliminate axial forces in the panels. Only the bottom connection of end panels must then transfer some vertical forces into the beam. As a key design problem of the outer damping system, the design of the interface damping layers can be carried out for the required damping ratio of the structure. This design becomes the primary parameter for controlling the overall structural vibration under extreme loading conditions. According to the required design damping ratio, the geometric size of the FRP plates, and the interface damping layer dimensions and properties will be determined by simple calculation.

In the design process of the outer FRP laminates, an idealized symmetric motion was assumed. Accordingly, the thickness of FRP laminates was designed to have rigid body motion to make idealized shear deformation in the constrained interface damping layers. That is, the laminate thickness could be determined from the maximum allowable interface deformation to insure the maximum shear

strain in the viscoelastic materials. The geometric size of the outer damping panels can be adjustable to the configuration of the constrained interface damping layers. In practice, an actual thickness will be larger than the design thickness due to the application of adhesive material. In this study, bonding effect of the interface layers was not considered, and perfect bond was assumed. From Fig. 6-9, the shear strain in the layers may be expressed as:

$$\gamma_v = \frac{\Delta b}{h t} \quad (6-1)$$

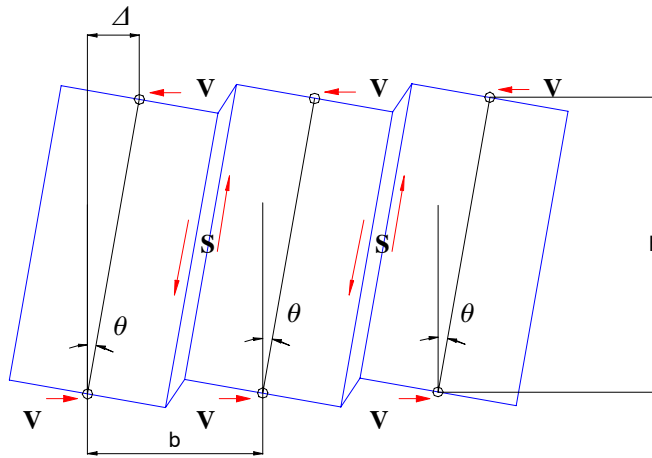


Figure 6-9 Deformed Geometry of the Damping Panel during Inter-story Drift

The parameters that need to be considered are: the shear strain, γ_v , inter-story displacement, Δ , thickness of the interface layer, t , and width, b , and height, h , of damping panel. Further, the static lateral stiffness of n interface layers may be expressed using the energy method.

For the external energy,

$$W_E = \frac{1}{2} K_{lat} \Delta^2 \quad (6-2)$$

and the internal energy,

$$W_I = \frac{1}{2} n G_v \gamma_v^2 V \quad (6-3)$$

where G_v , γ_v present shear modulus and strain of the interface layer, representatively, and V is the volume of an interface layer (i.e. $V = A_v$ (interface area) $\times t$ (thickness)).

Upon substituting γ_v and V into (6-3), then the internal strain energy is

$$W_I = \frac{1}{2} \left(\frac{n G_v A_v}{t} \right) \left(\frac{b}{h} \right)^2 \Delta^2 \quad (6-4)$$

Using the energy balance, $W_E = W_I$, k_{lat} can be evaluated, that is, the strain energy in the interface layer should now equal to the work by the applied loads. Finally, the static lateral stiffness produced by the interface layers is given as,

$$K_{lat} = \left(\frac{n G_v A_v}{t} \right) \left(\frac{b}{h} \right)^2 \quad (6-5)$$

Based on the concepts outlined in (6-1) and (6-5), the PMC panels were designed. Among design parameters, the interface layer thickness was determined by considering a desirable shear strain in both the viscoelastic materials and the commercial honeycomb size. Based on the selected layer thickness, the other design parameters were chosen here. Especially, the combining ratio of the polymer honeycomb and viscoelastic materials is a very important parameter in the design process of the constrained passive damping interface layers. To get the best combination factor, numerous coupon tests by representing different combining ratios were performed in section 5. Finally, the combining ratio of 0.6, was determined by the test results. Such a ratio is likely to be an economical design strategy for reducing the use of relatively expensive viscoelastic materials.

Fig. 6-10 presents the detailed design dimension of both the interface damping layer and a piece of outer FRP panel, respectively. In this study, considering the natural frequency of the undamped structure, 5–10% increased damping was considered as a design target due to expensive viscoelastic material and limited experimental results. Finally, the overall configuration of the multi-panel PMC infill system is shown in Fig. 6-11 and 6-12.

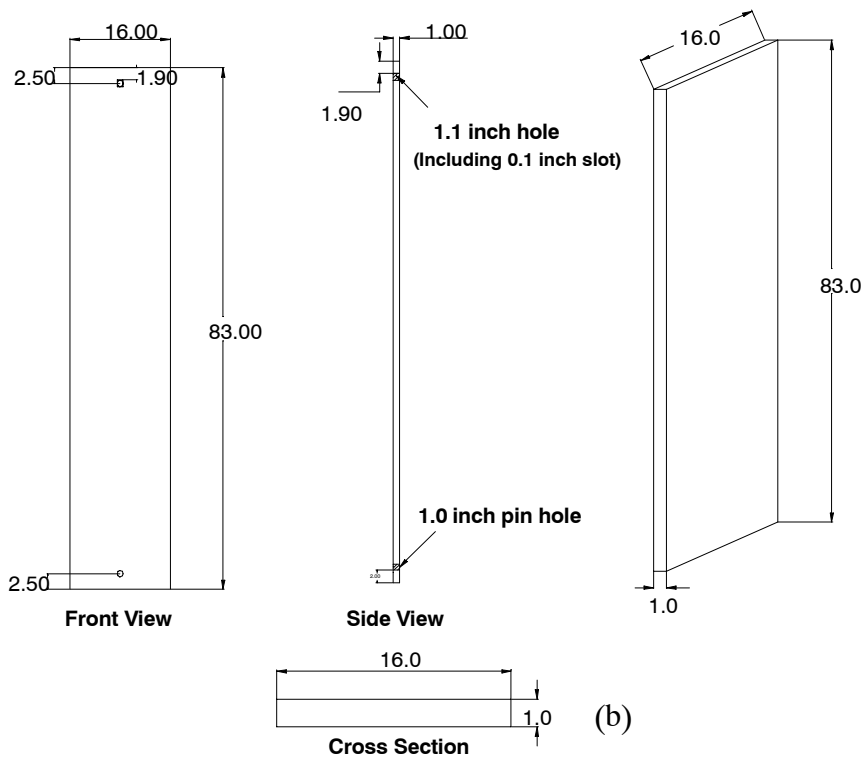
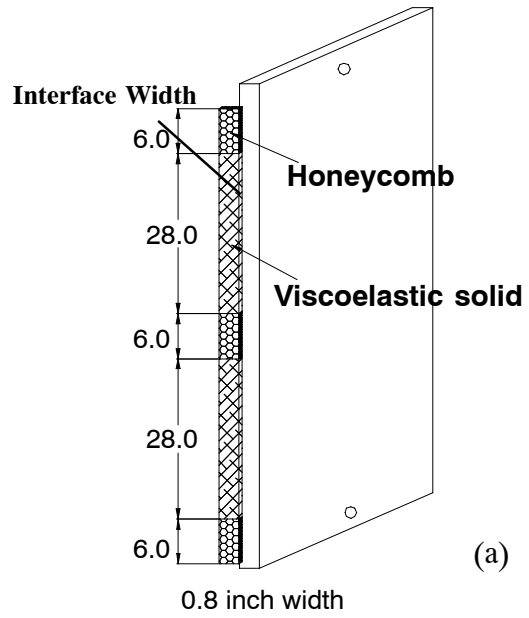


Figure 6-10 The Detail Dimension of a Damping Panel (unit=inch):
(a) Interface Damping Layer (b) FRP Laminate Plate

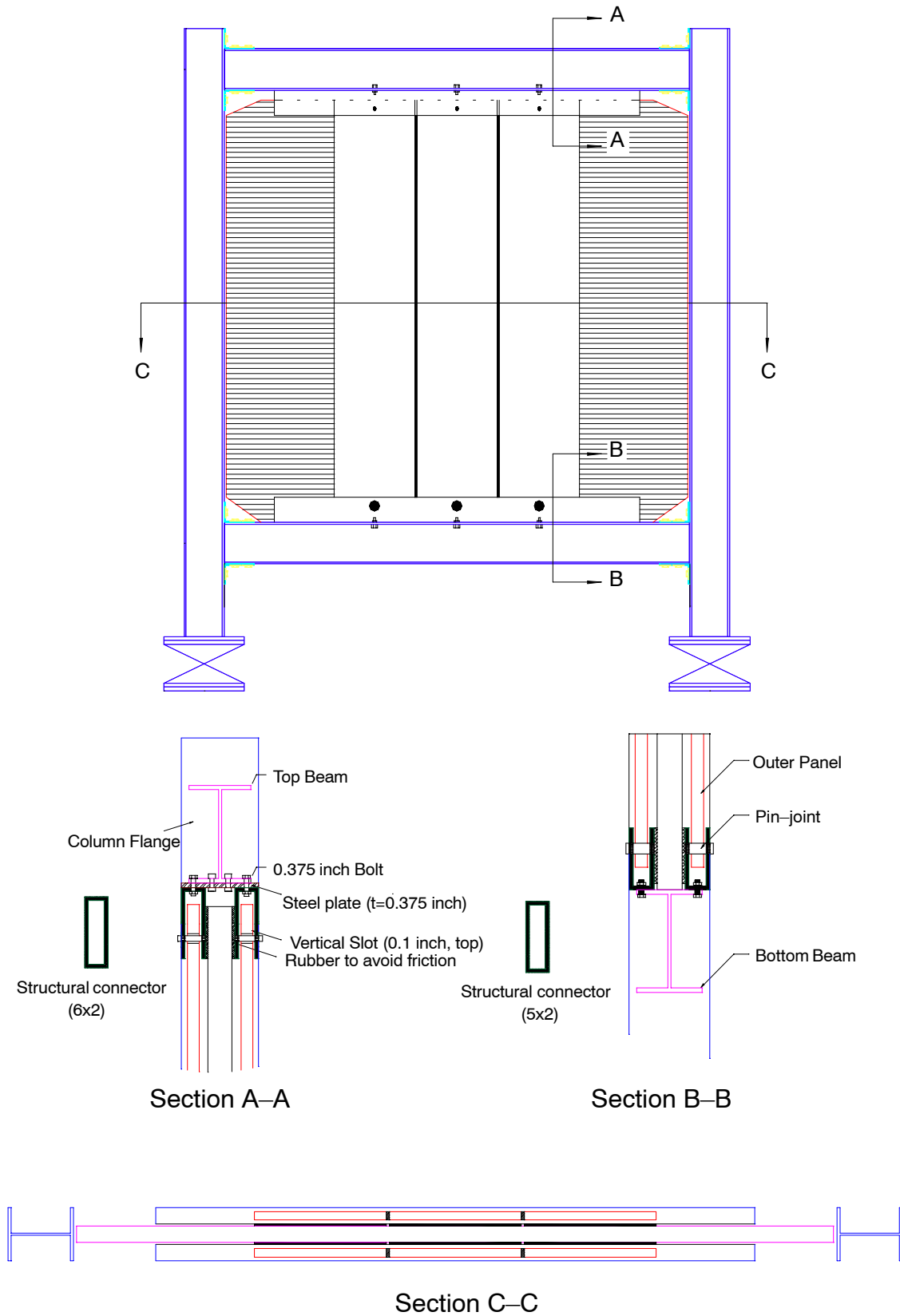


Figure 6-11 The Detail Configuration of Each Cross Section

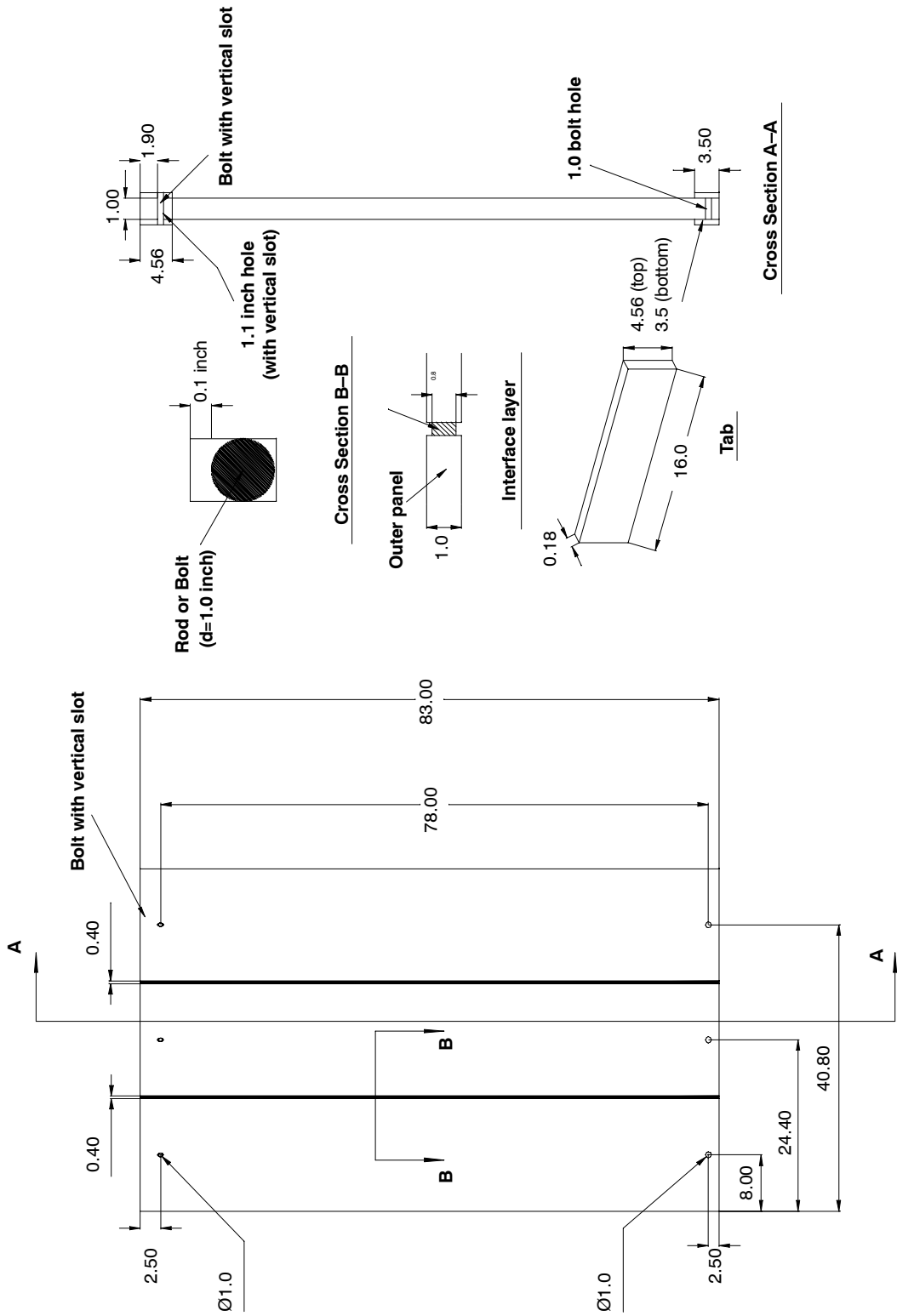


Figure 6-12 The Detail Dimension of Outer Panel (unit = inch)

6.2.2 Construction

Similar to the construction process of the multi-layer PMC infilled frame described in section 4, the PMC sandwich infill wall of the multi-panel infill system was constructed in collaboration with a local company (An-Cor Industrial plastics, Inc., North Tonawanda, NY). A product is formed to the desirable shape by the hand lay-up process. Applied reinforcing and resin materials were of Style 7781 E-glass (0.015" thickness/ply) and Derakane 411-350 Momentum clear with cure, respectively. Several layers were required and their reinforcing orientations were varied according to design. In the fabrication, one side of the foam at a time was considered in lay-up, with every other ply being carried out to completely cover the edge. When the other side is laid up, again carry out every other ply completely onto the edge. This should result in an edge thickness approximately the same as side thickness. Fig. 6-13 shows the completely fabricated PMC sandwich panel. For the purpose of experimental setup, lifting tabs were installed on the surface of the PMC sandwich panel at the top position as depicted in Fig. 6-13.



Figure 6-13 Fabrication of the PMC Sandwich Infill Panel

To get larger passive energy dissipation, the combined composite materials of honeycomb and solid viscoelastic materials were installed at the interface between outer FRP laminates. Based on the ori-

entation of stacking sequence depicted in Fig. 6-5, the fibers orientation for the outer FRP laminates was all in one direction, 90° and each laminate panel was simple flat stock 1.0 inch thickness using several plies of boat cloth on each side of interface. Fig. 6-14 shows the fabrication of the combined damping interface layers.



(c) Combining Polymer Honeycomb and 3M Viscoelastic Materials

Figure 6-14 Detailed Fabrication of the Interface Damping Layer

In the outer damping panel construction, pin joints were fabricated in order to connect the outer damping panel to the top and bottom steel beams. These joints are unavoidable in complex structures

because of their low cost, simplicity, and facilitation of disassembly for repair. Most commonly, these joints are formed by using mechanical fasteners.

In practice, it is important, however, to investigate the failure modes of these pinned connections. Uncertainties regarding the failure of joints in outer FRP laminates may lead to misleading results in the experimental works. According to previous research (Okutan et al., 2001; Ireman et al., 2000), there are, in general, three basic joint failure modes related to composite failure – namely, net-tension, shear out and bearing. In practice, a combination of these failure modes is possible. Typical damages due to each mechanism are shown in Fig. 6-15.

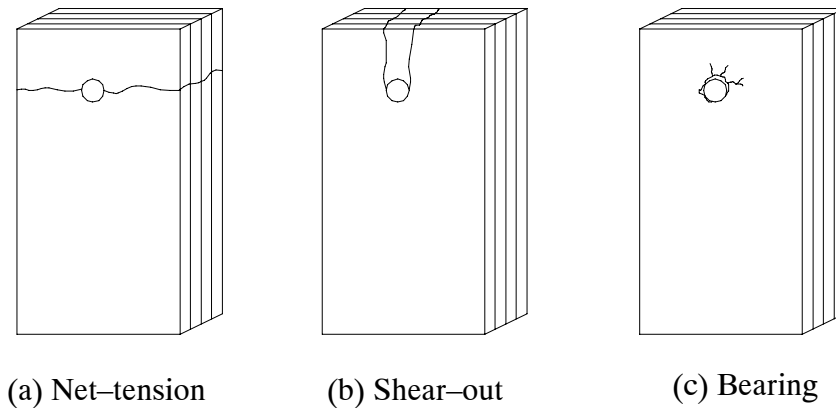


Figure 6-15 Typical Failure Mechanisms for the Pinned-joint Configuration

Joint failure modes for composite materials are generally not similar to those observed in metals, in which the metal exhibits considerable yielding prior to fracture. Yielding does not occur in FRP composites, but some form of pseudo-yielding can be experienced for certain lay-ups in which delamination and partial fiber breakage occurs before final failure. The behavior of the joint could be influenced by four groups of parameters.

Material parameter: fiber types and form, resin types, fiber orientation, laminate stacking sequence, etc.

Geometric parameters: specimen width (W) or ratio of width to hole diameter (W/D), edge distance (E) or ratio of the edge distance to hole diameter (E/D), specimen thickness (t), hole size (D).

Fastener parameter: fastener type, clamping area, hole size.

Design parameter: loading type, loading direction, failure criteria.

In the case of the multi-panel PMC infilled frame, ± 0.25 inch steel plates were sandwiched into the FRP laminate in order to avoid the above uncertain joint failures and a ± 0.5 slot joint with 1.0 inch diameter was considered to relieve the vertical force at the top of the FRP laminate. Fig. 6-16 and 6-17 show the joint connections used in the outer FRP laminates.

In the fabrication process of the sandwiched steel plates, there were three steps: (1) cutting 1/4 inch deep areas into foam to accept carbon steel, (2) squashing the steel into the cutting area, and (3) using thixotropy to fill out where necessary. Finally, each sandwiched steel plate, shown in Fig. 6-18, was assembled together in the hand lay-up process. From the transparent surface of outer FRP laminates, the holes of each joint connection were then drilled.

Fig. 6-19 shows the completed fabrication for the outer FRP panels. To protect the damage of the passive damping layers, 3M hot patches over each inter-panel joint were applied for shipping and rigging purposes.



Figure 6-16 Top Connection of the Outer Damping Panel (Slot)



Figure 6-17 Bottom Connection of Outer Damping Panel (Pin)

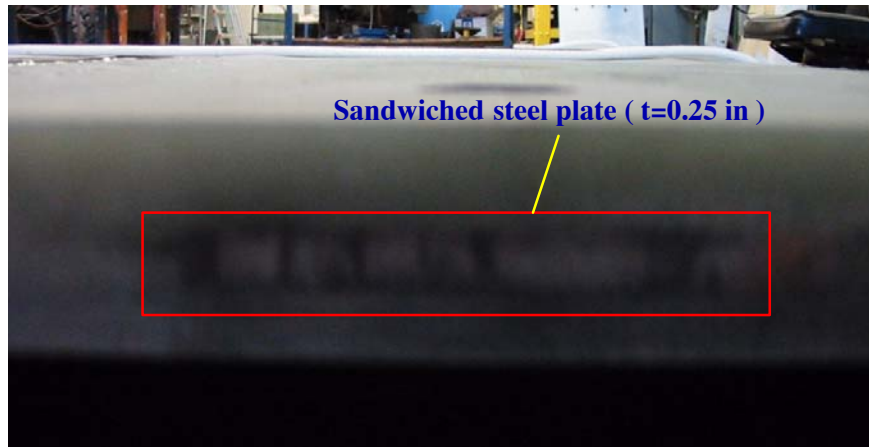


Figure 6-18 Sandwiched Steel Plate in the Outer Damping Panel Laminate



Figure 6-19 View of the Outer Damping Panel

6.3 Design of FRP Box Infill Systems

6.3.1 Design Concept and Structural Configuration

Light and flexible building systems often require specific design features for limiting damage and maximizing occupant comfort and safety. Numerous infill panel arrangements are possible in these design processes. With the same passive energy mechanical concept employed in the outer FRP damping panel in the multi-panel system, a tube-type infill system was proposed to have three FRP box panels instead of laminate plates. Fig. 6-20 shows the geometric configuration of the FRP box-type infill system.

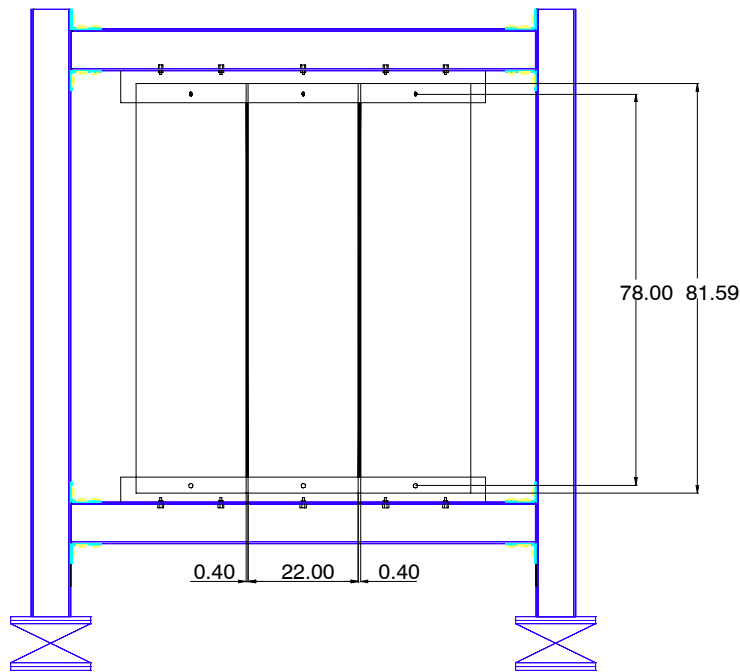


Figure 6-20 The Configuration of FRP Box Infill System (unit=inch)

In this case, significant increase in the damping of a steel frame may be expected by larger damping material space and some amount of initial stiffness will be produced before the polymer honeycomb breaks. In the conceptual design, the interface damping layers in the FRP box infill systems were arranged differently. The arrangement of the interface damping layers in the multi-panel infill panel system was in series, while the combining interface damping layers in the FRP box infill were arranged in parallel. This result may provide more information on the proper arrangement of the damp-

ing interface layers and their behaviors. The main emphasis herein is on quantifying the damping which arises from the cyclic straining of the damping materials in the primary lateral resistant system. Fig. 6-21 illustrates combined arrangement of the constrained passive interface damping layer in the FRP box infill.

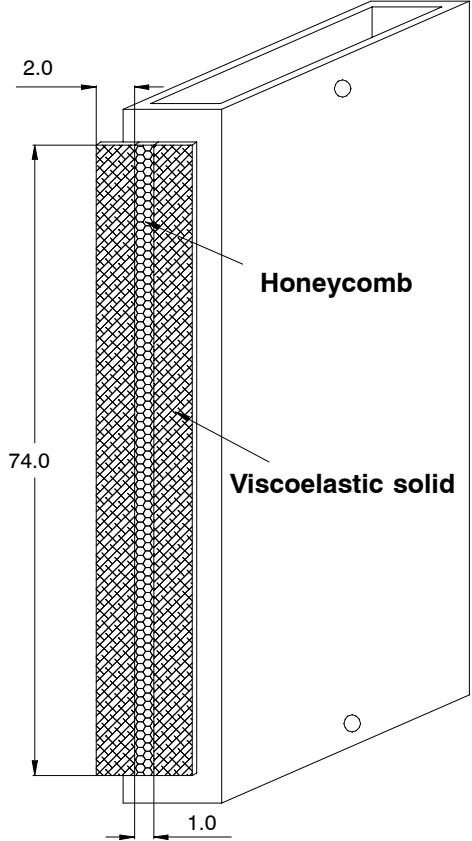


Figure 6-21 The Detail Dimension of Interface Layer (unit=inch)

In the design process of the FRP box infill system, the damping ratio and stiffness of the constrained interface layers are dominant factors. Similar to the design case of the outer FRP damping panel in the multi-panel PMC infill system, the required damping ratio is calculated by analyzing the undamped structure. By choosing the damping ratio, the geometric dimensions of the FRP box infill are designed. In such a case, it is assumed that the lateral resistance of the overall structure will be mainly provided by the steel frame. Although a limited amount of stiffness can be achieved by the

constrained interface damping layers, this may be dependent on the applied strain, the frequency, and the design of the interface properties.

Two cases of the FRP box infill systems were classified on the basis of the properties of the interface damping layers. First, the FRP box infill panel with a stiff and a flexible interface layers was considered. In such a case, a stiff interface layer, which was fabricated by woven-fabric epoxy coating on the surface, was intended to increase the lateral resistance by preventing sliding shear mechanism, while a flexible layer, which is not coated on the surface, was attributed to enhance the damping in the structure. Second, the FRP box damping panel with both flexible interface layers was designed to have a larger damping of the structure as well as comparison of the first case. Fig. 6-22 shows the configuration of each FRP box infill system.

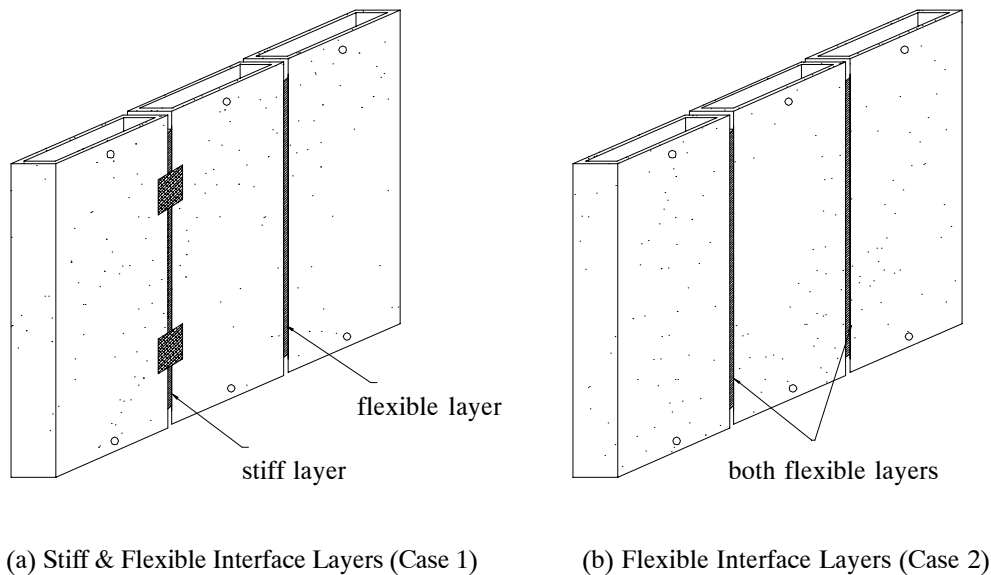


Figure 6-22 The Configuration of Two Types of FRP Box Infill Systems

For the design of the combined interface layers, since larger surface area was provided by the FRP box infill rather than the outer damping plates in the multi-panel PMC infill system described earlier, the applied area of composite damping materials at the interface between the FRP box panels was considered to be twice as large compared to the multi-panel PMC infill system. The designed shear strain of the viscoelastic material under applied static loading was approximately 200% at 2.5% drift. Finally, the FRP box infill was designed as shown in Fig. 6-23. For a given configuration of

the FRP box infills, designed damping ratio should be in the range of 0.1 and 0.4. Similarly, on both faces of the box panel, 0.25 inch thick steel plates were inserted in between the FRP box layers as in the multi-panel infilled frame structure to prevent unexpected pin connection failure.

The main scope of the FRP box infill is to produce shear deformation in the interface layer through the panel deformed shape, and relative lateral displacement. Accordingly, optimum ply stacking sequence and the total ply layer thickness are not important mechanically. In the design process, the chosen thickness of the FRP box section was 0.84 inch. This is the possible value to reduce the weight and costs when the sandwiched steel plates (0.25 inch) are considered. Finally, the stacking sequence with all $[\pm 90^{\circ}_{14}]_s$ was designed for increasing vertical resistance in the FRP box panel system. The ply thickness was 0.03 inch. Fig. 6-24 shows the stacking sequences and fiber orientation along the loading direction. More detailed structural configurations including the connection between the FRP box infill and steel beams are presented in Fig. 6-25. The width of the FRP box section was determined by considering the width of steel beam.

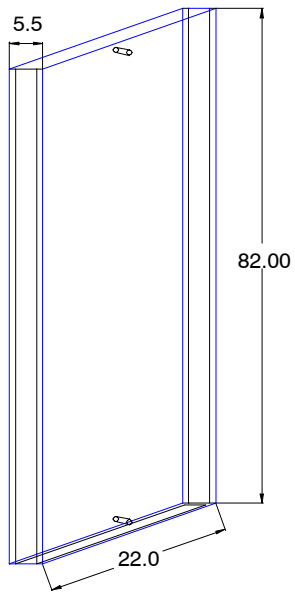
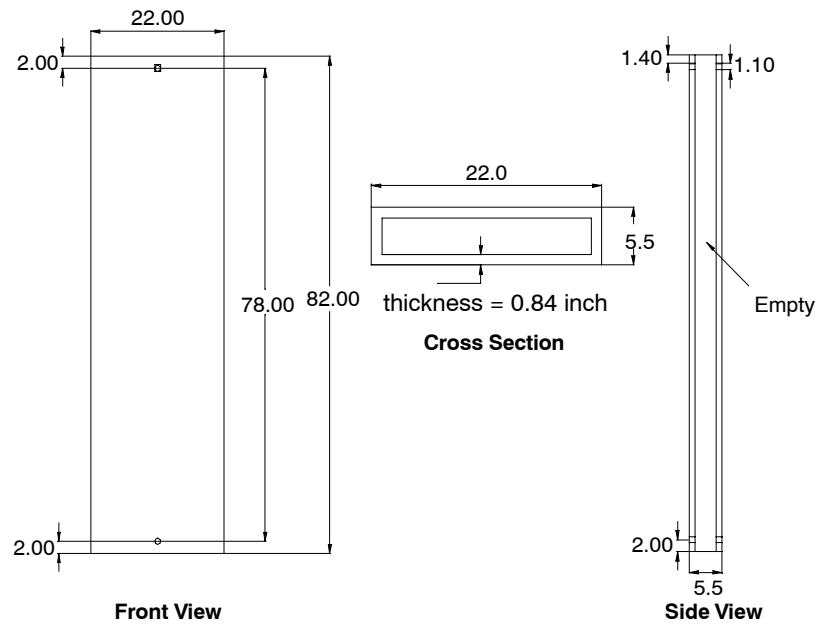


Figure 6-23 The Detailed Description of the FRP Box Infill System (unit=inch)

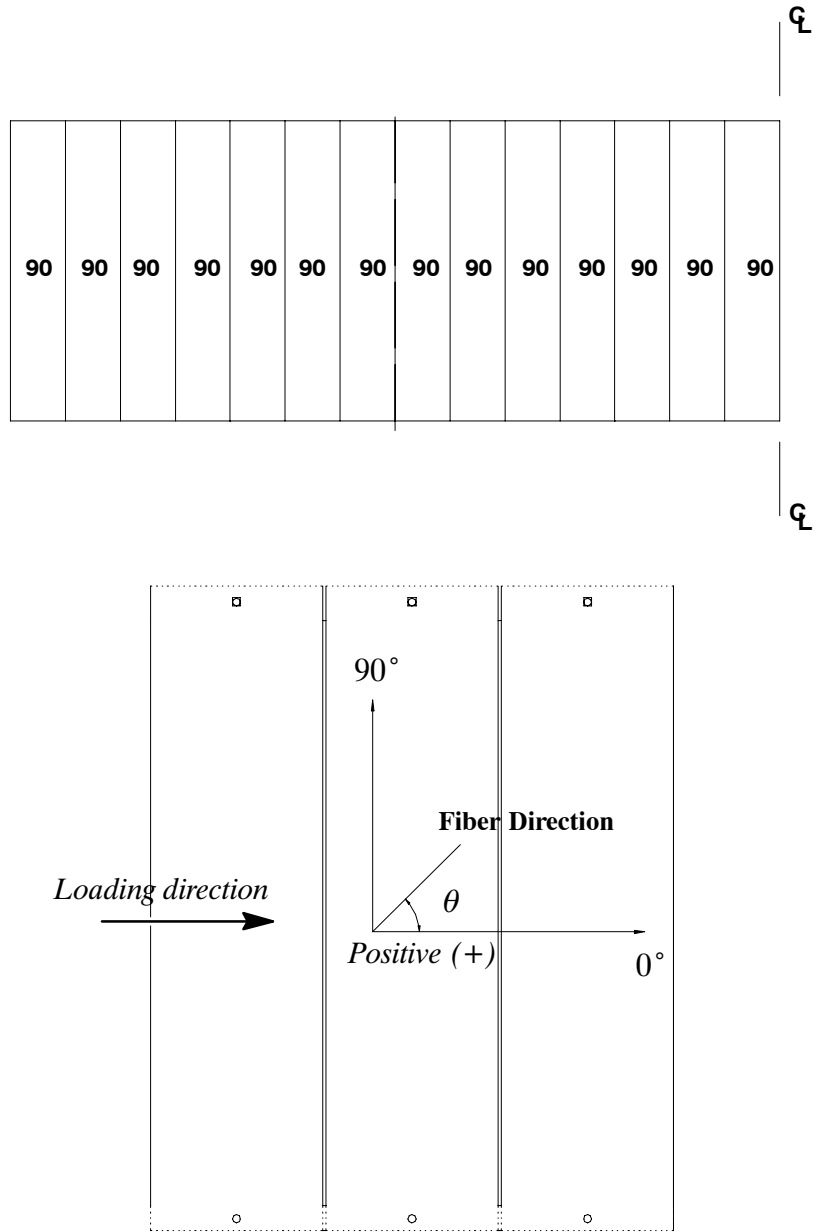
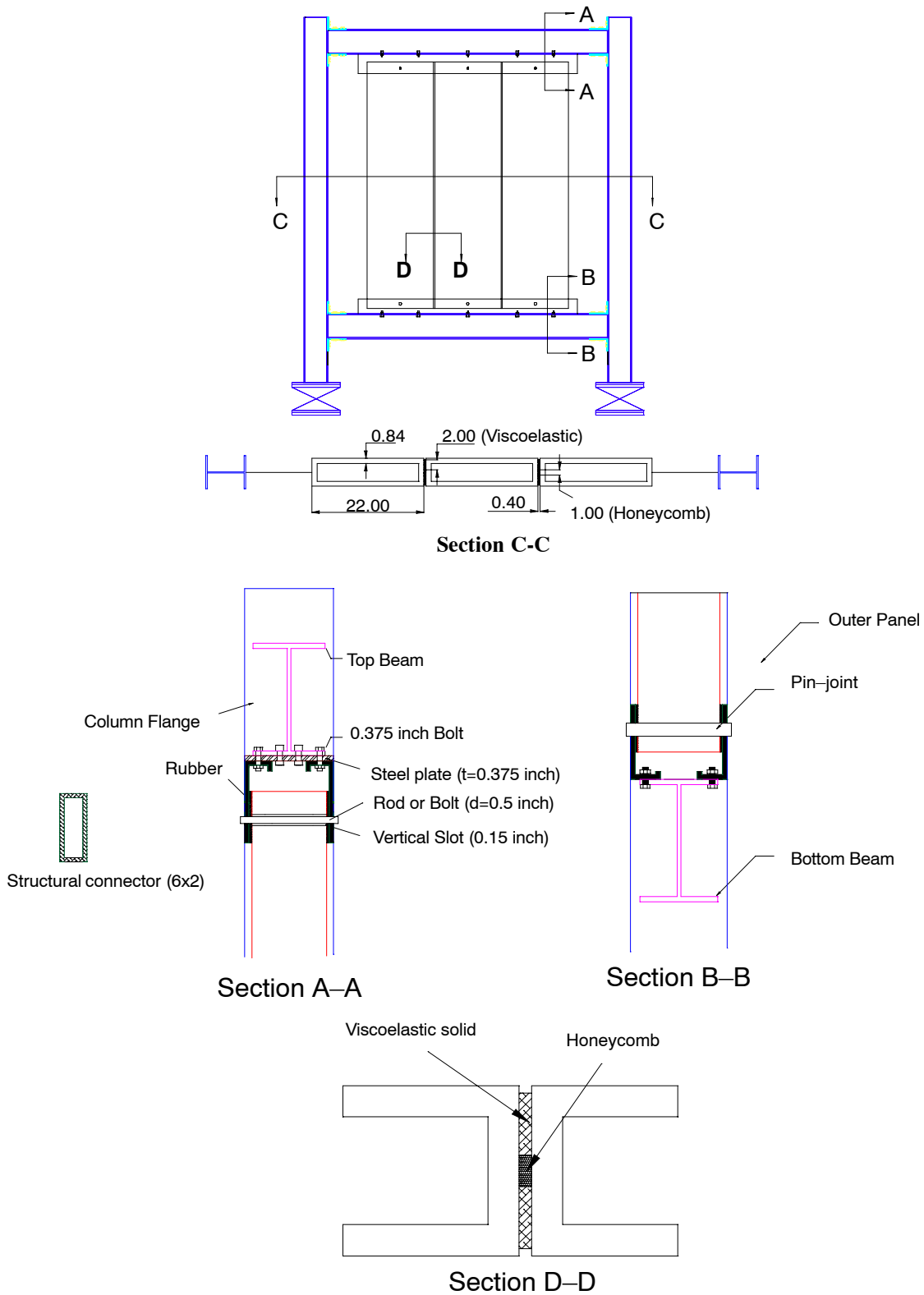


Figure 6-24 The Basic Orientation of FRP Box Infill (Each ply layer = 0.03 inch)



**Figure 6-25 The Configuration of the FRP Box Infill
(Each layer = 0.03 inch)**

6.3.2 Construction

The FRP box infill panel was also fabricated at An-Cor. Industrial Plastics, Inc. (North Tonawanda, NY). By using prefabricated mold composed of stacking layers of 3/4 inch thickness fiberwood, each rectangular composite box section was fabricated individually by the hand-process. The fiber reinforcement and resin materials were Style 7781 E-glass and Derakane 411–350 momentum clear cure, respectively. The Style 7781 E-glass is the same reinforcement used in the multi-panel infill system. Each layer of the laminate was constructed with a $[90^{\circ}_{14}]_S$ direction through the entire thickness of the laminate. The ply thickness was 0.015 inch. After fabricating the FRP box sections, three box sections were squashed together and the polymer honeycomb and 3M viscoelastic solid materials were placed in parallel between them by using a ply of boat cloth on each side of interface. Fig. 6-26 and 6-27 show the full configuration and cross section of the FRP box infill panel. With same mechanical concept of the outer damping panel of the multi-layer infilled frame, slot and pin holes depicted in Fig. 6-28 and 6-29 were also made at the top and bottom surface of each box section, respectively. To avoid premature fracture of these joint holes, 0.25 inch steel plates were also sandwiched into the FRP box infill as shown in Fig. 6-30.

At the interface a bonding adhesive, Dexter HYSOL (EA 9309NA, aerospace adhesive products) and DERAKANE 411–350 epoxy vinyl ester resin were used to provide superior toughness and increased strength. Dexter HYSOL (EA 9309NA) is a commonly used fluid for bonding metal, plastics, and glass. This adhesive is flexible and can resist water, salt spray, and excellent outstanding peel strength to the honeycomb bonding scrim. The high elongation characteristic of DERAKANE 411–350 material provides high bonding strength on the surface of viscoelastic materials during the testing. After completing the fabrication, the test specimen was applied by 3M hot patches over each inter-section joint for shipping and rigging purpose. Fig. 6-31 shows the interface layer made of a stiff by woven fabric-epoxy and resin coating on the surface of the interface layers.

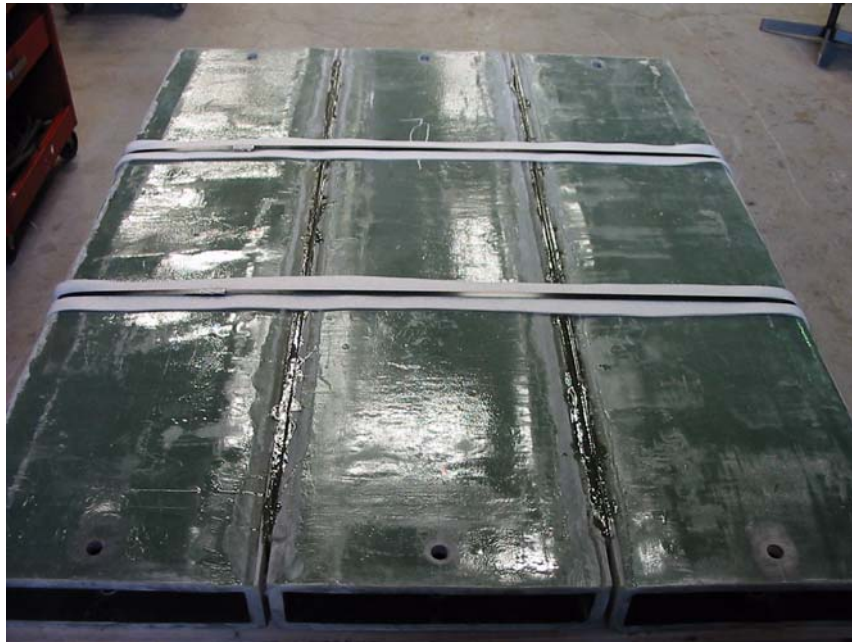


Figure 6-26 Fabricated FRP Box Infill Panel

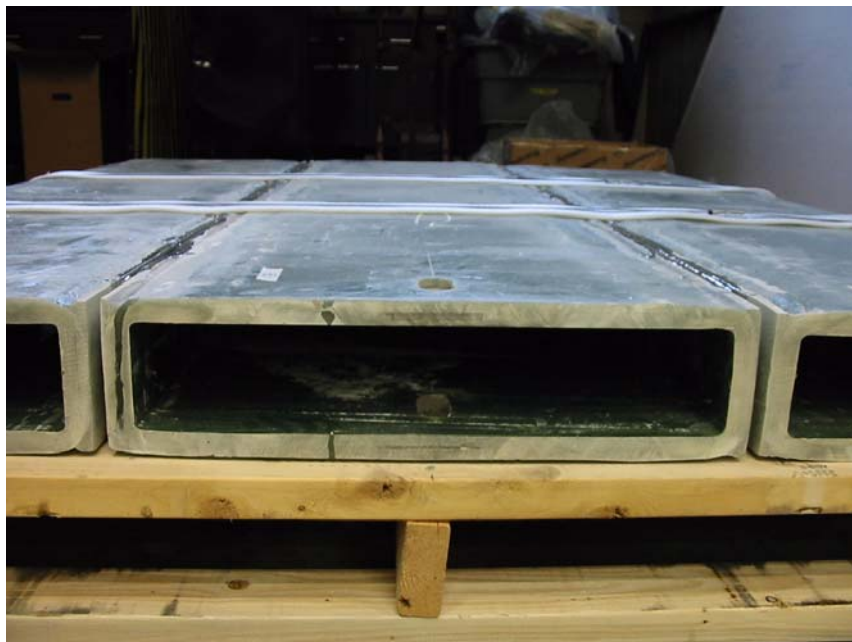


Figure 6-27 Cross Section of FRP Box Infill



Figure 6-28 Top Connection of the FRP Box Infill (Slot)



Figure 6-29 Bottom Connection of the FRP Box Infill (Pin)



Figure 6-30 Sandwiched Steel Plate in the FRP Box Panel

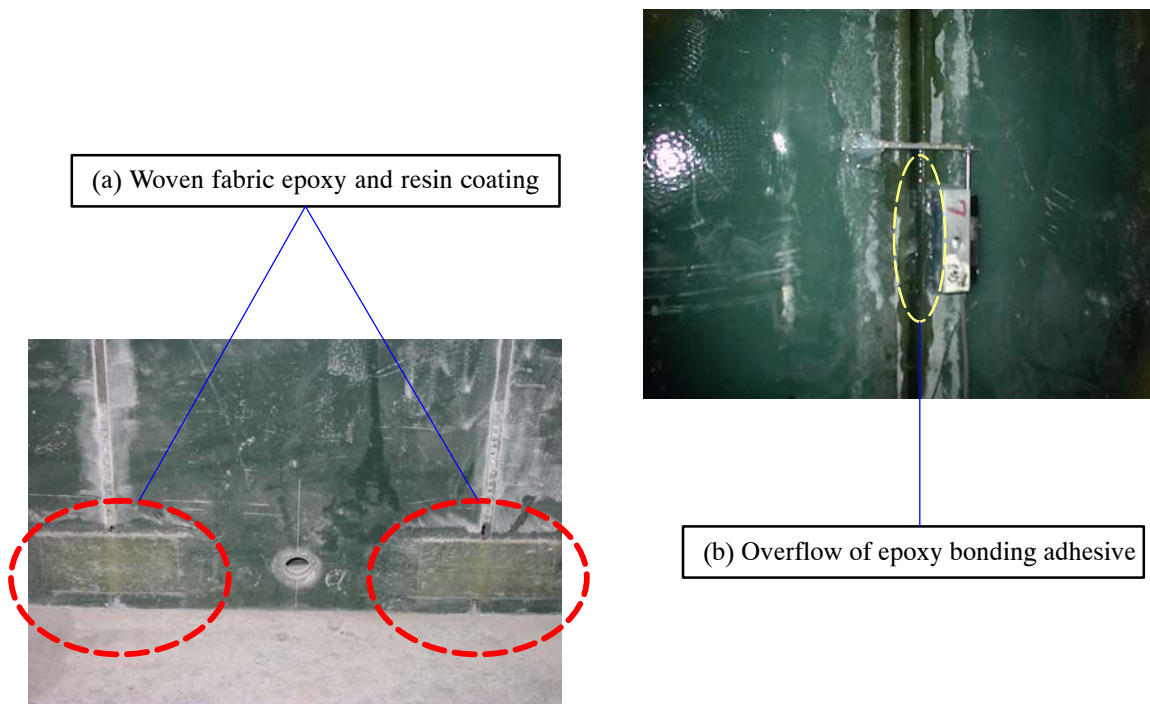


Figure 6-31 Configuration of the Proposed Stiff Layer of the Interface

6.4 Test Cases and Specimen Setup

In this section, two test specimens and the setup for each test are described.

Steel frame with a multi-panel PMC infill system

The multi-panel PMC infilled frame is composed of two structural components, outer panels and inner PMC sandwich panel. In the design process, each component was considered to have individual mechanical behavior upon loading the frame. Therefore, the multi-panel infilled frame test was divided into two stages; a steel frame (1) with the inner PMC sandwich panel and (2) with both inner and outer panels. Considering the experimental setup procedure, a steel frame with the PMC sandwich infill was tested first. Fig. 6-32 shows a steel frame in which a PMC sandwich infill has been placed. The objective of this test is to investigate the response of the PMC infill when allowing designing top and side gaps between the infill and the opening perimeter of the steel frame. As such, only push-over loading test was performed with a careful attention for inflecting any damage in the bolted angle connections. From this test, the expecting contact point obtained by numerical analysis will be investigated by experimental force-displacement relationship, and it is expected during the tests that the post action of the infill can be observed at specific lateral drift due to allowing initial gaps.

In order to achieve theoretically individual mechanism of each component and to erect the infill panel during the tests, wood and rubber spacers were used at the different gaps between the inner PMC sandwich infill and outer FRP damping panels. These materials were chosen to reduce the friction effect. 0.875 inch wood spacers were placed on the middle surface of the infill and 0.25 inch rubber pads were also attached at the angle connector areas. Fig. 6-33 shows the attached wood and rubber spacers using high strength adhesive plastic tapes after finishing the inner PMC sandwich panel test. Consequently, the outer damping panels were setup and tested to evaluate the overall response of the structure. Monotonic and cyclic loadings were applied in this test.



Figure 6-32 PMC Sandwich Infill Setup



Figure 6-33 Wood and Rubber Spacers

In order to set-up the outer damping panels to the steel frame structure, specific connectors were required in this study. By combining an L-shape angle (L 6 x 3.5 x 0.5) and a steel plate (PL 6 x 6 x 0.5), a beam-to-panel angle connector was developed. The beam-to-panel angle connectors can be attached to the top and bottom holes of the outer damping panels by using 1.0-inch high-strength A325 bolts. In the experimental phase, the outer FRP damping panels with beam-to-panel connectors were delivered into the opening of steel frame and fixed by welding with the steel beams. Fig 6-34 and 6-35 illustrate the geometric configuration and the setup process of the beam-to-panel connectors, respectively.

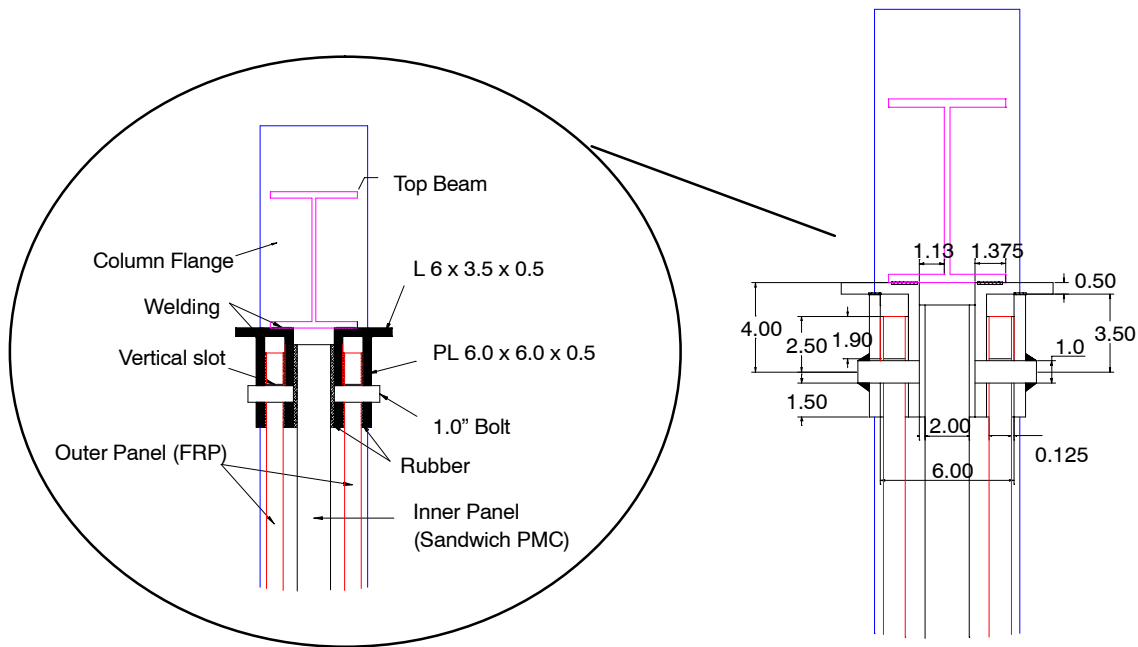
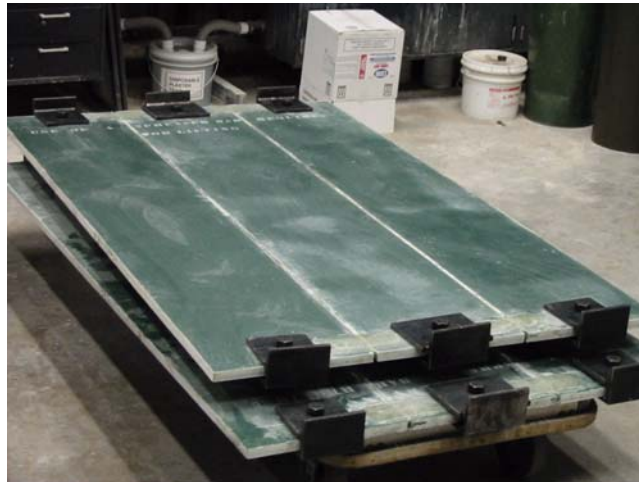


Figure 6-34 Design of Outer Damping Panel Connectors (unit=inch)

For easy installation of the outer damping panel, parts of structural components such as top beam and guide wheels were removed temporarily. Then, outer damping panels were placed on both sides of the PMC sandwich infill panel. The installation of outer panel on both sides will be helpful to provide larger buckling resistance by restraining out-of-plane behavior of the inner PMC sandwich infill. Fig. 6-36 shows the completed setup of the PMC sandwich infill panel and the FRP outer damping panel system.



(a) Fabricating Beam-to-panel Connector



(b) Installing Beam-to-panel Connector to Outer Damping Panel



(c) Setup Outer Damping Panel to the Tested Frame by weld

Figure 6-35 Fabrication Process of Beam-to-Panel Connector



Figure 6-36 Multi-panel PMC Infill Panel Setup

Steel frame with FRP box infills

A relatively flexible structural infill panel was applied to investigate the response under monotonic and cyclic loading conditions. The relatively flexible infill panel consists of FRP box sections and composite damping materials at the interface between them. In this study, three FRP box sections were employed due to high material costs.

Based upon the characteristics of the interface damping layers, two experimental cases were carried out here; a steel frame with (1) a stiff and a flexible damping interface layers, and (2) both flexible damping interface layers. After finishing the first case, woven fabric-epoxy coatings on the stiff interface were grinded away for making a flexible interface damping layer which allows shear deformation of the interface during the test.

The connection of the FRP box infill system to steel frame utilizes twelve sets of beam-to-panel connectors Fig. 6-37 shows the completed test specimen setup and the beam-to-panel connectors.

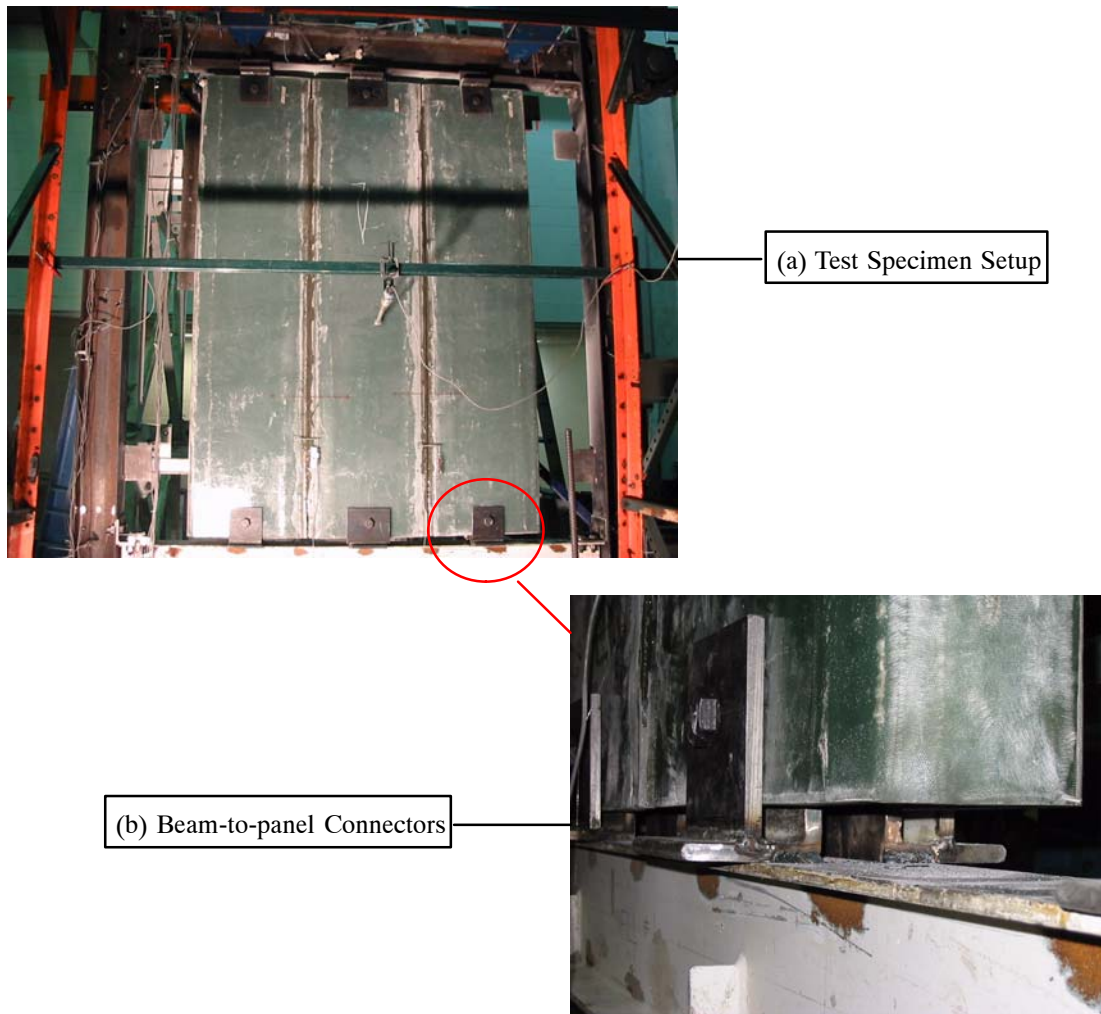


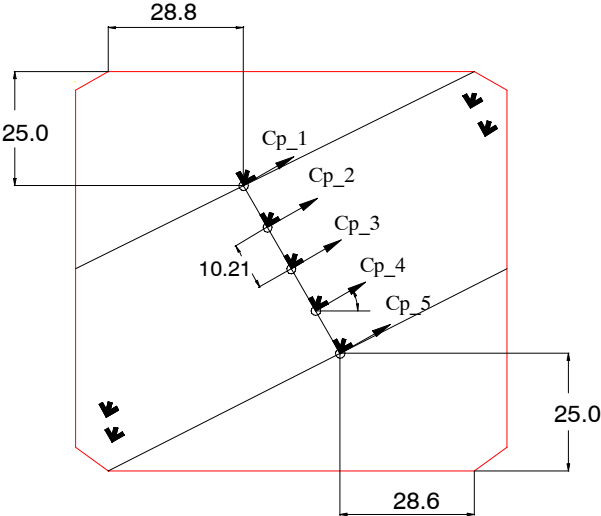
Figure 6-37 FRP Box Infill System Setup

6.5 Experimental Description

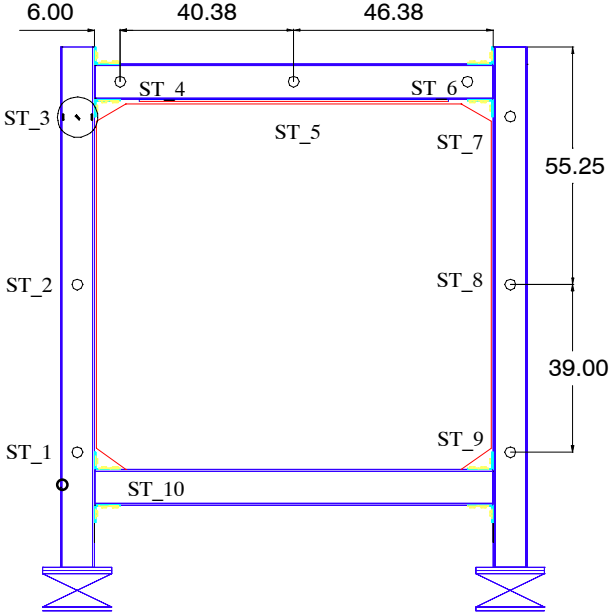
6.5.1 Instrumentations

The specimens were instrumented to provide key quantities to characterize the structural response of the frame, the infill walls, and the constrained interface layers. The typical instrumentations were already illustrated in section 4. (depicted in Fig. 4-23). In this stage, additional measurement instruments were used for each individual test depending on the geometrical configuration and the response of the infill walls. In the cases of the multi-panel PMC infilled frame test, more strain gauges were used to determine the compressive straining actions at the PMC sandwich infill panel and the steel frame. The location and evaluation of the strain gauges are shown in Fig. 6-38 and 6-39. Five

pairs of strain gages, that suited composite material, were bonded at the center of the inner PMC sandwich panels because the strut generally tends to be wider towards the center of the infill panel. These strain measurements were intended to determine the direction of the principal strains of the infill. Accordingly, the equivalent strut angle of the PMC infill could be predicted.



(a) PMC Sandwich Infill Panel



(b) Steel Frame

Figure 6-38 Strain Gage Location at the Inner Panel and the Steel Members (Cp: Composite strain pairs, ST: Steel strain pairs, unit=inch)

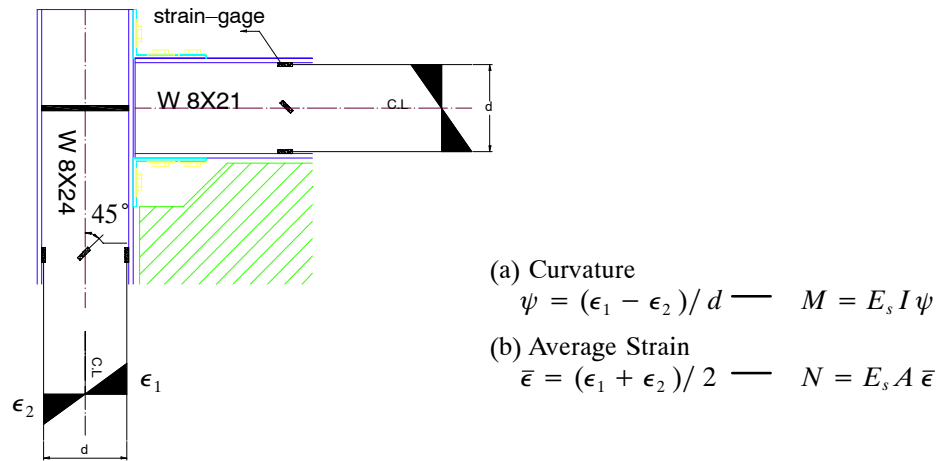


Figure 6-39 Calculation of the Steel Straining Actions

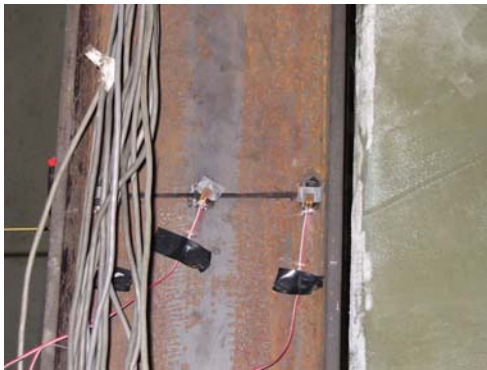
For steel frame members, 9 pairs of strain gages (ST_1 to ST_9) were used to determine moment distributions of steel members and, in particular, a pair of strain gages were attached to measure the moment-rotation relation at the end of the bottom beam. For each pair, three strain gages were bonded to the web of the steel column . Two gages designated 1 and 2 (one close to each flange) measured the strains along the axial direction of the member (ϵ_1, ϵ_2). From these gages, the curvature (ψ) and the average strain ($\bar{\epsilon}$) at that section were calculated as shown in Fig. 6-39. The chosen sign convention implies that positive curvature means tension and positive average strain implies axial tensile strain. The computed bending moment (M) and axial force (N) at any section are linearly proportional to the curvature (ψ) and average strain ($\bar{\epsilon}$) at that section. It is assumed that the strain and corresponding stress in the frame member for all the conducted experiments remained below elastic limit. Practically, because infilled frame, relative to the same non-infilled frame subjected to similar forces, is to reduce substantially the bending moments in the members, the steel frame has not developed a plastic collapse mechanism and still has considerable capacity to withstand higher stress while at the peak racking load. The experimental setup for applied strain gages was presented in Fig. 6-40.

The layout of the special instrumentation in the joint region is shown in Fig. 6-41 (a). First, two sets of linear potentiometers were placed on the top and bottom of the bolted semi-rigid connections. Two longitudinally mounted potentiometers (P1HS, P2HS) were used at the connection to measure

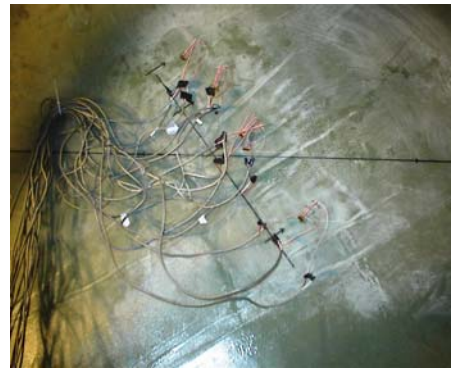
displacement related to the connection rotation. Fig. 6-42 presents local instrumentations for bolted top and seat angle connections. Determination of relative connection rotation (θ) is shown in Fig. 6-41 (b) The following is the function of connection rotation,

$$\theta = \frac{[\Delta(P1HS) - \Delta(P2HS)]}{d} \text{ or } \frac{[\Delta(P3VS) - \Delta(P4VS)]}{L} \quad (6-6)$$

Moreover, another set of linear potentiometers were used to capture the shear deformation of the interface damping materials when the structure was subjected to the applied force. The layout of the interface linear potentiometer is illustrated in Fig. 6-43.



(a) Strain Gages at the Column



(b) Strain Gages at the PMC Panel

Figure 6-40 Strain Gage Setup of the Test Specimen

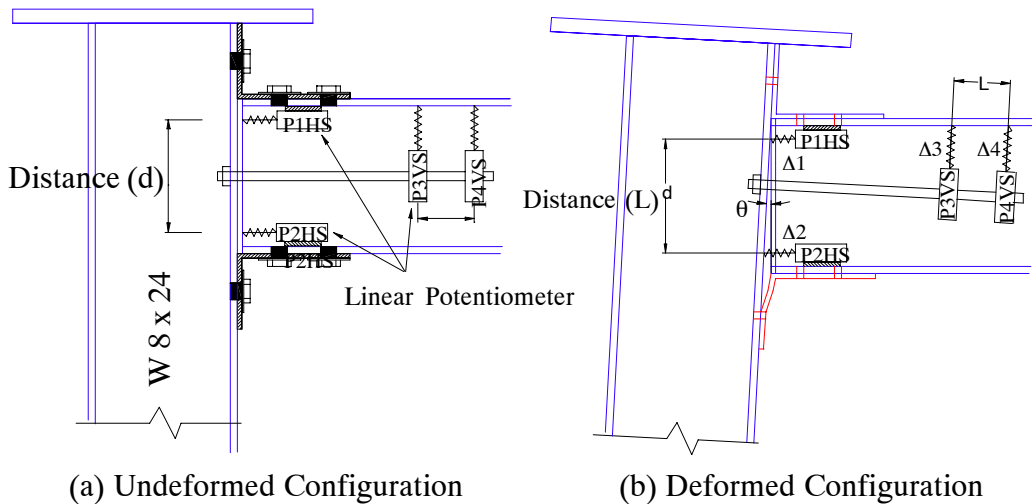


Figure 6-41 Joint Angle Connection Instrumentation

In the experimental setup, a linear potentiometer was bonded to one panel, and the rigid thin steel plate was fixed to the other panel. From such instrumentation setup, the relative displacement between them could be measured.

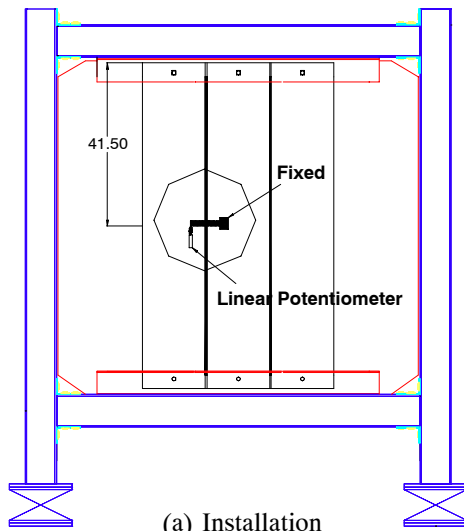


(a) LP at Joint Angle Connection

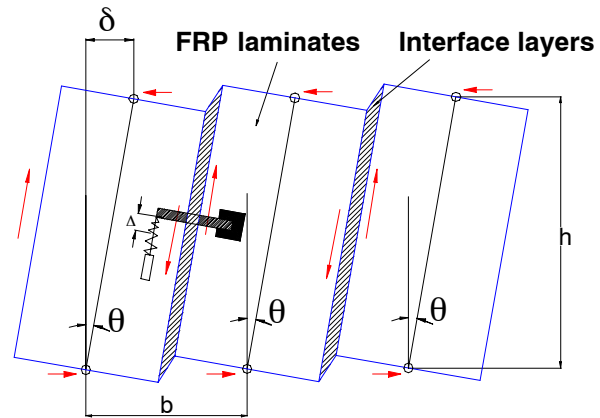


(b) LP at Interface Damping Layer

Figure 6-42 Linear Potentiometers for Special Measurements



(a) Installation



(b) Deformed Shape

Figure 6-43 Linear Potentiometer Setup at the Interface Layers

Two sets of linear variable differential transformers (LVDTs) were used to measure the absolute diagonal displacement as well as out-of-plane displacement of the infill panel. As shown in Fig. 6-44, LVDTs were placed along the diagonal and off-diagonal directions using magnetic bases. Out-of-plane LVDT measurement depicted in Fig. 4-23 (d) could be inconsistent and depended on the exact location of the buckling mode.

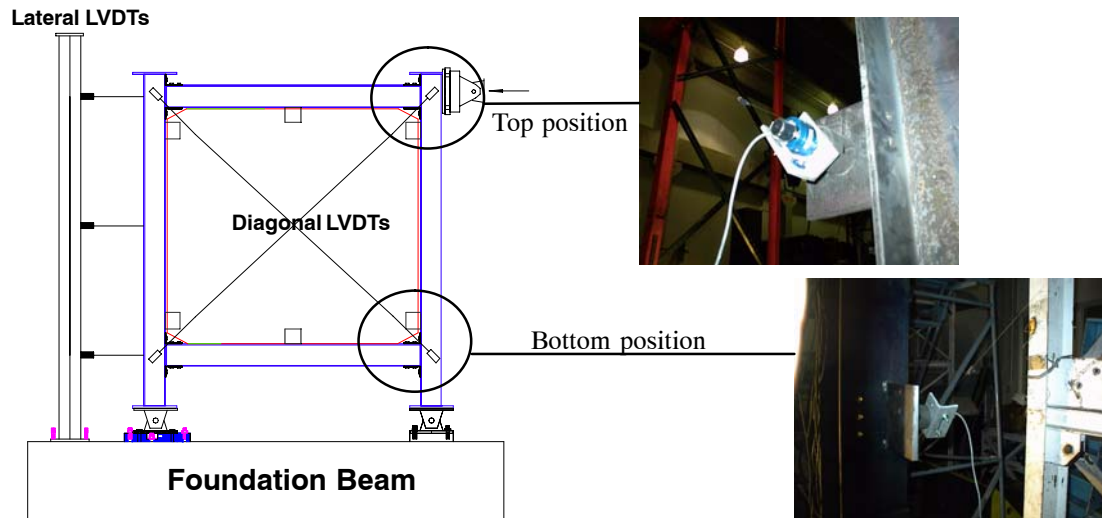


Figure 6-44 Design of Diagonal and Out-of-plane LVDTs

6.5.2 Loading System and History Protocol

The single-story frame specimen was subjected to sine-wave lateral displacement of constant amplitude. The load is applied to the top beam (W 8 x 21). A displacement feedback hydraulic actuator of 100 kips capacity with a stroke of ± 4 inches and a closed-loop MTS servo control system were used to control the actuator displacement. An externally mounted LVDTs on the specimen provided the necessary displacement feedback to the MTS controller. The displacement at the loaded point of the structure and the corresponding load are monitored and displayed using the graphical interface of the control software. The end of the actuator attached to the tested specimen allowed in-plane free rotation of the actuator axis with respect to the specimen. Therefore, there was no action applied due to rotational restraint from the actuator assembly.

The choice of the testing program and the associated loading history depends on the purpose of the experiment and the type of anticipated failure mode such as rapid or slow strength deterioration. Based on the multi-layer PMC infilled frame test described in section 4, multi-step test was also employed to allow for visual inspection. However, due to frequency effect of the viscoelastic material at the interface, the test specimens were cycled at least three times at assigned displacement under different frequencies. The displacement level was increased gradually by either 0.25% or 0.5% drift depending on the observed behavior of the structure. A sinusoidal wave form was then used to con-

control the input displacement histories. The applied amplitude of the test specimen for each lateral drift is illustrated in Table 6-3. Considering that the maximum velocity of the applied hydraulic actuator is 0.6 inch/sec, the possible frequency for each assigned displacement was shown in Table 6-4.

Table 6-3 The Applied Displacements of the Tests

Drift	Total Disp	Inter-story disp
0.25 & 0.5 % drift	0.295 in & 0.59 in (1.5 cm)	0.47 in (1.2cm)
1.0 % drift	1.18 in (3.0 cm)	0.94 in (2.4cm)
1.5 % drift	1.77 in (4.5 cm)	1.41 in (3.6cm)
2.0 % drift	2.36 in (6.0 cm)	1.88 in (4.79cm)
2.5% drift	2.95 in (7.5cm)	2.36 in (6.0 cm)
3.0% drift	3.54 in (9.0cm)	2.83 in (7.2 cm)

The test was paused after each test case so that the onset or progress of damage was visually inspected where the interface layers and the bolted semi-rigid angle connections were examined. Finally, the test was stopped when either the breaking of the bolted semi-rigid connections or buckling of PMC sandwich panel occurs. The applied displacement patterns consisted of two cycles of constant displacement histories as illustrated in Fig.6-45.

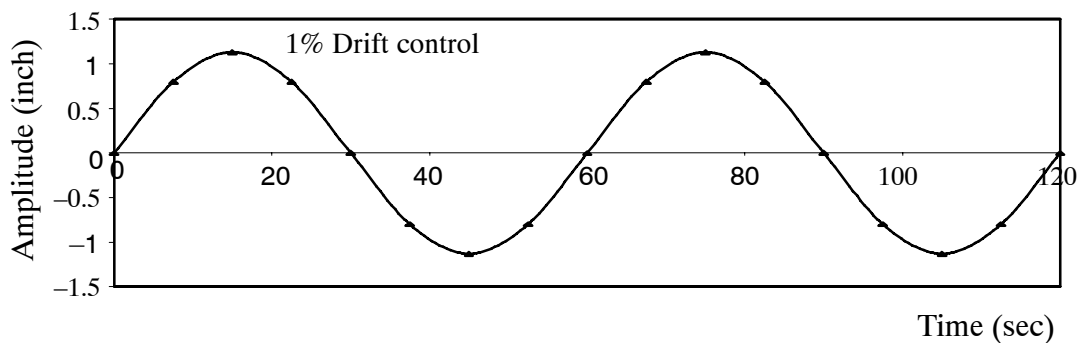


Figure 6-45 Displacement Pattern Applied Cyclic Loading

Table 6-4 Possible Frequency for Assigned Displacements

Total Displacement	0.12 in (0.1%)	0.19 in (0.16%)	0.3 in (0.25%)
Max. Velocity (in / sec)	0.6	0.6	0.6
Max. Freq (Hz)	0.81	0.5	0.324
Max. Period (T)	1 cycle / 1.24 sec	1 cycle / 2 sec	1 cycle / 3.1 sec
Min. Velocity (in / sec)	0.3	0.3	0.3
Min. Freq (Hz)	0.4	0.25	0.162
Min. Period (T)	1 cycle / 2.51 sec	1 cycle / 4 sec	1 cycle / 6.2 sec
Total Displacement	0.59 in (0.5%)	0.89 in (0.75%)	1.18 in (1.0%)
Max. Velocity (in / sec)	0.6	0.6	0.6
Max. Freq (Hz)	0.16	0.1	0.08
Max. Period (T)	1 cycle / 6.2 sec	1 cycle / 9.3 sec	1 cycle / 12.4 sec
Min. Velocity (in / sec)	0.3	0.3	0.3
Min. Freq (Hz)	0.08	0.05	0.04
Min. Period (T)	1 cycle / 12.4 sec	1 cycle / 20 sec	1 cycle / 25 sec
Total Displacement	1.77 in (1.5%)	2.36 in (2.0%)	3.54 in (3.0%)
Max. Velocity (in / sec)	0.6	0.6	0.6
Max. Freq (Hz)	0.054	0.04	0.027
Max. Period (T)	1 cycle / 18.5 sec	1 cycle / 25 sec	1 cycle / 37 sec
Min. Velocity (in / sec)	0.3	0.3	0.3
Min. Freq (Hz)	0.027	0.02	0.0135
Min. Period (T)	1 cycle / 37 sec	1 cycle / 50 sec	1 cycle / 74 sec

6.6 Results and Discussions

The purpose of experiments is to evaluate seismic performance of the proposed infill system as part of structures. Adequate performance implies that a component fulfills a set of specified performance requirements. These requirements may be based on various measures, such as, the stiffness and strength characteristics, deformation capacity, and energy dissipation characteristics. For a component this implies that its role within a structure needs to be identified and its capacities as well as the demands imposed by applied loading need to be quantified.

6.6.1 Results of Multi-panel PMC Infilled Frame Test

Testing of a Steel Frame with the inner PMC Sandwich Infill Panel

A static experiment on a steel frame with the PMC sandwich infill with monotonically increasing lateral load was conducted. The purposes of this test were to investigate in-plane behaviors of the PMC sandwich infill along with preset initial top and side gaps. The force-displacement relation obtained from the test clearly indicated that the contact point of the PMC infill with designing gaps was approximately 2.0 inch. Fig. 6-46 presents the force-displacement response of the PMC sandwich infill panel with allowing initial gaps. Beyond that point, there is a progressive increase in lateral load resistance as the contact area increases. The test result for the contact point is verified by finite element analysis as shown in Fig. 6-6.

As shown in Fig. 6-47, it was observed by the shape of the loading and unloading curve that hysteresis loops are apparent. This is an evidence of sliding shear mechanism as well as the potential bolted angle connections yielding before the contact. When the contact occurred, the test was stopped to avoid further damage of bolted angle connections since the contact will attract large forces and, hence, damage the connection. From the inter-story drift vs. joint rotation response (depicted in Fig. 6-48), it can be seen that the bottom rotation was relatively smaller than the top. The bottom joint appeared to be moving less probably due to some extra stiffening and strengthening in that corner of the PMC infill. Fig. 6-49 presents the moment-rotation relation of the PMC sandwich infilled frame at the top angle connection where the contact occurs under push-over load.

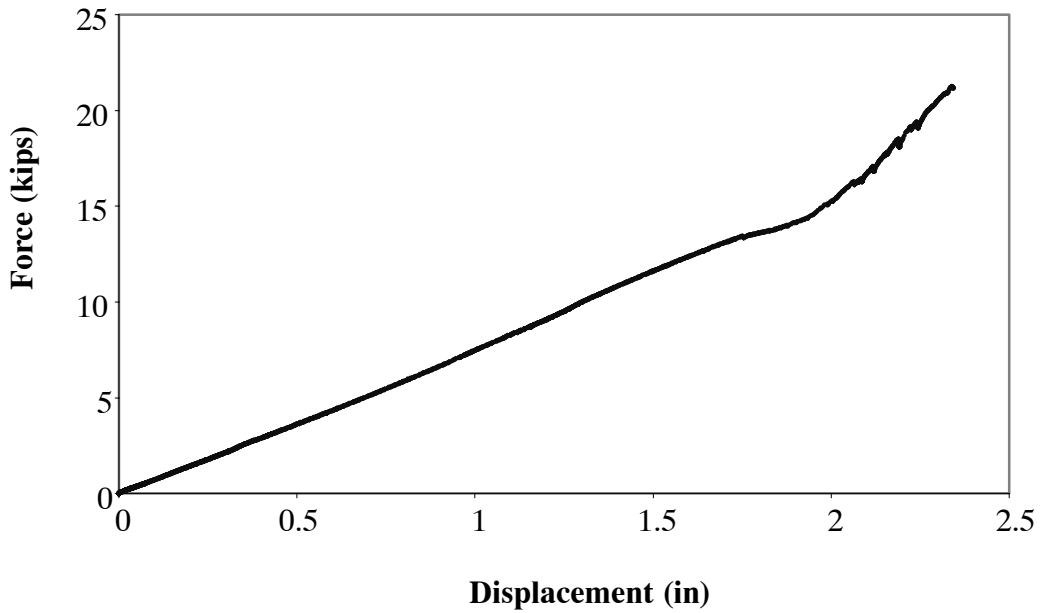


Figure 6-46 Force-displacement Relationship of the PMC Sandwich Infill Panel under Push-over load

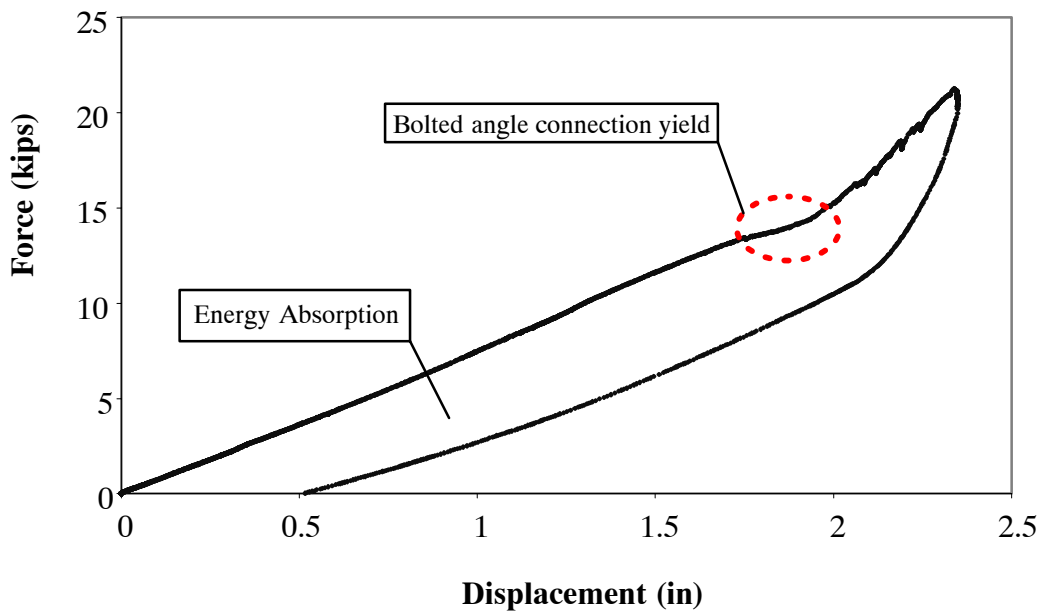


Figure 6-47 Loading and Unloading Relation of the PMC Sandwich Infill

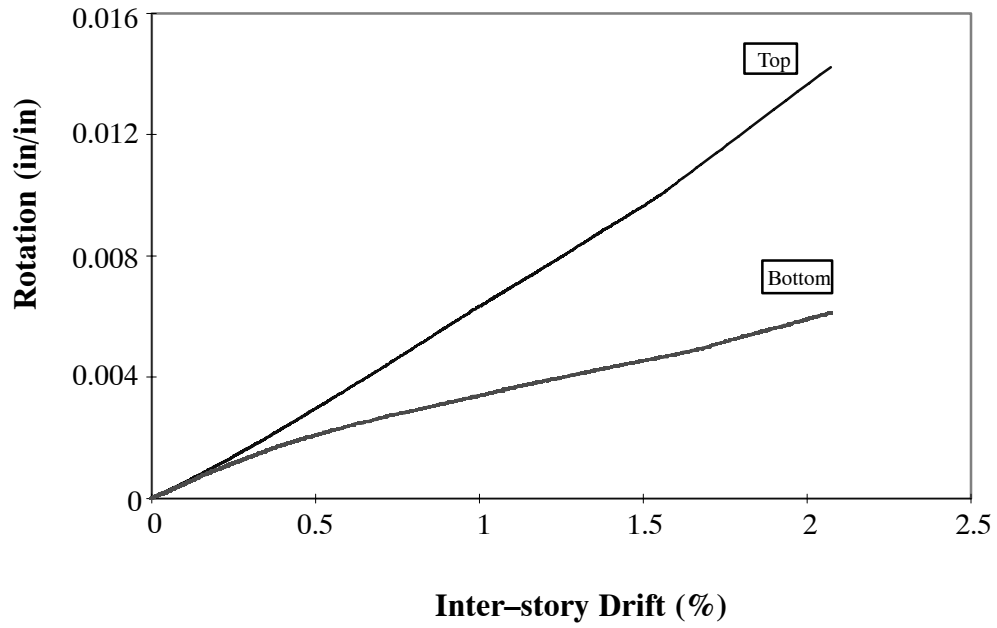


Figure 6-48 Comparison of Inter-story Drift - Rotation Relation of Each Joint Angle Connection

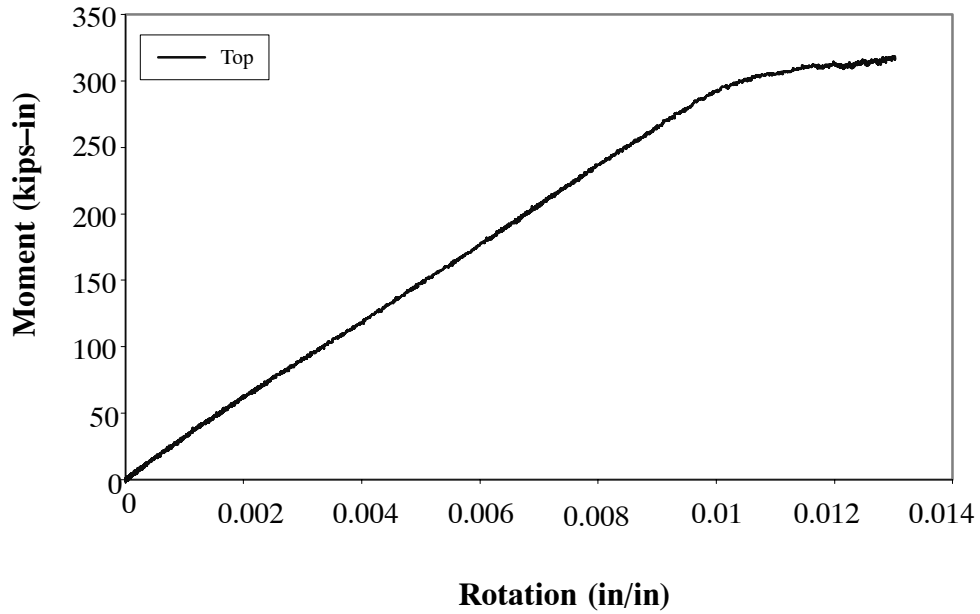


Figure 6-49 Moment-Rotation Relation of Top Joint Connection (PMC Sandwich Infilled Frame Test, Push-over Load)

In the PMC sandwich infill panel test, several pairs of strain gages were used at both columns and the upper beam. The location of each strain gage is illustrated in Fig. 6-38. This was necessary because it was not fully known as to how the frame would react with a PMC sandwich infill placed inside it. The moments at each strain gage location were captured when either maximum positive loading or maximum negative loading was applied. Fig. 6-50 and 6-51 indicate that the obtained maximum bending moment was less than section yield moment so that the frame members remained in the elastic range. Fig. 6-52 and 6-53 show the substantial reduction of bending moment on the structural frame members by the effect of the PMC infill.

The variation of the strain measurements at different locations on the PMC infill wall is illustrated in Fig. 6-54. It shows the variation of the corresponding strain amplitude on the PMC infill panel before and after the contact between the infill and steel frame under the push-over load. From these strain actions of the infill, an equivalent strut acting in compression can only be generally defined to represent the effect of the infill on the bounding frame members. However, in the laminate structures having orthotropic properties, the magnitude and direction of the stress and strain for the principal planes are varied through the layers.

In this study, an equivalent strut angle of the PMC infill panel was simply determined following the principal strain direction. More detailed discussions on the principal stress and strain directions of the FRP laminates are presented in the reference (Jones, 1999). The results for strut angle along principal material and global coordinates are between 35° and 40° as shown in Fig. 6-55 and Fig. 6-56, respectively. For the compressive strut angle with respect to the principal stress plane, the optimum angle obtained by summing total force will be recommended as a strut angle value. Practically, the strut angle for principal stress direction varies with the arranged stacking sequence of laminates.

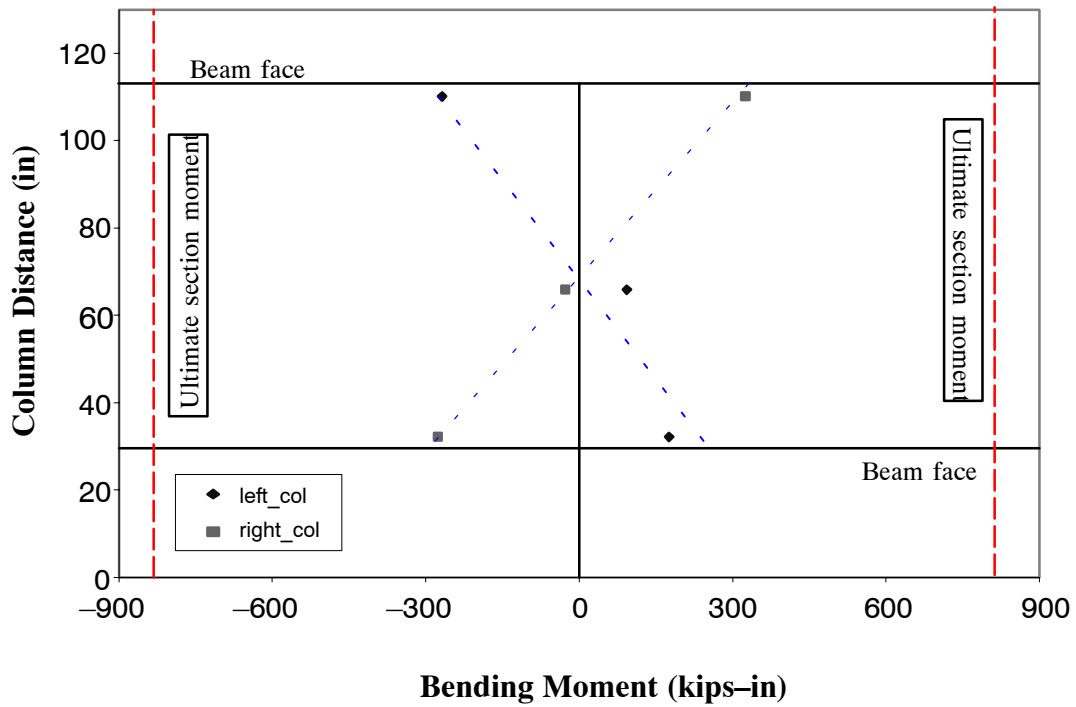


Figure 6-50 Maximum Moment Distribution of Steel Column under Push-over Test (2.0%)

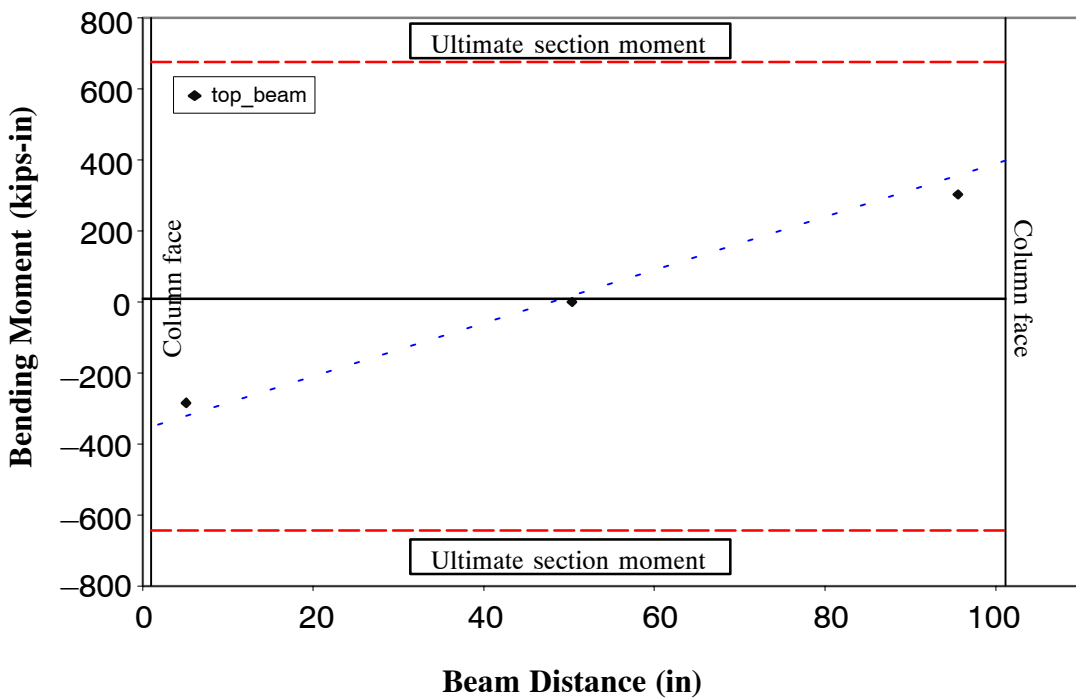


Figure 6-51 Maximum Moment Distribution of Steel Beam under Push-over Test (2.0%)

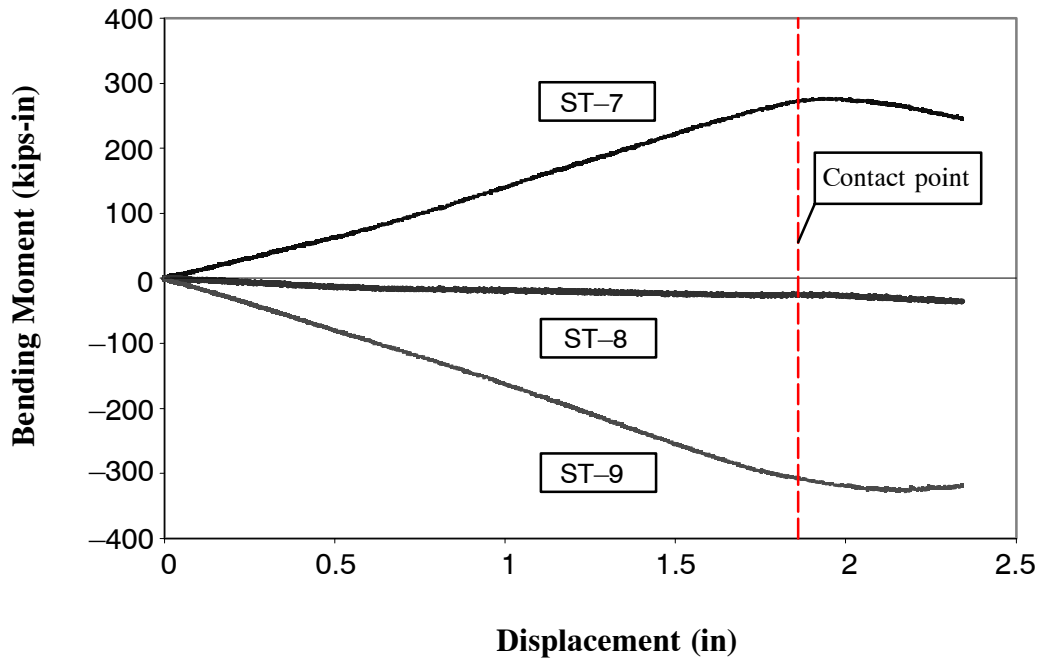


Figure 6-52 Reduction of Bending Moment at the Column after the Contact Point

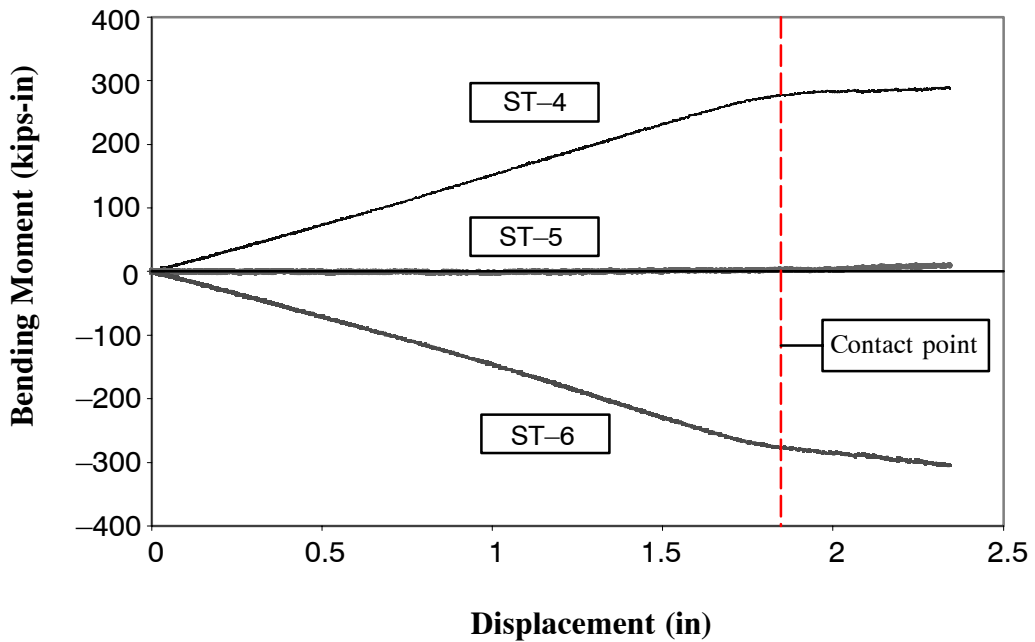


Figure 6-53 Reduction of Bending Moment at the Beam after the Contact Point

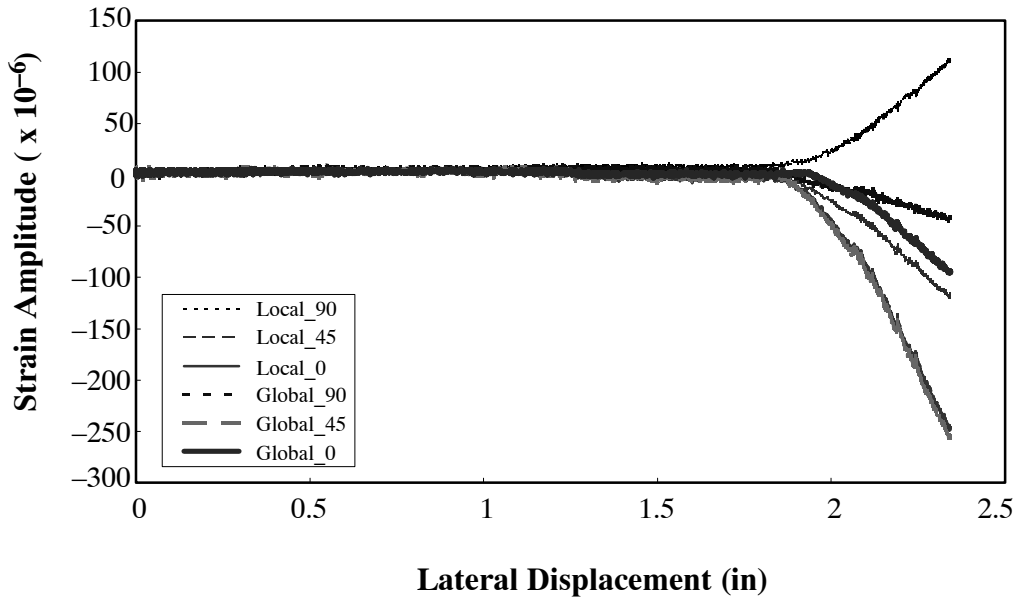


Figure 6-54 Strain Variation of the PMC Infill Panel

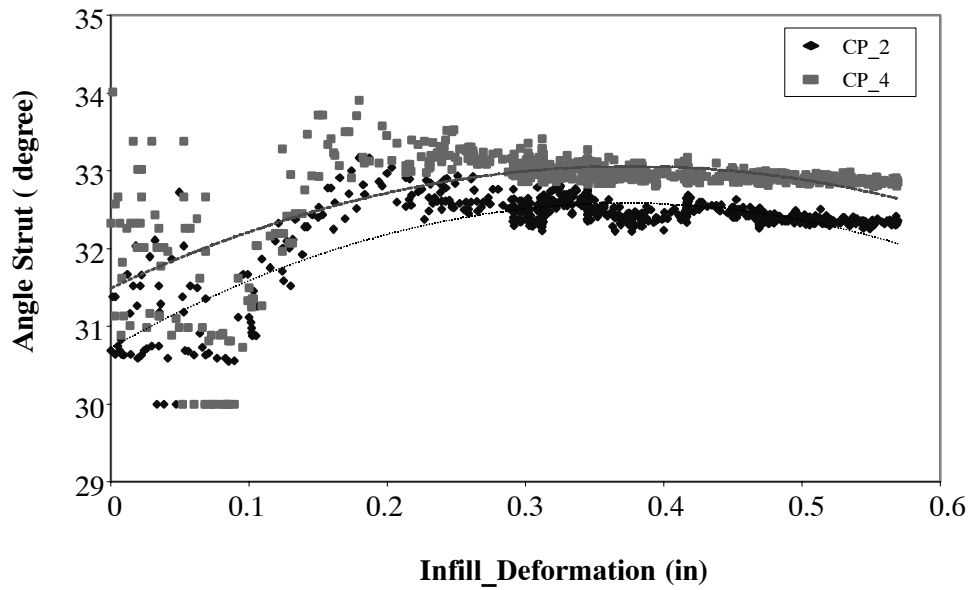


Figure 6-55 Strut Angle Distribution of the PMC Infill Panel along Principal Material Coordinate Direction

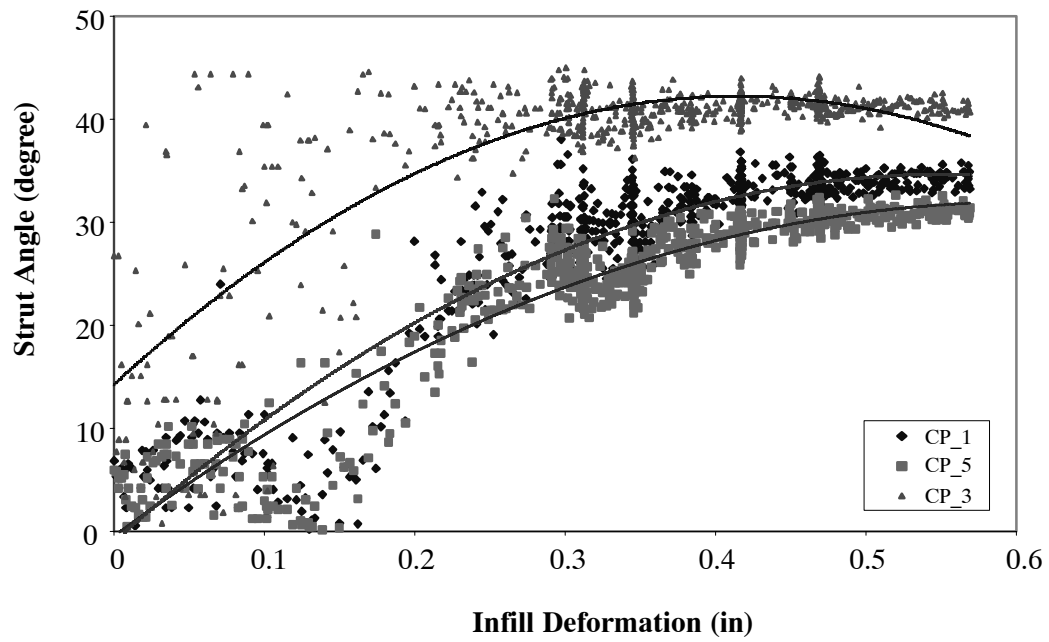


Figure 6-56 Strut Angle Distribution of the PMC Infill Panel along Global Coordinate Direction

Testing of Steel Frame with Multi-panel PMC Infill System

This part of testing involves the testing of both the inner PMC sandwich infill and the outer FRP panels.

Force-displacement Response

Monotonic tests were conducted at 0.5%, 1.0%, and 1.5% drift. Important information about in-plane stiffness and the effect of the interface layer can be obtained from such experiments. At first, a hydraulic actuator was driven slowly up to 0.5% drift. The aim of such a test was to investigate the initial stiffness of the structure having all multi-panel infill components, and to remove the effects of epoxy coating or overflowed adhesive on the surface of the interface layer. Fig. 6-57 shows the high initial stiffness induced by the effects of the polymer honeycomb contribution and a fraction of imperfection factors associated with overflow of adhesive on the viscoelastic layers that were caused by the hand-layup process.

After spalling off overflowed epoxy bonding on the interface layers and breakage of the honeycomb layers, the behavior of the structure was restored to the intended structural condition, which means the interface layers of 3M viscoelastic were acting only. Practically, the overall stiffness of the multi-panel infilled frame was considered in this range because the basic design criteria of the interface layer is to have sufficient strength to preclude its failure. As shown in Fig. 6-58, the measured overall stiffness of the multi-panel PMC infilled frame was larger than that of the steel frame. It is evident that the interface layer increased the lateral resistance by the contribution of the viscoelastic materials. The stiffness of the multi-panel infilled frame was found to vary from 5.5 *kips/in* to 7.7 *kips/in* during the test.

In the fabrication, bolt holes of each connector between the outer FRP panels and the steel beams were made 0.125 inch larger than the bolt shaft diameter. As such, there was a slippage between the bolt shank-to-bolt holes until locking the pin or slot connector in place. Once a desirable locking configuration is achieved, the interface layer will be subjected to shear force. Fig. 6-59 presents the shear deformation of the interface layer after locking the connectors.

The measured stiffness of steel frame was approximately 5.5 kips/in. Compared with the steel frame test in section 3, the overall stiffness was decreased. It is possible that accumulated fabrication errors at the bolted joint angle connections may become larger as the test specimen was successively subjected to monotonic and cyclic loading. Previously conducted experiments may have some effect on the inelastic strain distribution of the joint angle materials and the high restraint between angle and column face which arises from the clamping action of the bolts. Fig. 6-60 shows the comparison of moment-rotation behavior of the bolted angle connection before and after the multi-panel infilled frame testing.

Joint Rotation Response

Moment-rotation relationships were investigated under push-over and cyclic loads. As shown in Fig. 6-61, the measured rotational stiffness at the top and bottom connection exhibited slightly different response. This variation was attributed to the large racking force induced by the PMC infill concentrated at the bottom angle connection when a previous PMC sandwich infill system was tested. The bottom angle joint appeared to be moving less due to extra stiffening and strengthening in that corner of the infill. Fig. 6-62 and 6-63 show the cyclic displacement vs. joint rotation response for the top and bottom joints of the multi-panel PMC infilled frame tests. These figures show only the first cycle of each test.

Finally, based on measured data of joint rotations, the comparison of the top joint response before and after the contact between the infill and the steel members is presented in Fig. 6-64. Before contact initiated, a reduction in joint rotations cannot be seen under loading and reverse loading directions. However, after the initiation of contact, a reduction in joint rotation became apparent when the angle joint was closing in on the panel, whereas in the reverse direction, diagonal strut of the infill should help to open the angle joint more than the drift angle at the steel bare frame test. However, it is clear that significant hysteresis can be observed which indicates that angle connections had yielded.

Moment Distribution

In this section, the distribution of the bending moment induced by the outer FRP damping panels was investigated and compared with that of the bare frame. As shown in Fig. 6-65 to 6-67, it was observed that an increase in horizontal stiffness and enhanced damping by the constrained interface layers had reduced bending moment of steel members compared to the steel frame only. Moreover, the loaded corner exhibited an increase in stress and the bolted angle attracted more stress as the lateral drift was increased.

In general, relative to the bare frame subjected to similar force, additional effect of the infilling on the frame is to reduce substantially the bending moments in the members. In reality, the infill bears against the beam and column members over part of their lengths and induces bending moments in them. Saneinejad et al. (1995) presented that a single-panel infilled frame loaded diagonally up to the peak level would not undergo a plastic collapse mechanism, and develop only insignificant bending moments at the unloaded corners. As presented before, the PMC sandwich infill was also effective for reducing the bending moment on the structural members. The variation of bending moment in the PMC infilled frame members with applied lateral loading is highly nonlinear because of the continuous variation of the contact length between the infill and column members.

Typically, the effectiveness of energy dissipation is significantly reduced when the structural system undergoes inelastic action. The reasons being that – (a) de-tuning of the energy dissipation when inelastic action occurs, and (b) the enhancement of damping is insignificant in comparison to that generated by inelastic action (Constantinou et al., 1998). In the case of the multi-panel infill system, de-tuning of the energy dissipation may not be a problem and the reduction of structural drift by the outer damping panels and the increased stiffness by the PMC sandwich infill will prevent inelastic action of structural frame members.

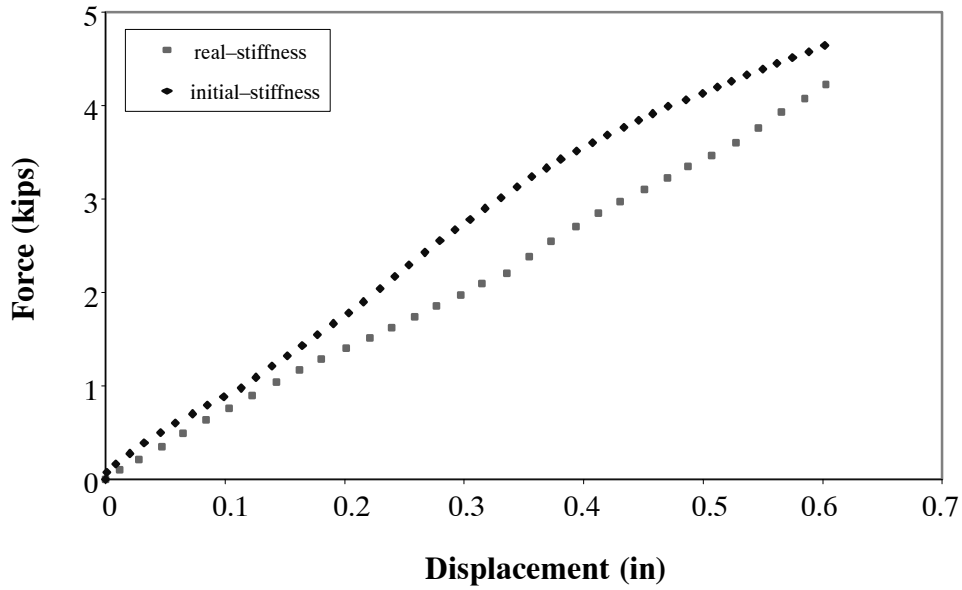


Figure 6-57 Initial Stiffness of the Multi-panel Infilled Frame Test (1% Drift, Push-over Test)

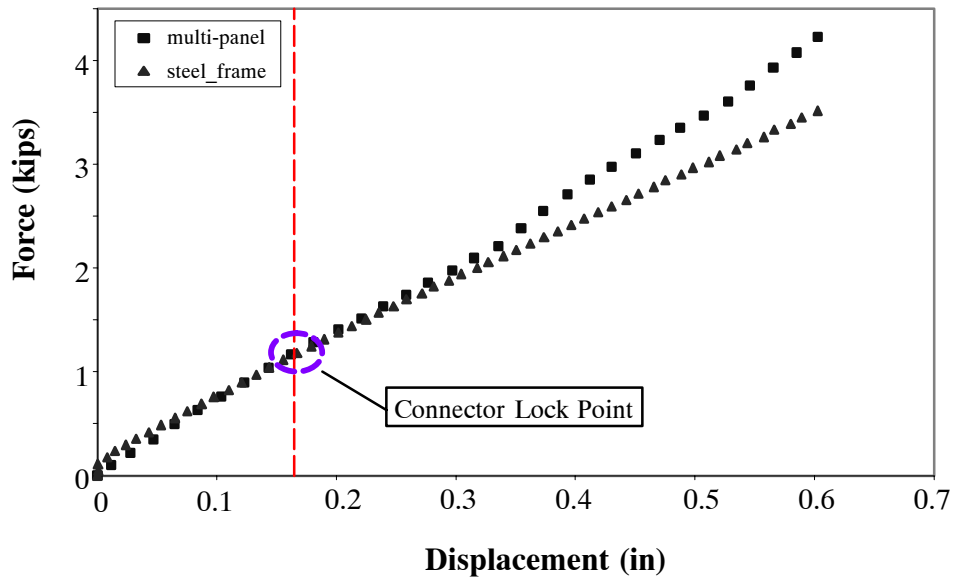


Figure 6-58 Enhanced Stiffness Effect of the Interface Damping Layers

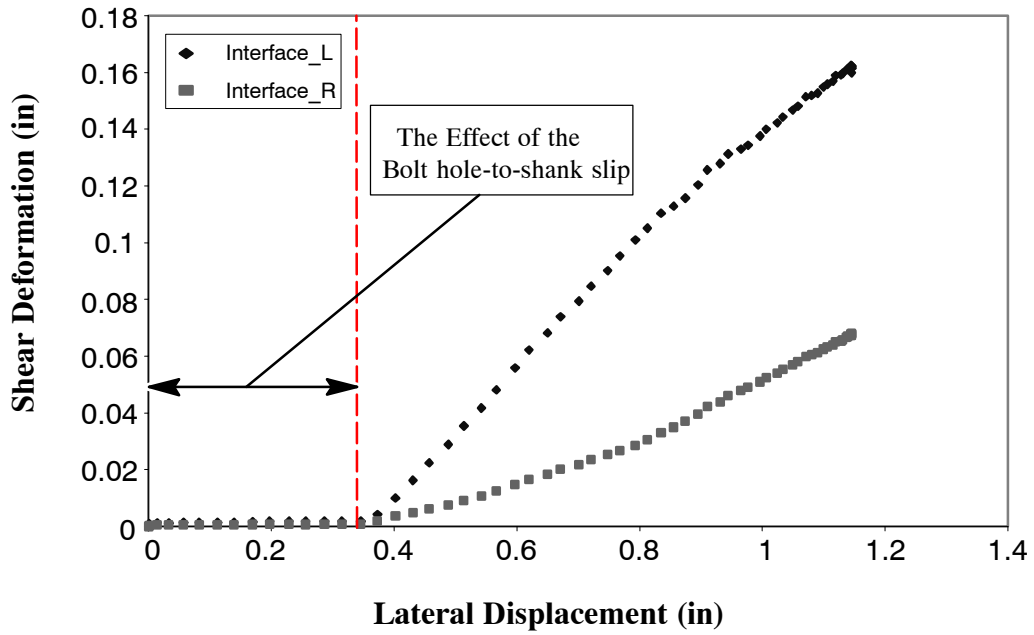


Figure 6-59 Shear Deformation of the Interface Damping Layer under Push-over Load (1.0%)

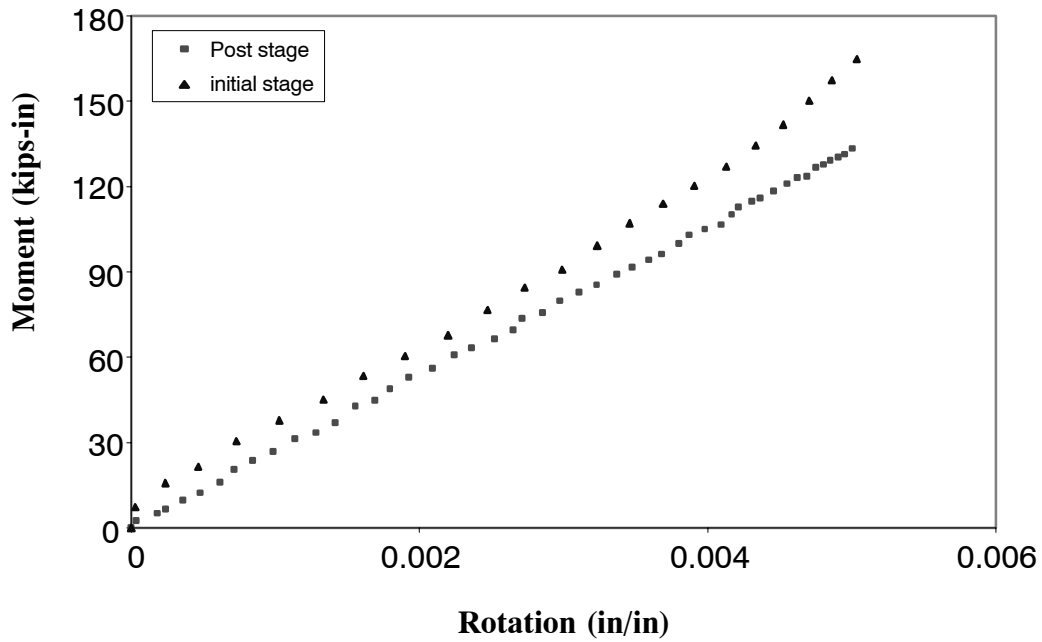


Figure 6-60 Comparison of Moment-Rotation Behavior of the Bare Frame before and after the the Multi-panel Infilled Frame Tests (1.0%, Push-over)

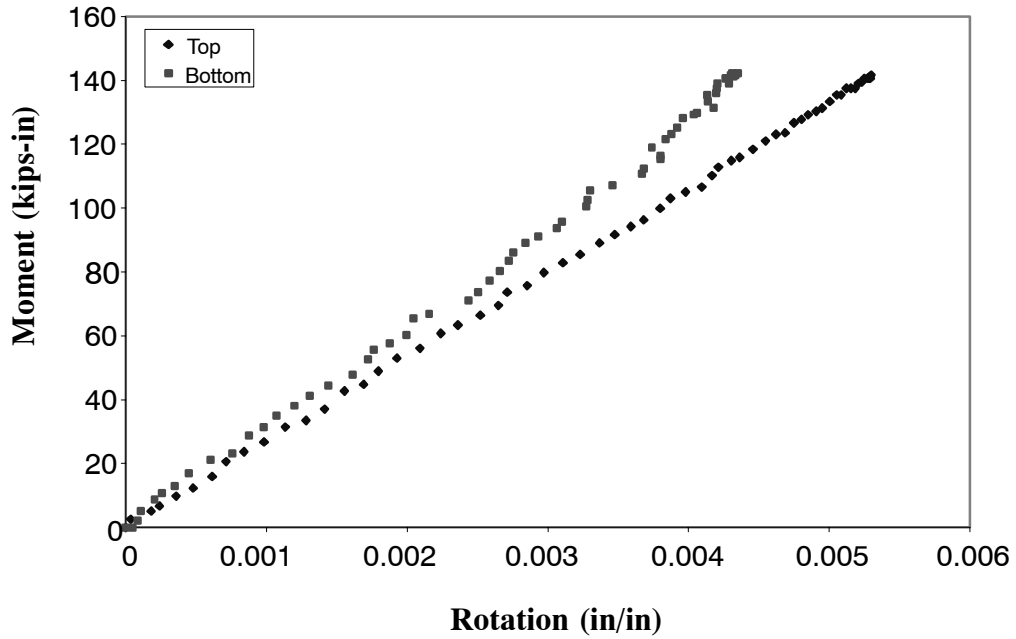


Figure 6-61 Moment-Rotation Relation of the Top and Seat Angle Connection in the Multi-panel Infill System (1.0%, Push-over)

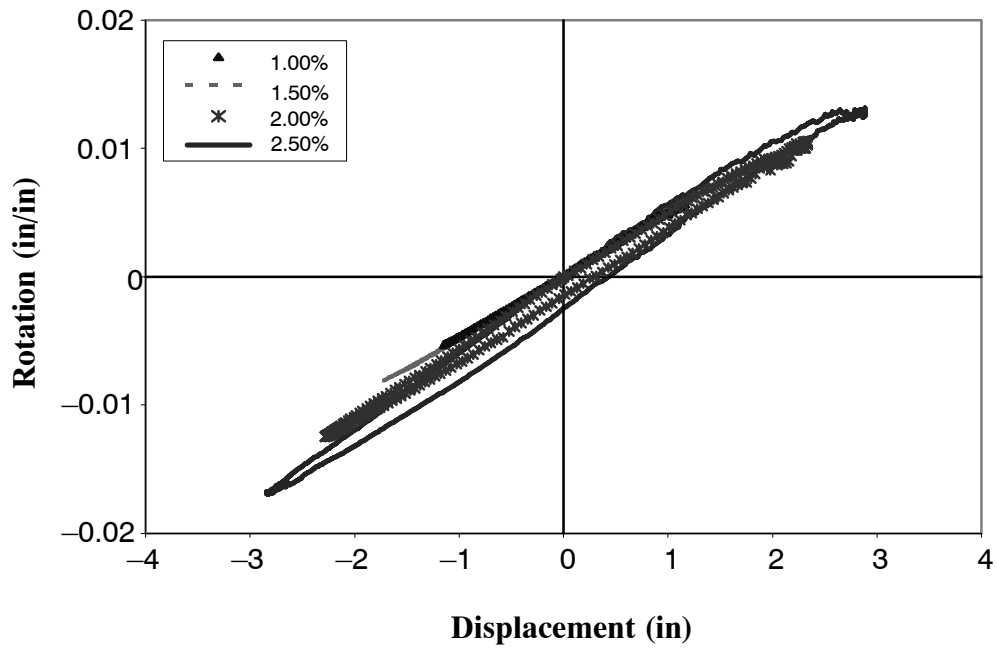


Figure 6-62 Top Joint Rotation Response of the Multi-panel PMC Infilled Frame under Cyclic Loading

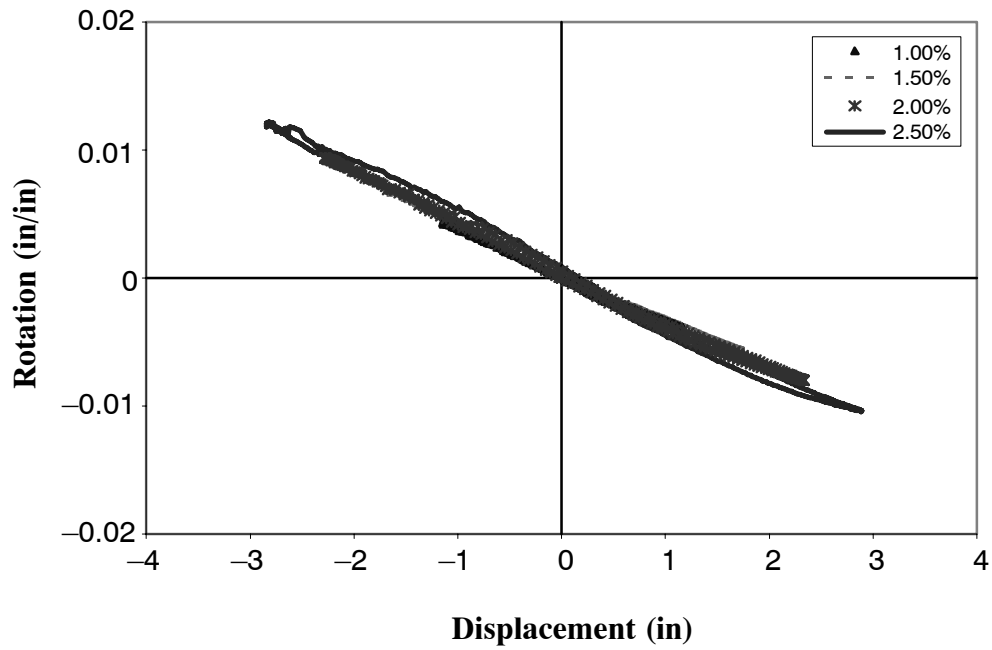


Figure 6-63 Bottom Joint Rotation Response of the Multi-panel PMC Infilled Frame under Cyclic Loading

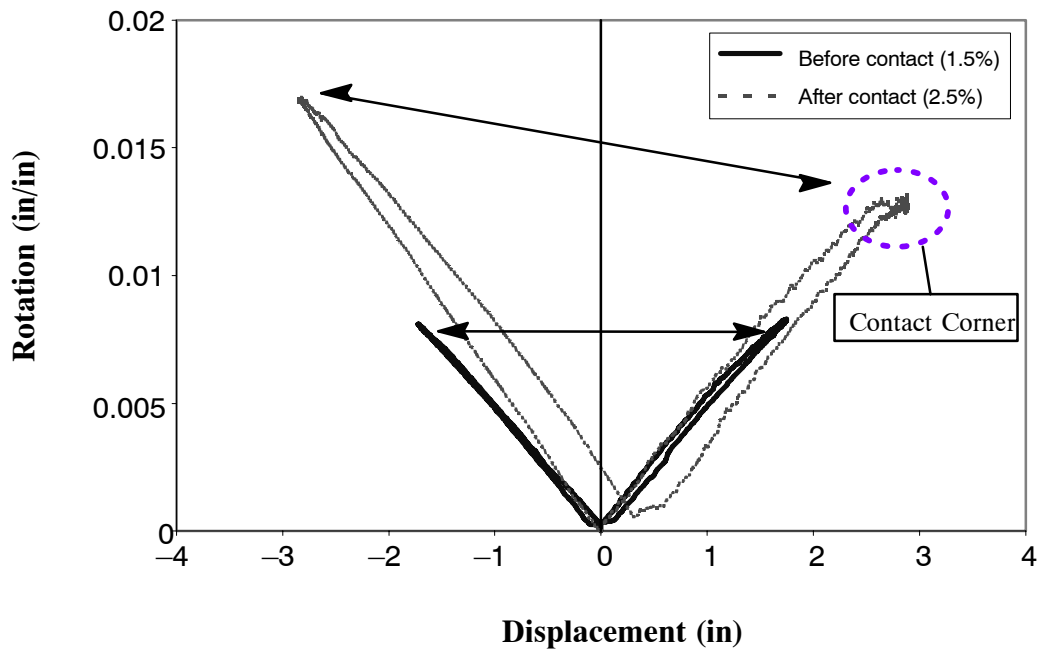


Figure 6-64 Comparison of Top Joint Rotation Response before and after the Infill contact in the Multi-panel PMC Infilled Frame

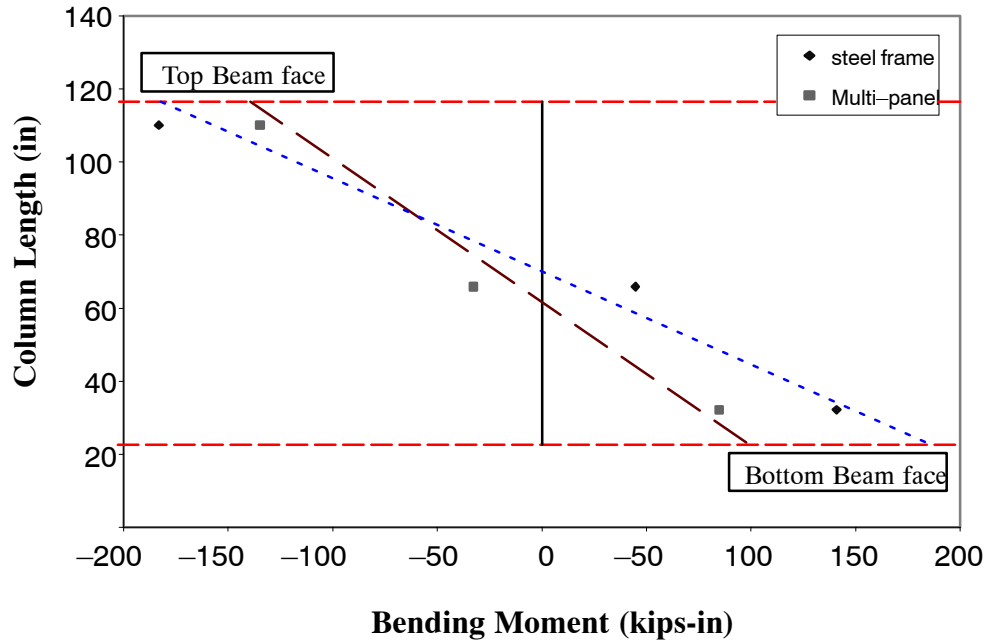


Figure 6-65 Comparison of Moment Distribution of the Left Steel Column (1.0%, Push-over)

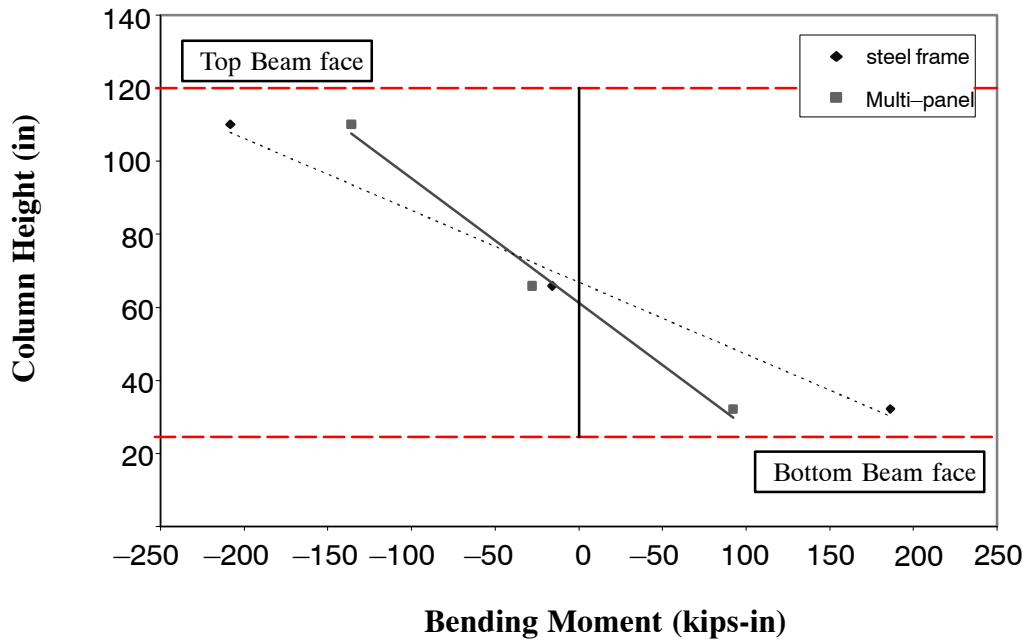


Figure 6-66 Comparison of Moment Distribution of the Right Steel Column (1.0%, Push-over)

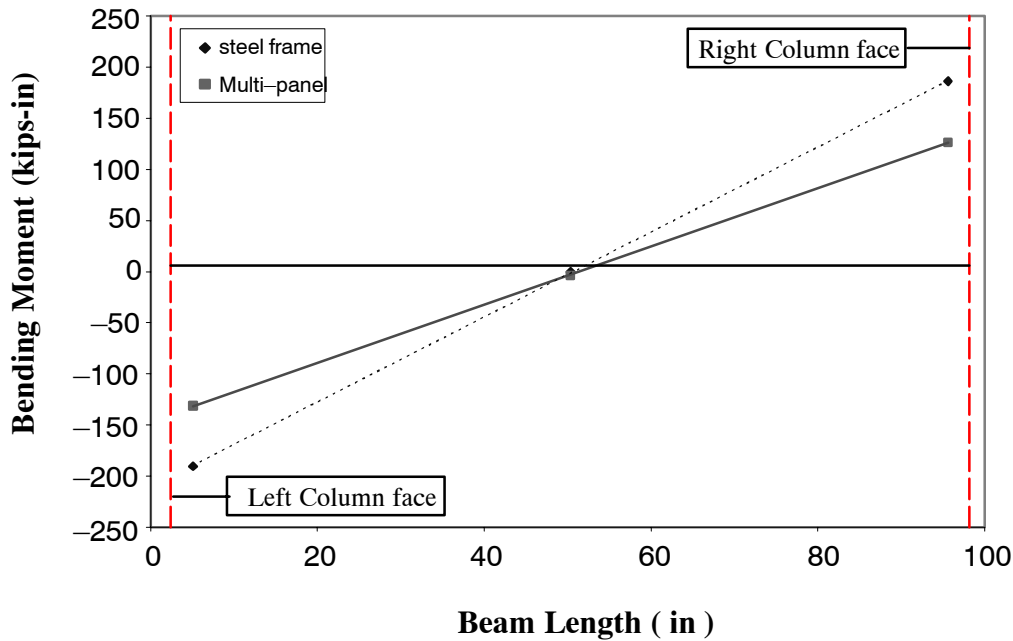


Figure 6-67 Comparison of Moment Distribution of the Top Steel Beam (1.0%, Push-over)

Energy Dissipation of the Interface Damping Layer

Attention is given to the experimental investigation of the energy dissipation which is present in the multi-panel infilled frame. Generally, resonant dynamic response is controlled by the overall damping exhibited by a structure. Such damping may arise from many sources, such as cyclic straining of structural and nonstructural elements, friction at interfaces, and nonlinear behavior. In this study, the damping arises from cyclic straining of the damping materials at the interface between the FRP laminates. Of concern herein is the availability of increasing the damping which arises from the cyclic straining of the materials in the composite frame and the feasibility of the design concept. Frictional and nonstructural sources are not considered herein. Therefore, the exact overall damping of a structure is not quantified.

The experimental results are evaluated by considering force-displacement curves, stiffness degradation under successively applied cycles, and dissipated energy. The experimental force-displacement

response is divided into two stages as depicted in Fig. 6-68 and 6-69. Both figures are represented by the hysteretic response before or after the PMC sandwich infill contacted the steel frame. It was observed that the outer FRP damping panels produced the damping without significant lateral resistance, while an increase in lateral resistance of the structure was provided by the PMC infill beyond the point where contact took place.

The hysteretic energy observed during the applied loading cycles was compared for the steel frame and the multi-panel PMC infilled frame. Because of rate dependent effect of the interface damping layer, the multi-panel PMC infilled frame tests were investigated for different frequencies. Fig. 6-70 to 6-75 present the comparison of the energy dissipation between both structures at 0.16%, 1.0%, and 1.5% drift. By comparing the performance of both specimens, some insights on the effect of interface damping layers at 0.16% drift can be obtained. However, significant hysteresis could not be captured as the lateral drift increased, because hysteretic envelopes of the multi-panel infilled frame were obtained under very low frequencies. In the experiment, the maximum velocity of the 100 kips MTS servo-controlled hydraulic actuator used in the tests was 0.6 inch/sec. The capacity of the applied frequency was varied with the assigned displacement so that the available maximum frequency was 0.5, 0.16, and 0.08 Hz at three levels of lateral drift; 0.16%, 0.5%, and 1.0% drift. Therefore, the obtained energy dissipations induced by the constrained interface damping layers were underestimated considering the available maximum performances. In this study, to predict an enhanced performance under high frequencies, finite element simulations were performed and presented in Fig. 6-76 and 6-77. The results show that the hysteretic energy response of the structure significantly increases as the applied loading rate increases.

Fig. 6-78 and 6-79 show shear deformations of the interface damping layers under successively increasing lateral cyclic drifts. The discrepancy in both results is due to the slippage of the bolt shank-to-bolt holes at the early stage of the loading (as shown in Fig. 6-59). The effective length of the connector lock was found to be approximately 0.18 inch, and little difference between the behaviors of the left and right interface layers therefore occurred during the tests. The difference between peak

point of the interface layers under push and pull loading may be due to the fact that the structure was not able to return exactly to its original position upon reverse loading.

In a viscoelastically damped structure, it is necessary to investigate the effect of frequencies and the environmental temperature within which they operate for practical applications. In general, the viscoelastic materials need to be designed for the expected maximum ambient temperature to ensure adequate damping for the structure at various conditions. However, the applied 3M viscoelastic materials were considered to operate at room temperature of approximately 20°C. Hence, only the variation of the structure's natural frequencies was considered in the study.

Fig. 6-80 compares the structural hysteretic responses under different frequencies and drifts. From this figure, little effect of the frequency for energy dissipation was observed experimentally even if the frequency may be a significant factor that controls the energy dissipation effect of 3M viscoelastic material. In the case of small drift and large frequency range such as 0.16% drift, because of the slip effect of the bolt shank-to-bolt holes, the viscoelastic material was not able to work well even though the applied frequency is adequate. For the other cases: such as 1.5% and 1.0%, the applied frequency during the tests was not adequate to investigate the frequency effect of the viscoelastic material. It is due to the fact that there was a limitation of the applied velocity of the hydraulic actuator used in cyclic loading tests. As such, it is advisable that the frequency response of the full test structure with viscoelastic materials should be studied in the future using a shaking table in order to investigate its real behavior and the corresponding effects under seismic excitation.

Finally, energy dissipation capacities were calculated based on the experimental results and presented in Fig. 6-81. By comparing these results, it can be seen that there is a slight difference and energy dissipation increases as the frequency increases. Fig. 6-82 presents hysteretic energy absorbed by test specimens at 1.0% drift. From the result, the net response of the multi-panel PMC infill system under applied various frequencies can be obtained by subtracting the steel bare frame response for a given lateral drift from the gross infilled frame response.

Degradation and Failure of Overall Structure

Fig. 6-83 shows the change in the effective stiffness of the structure under increasing displacement amplitude and number of cycles. It is evident that the bolted angle connections were already yielded and started to undergo plastic deformation.

After completion of the monotonic and cyclic loading tests, the specimen was tested to failure to examine its failure mode. The test was conducted by displacement control until the test specimen reached failure. Test result is shown in Fig. 6-84. The PMC infilled frame was designed based on the elastic buckling of the PMC infill. However, the progressive angle connection failure occurred during the test before the elastic buckling of the PMC sandwich infill. It was observed that by allowing large gaps around top and side places, a large slippage between the PMC infill and the bottom beams can be introduced. As the result, high pressure between the PMC infill and the bolted angle connection at left bottom side was generated when the infill slid across into the lower corner of the steel frame. The pressure between PMC infill and the bolted angle connection was gradually increased as the inter-story drift increased. Finally, larger compressive pressure to the bolted angle connection led to failure of the structure. The schematic representation of these failure modes is illustrated in Fig. 6-85.

In the design process, four edges of the PMC sandwich infill were cut off from its original shape to allow slipping distance between the PMC infill and the bottom beam. The cutting edge area was chosen based on the initial side gap distance. However, the verification of slippage can be complicated. For design purpose, slippage between the PMC infill and the bottom beams need to be investigated and considered as one of important design parameters. Finally, Fig. 6-86 shows the edge shape of the current PMC sandwich infill and the failure of the joint angle connection.

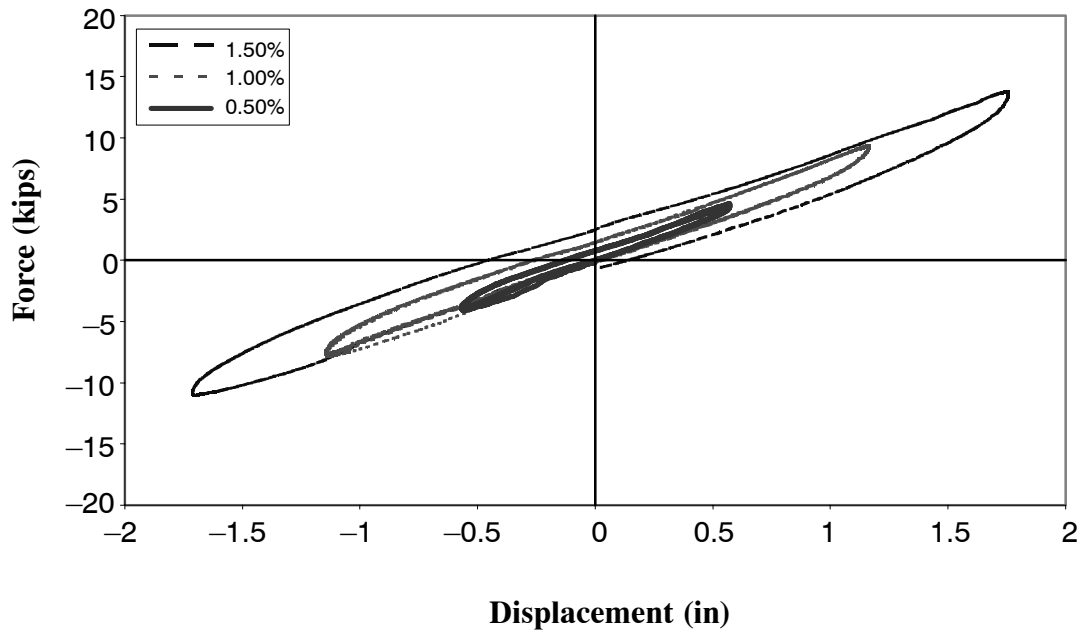


Figure 6-68 Hysteretic Response of the Multi-panel PMC Infilled Frame Before Making Contact with the PMC Sandwich Infill Panel

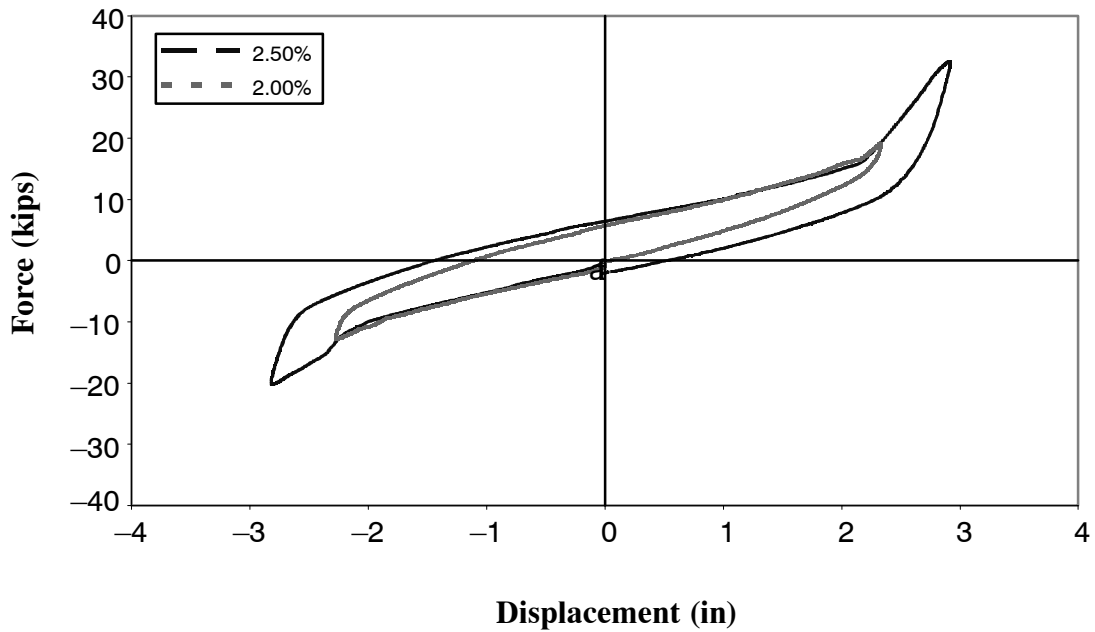


Figure 6-69 Hysteretic Response of the Multi-panel PMC Infilled Frame in Contact with the PMC Sandwich Infill Panel

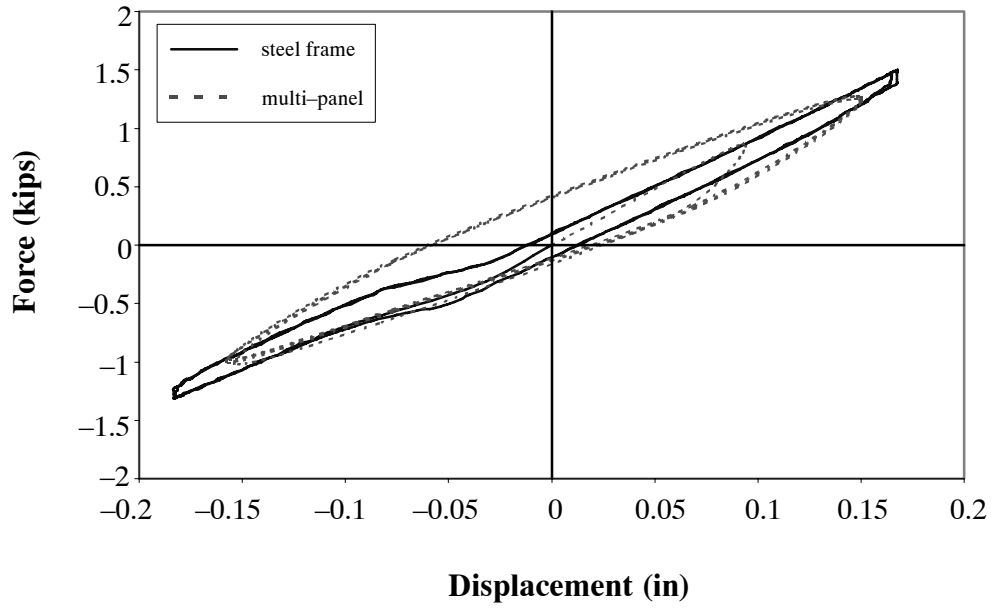


Figure 6-70 Comparison of Damping Performance between the Steel Frame and the Multi-panel Infill System (0.16%, $f = 0.5$ Hz)

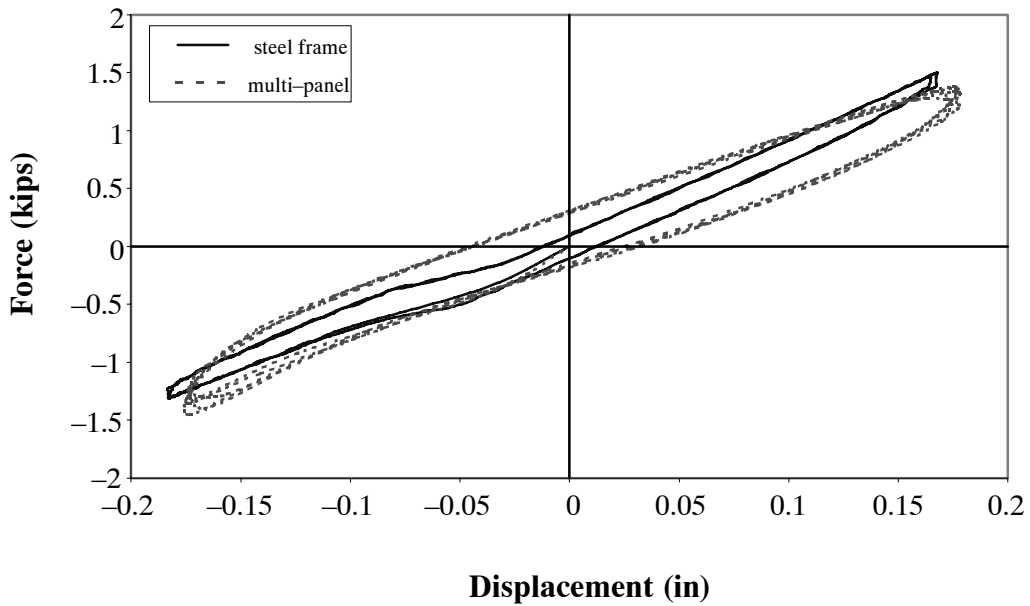


Figure 6-71 Comparison of Damping Performance between the Steel Frame and the Multi-panel Infill System (0.16%, $f = 0.25$ Hz)

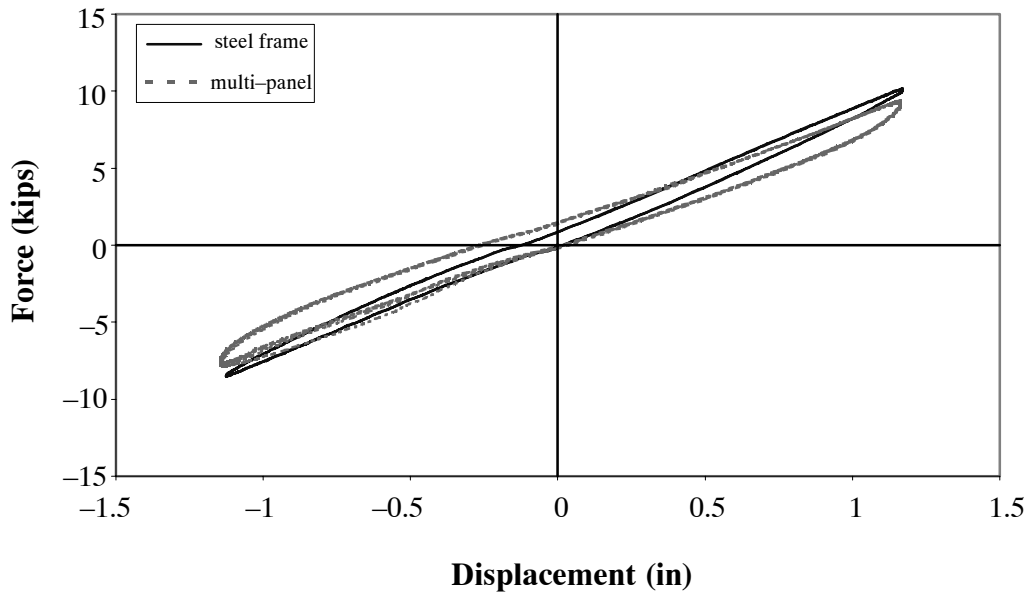


Figure 6-72 Comparison of Damping Performance between the Steel Frame and the Multi-panel Infill System (1.0%, $f = 0.08$ Hz)

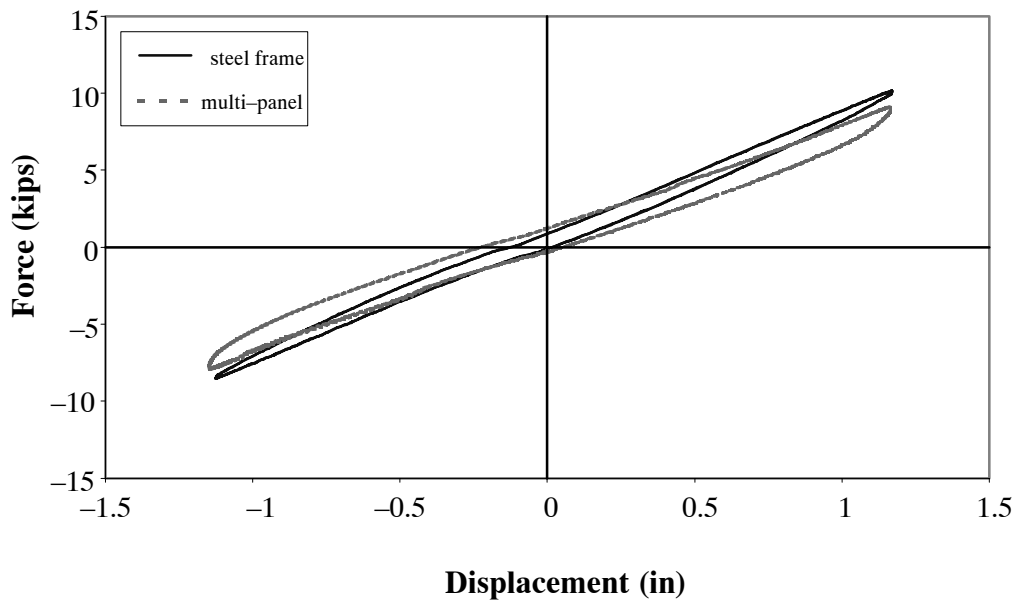


Figure 6-73 Comparison of Damping Performance between the Steel Frame and the Multi-panel Infill System (1.0%, $f = 0.04$ Hz)

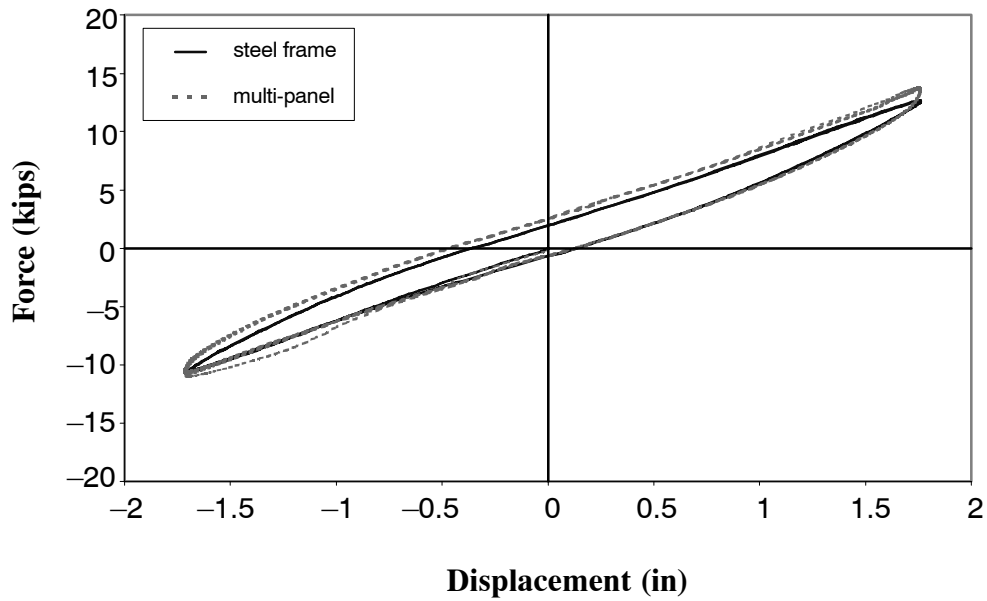


Figure 6-74 Comparison of Damping Performance between the Steel Frame and the Multi-panel Infill System (1.5%, $f = 0.054$ Hz)

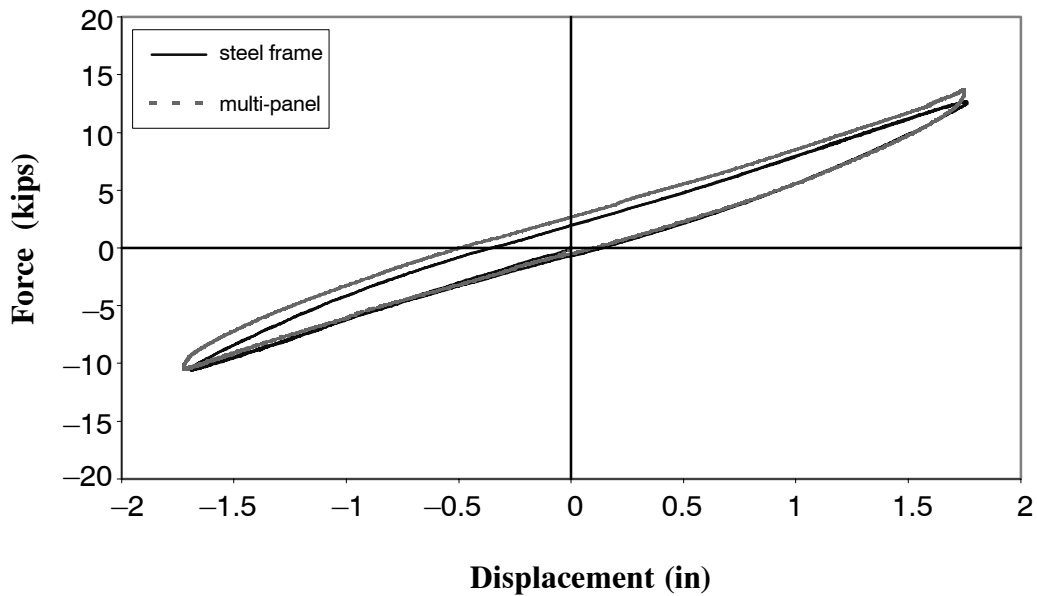


Figure 6-75 Comparison of Damping Performance between the Steel Frame and the Multi-panel Infill System (1.5%, $f = 0.027$ Hz)

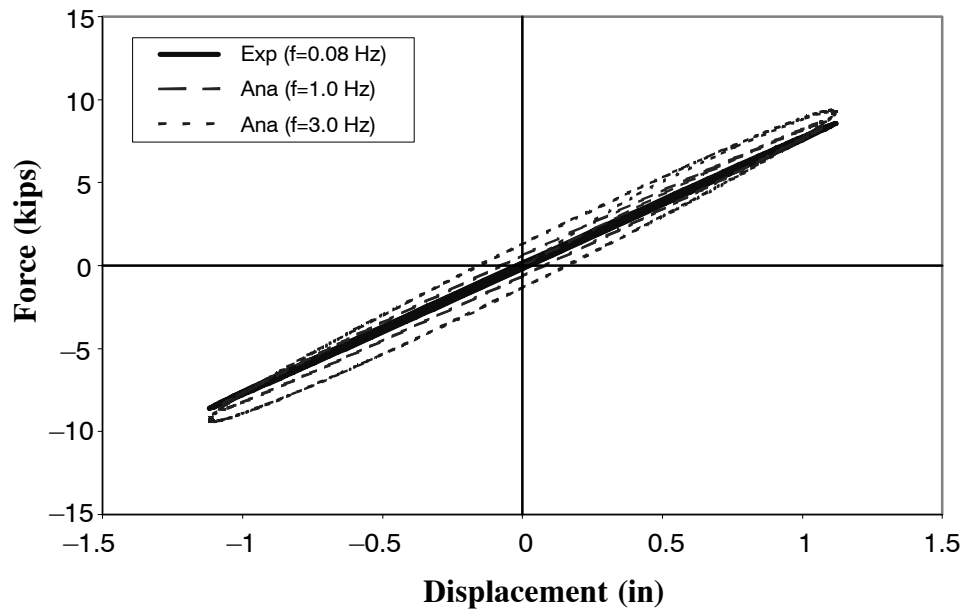


Figure 6-76 Comparison of Hysteretic Energy Dissipation Under Various Frequencies (1.0% drift)

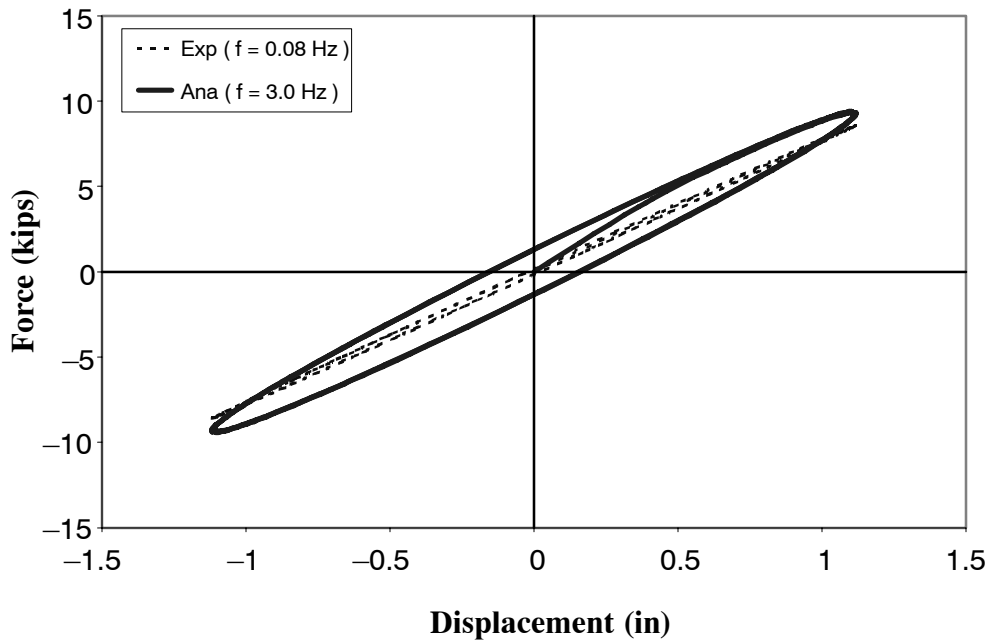


Figure 6-77 High Frequency Effect of the Outer FRP Damping Panel Systems (1.0% drift, $f = 3.0$ Hz)

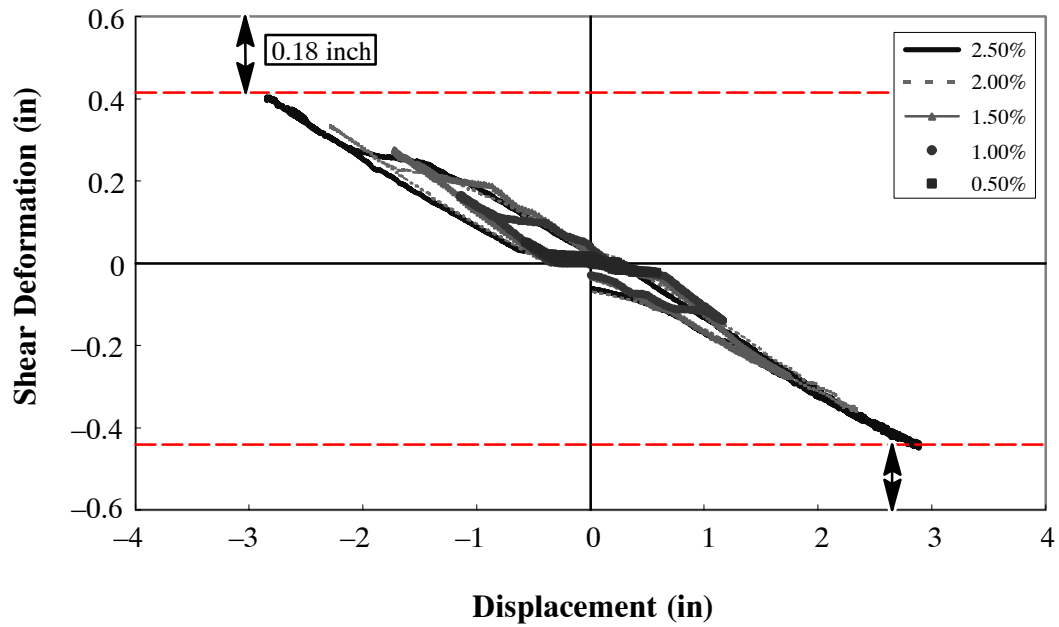


Figure 6-78 Variation of Shear Deformation of the Left Interface Damping Layer under Increasing Cyclic Loading Drift

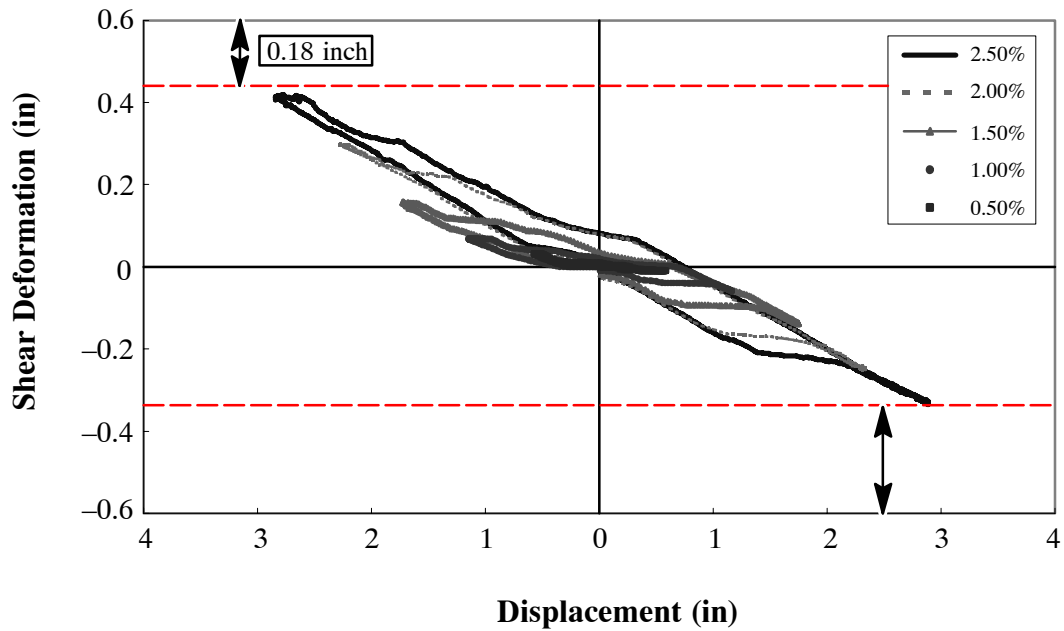


Figure 6-79 Variation of Shear Deformation of the Right Interface Damping Layer under Increasing Cyclic Loading Drift

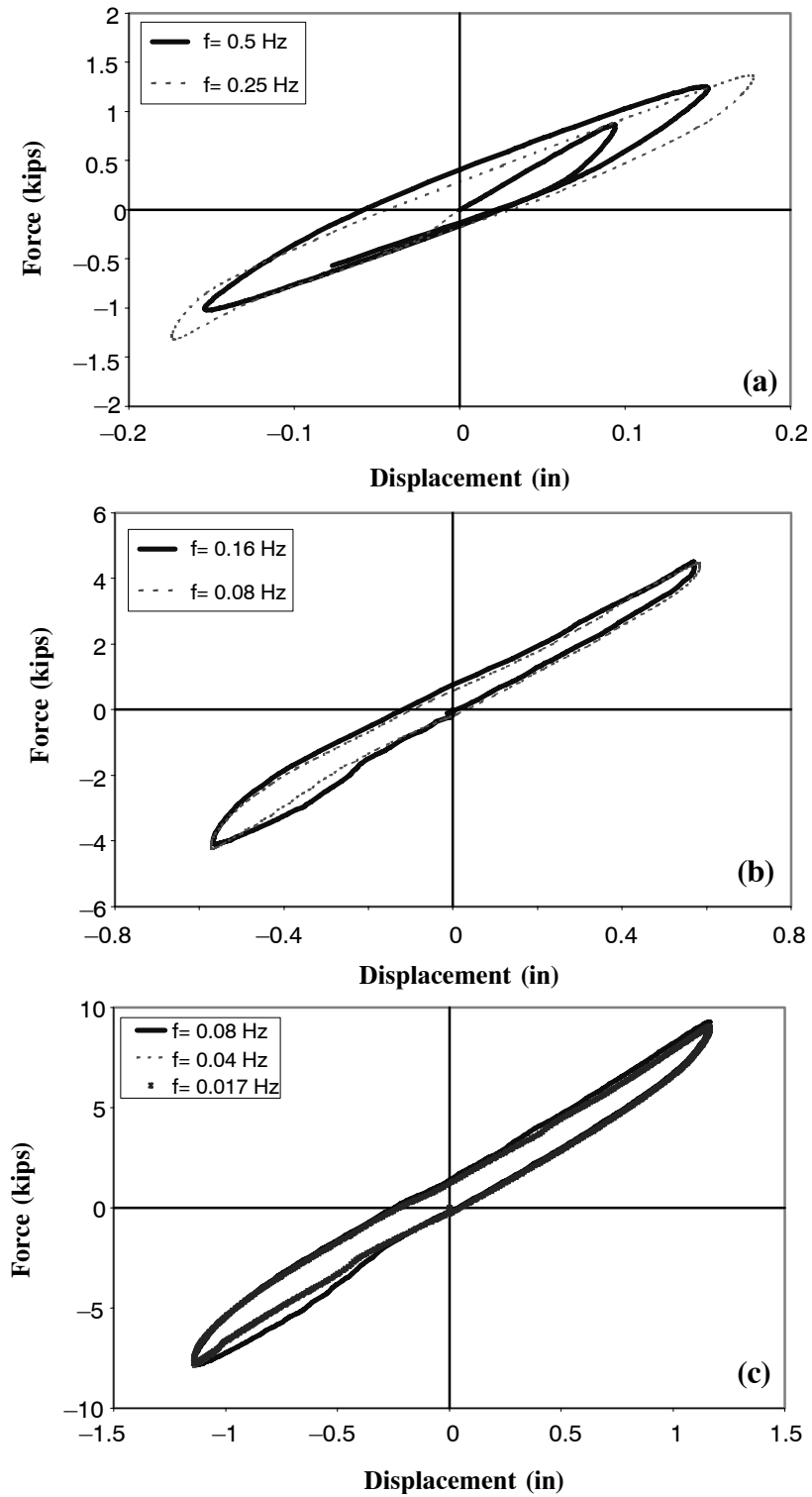


Figure 6-80 The Rate Effect of the Interface Damping Layer of the Multi-panel Infilled Frame: (a) 0.16%; (b) 0.5%; (c) 1.0% drift

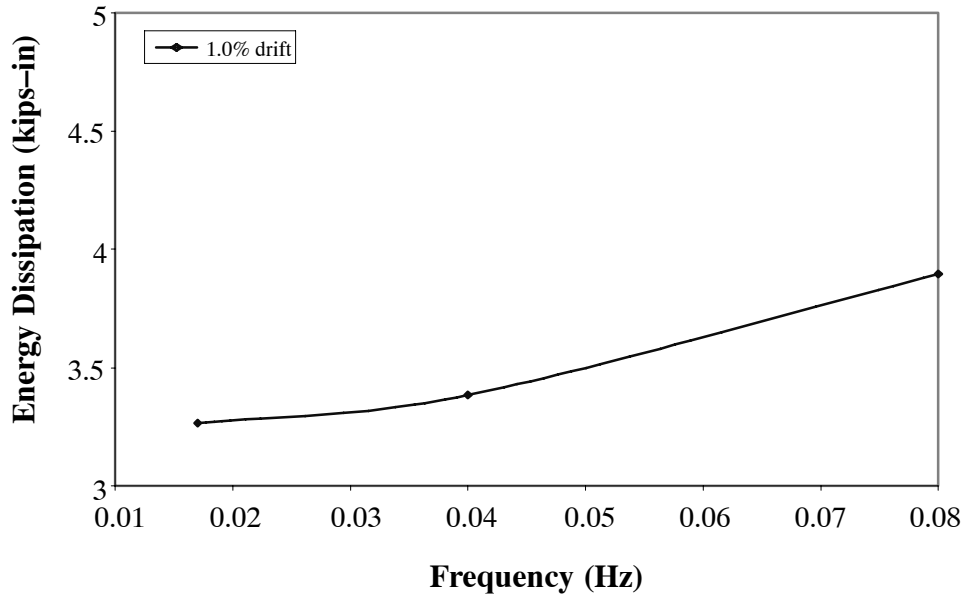


Figure 6-81 Frequency Effect of the Multi-panel Infill System under Cyclic Loading (1.0% drift)

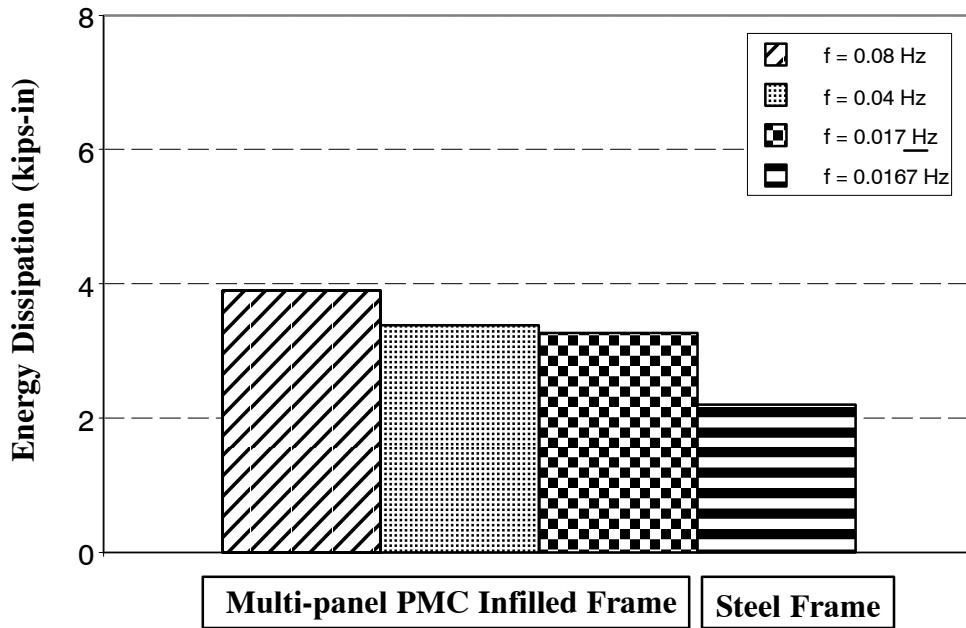


Figure 6-82 Comparison of Energy Dissipation Capacity for the Multi-panel Infill System and the Steel Frame (1.0% drift)

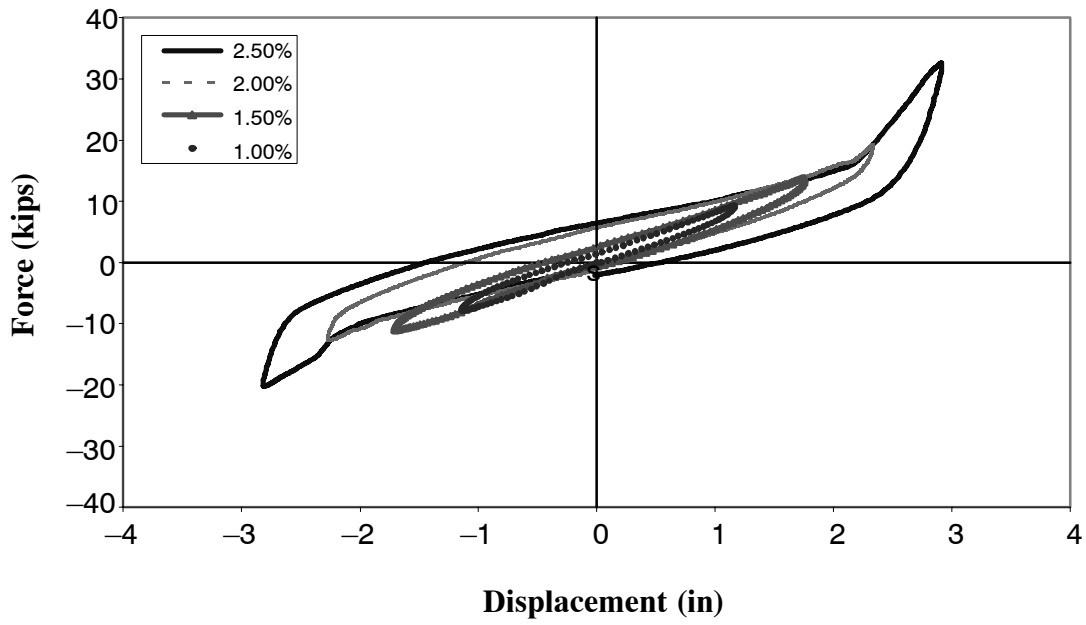


Figure 6-83 Stiffness Degradation of the Multi-panel Infill System under Successively Applied Cycles

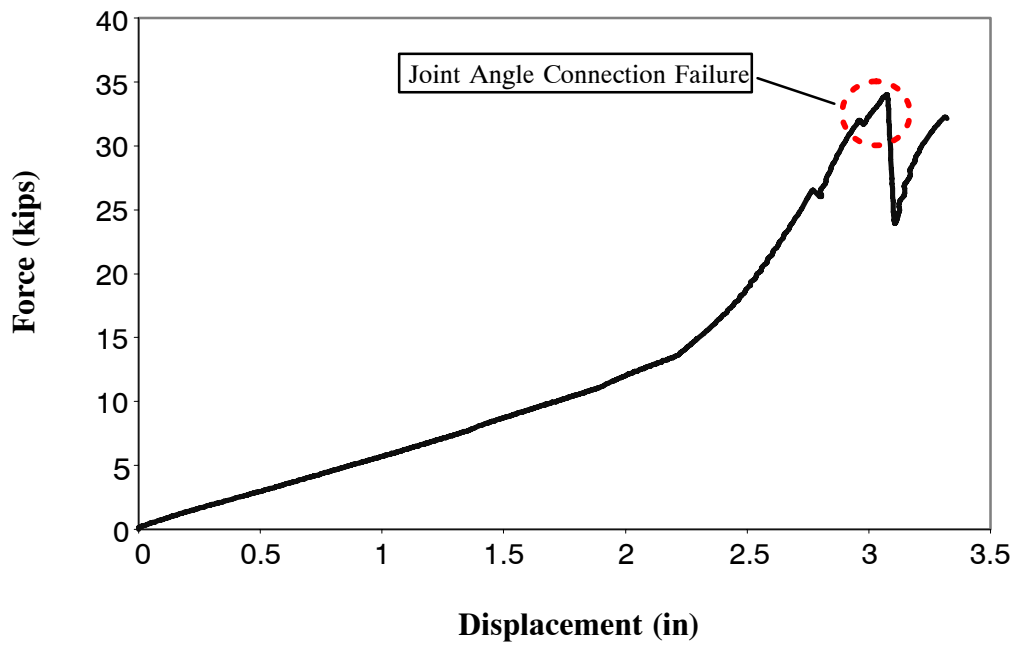


Figure 6-84 Destructive Test of the Multi-panel PMC Infilled Frame under Push-over Loading (Up to 3.0% drift)

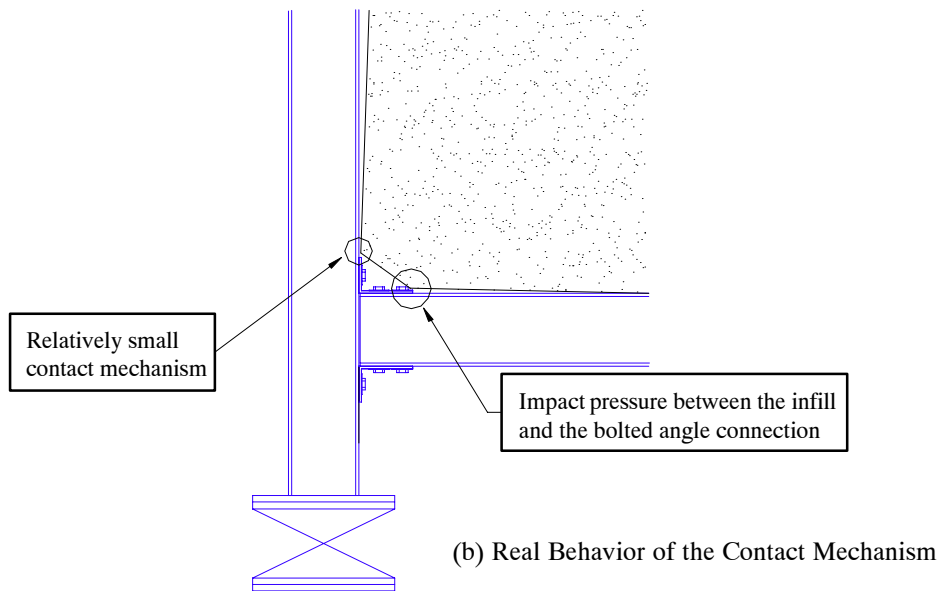
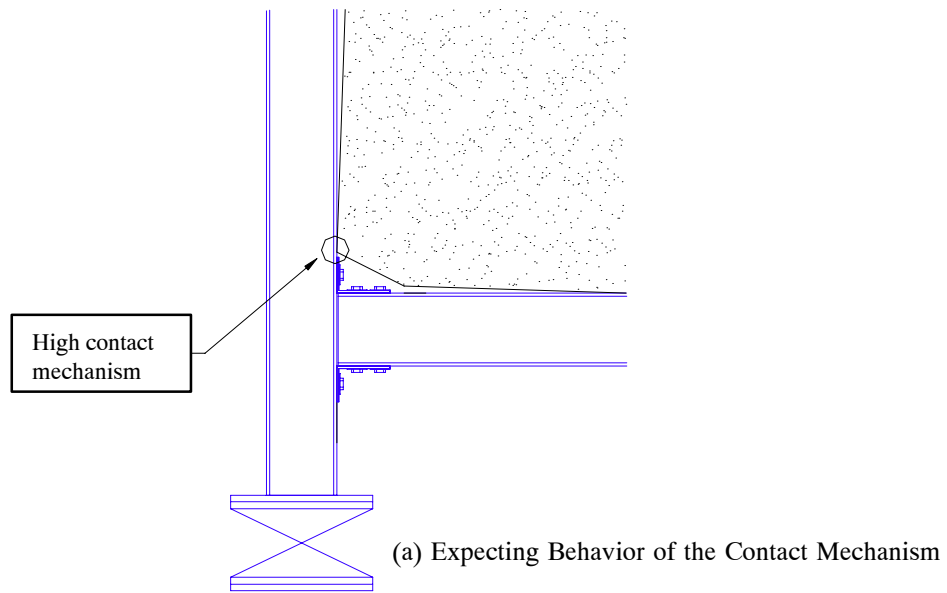
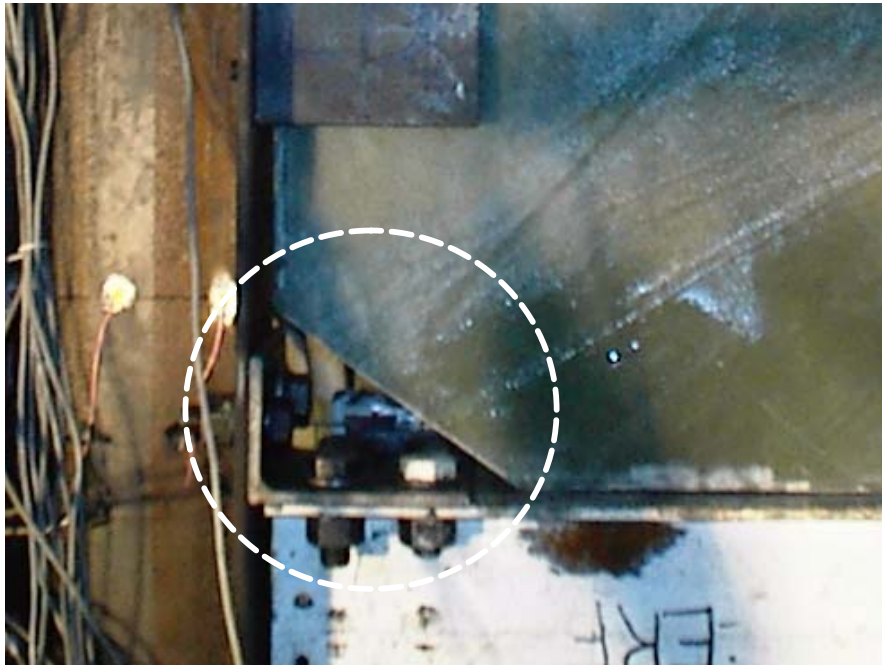
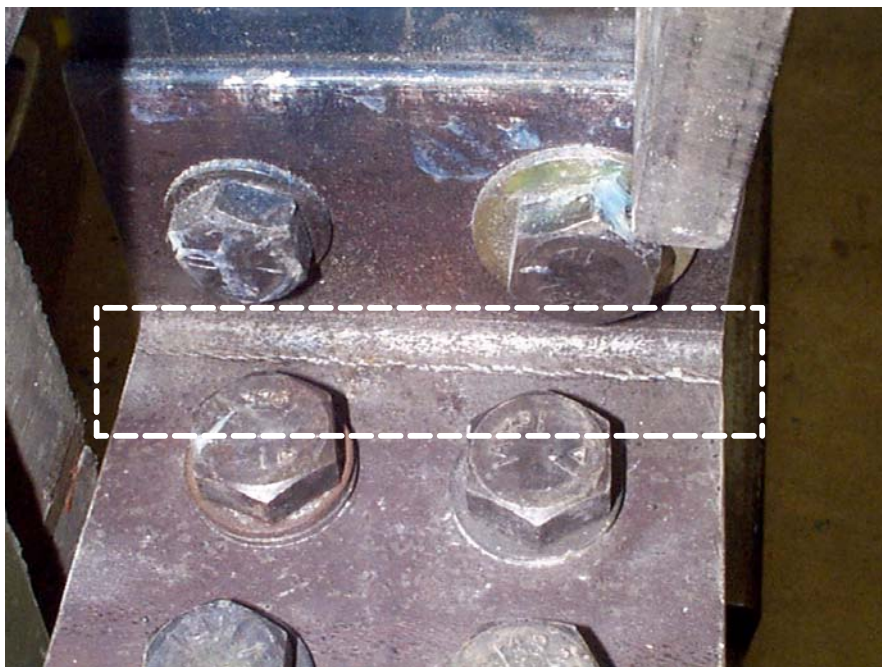


Figure 6-85 Schematic Representation of the Failure Caused by Impact Pressure Between the Bolted Angle Connection and the Infill



(a) Edge Shape of the PMC Sandwich Infill Panel



(b) Bolted Semi-rigid Joint Angle Connection Failure

Figure 6-86 The Failure of the Multi-panel PMC Infilled Frame Structure

6.6.2 Result of FRP Box Infill Panel Testing

A special specimen was tested for developing enhanced energy dissipating infill panel after completing the multi-panel infilled frame tests. The test specimen was composed of two constrained interface damping layers and was tested for two cases. Both test cases were identical in all respects except that the FRP box damping panel was installed with a stiff and a combining interface layers in one specimen test (Case 1) and with both viscoelastic interface layers in the other (Case 2).

The construction of the stiff layer was described in earlier section. From the testing of a steel frame with the FRP box infill panel system, the effectiveness of two different types of FRP box infills is addressed in terms of in-plane behavior and energy dissipation capacity. The local responses of the steel frame members could not be investigated due to severe damage of strain gages and plastic deformation at parts of the joint connections during previous tests. In this test, careful attention was paid to the behavior of the joint angle connections in order to obtain the hysteretic energy contribution of the damping panel system without failure of the joint connections.

Force-displacement Response of the Test Specimens

Both cases of the FRP box damping panel system were monotonically tested and compared to the response of the steel frame. Fig. 6-87 shows the force-displacement response of the test structures under push-over load. It is shown that the initial stiffness of case 1 was significantly enhanced by two sources. First, the polymer honeycomb material in the combining interface layer provided the lateral resistance for the structure. Second, the epoxy coating on the stiff layer prevented deformation of the interface layer leading to a large lateral resistance in the structure.

In the testing of case 2, the force-displacement response was measured after breaking the polymer honeycomb material on the stiff interface layer. In such a case, the initial stiffness was provided by the viscoelastic materials at both interface layers. The stiffness of case 1 was increased at the beginning of loading but the case 2 was stiffened after the bolt shank-to-bolt holes lock. As shown in Fig. 6-88, the gap of the bolt shank-to-bolt holes introduced slippage that the shear deformation of the

constrained interface layer did not commence. Based on the measurement of force-displacement response, results are summarized in Table. 6-5.

Table 6-5 The Comparison of the Initial Stiffness for the Steel Frame and Two Cases of the FRP Box Damping Panel Systems under Push-over Load

	Steel Frame	FRP Box – Case 1	FRP Box – Case 2
Stiffness (kips/in)	7.2	18.3	13.2

The hysteretic responses for both cases (1 and 2) of the FRP box damping panel are shown in Fig. 6-89 and 6-90, respectively. The tests were carried out based on the assigned cyclic displacement and the corresponding frequency. Careful attention was given to the test for case 1 and this test was stopped at 1.5% drift to avoid the progressive joint connection failure. From the testing of the structure in case 1, it is clear that preventing sliding shear at the stiff layer provided a large effective stiffness to the structure after locking at the pin connection. However, preventing shear deformation at the stiff interface layer may cause high pressure at the joint angle connection as the tests progressed and the lateral displacement increased. Fig. 6-90 presents the hysteretic loops of the structure (case 2) when both flexible interface layers undergo successively increasing lateral displacements. This figure also indicates that enclosed area obtained by the hysteretic loops became larger as the cyclic strain amplitude of the interface layers increases.

As shown in Fig. 6-91 and 6-92, these figures indicate the variation of shear deformation for two different interface cases. As expected, under the loading, the stiff interface layer was not deformed, whereas the combined flexible interface layer produced a large shear deformation. By comparing with the result obtained from the simplified design calculation (depicted in Fig. 6-9), 0.2 inch slip caused by the bolt shank-to-bolt hole gap was occurred at the response of the shear deformation in the combined flexible interface layer.

At the moment of reversed loading direction, a flat region was also observed due to the slippage at the contact surface between the measuring instrumentation and the attached plate. Fig. 6-93 and 6-94 present the variation of total measured shear deformation on the both interface cases under increas-

ing lateral cyclic displacements. It is evident by the enclosed area that there is an amount of energy dissipation in the combined interface layer upon loading the frame.

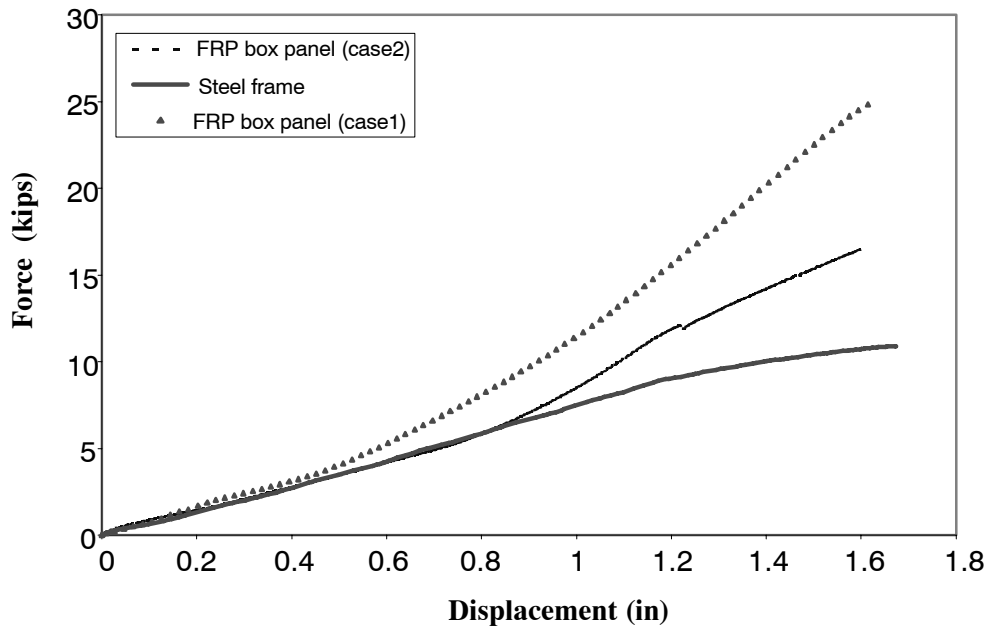


Figure 6-87 Force-Displacement Response of the FRP Box Infill Systems under Push-over Loading (1% drift)

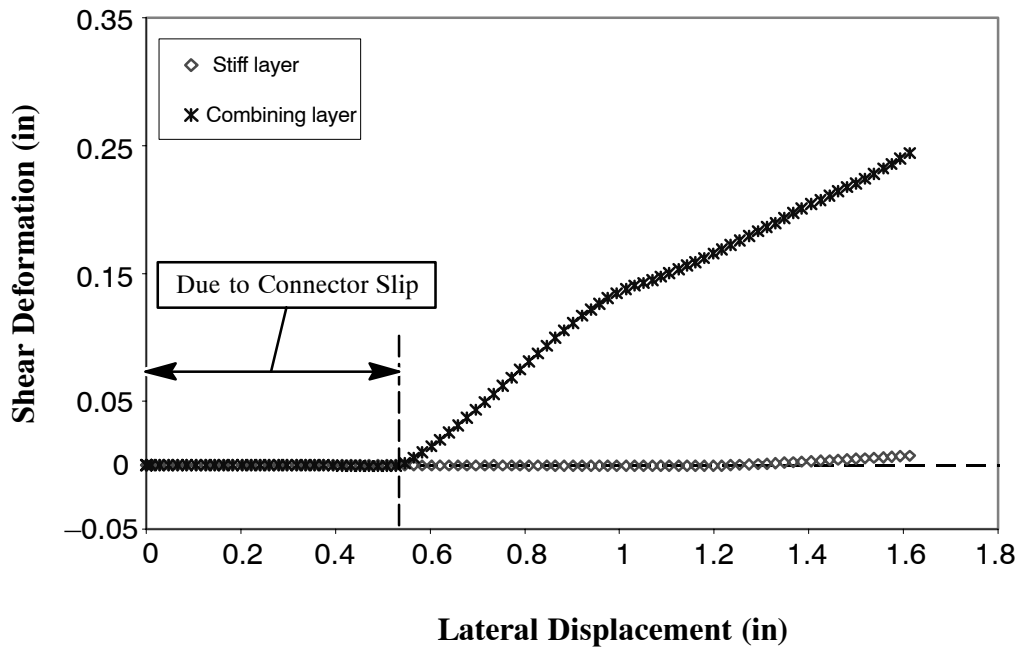


Figure 6-88 Variation of Shear Deformation of the Interface Layer in the FRP Box Infill Systems under Push-over Loading (1% drift)

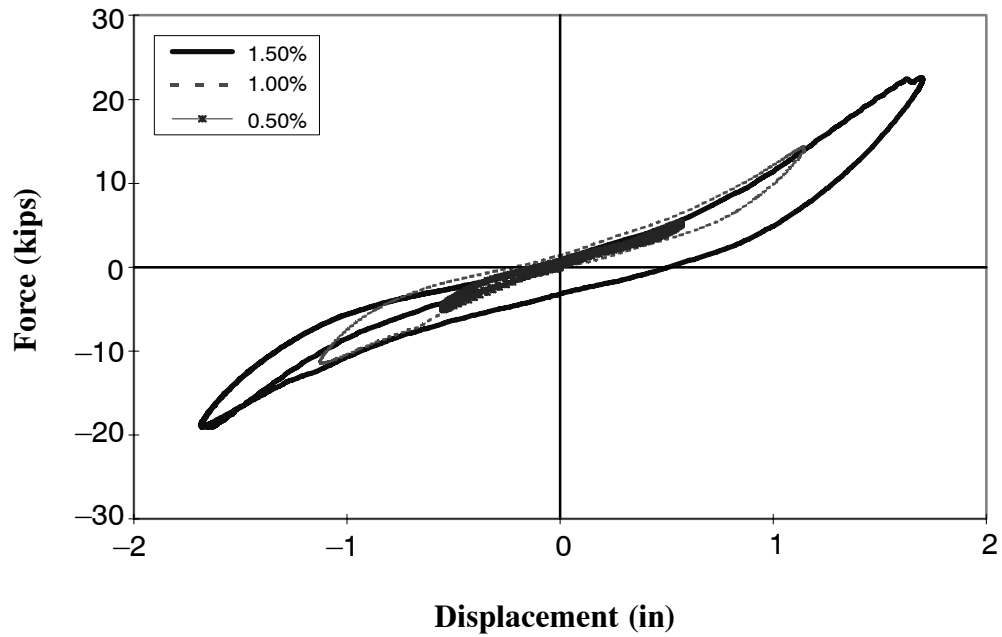


Figure 6-89 Hysteretic Response of the FRP Box Infill System (Case 1, High Frequency (3.0 Hz))

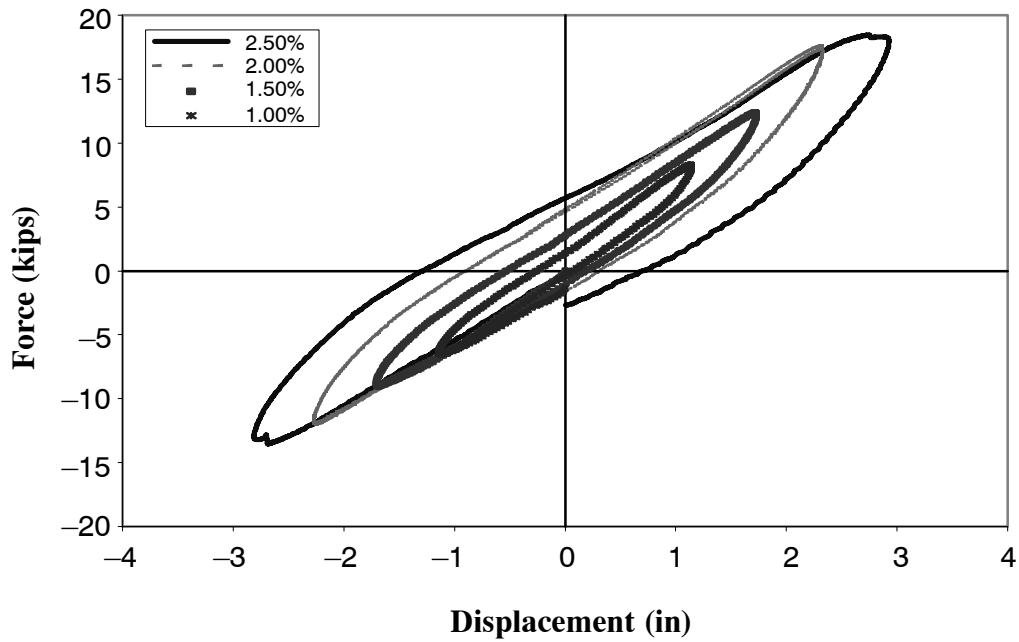


Figure 6-90 Hysteretic Response of the FRP Box Infill System (Case 2, High Frequency (3.0 Hz))

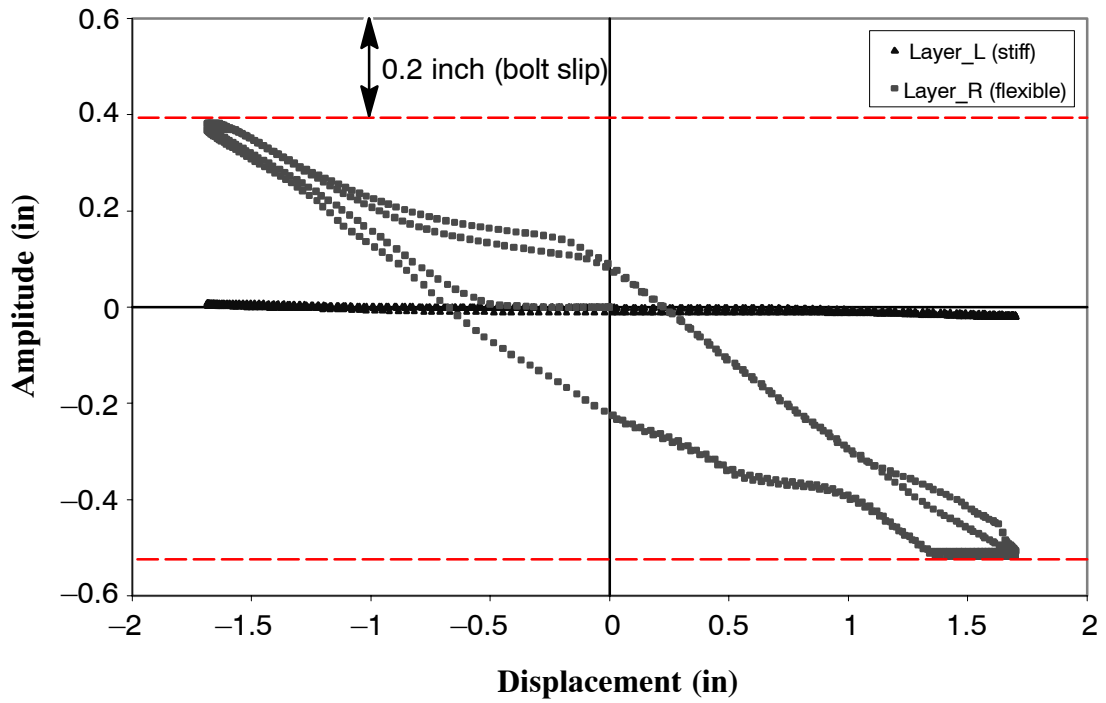


Figure 6-91 Shear Deformation of the Interface Layers of the Test Structure Case 1 (1.5% Drift)

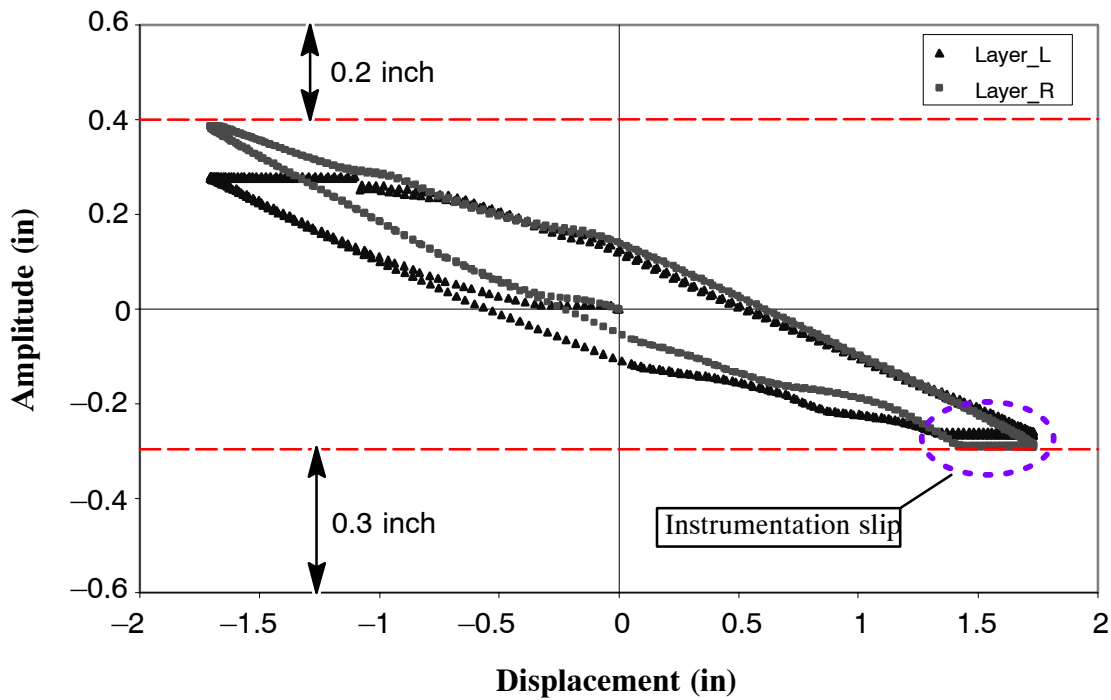


Figure 6-92 Shear Deformation of the Interface Layers of the Test Structure Case 2 (1.5% Drift)

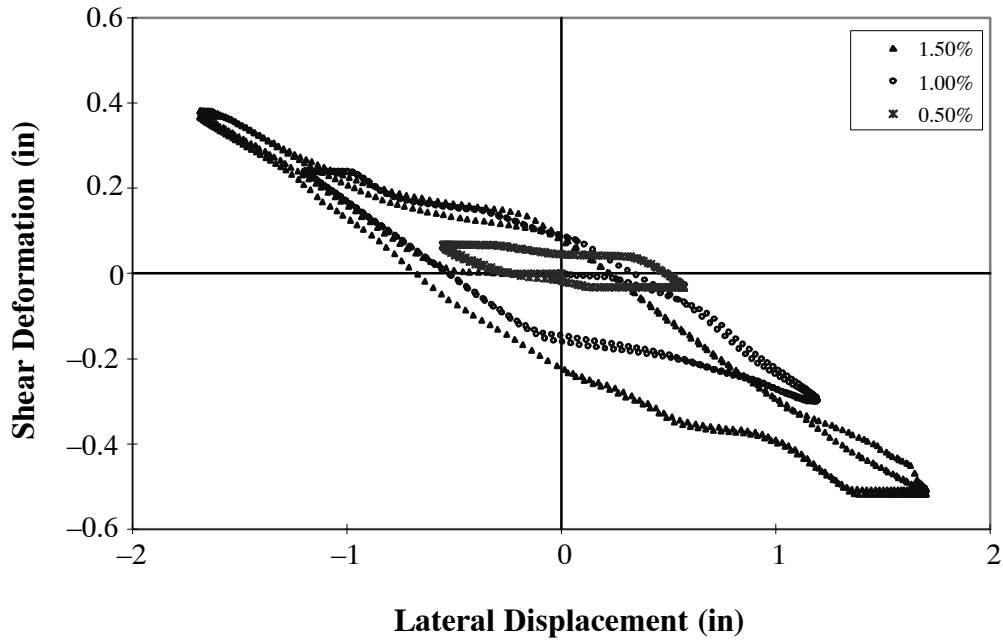


Figure 6-93 Variation of the Shear Deformation on the Combining Interface Layer under Cyclic Loading Tests (Case 1)

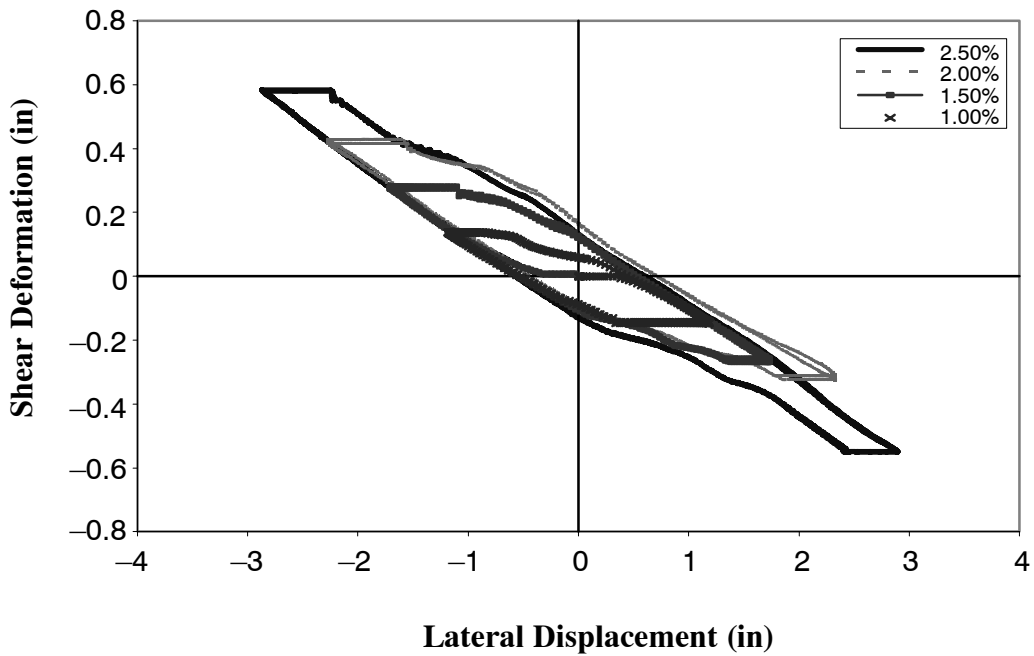


Figure 6-94 Variation of the Shear Deformation of the Interface Damping Layer under Cyclic Loading Tests (Case 2)

Energy Dissipation Capacity of the FRP Box Damping Panel

The combined interface layer of the FRP box panel consists of the polymer honeycomb and 3M viscoelastic materials. In general, viscoelastic solid material exhibits mechanical properties which are frequency and temperature dependent. The frequency effect for both cases of the FRP box infill systems was investigated at a high drift level in order not to consider the honeycomb effect and presented in Fig. 6-95 to 6-96. As shown in these figures, a significant effect was not found in the tests due to limited applied loading rate. The maximum velocity of the hydraulic actuator used in these tests was also 0.6 in/sec. For the static full-scale specimen test, it was difficult to represent the frequency effect under the applied actuator velocity. However, it is believed based on material testing that the energy dissipation capacity of the combined interface layers will be increased as the applied frequency increases. In section 5, the dependency of energy dissipation capacity on frequency was verified by experimental studies. Under seismic excitation, it would be expected that the interface damping layers may play an important role to reduce seismic response of the structure.

Energy dissipation capacity of both FRP box infill cases was evaluated at the available maximum frequency. From the test results, a slight increase in energy dissipation was observed compared to the steel bare frame response as shown in Fig. 6-97 to 6-100. On the basis of the measured hysteretic energy responses for a given drift, energy dissipation capacity was calculated and summarized in Fig. 6-101. In reality, larger energy dissipation capacity of the structure will occur as the frequency increases. In practical application, such frequency dependent damping performance will be effective to control structural vibration when the FRP box infill system is subjected to the wind environment or earthquake excitations.

The failure of the FRP box panel having a stiff and a combined interface layers was investigated after completing all test procedures. The displacement had been applied monotonically up to 2.0% drift. Fig. 6-102 shows the right top joint angle connection of steel frame failed by the stress concentration as a result of preventing sliding shear of the stiff interface layer.

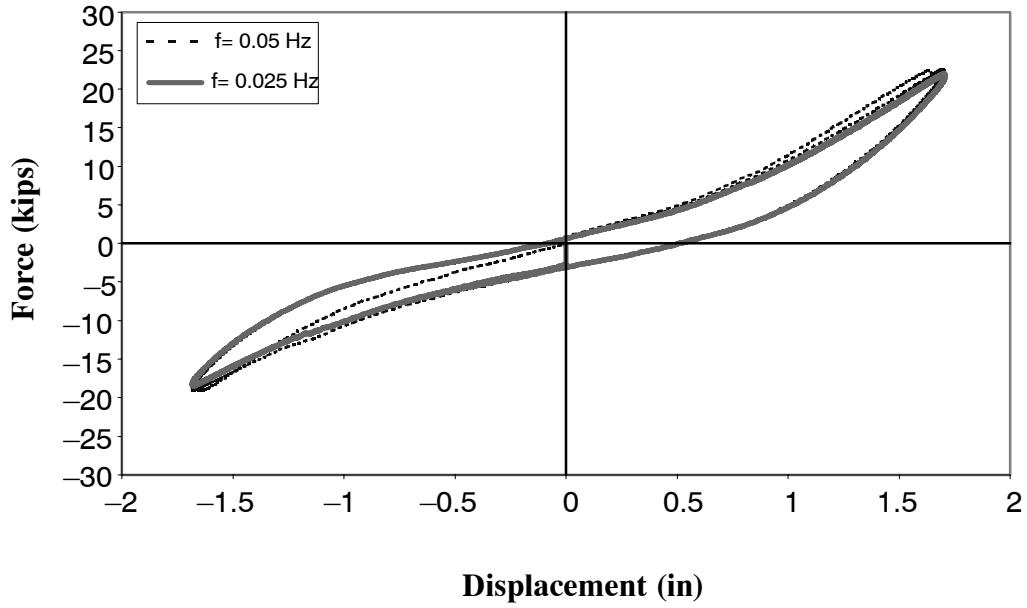


Figure 6-95 Frequency Effect of the Combining Interface Layer in the FRP Box Infill (Case 1, 1.5%)

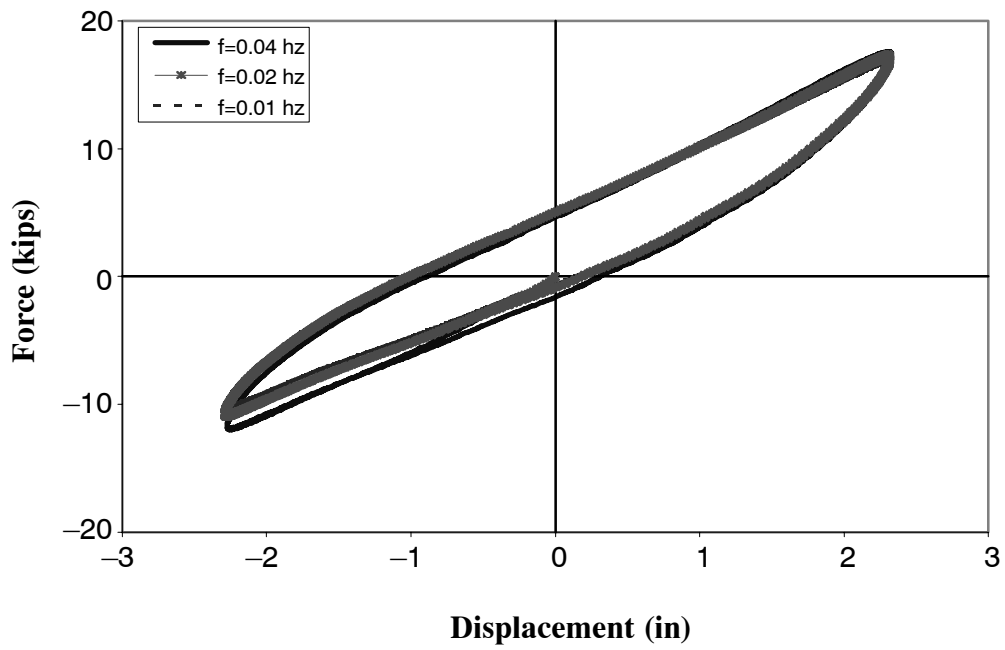


Figure 6-96 Frequency Effect of the Combining Interface Layer in the FRP Box Infill (Case 2, 2.0%)

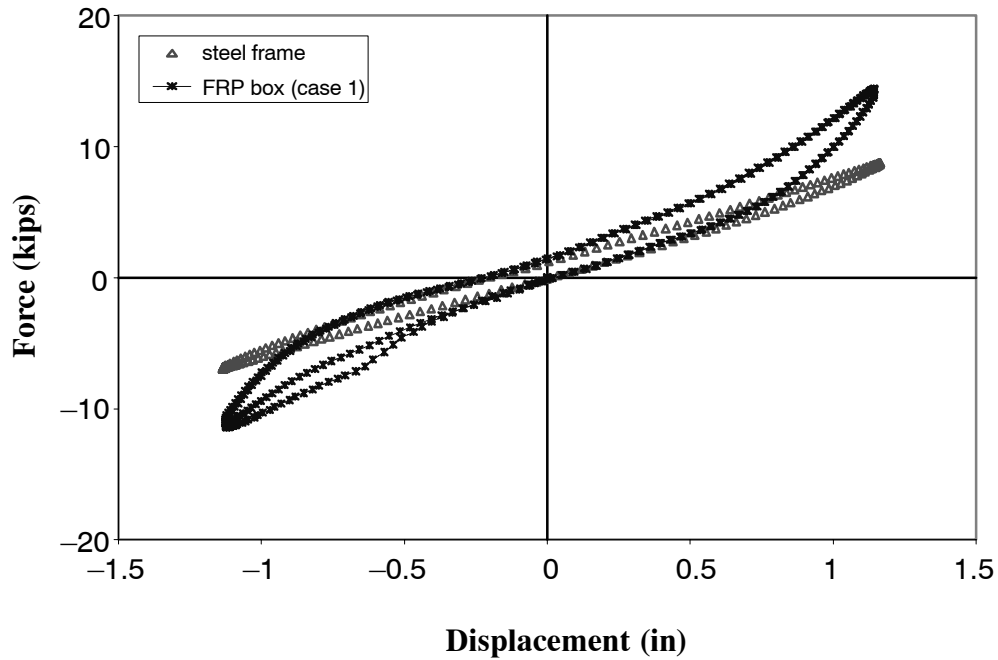


Figure 6-97 Comparison of the Hysteretic Energy for the FRP Box Infill (Case 1) and the Steel Frame (1.0% drift, $f = 0.08$ Hz)

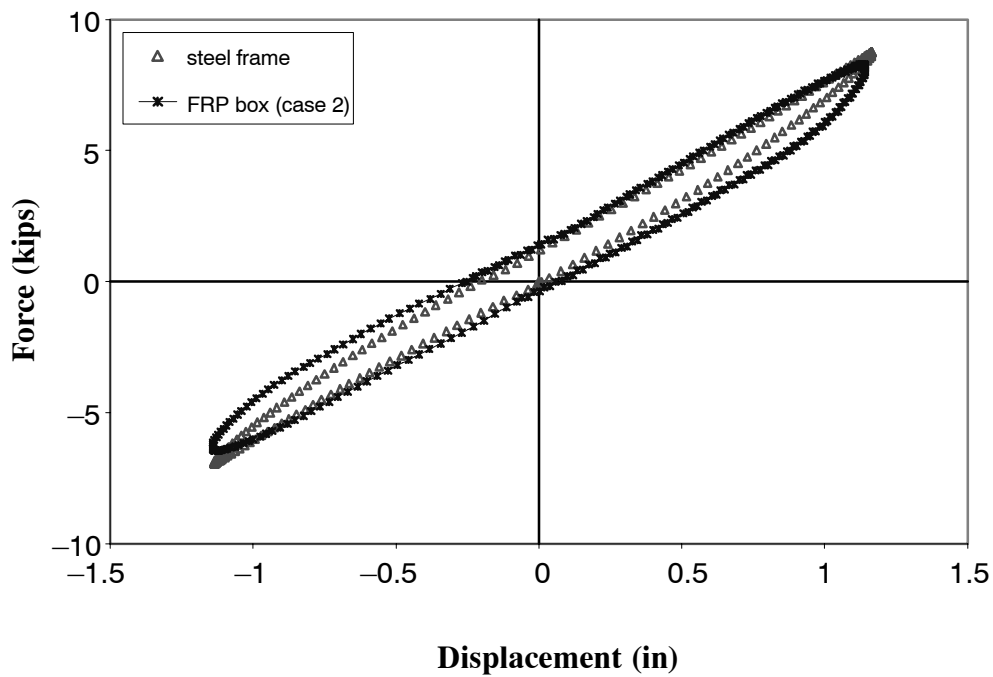


Figure 6-98 Comparison of the Hysteretic Energy for the FRP Box Infill (Case 2) and the Steel Frame (1.0% drift, $f = 0.08$ Hz)

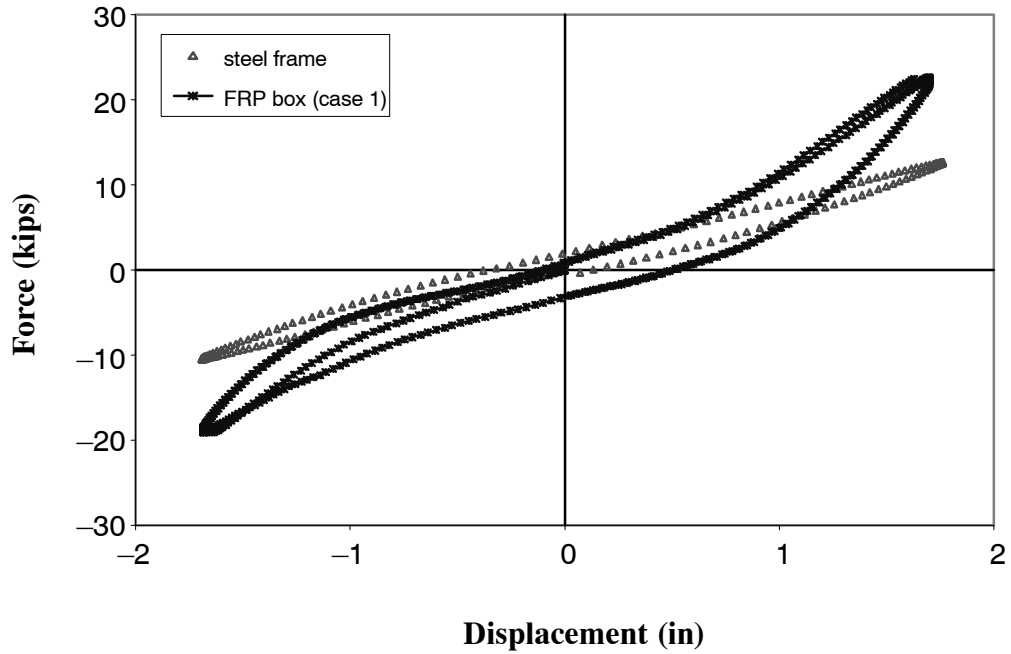


Figure 6-99 Comparison of the Hysteretic Energy for the FRP Box Infill (Case 1) and the Steel Frame (1.5% drift, $f = 0.054$ Hz)

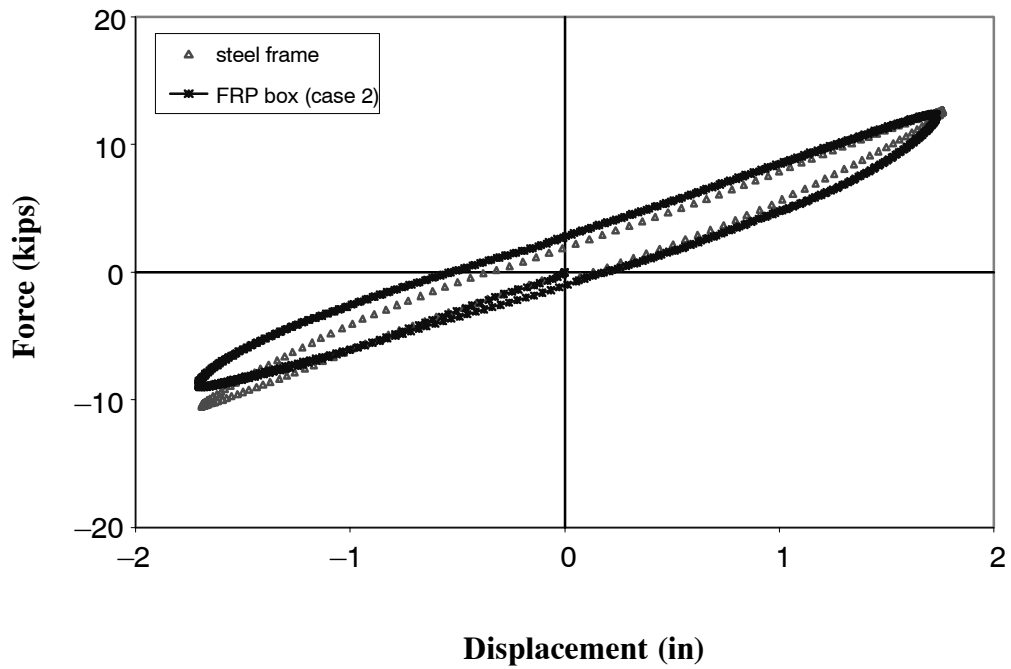


Figure 6-100 Comparison of the Hysteretic Energy for the FRP Box Infill (Case 2) and the Steel Frame (1.5% drift, $f = 0.054$ Hz)

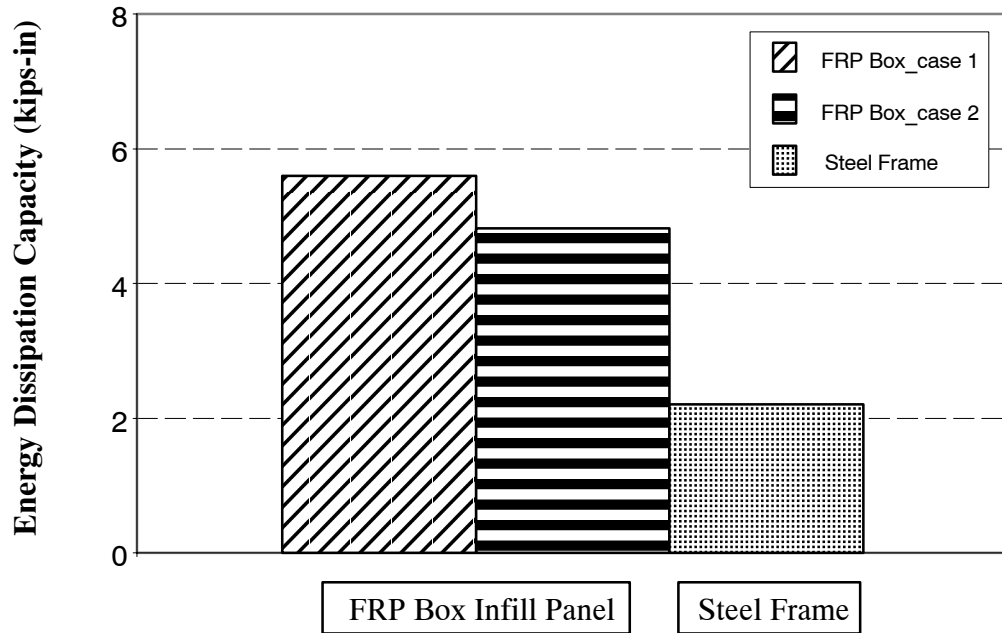


Figure 6-101 Comparison of Energy Dissipation Capacity for the FRP Box Panel Cases and the Steel Frame (1.0% drift, $f = 0.08$ Hz)

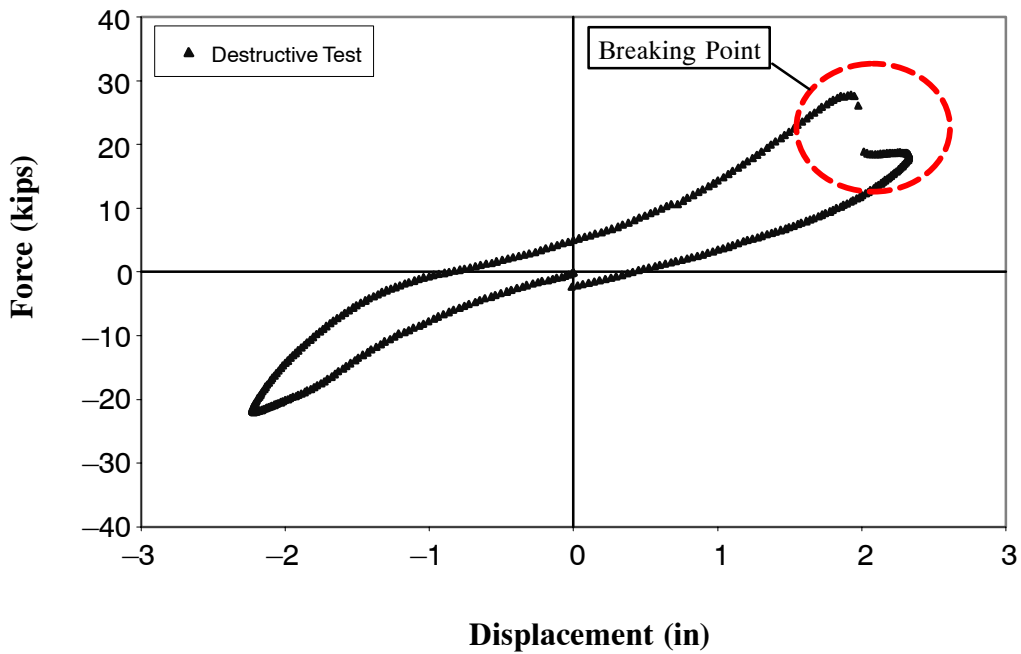


Figure 6-102 Failure of the FRP Box Infill having a Stiff and a Flexible Interface Layers under Cyclic Load (2.0% drift, $f = 0.04$ Hz)

Comparison and Discussion for the FRP Box Infill Systems (Case 1 & Case 2)

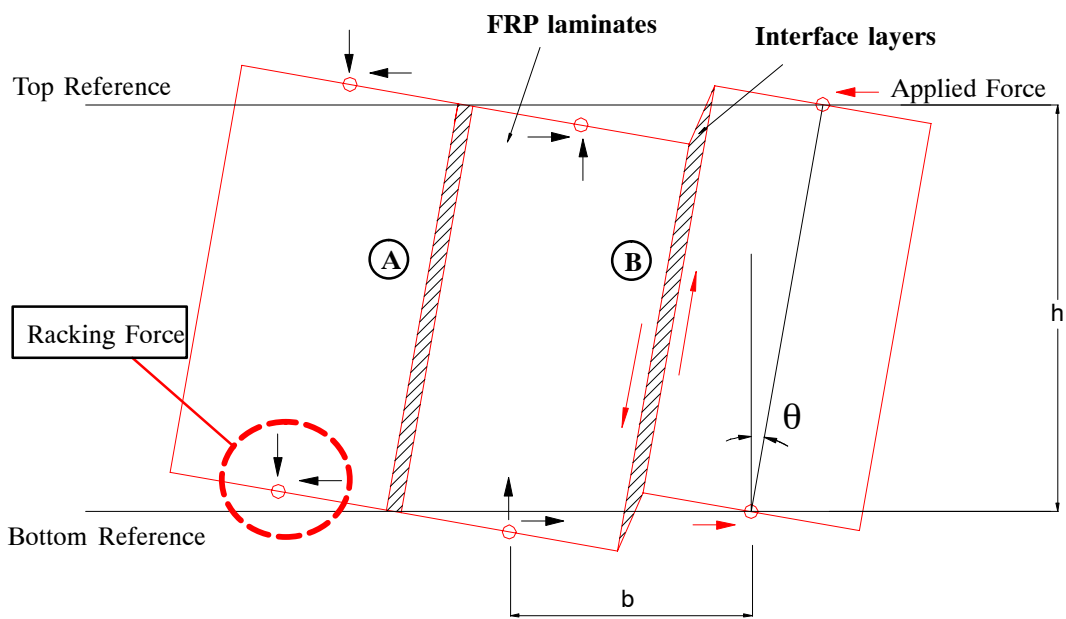
This section presents the comparison of the behavior of two cases of the FRP box infill systems. As mentioned before, basic configuration of FRP box infill system was composed of three FRP box panels and two constrained layers at the interface between them. Two FRP box infill systems were identical in all aspects except that one of the interface layers was stiffened in case 1, and both are flexible in case 2. Both systems were tested under static monotonic and cyclic loads, and all test results were presented in terms of the effective stiffness and energy absorption capacity.

When the FRP box infill system was subjected to the applied lateral force, two different deformed shapes were achieved; unsymmetric and symmetric interface deformations. This behavior can be predicted according to the characteristic of the interface layers. Fig. 6-103(a) and (b) show the possible schematic representation of deformed shape of both FRP box infill systems. In case 1, with a stiff interface layer, actual deformation is not easily defined because each layer was made up of different stiffness properties. This unsymmetric interface motion between the FRP box panels can produce a complex problem. At the top connection of the FRP box panel, the slot distance, which was used to reduce vertical forces, may also introduce an unknown factor and, thus, the exact deformed panel geometry is affected. However, the expected shear deformation of case 2 is easily determined by its symmetric motion as mentioned earlier.

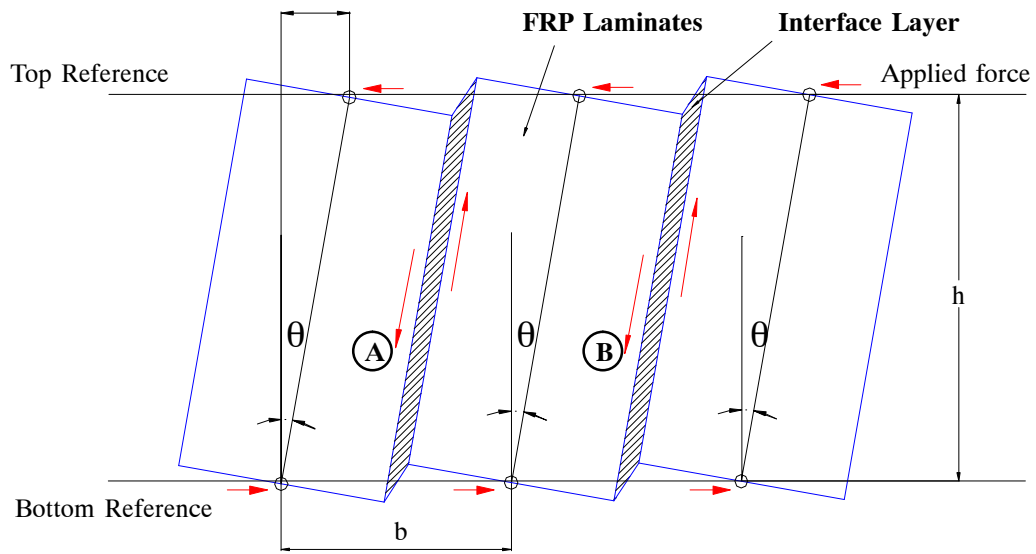
In order to investigate the effect of unsymmetric motion caused by a stiff interface layer in case 1, shear deformation of the flexible interface layer in both cases was measured experimentally under 1% inter-story drift of the applied lateral displacement. To reduce the stiffening effect of the honeycomb, the test was performed after breaking the honeycomb material in the combined interface layer. Fig. 6-104 shows the shear deformation of the interface layer at “B” location (depicted in Fig. 6-103) in case 1. The comparison of the results in both cases provides an indication of the effects produced by a stiff interface layer in case 1. It is evident in Fig. 6-105 that the shear deformation of case 1 is larger than that of case 2 because preventing shear by the stiff interface layer in case 1 produced an increase in shear deformation in the other side of interface layer.

The comparison of the hysteretic response of both cases of the FRP box infill is presented from Fig. 6-106 to 6-108. From these figures, significant increase for the stiffness/strength to the structure is clearly illustrated in case 1 because of preventing shear effect of one interface region in case 1. However, the hysteretic energy of both cases was not much different even though the number of applied interface layers in case 2 was twice as many as that of case 1. This is primarily due to the fact: (1) the shear deformation at interface layers in case 2 was relatively smaller than that of case 1, (2) the energy dissipation obtained by the inelastic action of the joint angle connection may become larger in case 1 than in case 2 because of a large stress concentration at the joint connection caused by preventing shear deformation in case 1, and (3) the lower frequency was applied during the tests.

Based upon the in-plane behavior, the overall response of the FRP box infill system with a stiff and a flexible layers (Case 1) is analogous to that of the multi-layer PMC infilled frame with the column-to-infill connections described in section 4. Practically, it is clear that preventing shear mechanism induced by either the stiff interface layer or the column-to-infill connections increases lateral resistance in the structure, but the corresponding stress concentration at the joint connections will lead to failure of the structure. The bolted joint angle connection failure induced by preventing shear deformation of the stiff interface layer is clearly shown in Fig. 6-109.



(a) FRP Box Infill with a Stiff and a Flexible Layers (Case 1)



(b) FRP Box Infill with Both Flexible Layers (Case 2)

Figure 6-103 Schematic Representation of the FRP Box Infill Geometry

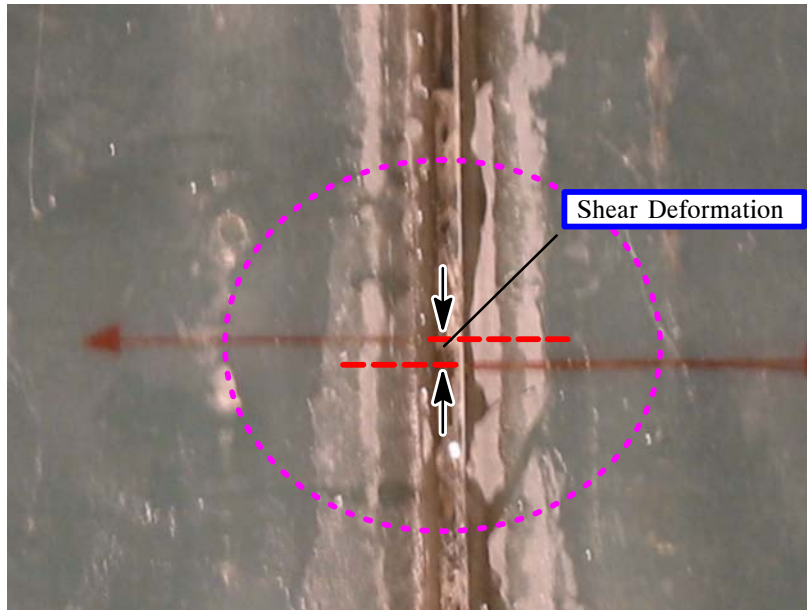


Figure 6-104 Shear Deformation of the Interface Layer at B Location (1.0% drift)

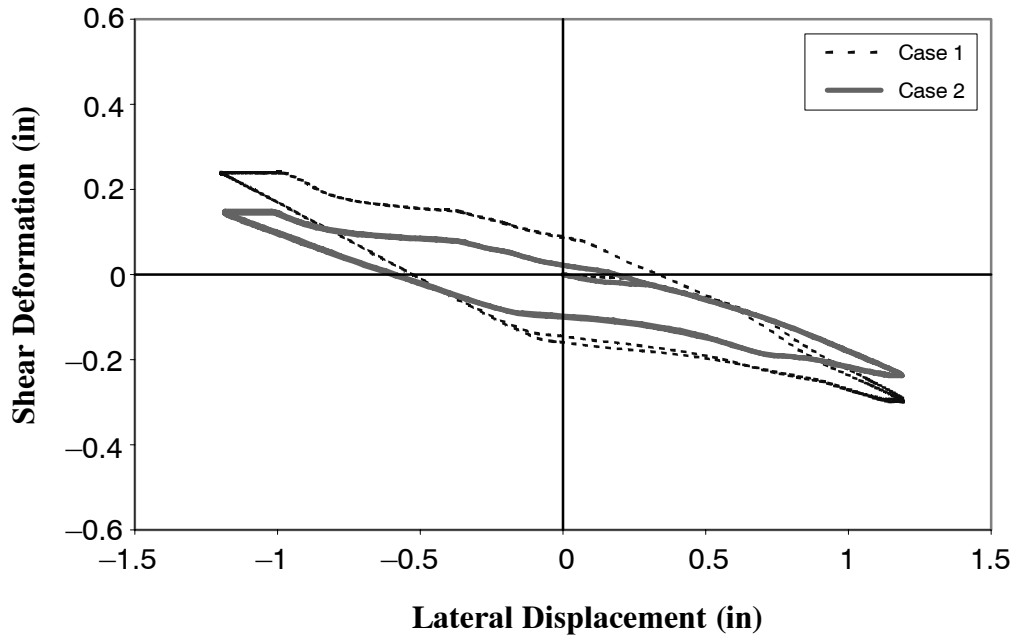


Figure 6-105 Comparison of Shear Deformation for the Interface Layers at B Location in Both Cases (1.0% drift)

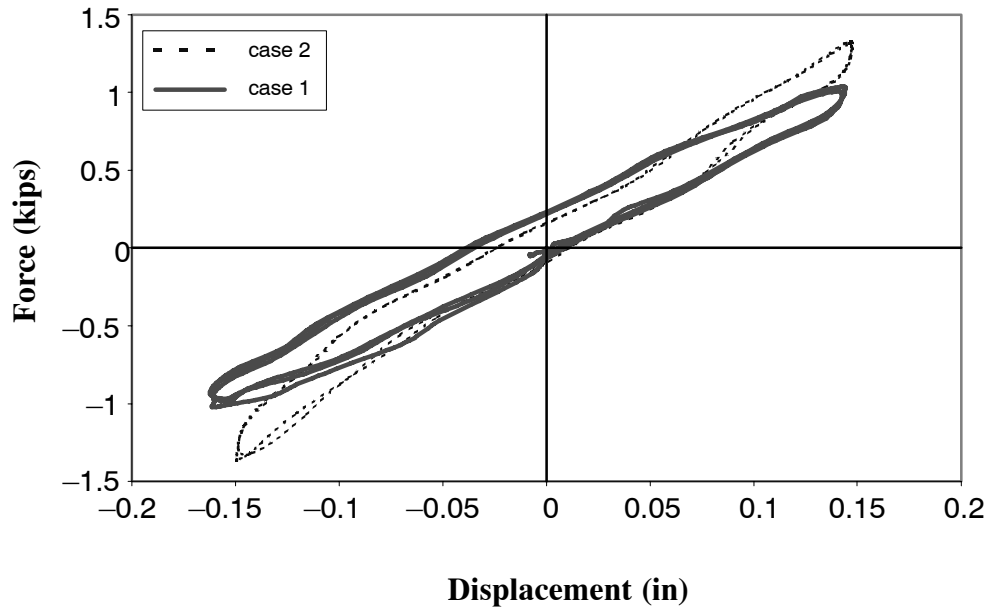


Figure 6-106 Comparison of Hysteretic Response for Both Cases of the FRP Box Infill Systems (0.16% drift)

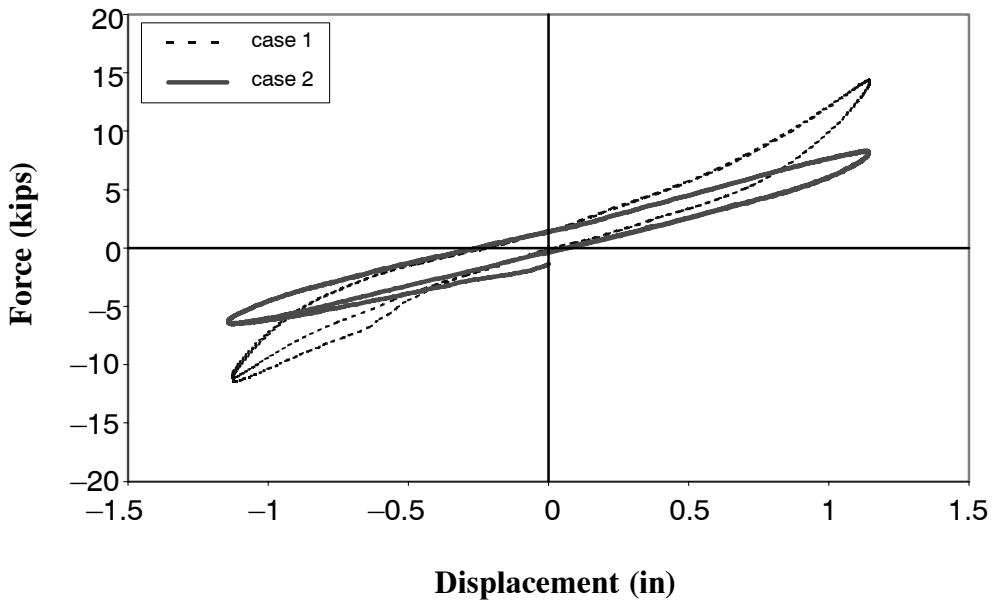


Figure 6-107 Comparison of Hysteretic Response for Both Cases of the FRP Box Infill System (1.0% drift)

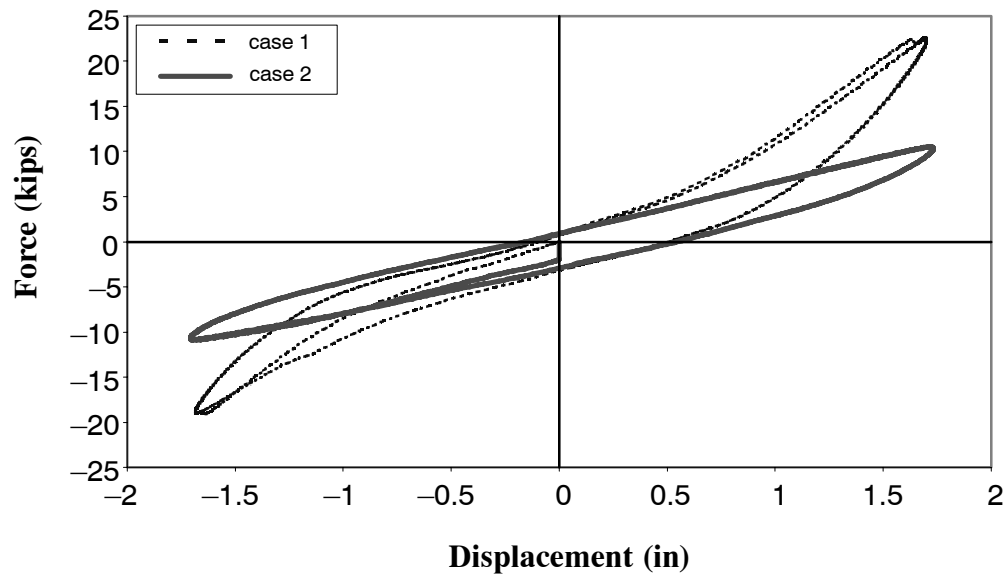


Figure 6-108 Comparison of Hysteretic Response for Both Cases of the FRP Box Infill System (1.5% drift)



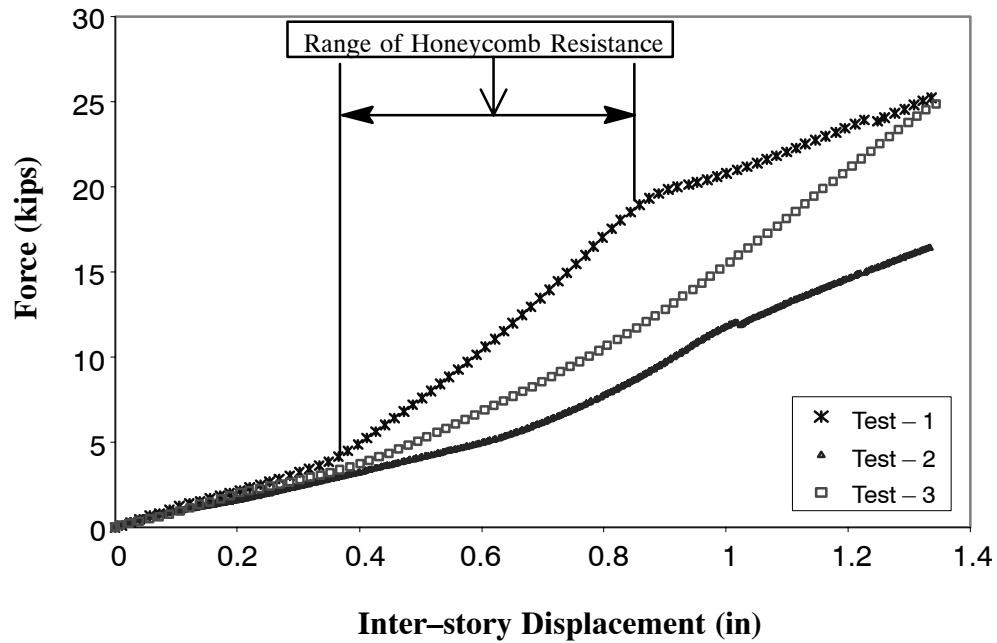
Figure 6-109 Failure of Joint Angle Connection by Preventing Shear Deformation of the FRP Box Infill System (Case 1, 1.5% Drift)

6.6.3 Honeycomb Effect of the Interface Damping Layers

In this study, the polymer honeycomb material was employed in the constrained interface layer to increase the initial lateral resistance/energy dissipation of the structure and reduce the fabricating cost. Fig. 6-110 shows total results for push-over static loading tests at the initial stage. As shown in this figure, the honeycomb primarily contributes to the overall lateral resistance up to its scrim layer failure, in the range between 0.15 –0.25 % strain. The resistant range matches well with material coupon test results. From design point of view, it will be desirable that the contribution of the polymer honeycomb in the interface layers may be adjustable depending on its thickness/area in the FRP box infill dimensions, but the durability of the honeycomb is questionable under prolonged cyclic loading. In the tests, it was found that additional energy was dissipated from friction between interface walls after breaking the honeycomb.

After loss of the polymer honeycomb resistance, the stiffness of the structure dropped rapidly. At the beginning of loading, the polymer honeycomb layer was subjected to in-plane shear deformation. When the honeycomb wall reached maximum shearing stress, the wall yielded and behaved nonlinearly. Finally, the honeycomb lost its capacity due to the scrim failure or delamination between surface sheet and honeycomb. Test 3 in Fig. 6-110 shows that the structure with only viscoelastic interface layers did cause a loss of stiffness, but it seemed tolerable and provided a relatively small fraction to the total lateral stiffness by interface friction between honeycomb walls.

In the design process, the honeycomb was considered as an additional component in the combined interface layers because the polymer honeycomb material does not have adequate fatigue strength for long term durability in the wind excitation. From a construction perspective, it is apparent that by applying advanced cellular materials, there is a possibility of making more advanced honeycomb material to achieve a desirable drift ratio to satisfy various design criteria..



Test – 1 : Combining Interface (Polymer Honeycomb) layers
 + Preventing sliding shear + Overflowed adhesive coating
 Test – 2 : Preventing sliding shear + Viscoelastic layers
 Test – 3 : Viscoelastic layers only

Figure 6-110 Stiffness Variation through the Honeycomb Effect of the Interface Layer (Case 1, 1.5% drift)

6.7 Summary

Light and flexible building systems often require specific design features for limiting damage and maximizing occupant comfort and safety. This section described two types of energy dissipating PMC infill systems for seismic retrofitting. By using the constrained interface damping layers, such panels were designed to form part or all of test structural system. The challenge in making these concepts is to achieve satisfactory input of passive energy dissipation to the steel frame in an existing building. To validate some of the proposed concepts, full-scale infill models were fabricated and tested within a steel frame.

Several important conclusions concerning proposed energy absorbing PMC infill panel are stated. For the multi-panel PMC infill system, the effectiveness of the PMC sandwich infill was examined first by analytical and experimental studies. The PMC sandwich infill was designed to provide considerable stiffness in the existing structure at specific lateral drift to avoid large excessive relative floor displacements that causes both structural and non-structural damage. In the design process, stacking sequence of FRP skin laminates as well as initial gaps between the infill and the opening of steel frame were considered as key parameters. By using numerous finite element simulations representing the lay-up, optimum stacking sequence was designed on the basis of maximum buckling resistance, and the commencement of the infill action was determined by a specified initial gap distance. Finally, the in-plane behavior of a steel frame infilled with the PMC sandwich panel was investigated by the experimental studies. The comparison of both numerical and experimental results was in a good agreement.

The outer FRP panels were designed to have the FRP laminate panels and the constrained interface layer at the interface between them. The constrained interface layers were fabricated by a combination of 3M viscoelastic solid and polymer honeycomb material. Combining ratio between these composite materials was studied in section 5, and the geometric dimensions were designed by the simplified calculation proposed by Gasparini et al.(1981) on the basis of required damping of the structure. After installing the outer FRP panels, overall behaviors of the multi-panel PMC infill sys-

tem were investigated under various frequencies in terms of the effective stiffness as well as energy dissipation. In the experimental studies, the comparative results with steel frame showed a slight increase of the damping in the multi-panel PMC infill system but these results may still be highly conservative. It is because that energy dissipation of the multi-panel PMC infill was limited by the loading rate available during the test. In the experimental phase of a full-scale specimen test, the maximum velocity of the hydraulic actuator used in this study was restricted within 0.6 in/sec, thus, the corresponding applied frequency was very low. Also, the frequency was decreased as the lateral drift increases. Considering that viscoelastic material in the combined interface layer is a frequency-dependent, the obtained energy dissipation was not accurately quantified from the tests. However, the multi-panel PMC infill system was proven numerically to have tremendous potential for increasing the damping as the applied frequency increases. It is also evident by test results that measured cyclic shear straining of the combined interface layers becomes larger as the lateral drift increases in the structure. The passive damping mechanism represented by the cyclic straining of the interface layers is a very important factor for evaluating the damping of the multi-panel PMC infill system.

From the failure of the multi-panel PMC infilled frame, some important observations were found in regard to the semi-rigidly bolted connection. In particular, the relation between the edge shape of the PMC sandwich infill and allowing initial gaps needs to be investigated. Allowing initial gaps in the current design required a large infill lifting into the corner of steel frame. When the infill slides into the corner, the impact between the infill and the bolt head on the surface of the angle connection had taken place before the contact between the infill and the steel column. This was a reason to reduce the contact length between the infill and the steel column, and hence it caused a high pressure on the joint angle connection.

In the installation of the outer panel into the steel frame, the gaps between the inner PMC sandwich infill and outer panels are sometimes disregarded. In this study, this gap was filled out by wood and rubber spacers before starting the tests in order to achieve an individual behavior in the PMC sandwich infill and the FRP outer panels, respectively. Sometimes, it would happen during the tests that the spacers tightly inserted in between the PMC sandwich and outer panels may interrupt a free

movement of the PMC sandwich infill to take place during the opening and closing of the initial gaps under cyclic loading condition.

For the studying the FRP box infill system, we considered two cases; (1) the FRP box infill with a stiff and a flexible interface layers (case 1), and (2) the FRP box infill with both flexible interface layers (case 2). A stiff layer was fabricated by a woven fabric coating on the surface of the interface layer. In the experimental studies, testing procedures and descriptions were similar to the multi-panel PMC infill system tests described earlier. The specimen in case 1 was tested up to 1.5% drift to avoid a progressive damage of the joint angle connections, while the specimen of case 2 was performed up to failure under various frequencies. The test results in both cases were examined in terms of effective stiffness as well as the energy dissipation. Significant increase in stiffness/strength to the structure induced by preventing shear deformation of the stiff interface layer was observed in case 1 by the experimental force-displacement response. However, preventing shear mechanism led to a large stress concentration to the bolted angle connections and finally to damage of the structure. Such a behavior was also observed in the multi-layer PMC infilled frame with the infill-to-column connections described in section 4.

From the experimental hysteretic energy response, the energy dissipations in both cases were still not taken because of lower applied loading rate. However, by considering the factors: (1) the enhanced energy dissipation capacity of the combined interface layers presented in section 5, (2) numerical simulation for hysteretic energy under high frequency, and (3) the evaluation of the cyclic straining in the combined interface layer under the cyclic load in present section, the FRP box infill system should have larger energy dissipation as the frequency increases. Finally, the effect of the polymer honeycomb was investigated in case 1. It was found by experimental studies that although the polymer honeycomb material does not have adequate fatigue strength for long term durability, the honeycomb primarily contributes to the initial lateral resistance up to its yield point. Therefore, in practical applications, the honeycomb was considered as an additional component in the combined interface layers.

In this section, even if significant energy dissipations of the proposed PMC infill systems were not apparent from the experimental studies, it is believed that these infill systems will provide considerable stiffness and/or enhanced energy dissipation capabilities when applied to mid-rise building or hospital structures under seismic excitation. The predictable seismic response of those PMC infill systems when subjected to real earthquake loading will be presented in another report.

SECTION 7

CONCLUSIONS AND RECOMMENDATIONS

7.1 Conclusions

By using polymer matrix composite (PMC) material, new conceptual designs for seismic retrofitting were developed for application in existing buildings. Similar to partial rehabilitation techniques using composite material such as column wrapping, the use of prefabricated PMC infill panel systems is a very efficient way to achieve seismic retrofitting of existing facilities because of the efficiency of the material and its ease of use in construction. PMC material has high stiffness-to-weight and strength-to-weight ratios. Thus, the addition of PMC infill panels into existing structures will not significantly alter the weight of the structure while providing substantial structural enhancements.

In this study, three prefabricated PMC infill panel systems for seismic retrofitting were proposed. The PMC infill panels were studied using analytical and experimental methods to assess their effectiveness and response under simulated earthquake loading. Applying the concept of combined interface damping layers to the proposed panel systems was found to be highly feasible in the seismic applications. Design and fabrication procedures for each PMC infill panel were presented, and a conceptual trial design was performed using finite element (FE) analysis. To validate the proposed systems in real situations, both monotonic- and cyclic-loading tests were performed on full-scale models. The results obtained from this research showed that the systems offer the potential to increase the damping as well as the lateral resistance of steel frames, with a relatively low cost of retrofitting.

7.1.1 General Advantages of Proposed PMC Infill Panel Systems

Fiber-reinforced polymeric (FRP) composites offer a significant potential for dramatic changes in the design and construction of civil structures ranging from bridges to buildings because of their ease of fabrication, high strength-to-weight and stiffness-to-weight ratios, and potentially high durability. From an architectural perspective, PMC materials enable the designer to produce highly efficient

structures, often utilizing the geometric form to provide stability and strength, while removing the inherent structural redundancy and lack of efficiency found in most conventional structures.

Compared to traditional infill wall materials, such as concrete, masonry, and brick, a PMC infill panel is much lighter, which can result in less weight being carried by columns and the foundation as well as a reduced seismic load because of the reduced mass added to the structure. Also, prefabricated PMC infill panels shorten the erection process while reducing the cost of construction, field inspection, and quality control, resulting in even greater construction efficiencies for these systems.

Compared to traditional infill systems, PMC infill panels can be much easier and faster to construct when they are used for seismic retrofitting of existing structures.

7.1.2 Multi-layer PMC Infilled Frame

To use PMC material in infill panel walls, several technical and cost challenges associated with the design of the PMC infill panel must be overcome. The current lack of design standards for infill panel walls made of PMC materials and many design variables that affect both the performance and cost of the infill panel were two of the most serious challenges encountered in this study. The design criteria of traditional infill panel systems, such as those constructed of concrete or masonry, were not applicable to the PMC infill panel systems because of the different material characteristics, relative stiffness, and initial gap between the steel column and the PMC infill panel.

To achieve high damping performance in the structure, a multi-layer PMC infill panel system was introduced. Such a system was designed with three components comprising the entire wall thickness — namely, the inner component, the outer component, and the interface. With a perfect bonding assumption, this multi-layer system was expected to allow in-plane shear deformation and, therefore, sliding along specific layers upon loading of the frame. The damage of the multi-layer PMC infill panel was intended to be concentrated in its honeycomb interface layers and, hence, energy dissipation would be produced within the panel system itself.

To achieve the expected behavior, a sandwich-type construction was chosen for the inner component, and the FRP laminate was fabricated as outer components on both sides of the inner component. At the interface between these inner and outer components, the polymer honeycomb material constitutes the link between the inner and outer component of the PMC infill panel and dissipates energy. The practical role of this inner component was to increase the structural rigidity of the composite panel, while the outer FRP laminates were designed to transfer the applied force to the interface layers.

The optimal design of inner and outer FRP laminates was obtained by weighing the structural performance and cost of the components. After selecting the fiber reinforcement, the FRP laminates were designed by considering several possible stacking sequences and constraints, such as cost and stiffness. By using numerous FE simulations representing different lay-up and geometric combinations of a variety of materials, the final choice of laminate architecture for the PMC infill panel was determined by stiffness rather than strength.

The experiments demonstrate that the multi-layer PMC infill panel system can play an important role in the strength and ductility of steel-frame structures. Several important results concerning energy dissipation of the PMC infill wall systems are summarized here.

The stiffness of the PMC-infilled frame was *three times* that of the bare steel frame. The load-carrying capacity of the PMC-infilled frame was *four times* that of the bare steel frame. For a second PMC-infilled frame, one in which column-to-infill connections were introduced, the stiffness was 1.43 times that of the PMC-infilled frame that lacked any connections to the columns. In terms of energy dissipation, the PMC-infilled frame could dissipate three times energy compared to the bare steel frame when subjected to small deformation at the honeycomb layers. The PMC infill panel wall contributed 65% of the overall energy-dissipation performance of the structure without significant degradation in stiffness or strength. The energy-dissipation capacity of the PMC-infilled frame may become greater when the honeycomb layers undergo large deformations. The test of the PMC-in-

filled frame with column-to-infill connections shows the enhanced contribution of the PMC infill panel honeycomb layers.

Initial gaps affect the behavior of the PMC-infilled frame. Similar to the frame infilled with traditional materials, the initial stiffness of the PMC-infilled frame was reduced by the presence of any initial gap. From a practical standpoint, reducing the size of the initial gap as much as possible in the PMC infill panel wall is preferred.

The main damage to the PMC-infilled frame structure was through elastic buckling of the inner panel at high drift values (2.5% or more) and consequent angle-connection damage. To increase the performance of the PMC infill panel wall system, new geometric shapes and dimensions of the inner and outer panel are being considered. For the outer panel, two facts are relevant. First, it was evident that by calculating a resistant force, assuming that a distributed stress acts on the surface area, the honeycomb layers provided a fraction of the total lateral and vertical stiffness in the PMC infill wall system. Second, it was shown that the current geometric shape of the outer panel is not an optimal solution for a cyclic-loading condition. These results indicate that further studies to optimize the shape of the outer panel by considering both the stiffness of the honeycomb material as well as the cyclic loading condition are warranted.

The test results presented in this study showed that the presence of the PMC infill panel greatly stiffened and strengthened the structural system. However, the results obtained also suggest some deficiencies, such as insufficient damping performance, of the structure. More researches on the larger energy-dissipation interface layers and their role in improving damping characteristics were required in this study. As such, the following section presents the study of advanced composite damping layers for more effective application in the infill wall.

7.1.3 Combining Interface Constrained Damping Layer

From the research conducted on the multi-layer panel, it was found that the honeycomb material may not be efficient at applying large interface damping, even if considerable stiffness in the struc-

ture was achieved. In addition, considering the feasibility of the constrained damping layer concept, the honeycomb layers at the interface did not have sufficient strength to preclude their failure during extreme loading conditions. To enhance the damping output of the interface damping layers, the material must have adequate fatigue strength as well as flexibility for long-term durability in wind- or earthquake-prone environments. It was illustrated that the inclusion of a passive material in the interface layer could provide more flexibility for the design and thereby satisfy different requirements of damping as well as stiffness.

A new concept with a passive hybrid constraining layer was proposed to improve the damping performance of the previously proposed stiff constrained layer system composed of honeycomb material. In this new configuration, the interface layer consists of two different types of composite materials. One is the polymer honeycomb material; the other is 3M™ viscoelastic solid material. Previous research (Cao, *et al.*, 1995) has shown that applying viscoelastic material in constrained layers within a mechanical structure is very effective in suppressing resonant vibration, excessive noise, and fatigue failure.

By combining both composite materials and adjusting the proportions of each material in the interface layer, maximum energy dissipation can be obtained from shear straining of the viscoelastic material and interface slip between the honeycomb cells. It is expected that the stiff portion of the honeycomb would fail in the early stages of earthquake loading without the presence of the damping properties afforded by a viscoelastic component, and, thus, the 3M viscoelastic material will effectively produce significant damping to the system. With this two-stage behavior that the combined interface layers are expected to perform, enhanced damping and stiffness can be adjusted and customized by the design. Thus, the capacity for customization in allowing stiffness and damping to be integrated into the design of one system is a novel and effective approach, as demonstrated in this study.

Experimental studies for individual materials forming the combined interface and hybrid constrained layer systems were performed to verify the feasibility of the damping concept and inves-

tigate its design parameters. Several experimental studies and quantitative design assessments were made to define the characteristics of the proposed damping interface system. Possible design parameters were considered in the experimental studies, and two parameters regarding the geometric arrangements — area and mixing ratios — were proven to be the most critical factors in determining the damping performance in the system. Finally, experimental studies conclusively show that the combined interface system is more effective than each individual material system. As a result, a new approach employing a combined interface damping layer could be adopted to provide a moderate level of vibration control in large structures.

In seismic applications, a minimum combination ratio of 60% viscoelastic material is recommended to provide an effective damping system. When less than 60% viscoelastic material is used, the effect of the honeycomb material becomes dominant, and the viscoelastic material provides only limited damping effects.

7.1.4 PMC Infill Panel Systems with Passive Energy Dissipation Mechanisms

When structures such as buildings and bridges are subjected to earthquakes, dissipating some of the input energy through predetermined and well-designed mechanisms is imperative. Recent earthquakes have demonstrated that a lack of energy absorption mechanisms is one of the major causes of poor building performance. The aim of this research was to propose a new seismic retrofitting strategy that places a priority on energy absorption and examine the effectiveness of the advanced PMC infill panel systems as part of this strategy. The research concentrated on two particular PMC infill panel systems that included passive energy-damping layers. In the first system, the multi-panel infill concept was introduced. FRP damping panels with vertical combined interface damping layers were positioned on both sides of a PMC sandwich infill panel. This PMC sandwich infill panel was designed to provide lateral stiffness at high lateral drift. In the second system, lightweight FRP box damping panels were designed, and passively combined interface-damping layers were installed in parallel between the FRP box sections.

For the multi-panel infill system, research focused on the mechanical behavior of strategically located component elements with reliable stiffness and damping properties that can modulate the response. The results of the study showed that the multi-panel PMC infill system had potential for improving seismic response of existing structures. It is believed that the corresponding behaviors shown under monotonic- and cyclic-loading tests demonstrate that the large shear deformation of the combined interface layers and PMC sandwich infill panel action provide enhanced damping as well as considerable stiffness in the structure. The FRP box infill panel system was designed to have relatively more flexible damping panels, given the advantage of the wide surface area of the box section. Although several types of structures are suitable for the application of such a concept, a tube-type structure lends itself best to the application because passive damping material can be easily installed in an existing structure such as a multi-story building.

On the basis of experimental investigations, the multi-panel PMC infill system was designed to provide considerable stiffness as well as enhanced damping properties. According to the numerical and experimental studies, using the passive concept of the combined interface damping layers provided enhanced damping characteristics through the outer damping panels. Also, as lateral drift increases, the contribution of the PMC sandwich infill panel can increase the stiffness when it wedges within the steel frame; thus, the additional contact and enhanced stiffness provide a mechanism to avoid excessively large relative floor displacements. Moreover, the influence of this stiffening by the PMC sandwich infill panel minimizes the $p-\Delta$ effect of the steel column.

In the experimental studies of the multi-panel PMC infill system, the energy dissipation characteristics did not show clear enhancement to structural damping. This apparently lackluster behavior was mainly attributable to the low rate of loading, a limitation imposed by the testing equipment. However, it was found numerically that the proposed systems should have the potential for significantly increasing the damping that arises from the cyclic straining of the interface damping layers when they are subjected to cyclic loads. It was also evident, and obviously anticipated, that the shear deformation of the interface damping layers becomes greater as the lateral drift increases in the struc-

ture, and the behaviors of the proposed PMC infill panels would therefore be expected to improve drastically. Moreover, the behavior of the interface layers is a very important factor for evaluating the effectiveness of the proposed PMC infill panel systems.

The main damage to a steel frame with the multi-panel PMC-infill system was the failure of the joint-angle connections at high drift values (2.75% or greater). To increase the performance of the multi-panel PMC infill system, two issues were considered in the design. First, the edge shapes of the PMC sandwich infill panel must be redesigned. By allowing initial gaps to be present in the current design, the large infill panel is permitted to lift into the corner of the steel frame. When the infill panel slides into the corner of the steel frame, the resulting impact between the edge of the infill panel and the bolts on the semi-rigid angle connection was occurring before the infill panel was in contact with the steel column. This was a direct cause of joint-angle connection failure. If the edge shape of the infill panel is properly designed to avoid this early impact, the infill panel making contact tightly into the corner of the joint-angle connection would reduce the rotation of the joint connection at that location. Second, the predominant factor for determining the overall resistance of PMC-infilled frame structures is the bolted semi-rigid connections. If the bolted semi-rigid angle connections have enough strength to produce buckling of the PMC sandwich infill panel, the overall performance of the structure will be significantly enhanced. To increase the bolted angle connection capacity, top-and-seat-angle connections with double web-angles are recommended because their rotational capacities would then be sufficient.

Significant potential for dramatic changes in the design and construction of civil structures was offered by using prefabricated PMC infill panel systems. Compared to traditional infill panel walls, such as those constructed of concrete, masonry, and brick, the proposed PMC infill panel systems will be easily designed to provide the desired damping limit in association with a light infilled frame structure through their constrained damping layers. In the design process of the proposed PMC infill panel systems, significant increases in the damping of existing structures may be realized by incorporating outer FRP laminate panels and combined damping layers at the interface between them.

The optimal damping panel can be easily designed by the simplified procedures previously described.

Mechanically, high values of initial stiffness are beneficial in areas dominated by wind loads or low seismicity. For the possible application of the structures under wind loads or low seismic zones, honeycomb materials were used in the PMC infill panel systems to make the structure stiff upon loading the frame. The results of the static experimental tests showed an increased initial lateral resistance of the structure through the honeycomb interface layers up to its failure. Otherwise, high values of stiffness for seismic loading may not necessarily be beneficial. Higher stiffness values are often associated with lower energy dissipation values, which are not beneficial for a structure under seismic loading. By designing the honeycomb material in the combined interface layers for the PMC infill panel systems, a desirable level of stiffness can be incorporated in the structure at the initial stage. After the honeycomb layers fail under their small elastic strain range, the polymer honeycomb material will be useful to the structure under seismic excitation because a slight amount of energy would be dissipated through the interface friction between the honeycomb cells.

As another important mechanism of the proposed multi-panel PMC infill systems, out-of-plane behavior or buckling resistance of the PMC-sandwich infill panel may be increased by placing the FRP rigid damping panels on both sides of the infill panel. Compared with the out-of-plane behavior of the steel frame with the PMC-sandwich infill panel only, the existence of the outer panels on both sides of the PMC sandwich infill panel may decrease out-of-plane behavior of the PMC-sandwich infill panel by adding their rigidity. Accordingly, it would be expected in the infilled frame structures that the buckling resistance of the multi-panel infill panel under racking load would be higher than that of the PMC-sandwich infill panel only. To achieve this performance, the connector elements between the FRP damping panels and steel beams must be conservatively designed to avoid premature failure of the angle connections.

Tube-type structures, as demonstrated in the FRP box infill system, prove to be relatively flexible, and they are very useful in areas of high seismic excitations. The shape of a box section can provide

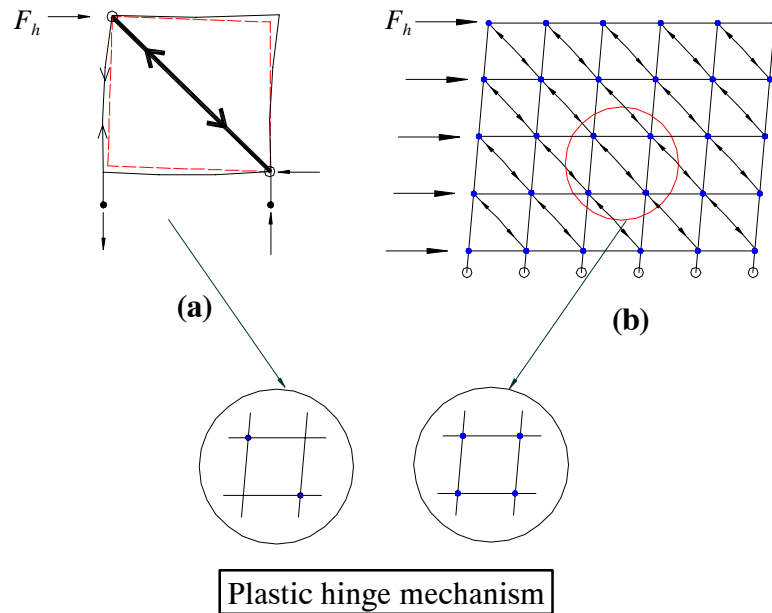
ample spaces for installing large numbers of viscoelastic layers. This type of damping panel system has three advantages: first; it is a simple method for designing such panel systems; second, it affords simple prediction for the effective damping and stiffness of such a system; and, third, it provides easy construction and practical retrofitting applications in existing structures by using prefabricated box damping panels.

In practical applications, more attention needs to be focused on the fabrication of the combined interface layers in both the multi-panel PMC infill and the FRP box infill systems. Sometimes, unexpected effects, such as the overflow of adhesive material in the honeycomb and/or epoxy-coated surface of the interface, may introduce a slightly stiffened structure under seismic excitation. In the experiments, the stiffening of the interface layers caused by these effects prevented the shear deformation of the viscoelastic layer and, finally, led to failure of the bolted angle connections during the FRP box infill system test.

7.2 Recommendation for Future Works

This study focused on the conceptual design, fabrication, and testing of energy-dissipating PMC infill panel systems. The scope of this research was aimed at examining the effectiveness and feasibility of these proposed infill systems. Even after performing extensive experimental and analytical studies, a need for a more complete understanding of PMC infill panel systems remains. The following is some recommendations for future research:

- Before the loss of the wall, the steel frame adds confining pressure to the wall and enhances its resistance. Thus, the actual effective forces on the steel frame components are probably minimal. As the frame components attempt to develop force, they deform and the stiffer infill panel components on the far side of the member pick up load. However, for the multi-panel PMC infill system, a one-story, semi-rigidly connected steel frame was applied, and its semi-rigid angle connections failed before the lateral resistance of the PMC infill panel reached its maximum capacity. Therefore, the maximum capacity of the PMC sandwich infill system was not assessed in the experimental studies. By the application of a prototype semi-rigidly connected steel frame used in a real hospital building structure, the lateral resistance of the PMC sandwich infill panel and the corresponding semi-rigid angle connection behavior will be investigated. Furthermore, numerical and experimental research for the multi-story steel frame infilled with the proposed PMC panels will be performed in the future and focus on the following: (1) in-plane behavior of the overall structure; (2) the behavior of the beam-to-column connections induced by their interaction with the infill panel; and (3) the plastic collapse mechanism if the semi-rigid connections have enough strength and ductility. The different plastic mechanisms between one-story and multi-story infilled frames were shown in Fig. 10-1.



**Figure 10-1 Plastic Hinge Mechanism:
(a) Single-story Steel Frame; (b) Multi-story Steel Frame**

- For the steel frame with the PMC infill panel systems, initial gaps are unavoidable in construction. As can be seen in the tests of the multi-panel PMC infill system, the presence of relatively large gaps or discontinuities between the prefabricated PMC infill panels and the frames led to problems such as different contact length and the impact between the infill panel edge and the joint-angle connections. Therefore, more research on the role of these initial gaps will be needed, taking into account the geometric configuration of the PMC sandwich infill panel. At the specific initial gap distance, the study of the corresponding behavior of the PMC infill panel system will be recommended in accordance with the various panel aspect ratios of the PMC infill panel. These results will be used for the practical application and the preliminary design with a proper evaluation of the connection.
- In the construction process, the PMC infill panels were fabricated by a hand lay-up procedure. This fabrication technique may affect the fiber volume fraction of composites and could result in some non-uniformity in material properties, section dimensions (including the panel thickness), and

adhesive properties. To reduce such fabrication errors during construction, it is recommended that a structural section be fabricated by an automated process, such as pultrusion.

- Damping of the proposed PMC infill panel systems is dependent on the applied frequencies. In the static experimental studies, larger hysteretic energy dissipation was not clearly demonstrated by the proposed damping systems because of the limited capacity of the applied actuator in the structural testing lab. Consequently, exact structural behaviors under cyclic loads, especially energy–dissipation capacity, cannot be evaluated accurately. Therefore, dynamic testing of such damping systems, using a shaking table and observation of earthquake response of the structure, should be conducted to evaluate the efficiency of the proposed PMC infill panel systems.

SECTION 8 REFERENCES

- ABAQUS / Standard User's Manual* (1997), Version 5.7 and 5.8., Hibbitt, Karlsson & Sorensen, Inc. Pawtucket, RI.
- ABAQUS/STANDARD User's Manual* (2000), Version 6.1., Hibbit, Karlsson & Sorensen, Inc., Pawtucket, RI.
- Annual Book of ASTM Standards* (1995), *The justification of ASTM Committee D-30 on High Modulus Fibers and Their Composites*, Vol. 15.03, Philadelphia, PA.
- Aiello, M. A., Ombres, L., (1997), "Local Buckling Loads of Sandwich Panels made with Laminate Faces", *Composite Structures*, 38, 191–201.
- Alberts TE, Xia H., (1995), "Design and Analysis of Fiber Enhanced Viscoelastic Damping Polymers", *Journal of Vibration and Acoustics*, 117, 398–404.
- Allen, H.G., (1969), "Analysis and design of structural sandwich panels", Pregamon Press, Oxford, U.K.
- Amos, K.A., (1985), "The shear strength of masonry infilled steel frames", MSc. thesis, University of New Brunswick, N.B., Canada.
- Angel, R., Abram, D.T., Shapiro, D., Uzarski, J., and Webster, M., (1994), "Behavior of Reinforced Concrete Frames with Masonry Infills", *Structural Research Series No. 589, UILU-ENG-942005*, University of Illinois at Urbana-Champaign.
- Aref, A. J., (1997), "A novel fiber reinforced composite bridge structural system." Ph.D. Thesis, University of Illinois at Urbana-Champaign.
- Aref, A.J., Jung, WY., (2001), "Polymer Matrix Composite Infill Walls for Seismic Retrofit", *Proceedings of the 2001 Structures Congress & Exposition*, ASCE, Washington, D.C., 21 – 23.

- Aref, A. J., Jung, W.Y., (2003), “Energy-dissipating Polymer Matrix Composite infill wall system for seismic retrofitting”, *J. Struct. Engrg.*, ASCE, 129(4), 440–448.
- Astaneh-Asl, A., (2001), “Seismic Behavior and Design of Steel Shear Walls – SEONC Seminar”, 2001 SEOANC Seminar, Structural Engineers Assoc. of Northern California, San Francisco, CA.
- Awkar, J.C., Lui, E.M., (1999), “Seismic analysis and response of multistory semirigid frames”, *Engineering Structures*, 21, 425–441.
- Baura, H.K. and Mallick, S.K., (1977), “Behavior of mortar infilled steel frame under lateral load”, *Building and Environment*, 12(3), 263–272.
- Benjamin, J.R. and Williams, H.A., (1957), “The behavior of one-story reinforced concrete shear walls”, *Journal of Structural division*, ASCE, 83, 1–35.
- Berman, J.W. and Bruneau, M., (2003), “Experimental investigation of light-gauge steel plate shear walls for the seismic retrofit of buildings,” Technical Report MCEER–03–0001, Multidisciplinary Center for Earthquake Engineering Research, State University of New York at Buffalo, NY.
- Cao, x., Mlejnek, H., (1995), “Computational prediction and redesign for viscoelastically damped structure”, *Comput. Methods Appl. Mech. Engrg.*, 125, 1–16.
- Carter, C., Stafford Smith, B., (1967), “On the structural behavior of masonry infilled frames subjected to racking loads”, *Int. Conf. Structural Masonry Systems*, University of Texas at Austin.
- Chang, K.C., Lai, M.L., Soong, T.T., Hao, D.S., and Yeh, Y.C., (1993), “Seismic behavior and design guideline for steel frame structure with added viscoelastic dampers,” Technical Report NCEER-93-0009, National Center of Earthquake Engineering Research, State University of New York at Buffalo, NY.
- Chopra, A. K., (2001), “Dynamic of Structures: Theory and Applications to Earthquake Engineering”, Prentice Hall, 2nd edition, Englewood Cliffs, NJ.
- Christensen, R. M., (1982), “Theory of Viscoelasticity”, Academic Press, New York.

- Constantinou, M.C., Soong, T.T, Dargush, G.F., (1998), "Passive Energy Dissipation Systems for Structural Design and Retrofit", Monograph Series, Multidisciplinary Center for Earthquake Engineering Research (MCEER), University at Buffalo, NY.
- Dawe, J.L. and Seah, C.K., (1989), "Behavior of masonry infill steel frames", Canadian Journal of Civil Engineering, 16, 865–876.
- Ehsani, M.R., Saadatmanesh, H., (1996), "Seismic Retrofitting of URM Walls with Fiber Composites", J. of The Masonry Society, 14(2), 63–72.
- Ehsani, M.R., Saadatmanesh, H., Velazquez–Dimas, J., (1999), "Behavior of retrofitted URM walls under simulated earthquake loading", J. of Composites for Construction, 3(3), 134–142.
- Elnashai, A.S., Elghazouli, A.Y., (1994), "Seismic behavior of semi–rigid steel frames", J. of Construction Steel Research, 29, 149–174.
- Federal Emergency Management Agency* (1997), NEHRP guidelines for the seismic rehabilitation of buildings, Rep. FEMA 273 (Guideline) and 274 (Commentary), Washington, DC.
- FEMA 356* (2000), Prestandard and commentary for the seismic rehabilitation of buildings, Washington, DC: Federal Emergency Management Agency.
- Ferry, J.D., (1980), "Viscoelastic properties of polymers", Wiley, New York.
- Flanagan, R. D., Bennett, R. M., (1999), "In-plane Behavior of Structural Clay Tile Infilled Frames", J. Struct. Engrg., ASCE, 125(6), 590–599.
- Frosch, R. J., Li, W., Jirsa, J. O., Kreger, M. E., (1996), "Retrofit of Non-ductile Moment-Resisting Frames Using Precast Infill Wall Panels", Earthquake Spectra, 12, 4, 741–760.
- Gasparini, Dario A., Debchaudhury, A.D., Curry, Lawrence W., (1980), "Damping of frames with constrained viscoelastic layers", Journal of the Structural Division, ASCE, 106(1), 115–131.
- Gasparini, Dario A., Curry, Lawrence W., Debchaudhury, Amitabha., (1981), "Damping of frames with viscoelastic infill panels", Journal of the Structural Division, ASCE, 107(5), 889–905.

- Ghassan, K., A., Gregory, E.L., (2002), “Design of Fiber-Reinforced Polymer (FRP) materials for seismic rehabilitation of infilled concrete structures”, No. CFM-A011, Engineering Research and Development Center (ERDC), U.S. Army Corps of Engineers.
- Gibson, L.J., Ashby, M.F., (1988), “Cellular solid structure and properties”, Pergamon press, England.
- Haroun, Medhat A, Ghoneam, Essam H., (1997), “Seismic performance testing of masonry-infilled frames retrofitted by fiber composite”, Proceedings of the International Modal Analysis Conference - IMAC, The International Society of Optical Engineering, 2, Orlando, FL, 1650–1656.
- Harris, H.G., Ballouz, G.R. and Kopatz, K.W., (1993), “Preliminary studies in seismic retrofitting of lightly reinforced concrete frames using masonry infills”, Proc. 6th North American Masonry Conf., Masonry Society (U.S.), Philadelphia, PA, 383–395.
- Hartley, A., Mullins, G. Sen, R., (1996), “Repair of concrete masonry block walls using carbon fiber”, Advanced Composite Materials in Bridges and Structures, Montreal, Quebec, 795 – 802.
- Hamilton, III, H.R., Dolan, C.W., (2001), “Flexural capacity of glass FRP strengthened concrete masonry walls”, Journal of Composites for Construction, 5, 170–178.
- Hendry, A. W., (1990), “Structural Masonry”, MacMillan Education, Ltd., London.
- Ireman, T., Ranvik, T., Eriksson, I., (2000), “On damage development in mechanically fasten composite laminates”, Composite Structures, 49, 151–171.
- Jones, Robert M., (1999), “Mechanics of composite materials”, Taylor & Francis, 2, Philadelphia, PA.
- Jung, W. Y., Aref . A. J., (2003), “A combined honeycomb and solid viscoelastic material for structural damping applications”, *Mechanics of Materials*, 35(8), 831–844.
- Kahn, L.F. and Hanson, R.D., (1979), “Infilled walls for earthquake strengthening”, Journal of Structural Division, ASCE, 105(2), 283–296.
- Kerwin E. M., (1959), “Damping of Flexural Waves by a Constrained Viscoelastic Layer”, Journal of Acoustical Society of America, 31(7), 952–962.

- Kesner, K. and Billington, S.L., (2005), "Development of seismic strengthening and retrofit strategies for critical facilities using engineered cementitious composite materials," Technical Report MCE-ER-05-0007, Multidisciplinary Center for Earthquake Engineering Research, State University of New York at Buffalo, NY.
- Kitane, Y., (2003), "Development of hybrid FRP-Concrete bridge superstructure system" Ph.D. Dissertation, State University of New York at Buffalo, U.S.
- Klingner, L.F. and Bertero, V.V., (1976), "Infilled frames in earthquake-resistant construction", Report No. EERC 76-32, Earthquake Engrg. Res. Ctr., U.C at Berkeley, CA.
- Kolsch, H.K., (1998), "Carbon fiber cement matrix (CFCM) overlay system for masonry strengthening", *Journal of Composites for Construction*, 2, 105-109.
- Laursen, P.T., Seible, F., Hegemier, G.A., and Innamorato, D., (1995), "Seismic Retrofit and Repair of Masonry Walls with Carbon Overlays", *Non-metallic (FRP) Reinforcement for Concrete Structure*. Edited by L. Taerwe, RILEM, 616-627.
- Liau, T.C. and Kwan, K.H., (1985), "Static and cyclic behaviors of multistory infilled frames with different interface conditions", *Journal of Sounds and Vibrations*, 99(2), 275-283.
- Lin, Y.Y., Tsai, M.H., Hwang, J.S., Chang, K.C., (2003), "Direct displacement-based design for building with passive energy dissipation systems", *Engineering Structures*, 25, 25-37.
- Mainstone, R.J., (1971), "On the stiffnesses and strengths of infilled frames", *Proc. Instn. of Civil Engrs Suppl.(iv)*, Institution of Civil Engineers (Great Britain), London, UK, 57-90.
- Mander, J.B, Nair, B., Wojtkowski, K. and Ma, J., (1993), "An Experimental study on the seismic performance of brick-infilled steel frames with and without retrofit," Technical Report NCEER-93-0001, National Center of Earthquake Engineering Research, State University of New York at Buffalo, NY, 1.1 – 3.1.
- Manos, G.C, Yasin, B. and Valiasis, T., (1993), "Small scale model simulation of the cyclic behavior of infill brick panels" *Proc. 6th North American Masonry Conf.*, Masonry Society (U.S.), Philadelphia, PA, 359-370.

- May, I.M., (1981), "Determination of collapse loads for unreinforced panels with and without openings", Proc., Instn. of Civ. Engrs., 71(2), London, UK, 215–233.
- Mehrabi, A.B., Shing, P.B., Schuller, M.P. and Noland, J.L., (1994), "Performance of masonry infilled R/C frames under in-plane lateral loads", Report CU/SR–94/6 Struct. Engrg. and Struct. Mech. Research Series, Dept. of Civ. Envir, and Arch. Engrg., Univ. of Colorado at Boulder, Colo.
- Moehle, J.P., (2000), "State of research on seismic retrofit of concrete building structure in the US" US-Japan Symposium and Workshop on Seismic Retrofit of Concrete Structure – State of Research and Practice, September, CA.
- Mosalam, K. M., White, R. N., and Gergely, P., (1997a), "Seismic evaluation of frames with infill walls using quasi-static experiments," Technical Report NCEER–97–0019, National Center of Earthquake Engineering Research, State University of New York at Buffalo, NY.
- Mosalam, K. M., White, R. N., and Gergely, P., (1997b), "Seismic evaluation of frames with infill walls using pseudo-dynamic experiments," Technical Report NCEER–97–0020, National Center of Earthquake Engineering Research, State University of New York at Buffalo, NY.
- Nelson, F.C., (1977), "Behavior of mortar infilled steel frame under lateral load", Building and Environment, 12(3), 263–272.
- Oberst H., (1952), "Uber die Damping der Biegeschwingungen dunner Bleche durch fest haftende Belage", Acustica, 2, 181 – 194
- Okutan, B., Aslan, Z., Karakuzu, R., (2001), "A study of the effects of various geometric parameters on the failure strength of pin-loaded woven-glass-fiber reinforced epoxy laminate", Composites Science and Technology, 61, 1491 – 1497.
- Paulay, T., Priestley, M.J.N., (1992), "Seismic Design of Reinforced Concrete and Masonry Building", John Wiley & Sons, New York, NY.
- Pong W.S., Tsai C.S., (1995), "Seismic Study of Buildings with Viscoelastic Dampers", Structural Engineering and Mechanics, 3(6), 569–581.

- Priestley, M.J.N., (1998), "Displacement based approaches to rational limit states design of new structures. In: Keynote address", Proceedings of the 11th European Conference on Earthquake Engineering, Paris, France.
- Riddington, J. R., (1984), "Influence of initial gaps on infilled frame behavior", Proceedings of the Institution of Civil Engineers, Institution of Civil Engineers (Great Britain), 77, London, UK, 295–310.
- Saadatmanesh, H., (1997), "Extending service life of concrete and masonry structures with fiber composites", Construction and Building Materials, 11(5–6), 327–335.
- Salazar, A.R., Haldar, A., (2001), "Energy Dissipation at PR Frame under Seismic Loading", J. of Struct. Engrg., ASCE, 127, 5, 588–592.
- Saneinejad A., Hobbs, B., (1995), "Inelastic Design of Infilled Frames", J. Struct. Engrg., ASCE, 121(4), 634–650.
- Schwegler, G., (1995), "Masonry Construction Strengthened with Fiber Composites in Seismic Endangered Zones", Proceedings of the 10th European Conference on Earthquake Engineering, Rotterdam, 2299–2303.
- Schwegler, G., Kelterborn, P., (1996), "Earthquake Resistance of Masonry Structure Strengthened with Fiber Composites", The 11th World Conference on Earthquake Engineering, Acapulco, Mexico.
- Soong, T.T., Dargush, G.F., (1997), "Passive energy dissipation systems in structural engineering", John Wiley & Sons Ltd., New York, NY.
- Staford-Smith, B., (1966), "Behavior of Square Infilled Frames", J. Struct. Engrg., ASCE, 92(1), 381–403.
- Staford-Smith, B., Carter, C., (1969), "A method for the analysis of infilled frames", Proc. Instn. Civ. Engrs, 44, 31–48.
- Thornton, P.H., Harwood, J.J., Beardmore, P., (1985), "Fiber-reinforced plastic composites for energy absorption purposes", Composite Science and Technology, 24(4), 275–298.

- Tumialan, J. G., Myers, J. J., and Nanni, A., (1997), "Field evaluation of masonry walls strengthened with FRP composites at the Malcolm Bliss Hospital," Technical Report CIES-99-12, Center for Infrastructure Engineering Studies, University of Missouri – Rolla, MO.
- Ungar E.E., Ross D., (1959), "Damping of Flexural Vibrations by Alternate Viscoelastic and Elastic Layers", Proceedings of the Fourth Conference on Solid Mechanics, University of Texas, Austin, TX.
- Valiasis, T., Stylianidis, K., (1989), "Masonry infilled R/C frames under horizontal loading Experimental results", *European Earthquake Engrg.*, 3, 10–20.
- Vian, D. and Bruneau, M., (2005), "Steel plate shear walls for seismic design and retrofit of building structures," Technical Report MCEER-05-0010, Multidisciplinary Center for Earthquake Engineering Research, State University of New York at Buffalo, NY.
- Wood, R.H., (1978), "Plastic composite action and collapse design of unreinforced shear wall panels in frames", *Proc., Instn. of Civ. Engrs.*, 65(2), London, UK, 381–411.
- Yang, J. N., Danielians, A., Liu, S. C. (1991), "Aseismic hybrid control systems for building structures", *Journal of Engineering Mechanics*, 117, 836–853.
- Zhang, R.H., Soong, T.T., Mahmoodi, P., (1989), "Seismic response of steel frame structures with added viscoelastic dampers", *Earthquake Engineering and Structural Dynamics*, 18, 389–396.
- Zhu, H.X., Mills, N.J., (2000), "The in-plane non-linear compression of regular honeycombs", *International Journal of Solid and Structures*, 37, 1931–1949.
- Zenkert, D., (1995), "An Introduction to sandwich construction", Engineering Materials Advisory Services (EMAS).

APPENDICES

APPENDIX A: CLASSICAL LAMINATION THEORY

A.1 Introduction

One of the main engineering advantages of composite materials is that designers can obtain the desired properties of materials in selected directions. The properties can be altered by the appropriate choice of fiber and matrix in the individual plies. However the greatest flexibility is obtained by arranging the various plies in various orientations during composite manufacturing process to obtain the overall thermomechanical properties. For example, in a unidirectional composite, the longitudinal strength (or stiffness) to the transverse strength (or stiffness) can be altered by changing the volume properties, the transverse properties are matrix dominated. A laminate is formed from two or more laminae (plies) bonded together to act as an integral structural element. However, as laminates are combinations of laminae that are oriented with respect to each other their design becomes critical in obtaining the final property of the composite.

A.2 Basic Assumptions

Classical lamination theory (CLT) embodies a collection of stress and deformation hypothesis. The basic assumptions are:

1. Each lamina is orthotropic and homogeneous.
2. Individual lamina properties (stiffness, compliance) specific to the angle of the ply with respect to loading axis are maintained.
3. Displacements are continuous across the laminae; however, the stress and strain need not be continuous.
4. Laminates are perfectly bonded, they are infinitely thin and not shear deformable. Thus at the interface (normal to z-direction) $\nu_{yz} = \nu_{xz} = \nu_{yz} = \nu_{xz} = 0$. Thus all the interlaminar shear stresses are zero.

5. Each lamina is elastic and no slip occurs between the lamina interfaces.

A.3 Strain and Stress in a Laminate

The stress-strain relation in principal material coordinates (1-2 axis, as shown in Fig. NO TAG) for a lamina of an orthotropic material under plane stress is expressed as,

$$\begin{Bmatrix} \sigma_1 \\ \sigma_2 \\ \tau_{12} \end{Bmatrix} = \begin{bmatrix} Q_{11} & Q_{12} & 0 \\ Q_{12} & Q_{22} & 0 \\ 0 & 0 & Q_{66} \end{bmatrix} \begin{Bmatrix} \epsilon_1 \\ \epsilon_2 \\ \gamma_{12} \end{Bmatrix} \quad (3)$$

where, Q_{ij} are reduced stiffnesses for a plane stress state.

$$\begin{aligned} Q_{11} &= \frac{E_1}{1 - \nu_{12}\nu_{21}} & Q_{22} &= \frac{E_2}{1 - \nu_{12}\nu_{21}} \\ Q_{12} &= \frac{\nu_{12}E_2}{1 - \nu_{12}\nu_{21}} = \frac{\nu_{21}E_1}{1 - \nu_{12}\nu_{21}} & Q_{66} &= G_{12} \end{aligned} \quad (4)$$

Alternatively,

$$\begin{Bmatrix} \epsilon_1 \\ \epsilon_2 \\ \gamma_{12} \end{Bmatrix} = \begin{bmatrix} S_{11} & S_{12} & 0 \\ S_{12} & S_{22} & 0 \\ 0 & 0 & S_{66} \end{bmatrix} \begin{Bmatrix} \sigma_1 \\ \sigma_2 \\ \tau_{12} \end{Bmatrix} \quad (5)$$

where S_{ij} are reduced compliances for a plane stress state.

$$\begin{aligned} S_{11} &= \frac{1}{E_1} & S_{22} &= \frac{1}{E_2} \\ S_{12} &= -\frac{\nu_{12}}{E_1} = -\frac{\nu_{21}}{E_2} & S_{66} &= \frac{1}{G_{12}} \end{aligned} \quad (6)$$

In any other coordinate system in the plane of the lamina, the stresses are

$$\begin{Bmatrix} \sigma_x \\ \sigma_y \\ \tau_{xy} \end{Bmatrix} = [T] \begin{Bmatrix} \sigma_1 \\ \sigma_2 \\ \tau_{12} \end{Bmatrix} \quad (7)$$

where $[T]$ is a transformed matrix that transforms stresses in the material principal axes to those in global (x-y) coordinates, and it is defined as follow:

$$[T] = \begin{bmatrix} \cos^2 \theta & \sin^2 \theta & -2 \sin \theta \cos \theta \\ \sin^2 \theta & \cos^2 \theta & 2 \sin \theta \cos \theta \\ \sin \theta \cos \theta & -\sin \theta \cos \theta & \cos^2 \theta - \sin^2 \theta \end{bmatrix} \quad (8)$$

where, θ is the angle from the global coordinate (x-axis) to the material principal coordinate (1-axis).

Finally, the stress-strain relations in the global coordinate (x-y axis) is expressed as follow:

$$\begin{Bmatrix} \sigma_x \\ \sigma_y \\ \tau_{xy} \end{Bmatrix} = \begin{bmatrix} \bar{Q}_{11} & \bar{Q}_{12} & \bar{Q}_{16} \\ \bar{Q}_{12} & \bar{Q}_{22} & \bar{Q}_{26} \\ \bar{Q}_{16} & \bar{Q}_{26} & \bar{Q}_{66} \end{bmatrix} \begin{Bmatrix} \epsilon_x \\ \epsilon_y \\ \gamma_{xy} \end{Bmatrix} \quad (9)$$

where the transformed reduced stiffnesses in terms of the reduced stiffnesses are

$$\begin{aligned} \bar{Q}_{11} &= Q_{11} \cos^4 \theta + 2(Q_{12} + 2Q_{66}) \sin^2 \theta \cos^2 \theta + Q_{22} \sin^4 \theta \\ \bar{Q}_{12} &= (Q_{11} + Q_{22} - 4Q_{66}) \sin^2 \theta \cos^2 \theta + Q_{12} (\sin^4 \theta + \cos^4 \theta) \\ \bar{Q}_{22} &= Q_{11} \sin^4 \theta + 2(Q_{12} + 2Q_{66}) \sin^2 \theta \cos^2 \theta + Q_{22} \cos^4 \theta \\ \bar{Q}_{16} &= (Q_{11} - Q_{12} - 2Q_{66}) \sin \theta \cos^3 \theta + (Q_{12} - Q_{22} + 2Q_{66}) \sin^3 \theta \cos \theta \\ \bar{Q}_{26} &= (Q_{11} - Q_{12} - 2Q_{66}) \sin^3 \theta \cos \theta + (Q_{12} - Q_{22} + 2Q_{66}) \sin \theta \cos^3 \theta \\ \bar{Q}_{66} &= (Q_{11} + Q_{22} - 2Q_{12} - 2Q_{66}) \sin^2 \theta \cos^2 \theta + Q_{66} (\sin^4 \theta + \cos^4 \theta) \end{aligned} \quad (10)$$

Both Equations (9) and (10) can be considered as stress-strain relations for the k^{th} layer of a multilayered laminate. Accordingly, the stress-strain relations can be rewritten as

$$\{\sigma\}_k = [\bar{Q}]_k \{\epsilon\}_k \quad (11)$$

The total variation of stresses and strains in the laminates will be the net effects of the above equation.

A.4 Stress and Strain Variation in a Laminate

The variation of stress and strain through the laminate thickness is essential to the definition of the extensional and bending stiffness of a laminate. From the definition of CLT, displacements are continuous across laminae boundaries. Each lamina exhibits individual properties based on its orientation.

If the laminate is thin, then Kirchhoff hypothesis is assumed whereby a line originally straight and perpendicular to the middle surface of the laminate is assumed to remain straight and perpendic-

ular to the middle surface when the laminate is extended or bent. This requirement is equivalent to ignoring shear strain in plane perpendicular to the middle surface, that is $\nu_{xz} = \nu_{yz} = 0$ where z is the direction of the normal of the surface. Also, the normals are presumed to have constant length so that ϵ_z is assumed to have zero.

Consider the Kirchhoff hypothesis and a side view of a plate in the Cartesian x - y - z coordinate system as shown in Fig. A.1, assume u_0, v_0 and w_0 to be displacements in the x -, y - and z -directions at mid-plane and u, v and w are the displacements at any points in the x -, y -, z -directions, respectively. At any point other than the midplane, the two displacements in the x - y plane will depend on the axial location of the point and the slope of the laminate midplane with the x - and y -direction.

$$u = u_0 - z\alpha \quad \text{where, } \alpha = \frac{\partial w_0}{\partial x} \quad (12)$$

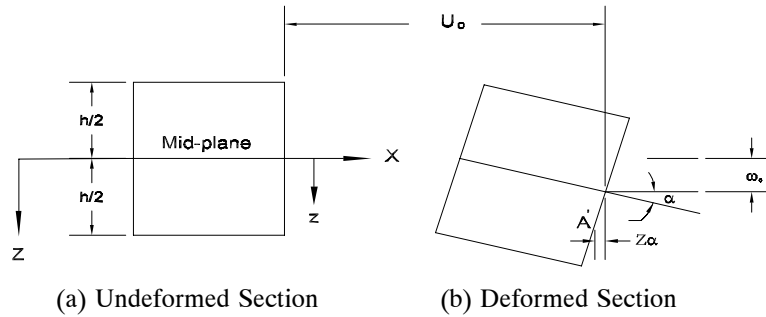


Figure A.1: Bending of Line Element in x - z Plane

The displacement u and v in the x - y direction are,

$$u = u_0 - z \frac{\partial w_0}{\partial x} \quad (13)$$

$$v = v_0 - z \frac{\partial w_0}{\partial y} \quad (14)$$

The middle surface of the laminate is usually considered as the reference surface. By using these displacement expressions, the strains in the laminate can be obtained as

$$\epsilon_x = \frac{\partial u}{\partial x} = \frac{\partial u_0}{\partial x} - z \frac{\partial^2 w_0}{\partial x^2} \quad (15)$$

$$\epsilon_y = \frac{\partial v}{\partial y} = \frac{\partial v_0}{\partial y} - z \frac{\partial^2 w_0}{\partial y^2} \quad (16)$$

$$\gamma_{xy} = \frac{\partial u}{\partial x} + \frac{\partial v}{\partial y} = \frac{\partial u_0}{\partial y} + \frac{\partial v_0}{\partial x} - 2z \frac{\partial w_0^2}{\partial x \partial y} \quad (17)$$

For the reference surface strains and curvatures as

$$\begin{Bmatrix} \epsilon_x \\ \epsilon_y \\ \gamma_{xy} \end{Bmatrix} = \begin{Bmatrix} \frac{\partial u_0}{\partial x} \\ \frac{\partial v_0}{\partial y} \\ \frac{\partial u_0}{\partial y} + \frac{\partial v_0}{\partial x} \end{Bmatrix} - z \begin{Bmatrix} -\frac{\partial^2 w_0}{\partial x^2} \\ -\frac{\partial^2 w_0}{\partial y^2} \\ -2 \frac{\partial^2 w_0}{\partial x \partial y} \end{Bmatrix} \quad (18)$$

Respectively, the laminate strains can be written as

$$\begin{Bmatrix} \epsilon_x \\ \epsilon_y \\ \gamma_{xy} \end{Bmatrix} = \begin{Bmatrix} \epsilon_x^0 \\ \epsilon_y^0 \\ \gamma_{xy}^0 \end{Bmatrix} + z \begin{Bmatrix} \kappa_x \\ \kappa_y \\ \kappa_{xy} \end{Bmatrix} \quad (19)$$

The term κ_{xy} is the twist curvature of the middle surface. The above analysis is valid only for plates. For shells, the ϵ_y term should be supplemented by a term $\frac{\omega_0}{r}$ where r is the radius of a circular shell. More complicated terms are needed to be added for other types of shells.

With the strain variation, the stress in the k^{th} layer can be obtained in terms of the reference surface strains and curvatures as

$$\begin{Bmatrix} \sigma_x \\ \sigma_y \\ \tau_{xy} \end{Bmatrix}_k = \begin{Bmatrix} \bar{Q}_{11} & \bar{Q}_{12} & \bar{Q}_{16} \\ \bar{Q}_{12} & \bar{Q}_{22} & \bar{Q}_{26} \\ \bar{Q}_{16} & \bar{Q}_{26} & \bar{Q}_{66} \end{Bmatrix} \begin{Bmatrix} \epsilon_x^0 \\ \epsilon_y^0 \\ \gamma_{xy}^0 \end{Bmatrix} + z \begin{Bmatrix} \bar{Q}_{11} & \bar{Q}_{12} & \bar{Q}_{16} \\ \bar{Q}_{12} & \bar{Q}_{22} & \bar{Q}_{26} \\ \bar{Q}_{16} & \bar{Q}_{26} & \bar{Q}_{66} \end{Bmatrix} \begin{Bmatrix} \kappa_x \\ \kappa_y \\ \kappa_{xy} \end{Bmatrix} \quad (20)$$

Since \bar{Q}_{ij} can be different for each layer of the laminate, the stress variation through the laminate thickness is not necessary linear, though the strain variation is linear.

A.5 Force and Moment Resultants in a Laminate

Force and moment resultants acting on a laminate can be obtained by integrating the stresses through the entire thickness of the laminate. Numerical approach assumes that a laminate arranged with the principal directions of each layer in different orientations. The various layers are assumed

to be rigidly bonded together. The section force and moment resultants per unit length in the normal basis directions in a given layer can be defined on this basis as

$$(N_x, N_y, N_{xy}) = \int_{-\frac{h}{2}}^{\frac{h}{2}} (\sigma_x, \sigma_y, \tau_{xy}) dz \quad (21)$$

$$(M_1, M_2, M_{12}) = \int_{-\frac{h}{2}}^{\frac{h}{2}} (\sigma_1, \sigma_2, \tau_{12}) z dz \quad (22)$$

where h is the thickness of the laminate. This leads to the relations

$$\begin{Bmatrix} N_1 \\ N_2 \\ N_{12} \\ M_1 \\ M_2 \\ M_{12} \\ V_1 \\ V_2 \end{Bmatrix} = \begin{bmatrix} A_{11} & A_{12} & A_{13} & B_{11} & B_{12} & B_{13} & 0 & 0 \\ A_{12} & A_{22} & A_{23} & B_{12} & B_{22} & B_{23} & 0 & 0 \\ A_{13} & A_{23} & A_{33} & B_{13} & B_{23} & B_{33} & 0 & 0 \\ B_{11} & B_{12} & B_{13} & D_{11} & D_{12} & D_{13} & 0 & 0 \\ B_{12} & B_{22} & B_{23} & D_{12} & D_{22} & D_{23} & 0 & 0 \\ B_{13} & B_{23} & B_{33} & D_{13} & D_{23} & D_{33} & 0 & 0 \\ 0 & 0 & 0 & 0 & 0 & 0 & E_{11} & E_{12} \\ 0 & 0 & 0 & 0 & 0 & 0 & E_{12} & E_{22} \end{bmatrix} \begin{Bmatrix} \epsilon_1 \\ \epsilon_2 \\ \gamma_{12} \\ \kappa_1 \\ \kappa_2 \\ \kappa_{12} \\ \gamma_{13} \\ \gamma_{23} \end{Bmatrix} \quad (23)$$

where A_{ij} , B_{ij} , and D_{ij} are extensional stiffnesses, bending-extension coupling stiffnesses, and bending stiffnesses, respectively. the components of this section stiffness matrix are given by

$$(A_{ij}, B_{ij}, D_{ij}) = \int_{-\frac{h}{2}}^{\frac{h}{2}} \bar{Q}_{ij}^m (1, Z, Z^2) dZ, \quad (i, j = 1, 2, 3) \quad (24)$$

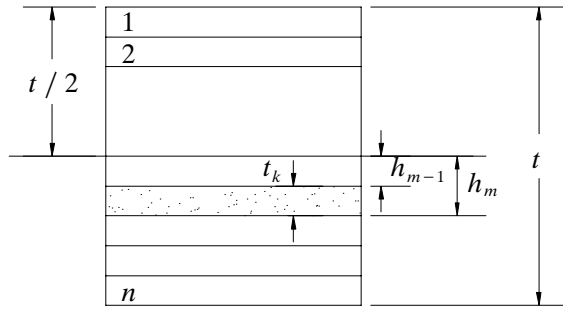
Here m indicates a particular layer. Thus, the \bar{Q}_{ij}^m depend on the material properties and fiber orientation of the m th layer. If there are n layers in the layup, the above equation can be rewritten as a summation of integrals over the n laminae. The material coefficients will then take the form

$$A_{ij} = \sum_{m=1}^n \bar{Q}_{ij}^m (h_m - h_{m-1}) \quad (25)$$

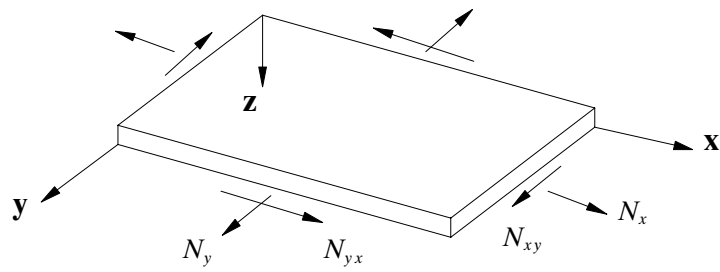
$$B_{ij} = \frac{1}{2} \sum_{m=1}^n \bar{Q}_{ij}^m (h_m^2 - h_{m-1}^2) \quad (26)$$

$$D_{ij} = \frac{1}{3} \sum_{m=1}^n \bar{Q}_{ij}^m (h_m^3 - h_{m-1}^3) \quad (27)$$

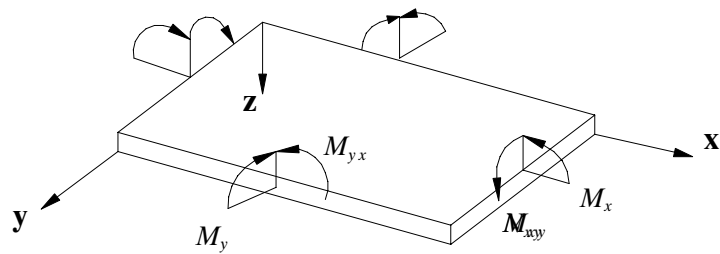
where the h_m and h_{m-1} in above equations indicate that the m th lamina is bounded by surface $z = h_m$ and $z = h_{m-1}$. The geometry and resultant force directions of the laminate are shown in Fig. A.2.



(a) Geometry of N-layered Laminate



(b) Force of a Laminate



(c) Moment of a Laminate

Figure A.2: Geometry and Resultant Forces of a Laminate

A.6 Determination of Laminate Stresses and Strains

Relation between the applied loads and the midplane strains and plate curvatures are provided by Eq. (23). These equations can be solved for the unknowns. The strains and curvatures are derived as explicit functions of applied loads. The general constitutive equations for a laminate are

$$\begin{Bmatrix} N \\ M \end{Bmatrix} = \begin{Bmatrix} A & B \\ B & D \end{Bmatrix} \begin{Bmatrix} \epsilon_0 \\ \kappa \end{Bmatrix} \quad (28)$$

Considering the equation for N and M,

$$\begin{aligned} \{N\} &= [A]\{\epsilon^0\} + [B]\{\kappa\} \\ \{M\} &= [B]\{\epsilon^0\} + [D]\{\kappa\} \end{aligned} \quad (29)$$

Solving the first term of Eq. (29) for midplane strains gives,

$$\{\epsilon_0\} = [A^{-1}]\{N\} - [A^{-1}][B]\{\kappa\} \quad (30)$$

Substituting Eq. (30) in Eq. (29)

$$\{M\} = [B][A^{-1}]\{N\} - [B][A^{-1}][B] - [D]\{\kappa\} \quad (31)$$

A partially inverted form of the laminate constitutive equation as follow

$$\begin{Bmatrix} \epsilon_0 \\ M \end{Bmatrix} = \begin{Bmatrix} A^* & B^* \\ C^* & D^* \end{Bmatrix} \begin{Bmatrix} N \\ \kappa \end{Bmatrix} \quad (32)$$

where

$$\begin{aligned} [A^*] &= [A^{-1}] \\ [B^*] &= -[A^{-1}][B] \\ [C^*] &= [B][A^{-1}] = -[B]^T \\ [D^*] &= [D] - [B][A^{-1}][B] \end{aligned} \quad (33)$$

Eq. (30) and (31) can be rewritten as

$$\begin{aligned}\{\epsilon_0\} &= [A^*]\{\epsilon^0\} + [B^*]\{\kappa\} \\ \{M\} &= [C^*]\{\epsilon^0\} + [D^*]\{\kappa\}\end{aligned}\quad (34)$$

Solving the second of Eq. (34) for plate curvatures gives

$$\{\kappa\} = [D^{*-1}]\{M\} - [D^{*-1}][C^*]\{N\}\quad (35)$$

Substituting Eq. (35) in the first relationship in Eq. (34) yields

$$\{\epsilon^0\} = \left[[A^*] - [B^*][D^{*-1}][C^*] \right] \{N\} - [B^*][D^{*-1}]\{M\}\quad (36)$$

Eq. (35) and (36) can be combined to obtain a fully inverted form of the laminated constitutive equations as follows:

$$\begin{Bmatrix} \epsilon_0 \\ M \end{Bmatrix} = \begin{Bmatrix} A' & B' \\ C' & D' \end{Bmatrix} \begin{Bmatrix} N \\ \kappa \end{Bmatrix} = \begin{Bmatrix} A' & B' \\ B' & D' \end{Bmatrix} \begin{Bmatrix} N \\ \kappa \end{Bmatrix}\quad (37)$$

where

$$\begin{aligned}[A'] &= [A^*] - [B^*][D^{*-1}][C^*] = [A^*] + [B^*][D^{*-1}][B^*]^T \\ [B'] &= [B^*][D^{*-1}] \\ [C'] &= -[D^{*-1}][C^*] = [B']^T = [B'] \\ [D'] &= [D^{*-1}]\end{aligned}\quad (38)$$

Multidisciplinary Center for Earthquake Engineering Research List of Technical Reports

The Multidisciplinary Center for Earthquake Engineering Research (MCEER) publishes technical reports on a variety of subjects related to earthquake engineering written by authors funded through MCEER. These reports are available from both MCEER Publications and the National Technical Information Service (NTIS). Requests for reports should be directed to MCEER Publications, Multidisciplinary Center for Earthquake Engineering Research, State University of New York at Buffalo, Red Jacket Quadrangle, Buffalo, New York 14261. Reports can also be requested through NTIS, 5285 Port Royal Road, Springfield, Virginia 22161. NTIS accession numbers are shown in parenthesis, if available.

- NCEER-87-0001 "First-Year Program in Research, Education and Technology Transfer," 3/5/87, (PB88-134275, A04, MF-A01).
- NCEER-87-0002 "Experimental Evaluation of Instantaneous Optimal Algorithms for Structural Control," by R.C. Lin, T.T. Soong and A.M. Reinhorn, 4/20/87, (PB88-134341, A04, MF-A01).
- NCEER-87-0003 "Experimentation Using the Earthquake Simulation Facilities at University at Buffalo," by A.M. Reinhorn and R.L. Ketter, to be published.
- NCEER-87-0004 "The System Characteristics and Performance of a Shaking Table," by J.S. Hwang, K.C. Chang and G.C. Lee, 6/1/87, (PB88-134259, A03, MF-A01). This report is available only through NTIS (see address given above).
- NCEER-87-0005 "A Finite Element Formulation for Nonlinear Viscoplastic Material Using a Q Model," by O. Gyebi and G. Dasgupta, 11/2/87, (PB88-213764, A08, MF-A01).
- NCEER-87-0006 "Symbolic Manipulation Program (SMP) - Algebraic Codes for Two and Three Dimensional Finite Element Formulations," by X. Lee and G. Dasgupta, 11/9/87, (PB88-218522, A05, MF-A01).
- NCEER-87-0007 "Instantaneous Optimal Control Laws for Tall Buildings Under Seismic Excitations," by J.N. Yang, A. Akbarpour and P. Ghaemmaghami, 6/10/87, (PB88-134333, A06, MF-A01). This report is only available through NTIS (see address given above).
- NCEER-87-0008 "IDARC: Inelastic Damage Analysis of Reinforced Concrete Frame - Shear-Wall Structures," by Y.J. Park, A.M. Reinhorn and S.K. Kunnath, 7/20/87, (PB88-134325, A09, MF-A01). This report is only available through NTIS (see address given above).
- NCEER-87-0009 "Liquefaction Potential for New York State: A Preliminary Report on Sites in Manhattan and Buffalo," by M. Budhu, V. Vijayakumar, R.F. Giese and L. Baumgras, 8/31/87, (PB88-163704, A03, MF-A01). This report is available only through NTIS (see address given above).
- NCEER-87-0010 "Vertical and Torsional Vibration of Foundations in Inhomogeneous Media," by A.S. Veletsos and K.W. Dotson, 6/1/87, (PB88-134291, A03, MF-A01). This report is only available through NTIS (see address given above).
- NCEER-87-0011 "Seismic Probabilistic Risk Assessment and Seismic Margins Studies for Nuclear Power Plants," by Howard H.M. Hwang, 6/15/87, (PB88-134267, A03, MF-A01). This report is only available through NTIS (see address given above).
- NCEER-87-0012 "Parametric Studies of Frequency Response of Secondary Systems Under Ground-Acceleration Excitations," by Y. Yong and Y.K. Lin, 6/10/87, (PB88-134309, A03, MF-A01). This report is only available through NTIS (see address given above).
- NCEER-87-0013 "Frequency Response of Secondary Systems Under Seismic Excitation," by J.A. HoLung, J. Cai and Y.K. Lin, 7/31/87, (PB88-134317, A05, MF-A01). This report is only available through NTIS (see address given above).
- NCEER-87-0014 "Modelling Earthquake Ground Motions in Seismically Active Regions Using Parametric Time Series Methods," by G.W. Ellis and A.S. Cakmak, 8/25/87, (PB88-134283, A08, MF-A01). This report is only available through NTIS (see address given above).

- NCEER-87-0015 "Detection and Assessment of Seismic Structural Damage," by E. DiPasquale and A.S. Cakmak, 8/25/87, (PB88-163712, A05, MF-A01). This report is only available through NTIS (see address given above).
- NCEER-87-0016 "Pipeline Experiment at Parkfield, California," by J. Isenberg and E. Richardson, 9/15/87, (PB88-163720, A03, MF-A01). This report is available only through NTIS (see address given above).
- NCEER-87-0017 "Digital Simulation of Seismic Ground Motion," by M. Shinozuka, G. Deodatis and T. Harada, 8/31/87, (PB88-155197, A04, MF-A01). This report is available only through NTIS (see address given above).
- NCEER-87-0018 "Practical Considerations for Structural Control: System Uncertainty, System Time Delay and Truncation of Small Control Forces," J.N. Yang and A. Akbarpour, 8/10/87, (PB88-163738, A08, MF-A01). This report is only available through NTIS (see address given above).
- NCEER-87-0019 "Modal Analysis of Nonclassically Damped Structural Systems Using Canonical Transformation," by J.N. Yang, S. Sarkani and F.X. Long, 9/27/87, (PB88-187851, A04, MF-A01).
- NCEER-87-0020 "A Nonstationary Solution in Random Vibration Theory," by J.R. Red-Horse and P.D. Spanos, 11/3/87, (PB88-163746, A03, MF-A01).
- NCEER-87-0021 "Horizontal Impedances for Radially Inhomogeneous Viscoelastic Soil Layers," by A.S. Veletsos and K.W. Dotson, 10/15/87, (PB88-150859, A04, MF-A01).
- NCEER-87-0022 "Seismic Damage Assessment of Reinforced Concrete Members," by Y.S. Chung, C. Meyer and M. Shinozuka, 10/9/87, (PB88-150867, A05, MF-A01). This report is available only through NTIS (see address given above).
- NCEER-87-0023 "Active Structural Control in Civil Engineering," by T.T. Soong, 11/11/87, (PB88-187778, A03, MF-A01).
- NCEER-87-0024 "Vertical and Torsional Impedances for Radially Inhomogeneous Viscoelastic Soil Layers," by K.W. Dotson and A.S. Veletsos, 12/87, (PB88-187786, A03, MF-A01).
- NCEER-87-0025 "Proceedings from the Symposium on Seismic Hazards, Ground Motions, Soil-Liquefaction and Engineering Practice in Eastern North America," October 20-22, 1987, edited by K.H. Jacob, 12/87, (PB88-188115, A23, MF-A01). This report is available only through NTIS (see address given above).
- NCEER-87-0026 "Report on the Whittier-Narrows, California, Earthquake of October 1, 1987," by J. Pantelic and A. Reinhorn, 11/87, (PB88-187752, A03, MF-A01). This report is available only through NTIS (see address given above).
- NCEER-87-0027 "Design of a Modular Program for Transient Nonlinear Analysis of Large 3-D Building Structures," by S. Srivastav and J.F. Abel, 12/30/87, (PB88-187950, A05, MF-A01). This report is only available through NTIS (see address given above).
- NCEER-87-0028 "Second-Year Program in Research, Education and Technology Transfer," 3/8/88, (PB88-219480, A04, MF-A01).
- NCEER-88-0001 "Workshop on Seismic Computer Analysis and Design of Buildings With Interactive Graphics," by W. McGuire, J.F. Abel and C.H. Conley, 1/18/88, (PB88-187760, A03, MF-A01). This report is only available through NTIS (see address given above).
- NCEER-88-0002 "Optimal Control of Nonlinear Flexible Structures," by J.N. Yang, F.X. Long and D. Wong, 1/22/88, (PB88-213772, A06, MF-A01).
- NCEER-88-0003 "Substructuring Techniques in the Time Domain for Primary-Secondary Structural Systems," by G.D. Manolis and G. Juhn, 2/10/88, (PB88-213780, A04, MF-A01).
- NCEER-88-0004 "Iterative Seismic Analysis of Primary-Secondary Systems," by A. Singhal, L.D. Lutes and P.D. Spanos, 2/23/88, (PB88-213798, A04, MF-A01).

- NCEER-88-0005 "Stochastic Finite Element Expansion for Random Media," by P.D. Spanos and R. Ghanem, 3/14/88, (PB88-213806, A03, MF-A01).
- NCEER-88-0006 "Combining Structural Optimization and Structural Control," by F.Y. Cheng and C.P. Pantelides, 1/10/88, (PB88-213814, A05, MF-A01).
- NCEER-88-0007 "Seismic Performance Assessment of Code-Designed Structures," by H.H-M. Hwang, J-W. Jaw and H-J. Shau, 3/20/88, (PB88-219423, A04, MF-A01). This report is only available through NTIS (see address given above).
- NCEER-88-0008 "Reliability Analysis of Code-Designed Structures Under Natural Hazards," by H.H-M. Hwang, H. Ushiba and M. Shinozuka, 2/29/88, (PB88-229471, A07, MF-A01). This report is only available through NTIS (see address given above).
- NCEER-88-0009 "Seismic Fragility Analysis of Shear Wall Structures," by J-W Jaw and H.H-M. Hwang, 4/30/88, (PB89-102867, A04, MF-A01).
- NCEER-88-0010 "Base Isolation of a Multi-Story Building Under a Harmonic Ground Motion - A Comparison of Performances of Various Systems," by F-G Fan, G. Ahmadi and I.G. Tadjbakhsh, 5/18/88, (PB89-122238, A06, MF-A01). This report is only available through NTIS (see address given above).
- NCEER-88-0011 "Seismic Floor Response Spectra for a Combined System by Green's Functions," by F.M. Lavelle, L.A. Bergman and P.D. Spanos, 5/1/88, (PB89-102875, A03, MF-A01).
- NCEER-88-0012 "A New Solution Technique for Randomly Excited Hysteretic Structures," by G.Q. Cai and Y.K. Lin, 5/16/88, (PB89-102883, A03, MF-A01).
- NCEER-88-0013 "A Study of Radiation Damping and Soil-Structure Interaction Effects in the Centrifuge," by K. Weissman, supervised by J.H. Prevost, 5/24/88, (PB89-144703, A06, MF-A01).
- NCEER-88-0014 "Parameter Identification and Implementation of a Kinematic Plasticity Model for Frictional Soils," by J.H. Prevost and D.V. Griffiths, to be published.
- NCEER-88-0015 "Two- and Three- Dimensional Dynamic Finite Element Analyses of the Long Valley Dam," by D.V. Griffiths and J.H. Prevost, 6/17/88, (PB89-144711, A04, MF-A01).
- NCEER-88-0016 "Damage Assessment of Reinforced Concrete Structures in Eastern United States," by A.M. Reinhorn, M.J. Seidel, S.K. Kunnath and Y.J. Park, 6/15/88, (PB89-122220, A04, MF-A01). This report is only available through NTIS (see address given above).
- NCEER-88-0017 "Dynamic Compliance of Vertically Loaded Strip Foundations in Multilayered Viscoelastic Soils," by S. Ahmad and A.S.M. Israil, 6/17/88, (PB89-102891, A04, MF-A01).
- NCEER-88-0018 "An Experimental Study of Seismic Structural Response With Added Viscoelastic Dampers," by R.C. Lin, Z. Liang, T.T. Soong and R.H. Zhang, 6/30/88, (PB89-122212, A05, MF-A01). This report is available only through NTIS (see address given above).
- NCEER-88-0019 "Experimental Investigation of Primary - Secondary System Interaction," by G.D. Manolis, G. Juhn and A.M. Reinhorn, 5/27/88, (PB89-122204, A04, MF-A01).
- NCEER-88-0020 "A Response Spectrum Approach For Analysis of Nonclassically Damped Structures," by J.N. Yang, S. Sarkani and F.X. Long, 4/22/88, (PB89-102909, A04, MF-A01).
- NCEER-88-0021 "Seismic Interaction of Structures and Soils: Stochastic Approach," by A.S. Veletsos and A.M. Prasad, 7/21/88, (PB89-122196, A04, MF-A01). This report is only available through NTIS (see address given above).
- NCEER-88-0022 "Identification of the Serviceability Limit State and Detection of Seismic Structural Damage," by E. DiPasquale and A.S. Cakmak, 6/15/88, (PB89-122188, A05, MF-A01). This report is available only through NTIS (see address given above).

- NCEER-88-0023 "Multi-Hazard Risk Analysis: Case of a Simple Offshore Structure," by B.K. Bhartia and E.H. Vanmarcke, 7/21/88, (PB89-145213, A05, MF-A01).
- NCEER-88-0024 "Automated Seismic Design of Reinforced Concrete Buildings," by Y.S. Chung, C. Meyer and M. Shinozuka, 7/5/88, (PB89-122170, A06, MF-A01). This report is available only through NTIS (see address given above).
- NCEER-88-0025 "Experimental Study of Active Control of MDOF Structures Under Seismic Excitations," by L.L. Chung, R.C. Lin, T.T. Soong and A.M. Reinhorn, 7/10/88, (PB89-122600, A04, MF-A01).
- NCEER-88-0026 "Earthquake Simulation Tests of a Low-Rise Metal Structure," by J.S. Hwang, K.C. Chang, G.C. Lee and R.L. Ketter, 8/1/88, (PB89-102917, A04, MF-A01).
- NCEER-88-0027 "Systems Study of Urban Response and Reconstruction Due to Catastrophic Earthquakes," by F. Kozin and H.K. Zhou, 9/22/88, (PB90-162348, A04, MF-A01).
- NCEER-88-0028 "Seismic Fragility Analysis of Plane Frame Structures," by H.H-M. Hwang and Y.K. Low, 7/31/88, (PB89-131445, A06, MF-A01).
- NCEER-88-0029 "Response Analysis of Stochastic Structures," by A. Kardara, C. Bucher and M. Shinozuka, 9/22/88, (PB89-174429, A04, MF-A01).
- NCEER-88-0030 "Nonnormal Accelerations Due to Yielding in a Primary Structure," by D.C.K. Chen and L.D. Lutes, 9/19/88, (PB89-131437, A04, MF-A01).
- NCEER-88-0031 "Design Approaches for Soil-Structure Interaction," by A.S. Veletsos, A.M. Prasad and Y. Tang, 12/30/88, (PB89-174437, A03, MF-A01). This report is available only through NTIS (see address given above).
- NCEER-88-0032 "A Re-evaluation of Design Spectra for Seismic Damage Control," by C.J. Turkstra and A.G. Tallin, 11/7/88, (PB89-145221, A05, MF-A01).
- NCEER-88-0033 "The Behavior and Design of Noncontact Lap Splices Subjected to Repeated Inelastic Tensile Loading," by V.E. Sagan, P. Gergely and R.N. White, 12/8/88, (PB89-163737, A08, MF-A01).
- NCEER-88-0034 "Seismic Response of Pile Foundations," by S.M. Mamoon, P.K. Banerjee and S. Ahmad, 11/1/88, (PB89-145239, A04, MF-A01).
- NCEER-88-0035 "Modeling of R/C Building Structures With Flexible Floor Diaphragms (IDARC2)," by A.M. Reinhorn, S.K. Kunnath and N. Panahshahi, 9/7/88, (PB89-207153, A07, MF-A01).
- NCEER-88-0036 "Solution of the Dam-Reservoir Interaction Problem Using a Combination of FEM, BEM with Particular Integrals, Modal Analysis, and Substructuring," by C-S. Tsai, G.C. Lee and R.L. Ketter, 12/31/88, (PB89-207146, A04, MF-A01).
- NCEER-88-0037 "Optimal Placement of Actuators for Structural Control," by F.Y. Cheng and C.P. Pantelides, 8/15/88, (PB89-162846, A05, MF-A01).
- NCEER-88-0038 "Teflon Bearings in Aseismic Base Isolation: Experimental Studies and Mathematical Modeling," by A. Mokha, M.C. Constantinou and A.M. Reinhorn, 12/5/88, (PB89-218457, A10, MF-A01). This report is available only through NTIS (see address given above).
- NCEER-88-0039 "Seismic Behavior of Flat Slab High-Rise Buildings in the New York City Area," by P. Weidlinger and M. Ettouney, 10/15/88, (PB90-145681, A04, MF-A01).
- NCEER-88-0040 "Evaluation of the Earthquake Resistance of Existing Buildings in New York City," by P. Weidlinger and M. Ettouney, 10/15/88, to be published.
- NCEER-88-0041 "Small-Scale Modeling Techniques for Reinforced Concrete Structures Subjected to Seismic Loads," by W. Kim, A. El-Attar and R.N. White, 11/22/88, (PB89-189625, A05, MF-A01).

- NCEER-88-0042 "Modeling Strong Ground Motion from Multiple Event Earthquakes," by G.W. Ellis and A.S. Cakmak, 10/15/88, (PB89-174445, A03, MF-A01).
- NCEER-88-0043 "Nonstationary Models of Seismic Ground Acceleration," by M. Grigoriu, S.E. Ruiz and E. Rosenblueth, 7/15/88, (PB89-189617, A04, MF-A01).
- NCEER-88-0044 "SARCF User's Guide: Seismic Analysis of Reinforced Concrete Frames," by Y.S. Chung, C. Meyer and M. Shinozuka, 11/9/88, (PB89-174452, A08, MF-A01).
- NCEER-88-0045 "First Expert Panel Meeting on Disaster Research and Planning," edited by J. Pantelic and J. Stoyke, 9/15/88, (PB89-174460, A05, MF-A01).
- NCEER-88-0046 "Preliminary Studies of the Effect of Degrading Infill Walls on the Nonlinear Seismic Response of Steel Frames," by C.Z. Chrysostomou, P. Gergely and J.F. Abel, 12/19/88, (PB89-208383, A05, MF-A01).
- NCEER-88-0047 "Reinforced Concrete Frame Component Testing Facility - Design, Construction, Instrumentation and Operation," by S.P. Pessiki, C. Conley, T. Bond, P. Gergely and R.N. White, 12/16/88, (PB89-174478, A04, MF-A01).
- NCEER-89-0001 "Effects of Protective Cushion and Soil Compliancy on the Response of Equipment Within a Seismically Excited Building," by J.A. HoLung, 2/16/89, (PB89-207179, A04, MF-A01).
- NCEER-89-0002 "Statistical Evaluation of Response Modification Factors for Reinforced Concrete Structures," by H.H-M. Hwang and J-W. Jaw, 2/17/89, (PB89-207187, A05, MF-A01).
- NCEER-89-0003 "Hysteretic Columns Under Random Excitation," by G-Q. Cai and Y.K. Lin, 1/9/89, (PB89-196513, A03, MF-A01).
- NCEER-89-0004 "Experimental Study of 'Elephant Foot Bulge' Instability of Thin-Walled Metal Tanks," by Z-H. Jia and R.L. Ketter, 2/22/89, (PB89-207195, A03, MF-A01).
- NCEER-89-0005 "Experiment on Performance of Buried Pipelines Across San Andreas Fault," by J. Isenberg, E. Richardson and T.D. O'Rourke, 3/10/89, (PB89-218440, A04, MF-A01). This report is available only through NTIS (see address given above).
- NCEER-89-0006 "A Knowledge-Based Approach to Structural Design of Earthquake-Resistant Buildings," by M. Subramani, P. Gergely, C.H. Conley, J.F. Abel and A.H. Zaghaw, 1/15/89, (PB89-218465, A06, MF-A01).
- NCEER-89-0007 "Liquefaction Hazards and Their Effects on Buried Pipelines," by T.D. O'Rourke and P.A. Lane, 2/1/89, (PB89-218481, A09, MF-A01).
- NCEER-89-0008 "Fundamentals of System Identification in Structural Dynamics," by H. Imai, C-B. Yun, O. Maruyama and M. Shinozuka, 1/26/89, (PB89-207211, A04, MF-A01).
- NCEER-89-0009 "Effects of the 1985 Michoacan Earthquake on Water Systems and Other Buried Lifelines in Mexico," by A.G. Ayala and M.J. O'Rourke, 3/8/89, (PB89-207229, A06, MF-A01).
- NCEER-89-R010 "NCEER Bibliography of Earthquake Education Materials," by K.E.K. Ross, Second Revision, 9/1/89, (PB90-125352, A05, MF-A01). This report is replaced by NCEER-92-0018.
- NCEER-89-0011 "Inelastic Three-Dimensional Response Analysis of Reinforced Concrete Building Structures (IDARC-3D), Part I - Modeling," by S.K. Kunnath and A.M. Reinhorn, 4/17/89, (PB90-114612, A07, MF-A01). This report is available only through NTIS (see address given above).
- NCEER-89-0012 "Recommended Modifications to ATC-14," by C.D. Poland and J.O. Malley, 4/12/89, (PB90-108648, A15, MF-A01).
- NCEER-89-0013 "Repair and Strengthening of Beam-to-Column Connections Subjected to Earthquake Loading," by M. Corazao and A.J. Durrani, 2/28/89, (PB90-109885, A06, MF-A01).

- NCEER-89-0014 "Program EXKAL2 for Identification of Structural Dynamic Systems," by O. Maruyama, C-B. Yun, M. Hoshiya and M. Shinozuka, 5/19/89, (PB90-109877, A09, MF-A01).
- NCEER-89-0015 "Response of Frames With Bolted Semi-Rigid Connections, Part I - Experimental Study and Analytical Predictions," by P.J. DiCorso, A.M. Reinhorn, J.R. Dickerson, J.B. Radzinski and W.L. Harper, 6/1/89, to be published.
- NCEER-89-0016 "ARMA Monte Carlo Simulation in Probabilistic Structural Analysis," by P.D. Spanos and M.P. Mignolet, 7/10/89, (PB90-109893, A03, MF-A01).
- NCEER-89-P017 "Preliminary Proceedings from the Conference on Disaster Preparedness - The Place of Earthquake Education in Our Schools," Edited by K.E.K. Ross, 6/23/89, (PB90-108606, A03, MF-A01).
- NCEER-89-0017 "Proceedings from the Conference on Disaster Preparedness - The Place of Earthquake Education in Our Schools," Edited by K.E.K. Ross, 12/31/89, (PB90-207895, A012, MF-A02). This report is available only through NTIS (see address given above).
- NCEER-89-0018 "Multidimensional Models of Hysteretic Material Behavior for Vibration Analysis of Shape Memory Energy Absorbing Devices, by E.J. Graesser and F.A. Cozzarelli, 6/7/89, (PB90-164146, A04, MF-A01).
- NCEER-89-0019 "Nonlinear Dynamic Analysis of Three-Dimensional Base Isolated Structures (3D-BASIS)," by S. Nagarajaiah, A.M. Reinhorn and M.C. Constantinou, 8/3/89, (PB90-161936, A06, MF-A01). This report has been replaced by NCEER-93-0011.
- NCEER-89-0020 "Structural Control Considering Time-Rate of Control Forces and Control Rate Constraints," by F.Y. Cheng and C.P. Pantelides, 8/3/89, (PB90-120445, A04, MF-A01).
- NCEER-89-0021 "Subsurface Conditions of Memphis and Shelby County," by K.W. Ng, T-S. Chang and H-H.M. Hwang, 7/26/89, (PB90-120437, A03, MF-A01).
- NCEER-89-0022 "Seismic Wave Propagation Effects on Straight Jointed Buried Pipelines," by K. Elhadi and M.J. O'Rourke, 8/24/89, (PB90-162322, A10, MF-A02).
- NCEER-89-0023 "Workshop on Serviceability Analysis of Water Delivery Systems," edited by M. Grigoriu, 3/6/89, (PB90-127424, A03, MF-A01).
- NCEER-89-0024 "Shaking Table Study of a 1/5 Scale Steel Frame Composed of Tapered Members," by K.C. Chang, J.S. Hwang and G.C. Lee, 9/18/89, (PB90-160169, A04, MF-A01).
- NCEER-89-0025 "DYNA1D: A Computer Program for Nonlinear Seismic Site Response Analysis - Technical Documentation," by Jean H. Prevost, 9/14/89, (PB90-161944, A07, MF-A01). This report is available only through NTIS (see address given above).
- NCEER-89-0026 "1:4 Scale Model Studies of Active Tendon Systems and Active Mass Dampers for Aseismic Protection," by A.M. Reinhorn, T.T. Soong, R.C. Lin, Y.P. Yang, Y. Fukao, H. Abe and M. Nakai, 9/15/89, (PB90-173246, A10, MF-A02). This report is available only through NTIS (see address given above).
- NCEER-89-0027 "Scattering of Waves by Inclusions in a Nonhomogeneous Elastic Half Space Solved by Boundary Element Methods," by P.K. Hadley, A. Askar and A.S. Cakmak, 6/15/89, (PB90-145699, A07, MF-A01).
- NCEER-89-0028 "Statistical Evaluation of Deflection Amplification Factors for Reinforced Concrete Structures," by H.H.M. Hwang, J-W. Jaw and A.L. Ch'ng, 8/31/89, (PB90-164633, A05, MF-A01).
- NCEER-89-0029 "Bedrock Accelerations in Memphis Area Due to Large New Madrid Earthquakes," by H.H.M. Hwang, C.H.S. Chen and G. Yu, 11/7/89, (PB90-162330, A04, MF-A01).
- NCEER-89-0030 "Seismic Behavior and Response Sensitivity of Secondary Structural Systems," by Y.Q. Chen and T.T. Soong, 10/23/89, (PB90-164658, A08, MF-A01).
- NCEER-89-0031 "Random Vibration and Reliability Analysis of Primary-Secondary Structural Systems," by Y. Ibrahim, M. Grigoriu and T.T. Soong, 11/10/89, (PB90-161951, A04, MF-A01).

- NCEER-89-0032 "Proceedings from the Second U.S. - Japan Workshop on Liquefaction, Large Ground Deformation and Their Effects on Lifelines, September 26-29, 1989," Edited by T.D. O'Rourke and M. Hamada, 12/1/89, (PB90-209388, A22, MF-A03).
- NCEER-89-0033 "Deterministic Model for Seismic Damage Evaluation of Reinforced Concrete Structures," by J.M. Bracci, A.M. Reinhorn, J.B. Mander and S.K. Kunnath, 9/27/89, (PB91-108803, A06, MF-A01).
- NCEER-89-0034 "On the Relation Between Local and Global Damage Indices," by E. DiPasquale and A.S. Cakmak, 8/15/89, (PB90-173865, A05, MF-A01).
- NCEER-89-0035 "Cyclic Undrained Behavior of Nonplastic and Low Plasticity Silts," by A.J. Walker and H.E. Stewart, 7/26/89, (PB90-183518, A10, MF-A01).
- NCEER-89-0036 "Liquefaction Potential of Surficial Deposits in the City of Buffalo, New York," by M. Budhu, R. Giese and L. Baumgrass, 1/17/89, (PB90-208455, A04, MF-A01).
- NCEER-89-0037 "A Deterministic Assessment of Effects of Ground Motion Incoherence," by A.S. Veletsos and Y. Tang, 7/15/89, (PB90-164294, A03, MF-A01).
- NCEER-89-0038 "Workshop on Ground Motion Parameters for Seismic Hazard Mapping," July 17-18, 1989, edited by R.V. Whitman, 12/1/89, (PB90-173923, A04, MF-A01).
- NCEER-89-0039 "Seismic Effects on Elevated Transit Lines of the New York City Transit Authority," by C.J. Costantino, C.A. Miller and E. Heymsfield, 12/26/89, (PB90-207887, A06, MF-A01).
- NCEER-89-0040 "Centrifugal Modeling of Dynamic Soil-Structure Interaction," by K. Weissman, Supervised by J.H. Prevost, 5/10/89, (PB90-207879, A07, MF-A01).
- NCEER-89-0041 "Linearized Identification of Buildings With Cores for Seismic Vulnerability Assessment," by I-K. Ho and A.E. Aktan, 11/1/89, (PB90-251943, A07, MF-A01).
- NCEER-90-0001 "Geotechnical and Lifeline Aspects of the October 17, 1989 Loma Prieta Earthquake in San Francisco," by T.D. O'Rourke, H.E. Stewart, F.T. Blackburn and T.S. Dickerman, 1/90, (PB90-208596, A05, MF-A01).
- NCEER-90-0002 "Nonnormal Secondary Response Due to Yielding in a Primary Structure," by D.C.K. Chen and L.D. Lutes, 2/28/90, (PB90-251976, A07, MF-A01).
- NCEER-90-0003 "Earthquake Education Materials for Grades K-12," by K.E.K. Ross, 4/16/90, (PB91-251984, A05, MF-A05). This report has been replaced by NCEER-92-0018.
- NCEER-90-0004 "Catalog of Strong Motion Stations in Eastern North America," by R.W. Busby, 4/3/90, (PB90-251984, A05, MF-A01).
- NCEER-90-0005 "NCEER Strong-Motion Data Base: A User Manual for the GeoBase Release (Version 1.0 for the Sun3)," by P. Friberg and K. Jacob, 3/31/90 (PB90-258062, A04, MF-A01).
- NCEER-90-0006 "Seismic Hazard Along a Crude Oil Pipeline in the Event of an 1811-1812 Type New Madrid Earthquake," by H.H.M. Hwang and C-H.S. Chen, 4/16/90, (PB90-258054, A04, MF-A01).
- NCEER-90-0007 "Site-Specific Response Spectra for Memphis Sheahan Pumping Station," by H.H.M. Hwang and C.S. Lee, 5/15/90, (PB91-108811, A05, MF-A01).
- NCEER-90-0008 "Pilot Study on Seismic Vulnerability of Crude Oil Transmission Systems," by T. Ariman, R. Dobry, M. Grigoriu, F. Kozin, M. O'Rourke, T. O'Rourke and M. Shinozuka, 5/25/90, (PB91-108837, A06, MF-A01).
- NCEER-90-0009 "A Program to Generate Site Dependent Time Histories: EQGEN," by G.W. Ellis, M. Srinivasan and A.S. Cakmak, 1/30/90, (PB91-108829, A04, MF-A01).
- NCEER-90-0010 "Active Isolation for Seismic Protection of Operating Rooms," by M.E. Talbott, Supervised by M. Shinozuka, 6/8/9, (PB91-110205, A05, MF-A01).

- NCEER-90-0011 "Program LINEARID for Identification of Linear Structural Dynamic Systems," by C-B. Yun and M. Shinozuka, 6/25/90, (PB91-110312, A08, MF-A01).
- NCEER-90-0012 "Two-Dimensional Two-Phase Elasto-Plastic Seismic Response of Earth Dams," by A.N. Yiagos, Supervised by J.H. Prevost, 6/20/90, (PB91-110197, A13, MF-A02).
- NCEER-90-0013 "Secondary Systems in Base-Isolated Structures: Experimental Investigation, Stochastic Response and Stochastic Sensitivity," by G.D. Manolis, G. Juhn, M.C. Constantinou and A.M. Reinhorn, 7/1/90, (PB91-110320, A08, MF-A01).
- NCEER-90-0014 "Seismic Behavior of Lightly-Reinforced Concrete Column and Beam-Column Joint Details," by S.P. Pessiki, C.H. Conley, P. Gergely and R.N. White, 8/22/90, (PB91-108795, A11, MF-A02).
- NCEER-90-0015 "Two Hybrid Control Systems for Building Structures Under Strong Earthquakes," by J.N. Yang and A. Danielians, 6/29/90, (PB91-125393, A04, MF-A01).
- NCEER-90-0016 "Instantaneous Optimal Control with Acceleration and Velocity Feedback," by J.N. Yang and Z. Li, 6/29/90, (PB91-125401, A03, MF-A01).
- NCEER-90-0017 "Reconnaissance Report on the Northern Iran Earthquake of June 21, 1990," by M. Mehrain, 10/4/90, (PB91-125377, A03, MF-A01).
- NCEER-90-0018 "Evaluation of Liquefaction Potential in Memphis and Shelby County," by T.S. Chang, P.S. Tang, C.S. Lee and H. Hwang, 8/10/90, (PB91-125427, A09, MF-A01).
- NCEER-90-0019 "Experimental and Analytical Study of a Combined Sliding Disc Bearing and Helical Steel Spring Isolation System," by M.C. Constantinou, A.S. Mokha and A.M. Reinhorn, 10/4/90, (PB91-125385, A06, MF-A01). This report is available only through NTIS (see address given above).
- NCEER-90-0020 "Experimental Study and Analytical Prediction of Earthquake Response of a Sliding Isolation System with a Spherical Surface," by A.S. Mokha, M.C. Constantinou and A.M. Reinhorn, 10/11/90, (PB91-125419, A05, MF-A01).
- NCEER-90-0021 "Dynamic Interaction Factors for Floating Pile Groups," by G. Gazetas, K. Fan, A. Kaynia and E. Kausel, 9/10/90, (PB91-170381, A05, MF-A01).
- NCEER-90-0022 "Evaluation of Seismic Damage Indices for Reinforced Concrete Structures," by S. Rodriguez-Gomez and A.S. Cakmak, 9/30/90, PB91-171322, A06, MF-A01).
- NCEER-90-0023 "Study of Site Response at a Selected Memphis Site," by H. Desai, S. Ahmad, E.S. Gazetas and M.R. Oh, 10/11/90, (PB91-196857, A03, MF-A01).
- NCEER-90-0024 "A User's Guide to Strongmo: Version 1.0 of NCEER's Strong-Motion Data Access Tool for PCs and Terminals," by P.A. Friberg and C.A.T. Susch, 11/15/90, (PB91-171272, A03, MF-A01).
- NCEER-90-0025 "A Three-Dimensional Analytical Study of Spatial Variability of Seismic Ground Motions," by L-L. Hong and A.H.-S. Ang, 10/30/90, (PB91-170399, A09, MF-A01).
- NCEER-90-0026 "MUMOID User's Guide - A Program for the Identification of Modal Parameters," by S. Rodriguez-Gomez and E. DiPasquale, 9/30/90, (PB91-171298, A04, MF-A01).
- NCEER-90-0027 "SARCF-II User's Guide - Seismic Analysis of Reinforced Concrete Frames," by S. Rodriguez-Gomez, Y.S. Chung and C. Meyer, 9/30/90, (PB91-171280, A05, MF-A01).
- NCEER-90-0028 "Viscous Dampers: Testing, Modeling and Application in Vibration and Seismic Isolation," by N. Makris and M.C. Constantinou, 12/20/90 (PB91-190561, A06, MF-A01).
- NCEER-90-0029 "Soil Effects on Earthquake Ground Motions in the Memphis Area," by H. Hwang, C.S. Lee, K.W. Ng and T.S. Chang, 8/2/90, (PB91-190751, A05, MF-A01).

- NCEER-91-0001 "Proceedings from the Third Japan-U.S. Workshop on Earthquake Resistant Design of Lifeline Facilities and Countermeasures for Soil Liquefaction, December 17-19, 1990," edited by T.D. O'Rourke and M. Hamada, 2/1/91, (PB91-179259, A99, MF-A04).
- NCEER-91-0002 "Physical Space Solutions of Non-Proportionally Damped Systems," by M. Tong, Z. Liang and G.C. Lee, 1/15/91, (PB91-179242, A04, MF-A01).
- NCEER-91-0003 "Seismic Response of Single Piles and Pile Groups," by K. Fan and G. Gazetas, 1/10/91, (PB92-174994, A04, MF-A01).
- NCEER-91-0004 "Damping of Structures: Part 1 - Theory of Complex Damping," by Z. Liang and G. Lee, 10/10/91, (PB92-197235, A12, MF-A03).
- NCEER-91-0005 "3D-BASIS - Nonlinear Dynamic Analysis of Three Dimensional Base Isolated Structures: Part II," by S. Nagarajaiah, A.M. Reinhorn and M.C. Constantinou, 2/28/91, (PB91-190553, A07, MF-A01). This report has been replaced by NCEER-93-0011.
- NCEER-91-0006 "A Multidimensional Hysteretic Model for Plasticity Deforming Metals in Energy Absorbing Devices," by E.J. Graesser and F.A. Cozzarelli, 4/9/91, (PB92-108364, A04, MF-A01).
- NCEER-91-0007 "A Framework for Customizable Knowledge-Based Expert Systems with an Application to a KBES for Evaluating the Seismic Resistance of Existing Buildings," by E.G. Ibarra-Anaya and S.J. Fennes, 4/9/91, (PB91-210930, A08, MF-A01).
- NCEER-91-0008 "Nonlinear Analysis of Steel Frames with Semi-Rigid Connections Using the Capacity Spectrum Method," by G.G. Deierlein, S-H. Hsieh, Y-J. Shen and J.F. Abel, 7/2/91, (PB92-113828, A05, MF-A01).
- NCEER-91-0009 "Earthquake Education Materials for Grades K-12," by K.E.K. Ross, 4/30/91, (PB91-212142, A06, MF-A01). This report has been replaced by NCEER-92-0018.
- NCEER-91-0010 "Phase Wave Velocities and Displacement Phase Differences in a Harmonically Oscillating Pile," by N. Makris and G. Gazetas, 7/8/91, (PB92-108356, A04, MF-A01).
- NCEER-91-0011 "Dynamic Characteristics of a Full-Size Five-Story Steel Structure and a 2/5 Scale Model," by K.C. Chang, G.C. Yao, G.C. Lee, D.S. Hao and Y.C. Yeh," 7/2/91, (PB93-116648, A06, MF-A02).
- NCEER-91-0012 "Seismic Response of a 2/5 Scale Steel Structure with Added Viscoelastic Dampers," by K.C. Chang, T.T. Soong, S-T. Oh and M.L. Lai, 5/17/91, (PB92-110816, A05, MF-A01).
- NCEER-91-0013 "Earthquake Response of Retaining Walls; Full-Scale Testing and Computational Modeling," by S. Alampalli and A-W.M. Elgamal, 6/20/91, to be published.
- NCEER-91-0014 "3D-BASIS-M: Nonlinear Dynamic Analysis of Multiple Building Base Isolated Structures," by P.C. Tsopelas, S. Nagarajaiah, M.C. Constantinou and A.M. Reinhorn, 5/28/91, (PB92-113885, A09, MF-A02).
- NCEER-91-0015 "Evaluation of SEAOC Design Requirements for Sliding Isolated Structures," by D. Theodossiou and M.C. Constantinou, 6/10/91, (PB92-114602, A11, MF-A03).
- NCEER-91-0016 "Closed-Loop Modal Testing of a 27-Story Reinforced Concrete Flat Plate-Core Building," by H.R. Somaprasad, T. Toksoy, H. Yoshiyuki and A.E. Aktan, 7/15/91, (PB92-129980, A07, MF-A02).
- NCEER-91-0017 "Shake Table Test of a 1/6 Scale Two-Story Lightly Reinforced Concrete Building," by A.G. El-Attar, R.N. White and P. Gergely, 2/28/91, (PB92-222447, A06, MF-A02).
- NCEER-91-0018 "Shake Table Test of a 1/8 Scale Three-Story Lightly Reinforced Concrete Building," by A.G. El-Attar, R.N. White and P. Gergely, 2/28/91, (PB93-116630, A08, MF-A02).
- NCEER-91-0019 "Transfer Functions for Rigid Rectangular Foundations," by A.S. Veletsos, A.M. Prasad and W.H. Wu, 7/31/91, to be published.

- NCEER-91-0020 "Hybrid Control of Seismic-Excited Nonlinear and Inelastic Structural Systems," by J.N. Yang, Z. Li and A. Daniellians, 8/1/91, (PB92-143171, A06, MF-A02).
- NCEER-91-0021 "The NCEER-91 Earthquake Catalog: Improved Intensity-Based Magnitudes and Recurrence Relations for U.S. Earthquakes East of New Madrid," by L. Seeber and J.G. Armbruster, 8/28/91, (PB92-176742, A06, MF-A02).
- NCEER-91-0022 "Proceedings from the Implementation of Earthquake Planning and Education in Schools: The Need for Change - The Roles of the Changemakers," by K.E.K. Ross and F. Winslow, 7/23/91, (PB92-129998, A12, MF-A03).
- NCEER-91-0023 "A Study of Reliability-Based Criteria for Seismic Design of Reinforced Concrete Frame Buildings," by H.H.M. Hwang and H-M. Hsu, 8/10/91, (PB92-140235, A09, MF-A02).
- NCEER-91-0024 "Experimental Verification of a Number of Structural System Identification Algorithms," by R.G. Ghanem, H. Gavin and M. Shinozuka, 9/18/91, (PB92-176577, A18, MF-A04).
- NCEER-91-0025 "Probabilistic Evaluation of Liquefaction Potential," by H.H.M. Hwang and C.S. Lee," 11/25/91, (PB92-143429, A05, MF-A01).
- NCEER-91-0026 "Instantaneous Optimal Control for Linear, Nonlinear and Hysteretic Structures - Stable Controllers," by J.N. Yang and Z. Li, 11/15/91, (PB92-163807, A04, MF-A01).
- NCEER-91-0027 "Experimental and Theoretical Study of a Sliding Isolation System for Bridges," by M.C. Constantinou, A. Kartoum, A.M. Reinhorn and P. Bradford, 11/15/91, (PB92-176973, A10, MF-A03).
- NCEER-92-0001 "Case Studies of Liquefaction and Lifeline Performance During Past Earthquakes, Volume 1: Japanese Case Studies," Edited by M. Hamada and T. O'Rourke, 2/17/92, (PB92-197243, A18, MF-A04).
- NCEER-92-0002 "Case Studies of Liquefaction and Lifeline Performance During Past Earthquakes, Volume 2: United States Case Studies," Edited by T. O'Rourke and M. Hamada, 2/17/92, (PB92-197250, A20, MF-A04).
- NCEER-92-0003 "Issues in Earthquake Education," Edited by K. Ross, 2/3/92, (PB92-222389, A07, MF-A02).
- NCEER-92-0004 "Proceedings from the First U.S. - Japan Workshop on Earthquake Protective Systems for Bridges," Edited by I.G. Buckle, 2/4/92, (PB94-142239, A99, MF-A06).
- NCEER-92-0005 "Seismic Ground Motion from a Haskell-Type Source in a Multiple-Layered Half-Space," A.P. Theoharis, G. Deodatis and M. Shinozuka, 1/2/92, to be published.
- NCEER-92-0006 "Proceedings from the Site Effects Workshop," Edited by R. Whitman, 2/29/92, (PB92-197201, A04, MF-A01).
- NCEER-92-0007 "Engineering Evaluation of Permanent Ground Deformations Due to Seismically-Induced Liquefaction," by M.H. Baziar, R. Dobry and A-W.M. Elgamel, 3/24/92, (PB92-222421, A13, MF-A03).
- NCEER-92-0008 "A Procedure for the Seismic Evaluation of Buildings in the Central and Eastern United States," by C.D. Poland and J.O. Malley, 4/2/92, (PB92-222439, A20, MF-A04).
- NCEER-92-0009 "Experimental and Analytical Study of a Hybrid Isolation System Using Friction Controllable Sliding Bearings," by M.Q. Feng, S. Fujii and M. Shinozuka, 5/15/92, (PB93-150282, A06, MF-A02).
- NCEER-92-0010 "Seismic Resistance of Slab-Column Connections in Existing Non-Ductile Flat-Plate Buildings," by A.J. Durrani and Y. Du, 5/18/92, (PB93-116812, A06, MF-A02).
- NCEER-92-0011 "The Hysteretic and Dynamic Behavior of Brick Masonry Walls Upgraded by Ferrocement Coatings Under Cyclic Loading and Strong Simulated Ground Motion," by H. Lee and S.P. Prawl, 5/11/92, to be published.
- NCEER-92-0012 "Study of Wire Rope Systems for Seismic Protection of Equipment in Buildings," by G.F. Demetriades, M.C. Constantinou and A.M. Reinhorn, 5/20/92, (PB93-116655, A08, MF-A02).

- NCEER-92-0013 "Shape Memory Structural Dampers: Material Properties, Design and Seismic Testing," by P.R. Witting and F.A. Cozzarelli, 5/26/92, (PB93-116663, A05, MF-A01).
- NCEER-92-0014 "Longitudinal Permanent Ground Deformation Effects on Buried Continuous Pipelines," by M.J. O'Rourke, and C. Nordberg, 6/15/92, (PB93-116671, A08, MF-A02).
- NCEER-92-0015 "A Simulation Method for Stationary Gaussian Random Functions Based on the Sampling Theorem," by M. Grigoriu and S. Balopoulou, 6/11/92, (PB93-127496, A05, MF-A01).
- NCEER-92-0016 "Gravity-Load-Designed Reinforced Concrete Buildings: Seismic Evaluation of Existing Construction and Detailing Strategies for Improved Seismic Resistance," by G.W. Hoffmann, S.K. Kunnath, A.M. Reinhorn and J.B. Mander, 7/15/92, (PB94-142007, A08, MF-A02).
- NCEER-92-0017 "Observations on Water System and Pipeline Performance in the Limón Area of Costa Rica Due to the April 22, 1991 Earthquake," by M. O'Rourke and D. Ballantyne, 6/30/92, (PB93-126811, A06, MF-A02).
- NCEER-92-0018 "Fourth Edition of Earthquake Education Materials for Grades K-12," Edited by K.E.K. Ross, 8/10/92, (PB93-114023, A07, MF-A02).
- NCEER-92-0019 "Proceedings from the Fourth Japan-U.S. Workshop on Earthquake Resistant Design of Lifeline Facilities and Countermeasures for Soil Liquefaction," Edited by M. Hamada and T.D. O'Rourke, 8/12/92, (PB93-163939, A99, MF-E11).
- NCEER-92-0020 "Active Bracing System: A Full Scale Implementation of Active Control," by A.M. Reinhorn, T.T. Soong, R.C. Lin, M.A. Riley, Y.P. Wang, S. Aizawa and M. Higashino, 8/14/92, (PB93-127512, A06, MF-A02).
- NCEER-92-0021 "Empirical Analysis of Horizontal Ground Displacement Generated by Liquefaction-Induced Lateral Spreads," by S.F. Bartlett and T.L. Youd, 8/17/92, (PB93-188241, A06, MF-A02).
- NCEER-92-0022 "IDARC Version 3.0: Inelastic Damage Analysis of Reinforced Concrete Structures," by S.K. Kunnath, A.M. Reinhorn and R.F. Lobo, 8/31/92, (PB93-227502, A07, MF-A02).
- NCEER-92-0023 "A Semi-Empirical Analysis of Strong-Motion Peaks in Terms of Seismic Source, Propagation Path and Local Site Conditions, by M. Kamiyama, M.J. O'Rourke and R. Flores-Berrones, 9/9/92, (PB93-150266, A08, MF-A02).
- NCEER-92-0024 "Seismic Behavior of Reinforced Concrete Frame Structures with Nonductile Details, Part I: Summary of Experimental Findings of Full Scale Beam-Column Joint Tests," by A. Beres, R.N. White and P. Gergely, 9/30/92, (PB93-227783, A05, MF-A01).
- NCEER-92-0025 "Experimental Results of Repaired and Retrofitted Beam-Column Joint Tests in Lightly Reinforced Concrete Frame Buildings," by A. Beres, S. El-Borgi, R.N. White and P. Gergely, 10/29/92, (PB93-227791, A05, MF-A01).
- NCEER-92-0026 "A Generalization of Optimal Control Theory: Linear and Nonlinear Structures," by J.N. Yang, Z. Li and S. Vongchavalitkul, 11/2/92, (PB93-188621, A05, MF-A01).
- NCEER-92-0027 "Seismic Resistance of Reinforced Concrete Frame Structures Designed Only for Gravity Loads: Part I - Design and Properties of a One-Third Scale Model Structure," by J.M. Bracci, A.M. Reinhorn and J.B. Mander, 12/1/92, (PB94-104502, A08, MF-A02).
- NCEER-92-0028 "Seismic Resistance of Reinforced Concrete Frame Structures Designed Only for Gravity Loads: Part II - Experimental Performance of Subassemblages," by L.E. Aycaardi, J.B. Mander and A.M. Reinhorn, 12/1/92, (PB94-104510, A08, MF-A02).
- NCEER-92-0029 "Seismic Resistance of Reinforced Concrete Frame Structures Designed Only for Gravity Loads: Part III - Experimental Performance and Analytical Study of a Structural Model," by J.M. Bracci, A.M. Reinhorn and J.B. Mander, 12/1/92, (PB93-227528, A09, MF-A01).

- NCEER-92-0030 "Evaluation of Seismic Retrofit of Reinforced Concrete Frame Structures: Part I - Experimental Performance of Retrofitted Subassemblages," by D. Choudhuri, J.B. Mander and A.M. Reinhorn, 12/8/92, (PB93-198307, A07, MF-A02).
- NCEER-92-0031 "Evaluation of Seismic Retrofit of Reinforced Concrete Frame Structures: Part II - Experimental Performance and Analytical Study of a Retrofitted Structural Model," by J.M. Bracci, A.M. Reinhorn and J.B. Mander, 12/8/92, (PB93-198315, A09, MF-A03).
- NCEER-92-0032 "Experimental and Analytical Investigation of Seismic Response of Structures with Supplemental Fluid Viscous Dampers," by M.C. Constantinou and M.D. Symans, 12/21/92, (PB93-191435, A10, MF-A03). This report is available only through NTIS (see address given above).
- NCEER-92-0033 "Reconnaissance Report on the Cairo, Egypt Earthquake of October 12, 1992," by M. Khater, 12/23/92, (PB93-188621, A03, MF-A01).
- NCEER-92-0034 "Low-Level Dynamic Characteristics of Four Tall Flat-Plate Buildings in New York City," by H. Gavin, S. Yuan, J. Grossman, E. Pekelis and K. Jacob, 12/28/92, (PB93-188217, A07, MF-A02).
- NCEER-93-0001 "An Experimental Study on the Seismic Performance of Brick-Infilled Steel Frames With and Without Retrofit," by J.B. Mander, B. Nair, K. Wojtkowski and J. Ma, 1/29/93, (PB93-227510, A07, MF-A02).
- NCEER-93-0002 "Social Accounting for Disaster Preparedness and Recovery Planning," by S. Cole, E. Pantoja and V. Razak, 2/22/93, (PB94-142114, A12, MF-A03).
- NCEER-93-0003 "Assessment of 1991 NEHRP Provisions for Nonstructural Components and Recommended Revisions," by T.T. Soong, G. Chen, Z. Wu, R-H. Zhang and M. Grigoriu, 3/1/93, (PB93-188639, A06, MF-A02).
- NCEER-93-0004 "Evaluation of Static and Response Spectrum Analysis Procedures of SEAOC/UBC for Seismic Isolated Structures," by C.W. Winters and M.C. Constantinou, 3/23/93, (PB93-198299, A10, MF-A03).
- NCEER-93-0005 "Earthquakes in the Northeast - Are We Ignoring the Hazard? A Workshop on Earthquake Science and Safety for Educators," edited by K.E.K. Ross, 4/2/93, (PB94-103066, A09, MF-A02).
- NCEER-93-0006 "Inelastic Response of Reinforced Concrete Structures with Viscoelastic Braces," by R.F. Lobo, J.M. Bracci, K.L. Shen, A.M. Reinhorn and T.T. Soong, 4/5/93, (PB93-227486, A05, MF-A02).
- NCEER-93-0007 "Seismic Testing of Installation Methods for Computers and Data Processing Equipment," by K. Kosar, T.T. Soong, K.L. Shen, J.A. HoLung and Y.K. Lin, 4/12/93, (PB93-198299, A07, MF-A02).
- NCEER-93-0008 "Retrofit of Reinforced Concrete Frames Using Added Dampers," by A. Reinhorn, M. Constantinou and C. Li, to be published.
- NCEER-93-0009 "Seismic Behavior and Design Guidelines for Steel Frame Structures with Added Viscoelastic Dampers," by K.C. Chang, M.L. Lai, T.T. Soong, D.S. Hao and Y.C. Yeh, 5/1/93, (PB94-141959, A07, MF-A02).
- NCEER-93-0010 "Seismic Performance of Shear-Critical Reinforced Concrete Bridge Piers," by J.B. Mander, S.M. Waheed, M.T.A. Chaudhary and S.S. Chen, 5/12/93, (PB93-227494, A08, MF-A02).
- NCEER-93-0011 "3D-BASIS-TABS: Computer Program for Nonlinear Dynamic Analysis of Three Dimensional Base Isolated Structures," by S. Nagarajaiah, C. Li, A.M. Reinhorn and M.C. Constantinou, 8/2/93, (PB94-141819, A09, MF-A02).
- NCEER-93-0012 "Effects of Hydrocarbon Spills from an Oil Pipeline Break on Ground Water," by O.J. Helweg and H.H.M. Hwang, 8/3/93, (PB94-141942, A06, MF-A02).
- NCEER-93-0013 "Simplified Procedures for Seismic Design of Nonstructural Components and Assessment of Current Code Provisions," by M.P. Singh, L.E. Suarez, E.E. Matheu and G.O. Maldonado, 8/4/93, (PB94-141827, A09, MF-A02).
- NCEER-93-0014 "An Energy Approach to Seismic Analysis and Design of Secondary Systems," by G. Chen and T.T. Soong, 8/6/93, (PB94-142767, A11, MF-A03).

- NCEER-93-0015 "Proceedings from School Sites: Becoming Prepared for Earthquakes - Commemorating the Third Anniversary of the Loma Prieta Earthquake," Edited by F.E. Winslow and K.E.K. Ross, 8/16/93, (PB94-154275, A16, MF-A02).
- NCEER-93-0016 "Reconnaissance Report of Damage to Historic Monuments in Cairo, Egypt Following the October 12, 1992 Dahshur Earthquake," by D. Sykora, D. Look, G. Croci, E. Karaesmen and E. Karaesmen, 8/19/93, (PB94-142221, A08, MF-A02).
- NCEER-93-0017 "The Island of Guam Earthquake of August 8, 1993," by S.W. Swan and S.K. Harris, 9/30/93, (PB94-141843, A04, MF-A01).
- NCEER-93-0018 "Engineering Aspects of the October 12, 1992 Egyptian Earthquake," by A.W. Elgamal, M. Amer, K. Adalier and A. Abul-Fadl, 10/7/93, (PB94-141983, A05, MF-A01).
- NCEER-93-0019 "Development of an Earthquake Motion Simulator and its Application in Dynamic Centrifuge Testing," by I. Krstelj, Supervised by J.H. Prevost, 10/23/93, (PB94-181773, A-10, MF-A03).
- NCEER-93-0020 "NCEER-Taisei Corporation Research Program on Sliding Seismic Isolation Systems for Bridges: Experimental and Analytical Study of a Friction Pendulum System (FPS)," by M.C. Constantinou, P. Tsopelas, Y-S. Kim and S. Okamoto, 11/1/93, (PB94-142775, A08, MF-A02).
- NCEER-93-0021 "Finite Element Modeling of Elastomeric Seismic Isolation Bearings," by L.J. Billings, Supervised by R. Shepherd, 11/8/93, to be published.
- NCEER-93-0022 "Seismic Vulnerability of Equipment in Critical Facilities: Life-Safety and Operational Consequences," by K. Porter, G.S. Johnson, M.M. Zadeh, C. Scawthorn and S. Eder, 11/24/93, (PB94-181765, A16, MF-A03).
- NCEER-93-0023 "Hokkaido Nansei-oki, Japan Earthquake of July 12, 1993, by P.I. Yanev and C.R. Scawthorn, 12/23/93, (PB94-181500, A07, MF-A01).
- NCEER-94-0001 "An Evaluation of Seismic Serviceability of Water Supply Networks with Application to the San Francisco Auxiliary Water Supply System," by I. Markov, Supervised by M. Grigoriu and T. O'Rourke, 1/21/94, (PB94-204013, A07, MF-A02).
- NCEER-94-0002 "NCEER-Taisei Corporation Research Program on Sliding Seismic Isolation Systems for Bridges: Experimental and Analytical Study of Systems Consisting of Sliding Bearings, Rubber Restoring Force Devices and Fluid Dampers," Volumes I and II, by P. Tsopelas, S. Okamoto, M.C. Constantinou, D. Ozaki and S. Fujii, 2/4/94, (PB94-181740, A09, MF-A02 and PB94-181757, A12, MF-A03).
- NCEER-94-0003 "A Markov Model for Local and Global Damage Indices in Seismic Analysis," by S. Rahman and M. Grigoriu, 2/18/94, (PB94-206000, A12, MF-A03).
- NCEER-94-0004 "Proceedings from the NCEER Workshop on Seismic Response of Masonry Infills," edited by D.P. Abrams, 3/1/94, (PB94-180783, A07, MF-A02).
- NCEER-94-0005 "The Northridge, California Earthquake of January 17, 1994: General Reconnaissance Report," edited by J.D. Goltz, 3/11/94, (PB94-193943, A10, MF-A03).
- NCEER-94-0006 "Seismic Energy Based Fatigue Damage Analysis of Bridge Columns: Part I - Evaluation of Seismic Capacity," by G.A. Chang and J.B. Mander, 3/14/94, (PB94-219185, A11, MF-A03).
- NCEER-94-0007 "Seismic Isolation of Multi-Story Frame Structures Using Spherical Sliding Isolation Systems," by T.M. Al-Hussaini, V.A. Zayas and M.C. Constantinou, 3/17/94, (PB94-193745, A09, MF-A02).
- NCEER-94-0008 "The Northridge, California Earthquake of January 17, 1994: Performance of Highway Bridges," edited by I.G. Buckle, 3/24/94, (PB94-193851, A06, MF-A02).
- NCEER-94-0009 "Proceedings of the Third U.S.-Japan Workshop on Earthquake Protective Systems for Bridges," edited by I.G. Buckle and I. Friedland, 3/31/94, (PB94-195815, A99, MF-A06).

- NCEER-94-0010 "3D-BASIS-ME: Computer Program for Nonlinear Dynamic Analysis of Seismically Isolated Single and Multiple Structures and Liquid Storage Tanks," by P.C. Tsopelas, M.C. Constantinou and A.M. Reinhorn, 4/12/94, (PB94-204922, A09, MF-A02).
- NCEER-94-0011 "The Northridge, California Earthquake of January 17, 1994: Performance of Gas Transmission Pipelines," by T.D. O'Rourke and M.C. Palmer, 5/16/94, (PB94-204989, A05, MF-A01).
- NCEER-94-0012 "Feasibility Study of Replacement Procedures and Earthquake Performance Related to Gas Transmission Pipelines," by T.D. O'Rourke and M.C. Palmer, 5/25/94, (PB94-206638, A09, MF-A02).
- NCEER-94-0013 "Seismic Energy Based Fatigue Damage Analysis of Bridge Columns: Part II - Evaluation of Seismic Demand," by G.A. Chang and J.B. Mander, 6/1/94, (PB95-18106, A08, MF-A02).
- NCEER-94-0014 "NCEER-Taisei Corporation Research Program on Sliding Seismic Isolation Systems for Bridges: Experimental and Analytical Study of a System Consisting of Sliding Bearings and Fluid Restoring Force/Damping Devices," by P. Tsopelas and M.C. Constantinou, 6/13/94, (PB94-219144, A10, MF-A03).
- NCEER-94-0015 "Generation of Hazard-Consistent Fragility Curves for Seismic Loss Estimation Studies," by H. Hwang and J-R. Huo, 6/14/94, (PB95-181996, A09, MF-A02).
- NCEER-94-0016 "Seismic Study of Building Frames with Added Energy-Absorbing Devices," by W.S. Pong, C.S. Tsai and G.C. Lee, 6/20/94, (PB94-219136, A10, A03).
- NCEER-94-0017 "Sliding Mode Control for Seismic-Excited Linear and Nonlinear Civil Engineering Structures," by J. Yang, J. Wu, A. Agrawal and Z. Li, 6/21/94, (PB95-138483, A06, MF-A02).
- NCEER-94-0018 "3D-BASIS-TABS Version 2.0: Computer Program for Nonlinear Dynamic Analysis of Three Dimensional Base Isolated Structures," by A.M. Reinhorn, S. Nagarajaiah, M.C. Constantinou, P. Tsopelas and R. Li, 6/22/94, (PB95-182176, A08, MF-A02).
- NCEER-94-0019 "Proceedings of the International Workshop on Civil Infrastructure Systems: Application of Intelligent Systems and Advanced Materials on Bridge Systems," Edited by G.C. Lee and K.C. Chang, 7/18/94, (PB95-252474, A20, MF-A04).
- NCEER-94-0020 "Study of Seismic Isolation Systems for Computer Floors," by V. Lambrou and M.C. Constantinou, 7/19/94, (PB95-138533, A10, MF-A03).
- NCEER-94-0021 "Proceedings of the U.S.-Italian Workshop on Guidelines for Seismic Evaluation and Rehabilitation of Unreinforced Masonry Buildings," Edited by D.P. Abrams and G.M. Calvi, 7/20/94, (PB95-138749, A13, MF-A03).
- NCEER-94-0022 "NCEER-Taisei Corporation Research Program on Sliding Seismic Isolation Systems for Bridges: Experimental and Analytical Study of a System Consisting of Lubricated PTFE Sliding Bearings and Mild Steel Dampers," by P. Tsopelas and M.C. Constantinou, 7/22/94, (PB95-182184, A08, MF-A02).
- NCEER-94-0023 "Development of Reliability-Based Design Criteria for Buildings Under Seismic Load," by Y.K. Wen, H. Hwang and M. Shinozuka, 8/1/94, (PB95-211934, A08, MF-A02).
- NCEER-94-0024 "Experimental Verification of Acceleration Feedback Control Strategies for an Active Tendon System," by S.J. Dyke, B.F. Spencer, Jr., P. Quast, M.K. Sain, D.C. Kaspari, Jr. and T.T. Soong, 8/29/94, (PB95-212320, A05, MF-A01).
- NCEER-94-0025 "Seismic Retrofitting Manual for Highway Bridges," Edited by I.G. Buckle and I.F. Friedland, published by the Federal Highway Administration (PB95-212676, A15, MF-A03).
- NCEER-94-0026 "Proceedings from the Fifth U.S.-Japan Workshop on Earthquake Resistant Design of Lifeline Facilities and Countermeasures Against Soil Liquefaction," Edited by T.D. O'Rourke and M. Hamada, 11/7/94, (PB95-220802, A99, MF-E08).

- NCEER-95-0001 “Experimental and Analytical Investigation of Seismic Retrofit of Structures with Supplemental Damping: Part I - Fluid Viscous Damping Devices,” by A.M. Reinhorn, C. Li and M.C. Constantinou, 1/3/95, (PB95-266599, A09, MF-A02).
- NCEER-95-0002 “Experimental and Analytical Study of Low-Cycle Fatigue Behavior of Semi-Rigid Top-And-Seat Angle Connections,” by G. Pekcan, J.B. Mander and S.S. Chen, 1/5/95, (PB95-220042, A07, MF-A02).
- NCEER-95-0003 “NCEER-ATC Joint Study on Fragility of Buildings,” by T. Anagnos, C. Rojahn and A.S. Kiremidjian, 1/20/95, (PB95-220026, A06, MF-A02).
- NCEER-95-0004 “Nonlinear Control Algorithms for Peak Response Reduction,” by Z. Wu, T.T. Soong, V. Gattulli and R.C. Lin, 2/16/95, (PB95-220349, A05, MF-A01).
- NCEER-95-0005 “Pipeline Replacement Feasibility Study: A Methodology for Minimizing Seismic and Corrosion Risks to Underground Natural Gas Pipelines,” by R.T. Eguchi, H.A. Seligson and D.G. Honegger, 3/2/95, (PB95-252326, A06, MF-A02).
- NCEER-95-0006 “Evaluation of Seismic Performance of an 11-Story Frame Building During the 1994 Northridge Earthquake,” by F. Naeim, R. DiSulio, K. Benuska, A. Reinhorn and C. Li, to be published.
- NCEER-95-0007 “Prioritization of Bridges for Seismic Retrofitting,” by N. Basöz and A.S. Kiremidjian, 4/24/95, (PB95-252300, A08, MF-A02).
- NCEER-95-0008 “Method for Developing Motion Damage Relationships for Reinforced Concrete Frames,” by A. Singhal and A.S. Kiremidjian, 5/11/95, (PB95-266607, A06, MF-A02).
- NCEER-95-0009 “Experimental and Analytical Investigation of Seismic Retrofit of Structures with Supplemental Damping: Part II - Friction Devices,” by C. Li and A.M. Reinhorn, 7/6/95, (PB96-128087, A11, MF-A03).
- NCEER-95-0010 “Experimental Performance and Analytical Study of a Non-Ductile Reinforced Concrete Frame Structure Retrofitted with Elastomeric Spring Dampers,” by G. Pekcan, J.B. Mander and S.S. Chen, 7/14/95, (PB96-137161, A08, MF-A02).
- NCEER-95-0011 “Development and Experimental Study of Semi-Active Fluid Damping Devices for Seismic Protection of Structures,” by M.D. Symans and M.C. Constantinou, 8/3/95, (PB96-136940, A23, MF-A04).
- NCEER-95-0012 “Real-Time Structural Parameter Modification (RSPM): Development of Innervated Structures,” by Z. Liang, M. Tong and G.C. Lee, 4/11/95, (PB96-137153, A06, MF-A01).
- NCEER-95-0013 “Experimental and Analytical Investigation of Seismic Retrofit of Structures with Supplemental Damping: Part III - Viscous Damping Walls,” by A.M. Reinhorn and C. Li, 10/1/95, (PB96-176409, A11, MF-A03).
- NCEER-95-0014 “Seismic Fragility Analysis of Equipment and Structures in a Memphis Electric Substation,” by J-R. Huo and H.H.M. Hwang, 8/10/95, (PB96-128087, A09, MF-A02).
- NCEER-95-0015 “The Hanshin-Awaji Earthquake of January 17, 1995: Performance of Lifelines,” Edited by M. Shinozuka, 11/3/95, (PB96-176383, A15, MF-A03).
- NCEER-95-0016 “Highway Culvert Performance During Earthquakes,” by T.L. Youd and C.J. Beckman, available as NCEER-96-0015.
- NCEER-95-0017 “The Hanshin-Awaji Earthquake of January 17, 1995: Performance of Highway Bridges,” Edited by I.G. Buckle, 12/1/95, to be published.
- NCEER-95-0018 “Modeling of Masonry Infill Panels for Structural Analysis,” by A.M. Reinhorn, A. Madan, R.E. Valles, Y. Reichmann and J.B. Mander, 12/8/95, (PB97-110886, MF-A01, A06).
- NCEER-95-0019 “Optimal Polynomial Control for Linear and Nonlinear Structures,” by A.K. Agrawal and J.N. Yang, 12/11/95, (PB96-168737, A07, MF-A02).

- NCEER-95-0020 “Retrofit of Non-Ductile Reinforced Concrete Frames Using Friction Dampers,” by R.S. Rao, P. Gergely and R.N. White, 12/22/95, (PB97-133508, A10, MF-A02).
- NCEER-95-0021 “Parametric Results for Seismic Response of Pile-Supported Bridge Bents,” by G. Mylonakis, A. Nikolaou and G. Gazetas, 12/22/95, (PB97-100242, A12, MF-A03).
- NCEER-95-0022 “Kinematic Bending Moments in Seismically Stressed Piles,” by A. Nikolaou, G. Mylonakis and G. Gazetas, 12/23/95, (PB97-113914, MF-A03, A13).
- NCEER-96-0001 “Dynamic Response of Unreinforced Masonry Buildings with Flexible Diaphragms,” by A.C. Costley and D.P. Abrams, 10/10/96, (PB97-133573, MF-A03, A15).
- NCEER-96-0002 “State of the Art Review: Foundations and Retaining Structures,” by I. Po Lam, to be published.
- NCEER-96-0003 “Ductility of Rectangular Reinforced Concrete Bridge Columns with Moderate Confinement,” by N. Wehbe, M. Saiidi, D. Sanders and B. Douglas, 11/7/96, (PB97-133557, A06, MF-A02).
- NCEER-96-0004 “Proceedings of the Long-Span Bridge Seismic Research Workshop,” edited by I.G. Buckle and I.M. Friedland, to be published.
- NCEER-96-0005 “Establish Representative Pier Types for Comprehensive Study: Eastern United States,” by J. Kulicki and Z. Prucz, 5/28/96, (PB98-119217, A07, MF-A02).
- NCEER-96-0006 “Establish Representative Pier Types for Comprehensive Study: Western United States,” by R. Imbsen, R.A. Schamber and T.A. Osterkamp, 5/28/96, (PB98-118607, A07, MF-A02).
- NCEER-96-0007 “Nonlinear Control Techniques for Dynamical Systems with Uncertain Parameters,” by R.G. Ghanem and M.I. Bujakov, 5/27/96, (PB97-100259, A17, MF-A03).
- NCEER-96-0008 “Seismic Evaluation of a 30-Year Old Non-Ductile Highway Bridge Pier and Its Retrofit,” by J.B. Mander, B. Mahmoodzadegan, S. Bhadra and S.S. Chen, 5/31/96, (PB97-110902, MF-A03, A10).
- NCEER-96-0009 “Seismic Performance of a Model Reinforced Concrete Bridge Pier Before and After Retrofit,” by J.B. Mander, J.H. Kim and C.A. Ligozio, 5/31/96, (PB97-110910, MF-A02, A10).
- NCEER-96-0010 “IDARC2D Version 4.0: A Computer Program for the Inelastic Damage Analysis of Buildings,” by R.E. Valles, A.M. Reinhorn, S.K. Kunnath, C. Li and A. Madan, 6/3/96, (PB97-100234, A17, MF-A03).
- NCEER-96-0011 “Estimation of the Economic Impact of Multiple Lifeline Disruption: Memphis Light, Gas and Water Division Case Study,” by S.E. Chang, H.A. Seligson and R.T. Eguchi, 8/16/96, (PB97-133490, A11, MF-A03).
- NCEER-96-0012 “Proceedings from the Sixth Japan-U.S. Workshop on Earthquake Resistant Design of Lifeline Facilities and Countermeasures Against Soil Liquefaction, Edited by M. Hamada and T. O’Rourke, 9/11/96, (PB97-133581, A99, MF-A06).
- NCEER-96-0013 “Chemical Hazards, Mitigation and Preparedness in Areas of High Seismic Risk: A Methodology for Estimating the Risk of Post-Earthquake Hazardous Materials Release,” by H.A. Seligson, R.T. Eguchi, K.J. Tierney and K. Richmond, 11/7/96, (PB97-133565, MF-A02, A08).
- NCEER-96-0014 “Response of Steel Bridge Bearings to Reversed Cyclic Loading,” by J.B. Mander, D-K. Kim, S.S. Chen and G.J. Premus, 11/13/96, (PB97-140735, A12, MF-A03).
- NCEER-96-0015 “Highway Culvert Performance During Past Earthquakes,” by T.L. Youd and C.J. Beckman, 11/25/96, (PB97-133532, A06, MF-A01).
- NCEER-97-0001 “Evaluation, Prevention and Mitigation of Pounding Effects in Building Structures,” by R.E. Valles and A.M. Reinhorn, 2/20/97, (PB97-159552, A14, MF-A03).
- NCEER-97-0002 “Seismic Design Criteria for Bridges and Other Highway Structures,” by C. Rojahn, R. Mayes, D.G. Anderson, J. Clark, J.H. Hom, R.V. Nutt and M.J. O’Rourke, 4/30/97, (PB97-194658, A06, MF-A03).

- NCEER-97-0003 "Proceedings of the U.S.-Italian Workshop on Seismic Evaluation and Retrofit," Edited by D.P. Abrams and G.M. Calvi, 3/19/97, (PB97-194666, A13, MF-A03).
- NCEER-97-0004 "Investigation of Seismic Response of Buildings with Linear and Nonlinear Fluid Viscous Dampers," by A.A. Seleemah and M.C. Constantinou, 5/21/97, (PB98-109002, A15, MF-A03).
- NCEER-97-0005 "Proceedings of the Workshop on Earthquake Engineering Frontiers in Transportation Facilities," edited by G.C. Lee and I.M. Friedland, 8/29/97, (PB98-128911, A25, MR-A04).
- NCEER-97-0006 "Cumulative Seismic Damage of Reinforced Concrete Bridge Piers," by S.K. Kunnath, A. El-Bahy, A. Taylor and W. Stone, 9/2/97, (PB98-108814, A11, MF-A03).
- NCEER-97-0007 "Structural Details to Accommodate Seismic Movements of Highway Bridges and Retaining Walls," by R.A. Imbsen, R.A. Schamber, E. Thorkildsen, A. Kartoum, B.T. Martin, T.N. Rosser and J.M. Kulicki, 9/3/97, (PB98-108996, A09, MF-A02).
- NCEER-97-0008 "A Method for Earthquake Motion-Damage Relationships with Application to Reinforced Concrete Frames," by A. Singhal and A.S. Kiremidjian, 9/10/97, (PB98-108988, A13, MF-A03).
- NCEER-97-0009 "Seismic Analysis and Design of Bridge Abutments Considering Sliding and Rotation," by K. Fishman and R. Richards, Jr., 9/15/97, (PB98-108897, A06, MF-A02).
- NCEER-97-0010 "Proceedings of the FHWA/NCEER Workshop on the National Representation of Seismic Ground Motion for New and Existing Highway Facilities," edited by I.M. Friedland, M.S. Power and R.L. Mayes, 9/22/97, (PB98-128903, A21, MF-A04).
- NCEER-97-0011 "Seismic Analysis for Design or Retrofit of Gravity Bridge Abutments," by K.L. Fishman, R. Richards, Jr. and R.C. Divito, 10/2/97, (PB98-128937, A08, MF-A02).
- NCEER-97-0012 "Evaluation of Simplified Methods of Analysis for Yielding Structures," by P. Tsopelas, M.C. Constantinou, C.A. Kircher and A.S. Whittaker, 10/31/97, (PB98-128929, A10, MF-A03).
- NCEER-97-0013 "Seismic Design of Bridge Columns Based on Control and Repairability of Damage," by C-T. Cheng and J.B. Mander, 12/8/97, (PB98-144249, A11, MF-A03).
- NCEER-97-0014 "Seismic Resistance of Bridge Piers Based on Damage Avoidance Design," by J.B. Mander and C-T. Cheng, 12/10/97, (PB98-144223, A09, MF-A02).
- NCEER-97-0015 "Seismic Response of Nominally Symmetric Systems with Strength Uncertainty," by S. Balopoulou and M. Grigoriu, 12/23/97, (PB98-153422, A11, MF-A03).
- NCEER-97-0016 "Evaluation of Seismic Retrofit Methods for Reinforced Concrete Bridge Columns," by T.J. Wipf, F.W. Klaiber and F.M. Russo, 12/28/97, (PB98-144215, A12, MF-A03).
- NCEER-97-0017 "Seismic Fragility of Existing Conventional Reinforced Concrete Highway Bridges," by C.L. Mullen and A.S. Cakmak, 12/30/97, (PB98-153406, A08, MF-A02).
- NCEER-97-0018 "Loss Assessment of Memphis Buildings," edited by D.P. Abrams and M. Shinozuka, 12/31/97, (PB98-144231, A13, MF-A03).
- NCEER-97-0019 "Seismic Evaluation of Frames with Infill Walls Using Quasi-static Experiments," by K.M. Mosalam, R.N. White and P. Gergely, 12/31/97, (PB98-153455, A07, MF-A02).
- NCEER-97-0020 "Seismic Evaluation of Frames with Infill Walls Using Pseudo-dynamic Experiments," by K.M. Mosalam, R.N. White and P. Gergely, 12/31/97, (PB98-153430, A07, MF-A02).
- NCEER-97-0021 "Computational Strategies for Frames with Infill Walls: Discrete and Smeared Crack Analyses and Seismic Fragility," by K.M. Mosalam, R.N. White and P. Gergely, 12/31/97, (PB98-153414, A10, MF-A02).

- NCEER-97-0022 "Proceedings of the NCEER Workshop on Evaluation of Liquefaction Resistance of Soils," edited by T.L. Youd and I.M. Idriss, 12/31/97, (PB98-155617, A15, MF-A03).
- MCEER-98-0001 "Extraction of Nonlinear Hysteretic Properties of Seismically Isolated Bridges from Quick-Release Field Tests," by Q. Chen, B.M. Douglas, E.M. Maragakis and I.G. Buckle, 5/26/98, (PB99-118838, A06, MF-A01).
- MCEER-98-0002 "Methodologies for Evaluating the Importance of Highway Bridges," by A. Thomas, S. Eshenaur and J. Kulicki, 5/29/98, (PB99-118846, A10, MF-A02).
- MCEER-98-0003 "Capacity Design of Bridge Piers and the Analysis of Overstrength," by J.B. Mander, A. Dutta and P. Goel, 6/1/98, (PB99-118853, A09, MF-A02).
- MCEER-98-0004 "Evaluation of Bridge Damage Data from the Loma Prieta and Northridge, California Earthquakes," by N. Basoz and A. Kiremidjian, 6/2/98, (PB99-118861, A15, MF-A03).
- MCEER-98-0005 "Screening Guide for Rapid Assessment of Liquefaction Hazard at Highway Bridge Sites," by T. L. Youd, 6/16/98, (PB99-118879, A06, not available on microfiche).
- MCEER-98-0006 "Structural Steel and Steel/Concrete Interface Details for Bridges," by P. Ritchie, N. Kaulh and J. Kulicki, 7/13/98, (PB99-118945, A06, MF-A01).
- MCEER-98-0007 "Capacity Design and Fatigue Analysis of Confined Concrete Columns," by A. Dutta and J.B. Mander, 7/14/98, (PB99-118960, A14, MF-A03).
- MCEER-98-0008 "Proceedings of the Workshop on Performance Criteria for Telecommunication Services Under Earthquake Conditions," edited by A.J. Schiff, 7/15/98, (PB99-118952, A08, MF-A02).
- MCEER-98-0009 "Fatigue Analysis of Unconfined Concrete Columns," by J.B. Mander, A. Dutta and J.H. Kim, 9/12/98, (PB99-123655, A10, MF-A02).
- MCEER-98-0010 "Centrifuge Modeling of Cyclic Lateral Response of Pile-Cap Systems and Seat-Type Abutments in Dry Sands," by A.D. Gadre and R. Dobry, 10/2/98, (PB99-123606, A13, MF-A03).
- MCEER-98-0011 "IDARC-BRIDGE: A Computational Platform for Seismic Damage Assessment of Bridge Structures," by A.M. Reinhorn, V. Simeonov, G. Mylonakis and Y. Reichman, 10/2/98, (PB99-162919, A15, MF-A03).
- MCEER-98-0012 "Experimental Investigation of the Dynamic Response of Two Bridges Before and After Retrofitting with Elastomeric Bearings," by D.A. Wendichansky, S.S. Chen and J.B. Mander, 10/2/98, (PB99-162927, A15, MF-A03).
- MCEER-98-0013 "Design Procedures for Hinge Restrainers and Hinge Sear Width for Multiple-Frame Bridges," by R. Des Roches and G.L. Fenves, 11/3/98, (PB99-140477, A13, MF-A03).
- MCEER-98-0014 "Response Modification Factors for Seismically Isolated Bridges," by M.C. Constantinou and J.K. Quarshie, 11/3/98, (PB99-140485, A14, MF-A03).
- MCEER-98-0015 "Proceedings of the U.S.-Italy Workshop on Seismic Protective Systems for Bridges," edited by I.M. Friedland and M.C. Constantinou, 11/3/98, (PB2000-101711, A22, MF-A04).
- MCEER-98-0016 "Appropriate Seismic Reliability for Critical Equipment Systems: Recommendations Based on Regional Analysis of Financial and Life Loss," by K. Porter, C. Scawthorn, C. Taylor and N. Blais, 11/10/98, (PB99-157265, A08, MF-A02).
- MCEER-98-0017 "Proceedings of the U.S. Japan Joint Seminar on Civil Infrastructure Systems Research," edited by M. Shinozuka and A. Rose, 11/12/98, (PB99-156713, A16, MF-A03).
- MCEER-98-0018 "Modeling of Pile Footings and Drilled Shafts for Seismic Design," by I. PoLam, M. Kapuskar and D. Chaudhuri, 12/21/98, (PB99-157257, A09, MF-A02).


- MCEER-99-0001 "Seismic Evaluation of a Masonry Infilled Reinforced Concrete Frame by Pseudodynamic Testing," by S.G. Buonopane and R.N. White, 2/16/99, (PB99-162851, A09, MF-A02).
- MCEER-99-0002 "Response History Analysis of Structures with Seismic Isolation and Energy Dissipation Systems: Verification Examples for Program SAP2000," by J. Scheller and M.C. Constantinou, 2/22/99, (PB99-162869, A08, MF-A02).
- MCEER-99-0003 "Experimental Study on the Seismic Design and Retrofit of Bridge Columns Including Axial Load Effects," by A. Dutta, T. Kokorina and J.B. Mander, 2/22/99, (PB99-162877, A09, MF-A02).
- MCEER-99-0004 "Experimental Study of Bridge Elastomeric and Other Isolation and Energy Dissipation Systems with Emphasis on Uplift Prevention and High Velocity Near-source Seismic Excitation," by A. Kasalanati and M. C. Constantinou, 2/26/99, (PB99-162885, A12, MF-A03).
- MCEER-99-0005 "Truss Modeling of Reinforced Concrete Shear-flexure Behavior," by J.H. Kim and J.B. Mander, 3/8/99, (PB99-163693, A12, MF-A03).
- MCEER-99-0006 "Experimental Investigation and Computational Modeling of Seismic Response of a 1:4 Scale Model Steel Structure with a Load Balancing Supplemental Damping System," by G. Pekcan, J.B. Mander and S.S. Chen, 4/2/99, (PB99-162893, A11, MF-A03).
- MCEER-99-0007 "Effect of Vertical Ground Motions on the Structural Response of Highway Bridges," by M.R. Button, C.J. Cronin and R.L. Mayes, 4/10/99, (PB2000-101411, A10, MF-A03).
- MCEER-99-0008 "Seismic Reliability Assessment of Critical Facilities: A Handbook, Supporting Documentation, and Model Code Provisions," by G.S. Johnson, R.E. Sheppard, M.D. Quilici, S.J. Eder and C.R. Scawthorn, 4/12/99, (PB2000-101701, A18, MF-A04).
- MCEER-99-0009 "Impact Assessment of Selected MCEER Highway Project Research on the Seismic Design of Highway Structures," by C. Rojahn, R. Mayes, D.G. Anderson, J.H. Clark, D'Appolonia Engineering, S. Gloyd and R.V. Nutt, 4/14/99, (PB99-162901, A10, MF-A02).
- MCEER-99-0010 "Site Factors and Site Categories in Seismic Codes," by R. Dobry, R. Ramos and M.S. Power, 7/19/99, (PB2000-101705, A08, MF-A02).
- MCEER-99-0011 "Restraint Design Procedures for Multi-Span Simply-Supported Bridges," by M.J. Randall, M. Saiidi, E. Maragakis and T. Isakovic, 7/20/99, (PB2000-101702, A10, MF-A02).
- MCEER-99-0012 "Property Modification Factors for Seismic Isolation Bearings," by M.C. Constantinou, P. Tsopelas, A. Kasalanati and E. Wolff, 7/20/99, (PB2000-103387, A11, MF-A03).
- MCEER-99-0013 "Critical Seismic Issues for Existing Steel Bridges," by P. Ritchie, N. Kauh and J. Kulicki, 7/20/99, (PB2000-101697, A09, MF-A02).
- MCEER-99-0014 "Nonstructural Damage Database," by A. Kao, T.T. Soong and A. Vender, 7/24/99, (PB2000-101407, A06, MF-A01).
- MCEER-99-0015 "Guide to Remedial Measures for Liquefaction Mitigation at Existing Highway Bridge Sites," by H.G. Cooke and J. K. Mitchell, 7/26/99, (PB2000-101703, A11, MF-A03).
- MCEER-99-0016 "Proceedings of the MCEER Workshop on Ground Motion Methodologies for the Eastern United States," edited by N. Abrahamson and A. Becker, 8/11/99, (PB2000-103385, A07, MF-A02).
- MCEER-99-0017 "Quindío, Colombia Earthquake of January 25, 1999: Reconnaissance Report," by A.P. Asfura and P.J. Flores, 10/4/99, (PB2000-106893, A06, MF-A01).
- MCEER-99-0018 "Hysteretic Models for Cyclic Behavior of Deteriorating Inelastic Structures," by M.V. Sivaselvan and A.M. Reinhorn, 11/5/99, (PB2000-103386, A08, MF-A02).

- MCEER-99-0019 "Proceedings of the 7th U.S.- Japan Workshop on Earthquake Resistant Design of Lifeline Facilities and Countermeasures Against Soil Liquefaction," edited by T.D. O'Rourke, J.P. Bardet and M. Hamada, 11/19/99, (PB2000-103354, A99, MF-A06).
- MCEER-99-0020 "Development of Measurement Capability for Micro-Vibration Evaluations with Application to Chip Fabrication Facilities," by G.C. Lee, Z. Liang, J.W. Song, J.D. Shen and W.C. Liu, 12/1/99, (PB2000-105993, A08, MF-A02).
- MCEER-99-0021 "Design and Retrofit Methodology for Building Structures with Supplemental Energy Dissipating Systems," by G. Pekcan, J.B. Mander and S.S. Chen, 12/31/99, (PB2000-105994, A11, MF-A03).
- MCEER-00-0001 "The Marmara, Turkey Earthquake of August 17, 1999: Reconnaissance Report," edited by C. Scawthorn; with major contributions by M. Bruneau, R. Eguchi, T. Holzer, G. Johnson, J. Mander, J. Mitchell, W. Mitchell, A. Papageorgiou, C. Scaethorn, and G. Webb, 3/23/00, (PB2000-106200, A11, MF-A03).
- MCEER-00-0002 "Proceedings of the MCEER Workshop for Seismic Hazard Mitigation of Health Care Facilities," edited by G.C. Lee, M. Ettouney, M. Grigoriu, J. Hauer and J. Nigg, 3/29/00, (PB2000-106892, A08, MF-A02).
- MCEER-00-0003 "The Chi-Chi, Taiwan Earthquake of September 21, 1999: Reconnaissance Report," edited by G.C. Lee and C.H. Loh, with major contributions by G.C. Lee, M. Bruneau, I.G. Buckle, S.E. Chang, P.J. Flores, T.D. O'Rourke, M. Shinozuka, T.T. Soong, C-H. Loh, K-C. Chang, Z-J. Chen, J-S. Hwang, M-L. Lin, G-Y. Liu, K-C. Tsai, G.C. Yao and C-L. Yen, 4/30/00, (PB2001-100980, A10, MF-A02).
- MCEER-00-0004 "Seismic Retrofit of End-Sway Frames of Steel Deck-Truss Bridges with a Supplemental Tendon System: Experimental and Analytical Investigation," by G. Pekcan, J.B. Mander and S.S. Chen, 7/1/00, (PB2001-100982, A10, MF-A02).
- MCEER-00-0005 "Sliding Fragility of Unrestrained Equipment in Critical Facilities," by W.H. Chong and T.T. Soong, 7/5/00, (PB2001-100983, A08, MF-A02).
- MCEER-00-0006 "Seismic Response of Reinforced Concrete Bridge Pier Walls in the Weak Direction," by N. Abo-Shadi, M. Saiidi and D. Sanders, 7/17/00, (PB2001-100981, A17, MF-A03).
- MCEER-00-0007 "Low-Cycle Fatigue Behavior of Longitudinal Reinforcement in Reinforced Concrete Bridge Columns," by J. Brown and S.K. Kunnath, 7/23/00, (PB2001-104392, A08, MF-A02).
- MCEER-00-0008 "Soil Structure Interaction of Bridges for Seismic Analysis," I. PoLam and H. Law, 9/25/00, (PB2001-105397, A08, MF-A02).
- MCEER-00-0009 "Proceedings of the First MCEER Workshop on Mitigation of Earthquake Disaster by Advanced Technologies (MEDAT-1), edited by M. Shinozuka, D.J. Inman and T.D. O'Rourke, 11/10/00, (PB2001-105399, A14, MF-A03).
- MCEER-00-0010 "Development and Evaluation of Simplified Procedures for Analysis and Design of Buildings with Passive Energy Dissipation Systems," by O.M. Ramirez, M.C. Constantinou, C.A. Kircher, A.S. Whittaker, M.W. Johnson, J.D. Gomez and C. Chrysostomou, 11/16/01, (PB2001-105523, A23, MF-A04).
- MCEER-00-0011 "Dynamic Soil-Foundation-Structure Interaction Analyses of Large Caissons," by C-Y. Chang, C-M. Mok, Z-L. Wang, R. Settgast, F. Waggoner, M.A. Ketchum, H.M. Gonnermann and C-C. Chin, 12/30/00, (PB2001-104373, A07, MF-A02).
- MCEER-00-0012 "Experimental Evaluation of Seismic Performance of Bridge Restrainers," by A.G. Vlassis, E.M. Maragakis and M. Saiid Saiidi, 12/30/00, (PB2001-104354, A09, MF-A02).
- MCEER-00-0013 "Effect of Spatial Variation of Ground Motion on Highway Structures," by M. Shinozuka, V. Saxena and G. Deodatis, 12/31/00, (PB2001-108755, A13, MF-A03).
- MCEER-00-0014 "A Risk-Based Methodology for Assessing the Seismic Performance of Highway Systems," by S.D. Werner, C.E. Taylor, J.E. Moore, II, J.S. Walton and S. Cho, 12/31/00, (PB2001-108756, A14, MF-A03).

- MCEER-01-0001 "Experimental Investigation of P-Delta Effects to Collapse During Earthquakes," by D. Vian and M. Bruneau, 6/25/01, (PB2002-100534, A17, MF-A03).
- MCEER-01-0002 "Proceedings of the Second MCEER Workshop on Mitigation of Earthquake Disaster by Advanced Technologies (MEDAT-2)," edited by M. Bruneau and D.J. Inman, 7/23/01, (PB2002-100434, A16, MF-A03).
- MCEER-01-0003 "Sensitivity Analysis of Dynamic Systems Subjected to Seismic Loads," by C. Roth and M. Grigoriu, 9/18/01, (PB2003-100884, A12, MF-A03).
- MCEER-01-0004 "Overcoming Obstacles to Implementing Earthquake Hazard Mitigation Policies: Stage 1 Report," by D.J. Alesch and W.J. Petak, 12/17/01, (PB2002-107949, A07, MF-A02).
- MCEER-01-0005 "Updating Real-Time Earthquake Loss Estimates: Methods, Problems and Insights," by C.E. Taylor, S.E. Chang and R.T. Eguchi, 12/17/01, (PB2002-107948, A05, MF-A01).
- MCEER-01-0006 "Experimental Investigation and Retrofit of Steel Pile Foundations and Pile Bents Under Cyclic Lateral Loadings," by A. Shama, J. Mander, B. Blabac and S. Chen, 12/31/01, (PB2002-107950, A13, MF-A03).
- MCEER-02-0001 "Assessment of Performance of Bolu Viaduct in the 1999 Duzce Earthquake in Turkey" by P.C. Roussis, M.C. Constantinou, M. Erdik, E. Durukal and M. Dicleli, 5/8/02, (PB2003-100883, A08, MF-A02).
- MCEER-02-0002 "Seismic Behavior of Rail Counterweight Systems of Elevators in Buildings," by M.P. Singh, Rildova and L.E. Suarez, 5/27/02. (PB2003-100882, A11, MF-A03).
- MCEER-02-0003 "Development of Analysis and Design Procedures for Spread Footings," by G. Mylonakis, G. Gazetas, S. Nikolaou and A. Chauncey, 10/02/02, (PB2004-101636, A13, MF-A03, CD-A13).
- MCEER-02-0004 "Bare-Earth Algorithms for Use with SAR and LIDAR Digital Elevation Models," by C.K. Huyck, R.T. Eguchi and B. Houshmand, 10/16/02, (PB2004-101637, A07, CD-A07).
- MCEER-02-0005 "Review of Energy Dissipation of Compression Members in Concentrically Braced Frames," by K.Lee and M. Bruneau, 10/18/02, (PB2004-101638, A10, CD-A10).
- MCEER-03-0001 "Experimental Investigation of Light-Gauge Steel Plate Shear Walls for the Seismic Retrofit of Buildings" by J. Berman and M. Bruneau, 5/2/03, (PB2004-101622, A10, MF-A03, CD-A10).
- MCEER-03-0002 "Statistical Analysis of Fragility Curves," by M. Shinozuka, M.Q. Feng, H. Kim, T. Uzawa and T. Ueda, 6/16/03, (PB2004-101849, A09, CD-A09).
- MCEER-03-0003 "Proceedings of the Eighth U.S.-Japan Workshop on Earthquake Resistant Design of Lifeline Facilities and Countermeasures Against Liquefaction," edited by M. Hamada, J.P. Bardet and T.D. O'Rourke, 6/30/03, (PB2004-104386, A99, CD-A99).
- MCEER-03-0004 "Proceedings of the PRC-US Workshop on Seismic Analysis and Design of Special Bridges," edited by L.C. Fan and G.C. Lee, 7/15/03, (PB2004-104387, A14, CD-A14).
- MCEER-03-0005 "Urban Disaster Recovery: A Framework and Simulation Model," by S.B. Miles and S.E. Chang, 7/25/03, (PB2004-104388, A07, CD-A07).
- MCEER-03-0006 "Behavior of Underground Piping Joints Due to Static and Dynamic Loading," by R.D. Meis, M. Maragakis and R. Siddharthan, 11/17/03, (PB2005-102194, A13, MF-A03, CD-A00).
- MCEER-03-0007 "Seismic Vulnerability of Timber Bridges and Timber Substructures," by A.A. Shama, J.B. Mander, I.M. Friedland and D.R. Allicock, 12/15/03.
- MCEER-04-0001 "Experimental Study of Seismic Isolation Systems with Emphasis on Secondary System Response and Verification of Accuracy of Dynamic Response History Analysis Methods," by E. Wolff and M. Constantinou, 1/16/04 (PB2005-102195, A99, MF-E08, CD-A00).


- MCEER-04-0002 “Tension, Compression and Cyclic Testing of Engineered Cementitious Composite Materials,” by K. Kesner and S.L. Billington, 3/1/04, (PB2005-102196, A08, CD-A08).
- MCEER-04-0003 “Cyclic Testing of Braces Laterally Restrained by Steel Studs to Enhance Performance During Earthquakes,” by O.C. Celik, J.W. Berman and M. Bruneau, 3/16/04, (PB2005-102197, A13, MF-A03, CD-A00).
- MCEER-04-0004 “Methodologies for Post Earthquake Building Damage Detection Using SAR and Optical Remote Sensing: Application to the August 17, 1999 Marmara, Turkey Earthquake,” by C.K. Huyck, B.J. Adams, S. Cho, R.T. Eguchi, B. Mansouri and B. Houshmand, 6/15/04, (PB2005-104888, A10, CD-A00).
- MCEER-04-0005 “Nonlinear Structural Analysis Towards Collapse Simulation: A Dynamical Systems Approach,” by M.V. Sivaselvan and A.M. Reinhorn, 6/16/04, (PB2005-104889, A11, MF-A03, CD-A00).
- MCEER-04-0006 “Proceedings of the Second PRC-US Workshop on Seismic Analysis and Design of Special Bridges,” edited by G.C. Lee and L.C. Fan, 6/25/04, (PB2005-104890, A16, CD-A00).
- MCEER-04-0007 “Seismic Vulnerability Evaluation of Axially Loaded Steel Built-up Laced Members,” by K. Lee and M. Bruneau, 6/30/04, (PB2005-104891, A16, CD-A00).
- MCEER-04-0008 “Evaluation of Accuracy of Simplified Methods of Analysis and Design of Buildings with Damping Systems for Near-Fault and for Soft-Soil Seismic Motions,” by E.A. Pavlou and M.C. Constantinou, 8/16/04, (PB2005-104892, A08, MF-A02, CD-A00).
- MCEER-04-0009 “Assessment of Geotechnical Issues in Acute Care Facilities in California,” by M. Lew, T.D. O’Rourke, R. Dobry and M. Koch, 9/15/04, (PB2005-104893, A08, CD-A00).
- MCEER-04-0010 “Scissor-Jack-Damper Energy Dissipation System,” by A.N. Sigaher-Boyle and M.C. Constantinou, 12/1/04 (PB2005-108221).
- MCEER-04-0011 “Seismic Retrofit of Bridge Steel Truss Piers Using a Controlled Rocking Approach,” by M. Pollino and M. Bruneau, 12/20/04 (PB2006-105795).
- MCEER-05-0001 “Experimental and Analytical Studies of Structures Seismically Isolated with an Uplift-Restraint Isolation System,” by P.C. Roussis and M.C. Constantinou, 1/10/05 (PB2005-108222).
- MCEER-05-0002 “A Versatile Experimentation Model for Study of Structures Near Collapse Applied to Seismic Evaluation of Irregular Structures,” by D. Kusumastuti, A.M. Reinhorn and A. Rutenberg, 3/31/05 (PB2006-101523).
- MCEER-05-0003 “Proceedings of the Third PRC-US Workshop on Seismic Analysis and Design of Special Bridges,” edited by L.C. Fan and G.C. Lee, 4/20/05, (PB2006-105796).
- MCEER-05-0004 “Approaches for the Seismic Retrofit of Braced Steel Bridge Piers and Proof-of-Concept Testing of an Eccentrically Braced Frame with Tubular Link,” by J.W. Berman and M. Bruneau, 4/21/05 (PB2006-101524).
- MCEER-05-0005 “Simulation of Strong Ground Motions for Seismic Fragility Evaluation of Nonstructural Components in Hospitals,” by A. Wanitkorkul and A. Filiatrault, 5/26/05 (PB2006-500027).
- MCEER-05-0006 “Seismic Safety in California Hospitals: Assessing an Attempt to Accelerate the Replacement or Seismic Retrofit of Older Hospital Facilities,” by D.J. Alesch, L.A. Arendt and W.J. Petak, 6/6/05 (PB2006-105794).
- MCEER-05-0007 “Development of Seismic Strengthening and Retrofit Strategies for Critical Facilities Using Engineered Cementitious Composite Materials,” by K. Kesner and S.L. Billington, 8/29/05 (PB2006-111701).
- MCEER-05-0008 “Experimental and Analytical Studies of Base Isolation Systems for Seismic Protection of Power Transformers,” by N. Murota, M.Q. Feng and G-Y. Liu, 9/30/05 (PB2006-111702).
- MCEER-05-0009 “3D-BASIS-ME-MB: Computer Program for Nonlinear Dynamic Analysis of Seismically Isolated Structures,” by P.C. Tsopelas, P.C. Roussis, M.C. Constantinou, R. Buchanan and A.M. Reinhorn, 10/3/05 (PB2006-111703).

- MCEER-05-0010 “Steel Plate Shear Walls for Seismic Design and Retrofit of Building Structures,” by D. Vian and M. Bruneau, 12/15/05 (PB2006-111704).
- MCEER-05-0011 “The Performance-Based Design Paradigm,” by M.J. Astrella and A. Whittaker, 12/15/05 (PB2006-111705).
- MCEER-06-0001 “Seismic Fragility of Suspended Ceiling Systems,” H. Badillo-Almaraz, A.S. Whittaker, A.M. Reinhorn and G.P. Cimellaro, 2/4/06 (PB2006-111706).
- MCEER-06-0002 “Multi-Dimensional Fragility of Structures,” by G.P. Cimellaro, A.M. Reinhorn and M. Bruneau, 3/1/06.
- MCEER-06-0003 “Built-Up Shear Links as Energy Dissipators for Seismic Protection of Bridges,” by P. Dusicka, A.M. Itani and I.G. Buckle, 3/15/06 (PB2006-111708).
- MCEER-06-0004 “Analytical Investigation of the Structural Fuse Concept,” by R.E. Vargas and M. Bruneau, 3/16/06 (PB2006-111709).
- MCEER-06-0005 “Experimental Investigation of the Structural Fuse Concept,” by R.E. Vargas and M. Bruneau, 3/17/06 (PB2006-111710).
- MCEER-06-0006 “Further Development of Tubular Eccentrically Braced Frame Links for the Seismic Retrofit of Braced Steel Truss Bridge Piers,” by J.W. Berman and M. Bruneau, 3/27/06.
- MCEER-06-0007 “REDARS Validation Report,” by S. Cho, C.K. Huyck, S. Ghosh and R.T. Eguchi, 8/8/06.
- MCEER-06-0008 “Review of Current NDE Technologies for Post-Earthquake Assessment of Retrofitted Bridge Columns,” by J.W. Song, Z. Liang and G.C. Lee, 8/21/06.
- MCEER-06-0009 “Liquefaction Remediation in Silty Soils Using Dynamic Compaction and Stone Columns,” by S. Thevanayagam, G.R. Martin, R. Nashed, T. Shenthan, T. Kanagalingam and N. Ecemis, 8/28/06.
- MCEER-06-0010 “Conceptual Design and Experimental Investigation of Polymer Matrix Composite Infill Panels for Seismic Retrofitting,” by W. Jung, M. Chiewanichakorn and A.J. Aref, 9/21/06.



EARTHQUAKE ENGINEERING TO EXTREME EVENTS

University at Buffalo, The State University of New York
Red Jacket Quadrangle ▪ Buffalo, New York 14261
Phone: (716) 645-3391 ▪ Fax: (716) 645-3399
E-mail: mceer@buffalo.edu ▪ WWW Site <http://mceer.buffalo.edu>



University at Buffalo *The State University of New York*

ISSN 1520-295X